

TARGETING THE MICROENVIRONMENT NICHE IN SOLID AND HEMATOLOGIC MALIGNANCIES: BASIC AND TRANSLATIONAL RESEARCH

EDITED BY: Cirino Botta, Marco Rossi, Niccolò Bolli and Niels Weinhold
PUBLISHED IN: Frontiers in Oncology





frontiers

Frontiers eBook Copyright Statement

The copyright in the text of individual articles in this eBook is the property of their respective authors or their respective institutions or funders. The copyright in graphics and images within each article may be subject to copyright of other parties. In both cases this is subject to a license granted to Frontiers.

The compilation of articles constituting this eBook is the property of Frontiers.

Each article within this eBook, and the eBook itself, are published under the most recent version of the Creative Commons CC-BY licence.

The version current at the date of publication of this eBook is CC-BY 4.0. If the CC-BY licence is updated, the licence granted by Frontiers is automatically updated to the new version.

When exercising any right under the CC-BY licence, Frontiers must be attributed as the original publisher of the article or eBook, as applicable.

Authors have the responsibility of ensuring that any graphics or other materials which are the property of others may be included in the CC-BY licence, but this should be checked before relying on the CC-BY licence to reproduce those materials. Any copyright notices relating to those materials must be complied with.

Copyright and source acknowledgement notices may not be removed and must be displayed in any copy, derivative work or partial copy which includes the elements in question.

All copyright, and all rights therein, are protected by national and international copyright laws. The above represents a summary only. For further information please read Frontiers' Conditions for Website Use and Copyright Statement, and the applicable CC-BY licence.

ISSN 1664-8714

ISBN 978-2-88974-541-8

DOI 10.3389/978-2-88974-541-8

About Frontiers

Frontiers is more than just an open-access publisher of scholarly articles: it is a pioneering approach to the world of academia, radically improving the way scholarly research is managed. The grand vision of Frontiers is a world where all people have an equal opportunity to seek, share and generate knowledge. Frontiers provides immediate and permanent online open access to all its publications, but this alone is not enough to realize our grand goals.

Frontiers Journal Series

The Frontiers Journal Series is a multi-tier and interdisciplinary set of open-access, online journals, promising a paradigm shift from the current review, selection and dissemination processes in academic publishing. All Frontiers journals are driven by researchers for researchers; therefore, they constitute a service to the scholarly community. At the same time, the Frontiers Journal Series operates on a revolutionary invention, the tiered publishing system, initially addressing specific communities of scholars, and gradually climbing up to broader public understanding, thus serving the interests of the lay society, too.

Dedication to Quality

Each Frontiers article is a landmark of the highest quality, thanks to genuinely collaborative interactions between authors and review editors, who include some of the world's best academicians. Research must be certified by peers before entering a stream of knowledge that may eventually reach the public - and shape society; therefore, Frontiers only applies the most rigorous and unbiased reviews.

Frontiers revolutionizes research publishing by freely delivering the most outstanding research, evaluated with no bias from both the academic and social point of view. By applying the most advanced information technologies, Frontiers is catapulting scholarly publishing into a new generation.

What are Frontiers Research Topics?

Frontiers Research Topics are very popular trademarks of the Frontiers Journals Series: they are collections of at least ten articles, all centered on a particular subject. With their unique mix of varied contributions from Original Research to Review Articles, Frontiers Research Topics unify the most influential researchers, the latest key findings and historical advances in a hot research area! Find out more on how to host your own Frontiers Research Topic or contribute to one as an author by contacting the Frontiers Editorial Office: frontiersin.org/about/contact

TARGETING THE MICROENVIRONMENT NICHE IN SOLID AND HEMATOLOGIC MALIGNANCIES: BASIC AND TRANSLATIONAL RESEARCH

Topic Editors:

Cirino Botta, University of Palermo, Italy

Marco Rossi, University of Catanzaro, Italy

Niccolò Bolli, University of Milan, Italy

Niels Weinhold, Heidelberg University, Germany

Citation: Botta, C., Rossi, M., Bolli, N., Weinhold, N., eds. (2022). Targeting the Microenvironment Niche in Solid and Hematologic Malignancies: Basic and Translational Research. Lausanne: Frontiers Media SA.

doi: 10.3389/978-2-88974-541-8

Table of Contents

- 05 Prognostic and Immunological Role of FUN14 Domain Containing 1 in Pan-Cancer: Friend or Foe?**
Qingchen Yuan, Na Sun, Jiayu Zheng, Yingxuan Wang, Xiaole Yan, Wujian Mai, Yuhua Liao and Xiao Chen
- 18 Neem Leaf Glycoprotein Restrains VEGF Production by Direct Modulation of HIF1 α -Linked Upstream and Downstream Cascades**
Akata Saha, Partha Nandi, Shayani Dasgupta, Avishek Bhuniya, Nilanjan Ganguly, Tithi Ghosh, Ipsita Guha, Saptak Banerjee, Rathindranath Baral and Anamika Bose
- 29 The Autonomic Regulation of Tumor Growth and the Missing Links**
Maricris Bautista and Anand Krishnan
- 36 GPI-AP: Unraveling a New Class of Malignancy Mediators and Potential Immunotherapy Targets**
Nada H. Hussein, Nada S. Amin and Hend M. El Tayebi
- 54 A Novel Blockade CD47 Antibody With Therapeutic Potential for Cancer**
Fangzhen Lin, Mengshang Xiong, Wei Hao, Yuewen Song, Ruoqi Liu, Yuanyuan Yang, Xiangfei Yuan, Dongmei Fan, Yizi Zhang, Mu Hao, Zhou Ye, Yang Lu, Yanjun Zhang, Jianxiang Wang and Dongsheng Xiong
- 62 Targeting Adrenomedullin in Oncology: A Feasible Strategy With Potential as Much More Than an Alternative Anti-Angiogenic Therapy**
Ramiro Vázquez, Maria E. Riveiro, Caroline Berenguer-Daizé, Anthony O’Kane, Julie Gormley, Olivier Touzelet, Keyvan Rezai, Mohamed Bekradda and L’Houcine Ouafik
- 85 P. aeruginosa Mediated Necroptosis in Mouse Tumor Cells Induces Long-Lasting Systemic Antitumor Immunity**
Jia-long Qi, Jin-rong He, Shu-mei Jin, Xu Yang, Hong-mei Bai, Cun-bao Liu and Yan-bing Ma
- 97 Pictilisib Enhances the Antitumor Effect of Doxorubicin and Prevents Tumor-Mediated Bone Destruction by Blockade of PI3K/AKT Pathway**
Chao Liang, Xijiao Yu, Naping Xiong, Zhichang Zhang, Zhenyu Sun and Yang Dong
- 112 Potential Roles of Acute Phase Proteins in Cancer: Why Do Cancer Cells Produce or Take Up Exogenous Acute Phase Protein Alpha1-Antitrypsin?**
Sabina Janciauskiene, Sabine Wrenger, Steffen Günzel, Anna Ricarda Gründing, Heiko Golpon and Tobias Welte
- 122 LRIG3 Suppresses Angiogenesis by Regulating the PI3K/AKT/VEGFA Signaling Pathway in Glioma**
Chenghao Peng, Hanmin Chen, Youwei Li, Hang Yang, Peizhong Qin, Baojun Ma, Qiuhong Duan, Baofeng Wang, Feng Mao and Dongsheng Guo

133 *HOTAIRM1 Promotes Malignant Progression of Transformed Fibroblasts in Glioma Stem-Like Cells Remodeled Microenvironment via Regulating miR-133b-3p/TGF β Axis*

Haiyang Wang, Haoran Li, Qianqian Jiang, Xuchen Dong, Suwen Li, Shan Cheng, Jia Shi, Liang Liu, Zhiyuan Qian and Jun Dong

146 *YTHDF1 Is a Potential Pan-Cancer Biomarker for Prognosis and Immunotherapy*

Jian Hu, Dongxu Qiu, Anze Yu, Jiao Hu, Hao Deng, Huihuang Li, Zhenglin Yi, Jinbo Chen and Xiongbing Zu



Prognostic and Immunological Role of FUN14 Domain Containing 1 in Pan-Cancer: Friend or Foe?

Qingchen Yuan^{1,2†}, Na Sun^{3†}, Jiayu Zheng^{1,2}, Yingxuan Wang^{1,2}, Xiaole Yan^{1,2}, Wuqian Mai^{1,2}, Yuhua Liao^{1,2*} and Xiao Chen^{1,2*}

¹ Department of Cardiology, Tongji Medical College, Union Hospital, Huazhong University of Science and Technology, Wuhan, China, ² Key Lab of Molecular Biological Targeted Therapies of the Ministry of Education, Tongji Medical College, Union Hospital, Huazhong University of Science and Technology, Wuhan, China, ³ Department of Pathogen Biology, School of Basic Medicine, Tongji Medical College, Huazhong University of Science and Technology, Wuhan, China

OPEN ACCESS

Edited by:

Niels Weinhold,
Heidelberg University, Germany

Reviewed by:

Christian Badr,
Massachusetts General Hospital,
Harvard Medical School,
United States
Shiv K. Gupta,
Mayo Clinic, United States

*Correspondence:

Yuhua Liao
liaoyh27@163.com
Xiao Chen
skycreeper@126.com

[†]These authors have contributed
equally to this work

Specialty section:

This article was submitted to
Cancer Molecular Targets and
Therapeutics,
a section of the journal
Frontiers in Oncology

Received: 15 September 2019

Accepted: 16 December 2019

Published: 10 January 2020

Citation:

Yuan Q, Sun N, Zheng J, Wang Y,
Yan X, Mai W, Liao Y and Chen X
(2020) Prognostic and Immunological
Role of FUN14 Domain Containing 1
in Pan-Cancer: Friend or Foe?
Front. Oncol. 9:1502.
doi: 10.3389/fonc.2019.01502

Background: FUN14 domain containing 1 (FUNDC1) plays a pivotal role in mitochondrial autophagy (mitophagy), which is closely associated with human immunity. However, the role of FUNDC1 in cancers remains unclear. This study aimed to visualize the prognostic landscape of FUNDC1 in pan-cancer and investigate the relationship between FUNDC1 expression and immune infiltration.

Methods: In this study, we explored the expression pattern and prognostic value of FUNDC1 in pan-cancer across multiple databases, including ONCOMINE, PrognScan, GEPIA, and Kaplan-Meier Plotter. Then, using the GEPIA and TIMER databases, we investigated the correlations between FUNDC1 expression and immune infiltration in cancers, especially liver hepatocellular carcinoma (LIHC), and lung squamous cell carcinoma (LUSC).

Results: In general, compared with that in normal tissue, tumor tissue had a higher expression level of FUNDC1. Although FUNDC1 showed a protective effect on pan-cancer, a high expression level of FUNDC1 was detrimental to the survival of LIHC patients. Although different from what was found for LUSC, for LIHC, there were significant positive correlations between FUNDC1 expression and immune infiltrates, including B cells, CD8+ T cells, CD4+ T cells, neutrophils, macrophages, and dendritic cells. Furthermore, markers of infiltrating immune cells, such as tumor-associated-macrophages (TAMs), exhibited different FUNDC1-related immune infiltration patterns.

Conclusion: The mitophagy regulator FUNDC1 can serve as a prognostic biomarker in pan-cancer and is correlated with immune infiltrates.

Keywords: mitophagy, pan-cancer, database, survival analysis, immune infiltration, tumor microenvironment

INTRODUCTION

As the power plants in the human cells mitochondria generate adenosine triphosphate by oxidative phosphorylation to fuel cellular activities while also producing reactive oxygen species, which damage them. To maintain a proper balance, mitochondria undergo fission-fusion cycles and eliminate damaged and redundant sections by mitochondrial autophagy (mitophagy), a process that requires various molecular interactions during mitochondrial quality control (1–3).

FUN14 domain containing 1 (FUNDC1), which anchors to the outer mitochondrial membrane, is pivotal in mitophagy (4, 5). FUNDC1 interacts with molecules like LC3B, which is found on the mitochondria-associated membrane of the endoplasmic reticulum, to maintain good mitochondrial quality by forming mitophagosomes (4). FUNDC1-related mitochondrial dysfunction contributes to various pathophysiological processes, such as heart diseases, metabolic disorders, and cancers (6–9). In cardiovascular and metabolic diseases, FUNDC1 is generally considered to be protective because FUNDC1-mediated mitophagy can alleviate damage caused by intracellular stress such as hypoxia and thus benefit overall outcomes (9, 10). However, unlike in non-cancerous diseases, the role of FUNDC1 in pan-cancer has been largely underexplored. Meanwhile, the role of FUNDC1 might be context dependent and could vary among different cancers. For example, FUNDC1 can promote tumor progression and predict poor prognosis in some cancer types; however, it can also suppress carcinogenesis through mitophagy (6, 7, 11). Thus, it remains unclear whether FUNDC1 can be characterized as a friend or foe in pan-cancer.

The tumor microenvironment (TME) contains various cells. Among them, infiltrating immune cells account for a large proportion (12). On the one hand, unlike the conventional view of immune cells as a component of an antitumor strategy, immune infiltration into the TME reflects a tactic tumor cells use to avoid being killed (13–15). For example, tumor-associated-macrophages (TAMs) can help tumor cells in several ways, including immune escape, tumor angiogenesis, and metastasis (16–19). In addition, aside from macrophages, almost all types of immune cells, including B cells, CD8⁺ T cells, CD4⁺ T cells, neutrophils, natural killer (NK) cells, and dendritic cells (DC), are found in the TME, and some participate in the development of cancers (12). In contrast, immunotherapy targeting interactions between immune cells and tumor cells, as an alternative approach to classic anticancer treatments, have been developed in recent years to reactivate adaptive and innate immune systems and create a robust antitumoral immune response. For example, cytotoxic T lymphocyte associated antigen 4 (CTLA4), programmed death-1 (PD-1), and programmed death ligand-1 (PD-L1) inhibitors were found to have promising antitumor effects on malignant melanoma and non-small-cell lung carcinoma (14, 20). However, only a limited proportion of patients with certain cancer types respond well to current immunotherapies (14). Thus, it is necessary to explore additional potential targets.

Abbreviations: BLCA, bladder urothelial carcinoma; BRCA, breast invasive carcinoma; CHOL, cholangiocarcinoma; COAD, colon adenocarcinoma; DFS, disease-free survival; DMFS, distant metastasis-free survival; DSS, disease-specific survival; FUNDC1, FUN14 domain containing 1; HNSC, head and neck squamous cell carcinoma; HNSC-HPVpos, head and neck squamous carcinoma-HPV positive; HR, hazard ratio; KICH, kidney chromophobe; KIRC, kidney renal clear cell carcinoma; LGG, brain lower grade glioma; LIHC, liver hepatocellular carcinoma; LUAD, lung adenocarcinoma; LUSC, lung squamous cell carcinoma; OS, overall survival; OV, ovarian cancer; PFS, progression-free survival; PRAD, prostate adenocarcinoma; READ, rectum adenocarcinoma; RFS, relapse-free survival; TAM, tumor-associated-macrophage; THCA, thyroid carcinoma; TME, tumor microenvironment; UCEC, uterine corpus endometrial carcinoma.

In this study, we visualized the prognostic landscape of FUNDC1 in pan-cancer using databases, including ONCOMINE, PrognoScan, GEPIA, and Kaplan-Meier Plotter. We then explored the potential relationships between FUNDC1 expression and immune infiltration levels using the TIMER and GEPIA databases. The findings from this study indicate that FUNDC1 influences the prognosis of patients with cancers, probably via its interaction with infiltrating immune cells.

MATERIALS AND METHODS

FUNDC1 Expression in Human Cancers in ONCOMINE

The mRNA expression of FUNDC1 in different cancer types was analyzed in the ONCOMINE database (www.oncomine.org). The thresholds were set as a *P*-value of 0.001 and fold change of 1.5.

Survival Analysis in PrognoScan, GEPIA, and Kaplan-Meier Plotter

The correlation between FUNDC1 expression and survival in pan-cancer was analyzed in PrognoScan (<http://dna00.bio.kyutech.ac.jp/PrognoScan/index.html>), Kaplan-Meier Plotter (<https://kmplot.com/analysis/>), and GEPIA (<http://gepia.cancer-pku.cn/>) (21–23). Specifically, the FUNDC1 expression level was searched in all available microarray datasets of PrognoScan to determine its relationship with prognosis, including overall survival (OS) and disease-free survival (DFS). The threshold was set as a Cox *P*-value < 0.05, and R software (version 3.25.0, www.r-project.org) with the “forestplot” package was utilized to summarize and visualize the survival analysis from PrognoScan. GEPIA is an interactive online platform with tumor sample information from TCGA and GTEx projects. We explored the effect of FUNDC1 expression on OS and DFS in each available cancer type (total number = 34). Kaplan-Meier Plotter is a powerful online tool that can be used to assess the effect of 54,000 genes on survival in 21 cancer types. We analyzed the relationship of FUNDC1 expression with overall survival (OS) and relapse-free survival (RFS) in liver hepatocellular carcinoma (LIHC), lung squamous cell carcinoma (LUSC), bladder carcinoma (BC), head and neck squamous cell carcinoma (HNSC), ovarian carcinoma (OV), breast invasive carcinoma (BRCA), lung adenocarcinoma (LUAD), and rectum adenocarcinoma (READ). Hazard ratios (HRs) with 95% confidence intervals (CI) and log-rank *P*-values were calculated.

Correlations Between FUNDC1 Expression and Immune Cells in TIMER and GEPIA

The relationship between FUNDC1 expression and immune infiltration was determined using the TIMER (<http://cistrome.org/TIMER/>) and GEPIA databases (23, 24). TIMER is an ideal resource for the systematic analysis of immune infiltration across diverse cancer types. TIMER applies a previously published statistical deconvolution method to infer the abundance of tumor-infiltrating immune cells from gene expression profiles (24). The TIMER database contains 10,897 samples across

32 cancer types from TCGA to allow the evaluation of the abundance of immune infiltration. We analyzed FUNDC1 expression with the abundance of all six types of immune infiltrating cells, including B cells, CD4+ T cells, CD8+ T cells, neutrophils, macrophages, and dendritic cells. The relationship between the expression level of FUNDC1 and tumor purity was also determined.

In addition to the general analysis of immune cell type, we also analyzed the correlation between FUNDC1 expression and several immune cell markers to identify the potential subtypes of infiltrating immune cells. Immune gene markers were selected from the website of R&D Systems (<https://www.rndsystems.com/cn/resources/cell-markers/immune-cells>). These gene markers include markers of B cells, CD8+ T cells, follicular helper T cells (Tfh), T-helper 1 (Th1) cells, T-helper 2 (Th2) cells, T-helper 9 (Th9) cells, T-helper 17 (Th17) cells, T-helper 22 (Th22) cells, Tregs, exhausted T cells, M1 macrophages, M2 macrophages, tumor-associated macrophages, monocytes, natural killer (NK) cells, neutrophils, and dendritic cells. The gene expression level was adjusted with \log_2 RSEM. FUNDC1 was plotted on the x-axis, while marker genes were plotted on the y-axis. Scatterplots were used to analyze correlations between FUNDC1 and each immune gene marker. Similarly, in GEPIA, gene expression correlation analysis was performed for given sets of TCGA expression data. The Spearman method was used to determine the correlation coefficient. FUNDC1 was plotted on the x-axis, while other genes of interest were plotted on the y-axis.

Statistical Analysis

The results generated in OncoPrint are presented with P-values determined in *t*-tests, fold changes, and gene ranks. The Kaplan-Meier method was used to estimate the survival curve. To compare survival curves, we used the log rank test to calculate the HR and logrank *P*-value in Kaplan-Meier Plotter and GEPIA. A univariate Cox regression model was used to calculate the HR and Cox *P* value in PrognScan. The correlation of gene expression was evaluated using Spearman's correlation. A *P* < 0.05 was considered statistically significant, if not specially noted.

RESULTS

mRNA Expression Level of FUNDC1 in Pan-Cancer

FUNDC1 mRNA expression levels were analyzed in OncoPrint to examine FUNDC1 expression over a cancer-wide range. The results revealed that compared with that in the respective normal groups, FUNDC1 expression was higher in cancer groups, including breast, cervical, colorectal, lung, ovarian, pancreatic, and prostate cancers as well as leukemia and lymphoma. Meanwhile, a lower expression of FUNDC1 was only found in one breast cancer dataset (Figure 1A). The details of FUNDC1 expression in multiple cancers are summarized in Supplementary Table 1.

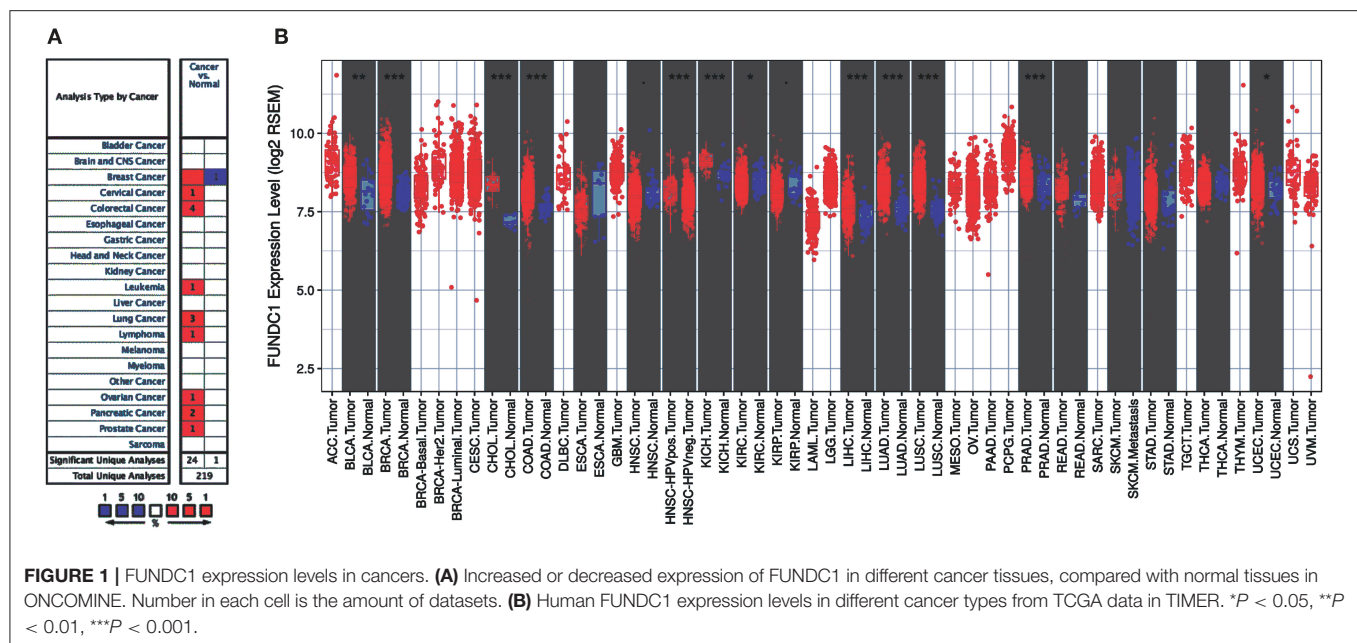
To further evaluate FUNDC1 expression in pan-cancer, we examined RNA sequencing data in TCGA using TIMER. The differential FUNDC1 expression patterns in tumor and

adjacent normal tissues are shown in Figure 1B. FUNDC1 expression was significantly lower in KIRC (kidney renal clear cell carcinoma) than in normal tissue. Meanwhile, FUNDC1 expression was significantly higher in BLCA (bladder urothelial carcinoma), BRCA (breast invasive carcinoma), CHOL (cholangiocarcinoma), COAD (colon adenocarcinoma), HNSC-HPV positive (head and neck squamous carcinoma-HPV positive), KICH (kidney chromophobe), LIHC (liver hepatocellular carcinoma), LUAD (lung adenocarcinoma), LUSC (lung squamous cell carcinoma), PRAD (prostate adenocarcinoma), and UCEC (uterine corpus endometrial carcinoma) than in their respective adjacent normal tissues.

Multifaceted Prognostic Value of FUNDC1 in Cancers

Next, we investigated the prognostic value of FUNDC1 for pan-cancer in different databases. In PrognScan, we explored the relationships between FUNDC1 expression and the prognosis of each cancer. The results are summarized in Supplementary Figure 1. Notably, FUNDC1 expression was significantly correlated with a total of eight cancer types, including bladder, brain, breast, colorectal, head and neck, lung, ovarian, and skin cancers (Figure 2). Among them, FUNDC1 played a detrimental role in five cancer types, including brain (OS: total number = 74, HR = 4.05, Cox *P* = 0.007261), breast [DMFS (distant metastasis-free survival): total number = 77, HR = 5.33, Cox *P* = 0.039723], colorectal [DFS (disease-free survival): total number = 55, HR = 2.48, Cox *P* = 0.015719; DSS (disease-specific survival): total number = 49, HR = 2.14, Cox *P* = 0.043165], head and neck [RFS (relapse-free survival): total number = 28, HR = 2.32, Cox *P* = 0.022573], and skin cancers (OS: total number = 38, HR = 4.29, Cox *P* = 0.031662). Meanwhile, FUNDC1 had a protective role in the other 3 cancer types, including bladder (DSS: total number = 165, HR = 0.54, Cox *P* = 0.002943), lung (OS: total number = 204, HR = 0.48, Cox *P* = 0.036986), and ovarian cancers (DFS: total number = 185, HR = 0.38, Cox *P* = 0.044859).

Using Kaplan-Meier Plotter, which is mainly based on Affymetrix microarray information from TCGA, we further assessed FUNDC1-related survival (OS and RFS) because the data in PrognScan are mainly extracted from the gene expression omnibus (GEO) database. Interestingly, we newly identified FUNDC1 as a detrimental prognostic factor in LIHC (OS: HR = 1.73, 95% CI from 1.21 to 2.46, logrank *P* = 0.0022; RFS, HR = 1.56, 95%CI from 1.12 to 2.17, logrank *P* = 0.0082) (Figures 3A,B). This finding may challenge the previously reported protective role of FUNDC1 in hepatocellular carcinogenesis (11). The findings for lung cancer were partly different from those using PrognScan, as a high expression of FUNDC1 only benefited LUSC (OS: HR = 0.64, 95 % CI from 0.48 to 0.85 logrank *P* = 0.0017; RFS: HR = 0.55, 95% CI from 0.33 to 0.91, logrank *P* = 0.019) (Figures 2C,D) and not LUAD (OS: HR = 0.8, 95% CI from 0.6 to 1.08, logrank *P* = 0.15; RFS: HR = 1.41, 95% CI from 0.91 to 2.19, logrank *P* = 0.13) (Figures 3M,N). For bladder cancer, FUNDC1 was found to have a protective effect on overall survival (OS: HR



= 0.59, 95% CI from 0.44 to 0.8, logrank $P = 0.00045$). However, FUNDC1 worsened relapse-free survival in bladder cancer (RFS: HR = 2.15, 95% CI from 1.01 to 4.58, logrank $P = 0.043$) (Figures 3E,F). For both head and neck squamous cell carcinoma (HNSC) and ovarian cancer (OV), FUNDC1 significantly influenced their overall survival (HNSC: OS, HR = 1.34, 95% CI from 1.02 to 1.75, logrank $P = 0.034$; OV: OS, HR = 0.66, 95% CI from 0.49 to 0.88, logrank $P = 0.0047$) but not relapse-free survival (HNSC: RFS, HR = 1.49, 95% CI from 0.7 to 3.17, logrank $P = 0.29$; OVC: RFS, HR = 0.74, 95% CI from 0.52 to 1.06, logrank $P = 0.095$) (Figures 3G–J). For BRCA, FUNDC1 had a protective effect on relapse-free survival (RFS: HR = 0.39, 95% CI from 0.21 to 0.74, logrank $P = 0.0029$) but did not have a significant effect on overall survival (OS: HR = 1.29, 95% CI from 0.93 to 1.77, logrank $P = 0.12$) (Figures 3K,L). In addition, for colorectal cancer, FUNDC1 only had a protective effect on RFS for rectum adenocarcinoma (READ) (OS: HR = 2.01, 95% CI from 0.6 to 6.7, logrank $P = 0.25$; RFS: HR = 0.18, 95% CI from 0.03 to 1.04, logrank $P = 0.033$) (Figures 3O,P).

In addition to the microarray analysis of FUNDC1 in Prognoscan and Kaplan-Meier Plotter, we also utilized GEPIA to analyze RNA sequencing data in TCGA. In GEPIA, we analyzed the role of FUNDC1 in each cancer type (number of cancer types = 33), as well as the overall effect of FUNDC1 on cancers. In general, FUNDC1 was a favorable prognostic marker in cancers (OS: total number = 9,496, HR = 0.72, logrank $P = 0$; DFS: total number = 9,496, HR = 0.8, logrank $P = 6.6E-09$) (Supplementary Figure 2A). Specifically, compared with a low expression level, a high expression level of FUNDC1 was correlated with a better OS in KIRC and LUSC and DFS in thyroid carcinoma (THCA). On the contrary, compared with a low expression level, a high expression level of FUNDC1 was correlated with a poorer OS in brain lower grade glioma (LGG) and LIHC. In addition, unlike the findings from Prognoscan and Kaplan-Meier Plotter, FUNDC1 expression impacted neither OS

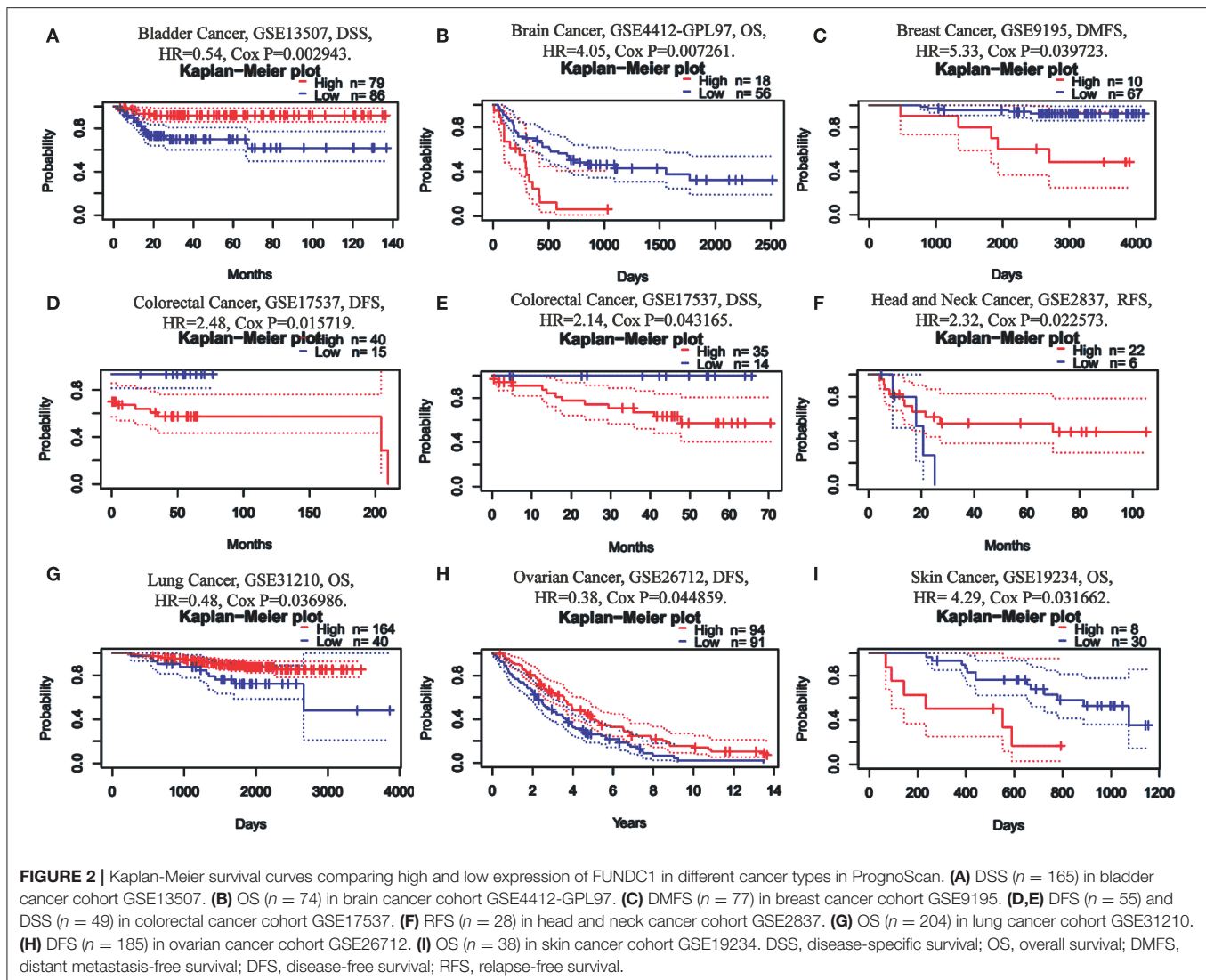
nor DFS in BRCA, CHOL, COAD, HNSC, KICH, LUAD, OV, READ, and UCEC (Supplementary Figure 2).

FUNDC1 Expression in a Stratified LIHC Population

Next, we explored the potential relevance and underlying mechanisms of FUNDC1 expression in cancers. By integrating clinical and pathological data in Kaplan-Meier Plotter, we investigated the relationship between FUNDC1 expression and several clinical features of patients with LIHC. For OS, FUNDC1 played a detrimental role in patients with LIHC with the following characteristics: male ($n = 246$, HR = 1.79, 95% CI from 1.14 to 2.83, $P = 0.011$), Asian ($n = 155$, HR = 2.33, 95% CI from 1.15 to 4.72, $P = 0.016$), no-alcohol consumption ($n = 202$, HR = 1.69, 95% CI from 1.03 to 2.75, $P = 0.035$), no hepatitis virus infection ($n = 167$, HR = 1.93, 95% CI from 1.09 to 3.4, $P = 0.021$), AJCC T3 stage ($n = 78$, HR = 2.06, 95% CI from 1.03 to 4.11, $P = 0.037$), and micro-vascular invasion ($n = 90$, HR = 2.97, 95% CI from 1.12 to 7.9, $P = 0.022$). On the contrary, FUNDC1 expression benefited LIHC patients at AJCC T2 stage ($n = 90$, HR = 0.44, 95% CI from 0.2 to 0.97, $P = 0.036$). For progression-free survival (PFS), FUNDC1 expression was significantly hazardous to LIHC patients without hepatitis virus infection ($n = 167$, HR = 2.1, 95% CI from 1.3 to 3.38, $P = 0.0019$) but became protective to LIHC patients at stage 2 ($n = 84$, HR = 0.52, 95% CI from 0.28 to 0.98, $P = 0.039$) and grade 3 ($n = 119$, HR = 0.6, 95% CI from 0.36 to 0.98, $P = 0.041$) (Figure 4).

Contradictory Results for LIHC and LUSC in Correlations of FUNDC1 Expression and Immune Infiltration

Immune cells in the TME can affect patient survival, and the above findings support a prognostic role of FUNDC1 in pancreatic cancer. Hence, it would be meaningful to explore the association



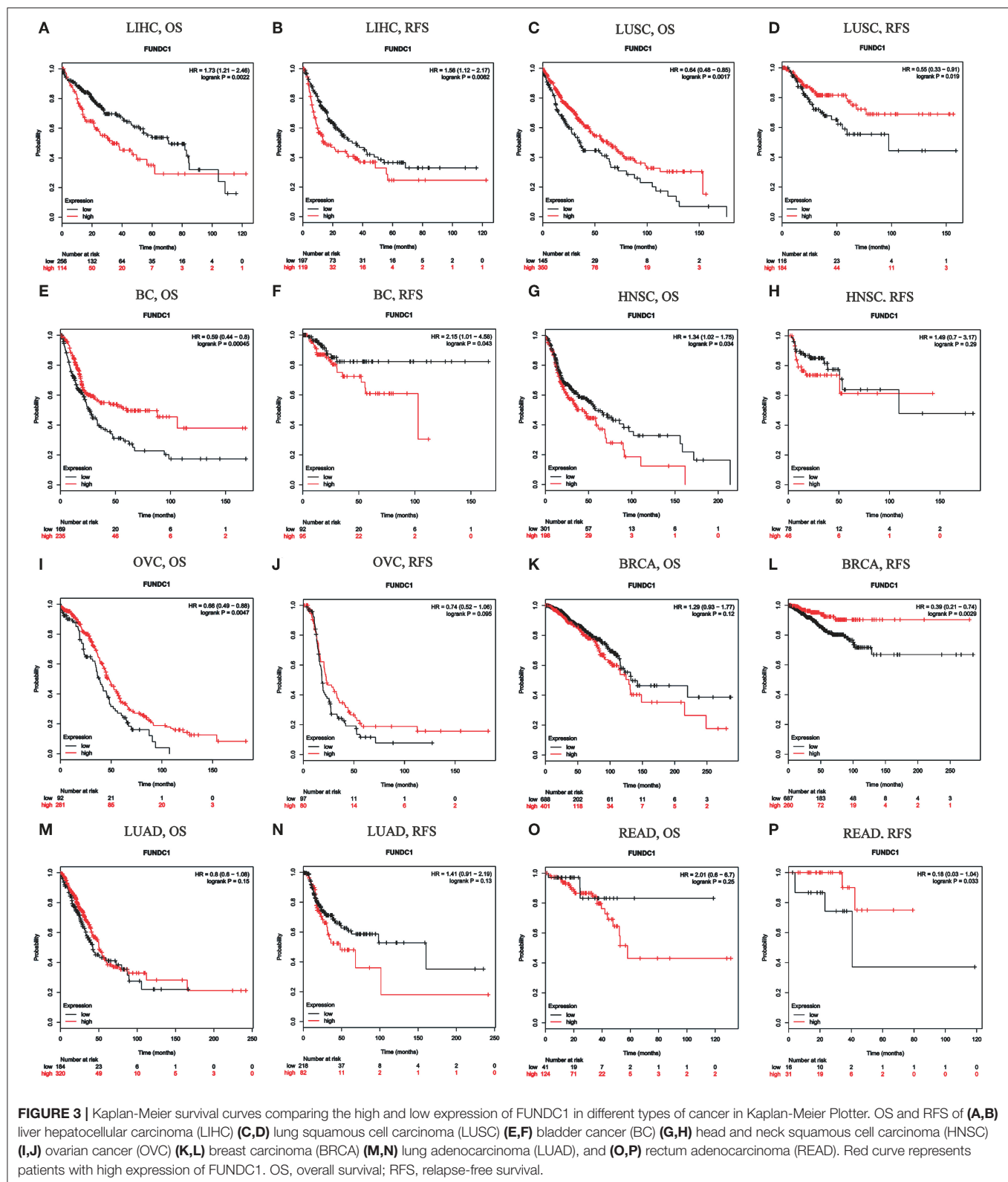
between immune infiltration and FUNDC1 expression. We determined whether FUNDC1 expression was correlated with the immune infiltration level in different cancers by calculating the coefficient of FUNDC1 expression and immune infiltration level in 39 cancer types in TIMER. The results indicated that FUNDC1 expression had significant correlations with tumor purity in 11 cancer types. Furthermore, FUNDC1 expression was also significantly correlated with the infiltration levels of B cells, CD8+ T cells, CD4+ T cells, macrophages, neutrophils, and dendritic cells in 10, 20, 16, 16, 19, and 19 cancer types, respectively (Figure 5 and Supplementary Figure 3).

TIMER and GEPIA contain most of the homologous data from TCGA. Based on the above findings in GEPIA, we chose LIHC to represent cancers with poor survival and LUSC to represent cancers with good survival when FUNDC1 had a high expression level. For LIHC, the FUNDC1 expression level had significant positive correlations with the infiltration levels of B cells ($R = 0.319$, $P = 1.42\text{E-}09$), CD8+ T cells ($R = 0.261$, $P = 9.99\text{E-}07$), CD4+ T cells ($R = 0.166$, $P = 2.06\text{E-}03$),

macrophages ($R = 0.308$, $P = 6.08\text{E-}09$), neutrophils ($R = 0.218$, $P = 4.34\text{E-}05$), and dendritic cells ($R = 0.266$, $P = 6.63\text{E-}07$) (Figure 5A). However, for LUSC, the FUNDC1 expression level had significant negative correlations with the infiltration levels of CD4+ T cells ($R = -0.279$, $P = 6.34\text{E-}10$), macrophages ($R = -0.196$, $P = 1.57\text{E-}05$), neutrophils ($R = -0.207$, $P = 5.38\text{E-}06$), and dendritic cells ($R = -0.234$, $P = 2.49\text{E-}07$) (Figure 5B). In addition, the FUNDC1 expression level in LIHC had no relation with tumor purity ($R = -0.086$, $P = 0.112$), while the FUNDC1 expression level in LUSC was positively correlated with tumor purity ($R = 0.12$, $P = 8.55\text{E-}03$) (Figure 5). These findings strongly suggest that FUNDC1 affects patient survival via interacting with immune infiltration in cancers like LIHC and LUSC.

Relationships Between FUNDC1 Expression and Immune Markers

To further explore the potential relationships between FUNDC1 and infiltrating immune cells, we examined the correlations



between FUNDC1 and several immune cell markers in TIMER and GEPIA. These markers were used to characterize immune cells, including B cells, CD8+ T cells, M1/M2 macrophages,

tumor-associated macrophages, monocytes, NK, neutrophils, and DCs in LIHC and LUSC. We also analyzed the different functional T cells such as Tfh, Th1, Th2, Th9, Th17, Th22, Treg,

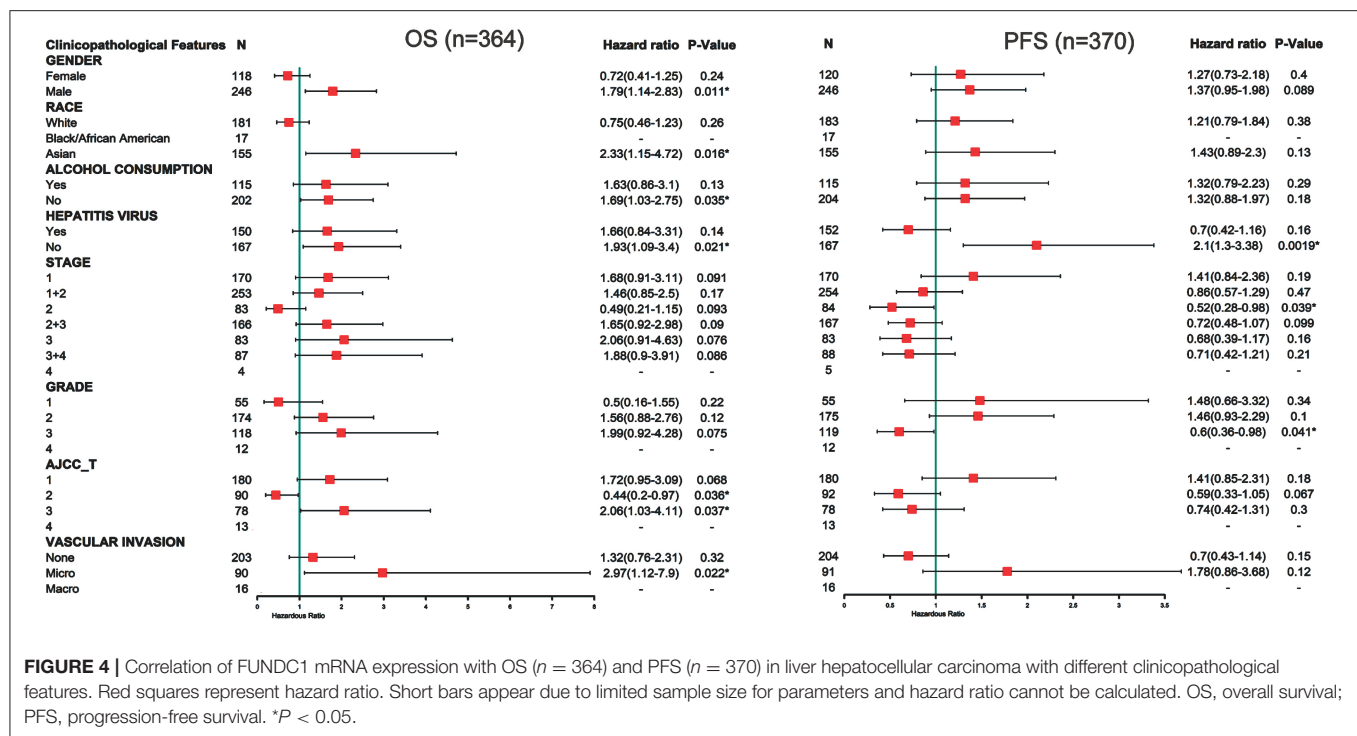
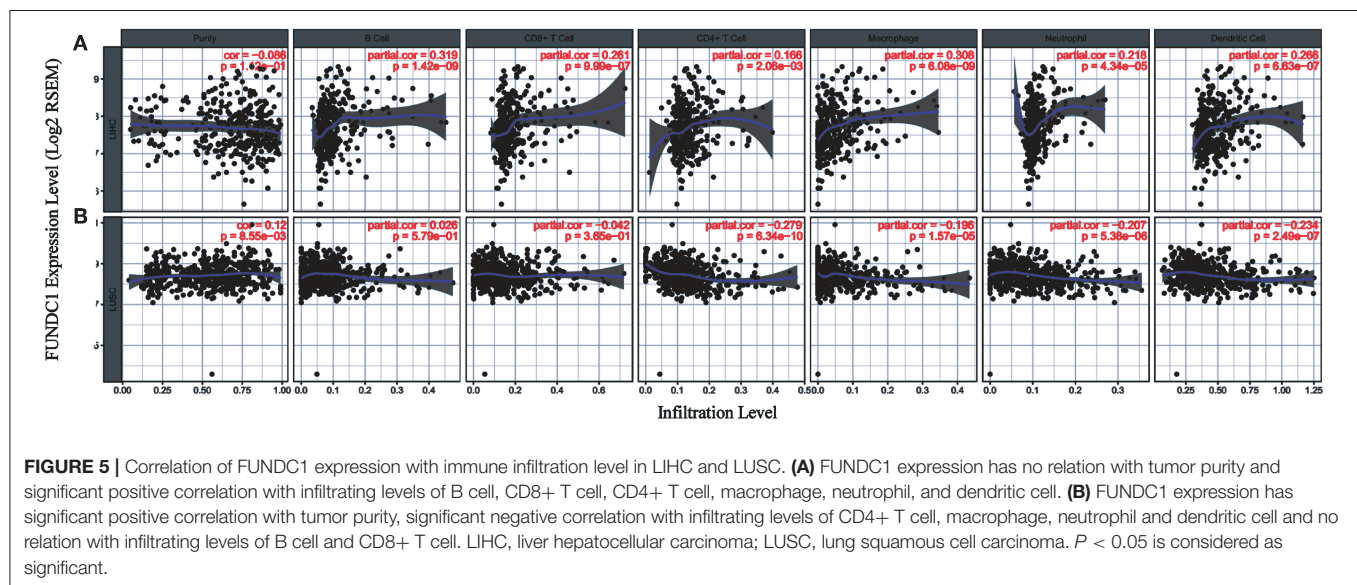


FIGURE 4 | Correlation of FUNDC1 mRNA expression with OS ($n = 364$) and PFS ($n = 370$) in liver hepatocellular carcinoma with different clinicopathological features. Red squares represent hazard ratio. Short bars appear due to limited sample size for parameters and hazard ratio cannot be calculated. OS, overall survival; PFS, progression-free survival. * $P < 0.05$.



and exhausted T cells (Table 1 and Figure 6). In TIMER, after adjustments for tumor purity, the FUNDC1 expression level was significantly correlated with 30 out of 45 immune cell markers in LIHC and 19 out of 45 immune cell markers in LUSC (Table 1).

As shown in Figure 5, in LIHC, B cells and macrophages were two immune cell types most strongly correlated with FUNDC1 expression. However, in LUSC, these two types were less significant. According to the results in Table 1, LIHC and LUSC also have different relationships between FUNDC1 expression and B cell/macrophage markers. Therefore, we further analyzed the correlations of FUNDC1 expression and B cell/macrophage

markers in tumor tissues of LIHC and LUSC in GEPIA. Notably, the results suggested that FUNDC1 correlates with tumor-associated macrophage infiltration in LIHC and LUSC (Table 2).

Moreover, FUNDC1 expression in LIHC and LUSC also relates differently with CD8+ T cell, Tfh, Th2, Th17, and Treg infiltration. The relationships of FUNDC1 with Th9 cells, Th22 cells, neutrophils, and NK cells were partially different between LIHC and LUSC. Additionally, FUNDC1 in LIHC also had significant correlations with exhausted T cell markers such as PD-1 and CTLA4, while FUNDC1 in LUSC did not have such a link (Table 1). Hence, these results confirm our speculation that

TABLE 1 | Correlations between FUNDC1 and Gene Markers of Immune Cells in TIMER.

Cell type	Gene marker	LIHC				LUSC			
		None		Purity		None		Purity	
		Cor	P	Cor	P	Cor	P	Cor	P
B cell	CD19	0.217	***	0.203	**	−0.118	*	−0.058	0.203
	CD20	0.085	0.102	0.064	0.235	−0.084	0.060	−0.023	0.609
	CD38	0.209	***	0.197	**	−0.113	0.011	−0.076	0.096
CD8+ T Cell	CD8A	0.159	*	0.119	0.027	−0.073	0.103	−0.044	0.333
	CD8B	0.193	**	0.161	*	0.024	0.589	0.035	0.447
Tfh	CXCR5	0.178	**	0.163	*	−0.147	**	−0.094	0.041
	ICOS	0.199	**	0.171	*	−0.120	*	−0.076	0.096
Th1	BCL-6	−0.219	***	−0.226	***	−0.006	0.888	−0.024	0.607
	IL12RB2	−0.056	0.279	−0.080	0.140	0.002	0.971	0.025	0.591
	WSX-1	0.297	***	0.275	***	−0.164	**	−0.148	*
Th2	T-BET	0.026	0.619	−0.009	0.867	−0.143	*	−0.105	0.022
	CCR3	0.231	***	0.217	***	−0.061	0.170	−0.035	0.439
	STAT6	−0.231	***	−0.246	***	0.015	0.745	0.025	0.584
Th9	GATA-3	0.229	***	0.207	**	−0.087	0.051	−0.060	0.191
	TGFB2	−0.194	**	−0.213	***	−0.298	***	−0.274	***
	IRF4	0.205	***	0.184	**	−0.178	***	−0.129	*
Th17	PU.1	0.263	***	0.270	***	−0.227	***	−0.197	***
	IL-21R	0.276	***	0.271	***	−0.225	***	−0.194	***
	IL-23R	0.047	0.370	0.026	0.624	−0.064	0.156	−0.033	0.468
Th22	STAT3	0.003	0.947	−0.022	0.686	−0.181	***	−0.158	**
	CCR10	0.275	***	0.249	***	−0.197	***	−0.167	**
	AHR	−0.296	***	−0.318	***	−0.160	**	−0.149	*
Treg	FOXP3	−0.014	0.787	−0.022	0.686	−0.176	***	−0.135	*
	CCR8	0.135	*	0.109	0.043	−0.197	***	−0.172	**
	CD25	0.197	**	0.183	**	0.024	0.559	0.081	0.077
T cell exhaustion	PD-1	0.271	***	0.246	***	−0.155	**	−0.116	0.011
	CTLA4	0.271	***	0.256	***	−0.126	*	−0.078	0.088
Macrophage	CD68	0.196	**	0.170	*	−0.202	***	−0.173	**
	CD11b	0.198	**	0.186	**	−0.232	***	−0.213	***
M1	NOS2	−0.084	0.105	−0.100	0.063	0.101	0.024	−0.087	0.057
	ROS	−0.135	*	−0.101	0.062	−0.191	***	−0.159	**
M2	ARG1	−0.252	***	−0.243	***	0.066	0.138	0.068	0.136
	MRC1	−0.097	0.063	−0.102	0.058	−0.226	***	−0.212	***
TAM	HLA-G	0.106	0.041	0.084	0.122	−0.063	0.159	−0.040	0.383
	CD80	0.253	***	0.247	***	−0.188	***	−0.161	**
	CD86	0.252	***	0.248	***	0.136	*	−0.098	0.032
Monocyte	CD14	−0.387	***	−0.037	***	−0.219	***	−0.190	***
	CD16	0.191	**	0.181	**	−0.167	**	−0.139	*
NK	XCL1	0.278	***	0.279	***	0.330	***	0.312	***
	KIR3DL1	0.003	0.951	−0.012	0.825	−0.050	0.264	−0.033	0.475
	CD7	0.239	***	−0.226	***	−0.170	0.017	−0.062	0.174
Neutrophil	CD15	0.357	***	0.329	***	−0.105	0.019	−0.060	0.194
	MPO	0.091	0.080	0.037	0.499	−0.132	*	−0.107	0.019
DC	CD1C	0.150	*	0.140	*	−0.078	0.081	−0.019	0.672
	CD141	−0.012	0.821	−0.059	0.277	−0.174	***	−0.169	**

LIHC, liver hepatocellular carcinoma; LUSC, lung squamous cell carcinoma; Tfh, follicular helper T cell; Th, T helper cell; Treg, regulatory T cell; TAM, tumor-associated- macrophage; NK, natural killer cell; DC, dendritic cell; None, correlation without adjustment; Purity, correlation adjusted for tumor purity; Cor, R value of Spearman's correlation. * $P < 0.01$; ** $P < 0.001$; *** $P < 0.0001$.

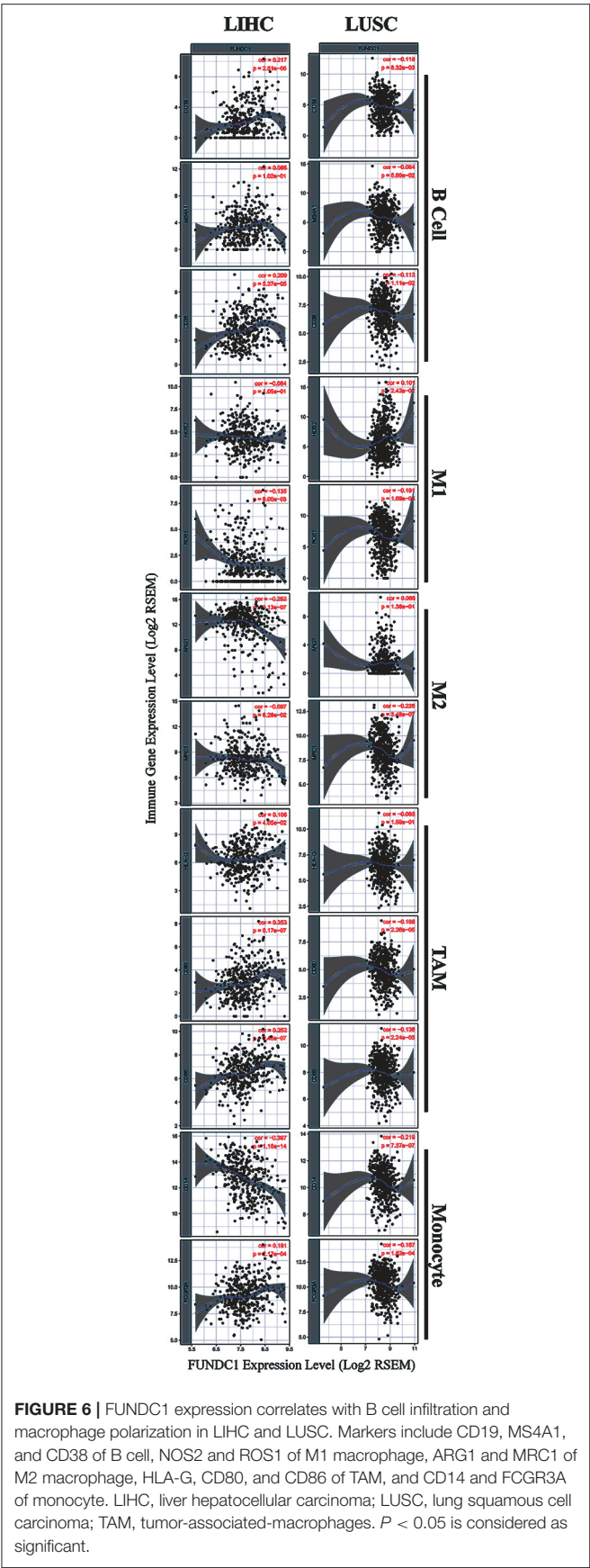


TABLE 2 | Correlations between FUNDC1 and genes markers of B cells, macrophages, and monocytes in GEPIA.

Cell type	Gene marker	LIHC				LUSC			
		Tumor		Normal		Tumor		Normal	
		R	P	R	P	R	P	R	P
B cell	CD19	0.280	***	0.320	***	−0.220	***	−0.048	0.380
	CD20	0.130	0.015	0.160	0.041	−0.180	***	−0.190	**
	CD38	0.300	***	0.220	**	−0.210	***	0.290	***
M1	NOS2	0.110	0.042	0.260	**	0.170	**	−0.300	***
	ROS	0.060	0.250	0.110	0.160	−0.130	*	0.360	***
M2	ARG1	−0.270	***	0.380	***	0.073	0.110	−0.160	*
	MRC1	0.039	0.450	0.350	***	−0.170	**	0.320	***
TAM	HLA-G	0.230	***	0.350	***	−0.150	**	0.130	0.021
	CD80	0.400	***	0.330	***	−0.210	***	−0.240	***
Monocyte	CD86	0.390	***	0.450	***	−0.180	***	0.016	0.770
	CD14	−0.410	***	0.190	0.015	−0.230	***	0.140	*
	CD16	0.340	***	0.480	***	−0.180	***	0.320	***

LIHC, liver hepatocellular carcinoma; LUSC, lung squamous cell carcinoma; TAM, tumor-associated-macrophage; Tumor, correlation analysis in tumor tissue of TCGA; Normal, correlation analysis in normal tissue of TCGA. * $P < 0.01$; ** $P < 0.001$; *** $P < 0.0001$.

FUNDC1 expression in LIHC and LUSC correlates with immune cell infiltration in different manners, which can help explain the differences in patient survival.

DISCUSSION

Mitochondria are essential for human immunity, and aberrant mitochondrial activity affects immune responses. For example, some studies have demonstrated that viruses (e.g., HBV in LIHC) can manipulate mitophagy, which enables viruses to promote persistent infection and attenuate the innate immune responses (25). FUNDC1 is an integral mitochondrial outer-membrane protein and a receptor for hypoxia-induced mitophagy. Unlike ubiquitin-dependent mitophagy, which is mainly mediated by PINK1 (PTEN induced kinase-1)-PRKN/PARK2 (parkin RBR E3 ubiquitin protein ligase), FUNDC1 is an LC3 interacting region-containing receptors that can directly induce mitophagy (26). FUNDC1-mediated mitophagy is negatively regulated by the phosphorylation of FUNDC1, as the phosphorylation of Tyr 18 in the FUNDC1 LC3-interacting region motif can weaken the binding affinity of FUNDC1 to LC3 (5). Meanwhile, it is now clear that hypoxia, a common feature of cancers, can induce extensive mitochondrial degradation in a FUNDC1-dependent manner (27). Hypoxia can induce FUNDC1 dephosphorylation and therefore enhance its selective interaction with LC3 (4, 5). In contrast, hypoxia can also promote the ubiquitylation of FUNDC1 at lysine 119 and subsequent degradation of redundant FUNDC1 through MARCH5, a mitochondrial ubiquitin ligase that fine-tunes hypoxia-induced mitophagy. However, severe hypoxic stress still leads to the dephosphorylation of FUNDC1 and increased mitophagic flux (28).

Although FUNDC1 has not been well-studied in immunology, several studies have been conducted. It is now

acknowledged that mitophagy is closely related to human immunity. Moreover, to the best of our knowledge, the relationship between FUNDC1 expression and tumor cell proliferation has been proved in cervical and breast cancers (6, 29). Thus, it is reasonable to surmise that FUNDC1 expression may influence patient survival through tumor cell proliferation. However, the role of FUNDC1 in other important aspects like tumor metastasis has not been thoroughly studied. As indicated by previous reports and our findings, it should also be noted that the role of FUNDC1 may vary in different contexts. Although this study offers a broad view related to patient survival, additional downstream mechanism studies are still warranted. One previous study has demonstrated that FUNDC1-mediated mitophagy can suppress hepatocarcinogenesis (11). This study found that the specific knockout of FUNDC1 in hepatocytes promotes the initiation and progression of chemical carcinogen diethylnitrosamine-induced HCC. The study also found that FUNDC1 transgenic hepatocytes protect against the development of HCC. However, according to our study, FUNDC1 is an unfavorable prognostic factor for LIHC patients (**Figure 3**), though the situation may vary according to different characteristics such as gender, race, alcohol consumption, hepatitis infection, tumor grade, tumor stage, or vascular invasion (**Figure 4**). The differences between our study using a cancer patient cohort and previous study using an animal model necessitate more comprehensive and precise studies in the future to explain tumor development. Understanding the tumor microenvironment, including immune cell infiltration, can probably help decipher the mechanisms behind tumor development. As shown in **Figures 5, 6**, we did find significant correlations between tumor FUNDC1 expression and immune cell infiltration, even though a cause-effect relationship could not be established in the current study. Besides, FUNDC1 expression is not related with the tumor purity in LIHC, while it does have significant positive correlation with the tumor purity in LUSC (**Figure 5**). Such difference may be attributable to the different enrichment patterns of FUNDC1 in the tumor microenvironment. Tumor microenvironment is a complex milieu of non-cancerous cells mainly consisting of immune cells around tumor cells. Genes highly expressed in cells in the microenvironment are believed to have negative associations with tumor purity. In contrast, genes highly expressed in the tumor cells are expected to have positive association with tumor purity. In this study, as an essential regulator of mitophagy, FUNDC1 expression have different relationships with tumor purity in different contexts, which suggests FUNDC1-related differences in various aspects such as carcinogenesis, metastasis, treatment strategies, etc. Future studies using more precise techniques such as single cell RNA sequencing and exploring direct interactions at the cellular and molecular levels are needed.

In this study, we demonstrated the prognostic value of FUNDC1 in pan-cancer. Compared with a low expression level, a high expression level of FUNDC1 correlated with a better prognosis in lung, ovarian, kidney, and thyroid cancers and a poorer prognosis in brain, skin, and liver cancers. Interestingly, increased FUNDC1 expression can specifically impact the prognosis of LIHC patients with the following characteristics:

male, Asian, no alcohol consumption, no hepatitis virus infection, stage 2, grade 3, AJCC T2 and T3, and micro-vascular invasion. Our analysis also revealed that LIHC and LUSC have different patterns with respect to correlations between immune infiltration and FUNDC1 expression. Hence, this study provides insights into the use of the mitophagy regulator FUNDC1 as a prognostic marker in pan-cancer from an immuno-oncological perspective, which could benefit future mechanistic studies and aid in the development of immunotherapies.

This study explored the expression levels of FUNDC1 and visualized the prognostic landscape in pan-cancer using independent datasets in ONCOMINE and PROGNOSCAN and TCGA data in GEPIA and TIMER. In ONCOMINE, we found that FUNDC1, compared with expression levels in normal tissues, was highly expressed in breast, cervical, colorectal, lung, ovarian, pancreatic, and prostate cancers, as well as in leukemia and lymphoma, while only one dataset showed that FUNDC1 had a lower expression level in breast cancer (**Figure 1A**). However, analysis of TCGA data in TIMER revealed that FUNDC1 expression was higher in BLCA, BRCA, CHOL, COAD, LIHC, LUAD, LUSC, PRAD, and UCEC and lower in KIRC compared with that in normal adjacent tissues (**Figure 1B**). These discrepant FUNDC1 expression levels in cancers across different databases are the result of heterogeneous data collection approaches, as well as underlying mechanisms with distinct biological properties. However, across databases, we identified the consistent prognostic value of FUNDC1 expression in LIHC and LUSC. For patient prognosis, analysis of FUNDC1 in Kaplan-Meier Plotter and GEPIA revealed that increased FUNDC1 expression correlated with a favorable prognosis in LUSC as well as an overall beneficial effect on cancers. In contrast, a high expression level of FUNDC1 in LIHC was correlated with a poor prognosis. In 8 datasets in PrognScan, high FUNDC1 expression levels could be used as an independent risk factor for a poor prognosis in brain, breast, colorectal, and skin cancers (**Figure 2**). In addition, a high level of FUNDC1 expression was shown to be related to a poor prognosis in LIHC with micro-vascular invasion but a favorable prognosis in LIHC with AJCC T2 (**Figure 4**). Taken together, these findings strongly suggest that FUNDC1 can serve as a prognostic biomarker in pan-cancer.

Another major finding from this study is that FUNDC1 expression correlates with diverse immune infiltration levels in cancers, especially in LIHC and LUSC. Our findings demonstrate that FUNDC1 expression has significant relationships with the infiltration level of CD4⁺ T cells, macrophages, neutrophils, and DCs in LIHC and LUSC (**Figure 5**). LIHC has positive coefficients between immune infiltration and the FUNDC1 expression level, but LUSC generally has negative ones. As we expected, the relationships between FUNDC1 expression and certain immune cell markers, such as NOS2, ROS1, ARG1, MRC1, and CD14, are not always the same as the overall trend, suggesting that specific interactions between FUNDC1 and certain immune cell subtypes (**Figure 5** and **Table 1**). Interestingly, the FUNDC1 expression level in LIHC is not related to tumor purity, suggesting that it is equally expressed in tumor cells and the tumor microenvironment. However, in LUSC, the FUNDC1 expression level had a significant

positive correlation with tumor purity, indicating its comparative enrichment in tumor cells. As important antigen presenting cells, B cells and macrophages were the cell types that most significantly correlated with FUNDC1 expression in LIHC; however, in LUSC, B cells had no relation to FUNDC1, and macrophages had the lowest coefficient with FUNDC1 among all significantly correlated cells (**Figure 5**). These differences suggest heterogeneities among tumors in recruiting antigen presenting cells to the TME. Moreover, after adjustment for tumor purity, FUNDC1 in LIHC had no relation to M1 macrophages but negatively correlated with ARG1+ M2 macrophages, while FUNDC1 in LUSC negatively correlated with ROS+ M1 macrophages and MRC1+ M2 macrophages. For infiltrating TAMs, after adjustment for tumor purity, in LIHC, FUNDC1 was positively correlated with CD80 and CD86, and in LUSC, FUNDC1 negatively correlated with CD80, indicating the constitutive effect of TAMs on differences in tumor cell survival (**Table 1**). Taken together, these findings suggest that FUNDC1 plays an important role in the recruitment and regulation of immune infiltrating cells in cancers, which may eventually influence patient survival.

Recent studies provide possible mechanisms explaining why FUNDC1 expression correlates with immune infiltration and different prognoses in pan-cancer. Initial theories assumed that immune cells helped resisting tumors. Indeed, it is still acknowledged that in the early phase of carcinogenesis, the immune system attacks tumor cells by activating T cells and macrophages to prevent the development of cancer. However, once a tumor progress past this early stage, the immune TME switches to supporting cancer cells and promoting tumor progression while suppressing immune cell-mediated cytotoxicity (12). FUNDC1 is a key regulator of mitophagy, which has been proved to participate in immunity (26). Several studies have linked mitophagy to mitochondrial antigen presentation (26, 30). Our study also provided evidence that the immune infiltration levels of antigen presenting cells (B cells and macrophages) are significantly correlated with the FUNDC1 expression level in cancers. The role of mitophagy in antigen presentation remains unclear. While one study reported that mitophagy can reduce CD8+ T cell activation, another study showed its facilitating role in the mitochondrial antigen presentation of glycoproteins. Aside from antigen presentation, mitophagy is also involved in the development and differentiation of immune cells, including T cells, natural killer (NK) cells, and macrophages (26).

Apart from interactions among immune cells, tumor cells can influence immune cells by producing lactic acid (31). This signal can induce the M2-like polarization of tumor-associated macrophages. In turn, the lactate-induced expression of arginase 1 by macrophages also plays an important role in tumor growth. Macrophages can also promote carcinogenesis by producing pro-inflammatory mediators such as IL-6, tumor necrosis factor, interferon- γ , proteases, ROS, and nitrogen species (32, 33). Specifically, TAMs can directly help tumor cell migration via a paracrine loop between macrophages and tumor cells that involves the secretion of EGF family ligands from macrophages and CSF1 from tumor cells. TAMs can also produce cathepsins

and matrix-remodeling enzymes to stimulate such process and increase tumor invasiveness (34–36). These interactions between tumor cells and infiltrating immune cells help explain the findings from this study indicating that TAMs have a positive correlation with FUNDC1 expression in LIHC and that the high expression of FUNDC1 is associated with a worse LIHC patient prognosis. For other immune cell types, T helper 2 (TH2) cells in the microenvironment can educate macrophages to become pro-tumoral and alter the immune response from a cytotoxic to a supportive role (15). Tumor-associated neutrophil and plasma cell signatures can also serve as significant but opposite predictors of survival for diverse solid tumors (37). Therefore, it is reasonable to surmise that immune infiltration can interact with FUNDC1-mediated activities in both immune cells and tumor cells.

However, even though we integrated information across multiple databases, this study still had limitations. First, a large proportion of the microarray and sequencing data were collected by analyzing tumor tissue information. Thus, the cell-level analysis of immune cell markers could have introduced systematic bias. To overcome this issue, future studies with a higher resolution, such as with the use of single cell RNA sequencing, should be performed (38, 39). Second, there is no information in these databases reflecting the post-translational modification of FUNDC1. As discussed above, both phosphorylation and ubiquitination can interfere with the molecular function of FUNDC1. Third, we still cannot define FUNDC1 as a friend or foe because of some conflicting findings from different databases. Fourth, this study only conducted a bioinformatics analysis of FUNDC1 expression and patient survival across different databases, and *in vivo/in vitro* experiments were not performed. Future mechanistic studies on FUNDC1 at the cellular and molecular levels could help clarify the role of FUNDC1. Fifth, despite the finding that FUNDC1 expression correlates with both immune cell infiltration and patient survival in cancers, we could not prove that FUNDC1 affects patient survival through immune infiltration. Future prospective studies focusing on FUNDC1 expression and immune infiltration in a cancer population could help provide a definitive answer.

In summary, FUNDC1 can affect pan-cancer prognosis and correlate with immune infiltration. Specially, for LIHC and LUSC, FUNDC1 is related to different TAM patterns in the TME. FUNDC1 can serve as a prognostic biomarker in pan-cancer. These findings may provide an immuno-based anti-tumor strategy involving manipulating the energy system of either tumor cells or tumor microenvironment infiltrates.

DATA AVAILABILITY STATEMENT

Publicly available datasets were analyzed in this study. This data can be found here: www.oncomine.org, <http://dna00.bio.kyutech.ac.jp/Prognoscan/index.html>, <https://kmplot.com/analysis/>, <http://gepia.cancer-pku.cn>, <http://cistrome.org/TIMER/>.

AUTHOR CONTRIBUTIONS

QY, NS, and XC designed this study. NS, JZ, YW, XY, and WM extracted the information from the databases. QY and NS analyzed the data. YL and XC supervised the entire study. QY wrote the manuscript. All authors revised the manuscript.

ACKNOWLEDGMENTS

We are grateful for the support from grants from the National Natural Science Foundation of China (No. 81670461;

81974106 to XC and No. 91439207 to YL). We thank Dr. Balazs Gyorffy, the project leader of Kaplan-Meier Plotter, for his technical support during our study. In addition, we sincerely thank the public databases, including Oncomine, GEPIA, Kaplan-Meier Plotter, and PrognScan, for providing open access.

SUPPLEMENTARY MATERIAL

The Supplementary Material for this article can be found online at: <https://www.frontiersin.org/articles/10.3389/fonc.2019.01502/full#supplementary-material>

REFERENCES

- Liu L, Feng D, Chen G, Chen M, Zheng Q, Song P, et al. Mitochondrial outer-membrane protein FUNDC1 mediates hypoxia-induced mitophagy in mammalian cells. *Nat Cell Biol.* (2012) 14:177–85. doi: 10.1038/ncb2422
- Chen M, Chen Z, Wang Y, Tan Z, Zhu C, Li Y, et al. Mitophagy receptor FUNDC1 regulates mitochondrial dynamics and mitophagy. *Autophagy.* (2016) 12:689–702. doi: 10.1080/15548627.2016.1151580
- Wu W, Li W, Chen H, Jiang L, Zhu R, Feng D. FUNDC1 is a novel mitochondrial-associated-membrane (MAM) protein required for hypoxia-induced mitochondrial fission and mitophagy. *Autophagy.* (2016) 12:1675–6. doi: 10.1080/15548627.2016.1193656
- Lv M, Wang C, Li F, Peng J, Wen B, Gong Q, et al. Structural insights into the recognition of phosphorylated FUNDC1 by LC3B in mitophagy. *Protein Cell.* (2017) 8:25–38. doi: 10.1007/s13238-016-0328-8
- Kuang Y, Ma K, Zhou C, Ding P, Zhu Y, Chen Q, et al. Structural basis for the phosphorylation of FUNDC1 LIR as a molecular switch of mitophagy. *eLife.* (2016) 12:2363–73. doi: 10.1080/15548627.2016.1238552
- Wu L, Zhang D, Zhou L, Pei Y, Zhuang Y, Cui W, et al. FUN14 domain-containing 1 promotes breast cancer proliferation and migration by activating calcium-NFATC1-BMI1 axis. *EBioMedicine.* (2019) 41:384–94. doi: 10.1016/j.ebiom.2019.02.032
- Schols A, Kneppers AEM, Kelders M, de Theije CC, Lainscak M, Gosker HR, et al. Hydrogen peroxide-induced mitophagy contributes to laryngeal cancer cells survival via the upregulation of FUNDC1. *Scient Rep.* (2019) 21:596–606. doi: 10.1007/s12094-018-1958-5
- Wu H, Wang Y, Li W, Chen H, Du L, Liu D, et al. Deficiency of mitophagy receptor FUNDC1 impairs mitochondrial quality and aggravates dietary-induced obesity and metabolic syndrome. *Autophagy.* (2019) 2019:1–17. doi: 10.1080/15548627.2019.1596482
- Zhang W, Siraj S, Zhang R, Chen Q. Mitophagy receptor FUNDC1 regulates mitochondrial homeostasis and protects the heart from I/R injury. *Autophagy.* (2017) 13:1080–1. doi: 10.1080/15548627.2017.1300224
- Fu T, Xu Z, Liu L, Guo Q, Wu H, Liang X, et al. Mitophagy directs muscle-adipose crosstalk to alleviate dietary obesity. *Cell Rep.* (2018) 23:1357–72. doi: 10.1016/j.celrep.2018.03.127
- Li W, Li Y, Siraj S, Jin H, Fan Y, Yang X, et al. FUN14 domain-containing 1-mediated mitophagy suppresses hepatocarcinogenesis by inhibition of inflammasome activation in mice. *EMBO J.* (2019) 69:604–21. doi: 10.1002/hep.30191
- Bindea G, Mlecnik B, Tosolini M, Kirilovsky A, Waldner M, Obenauf AC, et al. Spatiotemporal dynamics of intratumoral immune cells reveal the immune landscape in human cancer. *Immunity.* (2013) 39:782–95. doi: 10.1016/j.immuni.2013.10.003
- Gajewski TF, Schreiber H, Fu YX. Innate and adaptive immune cells in the tumor microenvironment. *Nat Immunol.* (2013) 14:1014–22. doi: 10.1038/ni.2703
- Topalian SL, Drake CG, Pardoll DM. Immune checkpoint blockade: a common denominator approach to cancer therapy. *Cancer Cell.* (2015) 27:450–61. doi: 10.1016/j.ccell.2015.03.001
- Quail DF, Joyce JA. Microenvironmental regulation of tumor progression and metastasis. *Nat Med.* (2013) 19:1423–37. doi: 10.1038/nm.3394
- Zhu Y, Yang J, Xu D, Gao XM, Zhang Z, Hsu JL, et al. Disruption of tumour-associated macrophage trafficking by the osteopontin-induced colony-stimulating factor-1 signalling sensitises hepatocellular carcinoma to anti-PD-L1 blockade. *Gut.* (2019) 68:1653–66. doi: 10.1136/gutjnl-2019-318419
- De Palma M, Biziato D, Petrova TV. Microenvironmental regulation of tumour angiogenesis. *Nat Rev Cancer.* (2017) 17:457–74. doi: 10.1038/nrc.2017.51
- Li X, Yao W, Yuan Y, Chen P, Li B, Li J, et al. Targeting of tumour-infiltrating macrophages via CCL2/CCR2 signalling as a therapeutic strategy against hepatocellular carcinoma. *Gut.* (2017) 66:157–67. doi: 10.1136/gutjnl-2015-310514
- Cully M. Cancer: re-educating tumour-associated macrophages with nanoparticles. *Nat Rev Drug Disc.* (2018) 17:468. doi: 10.1038/nrd.2018.102
- Gordon SR, Maute RL, Dulken BW, Hutter G, George BM, McCracken MN, et al. PD-1 expression by tumour-associated macrophages inhibits phagocytosis and tumour immunity. *Nature.* (2017) 545:495–9. doi: 10.1038/nature22396
- Mizuno H, Kitada K, Nakai K, Sarai A. PrognScan: a new database for meta-analysis of the prognostic value of genes. *BMC Med Genomics.* (2009) 2:18. doi: 10.1186/1755-8794-2-18
- Nagy A, Lanczky A, Menyhart O, Gyorffy B. Validation of miRNA prognostic power in hepatocellular carcinoma using expression data of independent datasets. *Scient Rep.* (2018) 8:9227. doi: 10.1038/s41598-018-29514-3
- Tang Z, Li C, Kang B, Gao G, Li C, Zhang Z. GEPIA: a web server for cancer and normal gene expression profiling and interactive analyses. *Nucleic Acids Res.* (2017) 45:W98–W102. doi: 10.1093/nar/gkx247
- Li B, Severson E, Pignon JC, Zhao H, Li T, Novak J, et al. Comprehensive analyses of tumor immunity: implications for cancer immunotherapy. *Genome Biol.* (2016) 17:174. doi: 10.1186/s13059-016-1028-7
- Zhang L, Qin Y, Chen M. Viral strategies for triggering and manipulating mitophagy. *Autophagy.* (2018) 14:1665–73. doi: 10.1080/15548627.2018.1466014
- Wu G, Ganley IG, Hill JA, Yin XM, Dong Z, Xu Y, et al. Emerging views of mitophagy in immunity and autoimmune diseases. *Autophagy.* (2019) 2019:1–15. doi: 10.1080/15548627.2019.1603547
- Zhang W, Ren H, Xu C, Zhu C, Wu H, Liu D, et al. Hypoxic mitophagy regulates mitochondrial quality and platelet activation and determines severity of I/R heart injury. *eLife.* (2016) 5:e21407. doi: 10.7554/eLife.21407
- Chen Z, Siraj S, Liu L, Chen Q. MARCH5-FUNDC1 axis fine-tunes hypoxia-induced mitophagy. *Autophagy.* (2017) 13:1244–5. doi: 10.1080/15548627.2017.1310789
- Hou H, Er P, Cheng J, Chen X, Ding X, Wang Y, et al. High expression of FUNDC1 predicts poor prognostic outcomes and is a promising target to improve chemoradiotherapy effects in patients with cervical cancer. *Cancer Med.* (2017) 6:1871–81. doi: 10.1002/cam4.1112
- Matheoud D, Sugiura A, Bellemare-Pelletier A, Laplante A, Rondeau C, Chemali M, et al. Parkinson's disease-related proteins PINK1 and

- parkin repress mitochondrial antigen presentation. *Cell*. (2016) 166:314–27. doi: 10.1016/j.cell.2016.05.039
31. Colegio OR, Chu NQ, Szabo AL, Chu T, Rhebergen AM, Jairam V, et al. Functional polarization of tumour-associated macrophages by tumour-derived lactic acid. *Nature*. (2014) 513:559–63. doi: 10.1038/nature13490
 32. Moore RJ, Owens DM, Stamp G, Arnott C, Burke F, East N, et al. Mice deficient in tumor necrosis factor- α are resistant to skin carcinogenesis. *Nat Med*. (1999) 5:828–31. doi: 10.1038/10552
 33. Canli O, Nicolas AM, Gupta J, Finkelmeier F, Goncharova O, Pesic M, et al. Myeloid cell-derived reactive oxygen species induce epithelial mutagenesis. *Cancer Cell*. (2017) 32:869–83 e5. doi: 10.1016/j.ccell.2017.11.004
 34. Goswami S, Sahai E, Wyckoff JB, Cammer M, Cox D, Pixley FJ, et al. Macrophages promote the invasion of breast carcinoma cells via a colony-stimulating factor-1/epidermal growth factor paracrine loop. *Cancer Res*. (2005) 65:5278–83. doi: 10.1158/0008-5472.CAN-04-1853
 35. Wyckoff J, Wang W, Lin EY, Wang Y, Pixley F, Stanley ER, et al. A paracrine loop between tumor cells and macrophages is required for tumor cell migration in mammary tumors. *Cancer Res*. (2004) 64:7022–9. doi: 10.1158/0008-5472.CAN-04-1449
 36. Hernandez L, Smirnova T, Kedrin D, Wyckoff J, Zhu L, Stanley ER, et al. The EGF/CSF-1 paracrine invasion loop can be triggered by heregulin beta1 and CXCL12. *Cancer Res*. (2009) 69:3221–7. doi: 10.1158/0008-5472.CAN-08-2871
 37. Gentles AJ, Newman AM, Liu CL, Bratman SV, Feng W, Kim D, et al. The prognostic landscape of genes and infiltrating immune cells across human cancers. *Nat Med*. (2015) 21:938–45. doi: 10.1038/nm.3909
 38. Giladi A, Amit I. Single-cell genomics: a stepping stone for future immunology discoveries. *Cell*. (2018) 172:14–21. doi: 10.1016/j.cell.2017.11.011
 39. Papalexi E, Satija R. Single-cell RNA sequencing to explore immune cell heterogeneity. *Nat Rev Immunol*. (2018) 18:35–45. doi: 10.1038/nri.2017.76

Conflict of Interest: The authors declare that the research was conducted in the absence of any commercial or financial relationships that could be construed as a potential conflict of interest.

Copyright © 2020 Yuan, Sun, Zheng, Wang, Yan, Mai, Liao and Chen. This is an open-access article distributed under the terms of the Creative Commons Attribution License (CC BY). The use, distribution or reproduction in other forums is permitted, provided the original author(s) and the copyright owner(s) are credited and that the original publication in this journal is cited, in accordance with accepted academic practice. No use, distribution or reproduction is permitted which does not comply with these terms.



Neem Leaf Glycoprotein Restrains VEGF Production by Direct Modulation of HIF1 α -Linked Upstream and Downstream Cascades

Akata Saha, Partha Nandi, Shayani Dasgupta, Avishek Bhuniya, Nilanjan Ganguly, Tithi Ghosh, Ipsita Guha, Saptak Banerjee, Rathindranath Baral and Anamika Bose *

Department of Immunoregulation and Immunodiagnostics, Chittaranjan National Cancer Institute (CNCI), Kolkata, India

OPEN ACCESS

Edited by:

Marco Rossi,
University of Catanzaro, Italy

Reviewed by:

Paolo Armando Gagliardi,
University of Bern, Switzerland
Fabrizio Martelli,
Istituto Superiore di Sanità (ISS), Italy

*Correspondence:

Anamika Bose
anamikabose2@gmail.com

Specialty section:

This article was submitted to
Cancer Molecular Targets and
Therapeutics,
a section of the journal
Frontiers in Oncology

Received: 18 November 2019

Accepted: 14 February 2020

Published: 06 March 2020

Citation:

Saha A, Nandi P, Dasgupta S,
Bhuniya A, Ganguly N, Ghosh T,
Guha I, Banerjee S, Baral R and
Bose A (2020) Neem Leaf
Glycoprotein Restrains VEGF
Production by Direct Modulation of
HIF1 α -Linked Upstream and
Downstream Cascades.
Front. Oncol. 10:260.
doi: 10.3389/fonc.2020.00260

Neem Leaf Glycoprotein (NLGP) is a natural immunomodulator, have shown sustained tumor growth restriction as well as angiogenic normalization chiefly by activating CD8⁺ T cells. Here, we have investigated the direct role of NLGP as a regulator of tumor microenvironmental hypoxia and associated vascular endothelial growth factor (VEGF) production. We observed a significant reduction in VEGF level in both *in vivo* murine tumor and *in vitro* cancer cells (B16Mel, LLC) and macrophages after NLGP treatment. Interestingly, NLGP mediated VEGF downregulation in tumor cells or macrophages within hypoxic chamber was found at an early 4 h and again at late 24 h in mRNA level. Our data suggested that NLGP prevented hypoxia-induced strong binding of HIF1 α with its co-factors, CBP/p300 and Sp3, but not with Sp1, which eventually limit the binding of HIF1 α -transcriptional complex to hypoxia responsive element of VEGF promoter and results in restricted early VEGF transcription. On the otherhand, suppressed phosphorylation of Stat3 by NLGP results reduction of HIF1 α at 24 h of hypoxia that further support sustained VEGF down-regulation. However, NLGP fails to regulate VHL activity as observed by both *in vivo* and *in vitro* studies. Therefore, this study for the first time reveals a mechanistic insight of NLGP mediated inhibition of angiogenesis by suppressing VEGF, which might help in vascular normalization to influence better drug delivery.

Keywords: hypoxia, VEGF, HIF1 α , STAT3, tumor-microenvironment, NLGP

SUMMARY

NLGP downregulates VEGF at 4 h transcriptionally and both VEGF and HIF1 α at 18 h translationally. Co-factors of HIF1 α -transcriptional-complex downregulated at 4 h in hypoxia by NLGP. Downregulation of pStat3 by NLGP downregulates HIF1 α resulting in a sustained VEGF reduction in hypoxia.

INTRODUCTION

Malignant solid tumor progression needs aberrant angiogenic stimuli for rapid neovascularization to maintain nutrient and oxygen supply to proceed beyond 2 mm³ (1, 2). Among various pro-angiogenic factors, vascular endothelial growth factor (VEGF) is the most influential factor responsible for promoting tumor angiogenesis despite the nature and origin of tumor. Thus, VEGF targeting has efficacy in several cancer management (3, 4). Rapid tumor cell proliferation creates hypoxia or oxygen deficit (5) and stabilizes HIF1 α , the main VEGF regulator along with growth factors and oncogenes (6, 7). Within the tumor microenvironment (TME), tumor cells themselves along with non-tumor stromal cells serves as the source of VEGF (8).

HIFs are basic helix-loop-helix transcription factors belonging to the PAS (PER/aryl hydrocarbon receptor nuclear translocator) family. It has two subunits, an oxygen-sensitive α -subunit and a constitutively expressed β -subunit (9). In normoxia, α -subunit undergoes post-transcriptional modifications with prolyl-hydroxylase (PHD) and von-Hippel-Lindau (VHL) leading to proteosomal degradation via E3 ubiquitin ligase (10). However, in hypoxia, HIF1 α becomes stable and translocate to the nucleus where it forms a heterodimer with HIF1 β and many other co-factors to activate more than 124 significant genes (11). In addition to hypoxia, several other factors are potent stimulator of either HIF1 α or VEGF or both. Growth factors, cytokines etc. by increase HIF1 α protein synthesis via activation of PI3K/AKT (12) or ERK/MAPK pathways (13) or STAT3 signaling pathway (14, 15). Interestingly, recent work suggested a co-operative role of STAT3 and HIF1 α in VEGF upregulation (16). VEGF expression can also be induced by HIF1 α independent manner by STAT3, AP1, Sp1, and cAMP etc. (16, 17).

Targeting VEGF by many agents, including anti-VEGF monoclonal antibodies, have been developed showing promising effect *in vitro*, but their effects *in vivo* settings or in cancer patients are limited due several adverse effects, such as hypertension, gastrointestinal-perforation, bleeding, impairment of wound healing etc. (18). On the other hand, several plant based natural molecules or anti-oxidants show promises in reducing VEGF but their mechanisms are largely unknown. Neem leaf glycoprotein (NLGP), a non-toxic immune-modulator, show sustained tumor growth restriction in multiple murine cancer settings primarily by activating CD8⁺ cytotoxic T cells (19, 20). We also reported normalization of aberrant angiogenesis in murine carcinoma and melanoma hosts in an immune dependent manner (21). Therefore, this is of immense interest to study whether and how NLGP restricts VEGF synthesis and secretion from tumor resident cells.

Herein, we show that NLGP primarily targets VEGF synthesis by disrupting the binding of HIF1 α with its co-factors, which ultimately prevents binding of HIF1 α - transcriptional complex to the HRE region of VEGF. Additionally, NLGP prevents Stat3 activation and STAT3-dependent HIF1 α transcription. Both of these events simultaneously mitigate VEGF secretion from tumor and non-tumor stromal cells.

MATERIALS AND METHODS

Antibodies and Reagents

DMEM-high glucose medium and Fetal bovine serum (FBS) were obtained from Invitrogen (NY, USA). Purified anti-mouse antibodies (VEGF, HIF1 α , Sp1, Sp3, p300, CBP, pAKT, pERK, STAT3, pSTAT3) and Stat3 siRNA were procured from Santa Cruz Biotechnology (Dallas, TX, USA). Anti-mouse/rabbit fluorescence conjugated secondary antibodies (FITC and PE conjugate) were purchased from Sigma Aldrich (St. Louis, US). RT-PCR primers were designed and procured from Eurofins, Bangalore, India. Trizol reagent for RNA isolation and Revert AidTM cDNA synthesis kit were procured from Invitrogen (Carlsbad, CA, USA) and Fermentas (Waltham, MA, USA), respectively.

Maintenance of Cell Lines

B16F10 murine melanoma cells (B16Mel) were purchased from the National Center for Cell Sciences (NCCS), Pune, India. Lewis Lung Carcinoma (LL/2 (LLC1) were purchased directly from American Type Cell Culture (ATCC[®] CRL1642TM, Manassas, VA, USA). Macrophages were collected from peritoneal cavity of C57BL/6J mice and tumor conditioned using B16Mel tumor lysate. Cells were maintained at 70% confluency in complete DMEM high glucose media supplemented with 10% (v/v) heat inactivated FBS, 2mM L-glutamine, 100 U/ml penicillin and 100 μ g/ml streptomycin at 37°C with the supply of 5% CO₂. Authentication is done using STR method in the cell banks. All cells were maintained for 10 to 12 passages and all handling procedure was done according to guidelines provided by ATCC. B16Mel cells were tested for mycoplasma contamination using mycoplasma detection kit (EZdetectTM PCR Kit for Mycoplasma Detection; based on 16s-23s rRNA spacer region, Himedia, India). All experiments were done within 6 months of purchase.

Mice and Tumor Inoculation

Inbred female C57BL/6J mice (age, 4–6 weeks, average body weight 21 g) were obtained and maintained as described (21). All experiments were performed in accordance with the guidelines provided by the Institutional Animal Care and Ethics Committee (Approval No. IAEC-1774/RB-7/2016/3).

Neem Leaf Glycoprotein

Neem leaf glycoprotein (NLGP) was prepared from neem leaves (*Azadirachta indica*), by the method as described previously (21). A standard protocol was followed as described (22).

Generation of Hypoxic Environment *in vitro*

B16Mel cells were kept in a hypoxia chamber (Stem Cell Technologies, Canada) to mimic artificial tumor hypoxic environment. The later was generated by passing a hypoxia gas mixture of 5% O₂, 85% N₂, and 10% CO₂, at 20psi pressure for 4 min. According to manufacturer's protocol, this time is required to completely replace the atmospheric gas inside the chamber with the desired gas mixture.

Histology and Immunohistochemistry

Tumors were fixed to stain with VEGF according to method described (19). In some cases, VEGF positive regions were selected and dissected using laser capture microscopy.

Cytokine Detection Assay

Cytokines secreted from B16Mel cells within culture supernatant both in hypoxia and normoxia w/o NLGP, were measured by ELISA as described (19).

Co-localization Studies

B16Mel cells were grown in chamber slides in hypoxia, w/o NLGP, fixed with paraformaldehyde and permeabilized in 0.1% Triton X-100. After methodical washing with PBS-Tween 20 and PBB (0.5% BSA + PBS) blocking was done using 2% BSA. Primary antibodies for Sp1, Sp3, CBP, p300 and HIF1 α were added in dilution range 1:200 to 1:500 and incubated in a moist chamber, overnight. Secondary antibody was added and incubated for 1 h. Slides were finally mounted with DAPI and images were acquired using Leica DM 1000, Fluorescent Microscope (Leica, BM 4000B, Germany).

Nuclear and Cytosolic Extraction

B16Mel cells were scraped using chilled PBS, centrifuged and cell pellet was re-suspended in ice-cold EMSA buffer to incubate for 1 h at 4°C. Nuclear and cytosolic fractions were carried out according to the protocol described (19).

RT-PCR

Cellular RNA was isolated using Trizol (Invitrogen, Camarillo, CA) and random hexamers were used to generate corresponding cDNA (First Strand cDNA Synthesis Kit; Fermentas, Hanover, MD). Amplification was done according to protocol described (22).

Co-immunoprecipitation and Western Blot

B16Mel cells were subjected to hypoxia w/o NLGP for 4 h, and Co-IP of Sp1/3, CBP, p300 with HIF1 α was performed as described (23).

Chromatin Immunoprecipitation (ChIP) Assay

ChIP assays were conducted following the manufacturer's protocol (Millipore, Darmstadt, Germany). B16Mel cells (1×10^6) were subjected to normoxia and hypoxia w/o NLGP as described (23) was followed. DNA was extracted using phenol/chloroform to conduct PCR using promoter specific primers: HRE region in the promoter of VEGF (HIF1 α binding site): sense 5'-CCACAGTGCATACGTGGGCTC-3', antisense 5'-GGTGTACGTATGCACCCGAG-3'.

si-RNA Mediated STAT3 Silencing

STAT3 specific si-RNA (Santacruz Biotechnology, Dallas, TX) was added in 70% confluent B16Mel culture as described (23). Finally, expression of *stat3* and *hif1 α* was checked both in untreated, NLGP treated and siRNA transfected B16Mel cells by RT-PCR.

Flow-Cytometric Staining

Flow-cytometry of pAKT, pERK and pSTAT3 was done as described (24).

Statistical Analysis

All reported results represent the mean \pm SD of data obtained in either six (for *in vivo* analysis) or three to six (*in vitro* assays) independent experiments. Statistical significance was established by unpaired *t*-test using INSTANT 3 Software (Graphpad Inc., USA), with differences between groups attaining a *p*-value < 0.01 considered as significant.

RESULTS

NLGP Mediated Tumor Growth Restriction Is Associated With Downregulation of VEGF in Immune and Tumor Cells

In continuation to our previous research in understanding the mechanism of NLGP mediated tumor growth restriction, we have reported that therapeutic NLGP treatment significantly reduces the availability of VEGF in tumor hosts, in an immune dependent (CD8⁺ T cells and IFN γ) manner (21). To analyze the detailed molecular mechanism behind NLGP mediated modulation of VEGF, here, first we studied the cellular source of VEGF, those are targeted by NLGP. Laser-capture-microdissection of tumor tissues followed by RT-PCR analysis suggested that *in vivo* NLGP treatment showed no change in melanoma (gp100) and dendritic cell (DC) (CD11c) marker, but an increase in macrophage marker (CD11b) (Figure 1C). Thus, observed reduction in VEGF as shown in Figure 1A might be due to NLGP's inhibition on VEGF secretion from B16Mel and macrophage cells (Figures 1A–D). This observation is suggestive that VEGF reduction is not due to direct killing of the tumor cells but rather NLGP could modulate tumor cells to restrict VEGF production.

Based on this *in vivo* result, next we studied VEGF expression of B16Mel and LLC cells and in macrophages under normoxia and hypoxia with NLGP treatment. RT-PCR and ELISA suggested a significant decrease in *veg*f gene as well as protein expression after 6 h and 48 h of NLGP treatment, respectively, in all cells studied. The extent of VEGF reduction was prominent under hypoxic condition with no change in normoxia (Figures 1E–G).

NLGP Modulates HIF1 α in Tumor Cells to Restrain VEGF Production

Given the direct effect of NLGP in reduction of VEGF in hypoxic condition, next we checked the involvement of HIF1 α , the main regulator of VEGF and also the exact time point at which VEGF is downregulated. B16Mel, LLC and macrophage cells were exposed to normoxic and hypoxic conditions for various time points (0 min, 30 min, 1 h, 4 h, 18 h, and 24 h) in presence or absence of NLGP (1.5 μ g/ml). RT-PCR analysis suggested downregulation of *veg*f started at 4 h and reached a maximum decrease at 24 h (Figures 2A,B), whereas downregulation of *hif1 α* was observed only at 24 h. Western blot analysis suggested a downregulation of total VEGF started at 18 h of NLGP treatment under hypoxia

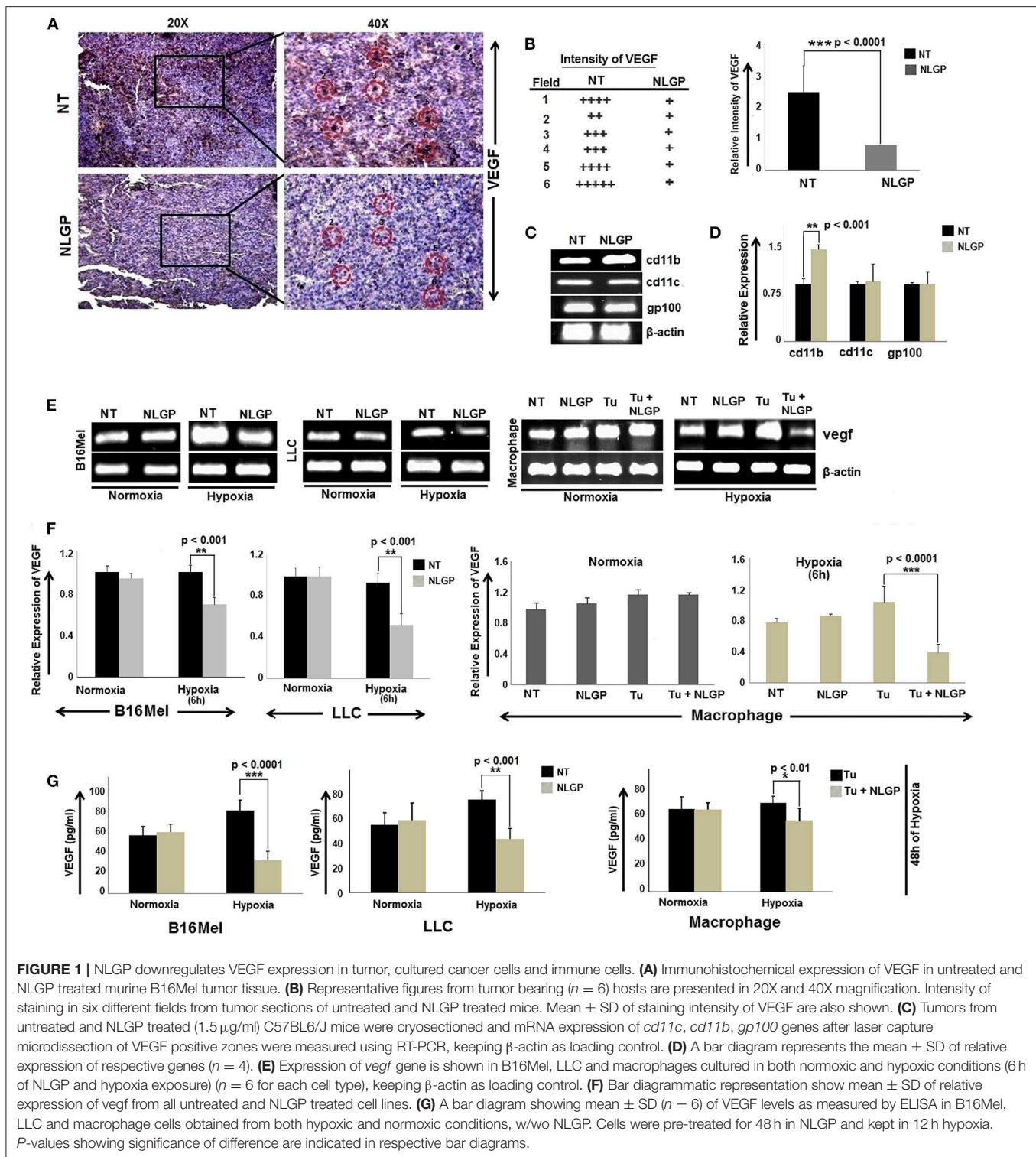


FIGURE 1 | NLGP downregulates VEGF expression in tumor, cultured cancer cells and immune cells. **(A)** Immunohistochemical expression of VEGF in untreated and NLGP treated murine B16Mel tumor tissue. **(B)** Representative figures from tumor bearing ($n = 6$) hosts are presented in 20X and 40X magnification. Intensity of staining in six different fields from tumor sections of untreated and NLGP treated mice. Mean \pm SD of staining intensity of VEGF are also shown. **(C)** Tumors from untreated and NLGP treated (1.5 μ g/ml) C57BL/6/J mice were cryosectioned and mRNA expression of *cd11c*, *cd11b*, *gp100* genes after laser capture microdissection of VEGF positive zones were measured using RT-PCR, keeping β -actin as loading control. **(D)** A bar diagram represents the mean \pm SD of relative expression of respective genes ($n = 4$). **(E)** Expression of *veg* gene is shown in B16Mel, LLC and macrophages cultured in both normoxic and hypoxic conditions (6 h of NLGP and hypoxia exposure) ($n = 6$ for each cell type), keeping β -actin as loading control. **(F)** Bar diagrammatic representation show mean \pm SD of relative expression of *veg* from all untreated and NLGP treated cell lines. **(G)** A bar diagram showing mean \pm SD ($n = 6$) of VEGF levels as measured by ELISA in B16Mel, LLC and macrophage cells obtained from both hypoxic and normoxic conditions, w/o NLGP. Cells were pre-treated for 48 h in NLGP and kept in 12 h hypoxia. *P*-values showing significance of difference are indicated in respective bar diagrams.

(Figures 2C,D; Supplementary Material). As hypoxia stabilizes HIF1 α protein and promotes its translocation to nucleus from cytoplasm, next we studied its expression in both cases. Although cytosolic HIF1 α expression remains low in all the conditions but hypoxia increases HIF1 α expression in nucleus of B16Mel

cells, while, NLGP treatment reduced stable HIF1 α expression at 24 h (Figures 2C,D). Therefore, collectively these data suggest that NLGP does not affect HIF1 α expression in either protein or mRNA level at 4 h to control their VEGF production in tumor cells.

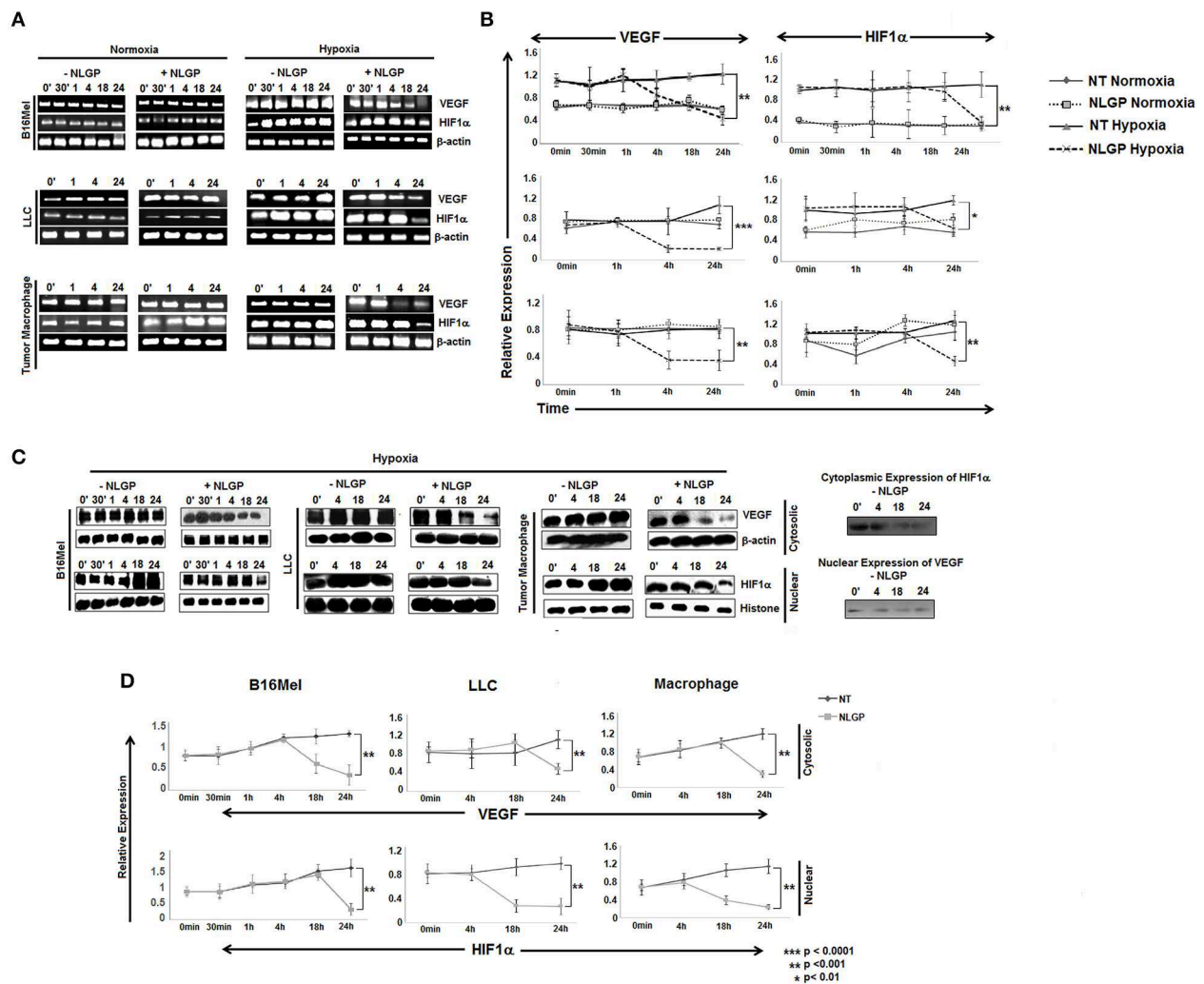


FIGURE 2 | NLGP modulates HIF1 α to restrain VEGF secretion in hypoxia. **(A)** B16Mel, LLC, and macrophages were treated w/wo NLGP and subjected to either hypoxia or kept in normoxia for different time periods. (A1) Representative data from $n = 6$ are shown, exhibiting mRNA for *vegfr* and *hif1 α* gene were studied by RT-PCR. β -actin was kept as a loading control. **(B)** A line graph showing different time points (0 min, 30 min, 1 h, 4 h, 18 h, and 24 h) represents the mean \pm SD of relative expression of *vegfr* and *hif1 α* genes. p -value significance of hypoxia exposed sample are shown in all graphs, no significant change was observed in normoxic samples. **(C)** Western blotting was performed to check the protein level expression of VEGF and HIF1 α in hypoxia for both untreated and NLGP treated cells at various time points. In the upper panel, cytosolic expression of VEGF is shown for various time points, β -actin was kept as loading control. Lower panel represents the nuclear expression of HIF1 α keeping histone H3 as loading control. Basal level of cytosolic expression of HIF1 α and nuclear VEGF expression in controlled condition is shown alongside the panel. **(D)** A line graph ($n = 6$) represents the mean \pm SD of cytosolic VEGF and nuclear HIF1 α expression w/wo NLGP treatment in hypoxia. p -values showing significance of difference are indicated in the figure.

NLGP Neither Affects Hypoxia-Induced HIF1 α Stabilization nor O₂/VHL-Dependent HIF1 α Degradation

NLGP mediated downregulation of VEGF gene transcription was achieved after 4 h. However, NLGP is unable to reduce stable HIF1 α expression in B16Mel cells at this time point, which was observed only at 24 h in both transcriptional and translational levels. This result clearly pointed out that NLGP treatment does not affect the HIF1 α stabilization in hypoxic condition.

Next, we look at VHL expression, an important tumor suppressor gene. In presence of O₂, VHL ubiquitinates HIF1 α for its subsequent proteosomal degradation. However, neither

in vivo (Figure 3A) nor *in vitro* (Figure 3B) NLGP treatment shows any effect in VHL expression in tumor tissues or in B16Mel cells, respectively, and suggested that NLGP mediated VEGF downregulation is not associated with VHL-dependent HIF1 α degradation (Figures 3A,B).

NLGP Targets the Binding of HIF1 α to Its Co-activator and Prevents Formation of Active HIF1 α Transcriptional Complex

HIF1 α binds with HIF1 β and other co-activators (like, Sp1, CBP/p300, etc.) to form active transcriptional complex after translocating to the nucleus and bind with hypoxia responsive

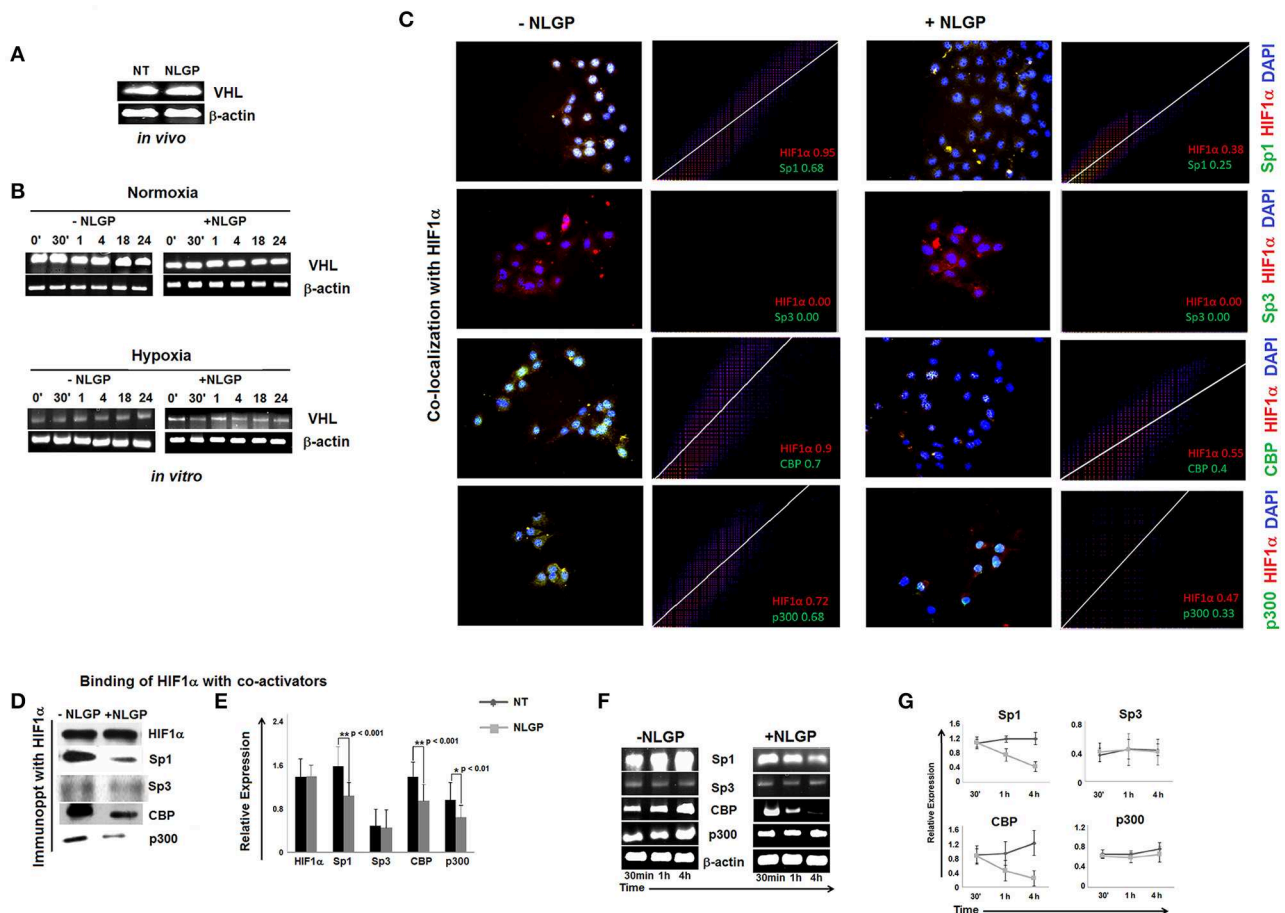


FIGURE 3 | Effect of NLGP on VHL and HIF1 α activation. **(A)** mRNA expression of tumor suppressor gene, *vhl* from both *in vivo* hosts **(A)** and *in vitro* B16Mel cells exposed to normoxia and hypoxia at different time points **(B)**, w/o NLGP, was assessed by RT-PCR. β -actin was used as a loading control in all cases. **(C)** Co-localization of HIF1 α and its co-activators in presence or absence of NLGP in hypoxia were determined by immunofluorescence microscopy and analyzed by *Image J* software as 2D histogram pictorial. Nuclei were stained with DAPI. HIF1 α and co-activators, Sp1, Sp3, CBP, and p300 were detected with anti-mouse PE and anti-rabbit FITC, respectively. Representative data from $n = 6$ are presented. Mander's tM1 value greater than 0.6 indicates higher co-localization, tM1 value within 0.5–0.6 range indicates moderate co-localization and values below 0.5 indicates weak co-localization. tM1 values for each co-factors are mentioned in respective pictures. **(D)** Co-immunoprecipitation and western blot analysis of hypoxia (4 h) treated B16Mel cells from w/o NLGP treatment as indicated. **(E)** A representative bar diagram showing mean \pm SD from $n = 6$ are presented. **(F)** Representative data from $n = 6$ are shown, exhibiting mRNA expression using RT-PCR of *sp1*, *sp3*, *cbp*, and *p300* genes in hypoxia w/o NLGP treatment at 3 different time points (30 min, 1 h, and 4 h). β -actin was used as a loading control. **(G)** A line diagram showing mean \pm SD ($n = 6$) representing change in expression with NLGP treatment from untreated samples are shown for three different time points (30 min, 1 h, and 4 h) of hypoxic condition.

elements (HRE) of VEGF promoter (25). As NLGP treatment does not show any effect on HIF1 α stabilization, we assessed the binding of HIF1 α with its co-activator(s). Accordingly, B16Mel cells were exposed to hypoxia w/o NLGP (1.5 μ g/ml) for 4 h and co-localization and co-immunoprecipitation assays were performed. Co-localization assay of B16Mel cells grown-on chamber slide in hypoxic environment demonstrated that NLGP significantly prevents co-localization of HIF1 α with Sp1, CBP, and p300. Analysis of co-localization by *Image J* software of HIF1 α with Sp1, CBP, and p300 shows higher Mander's tM1 value for all hypoxia treated cohorts (>0.6) compared to NLGP-treated cohorts (<0.5) (Figure 3C). Co-immunoprecipitation assay also supported that NLGP treatment is able to reduce protein-protein interaction of HIF1 α with its co-activators (Figures 3D,E; Supplementary Material),

whereas the binding between HIF1 α and Sp3 (a competitive inhibitor of Sp1) showed no change in NLGP treated B16Mel cells (Figures 3C,D). Interestingly, NLGP treatment also downregulates transcriptional expression of both Sp1, CBP and p300 in B16Mel cells under hypoxic condition after 4 h (Figures 3E,G). Therefore, the overall data suggest that NLGP is able to prevent the formation of active HIF1 α transcriptional complex required for VEGF transcription.

NLGP Prevents Binding of HIF1 α Transcriptional Complexes to VEGF Promoter in Hypoxia

As NLGP prevents the nuclear translocation of HIF1 α and the formation of active HIF1 α complex, next we assessed its

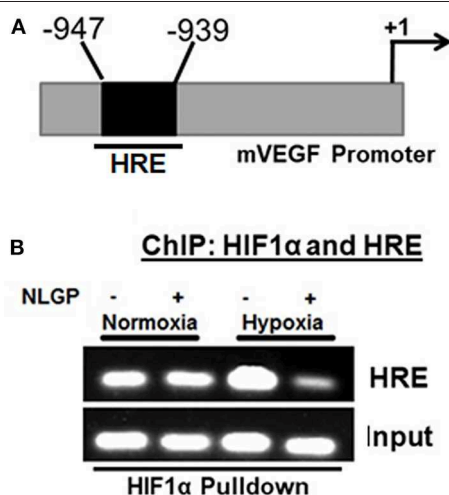


FIGURE 4 | NLGP prevents nuclear binding of HIF complex to HRE. **(A)** Potential Hypoxia Responsive Element (HRE) within mouse *vegf* gene promoter. Indicated arrows are for PCR primer positions used in ChIP assay. **(B)** Representative data of mRNA expression using RT-PCR of HIF1 α /co-activator complex recruitment to the HRE region of *vegf* promoter in NLGP treated or non-treated B16Mel cells in hypoxia. Input lanes are prepared from 10% of samples used in IPs, with control IgG and HIF1 α activation complex.

binding with cognate HRE sequence at VEGF promoter using chromatin immune-precipitation (ChIP) assay. Results obtained from ChIP assay suggested that hypoxia remarkably promoted the binding of HIF1 α with VEGF promoter in B16Mel cells whereas, NLGP treatment caused a significant reduction in binding of HIF1 α with VEGF promoter in hypoxic condition (Figures 4A,B).

NLGP Targets Stat3-Dependent Transcription of HIF1 α to Reduce VEGF

Although NLGP treatment downregulates VEGF primarily by targeting HIF1 α binding with VEGF promoter, it also causes a significant downregulation of HIF1 α in transcription level at 24 h. Several transcription factors or oncogenic stimuli are reported to have HIF1 α promoting activity like Stat3, NF- κ B, AKT, ERK etc. To study the target molecule(s) in our settings, we have checked the activation status of different HIF1 α -linked up-stream transcription factors in NLGP-treated B16Mel cells w/o hypoxia by flow-cytometry and western blot analysis. Both the assays suggested that after 30 min of NLGP treatment there was a significant downregulation of pStat3 expression, which further showed a decrease at 1 h and maintained a reduced pStat3 expression till 4 h in hypoxia-exposed tumor cells (Figures 5A–D). However, other factors like AKT, ERK show no significant changes after NLGP treatment

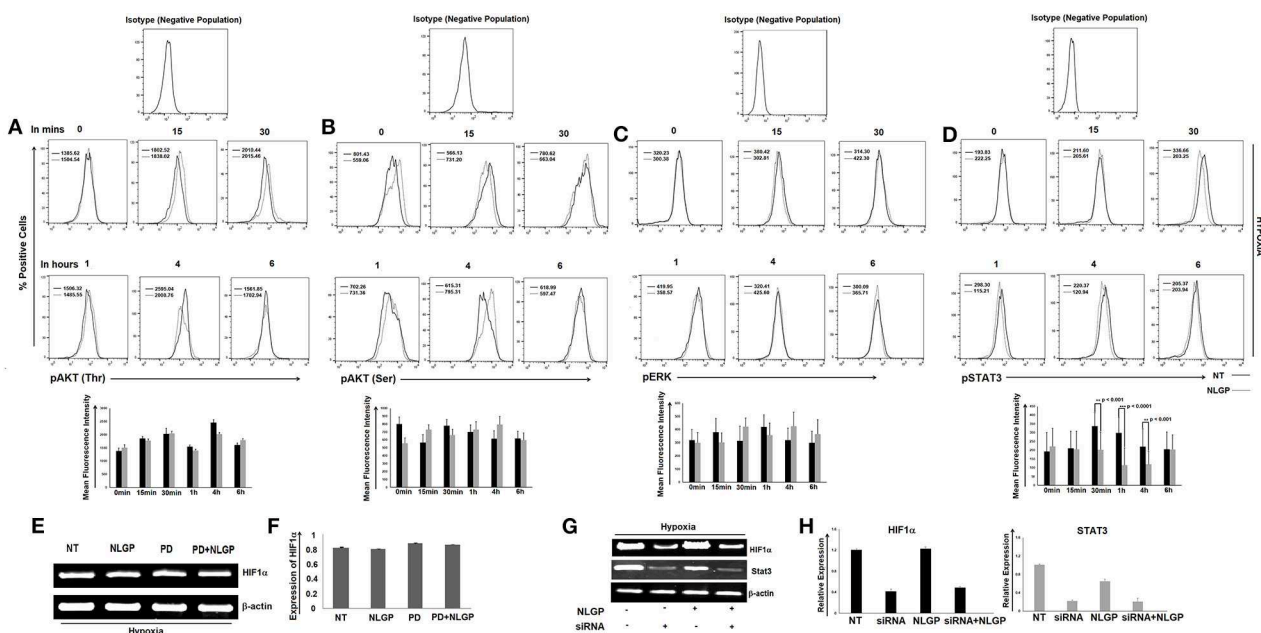


FIGURE 5 | NLGP targets HIF1 α upstream signaling cascade. **(A)** Responsible factors for regulating HIF1 α at protein level was determined by a time kinetics experiment. B16Mel cells were exposed to hypoxia w/o NLGP treatment for various time points (0 min, 15 min, 30 min, 1 h, 4 h, and 6 h) and expression pAKT(Thr) **(A)**, pAKT(Ser) **(B)**, pERK **(C)**, and pSTAT3 **(D)** was checked by flow cytometry. Illustrative histograms show percent positive cells for respective upstream signaling molecules ($n = 6$). Mean Fluorescence Intensity (MFI) measuring the mean level of phosphorylation is indicated in each histogram with a bar diagram showing mean \pm SD of $n = 4$ samples. **(E)** mRNA expression of *hif1 α* gene after blocking with inhibitor PD was checked w/o NLGP treatment, keeping β -actin as loading control. **(F)** Representative data and bar diagram showing mean \pm SD ($n = 6$) of HIF1 α expression by RT-PCR are presented. **(G)** B16Mel cells were either treated with NLGP or Stat3 siRNA or both in presence of hypoxia. mRNA expression by RT-PCR was checked for *hif1 α* gene expression. Level of Stat3 was also checked to see efficacy of the silencing experiment. **(H)** Representative bar diagram showing mean \pm SD of relative expression ($n = 6$) for respective genes are presented.

(Figures 5A–C), even after blocking them (Figures 5E,F). But, inhibition of Stat3 by Stat3-specific siRNA treatment significantly abrogated this NLGP mediated downregulation of HIF1 α after 24 h (Figures 5G,H).

DISCUSSIONS

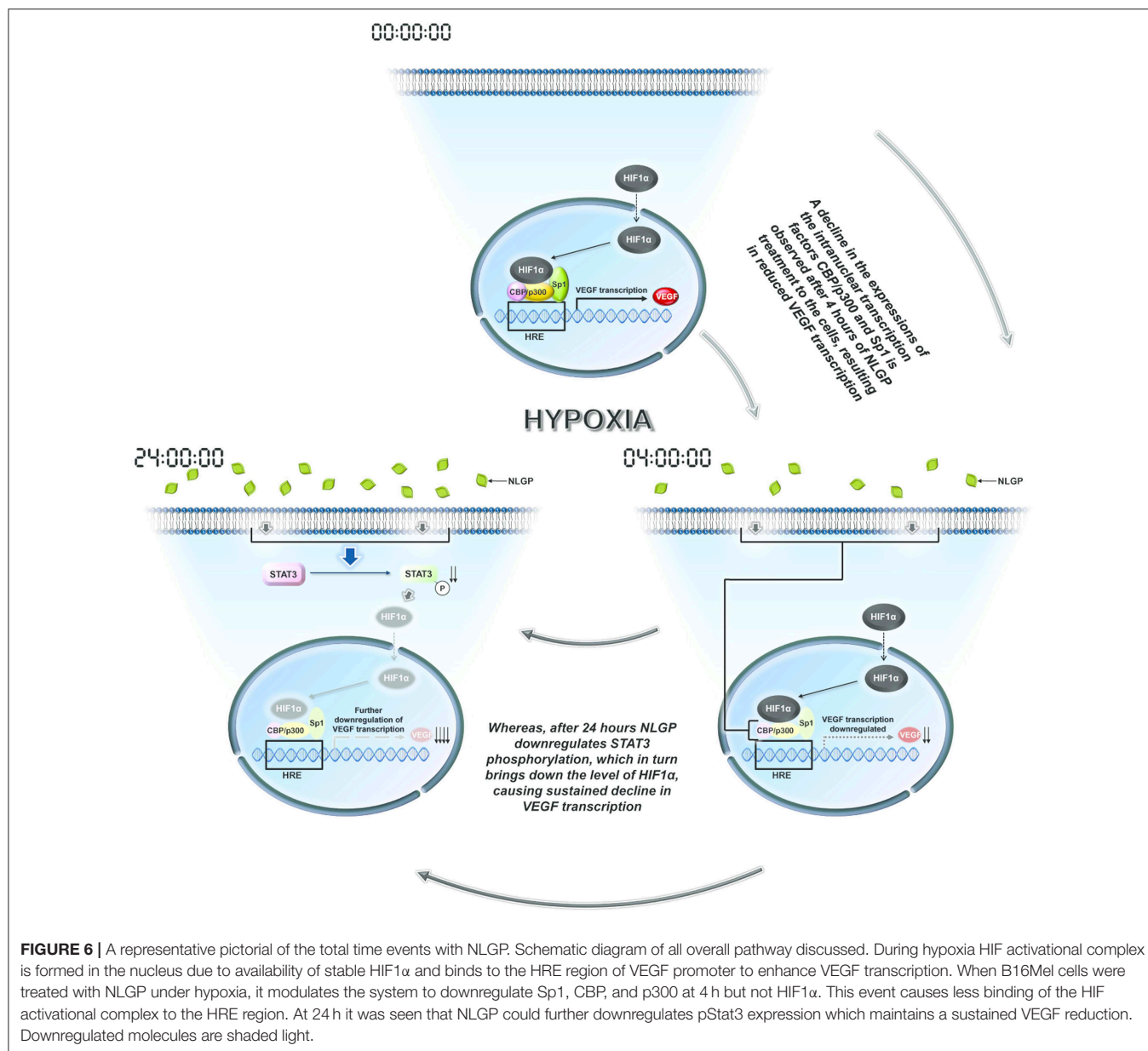
Angiogenesis plays a critical role in tumor growth by inducing VEGF secretion, which ultimately creates hypoxia and fosters tumor-promoting events and metastasis (26). Therefore, angiogenesis inhibitors specifically VEGF antagonist gained special interest in cancer management. However, these synthetic drugs generate toxicity as well as resistance. While non-toxic plant-based molecules seem more promising, detailed molecular mechanisms of action of plant based anti-angiogenic molecules are largely unknown. We reported a non-toxic immunomodulator, NLGP, having sustained effect on tumor growth restriction (27–30) and vascular normalization (21). These are primarily mediated by (i) activation of cytotoxic CD8⁺ T cells (20, 27, 29) and their interaction with CD4⁺ helper T cells (31), (ii) downregulation of immunosuppressive cytokines (IL-6, IL-10, TGF β , etc.) (20, 24, 28, 32), (iii) decrease in suppressor cell (Treg, TAM, DC2, MDSC) accumulation and their functions (32–34), (iv) generation of central and effector memory T cells (19). However, this molecule failed to induce any direct cytotoxic effect to the tumor cells (35). Here, for the first time we have shown that NLGP can directly modulate tumor cell property, which might switch the hostile TME.

A substantial reduction in uncontrolled angiogenesis is demonstrated recently after NLGP treatment in tumor bearing mice by downregulating intratumoral VEGF (21). Accordingly, the present work is initiated to understand how NLGP reduces VEGF within TME where tumor and tumor associated stromal cells including immune cells are major VEGF sources (36) and therefore could be potential targets of NLGP. To better understand the cellular target of NLGP, we looked inside a tumor tissue architecture and laser capture microdissection aided that NLGP can reduce VEGF secretion by modulating both macrophages and tumor cells. As reported earlier, NLGP significantly reduces of M2-type macrophages (24) and suppressor MDSCs (34). NLGP cannot directly kill macrophages or tumor cells thus it could modify the VEGF promoting factors like hypoxia (21). To understand the cellular and molecular mechanisms more precisely, we opt for *in vitro* culture of B16Mel, LLC, and macrophage cells, where we observed significant reduction of VEGF in tumor cells and macrophages after NLGP treatment as early as 4 h at mRNA level with more prominent result in hypoxia than normoxia, suggesting hypoxia as a major factor that NLGP targets. HIF1 α a major angiogenesis inducer in tumor cells (carcinoma and melanoma) both *in vitro* and *in vivo*. Hence, those conditions known to activate HIF1 α can upregulate VEGF production by recruiting other cofactors forming HIF activation complex (37). Therefore, possible mechanisms by which NLGP inhibits VEGF gene expression could include (i) Promotion of degradation of HIF1 α protein, (ii) Reduction of HIF1 α protein synthesis, (iii) Prevention of nuclear translocation of HIF1 α , (iv) Hindrance in active HIF1 α complex formation

by preventing binding between HIF1 α and partner(s), (v) Direct block in binding of HIF1 α complex to HRE region of VEGF promoter. As we carried out our experiments in hypoxia, which stabilizes HIF1 α , we did not find any changes in expression of HIF1 α mRNA and protein up to 24 h with NLGP treatment, so the first possibility is obsolete. Furthermore, degradation of HIF1 α protein requires obligatory presence of VHL (38), NLGP has no effect *in vivo* or *in vitro* over VHL expression. The second possibility at least for early (at 4 h) is ruled out since NLGP can only reduce HIF1 α protein expression after 18 h. NLGP treatment failed to reduce the accumulation of nuclear HIF1 α and can downregulate the same only after 24 h, excluding the third possibility for early VEGF downregulation. Next, we look further into the binding capacity of HIF1 α with other cofactors, like Sp1, CBP, p300, and we found that NLGP prevents co-localization of HIF1 α with CBP, p300 and Sp1 but not with Sp3, which can competitively target HIF1 α and Sp1 binding. Sp1 and Sp3 compete for binding to the HRE region as they share more than 90% sequence homology (39–41). Consequently, we observed significant less binding of active HIF1 α complex with HRE region. Moreover, this effect is more global as NLGP treatment shows downregulated expression of other HIF1 α target genes (PDK1 and EPO) (data not shown).

Many plant-based molecules show inhibitory effects toward VEGF mainly by modulating HIF1 α protein synthesis or degradation (42–49). On the other hand, NLGP initially target and destabilizes HIF1 α -HIF1 β -Sp1-CBP-p300 active transcriptional complex formation at 4 h, while at late hours it downregulates HIF1 α protein synthesis. Several signaling pathways are responsible for downregulation of HIF1 α , like AKT, ERK, MAPK, STAT3, etc. The status of AKT and ERK phosphorylation in B16Mel cells did not show any NLGP induced changes in either normoxia or hypoxia. However, NLGP causes significant reduction in Stat3 phosphorylation under hypoxia. Consistent with our previous reports, we observed downregulation of pStat3 by NLGP and siRNA mediated knock-down of stat3, both of which mimics NLGP's effect. Recent studies suggest that HIF1 α is regulated by STAT3 as the later increases the half-life of the transcription factor in both human and mouse melanoma cells (50). STAT3 can directly bind to HIF1 α promoter and upregulates its expression post-translationally (51). A pictorial shown in Figure 6 demonstrates how NLGP regulates VEGF in hypoxic TME at 4 and 24 h.

A significant reduction of HIF1 α -VEGF signaling axis within tumor by NLGP treatment has immense importance even from immunological perspective, where efficacy of NLGP is already proven. Moreover, effect of NLGP is dependent on CD8⁺ T cells and reduced hypoxia-and related factors may promote susceptibility of tumor cells toward T and NK cell mediated killing via induction of autophagy as well as more efficient functioning of several immune cells by downregulating CTLA4 on T cells and PDLs on tumor cells. However, here we are unable to explore how NLGP interact with macrophage or tumor cells to reduce stat3, which may eventually prevent the formation of active HIF1 α -transcriptional complex. This study adds new insight into the potential mechanism of NLGP's activity besides immunomodulation which may



intensify its prospective acceptance as a novel strategy for cancer management.

DATA AVAILABILITY STATEMENT

All datasets generated for this study are included in the article/**Supplementary Material**.

ETHICS STATEMENT

All experiments were performed in accordance with the guidelines provided by the (Chittaranjan National Cancer Institute, Kolkata) Institutional Animal Care and Ethics Committee (Approval No. IAEC-1774/RB-7/2016/3).

AUTHOR CONTRIBUTIONS

AS, ABo, and RB: experimental design of the study, planning and execution, analysis of data, and manuscript preparation. AS, PN, and SD: performed majority research. ABh, NG, TG, IG, and SB: performed minor research work and helped in providing resources. ABo and RB: supervised the project and acquired funds. All authors approved the manuscript.

FUNDING

This work was supported by Council of Scientific and Industrial Research, New Delhi (37(1524)/12/EMR-II).

It was also partially supported by Chittaranjan National Cancer Institute, Kolkata, India. The funders have no role in experimental designs, data collection and analysis, decision to publish or preparation of the manuscript.

REFERENCES

- Viallard C, Larrivée B. Tumor angiogenesis and vascular normalization: alternative therapeutic targets. *Angiogenesis*. (2017) 20:409–26. doi: 10.1007/s10456-017-9562-9
- Yuan Y, Jiang YC, Sun CK, Chen QM. Role of the tumor microenvironment in tumor progression and the clinical applications. *Oncol Rep*. (2016) 35:2499–515. doi: 10.3892/or.2016.4660
- Wu JB, Tang YL, Liang XH. Targeting VEGF pathway to normalize the vasculature: an emerging insight in cancer therapy. *Onco Targets Ther*. (2018) 11:6901–9. doi: 10.2147/OTT.S172042
- Ramjiawan RR, Griffioen AW, Duda DG. Anti-angiogenesis for cancer revisited: is there a role for combinations with immunotherapy? *Angiogenesis*. (2017) 20:185–204. doi: 10.1007/s10456-017-9552-y
- Eales KL, Hollinshead KER, Tennant DA. Hypoxia and metabolic adaptation of cancer cells. *Oncogenesis*. (2016) 5:e190. doi: 10.1038/oncsis.2015.50
- Masoud GN, Li W. HIF-1 α pathway: role, regulation and intervention for cancer therapy. *Acta Pharm Sin B*. (2015) 5:378–89. doi: 10.1016/j.apsb.2015.05.007
- Ziello JE, Jovin IS, Huang Y. Hypoxia-Inducible Factor (HIF)-1 regulatory pathway and its potential for therapeutic intervention in malignancy and ischemia. *Yale J Biol Med*. (2007) 80:51–60.
- Barbera-Guillem E, Nyhus JK, Wolford CC, Friece CR, Sampsel JW. Vascular endothelial growth factor secretion by tumor-infiltrating macrophages essentially supports tumor angiogenesis, and IgG immune complexes potentiate the process. *Cancer Res*. (2002) 62:7042–49.
- Semenza GL, Agani F, Booth G, Forsythe J, Iyer N, Jiang BH, et al. Structural and functional analysis of hypoxia-inducible factor 1. *Kidney Int*. (1997) 51:553–55. doi: 10.1038/ki.1997.77
- Weidemann A, Johnson RS. Biology of HIF-1 α . *Cell Death Differ*. (2008) 15:621–7. doi: 10.1038/cdd.2008.12
- Dengler VL, Galbraith MD, Espinosa JM. Transcriptional regulation by hypoxia inducible factors. *Crit Rev Biochem Mol Biol*. (2014) 49:1–15. doi: 10.3109/10409238.2013.838205
- Stegeman H, Span PN, Peeters WJ, Verheijen MM, Grénman R, Meijer TW, et al. Interaction between hypoxia, AKT and HIF-1 signaling in HNSCC and NSCLC: implications for future treatment strategies. *Fut Sci OA*. (2016) 2:FSO84. doi: 10.4155/fso.15.84
- Liu L, Zhang H, Sun L, Gao Y, Jin H, Liang S, et al. ERK/MAPK activation involves hypoxia-induced MGr1-Ag/37LRP expression and contributes to apoptosis resistance in gastric cancer. *Int J Cancer*. (2010) 127:820–29. doi: 10.1002/ijc.25098
- Noman MZ, Buart S, Van Pelt J, Richon C, Hasmin M, Leleu N, et al. The cooperative induction of hypoxia-inducible factor-1 α and STAT3 during hypoxia induced an impairment of tumor susceptibility to CTL-mediated cell lysis. *J Immunol*. (2009) 182:3510–21. doi: 10.4049/jimmunol.0800854
- Pawlus MR, Wang L, Hu CJ. STAT3 and HIF1 α cooperatively activate HIF1 target genes in MDA-MB-231 and RCC4 cells. *Oncogene*. (2014) 33:1670–9. doi: 10.1038/ncr.2013.115
- Jung JE, Kim HS, Lee CS, Shin YJ, Kim YN, Kang GH, et al. STAT3 inhibits the degradation of HIF-1 α by pVHL-mediated ubiquitination. *Exp Mol Med*. (2008) 40:479–85. doi: 10.3858/emmm.2008.40.5.479
- Pages G, Pouyssegur J. Transcriptional regulation of the vascular endothelial growth factor gene—a concert of activating factors. *Cardiovasc Res*. (2005) 65:564–73. doi: 10.1016/j.cardiores.2004.09.032
- Lupo G, Caporarello N, Olivieri M, Cristaldi M, Motta C, Bramanti V, et al. Anti-angiogenic therapy in cancer: downsides and new pivots for precision medicine. *Front Pharmacol*. (2017) 7:519. doi: 10.3389/fphar.2016.00519
- Ghosh S, Sarkar M, Ghosh T, Guha I, Bhuniya A, Saha A, et al. Neem leaf glycoprotein promotes dual generation of central and effector memory CD8+ T cells against sarcoma antigen vaccine to induce protective anti-tumor immunity. *Mol Immunol*. (2016) 71:42–53. doi: 10.1016/j.molimm.2016.01.007
- Barik S, Banerjee S, Mallick A, Goswami KK, Roy S, Bose A, Baral R. Normalization of tumor microenvironment by neem leaf glycoprotein potentiates effector T cell functions and therapeutically intervenes in the growth of mouse sarcoma. *PLoS ONE*. (2013) 8:e66501. doi: 10.1371/journal.pone.0066501
- Banerjee S, Ghosh T, Barik S, Das A, Ghosh S, Bhuniya A, et al. Neem leaf glycoprotein prophylaxis transduces immune dependent stop signal for tumor angiogenic switch within tumor microenvironment. *PLoS ONE*. (2014) 9:e110040. doi: 10.1371/journal.pone.0110040
- Goswami KK, Sarkar M, Ghosh S, Saha A, Ghosh T, Guha I, et al. Neem leaf glycoprotein regulates function of tumor associated M2 macrophages in hypoxic tumor core: critical role of IL-10/STAT3 signaling. *Mol Immunol*. (2016) 80:1–10. doi: 10.1016/j.molimm.2016.10.008
- Ghosh T, Barik S, Bhuniya A, Dhar J, Dasgupta S, Ghosh S, et al. Tumor-associated mesenchymal stem cells inhibit naïve T cell expansion by blocking cysteine export from dendritic cells. *Int J Cancer*. (2016) 139:2068–81. doi: 10.1002/ijc.30265
- Goswami KK, Barik S, Sarkar M, Bhowmick A, Biswas J, Bose A, et al. Targeting STAT3 phosphorylation by neem leaf glycoprotein prevents immune evasion exerted by supraglottic laryngeal tumor induced M2 macrophages. *Mol Immunol*. (2014) 59:119–27. doi: 10.1016/j.molimm.2014.01.015
- Olenyuk BZ, Zhang GJ, Klco JM, Nickols NG, Kaelin WG, Dervan PB. Inhibition of vascular endothelial growth factor with a sequence-specific hypoxia response element antagonist. *Proc Natl Acad Sci USA*. (2004) 101:16768–73. doi: 10.1073/pnas.0407617101
- Manalo DJ, Rowan A, Lavoie T, Natarajan L, Kelly BD, Shui QY, et al. Transcriptional regulation of vascular endothelial cell responses to hypoxia by HIF-1. *Blood*. (2005) 105:659–69. doi: 10.1182/blood-2004-07-2958
- Mallick A, Barik S, Ghosh S, Roy S, Sarkar K, Bose A, et al. Immunotherapeutic targeting of established sarcoma in Swiss mice by tumor-derived antigen-pulsed NLGP matured dendritic cells is CD8+ T-cell dependent. *Immunotherapy*. (2014) 6:821–31. doi: 10.2217/imt.14.53
- Chakraborty T, Bose A, Barik S, Goswami KK, Banerjee S, Goswami S, et al. Neem leaf glycoprotein inhibits CD4+ CD25+ Foxp3+ Tregs to restrict murine tumor growth. *Immunotherapy*. (2011) 3:949–69. doi: 10.2217/imt.11.81
- Mallick A, Barik S, Goswami KK, Banerjee S, Ghosh S, Sarkar K, et al. Neem leaf glycoprotein activates CD8+ T cells to promote therapeutic anti-tumor immunity inhibiting the growth of mouse sarcoma. *PLoS ONE*. (2013) 8:e47434. doi: 10.1371/journal.pone.0047434
- Barik S, Bhuniya A, Banerjee S, Das A, Sarkar M, Paul T, et al. Neem leaf glycoprotein is superior than Cisplatin and Sunitinib malate in restricting melanoma growth by normalization of tumor microenvironment. *Int Immunopharmacol*. (2013) 17:42–9. doi: 10.1016/j.intimp.2013.05.005
- Ghosh S, Sarkar M, Ghosh T, Guha I, Bhuniya A, Biswas J, et al. Absence of CD4+ T cell help generates corrupt CD8+ effector T cells in sarcoma-bearing Swiss mice treated with NLGP vaccine. *Immunol Lett*. (2016) 175:31–9. doi: 10.1016/j.imlet.2016.05.004
- Chakraborty T, Bose A, Goswami KK, Goswami S, Chakraborty K, Baral R. Neem leaf glycoprotein suppresses regulatory T cell mediated suppression of monocyte/macrophage functions. *Int Immunopharmacol*. (2012). 12:326–33. doi: 10.1016/j.intimp.2011.12.002

SUPPLEMENTARY MATERIAL

The Supplementary Material for this article can be found online at: <https://www.frontiersin.org/articles/10.3389/fonc.2020.00260/full#supplementary-material>

33. Goswami S, Bose A, Sarkar K, Roy S, Chakraborty T, Sanyal U, et al. Neem leaf glycoprotein matures myeloid derived dendritic cells and optimizes anti-tumor T cell functions. *Vaccine*. (2010) 28:1241–52. doi: 10.1016/j.vaccine.2009.11.018
34. Sarkar M, Ghosh S, Bhuniya A, Ghosh T, Guha I, Barik S, et al. Neem leaf glycoprotein prevents post-surgical sarcoma recurrence in Swiss mice by differentially regulating cytotoxic T and myeloid-derived suppressor cells. *PLoS ONE*. (2017) 12:e0175540. doi: 10.1371/journal.pone.0175540
35. Bose A, Haque E, Baral R. Neem leaf preparation induces apoptosis of tumor cells by releasing cytotoxic cytokines from human peripheral blood mononuclear cells. *Phytother Res*. (2007) 21:914–20. doi: 10.1002/ptr.2185
36. Sennino B, Kuhnert F, Tabruyn SP, Mancuso MR, Hu-Lowe DD, Kuo CJ, et al. Cellular source and amount of vascular endothelial growth factor and platelet-derived growth factor in tumors determine response to angiogenesis inhibitors. *Cancer Res*. (2009) 69:4527–36. doi: 10.1158/0008-5472.CAN-08-3779
37. Krock BL, Skuli N, Simon MC. Hypoxia-induced angiogenesis: good and evil. *Genes Cancer*. (2011) 2:1117–33. doi: 10.1177/1947601911423654
38. Tanimoto K, Makino Y, Pereira T, Poellinger L. Mechanism of regulation of the hypoxia-inducible factor-1 α by the von Hippel-Lindau tumor suppressor protein. *EMBO J*. (2000) 19:4298–309. doi: 10.1093/emboj/19.16.4298
39. Koizume S, Miyagi Y. Diverse mechanisms of Sp1-dependent transcriptional regulation potentially involved in the adaptive response of cancer cells to oxygen-deficient conditions. *Cancers*. (2016) 8:2. doi: 10.3390/cancers8010002
40. Yu B, Datta PK, Bagchi S. Stability of the Sp3–DNA complex is promoter-specific: Sp3 efficiently competes with Sp1 for binding to promoters containing multiple Sp-sites. *Nucleic Acids Res*. (2003) 31:5368–76. doi: 10.1093/nar/gkg706
41. Koizume S, Ito S, Nakamura Y, Yoshihara M, Furuya M, Yamada R, et al. Lipid starvation and hypoxia synergistically activate ICAM1 and multiple genes in an Sp1-dependent manner to promote the growth of ovarian cancer. *Mol Cancer*. (2015) 14:77. doi: 10.1186/s12943-015-0351-z
42. Lu J, Zhang K, Nam S, Anderson RA, Jove R, Wen W. Novel angiogenesis inhibitory activity in cinnamon extract blocks VEGFR2 kinase and downstream signaling. *Carcinogenesis*. (2009) 31:481–88. doi: 10.1093/carcin/bgp292
43. Chen MC, Hsu WL, Hwang PA, Chou TC. Low molecular weight fucoidan inhibits tumor angiogenesis through downregulation of HIF-1/VEGF signaling under hypoxia. *Mar Drugs*. (2015) 13:4436–51. doi: 10.3390/md13074436
44. Parveen A, Subedi L, Kim HW, Khan Z, Zahra Z, Farooqi MQ, et al. Phytochemicals targeting VEGF and VEGF-related multifactors as anticancer therapy. *J Clin Med*. (2019) 8:350. doi: 10.3390/jcm8030350
45. Lu K, Bhat M, Basu S. Plants and their active compounds: natural molecules to target angiogenesis. *Angiogenesis*. (2016) 19:287–95. doi: 10.1007/s10456-016-9512-y
46. Zhang Q, Tang X, Lu Q, Zhang Z, Rao J, Le AD. Green tea extract and (–)-epigallocatechin-3-gallate inhibit hypoxia-and serum-induced HIF-1 α protein accumulation and VEGF expression in human cervical carcinoma and hepatoma cells. *Mol Cancer Ther*. (2006) 5:1227–38. doi: 10.1158/1535-7163.MCT-05-0490
47. Fang J, Xia C, Cao Z, Zheng JZ, Reed E, Jiang BH. Apigenin inhibits VEGF and HIF-1 expression via PI3K/AKT/p70S6K1 and HDM2/p53 pathways. *FASEB J*. (2005) 19:342–53. doi: 10.1096/fj.04-2175com
48. Fan TP, Yeh JC, Leung KW, Yue PY, Wong RN. Angiogenesis: from plants to blood vessels. *Trends Pharmacol Sci*. (2006) 27:297–309. doi: 10.1016/j.tips.2006.04.006
49. Guo Y, Wang S, Hoot DR, Clinton SK. Suppression of VEGF-mediated autocrine and paracrine interactions between prostate cancer cells and vascular endothelial cells by soy isoflavones. *J Nutr Biochem*. (2007) 18:408–17. doi: 10.1016/j.jnutbio.2006.08.006
50. Niu G, Briggs J, Deng J, Ma Y, Lee H, Kortylewski M, et al. Signal transducer and activator of transcription 3 is required for hypoxia-inducible factor-1 α RNA expression in both tumor cells and tumor-associated myeloid cells. *Mol Cancer Res*. (2008) 6:1099–105. doi: 10.1158/1541-7786.MCR-07-2177
51. Xu Q, Briggs J, Park S, Niu G, Kortylewski M, Zhang S, et al. Targeting Stat3 blocks both HIF-1 and VEGF expression induced by multiple oncogenic growth signaling pathways. *Oncogene*. (2005) 24:5552–60. doi: 10.1038/sj.onc.1208719

Conflict of Interest: The authors declare that the research was conducted in the absence of any commercial or financial relationships that could be construed as a potential conflict of interest.

Copyright © 2020 Saha, Nandi, Dasgupta, Bhuniya, Ganguly, Ghosh, Guha, Banerjee, Baral and Bose. This is an open-access article distributed under the terms of the Creative Commons Attribution License (CC BY). The use, distribution or reproduction in other forums is permitted, provided the original author(s) and the copyright owner(s) are credited and that the original publication in this journal is cited, in accordance with accepted academic practice. No use, distribution or reproduction is permitted which does not comply with these terms.



The Autonomic Regulation of Tumor Growth and the Missing Links

Maricris Bautista^{1,2} and Anand Krishnan^{1,2*}

¹ Department of Anatomy, Physiology, and Pharmacology, College of Medicine, University of Saskatchewan, Saskatoon, SK, Canada, ² Cameco MS Neuroscience Research Centre (CMSNRC), University of Saskatchewan, Saskatoon, SK, Canada

Accumulating evidence now indicates that peripheral nerves and solid tumors mutually support the growth of each other. Tumor-derived molecular cues guide nerve infiltration to the tumor milieu, while the tumor-infiltrating nerves provide molecular support to promote tumor growth and dissemination. In this mini-review, we discuss the unique roles of sympathetic and parasympathetic nerves in promoting tumor growth and metastasis. The contribution of adrenergic and cholinergic signals, the specific receptors involved, and the downstream molecular links in both cancer cells and stromal cells are discussed for their intrinsic capacity to modulate tumor growth. We identified unappreciated niche areas in the field, an investigation of which are critical to filling the knowledge gap in understanding the biology of neuromodulation of cancers.

Keywords: nerve-tumor interface, nerve-tumor crosstalk, nerve-dependence of cancers, metastasis, norepinephrine, acetylcholine, neurotrophic factors

OPEN ACCESS

Edited by:

Marco Rossi,
University of Catanzaro, Italy

Reviewed by:

Luca Filippi,
University of Florence, Italy
Massimo Dal Monte,
University of Pisa, Italy

*Correspondence:

Anand Krishnan
anand.krishnan@usask.ca

Specialty section:

This article was submitted to
Cancer Molecular Targets and
Therapeutics,
a section of the journal
Frontiers in Oncology

Received: 15 March 2020

Accepted: 20 April 2020

Published: 13 May 2020

Citation:

Bautista M and Krishnan A (2020) The
Autonomic Regulation of Tumor
Growth and the Missing Links.
Front. Oncol. 10:744.
doi: 10.3389/fonc.2020.00744

INTRODUCTION

The tumor microenvironment significantly influences the progression of solid tumors (1). Therefore, there has been a long-standing interest in understanding the functions of stromal cells in the tumor milieu. An immense interest has been recently developed in understanding the functions of peripheral nerves in the tumor microenvironment. For many decades, nerves were only recognized as pain carriers of tumors. However, recent studies demonstrated that peripheral nerves modulate tumor growth and dissemination. The widely recognized belief now is that the tumors attract nerves by stimulating nerve growth, and in turn, the nerves feed both cancer and stromal cells in the tumor milieu (2, 3).

The nerve-derived molecules supporting tumor growth have been reviewed in much detail (2, 3). In this regard, the neurotransmitters released from autonomic nerves have gained much attention, and clinical trials are now underway by blocking the corresponding receptors to managing a variety of solid tumors. Here, we review the nerve-tumor interface with particular attention to the unique contribution of autonomic signaling to tumor growth and dissemination. We also discuss the missing links in the current state of knowledge in understanding the biology of neuromodulation of cancers.

THE NERVE-TUMOR CROSSTALK: THE MILESTONES

The nerve-dependence of tumors received initial attention due to the occurrence of perineural invasion (PNI), in which cancer cells migrate around and invade nerves (4–6). Although PNI was recognized much earlier as a complex physical interaction between cancer cells and nerves, a mutual growth stimulatory interaction between the cancer cells and neurons was experimentally demonstrated within the past two decades. In an elegant study, Ayala et al. showed that the

outgrowth and directionality of sensory neurons and the proliferation and migration of prostate cancer cells were mutually benefitted when they were cultured together (7). This observation kickstarted serious investigations to understanding the nerve-tumor interface.

In the early 2000, clinicians also found an association between underlying stress and poor prognosis of cancer patients (8). Supporting this association, a study by Thaker et al. showed that stress-activated adrenergic signals promote tumor growth, signifying the critical involvement of sympathetic nerves in tumor progression (9). Another breakthrough occurred in 2013 when Magnon et al. demonstrated that adrenergic signals in stromal cells are indeed essential for tumorigenesis (10). The tumor promoting roles of cholinergic signals were also established around this time when it was discovered that cholinergic muscarinic receptors facilitate tumorigenesis and metastasis (10, 11). These discoveries then fuelled a broader interest in understanding the roles of autonomic signals in tumor microenvironment.

SYMPATHETIC DISTRIBUTION IN THE TUMOR MICROENVIRONMENT

Sympathetic nerve innervation in tumors has been demonstrated in prostate, ovarian, and breast tumors by specifically staining the adrenergic neurons with tyrosine hydroxylase (10, 12–14). In addition, animal tumor models of the prostate, melanoma and ovarian cancers showed increased levels of the sympathetic neurotransmitter norepinephrine (NE), indicating that sympathetic activity is enhanced in solid tumors (12, 13, 15). NE has also been implicated in stress-mediated melanoma and ovarian tumor progression (13, 16). The specific receptors for NE, the adrenergic β receptors (Adrb), are widely distributed in both cancer and stromal cells. For example, the Adrb are expressed in the prostate, melanoma, ovarian, pancreatic, colon and breast cancer cells, and pericytes, endothelial cells, lymphocytes, and myeloid cells (10, 12–14, 17–22). Among the Adrb, varying expressions and levels of Adrb1/ β 2/ β 3 are reported in several cancer types (23).

ADRENERGIC SIGNALS AS TUMOR PROMOTERS: MOLECULAR MECHANISMS

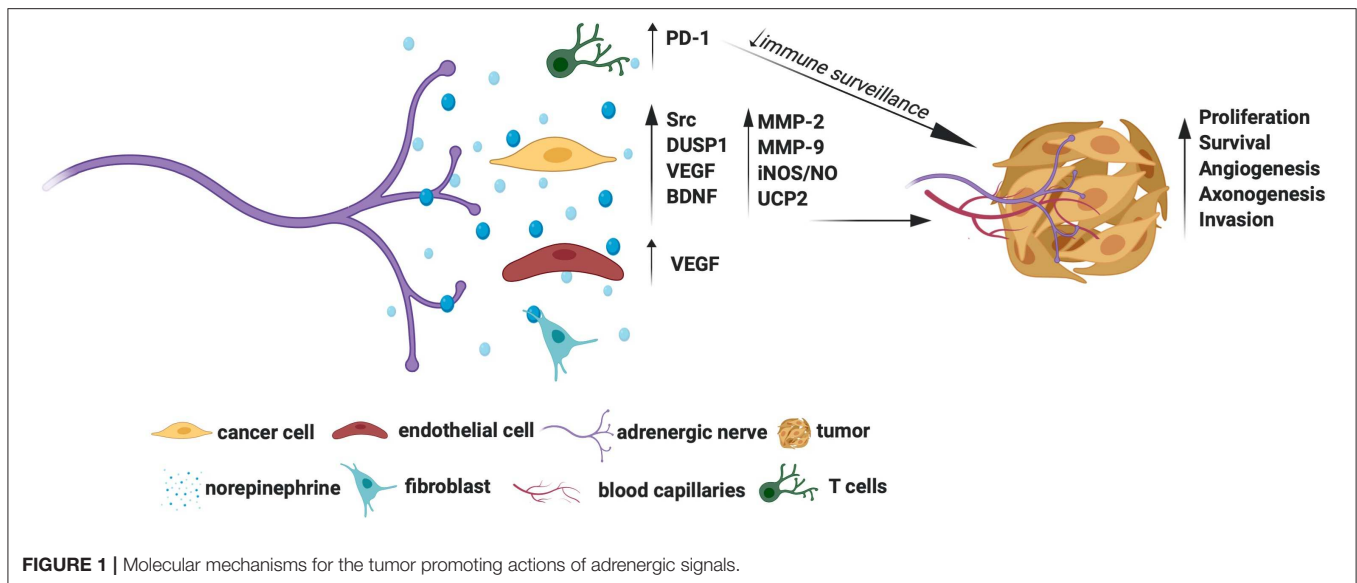
Several growth signaling cascades are activated downstream of Adrb. For example, Adrb2 activation was shown to trigger Src kinase to promote ovarian cancer cell proliferation, migration, and invasion (19). A positive association between NE and Src activation was also demonstrated in human ovarian tumors substantiating the tumor promoting roles of the NE-Src axis (19). Adrb2 also enables cancer cells to escape chemotherapy-induced cytotoxicity. For instance, Adrb2 signals have shown to activate the survival phosphatase, DUSP1, which in turn dephosphorylates JNK and c-jun to promote ovarian cancer cell survival pre-treated with cisplatin or paclitaxel (24). Thaker et al. showed that activation of Adrb2 by NE induces VEGF in ovarian

cancer cells (9). The VEGF, in turn, signals endothelial cells to facilitate angiogenesis, which is an example of how NE promotes tumor angiogenesis indirectly (9). Interestingly, NE dependent activation of Adrb3 in ovarian cancer cells induces BDNF through cAMP/JNK activation (13). The BDNF then signals TrkB receptors in the nearby nerves to promote axonogenesis, which is an example of how NE promotes tumor axonogenesis indirectly. A positive association between NE and BDNF was also observed in human ovarian carcinoma, further indicating that the NE-BDNF axis promotes tumors (13).

The tumor-promoting roles of Adrb3, and the mechanisms involved, have been extensively studied in melanoma. In line with this, Dal Monte et al. showed that blockade of Adrb3 induces apoptosis of melanoma cells through downregulation iNOS (inducible nitric oxide synthase) mediated NO synthesis (25, 26). Calvani et al. showed that various cellular stresses, such as hypoxia, ischemia, or glucose deprivation induce Adrb3 in melanoma cells, suggesting that these natural triggers may drive higher production of Adrb3 in the tumor milieu (21). Strikingly, Adrb3 promotes the classical Warburg effect (preferred glycolysis) in melanoma stem cells by upregulating UCP2 (uncoupling protein 2) (27). Adrb3 was also shown to regulate the stemness of neuroblastoma cells wherein Adrb3 inhibition promoted their differentiation by disrupting the sphingosine kinase 2(sk2)-sphingosine-1-phosphatase receptor 2 (S1P2) axis, which is a lipid metabolic axis otherwise crucial for these cells' stemness and proliferation (28).

The Adrb have stromal cell-specific actions too. Selective depletion of Adrb2 and/or Adrb3 in the stromal compartment prevented the occurrence and early growth of prostate cancer, indicating that stromal cell-specific Adrb is essential for maturation of oncogenic signals (10). Adrb2 also facilitates aerobic glycolysis in endothelial cells and promote tumor angiogenesis (12). Both CD4⁺ and CD8⁺ T lymphocytes express Adrb2, while sympathetic deprivation of these cells downregulates the immune checkpoint protein PD-1 and favor better immune surveillance of breast cancer (14). The Adrb3 is also expressed in stromal cells, especially fibroblasts, endothelial cells, and immune cells and support tumors and angiogenesis (21, 29). Specific blockade of Adrb3 was shown to impair endothelial cell survival in melanoma (25). Besides, blockade of Adrb3 was shown to accentuate the levels of cytotoxic T lymphocytes and natural killer (NK) cells and attenuate the levels of tumor favoring regulatory T cells (Tregs) and myeloid-derived suppressor cells (MDSCs) in melanoma, promoting a favorable immune surveillance (29). Interestingly, Adrb3 inhibition in myeloid cells switches macrophage and neutrophil phenotypes to immunocompetent M1 and N1 types, respectively, indicating additional mechanisms of Adrb3 blockers in checking tumors (29). Adrb3 signals also enrich stromal population by recruiting and maintaining hemopoietic (HSC) and mesenchymal stem cells (MSC) favoring tumor aggression, while Adrb3 blockade was shown to promote local differentiation of HSC to lymphoid/myeloid lineages and MSC to adipocyte lineages in melanoma favoring a less aggressive tumor milieu (30).

The adrenergic signals also promote migration and invasion of cancer cells. Activation of Adrb in ovarian and pancreatic



cancer cells upregulates MMP-2, MMP-9 and VEGF to facilitate cell migration and invasion (18, 31). A phase II trial showed that a combination of propranolol (a non-specific $\text{Adr}\beta$ blocker) and etodolac (a non-steroidal anti-inflammatory drug) reduces the levels of epithelial-mesenchymal transition (EMT) genes involved with breast cancer metastasis, suggesting a potential clinical benefit of using β -blockers in fighting metastasis (32). This trial also showed immune profile changes in the treatment cohort (32). However, due to the combined treatment protocol used in this trial, the exact contribution of β -blockers in generating this gene profile is not known. Nonetheless, retrospective analyses showed that β -blockers slow down the progression of multiple myeloma, prostate, melanoma, lung, and ovarian cancers, indicating an apparent additional benefit of targeting adrenergic signals for prolonging disease-free survival (33–37).

Overall, $\text{Adr}\beta$ receptors, especially the $\text{Adr}\beta_2$ and $\text{Adr}\beta_3$, show promise as cancer therapeutic targets. The molecular mechanisms by which adrenergic signals promote tumor growth are summarized in **Figure 1**. However, it remains to be established whether targeting $\text{Adr}\beta$ is beneficial in treating all cancer types. For example, inhibition of $\text{Adr}\beta_2$ showed no effect in gastric tumors (38). Moreover, although NE levels were shown to increase in animal tumors, such an increase in its levels was established only in human ovarian carcinoma (13). Quantification of NE in other tumor types also is warranted to identify its general activation profile in human cancers. Similarly, although $\text{Adr}\beta_3$ was shown to maintain stem cell traits in tumor milieu, more understanding is required to elucidate the responsible mechanisms.

PARASYMPATHETIC DISTRIBUTION IN THE TUMOR MICROENVIRONMENT

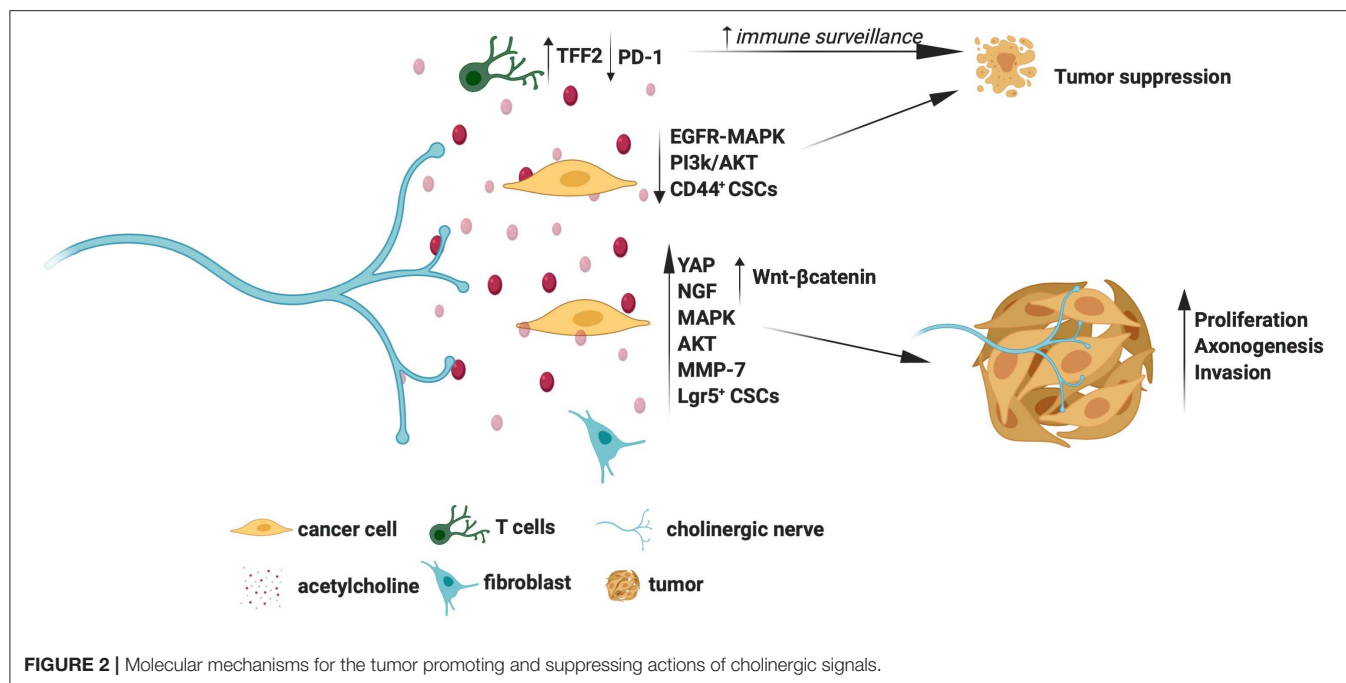
In contrast to sympathetic signals, the parasympathetic signals offer both tumor suppressing and promoting functions. The

parasympathetic innervation has been demonstrated in gastric, prostate and breast cancers using choline acetyltransferase (ChAT) or vesicular acetylcholine transporter (VAChT) as specific markers (10, 14, 38). The specific receptors of the parasympathetic neurotransmitter acetylcholine, the cholinergic muscarinic receptors (Chrms), are shown to express in gastric, pancreatic, lung, cervical, and colon cancer cells (38–42). Interestingly, lung, pancreatic, cervical and colon cancer cells, and gastric epithelial tuft cells express acetylcholine, independent of nerves (38, 40, 43).

CHOLINERGIC SIGNALS AS TUMOR SUPPRESSORS: MOLECULAR MECHANISMS

Early studies in the '80s showed that cholinergic deprivation resulting from vagotomy facilitates gastric tumorigenesis, suggesting that cholinergic signals are essential for tumor suppression (44, 45). Similarly, a recent study by Renz et al. showed that vagotomy promotes pancreatic tumor progression whereas selective activation of Chrm1 reduced tumor incidence (42). Using RNA sequencing studies, the authors showed that Chrm1 signals perturb EGFR/MAPK and PI3K/AKT cascade in cancer cells to inhibit tumor growth (42). Chrm1 activation was also shown to suppress cancer stem cells (CSCs), which is an additional mechanism by which cholinergic signals suppress tumors (42).

The cholinergic signals also modulate the neuro-immune axis. In line with this, Dubeykovskaya et al. showed that cholinergic activation induces trefoil factor 2 (TFF2) secretion by memory T cells, which in turn suppresses MDSC to prevent colorectal cancer progression (46). Similarly, Kamia et al. showed that parasympathetic stimulation of T lymphocytes, which express Chrm1, reduces the immune checkpoint protein PD-1, leading to suppression of breast cancer (14). The cholinergic-immune axis is also essential for suppressing pancreatic cancer. For instance,



cholinergic deprivation was shown to increase macrophage influx and production of $\text{TNF}\alpha$, resulting in pancreatic tumor progression (47).

CHOLINERGIC SIGNALS AS TUMOR PROMOTERS: MOLECULAR MECHANISMS

Through selective depletion studies, Zhao et al. demonstrated that a lack of cholinergic transmission prevents gastric tumorigenesis, while Magnon et al. showed that the lack of these signals in stromal cells prevents prostate cancer metastasis (10, 11). There are multiple mechanisms that account for the tumor promoting actions of cholinergic signals. For instance, in gastric cancer cells, activated *Chrm3* induces Wnt- β -catenin signals downstream of the transcriptional co-activator YAP (38). The Wnt- β -catenin signals then expand cancer stem cells (CSCs) to promote gastric tumor growth (11). *Chrm3* was also shown to induce NGF in gastric cancer cells, and the NGF then acts on TrkA receptors in the nearby nerves to facilitate tumor innervation, which is an example of how cholinergic signals promote tumor axonogenesis indirectly (38). Expression of NGF and YAP was also associated with advanced stages of gastric tumors, which further substantiates the critical roles of *Chrm3*-NGF and *Chrm3*-YAP axes in tumor pathology (38). A retrospective study showed that vagotomy, and associated cholinergic deprivation, reduces gastric cancer incidence, suggesting a potential utility of cholinergic blockers in preventing gastric cancers (11). *Chrm3* was also shown to promote Small Cell Lung Carcinoma (SCLC) by activating MAPK and Akt signals (40). *Chrm3* promotes the invasion of cancer cells too. For instance, *Chrm3* was shown to activate ERBB receptors downstream of MMP-7 in colon cancer cells,

which, in turn, triggered MAPK and Akt signaling to induce cell invasion (41). Besides, inhibition of *Chrm3* was shown to attenuate small intestinal neoplasia, further confirming the therapeutic utility of *Chrm3* blockers in intestinal cancers (48).

In contrast to the findings by Renz et al., which showed that *Chrm1* suppresses pancreatic cancer, a study by Magnon et al. showed that stromal cells-specific *Chrm1* is indeed essential for prostate cancer metastasis, indicating that *Chrm1* is a potential therapeutic target for prostate cancer (10, 42). A study by Coarfa et al. also supported the idea that cholinergic blockers are effective in prostate cancer by demonstrating that Botox mediated depletion of cholinergic signals improves prostate cancer outcomes (49).

The molecular mechanisms by which cholinergic signals promote or suppress tumors are summarized in **Figure 2**. Overall, the Chrms, especially the *Chrm1* and *Chrm3*, appear as promising targets for cancer therapy. However, it is still puzzling how the cholinergic signals elicit contrasting effects in tumors, for example, they promote and suppress gastric and pancreatic cancers, respectively (11, 38, 42). The wide expression of Chrms in cancer and stromal cells and the nerve-independent sources of acetylcholine pose hurdles in selectively studying the contribution of cholinergic nerves in tumors. Understanding of the distribution pattern of Chrms sub-types, and the various sources of acetylcholine in specific tumor types would further delineate the unique contribution of cholinergic signals in distinct tumors.

DISCUSSION AND FUTURE PERSPECTIVES

Accumulating evidence beyond doubt indicates that nerves offer trophic support to adult tissues. For instance, nerves maintain the

adult stem cell niche, participate in wound healing, and facilitate regeneration of adult tissues (50–54). While nerves execute these functions in a controlled manner—they know when to outset and dismiss trophic secretions—it seems it is not the case when they encounter tumors, although more studies are required to make definite conclusions. No studies, however, claim that nerve-derived signals on its own are tumorigenic, but instead amplify an underlying tumor pathology (10, 11, 38, 42).

Landmark studies that addressed nerve-dependence of tumors used experimental denervation to show that lack of nerves prevents tumorigenesis (10, 11). However, the pathophysiological consequences that follow nerve damage has not been taken into account in these studies. For instance, peripheral nerve injury leads to Wallerian degeneration of nerves, recruitment of myeloid cells, and initiation of Schwann cell (SC) proliferation (55). These functional consequences may hinder experimental tumorigenesis. For instance, vagotomy was shown to induce chemokine signaling and leukocytes recruitment, similar to that occur during Wallerian degeneration, in gastric tumors (11). Denervation also induces extensive genotypic changes in healthy tissues (49). Therefore, denervation studies may be interpreted with caution when defining the mechanisms of nerve dependence of cancers.

Adult tissue function and homeostasis are maintained by coordinated actions of autonomic, sensory, and motor neurons. Therefore, a more holistic approach of considering the roles of both sensory and autonomic nerves will give additional insights into the overall effects of peripheral nerves on tumor dynamics. Sensory neurons are likely the first responders to changes in the local environment, and therefore, it is critical to understand

how these neurons respond to malignant proliferation. We found that sensory neurons promote proliferation of mature macrophages and glial cells (56). Sensory nerves are also rich source of growth factors, such as NGF, BDNF, and GDNF, and interestingly, several studies demonstrated tumor-specific expression of these growth factors and their receptors (13, 38, 57). Sensory neurons also express tumor suppressor proteins and DNA repair proteins, indicating that they are equipped with tumor suppressor machinery too (58–60). Although both tumor promoting and suppressing roles are attributed to sensory neurons, more studies are required in this direction to make definite conclusions (61–63). Finally, while most studies demonstrated nerve innervation in human tumor samples, a future examination of differential distribution of sympathetic, parasympathetic, and sensory neurons may provide additional insights into whether adrenergic, cholinergic, or sensory nerve on its own is tumor permissive or suppressive.

AUTHOR CONTRIBUTIONS

MB participated in developing the concept, collected the literature, and composed the preliminary draft. AK formulated the concept, revised the draft extensively, composed the figures, and finalized the manuscript.

ACKNOWLEDGMENTS

College of Medicine, and Office of the Vice-Provost, Faculty Relations, University of Saskatchewan for the Research start-up fund to AK.

REFERENCES

- Bussard KM, Mutkus L, Stumpf K, Gomez-Manzano C, Marini FC. Tumor-associated stromal cells as key contributors to the tumor microenvironment. *Breast Cancer Res.* (2016) 18:84. doi: 10.1186/s13058-016-0740-2
- Jobling P, Pundavela J, Oliveira SM, Roselli S, Walker MM, Hondermarck H. Nerve-cancer cell cross-talk: a novel promoter of tumor progression. *Cancer Res.* (2015) 75:1777–81. doi: 10.1158/0008-5472.Can-14-3180
- Boilly B, Faulkner S, Jobling P, Hondermarck H. Nerve dependence: from regeneration to cancer. *Cancer Cell.* (2017) 31:342–54. doi: 10.1016/j.ccell.2017.02.005
- Villers A, McNeal JE, Redwine EA, Freiha FS, Stamey TA. The role of perineural space invasion in the local spread of prostatic adenocarcinoma. *J Urol.* (1989) 142:763–8. doi: 10.1016/s0022-5347(17)38881-x
- Li R, Wheeler T, Dai H, Ayala G. Neural cell adhesion molecule is upregulated in nerves with prostate cancer invasion. *Hum Pathol.* (2003) 34:457–61. doi: 10.1016/s0046-8177(03)00084-4
- Shimada K, Nara S, Esaki M, Sakamoto Y, Kosuge T, Hiraoka N. Intrapancratic nerve invasion as a predictor for recurrence after pancreaticoduodenectomy in patients with invasive ductal carcinoma of the pancreas. *Pancreas.* (2011) 40:464–8. doi: 10.1097/MPA.0b013e31820b5d37
- Ayala GE, Wheeler TM, Shine HD, Schmelz M, Frolov A, Chakraborty S, et al. *In vitro* dorsal root ganglia and human prostate cell line interaction: redefining perineural invasion in prostate cancer. *Prostate.* (2001) 49:213–23. doi: 10.1002/pros.1137
- Ben-Eliyahu S. The promotion of tumor metastasis by surgery and stress: immunological basis and implications for psychoneuroimmunology. *Brain Behav Immun.* (2003) 17 Suppl 1:S27–36. doi: 10.1016/s0889-1591(02)00063-6
- Thaker PH, Han LY, Kamat AA, Arevalo JM, Takahashi R, Lu C, et al. Chronic stress promotes tumor growth and angiogenesis in a mouse model of ovarian carcinoma. *Nat Med.* (2006) 12:939–44. doi: 10.1038/nm1447
- Magnon C, Hall SJ, Lin J, Xue X, Gerber L, Freedland SJ, et al. Autonomic nerve development contributes to prostate cancer progression. *Science.* (2013) 341:1236361. doi: 10.1126/science.1236361
- Zhao CM, Hayakawa Y, Kodama Y, Muthupalani S, Westphalen CB, Andersen GT, et al. Denervation suppresses gastric tumorigenesis. *Sci Transl Med.* (2014) 6:250ra115. doi: 10.1126/scitranslmed.3009569
- Zahalka AH, Arnal-Estape A, Maryanovich M, Nakahara F, Cruz CD, Finley LWS, et al. Adrenergic nerves activate an angio-metabolic switch in prostate cancer. *Science.* (2017) 358:321–6. doi: 10.1126/science.aah5072
- Allen JK, Armaiz-Pena GN, Nagaraja AS, Sadaoui NC, Ortiz T, Dood R, et al. Sustained Adrenergic signaling promotes intratumoral innervation through BDNF induction. *Cancer Res.* (2018) 78:3233–42. doi: 10.1158/0008-5472.Can-16-1701
- Kamiya A, Hayama Y, Kato S, Shimomura A, Shimomura T, Irie K, et al. Genetic manipulation of autonomic nerve fiber innervation and activity and its effect on breast cancer progression. *Nat Neurosci.* (2019) 22:1289–305. doi: 10.1038/s41593-019-0430-3
- Sereni F, Dal Monte M, Filippi L, Bagnoli P. Role of host beta1- and beta2-adrenergic receptors in a murine model of B16 melanoma: functional involvement of beta3-adrenergic receptors. *Naunyn Schmiedeberg Arch Pharmacol.* (2015) 388:1317–31. doi: 10.1007/s00210-015-1165-7
- Sanzo M, Colucci R, Arunachalam M, Berti S, Moretti S. Stress as a possible mechanism in melanoma progression. *Dermatol Res Pract.* (2010) 2010:483493. doi: 10.1155/2010/483493
- Perrone MG, Notarnicola M, Caruso MG, Tutino V, Scilimati A. Upregulation of beta3-adrenergic receptor mRNA in human colon

- cancer: a preliminary study. *Oncology*. (2008) 75:224–9. doi: 10.1159/000163851
18. Guo K, Ma Q, Wang L, Hu H, Li J, Zhang D, et al. Norepinephrine-induced invasion by pancreatic cancer cells is inhibited by propranolol. *Oncol Rep*. (2009) 22:825–30. doi: 10.3892/or.00000505
 19. Armaiz-Pena GN, Allen JK, Cruz A, Stone RL, Nick AM, Lin YG, et al. Src activation by beta-adrenoreceptors is a key switch for tumour metastasis. *Nat Commun*. (2013) 4:1403. doi: 10.1038/ncomms2413
 20. Moretti S, Massi D, Farini V, Baroni G, Parri M, Innocenti S, et al. beta-adrenoceptors are upregulated in human melanoma and their activation releases pro-tumorigenic cytokines and metalloproteases in melanoma cell lines. *Lab Invest*. (2013) 93:279–90. doi: 10.1038/labinvest.2012.175
 21. Calvani M, Pelon F, Comito G, Taddei ML, Moretti S, Innocenti S, et al. Norepinephrine promotes tumor microenvironment reactivity through beta3-adrenoreceptors during melanoma progression. *Oncotarget*. (2015) 6:4615–32. doi: 10.18632/oncotarget.2652
 22. Choy C, Raytis JL, Smith DD, Duenas M, Neman J, Jandial R, et al. Inhibition of beta2-adrenergic receptor reduces triple-negative breast cancer brain metastases: the potential benefit of perioperative beta-blockade. *Oncol Rep*. (2016) 35:3135–42. doi: 10.3892/or.2016.4710
 23. Rains SL, Amaya CN, Bryan BA. Beta-adrenergic receptors are expressed across diverse cancers. *Oncoscience*. (2017) 4:95–105. doi: 10.18632/oncoscience.357
 24. Kang Y, Nagaraja AS, Armaiz-Pena GN, Dorniak PL, Hu W, Rupaimoole R, et al. Adrenergic stimulation of DUSP1 impairs chemotherapy response in ovarian cancer. *Clin Cancer Res*. (2016) 22:1713–24. doi: 10.1158/1078-0432.Ccr-15-1275
 25. Dal Monte M, Casini G, Filippi L, Nicchia GP, Svelto M, Bagnoli P. Functional involvement of beta3-adrenergic receptors in melanoma growth and vascularization. *J Mol Med*. (2013) 91:1407–19. doi: 10.1007/s00109-013-1073-6
 26. Dal Monte M, Fornaciari I, Nicchia GP, Svelto M, Casini G, Bagnoli P. beta3-adrenergic receptor activity modulates melanoma cell proliferation and survival through nitric oxide signaling. *Naunyn-Schmiedeberg's Arch Pharmacol*. (2014) 387:533–43. doi: 10.1007/s00210-014-0969-1
 27. Calvani M, Cavallini L, Tondo A, Spinelli V, Ricci L, Pasha A, et al. beta3-adrenoreceptors control mitochondrial dormancy in melanoma and embryonic stem cells. *Oxid Med Cell Longev*. (2018) 2018:6816508. doi: 10.1155/2018/6816508
 28. Bruno G, Cencetti F, Pini A, Tondo A, Cuzzubbo D, Fontani F, et al. beta3-adrenoreceptor blockade reduces tumor growth and increases neuronal differentiation in neuroblastoma via SK2/S1P2 modulation. *Oncogene*. (2020) 39:368–84. doi: 10.1038/s41388-019-0993-1
 29. Calvani M, Bruno G, Dal Monte M, Nassini R, Fontani F, Casini A, et al. beta3-Adrenoceptor as a potential immuno-suppressor agent in melanoma. *Br J Pharmacol*. (2019) 176:2509–24. doi: 10.1111/bph.14660
 30. Calvani M, Bruno G, Dabroia A, Subbiani A, Bianchini F, Fontani F, et al. beta3-Adrenoreceptor blockade induces stem cells differentiation in melanoma microenvironment. *Int J Mol Sci*. (2020) 21:21041420. doi: 10.3390/ijms21041420
 31. Sood AK, Bhatti R, Kamat AA, Landen CN, Han L, Thaker PH, et al. Stress hormone-mediated invasion of ovarian cancer cells. *Clin Cancer Res*. (2006) 12:369–75. doi: 10.1158/1078-0432.Ccr-05-1698
 32. Shaashua L, Shabat-Simon M, Halder R, Matzner P, Zmora O, Shabtai M, et al. Perioperative COX-2 and beta-adrenergic blockade improves metastatic biomarkers in breast cancer patients in a phase-II randomized trial. *Clin Cancer Res*. (2017) 23:4651–61. doi: 10.1158/1078-0432.Ccr-17-0152
 33. De Giorgi V, Grazzini M, Gandini S, Benemei S, Lotti T, Marchionni N, et al. Treatment with beta-blockers and reduced disease progression in patients with thick melanoma. *Arch Intern Med*. (2011) 171:779–81. doi: 10.1001/archinternmed.2011.131
 34. Diaz ES, Karlan BY, Li AJ. Impact of beta blockers on epithelial ovarian cancer survival. *Gynecol Oncol*. (2012) 127:375–8. doi: 10.1016/j.ygyno.2012.07.102
 35. Grytli HH, Fagerland MW, Fossa SD, Tasken KA, Haheim LL. Use of beta-blockers is associated with prostate cancer-specific survival in prostate cancer patients on androgen deprivation therapy. *Prostate*. (2013) 73:250–60. doi: 10.1002/pros.22564
 36. Wang HM, Liao ZX, Komaki R, Welsh JW, O'Reilly MS, Chang JY, et al. Improved survival outcomes with the incidental use of beta-blockers among patients with non-small-cell lung cancer treated with definitive radiation therapy. *Ann Oncol*. (2013) 24:1312–9. doi: 10.1093/annonc/mts616
 37. Hwa YL, Shi Q, Kumar SK, Lacy MQ, Gertz MA, Kapoor P, et al. Beta-blockers improve survival outcomes in patients with multiple myeloma: a retrospective evaluation. *Am J Hematol*. (2017) 92:50–5. doi: 10.1002/ajh.24582
 38. Hayakawa Y, Sakitani K, Konishi M, Asfaha S, Niikura R, Tomita H, et al. Nerve growth factor promotes gastric tumorigenesis through aberrant cholinergic signaling. *Cancer Cell*. (2017) 31:21–34. doi: 10.1016/j.ccell.2016.11.005
 39. Kodaira M, Kajimura M, Takeuchi K, Lin S, Hanai H, Kaneko E. Functional muscarinic m3 receptor expressed in gastric cancer cells stimulates tyrosine phosphorylation and MAP kinase. *J Gastroenterol*. (1999) 34:163–71. doi: 10.1007/s005350050238
 40. Song P, Sekhon HS, Lu A, Arredondo J, Sauer D, Gravett C, et al. M3 muscarinic receptor antagonists inhibit small cell lung carcinoma growth and mitogen-activated protein kinase phosphorylation induced by acetylcholine secretion. *Cancer Res*. (2007) 67:3936–44. doi: 10.1158/0008-5472.Can-06-2484
 41. Belo A, Cheng K, Chahdi A, Shant J, Xie G, Khurana S, et al. Muscarinic receptor agonists stimulate human colon cancer cell migration and invasion. *Am J Physiol Gastrointest Liver Physiol*. (2011) 300:G749–760. doi: 10.1152/ajpgi.00306.2010
 42. Renz BW, Tanaka T, Sunagawa M, Takahashi R, Jiang Z, Macchini M, et al. Cholinergic signaling via muscarinic receptors directly and indirectly suppresses pancreatic tumorigenesis and cancer stemness. *Cancer Discov*. (2018) 8:1458–73. doi: 10.1158/2159-8290.Cd-18-0046
 43. Cheng K, Samimi R, Xie G, Shant J, Drachenberg C, Wade M, et al. Acetylcholine release by human colon cancer cells mediates autocrine stimulation of cell proliferation. *Am J Physiol Gastrointest Liver Physiol*. (2008) 295:G591–597. doi: 10.1152/ajpgi.00055.2008
 44. Tatsuta M, Yamamura H, Iishi H, Ichii M, Noguchi S, Baba M, et al. Promotion by vagotomy of gastric carcinogenesis induced by N-methyl-N'-nitro-N-nitrosoguanidine in Wistar rats. *Cancer Res*. (1985) 45:194–7.
 45. Tatsuta M, Iishi H, Yamamura H, Baba M, Taniguchi H. Effects of bilateral and unilateral vagotomy on gastric carcinogenesis induced by N-methyl-N'-nitro-N-nitrosoguanidine in Wistar rats. *Int J Cancer*. (1988) 42:414–8. doi: 10.1002/ijc.2910420318
 46. Dubeykovskaya Z, Si Y, Chen X, Worthley DL, Renz BW, Urbanska AM, et al. Neural innervation stimulates splenic TFF2 to arrest myeloid cell expansion and cancer. *Nat Commun*. (2016) 7:10517. doi: 10.1038/ncomms10517
 47. Partecke LI, Kading A, Trung DN, Diedrich S, Sessler M, Weiss F, et al. Subdiaphragmatic vagotomy promotes tumor growth and reduces survival via TNFalpha in a murine pancreatic cancer model. *Oncotarget*. (2017) 8:22501–12. doi: 10.18632/oncotarget.15019
 48. Raufman JP, Shant J, Xie G, Cheng K, Gao XM, Shiu B, et al. Muscarinic receptor subtype-3 gene ablation and scopolamine butylbromide treatment attenuate small intestinal neoplasia in Apcmin/+ mice. *Carcinogenesis*. (2011) 32:1396–402. doi: 10.1093/carcin/bgr118
 49. Coarfa C, Florentin D, Putluri N, Ding Y, Au J, He D, et al. Influence of the neural microenvironment on prostate cancer. *Prostate*. (2018) 78:128–39. doi: 10.1002/pros.23454
 50. Cheng C, Singh V, Krishnan A, Kan M, Martinez JA, Zochodne DW. Loss of innervation and axon plasticity accompanies impaired diabetic wound healing. *PLoS ONE*. (2013) 8:e75877. doi: 10.1371/journal.pone.0075877
 51. Knox SM, Lombaert IM, Haddox CL, Abrams SR, Cotrim A, Wilson AJ, et al. Parasympathetic stimulation improves epithelial organ regeneration. *Nat Commun*. (2013) 4:1494. doi: 10.1038/ncomms2493
 52. Rinkevich Y, Montoro DT, Muhonen E, Walmsley GG, Lo D, Hasegawa M, et al. Clonal analysis reveals nerve-dependent and independent roles on mammalian hind limb tissue maintenance and regeneration. *Proc Natl Acad Sci USA*. (2014) 111:9846–51. doi: 10.1073/pnas.1410097111
 53. Tong CK, Chen J, Cebrian-Silla A, Mirzadeh Z, Obernier K, Guinto CD, et al. Axonal control of the adult neural stem cell niche. *Cell Stem Cell*. (2014) 14:500–11. doi: 10.1016/j.stem.2014.01.014
 54. Carr MJ, Toma JS, Johnston APW, Steadman PE, Yuzwa SA, Mahmud N, et al. Mesenchymal precursor cells in adult nerves contribute to mammalian

- tissue repair and regeneration. *Cell Stem Cell*. (2019) 24:240–56.e249. doi: 10.1016/j.stem.2018.10.024
55. Krishnan A, Duraikannu A, Zochodne DW. Releasing 'brakes' to nerve regeneration: intrinsic molecular targets. *Eur J Neurosci*. (2016) 43:297–308. doi: 10.1111/ejn.13018
 56. Krishnan A, Bhavanam S, Zochodne D. An intimate role for adult dorsal root ganglia resident cycling cells in the generation of local macrophages and satellite glial cells. *J Neuropathol Exp Neurol*. (2018) 77:929–41. doi: 10.1093/jnen/nly072
 57. He S, Chen CH, Chernichenko N, He S, Bakst RL, Barajas F, et al. GFR α 1 released by nerves enhances cancer cell perineural invasion through GDNF-RET signaling. *Proc Natl Acad Sci USA*. (2014) 111:E2008–17. doi: 10.1073/pnas.1402944111
 58. Christie KJ, Krishnan A, Martinez JA, Purdy K, Singh B, Eaton S, et al. Enhancing adult nerve regeneration through the knockdown of retinoblastoma protein. *Nat Commun*. (2014) 5:3670. doi: 10.1038/ncomms4670
 59. Singh B, Singh V, Krishnan A, Koshy K, Martinez JA, Cheng C, et al. Regeneration of diabetic axons is enhanced by selective knockdown of the PTEN gene. *Brain*. (2014) 137(Pt 4):1051–67. doi: 10.1093/brain/awu031
 60. Krishnan A, Purdy K, Chandrasekhar A, Martinez J, Cheng C, Zochodne DW. A BRCA1-Dependent DNA damage response in the regenerating adult peripheral nerve milieu. *Mol Neurobiol*. (2018) 55:4051–67. doi: 10.1007/s12035-017-0574-7
 61. Erin N, Duymus O, Ozturk S, Demir N. Activation of vagus nerve by semapimod alters substance P levels and decreases breast cancer metastasis. *Regul Pept*. (2012) 179:101–8. doi: 10.1016/j.regpep.2012.08.001
 62. Peterson SC, Eberl M, Vagnozzi AN, Belkadi A, Veniaminova NA, Verhaegen ME, et al. Basal cell carcinoma preferentially arises from stem cells within hair follicle and mechanosensory niches. *Cell Stem Cell*. (2015) 16:400–12. doi: 10.1016/j.stem.2015.02.006
 63. Sinha S, Fu YY, Grimont A, Ketcham M, Lafaro K, Saglimbeni JA, et al. PanIN neuroendocrine cells promote tumorigenesis via neuronal cross-talk. *Cancer Res*. (2017) 77:1868–79. doi: 10.1158/0008-5472.Can-16-0899-t

Conflict of Interest: The authors declare that the research was conducted in the absence of any commercial or financial relationships that could be construed as a potential conflict of interest.

Copyright © 2020 Bautista and Krishnan. This is an open-access article distributed under the terms of the Creative Commons Attribution License (CC BY). The use, distribution or reproduction in other forums is permitted, provided the original author(s) and the copyright owner(s) are credited and that the original publication in this journal is cited, in accordance with accepted academic practice. No use, distribution or reproduction is permitted which does not comply with these terms.



GPI-AP: Unraveling a New Class of Malignancy Mediators and Potential Immunotherapy Targets

Nada H. Hussein[†], Nada S. Amin[†] and Hend M. El Tayebi^{*†}

Molecular Pharmacology Research Group, Department of Pharmacology and Toxicology, Faculty of Pharmacy and Biotechnology, German University in Cairo, Cairo, Egypt

OPEN ACCESS

Edited by:

Niels Weinhold,
Heidelberg University, Germany

Reviewed by:

Qiong Zhang,
Affiliated Hospital of Nantong
University, China
Luis E. Arias-Romero,
National Autonomous University of
Mexico, Mexico

*Correspondence:

Hend M. El Tayebi
hend.saber@guc.edu.eg

*ORCID:

Nada H. Hussein
orcid.org/0000-0003-4346-1520
Nada S. Amin
orcid.org/0000-0002-9541-549X
Hend M. El Tayebi
orcid.org/0000-0002-6896-6018

Specialty section:

This article was submitted to
Cancer Molecular Targets
and Therapeutics,
a section of the journal
Frontiers in Oncology

Received: 11 March 2020

Accepted: 19 October 2020

Published: 04 December 2020

Citation:

Hussein NH, Amin NS and
El Tayebi HM (2020)
GPI-AP: Unraveling a New Class
of Malignancy Mediators and
Potential Immunotherapy Targets.
Front. Oncol. 10:537311.
doi: 10.3389/fonc.2020.537311

With millions of cases diagnosed annually and high economic burden to cover expensive costs, cancer is one of the most difficult diseases to treat due to late diagnosis and severe adverse effects from conventional therapy. This creates an urgent need to find new targets for early diagnosis and therapy. Progress in research revealed the key steps of carcinogenesis. They are called cancer hallmarks. Zooming in, cancer hallmarks are characterized by ligands binding to their cognate receptor and so triggering signaling cascade within cell to make response for stimulus. Accordingly, understanding membrane topology is vital. In this review, we shall discuss one type of transmembrane proteins: Glycosylphosphatidylinositol-Anchored Proteins (GPI-APs), with specific emphasis on those involved in tumor cells by evading immune surveillance and future applications for diagnosis and immune targeted therapy.

Keywords: glycosylphosphatidylinositol, glycosylphosphatidylinositol-anchored protein, immunotherapy, cancer, immunology

INTRODUCTION

Cancer is one of the most aggressive diseases responsible for thousands of deaths annually and millions newly diagnosed (1). The major problems are family history, unhealthy lifestyle, late diagnosis, and the detrimental side effects of chemotherapy and radiotherapy (2). Consequently, thanks to rigorous research, scientists were able to develop characteristic hallmarks for transformation of normal cell into cancerous cell, with classic hallmarks published in 2000 (3). Classical hallmarks include apoptosis resistance to sustained growth, metastasis and angiogenesis (3). Lastly, increased telomerase activity empowers the tumor cell against senescence (3). Decade later, research suggested the involvement of additional hallmarks in cancer pathogenesis (4). Next-Generation Cancer hallmarks include metabolic reprogramming, escaping immune surveillance, tumor promoting inflammation and genome instability (4).

Zooming in, the detailed molecular pathway for each hallmark showed that all pathways are initiated by ligands binding to membrane-anchored proteins, thus activating a signaling pathway (4). This alters the expression of certain genes, leading to cellular response (**Figure 1**). Specifically, membrane-anchored proteins are either peripheral or integral. Peripheral proteins are superficially attached to the cell membrane. However, integral proteins have their heads exposed to extracellular matrix, and the tail is embedded in the phospholipid bilayer. Integral membrane proteins are further classified into Type-I transmembrane, Type-II transmembrane, Type-III transmembrane, Type-IV

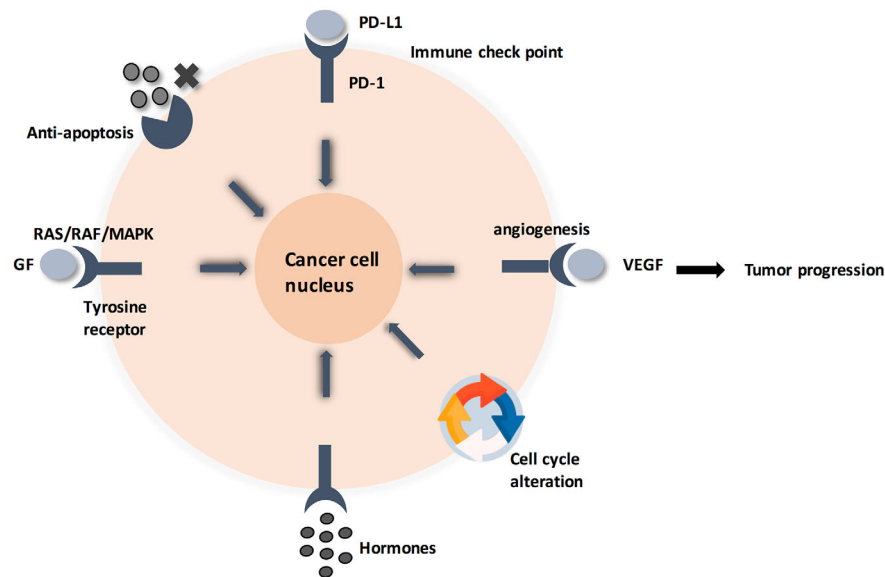


FIGURE 1 | Cancer cell circuit. When treating cancer as a minimalist/reductionalist view, tumor tissue consists of parenchyma and stroma that contain distinct cell types and subtypes that collectively enable tumor growth and progression. These cells communicate via signaling molecules, which are received by membrane anchored receptors, followed by pathway cascade to support tumor progression.

transmembrane, Type-V GPI-anchored proteins, and Type-VI transmembrane (Supplementary Figure 1) (5, 6). Consequently, predicting the type of a membrane-anchored protein is a challenging task due to the complexity of biosynthesis process. Specifically, biosynthesis process begins with joining early polypeptide chain and transmembrane area components in the ER, followed by recognizable proof and appropriate plan of TM areas, and lastly by reconciliation of TM spaces into the lipid bilayer (7, 8).

Based on the above information, studying membrane-anchored proteins is crucial in order to understand carcinogenesis and, therefore, deduce appropriate diagnosis and personalized therapy. In this review, we shall focus on Type-V GPI-anchored proteins (GPI-APs). We specifically chose this class of membrane-anchored proteins due to the expansion of investigations depicting their immune-modulatory role in cancer and current developments in immune targeted therapy. Briefly, GPI biochemical pathway consists of three phases: GPI anchor synthesis, joining protein moiety to GPI anchor, and final remodeling (9). Most of the literature emphasized on the role of GPI-APs in neurological and congenital disorders (10). However, only a few of the numerous examples of GPI-APs were studied for their role in cancer pathogenesis. For instance, CD-55 and CD-59 are crucial complement regulatory proteins elevated in various cancers, while Carcino-embryonic antigen (CEA) is a highly specific cancer biomarker, whose targeted immunotherapies are still in the early clinical trials (11). CEA mediates metastasis through binding to selectins in colon carcinomas (11). In addition, Mesothelin (MSLN) and Glypican-3 (GPC-3) are oncogenic GPI-APs over-expressed in multiple tumors, whose targeted

immunotherapies are showing promising results in clinical trials (12). Specifically, MSLN promotes cancer proliferation and apoptosis resistance through NF- κ B activation, while GPC-3 promotes cancer proliferation through sulfatase/Wnt-signaling pathway (12).

Therefore, this review highlights links between GPI-APs and GPI biochemical pathway. This represents a huge opportunity for molecular targeting whether by blocking GPI-AP as a whole or by blocking members of GPI pathway, unlike other oncogenic proteins that have only few molecular targets. This is because GPI pathway involves 26 genes and at least 150 proteins are confirmed as GPI-APs (9). Moreover, our review sheds light on the use of GPI-APs and GPI pathway members as cancer biomarkers. The outline of our review starts with GPI pathway definition, followed by an insightful discussion of examples of established GPI-APs; highlighting pros and cons of immune targeted therapies and possible future applications.

GPI-ANCHORED PROTEINS

Discovery

GPI proteins were first discovered in 1963 through studying selective cleavage of Alkaline Phosphatase by bacterial phospholipase-C (PL-C). Two decades later, hypothetical GPI-AP structure was confirmed by isolating actual GPI-APs, such as acetylcholinesterases, from different organisms (13, 14). Finally, variant surface glycoprotein (VSG) ectopic expression in African trypanosome system was used as a model to dissect the GPI biochemical pathway and GPI-linked proteins/glycoproteins characteristics (15).

Structure

Based on the substance to be anchored, GPIs are currently classified into protein-linked GPIs and non-protein-linked GPIs. Protein-linked GPIs consist of protein or glycoprotein attached to GPI anchor, while non-protein-linked GPIs consist of GPI anchor and non-protein extracellular glycol conjugates (13–15). All GPIs share a common structure, starting with a lipid tail attached to cell membrane, followed by glycan core, and finally anchored substance. Zooming in, the lipid tail consists of a lipid moiety attached to the inositol ring by a phosphodiester bridge. Depending on the organism, there are various types of lipid moieties such as ceramide (slime mold proteins), diacylglycerol (protozoa), and 1-alkyl-2-acylglycerol (most mammalian proteins) (11–13). The conserved glycan core consists of $\text{Man}\alpha(1\rightarrow2)\text{Man}\alpha(1\rightarrow6)\text{Man}\alpha(1\rightarrow4)\text{GlcNH}_2\alpha(1\rightarrow6)\text{-myo-Inositol-1-PO}_4\text{-lipid}$. Finally, the C-terminus of polypeptide chain is conjugated to the 6-O-position of the non-reducing-end mannose of GPIs through a phosphoethanol amine group (P-OEtNH₂) (14, 15) (**Supplementary Figure 2**).

Characteristics/Identification

GPI-APs feature a NH₂-terminal signal peptide and a COOH-terminal GPI signal peptide, where these peptides can be utilized for computational examination to forecast whether a certain gene produces a GPI-anchored protein or not, such as the Web-based “enormous P indicator” calculation (11, 12). Another key component is affectability of GPI-APs to phospholipases, which can be applied in different tests for recognizing GPI-APs, like the migration of proteins from the pellet to the supernatant after treating cells with PI-PLC. Moreover, PI-PLC cleavage produces cross-responding determinant inositol-1,2-cyclic monophosphate; consequently, applying immune-based assays to detect the cross-reacting determinant serves as a test to identify GPI-AP. It should be noted, however, that some GPI-APs are impervious to PI-PLC cleavage due to C-2 inositol acylation. On the other hand, all GPI-anchored proteins are labile to serum GPI-phospholipase-D (GPI-PLD). Cleavage by GPI-PLD, however, does not produce “cross-responding determinant.” Instead, it produces the inositol acyl gathering (one unsaturated fat connected to the protein) which may avoid total Triton X-114 Phase separation after GPI-PLD digestion, therefore yielding false-negative results for GPI proteins identification by Triton X Phase separation test (13–16).

GPI-APs can additionally be traced by radioactively labeled constituents, such as [3H]myo-inositol, [3H]mannose-, [3H]glucosamine-, and [3H]inositol. Lastly, a unique chemical test for GPI-APs is deamination of glucosamine moiety by nitrous acid, which results in a very specific cleavage at the glucosamine-inositol glycosidic bond. The products of this reaction are a phosphatidyl inositol part, and a free reducing end on the GPI glycan (2,5-anhydromannose), where the former can be identified by solvent partition coupled to mass spectrometry. Meanwhile, the sugar end is additionally reduced to [1-3H]2,5-anhydromannitol (AHM) by sodium borotritide. AHM is then attached to a radiolabel or fluorophore to be assayed by different identification techniques, such as sequencing, after treatment with exoglycosidases and tandem mass spectrometry (13).

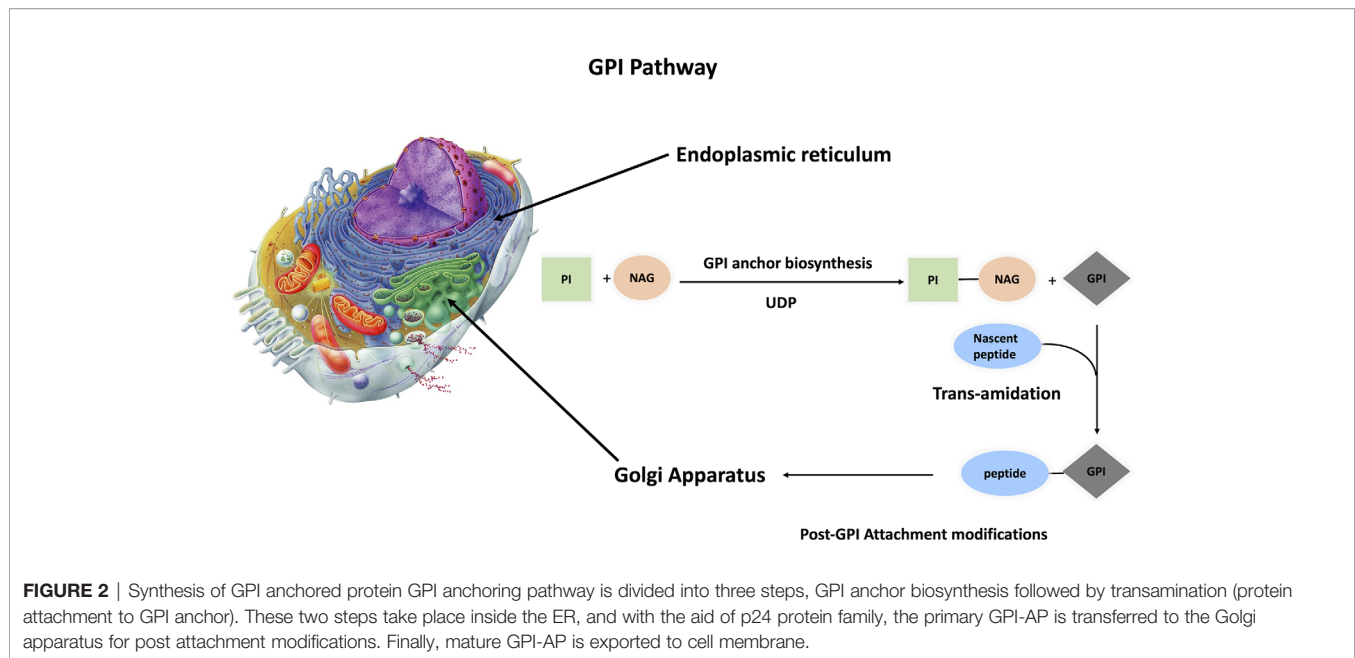
The last characteristic is endocytic targeting, by which, like all extracellular proteins, they are downregulated and degraded by endocytosis. In fact, the proof demonstrates that, in spite of lacking a cytoplasmic tail, GPI-APs can be degraded by clathrin-dependent endocytosis. This paradox has been unraveled by studying clathrin-dependent endocytosis of PrP and the GPI-anchored urokinase plasminogen activator receptor (uPAR), where internalization was achieved by association with the transmembrane LDL receptor-related protein. Other mechanisms of endocytosis for GPI-anchored proteins exist, where GPI-APs undergo endocytosis through caveolae, a gathering of lipid pontoons coated with caveolin. Yet, this claim has been nullified for different reasons. Firstly, GPI-APs are poor in caveolae. Additionally, regular endocytosis requires cutting of the endocytic vesicle from the cell membrane by a GTPase, dynamin which is repudiated by different investigations. Likewise, it is proposed that GPI-anchored proteins are broken down by a pathway called GPI-anchored protein-advanced early endosomal compartments (GEEC) pathway. Finally, a novel pathway involving the raft protein—Flotillin-1—is suggested for GPI-APs endocytosis (13–15).

GPI Anchoring Pathway

The conserved glycan core of GPI anchors suggests a generally conserved biosynthetic pathway among different species (13). This is a crucial pathway because a minimum of 150 different human proteins are anchored to the extracellular layer of cell membrane via glycosylphosphatidylinositol (GPI). GPI-AP synthesis is divided into three parts: biosynthesis, protein attachment to GPI, and GPI-AP remodeling. This complex process is performed in 15 steps, involving 26 genes that code for 15 enzymes, with twenty-two phosphatidyl inositol glycan (PIG) genes responsible for biosynthesis and polypeptide chain attachment to GPI, while four post-GPI attachment to proteins (PGAP) genes are responsible for GPI modifications (16–20) (**Supplementary Table 1** and **Figure 2**). The roles of these genes were tested by gain-and-loss-of-function experiments in different organisms, impacting the capability of protein attachment to plasma membrane regardless of expression level inside the cell.

Signaling Functions

GPI-anchored proteins are involved in multiple cellular functions as shown in **Supplementary Table 2**. First of all, analogous to bacterial phospholipase-C, phospholipases exist endogenously in order to release a protein from the membrane in response to a stimulus. The detached protein may have the same or slightly different functions compared to the membrane-anchored precursor. Interestingly, several GPI-anchored proteins are found to be secreted as well as having cross-reacting determinant, which further supports PI-PLC cleavage. Other enzymes are suggested, such as GPI-specific phospholipase-D, which is present in the blood and has proved promising activity *in vitro*. Notch is a Wnt signaling inhibitor, has also been proven to cleave the GPI anchor of many proteins such as glypican family, which regulate Wnt signaling. Finally, angiotensin-converting enzyme (ACE) is a promising option that



is still under study. In conclusion, these enzymatic reactions result in controlled release of GPI-AP (13–15, 17).

GPI pathway is additionally responsible for anchoring the molecule of interest to membrane microdomains called lipid rafts, which are rich in sphingomyelin, glycosphingolipids, and cholesterol. Lipid rafts serve as compartments for myriads of functions such as endocytosis and cell signaling. GPI proteins are enriched in lipid rafts due to favorable hydrophobic interactions between saturated GPI anchor fatty acid chains and lipid raft-resident membrane lipids forming a more tightly packed gel-like phase than the surrounding semifluid phospholipid bilayer. As a result, lipid rafts are partially resistant to nonionic detergents, which serve as a base for Triton X Phase separation test described in the Identification section (13–15).

Furthermore, GPI signal sequence is used to determine whether the protein is placed in the basolateral or apical side of the membrane, as demonstrated by multiple studies. A signal peptide for either the folate receptor or PrP was conjugated to the C-terminus of green fluorescent protein (GFP), and then the cells were imaged. Interestingly, the GFP-folate receptor fusion was localized in the apical surface, while GFP-PrP fusion was localized in the basolateral surface. Of note, it is speculated that the surrounding lipid environment plays a role in this sorting (14, 15, 18).

Finally, binding of GPI-AP to its antibody causes a rise in intracellular Ca^{2+} , tyrosine phosphorylation, proliferation, cytokine induction and oxidative burst, triggering signal transduction pathways. This was illustrated by replacing GPI anchor with a transmembrane domain, which abolished the signaling cascade. This is supported by further evidence, where enrichment of signaling molecules coupled to GPI-anchored proteins is critical for lipid rafts signaling function. However, the mechanism of how GPI anchor transduces signals is not fully

understood yet. One possible explanation is direct attachment of GPI-AP to signaling transmembrane proteins within lipid rafts. This was proved by replacing the GPI anchor motif of differentiation-promoting neural cell adhesion molecule (NCAM) with the signal sequence from carcinoembryonic antigen (CEA), producing a hybrid protein with NCAM ectodomain, but CEA-like antidifferentiation activity (10). Another explanation is that these antibody-induced signaling events depend on the induction and coalescence of lipid raft nanoclusters. Accordingly, GPI-APs function as hydrolytic enzymes, receptors, adhesion molecules, complement regulatory proteins, and other immunologically important proteins, many of which are implicated in many diseases (14, 15, 17).

GPI Mutations in Diseases

Mutations of GPI pathway genes are well documented in neurological and congenital disorders (9, 10). To start with, clinical data of 152 individual patients was reviewed and compared against the phenotypic information obtained from Human Phenotype Ontology (HPO). Statistically significant difference was observed between the GPI pathway genes and frequencies of phenotypes in the musculoskeletal system, cleft palate, nose phenotypes, and cognitive disability (21). These phenotypes are congruent with inherited GPI deficiencies (IGDs) (21). Getting deeper, non-synonymous variant (c.968A > G) in the seventh exon of GPAA1 causes inherited vascular anomalies (VAs). VAs comprise a wide spectrum of abnormalities, from blood vessels, to angiogenesis in different tumors subtypes due to variation in multiple tyrosine kinase (TK) receptor signaling pathways, such as TIE2, PIK3CA and GNAQ/11 (22). Another example, PIG-O biallelic variation, was observed in Mabry disease (23). Mabry disease symptoms include intellectual disability, distinctive facial features,

intractable seizures, and hyperphosphatasia (23). In addition, compound heterozygous variants in PIG-S:c.148C > T and c.1141_1164 resulted in infantile spasms (ISs), severe global developmental delay, hearing loss, visual impairment (cortical blindness), hypotonia, and intellectual disability (24). Furthermore, two subsets of mutations were associated with early infantile epileptic-dyskinetic encephalopathy; first is the homozygous c.384del variant of PIG-P gene (25), which led to the frame shift of 6 codons before the expected stop signal (25), and second are PIG-Q mutations, particularly PIG-Q novel variants, which included two missense mutations (p.G17R; p.G449R), a canonical splice site substitution (c.942+1G>A), an in-frame deletion (p.A377_S389del) and three frameshifts (p.Q527Afs*75, p.R538Afs*24 and p.G557Dfs*) (26). Finally, mutational analysis of PIGA identified 124 PIG-A mutations in 92% of paroxysmal nocturnal hemoglobinuria (PNH) patients, of which 101 were distinct mutations and 23 were recurrent (27).

Some studies tested the impact of GPI pathway manipulation on dependent GPI-anchored complement regulatory protein, CD-59, which was found to be under expressed in congenital and neurological disorders, as well as PNH (21–27). CD-59 was, however, overexpressed in most solid tumors (28). Weighted gene co-expression network analysis (WGCNA) was used to identify the hub gene in Kirsten-rat sarcoma viral oncogene homolog (KRAS) mutant colorectal cancer (CRC) patients (29). Surprisingly, PIG-U was under expressed in KRAS mutant CRC compared to normal controls (29). Specifically, KRAS mutant patients had a poor prognosis and PIG-U low expressing samples show elevated MAPK signaling activity (29). Contrastingly, our recent work showed that PIG-C is overexpressed in breast cancer (30). Also, PIG-C SNP was observed in HCC (31). Moreover, gain of chromosome copy number in breast cancer results in elevated expression of transamidase subunits such as GPI anchor attachment protein 1 (GPAA1) and GPI class T (PIG-T) (32). Therefore, more studies are required to depict the role of GPI pathway in cancer. In the next section, functions of GPI anchored proteins and immune therapies will be discussed in detail.

GPI-ANCHORED PROTEINS IN CANCER IMMUNOMODULATION AND TARGETED THERAPY

Complement Regulatory Proteins: CD55 and CD59

Structure and History

Complement regulatory proteins are CD-46, CD-55, and CD-59. Our scope includes the GPI-APs: CD-55 and CD-59. CD-55 is called Decay Accelerating Factor (DAF), while CD-59 is called Membrane Attack Complex Inhibitor (MAC-i). CD-55 has an extracellular domain that is composed of 4 short consensus repeat (SCR) domains (33). CD-59 is a LY-6 like protein, with molecular weight 18–20 KDa (34).

Pathway and Function

Complement system is a powerful soldier in innate immune system attack, which serves as first defense line against infections. DAF is a complement regulatory protein (CRP). CRPs are crucial in order to keep nearby normal cells safe from bystander killing and complement-mediated damage. CD55 accelerates the dissociation and decay of C3 convertases (C4bC2a and C3bBb) and in turn the C5 convertases into their building units, after which they are no longer able to rejoin. Of note, DAF does not work in a proteolytic manner (35–37). Specifically, CD55 is a ligand for CD97, where CD55 binds to CD97 at EGF domain region (37–39). The EGF domain requires calcium to maintain conformational stability, making cells highly resistant to complement activation pathway (39). Consequently, this enables cancer cells to escape immune system attack.

Similar to CD55, MAC-i is a complement regulatory protein. After CD46 and CD55, CD59 acts as last line of defense against complement activation, where it sequesters C8 and C9 components, therefore preventing C9 polymerization into the pore-forming membrane attack complex (40). Specifically, CD59 binds to the α -chain of C8 and to the β domain of C9. In an attempt to decipher CD-59 molecular pathway, Murray and Robins tested the proteins that underwent phosphorylation upon stimulation of CD59 in THP-1 and U937 hematopoietic cell lines (41). Indeed, protein tyrosine kinase family (Src) phosphorylation was observed upon CD59 activation (41). Sequentially, Src resulted in tyrosine phosphorylation of the adaptor proteins p120cbl and Shc, the cytoplasmic non receptor tyrosine kinase Syk, and its close relative Zap-70 (41). Interestingly, interaction of Phospho-Syk with Grb2 induced the MAP kinase (ERK1/ERK2) pathway (42). Moreover, the study observed inositol-5- phosphatase SHIP (43), in immunoprecipitations of Shc upon CD59 activation. SHIP phosphorylation appears to be triggered by various growth factors and cytokines (43) and may be involved in apoptosis and growth regulation (44).

Expression Level

Elevated CD55 is correlated with poor prognosis of colorectal, breast, pancreatic, gallbladder (IHCC), and gastric cancers. Paradoxically, CD55 expression is decreased in ovarian cancer and lung cancer, with certain SNPs associated with higher risk such as rs2564978 variant and rs2564978 (36, 37, 39, 45). As for CD59, it was found to be overexpressed in head and neck, colorectal, ovarian, (28, 46, 47), and in cervical cancer as well (48). In these cases, overexpression appears to be correlated to poorer prognosis (28, 46, 47).

In Vivo Model

In terms of immune-based therapy, antibodies raised against CD55 did not show overall consistent results; while 791T showed marvelous results in preclinical trials when conjugated to ricin-A chain, it failed phase I clinical trials. It was believed that therapeutic antibodies against CD55 should target SCR-3, while the use antibodies targeting other SCRs should only be restricted to immune-based assays. Until 2017, a patent illustrated that 791T antibody binds to epitopes located in

SCR1 and SCR2, therefore opening the door for using more epitopes to raise antibodies against DAF. Interestingly, 791T was used to raise 105 AD7, a human anti-idiotypic monoclonal antibody that mimics CD55. In 2000, the use of 105 AD7 as a peptide vaccine was first reported. Indeed, it stimulated anti-tumor immune reactions in patients with HLA/ A1,3,24 and HLA/DR1,3,7 haplotypes. In 2005, Ziller et al. reported mini antibodies MB-55 (against CD55) and MB-59 (against CD59) that increased lysis of Karpas 422 and Hu-SCID1 lymphoma cell lines when combined with Rituximab. In 2007, Macor et al. reported the same findings *in vivo* using LCL2 lymphoma cells in female SCID mice (49–52).

Strategy of CD59 blockade is showing promising results, where *ex vivo* treatment of colorectal cancer patients' T-cells with CD59-specific antibodies, MEM-43, and HC-1 has shown significantly enhanced antitumor immune response (53). Another study compared the effect of CD59 silencing on HT-29 cells viability when treated with 5-fluorouracil or oxaliplatin. Indeed, silencing of CD59 enhanced the sensitivity of HT-29 cells to 5-fluorouracil and oxaliplatin (54). In addition, CD-20+ -Lymphoma mice treated with MB-55 and MB-59 had improved response for rituximab immunotherapy, where 70% of mice survived when treated with rituximab and MB-59 or MB-55 combination, while 30% of mice survived when treated with rituximab alone (55). One possible clue is a study showing that CD55 and CD59 expression guards HER2-breast cancer cells from trastuzumab-induced complement-dependent cytotoxicity (56). However, account should be taken as targeted CD-59 depletion in mouse embryonic cells resulted in mice with increased RBCs count and higher susceptibility to complement lysis (57).

Insights

CD-59 is a promising marker as demonstrated by non-invasive graphene oxide based immune sensor with detection range 1fg/ml to 10 ng/ml (58). However, therapeutic potential for CD-59 blockade in tumors still requires more testing *in vivo*. Current evidence supports adjuvant use of CD-59 blockade in order to enhance efficacy of anti-cancer immune therapies (54, 55). However, caution should be taken, as adverse CD-59 blockade may cause paroxysmal nocturnal hemoglobinuria (PNH), which is characterized by elevated complement activity, RBCs lysis and CD-59 decreased expression (59). One possible refutation is the study using CD59 knockout and CD-59/CD-55 double-knockout mouse models (60). Surprisingly, Crry (complement receptor 1 (CR1)-related gene), neither CD59 nor DAF, was indispensable for murine erythrocyte protection *in vivo* from spontaneous complement attack, despite murine RBCs sensitivity to antibody-induced complement lysis *in vitro*. This proves that C3 inhibition is more critical *in vivo* rather than C8 and C9.

On the brighter side, C5 inhibitor eculizumab showed success and improvements in some PNH case reports, owing to the restoration of CD-59 activity (61). Nevertheless, eculizumab still faces challenges, including persistent anemia with some patients requiring transfusions, and incomplete C5 inhibition with breakthrough hemolysis (61). This prompted the investigation of several second-generation C5 inhibitors (new mAb, siRNAs

and small molecules) (62). Altogether, this ultimately justifies the rationale behind the use of CD-55 and CD-59 silencing as anti-cancer therapy, especially with establishment of CD-59 knocked out cancer cell lines which can be used for further *in vivo* investigations (63).

(CD66) Carcinoembryonic Antigen (CEA) Structure and History

CEA was discovered in 1965 by Gold and Freedman as a surface protein found in gastrointestinal cancer cells. The human CEA family consists of 29 genes, out of which 18 are expressed. The expressed proteins are further classified into CEA subgroup (7 proteins) and pregnancy-specific glycoprotein subgroup (11 proteins) (11, 64). Our scope, once again, is GPI anchored CEAs: CEA-CAM 6 and CEA-CAM 5, which is also known as CD66e (11).

Pathway and Function

Due to unique sialofucosylated glycoforms within its GPI anchor, CEA was found to bind to L-selectin and E-selectin, therefore mediating cell adhesion. CEA-CAM 1 is tumor suppressing through decreasing cell proliferation and metastasis, while CEA-CAM-5 is tumor promoting through inhibiting colon cell differentiation, anoikis and apoptosis (65, 66). This is attributed to CEA-CAM-5 co-localization and subsequent activation of $\alpha 5 \beta 1$ integrin signal transduction, triggering PI3K/AKT activity (67). CEA-CAM 6 oncogenic activity is due to mediating metastasis and resisting apoptosis. Increasing metastasis is through CEA-CAM 6 signaling induced SRC activity. SRC is a non-receptor Tyrosine kinase, which in turn phosphorylates focal adhesion kinase (FAK) and stimulates IGF-1 secretion. As a result, PI3K/AKT pathway is activated, consequently inducing epithelial mesenchymal transition (11, 68). Surprisingly, TGF-B/type II receptor (TBR2) interaction functions as a positive feedback, where TBR2 forms a heterodimer with TBR1, which increases PI3K/AKT pathway activity and SMAD-3 phosphorylation. Phospho-SMAD-3 then forms a complex with Co-SMAD-4. This complex translocates to the nucleus and binds to CEA-CAM 6 gene promoter, elevating its expression (11).

Expression Level

Stoichiometric expression of CEA family members (CEA-CAMS 1,5,6) on epithelial cell guards normal tissue architecture through micro-environment interactions described above. Interestingly, CEA-CAM 1 is under expressed in CRC, breast cancer, prostate cancer and hepatoma (69). On the other hand, 70% of epithelial tumors over express CEA-CAM 6 rather than CEA-CAM 5 (11, 70, 71). Specifically, CD66 is elevated in colorectal, pancreas, liver, breast, ovary, and lung cancer (11, 70, 71). Interestingly, CEA-CAM 5 is temporarily produced during fetal development until birth. This encourages the use of CEA in diagnosis and targeted therapy.

In Vivo Models

In 2015, Li et al. reported a bispecific antibody that targets CD3 and CEA. It was produced by genetically linking an anti-carcino

embryonic domain (variable heavy H) to the C-terminal end of an anti-CD3 variable heavy, constant heavy 1, followed by co-transduction with anti-CD3 variable light-constant light in bacteria. The produced protein (antibody) is called S-FAB. To demonstrate *in vitro* efficacy of S-FAB, CEA-expressing human colorectal cancer cell lines HT29 and LS174T were exposed to human peripheral blood mononuclear cells (PBMCs) or isolated T-cells in the presence and absence of S-FAB. In absence of S-FAB, no cytotoxicity occurred, while treatment with S-FAB resulted in cytotoxicity, where cell viability was assayed using Cell Counting Kit (CCK) reagent. Accordingly, this study advanced to *in vivo* level, where NOD/SCID mice were subcutaneously injected with a mixture consisting of 1×10^6 LS174T cells and 5×10^6 fresh human PBMCs. An hour later, mice were IP injected with 20 μ g S-FAB. Indeed, S-FAB successfully inhibited tumor growth, even better than anti-CD3 FAB (72). A similar bispecific antibody called CEA TCB has shown promising results *in vitro* and *in vivo* and is now tested in phase-I clinical trials (73). Other CEA-CAM targeting antibodies are MN-3, MN-14 and MN-15. Xenograft colorectal cancer mice showed higher survival, decreased adhesion to the extracellular matrix (ECM), and lower metastatic activity when treated with MN-3 and MN-15 (11, 71). However, these mAbs did not have a significant impact on tumor growth (11, 71). This called for testing other immune therapeutic strategies. For instance, By114-saporin is an immunotoxin tested on pancreatic xenograft

model, where antibody mediated crosslinking increased apoptosis, enhancing the efficacy of saporin immunotherapy (74). Another study involved the use of Ab-IRDye where CEA antibody targets photosensitizer to cancer cells, thus, when cells are exposed to near-IR rays, oxidative burst occurred selectively in cancer cells causing their death, leaving normal cells intact. The efficacy of Ab-IRDye was tested *in vivo* using nude mice carrying gastric carcinoma xenograft (75). In addition, Silencing CEA-CAM 6 by RNAs decreased tumor proliferation by 68% in pancreatic cancer xenograft mice compared to control siRNAs (f. 88-90). Other observations were impaired angiogenesis, increased apoptosis, suppressed metastasis (0% treated versus 60% untreated, $p < 0.05$), and improved survival without toxicity.

Clinical Trials

For details on clinical trials targeting CEA, clinicaltrials.gov was searched, and data were collected in **Table 1**. PANVAC-F (falimarev) vaccine and PANVAC-V (inalimarev) are therapeutic vaccines expressing CEA, where PANVAC-V is derived from vaccinia virus, while PANVAC-F is derived from fowlpox virus. In addition, a recent study reported first-generation CAR-T therapy against CEA. It was evaluated in phase-I clinical trials for CEACAM5+ lung cancer patients. Unfortunately, no significant clinical improvement was observed and the CAR-T cells lived for 14 days only. However,

TABLE 1 | CEA clinical trials.

NCT Number	Conditions	Interventions	Results
NCT00088413	Adenocarcinoma Colorectal Cancer Ovarian Cancer Breast Cancer	PANVAC-V and PANVAC-F Plus Sargramostim	For breast cancer *Median OS=13.7 m. *Median PFS=2.5 m. For ovarian cancer *Median OS=15 m. *Median PFS=2 m. *1patient showed complete response *1patient showed 17% reduction in mediastinal mass *SE: mild injection-site reactions *No dose limiting toxicities *Partial Disease :7/21 *stable disease:14/21
NCT00408590	Ovarian Cancer Primary Peritoneal Cavity Cancer	CEA-expressing measles virus	For PANVAC +DOC. *Median PFS= 6.6 m. *SE=23/25 For DOC. *Median PFS= 3.8 m. *SE=25/25 *SEs observed were anemia, tachycardia, and vomiting for DOX treated group. For PANVAC +SARG. *recurrence free surv.= 55% For DC +SARG. *recurrence free survival= 47% *Immune response by T-cell against CEA was statistically similar between study arms.
NCT00179309	Breast Cancer	PANVAC-V and PANVAC-F Docetaxel Sargramostim	For cT84.66+Flox 0.10 mg/kg/Day: *Median OS.= 23.2 m. For cT84.66+Flox 0.15 mg/kg/Day: *Median OS.= 73.2 m. For cT84.66+Flox 0.20 mg/kg/Day: *Median OS.= 41.2 m. (MTD) of HAI FudR=0.20 mg/kg/Day
NCT00103142	Colorectal Cancer Metastatic Cancer	Falimarev Inalimarev Sargramostim Autologous dendritic cells	
NCT00645710	Liver Metastases Recurrent Colon Cancer Recurrent Rectal Cancer Stage IV Colon Cancer Stage IV Rectal Cancer	Anti-CEA mAb cT84.66 Gemcitabine hydrochloride Floxuridine Radiation: yttrium Y 90	

OS, overall survival; PFS, progression-free survival; SE, side effects; MTD, maximum tolerated dose.

rising levels of systemic IFN γ and IL-6 indicate the presence of immune response when patients were pretreated with cyclophosphamide and fludarabine, as well as systemic IL-2 during CAR-T therapy. This means that CAR-T therapy targeting CEA is promising, but future studies should try to develop other CAR designs and T-cell production methods (76). A phase-I clinical trial was done to study the safety of anti-CEA second-generation CAR-T scfv-CD28/CD3z (Tandem), in which CAR-T therapy was delivered by infusion into hepatic artery. The results were promising; coadministration of IL-2 with CAR-T therapy has decreased CEA levels and increased serum IFN γ levels. Also, no patient suffered from severe adverse effects (77).

Insights

Finally, CEA has a unique expression pattern, making it a treasure for diagnosis using *in vivo* fluorescent imaging and immunosensing using nanomaterial-based electrochemical immunoassay, photoelectrochemical immunoassay, and optical immunoassay (78, 79). In addition, numerous studies combine CEA with other biomarkers for better diagnosis (80–83). As for prognosis, drop in CEA level can be used as a posttreatment watch (81, 82, 84). Clinical trials data prove the efficacy and safety of CEA-targeted immune therapy. However, they cannot be used as a single agent for treatment of different tumor types, where conventional chemotherapy is still needed to relieve tumor compact structure and add a synergistic tumor-killing effect. Finally, the use of anti-CEA as an adjuvant therapy decreased adverse effects compared to the use of standard therapies alone. More importantly, no serious adverse effects were observed in CEA-immune-based therapy.

Glypican-3

Structure and History

Glypican-3 (GPC3) is a member of the glypican family, which are a group of GPI-APs. So far, 6 types (GPC1–GPC6) have been identified in mammals. Glypicans were shed in serum upon cleavage by Notum (a lipase for GPI anchors). Moreover, GPC3 has two heparan sulphate (HS) glycan chains attached to the C-terminus. GPC3 gene codes for a 70 kDa precursor core protein with 580 amino acids, which can be cleaved by furin producing a 40 kDa amino (N)-terminal protein and a 30 kDa membrane-bound carboxyl- (C-) terminal protein. Furin cleavage between Arg358 and Ser359 was found to be crucial for GPC3 activity in zebrafish, but not in HCC. It was also predicted that cleavage for GPI anchor occurs at serine 560 (85, 86).

Pathway and Function

GPC3 knockout mice showed a distinctive phenotype: Simpson-Golabi-Behmel Syndrome (SGBS), an X-linked disorder characterized by pre- and postnatal overgrowth. This gave a hint that GPC3 is somehow involved in cancer cell proliferation. One possibility is that HS proteoglycans (HSPGs) may act as supporting receptors or storage for growth factors such as Hedgehogs, bone morphogenetic proteins, and fibroblast growth factors (FGFs). A various amount of evidence supports this point of view, where sulfatase 2 (SULF2) was elevated in breast cancer and HCC. For elaboration, sulfatase 2 enzyme

cleaves HSPGs at 6-O-sulphate site. Also, SULF2 knockout decreased tumorigenesis of pancreatic cancer cell lines. A study investigated the SULF2-GPC3-Wnt signaling triad. It concluded that sulfatase 2 cleaves GPC3/Wnt complex at the HS region, therefore releasing Wnt protein to initiate signaling cascade (**Figure 3**). Interestingly, GPC3 can interact with Wnt molecules independent of HS chains and accelerate cancer cell division by activation of canonical Wnt signaling pathway. These results indicate that GPC3/Wnts complex acts as a growth factor by binding to other proteins (coreceptors for either GPC3 or Wnts) (18, 86, 87). On the other hand, GPC-3 is possibly a tumor suppressor where ectopic expression increased apoptosis in A549 and NCI-H460 cell lines (88).

Expression Level

GPC3 gene is expressed in a time-specific manner, where it reaches peak expression during development, followed by gradual decline after birth, thus its expression is down regulated in normal tissues (86). GPC3 is uniquely over-expressed in HCC with poor prognosis correlation in late stage (89, 90). It is also over expressed in oral, colorectal and ovarian cancers (91–93). Controversially, GPC3 gene hyper methylation is observed in adult cancers, which supports argument GPC3 is under expressed in mesothelioma and neuroblastoma (94, 95).

In Vivo Models

The first antibodies against GPC3 were of murine origin, and they did not advance for therapeutic use due to immunogenicity risk. Instead, they are currently evaluated for their use in assaying GPC3 in serum and tissue (i.e., diagnostic use) (12, 86). The first therapeutic mAb against GPC3, called GC33 (IgG2a, κ) was reported in 2008. Its epitope is located near the C-terminus (residues: 524–563). It was raised in mice and effectively induced antibody-dependent cellular cytotoxicity (ADCC) against subcutaneously transplanted HepG2 and HuH-7 xenografts (12, 86). Accordingly, GC33 was modified by recombinant technology yielding humanized GC33 (hGC-33/codrituzumab) (12, 86). Interestingly, Hep-G2 expressed higher levels of GPC3 compared to Huh-7 based on fluorescence-activated cell sorting (FACS) analysis, where Hep-G2 expressed 1.5×10^6 GPC3 molecules per cell, while HuH-7 expressed 4.0×10^4 GPC3 molecules per cell. These findings are extrapolated *in vivo*, where Huh-7 mice xenograft models demonstrated significant tumor reduction from 3000 mm³ to 1500 mm³ when treated with 1mg/kg GC33, and to 1000 mm³ when treated with 5 mg/kg GC33, compared to untreated control. Similarly, Hep-G2 xenograft models demonstrated significant tumor reduction from 1200 mm³ to 600 mm³ when treated with 1mg/kg GC33 and to 100 mm³ when treated with 5 mg/kg GC33, compared to untreated control. Testing the efficacy of sorafenib/GC33 combination on Hep-G2 xenograft model revealed that, indeed, tumor volume was significantly decreased from 1000 mm³ to 200 mm³ when treated with 1 mg/kg GC33 plus 80 mg/kg sorafenib, compared to untreated control. Meanwhile, sorafenib and GC33 had equal tumor reduction ability with tumor volume reduced to 450 mm³. The study also evaluated the efficacy of doxorubicin/GC33 combination on Huh-7 xenograft model. This

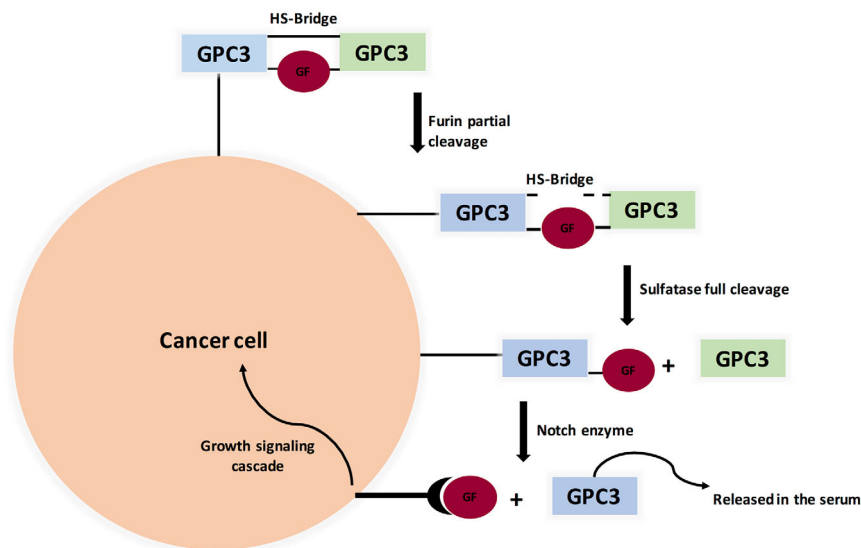


FIGURE 3 | Proposed Model for Glypicans Due to Heparan Sulfate bridge (HS), GPC3 is not fully cleaved by Furin (unlike MSLN). Full cleavage is achieved when HS bonds are broken by Sulfatase 1 or Sulfatase 2. Interestingly, Sulfatase 1 has anti-oncogenic properties while Sulfatase 2 favors tumor progression by releasing growth factors, therefore binding to its cognate receptor and initiating signaling cascade. (GF=Growth Factor).

showed that tumor volume was significantly decreased from 3000 mm³ to 1000 mm³ when treated with 5 mg/kg GC33 plus 3 mg/kg doxorubicin compared to untreated control, whereas doxorubicin and GC33 also had equal tumor reduction ability with tumor volume reduced to 1750 mm³ (96).

Clinical Trials

Currently GC33 is under clinical trials. Encouragingly, a phase-I clinical trial showed no maximum tolerated dose (MTD) because no dose-limiting toxicities (DLTs) happened. However, reported side effects included fatigue, constipation, headache, and decreased sodium level. Another ongoing clinical trial studies the combination of hGC33 with sorafenib. Meanwhile, a phase-I clinical trial consisting of advanced HCC patients showed that murine GC33 can be safely administered intravenously up to 20 mg/kg weekly (97, 98).

In addition, a GPC3 peptide vaccine was reported to induce CD8⁺ activity in HLA-A2.1 transgenic mice without causing autoimmune side reactions, where treatment of NOD/SCID mice with the cytotoxic T-lymphocytes (CTLs) significantly inhibited the growth of human HCC xenografts. Therefore, phase-I clinical trials were initiated, with the vaccine consisting of two GPC3-derived peptides and an incomplete Freund's adjuvant in advanced HCC patients. Spectacular results were achieved as the vaccine was well tolerated and 30 out of 33 patients demonstrated a significant quantified immune response. Furthermore, a correlation between the intensity of immune response and overall survival was observed. Consequently, the vaccine has advanced to phase-II clinical trials and has also been evaluated in combination with chemotherapy (99). For details about clinical trials, see **Table 2**.

Insights

As per methylation analysis performed by Boily et al. (95), where methylation abnormalities were present only in female neuroblastoma samples (loss of methylation) and mainly in male WT samples (gain of methylation) (95). Therefore, these results suggest that DNA methylation of the promoter region is not essential for the transcriptional repression of the GPC3 gene and that the methylation observed in females is probably linked to the inactive X chromosome. Other possible regulators are micro-RNAs, where MiR-219-5p targeted GPC3 and inhibited HCC cell line proliferation (100). GPC3 is an attractive target for immune-based therapy due to its high expression in HCC and especially that GPC3 was found in cancerous liver cells but not normal ones (89).

Mesothelin (MSLN)

Structure and History

Mesothelin is a glycosylphosphatidylinositol (GPI) fixed cell surface protein. The human MSLN is a ~71 kDa antecedent protein of 622 amino acids, which is separated by furin into 31 kDa N-terminal megakaryocyte potentiating factor (MPF) and 40 kDa mature mesothelin attached to the cell surface (101) (**Supplementary Figure 3**). MSLN was discovered in the mid-1990s, in an investigation initiated by Ira Pastan and Mark Willingham (National Cancer Institute, NIH) aiming to find new therapeutic target to treat ovarian cancer, where they started by screening for novel antibodies that target proteins significantly overexpressed in cancer cells compared to normal cells (102). Then, different mAbs were produced by Hybridoma technology (102). Candidate mAbs were evaluated by immunohistochemistry, bringing about the revelation of

TABLE 2 | Glypican-3 clinical trials.

NCT Number	Conditions	Interventions	Results
NCT02748837	Solid Tumors	ERY974 Phase I	Just completed Aug 2019
NCT02395250	HCC	anti-GPC3 CAR T	Just completed Aug 2019
NCT02723942	GPC3 Positive HCC	CAR-T cell immunotherapy	No data update since 2017
NCT00976170	HCC	RO5137382 (GC33) and sorafenib (Phase I b) Codrituzumab	*Drug limiting toxicities were: grade 3 hyponatremia and hypona hyperglycemia *MTD for GC-33/sorafenib combination was 1600 mg q2w and 400 mg bid.
NCT01507168	Metastatic HCC	RO5137382 (GC33) VS. Placebo (Phase 2)	*Median PFS in the codrituzumab vs. placebo groups were: 2.6 vs. 1.5 (hazard ratios 0.97, $p=0.87$), in months *Median OS was 8.7 vs. 10 (hazard ratios 0.96, $p=0.82$).

OS, overall survival; PFS, progression-free survival; SE, side effects; MTD, maximum tolerated dose.

mAb-K1 in 1992 (102). Since mAb-K1 binding protein is expressed in typical mesothelial cells, it was called mesothelin, where it was the first characterized 125I fractionation and phospholipase-C treatment. MSLN was also identified by western blot, with molecular weight 40 kDa, present in both OVCAR3 and Hela cells. Consequently, the K1 mAb was employed to screen a lambda cDNA library containing Hela cells genome. MSLN cDNA encoded a 69 kDa protein, which, when transfected in 3T3 cells, caused a noteworthy 40 kDa band and a minor 69 kDa band to be distinguished showing that the 40 kDa band was derived from a larger parent protein (102).

Pathway and Function

The biological role of mesothelin is still anonymous because mesothelin knockout mice do not show a significant phenotypic change (12, 103). Therefore, investigations were principally done on ovarian cancer and pancreatic cancer cell lines (12). MSLN plays a pivotal role in cancer cell survival/proliferation by NF- κ B activation which induces IL-6 expression. IL-6 acts as a growth factor via a new auto/paracrine IL-6/sIL-6R signaling pathway (104). In addition, MSLN enables cancer cell survival, despite inflammation, due to resisting TNF- α -induced apoptosis, through elevating Akt/PI3K/NF- κ B and IL-6/MCL-1 axes (12, 101, 103). Studies on ovarian cancer cell lines showed that

mesothelin is involved in tumor adhesion and metastasis based on its binding to MUC16 (also known as CA125), due to its rich glycosylation, where O-linked and N-linked MUC-16 oligosaccharides triggered heterotypic cell adhesion (103). It was recently found that immune-reactivity against mature MSLN involved IFN- γ , IL-2, and IL-7 and was positively correlated with the survival of secondary brain-cancer patients (105). An interesting finding states that MSLN is specifically increased in CCA while Glypican-3 is specifically increased in HCC, therefore shedding light on their use as diagnostic markers differentiating HCC from CCA (12) (see **Figure 4**).

Expression Level

In addition to its protumorigenic role described above, mesothelin is a valuable target for various immunotherapeutic strategies due to its high presence in ovarian, uterine, and pancreatic cancers. Recent papers show that it is also elevated in triple-negative breast cancer (TNBC)—in addition to the possession of a highly immunogenic region (Region I) (12, 103, 106, 107).

In Vivo Models

To compare the uptake of mAb-K1 in cancer and normal cells, mice were subcutaneously injected with human mesothelin-expressing tumors and then treated with Indium-labeled

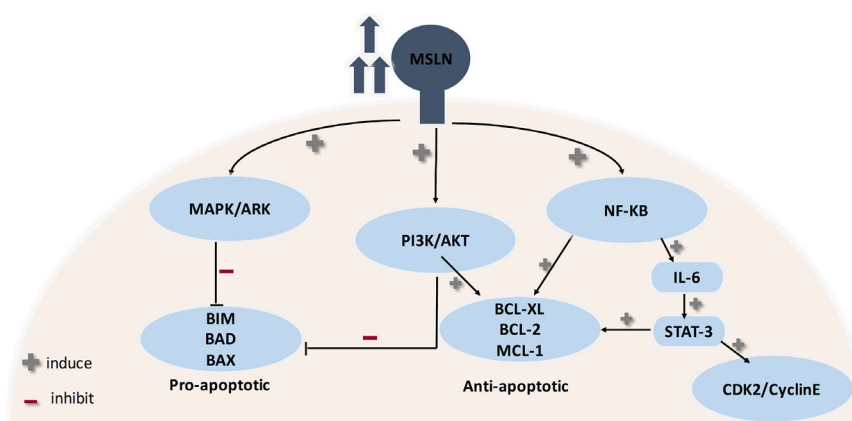


FIGURE 4 | Role of MSLN in cancer progression. MSLN elevation activates MAPK/ERK, PI3K/Akt pathways therefore making cancer cells resistant to apoptosis. Also, MSLN overexpression induces NF- κ B which leads to higher IL-6 production. High IL-6 induces the transcription protein 3 (Stat3), resulting in increased expression levels of the cyclin E/cyclin-dependent kinase (CDK2) complex, therefore speeding the G1-S transition resulting in enhanced cell proliferation.

mAb-K1. The results were promising and, accordingly, antitumor activity was tested by conjugating mAb-K1 to *Pseudomonas* exotoxin A (PE). This was the first immunotoxin, named K1-LysPE38QQR, and indeed it showed an excellent *in vitro* and *in vivo* activity. However, K1 antibody has a low affinity for mesothelin; therefore, mice were immunized with a mesothelin-expressing cDNA construct, and produced antibodies were isolated by phage display. The new antibody SS was produced. The low affinity of SS was overcome by mutagenizing CDR3 residues of the heavy chain of the Fv using hotspot mutagenesis method, increasing Kd to about 1 nmol/L. This was called SS1. SS1 Fv was fused to a PE fragment producing the recombinant immunotoxin SS1P. SS1P kills cells by binding to mesothelin, followed by endocytosis, and inactivating elongation factor 2, then halting protein synthesis, and initiating programmed cell death (12, 102, 103).

Another example is MORAb-009 (amatuximab), a recombinant humanized antibody consisting of murine SS1 Fv and human constant region (IgG1κ). *In vitro* studies illustrated that MORAb-009 kills cancer cells by ADCC and blocking mesothelin/MUC-16 interaction. *In vivo* investigations combining amatuximab with chemotherapy showed significant growth deceleration of mesothelin-positive tumors in nude mice compared to chemotherapy or MORAb-009 treatment alone (102). Another investigation was performed using pancreatic cancer xenograft model, where administration of 200 mg/kg amatuximab lowered tumor volume by 75% and tumor mass by 6 folds. The study was extended to test amatuximab efficacy as combinatorial therapy with gemcitabine. Indeed, a synergistic effect was observed, where when combined with gemcitabine, tumor mass and tumor volume were reduced to 200 mg and 400 mg. Gemcitabine reduced tumor to 600 mg and 1750 mm³ compared to untreated control (600 mg, 1200mm³) (108).

Continuous developments in antibody production have led to the discovery of the first human antibody against MSLN. It is designated as m912. M912 is believed to kill cancer cells by ADCC. In another study, a high-affinity human single-chain Fv (named HN1, unique against mesothelin) was obtained from a naïve human single-chain Fv (scFv) phage display library. To assess the therapeutic potential of HN1, a fully human IgG1κ and immunotoxin (HN1 scFv + *Pseudomonas* exotoxin) were produced. The HN1 demonstrated a very strong ADCC and also blocked MSLN binding to MUC-16, while HN1 immunotoxin acted similar to SS1P (12, 102).

BAY 94-9343 is an antibody drug conjugate consisting of humanized immunoglobulin G1 anti-mesothelin mAb and maytansine derivative DM4 (a tubulin polymerase inhibitor) while MDX-1382 MED2460 (Medarex) consists of MSLN mAb conjugated to duocarmycin (a DNA-alkylating agent). Antibody drug conjugate (ADC) is based on the concept that the drugs will be released into the cytoplasm after antibody drug conjugate endocytosis. Interestingly, *in vitro* studies of BAY 94-9343 showed that it was able to kill adjacent MSLN-lacking tumor cells with no effect on quiescent cells; a possible explanation is multiple targeting as tumor cells express heterogeneous antigens. ADCs are still in phase-I clinical studies (102, 109, 110).

Clinical Trials

Immunotherapy targeting MSLN includes the use of tumor vaccines, antibody-based therapies, and adoptive T-cell therapy (CAR-T cells), some of which have demonstrated outstanding results in early clinical studies. However, antibodies targeting region I do not inhibit cancer cell proliferation. Furthermore, obtaining mAbs targeting MSLN domains outside region I is a difficult task. This calls for the possibility of controlling MSLN expression through genetic targeting either by miRNAs or by CRISPR/CAS (12, 103).

To evaluate SS1P efficacy and safety, phase-I clinical trials were conducted by administering SS1P intravenously; the dose-limiting side effect was pleuritis, and unfortunately 90% of patients developed neutralizing antibodies against toxin part. Neutralizing antibodies problem was tackled by immunosuppressive regimen of pentostatin and cyclophosphamide. An interesting approach is to use recombinant technology to deduce and remove B- and T-cell epitopes in SS1P, therefore decreasing its immunogenicity. A new immunotoxin resulted from deletion of PE domain II and six residues in domain III substituted with alanine. Loss of domain II rendered the new immunotoxin small and was rapidly filtered by the kidney. This was solved by replacing the Fv with a Fab to make RG7787. Interestingly, results obtained from RG7787 were promising, where large doses were safely administered to mice, with a lower risk of capillary leak syndrome in rats, and it has significant antitumor activity in mice bearing several types of mesothelin-positive tumors. Consequently, RG7787 advanced to Phase-I clinical trials (102, 109–112).

Another drawback was the large size coupled with relatively short life in circulation (20 min in mice and 2–8 h in humans), which resulted in poor penetration into solid tumors. A possible solution is combination with chemotherapy, where preclinical studies showed that chemotherapy relaxes tumor cell compact structure and lowers intratumoral fluid pressure, therefore allowing immunotoxin to reach more cells within the tumor, and produce better antitumor responses. Using confocal microscopy, SS1P penetration was studied in 3D tumor mesothelioma spheroids. Sensitivity to SS1P of spheroids was 100 times lower compared to primary cell lines grown as monolayer. This finding was explained by significant rise in the count of tight junctions inside the spheroids, with specific elevation of E-cadherin gene. This was supported by enhanced SS1P immunotoxin therapy *in vitro* when combined with small interfering RNA silencing and antibody inhibition targeting E-cadherin (102, 109).

Phase-I clinical trials proved the safety of amatuximab, where maximum tolerated dose was established as 200 mg/m². Unfortunately, a randomized phase-II clinical trial of amatuximab/gemcitabine combination failed to show additive advantage in pancreatic cancer population compared to gemcitabine alone. However, in a nonrandomized clinical trial involving advanced unresectable pleural mesothelioma patients, amatuximab was co-administered with pemetrexed and cisplatin. Results showed improvement in overall quality of life, despite failure in increasing progression-free survival as compared with historical controls (102, 109, 113–115).

Based on the promising results obtained from MSLN mAbs, immunotoxins, and ADCs, there is a growing interest in exploring MSLN as a target for CAR-T cell therapy, where T-cells are manipulated to produce variable chain/T-cell receptor hybrid so that cancer cell is recognized by CAR-T cell binding to the tumor antigen, which activates T-cell signaling and results in cancer-cell killing. Currently, there are two approaches for anti-mesothelin CAR-T cells synthesis: either direct treatment with antimesothelin modified lymphocytes or autologous redirection (where patients' T-cells are edited for Fv against MSLN and then returned back) (53, 59, 66).

The feasibility of MSLN CAR T-cell therapy was evaluated *in vivo* using subcutaneous or orthotopic mouse models of mesothelioma, ovarian cancer, and lung cancer, where local administration of CAR-T cells produced better results due to earlier antigen recognition, which is reflected as increased CD8+ CAR-T cell proliferation and function. Therefore, various clinical trials for MSLN CAR-T cells were started either alone or combined with chemotherapy to determine the safety and the maximum tolerated dose. A major challenge limiting the safety of CAR-T therapy is on-target/off-tumor toxicity, which is tackled by transfection of mRNA that encodes MSLN CAR into patients' T-cells and then returning it back (i.e., autologous). Indeed, this idea demonstrated positive results in preclinical models and therefore advanced to clinical trials' stage. The only problem for this method is that the effect is transient, lasting only for few days. Luckily, a clinical trial involving multiple infusions of MSLN CAR-T cells (SS1-4-1BB) was safe without toxicity observed. Even better, MSLN CAR T-cell therapy caused transient elevation of inflammatory cytokines in the sera, including IL-12, IL-6, G-CSF, MIP1 β , MCP1, IL1RA, and RANTES. Consequently, tumor lysis and inflammation occurred, which led to the release of multiple antigens, stimulating immune response. As a result, a polyclonal IgG antibody response was detected. This phenomenon is called epitope spreading. Unfortunately, only one patient suffered from a severe anaphylactic shock and cardiac shock due to high production of IgE against MSLN CAR-T cells (102, 109, 116, 117).

An alternative strategy is increasing T-cell safety through a suicide gene to remove T-cells as soon as an adverse event occurs, such as drug-induced activation of a suicide gene, for example, the herpes simplex thymidine kinase (HSV-TK) gene, inducible caspase-9 (iCaspase-9), or EGFR Δ gene. This concept of "safety-switch systems" has succeeded in clinical investigation and is currently put under clinical trial. Preclinical studies proved the safety of suicide gene in CAR-T therapy where a single dose of the AP1903 small molecule (clinical-grade construct with an iCaspase-9 safety switch) successfully removed MSLN CAR-T cells at the peak of their proliferation. Furthermore, a particular concern regarding MSLN CAR-T cells is cross-reaction with soluble MSLN related peptide (SMRP), which could occupy and block the scFv portion, therefore causing loss of CAR-T cell activity, especially with MSLN and SMRP having identical sequence. Reassuringly, MSLN CAR-T cell activation (cytokine secretion and cytotoxic activity) depends on MSLN attached to the cell surface, where the presence of serum SMRP at high level did not alter MSLN CAR-T cell efficiency neither *in vitro* nor *in vivo* (102, 118).

Ultimately, the sole mesothelin vaccine now in clinical trials is CRS-207. It is a live attenuated vaccine produced using *Listeria monocytogenes* vector that overexpresses human MSLN. So far, the suitability of this immunization was assessed in stage-I clinical trials in patients with mesothelin-positive-resisting tumors. A stage-II clinical trial comprised of advanced pancreatic cancer population yielded noteworthy outcomes, where patients were administered either six cycles of GVAX (allogeneic pancreatic cell lines secreting granulocyte macrophage colony stimulating factor) alone or two rounds of GVAX followed by four cycles of CRS-207 every 3 weeks. After a median follow-up of 7.8 months, the median overall survival of patients treated with GVAX/CRS-207 was 6.1 months versus 3.9 months for patients treated with GVAX alone ($P=0.011$). However, this study included just 90 patients. Subsequently, approval in a larger stage-III setting is required (102, 119, 120). For a summary of MSLN immunotherapies, see **Table 3**.

Insights

MSLN immunotherapy is the most promising among GPI-AP immunotherapy, with variety of models currently tested in clinical trials. However, further studies are required for its use as biomarker to decipher its sensitivity and specificity. Currently, SMRP and MSLN are recommended in combination with other serological biomarkers. Surprisingly, significant MSLN promoter hypo-methylation was observed in mesothelioma and lung cancer patients with previous asbestos exposure. However, no correlation was found between MSLN hypo-methylation and SMRP serum levels. These findings do not only account for MSLN over expression in multiple tumors, but more importantly they support MSLN regulation by other epigenetic methods. For instance, our investigation proved that miR-2355 targeted PIG-C and MSLN mRNAs (121). Another example is MSLN targeting by miR-21-5p that decreased MERO-14 cells proliferation (122). Other examples are miR-611 and miR-877 that were tested in mesothelioma cell lines. Astonishingly, miR-611 could not degrade MSLN harboring SNP rs1057147 (123).

PRACTICAL IMPLICATIONS

Immune Painting

A rising star in targeted immunotherapy is increasing the levels of costimulatory proteins within cancer cells in order to reverse immune suppression. This can be achieved by attaching GPI anchor sequence to costimulatory proteins such as CD80, ICAM-1, and CD86, which are originally Type-I transmembrane protein. The GPI anchor is obtained from naturally occurring GPI anchoring proteins. This is called immune painting. There are two options for immune surface painting, either genetic engineering or protein engineering. Genetic engineering is construction of plasmid consisting of the DNA sequence coding for the GPI anchor attached to the sequence encoding the protein of interest, whereas protein engineering means that GPI-modified protein is directly

TABLE 3 | MSLN targeted therapy in clinical trials.

NCT Number	Conditions	Interventions	Results
NCT00570713	Pancreatic Cancer	Phase 2: <ul style="list-style-type: none"> • MORAb-009 • Placebo • Gemcitabine 	mAb-009+Gemcitabine 1-OS=6.5 mon. (4.5 to 8.10) 2-AE=67.12% Placebo+Gemcitabine 1-OS=6.9 mon. (5.4to 8.8) 2-AE=72%
NCT01018784	mesothelin-positive solid tumors	MORAb-009 (Phase 1)	1-MTD=200 mg/m2 2-AEs=76.5% grade 1 fatigue and pyrexia
NCT00006981	Mesothelin positive tumours	• SS1P	1-MTD = 25 microg/kg/d x10 2- Serious AE: 1/6 reversible vascular leak syndrome 3-all patients developed antibodies against SS1P
NCT01362790	<ul style="list-style-type: none"> • Mesothelioma • Adenocarcinoma of Lung • Pancreatic Neoplasms 	<ul style="list-style-type: none"> • SS1P • Pentostatin • cyclophosphamide 	For SS1P then pento 1- Response Assessment: 18.2% partial response, 45.5% stable disease,27.3% progressive 2-DOR = 16.3mon. (10.6 to 26.2) 3-OS= 11.8 months(1.6 to 13.6) For pento then SS1P 1- Response Assessment: 75% stable disease,12.5%progressive 2-OS = 8.8 mon. (0.6 to 13.0) • 21 infusions were administered • 1 patient had serious AE • 1 patient had minimal arthralgias and fatigue For Cy/GVAX + CRS-207: 1-OS = 6.28 months (4.47 to 9.40) 2-Serious AE: 29/64 For Cy or GVAX alone: 1-OS = 4.07 months (3.32 to 5.42) 2-Serious AE: 10/29 For Cy/GVAX + CRS-207 1-OS = 3.8 months (2.9 to 5.3) 2-Serious AE: 44/94 For CRS-207 1-OS=5.4 months (4.2 to 6.9) 2-Serious AE: 32/87 For Gemcitabine 1-OS=4.6 months (4.2 to 5.8) 2-Serious AE: 15/52
NCT01355965	Malignant Pleural Mesothelioma	autologous transfected anti-mesothelin CAR T cells	
NCT01417000	• Metastatic Pancreatic Cancer	<ul style="list-style-type: none"> • GVAX Vaccine (CRS-207) • Cyclophosphamide 	
NCT02004262	• 2nd-line, 3rd-line and greater metastatic pancreatic cancer	<ul style="list-style-type: none"> • GVAX Vaccine • CRS-207 • Gemcitabine • Cyclophosphamide 	

OS, overall survival; PFS, progression-free survival; SE, side effects; MTD, maximum tolerated dose.

incorporated into the cell membrane; this is based on the fact that GPI-anchored proteins can be exchanged between cells. Both strategies have shown amazing results in terms of elevating immune response; plasmids are being studied as DNA vaccine and possible use in oncolytic virus therapy, whereas protein engineering is used in cases where limited biochemical information renders specific enrichment difficult, for example, in case of enveloped viruses (124).

Noninvasive Tests

An interesting thought is to benefit from GPI-APs in noninvasive tests, which assay binding of membrane GPIs to enzymes such as alpha-toxin and aerolysin upon cell lysis (125–127). An interesting thought for MSLN is to assay SMRP (MSLN shed in serum, identical sequence) using ELISA; this is possible because MSLN overexpression is directly reflected in serum as elevated SMRP (102, 128–131). Indeed, this rationale

can be extended for GPI-shed proteins such as serum CD55, serum CD59, and serum Glypican-3. Together, these features shed light on new noninvasive tests. An outlaw, however, is the utility of Glypican-3 in the diagnosis of HCC, where it is found to indicate poor differentiation, and, is therefore not useful as an early biomarker.

Chemical Synthesis

A challenging task in the attempt to study the structure activity relationship (SAR) of GPI-anchored proteins was the chemical synthesis of GPI anchor that started in the late 90s–early 2000s, especially after the discovery of VSG in 1988 by Ferguson et al. Simply, GPI building blocks (mannose, glucosamine, inositol, and phospholipids) are connected together through a series of chemical reactions. However, there are some obstacles. First of all, the chirality of molecules is critical for GPI-AP protein function. Moreover, oxidation and reduction complexity

affect the lipid tail. Such drawbacks were tackled by the use of modern blocking methods rather than global blocking (15, 132). This resulted in the successful synthesis of naturally occurring GPI-AP and semisynthetic/synthetic derivatives containing unsaturated lipids (e.g., click chemistry tags), or highly branched structures (132). In fact, a chemical method, designated one pot ligation (OPL), was used to achieve semi-synthetic GPI anchored eGFP, Thy1, and the *Plasmodium berghei* protein MSP1₁₉. Interestingly, GPI attachment did not cause a change in peptide structure, but it resulted in a strong inflammatory response in vitro (133).

OVERALL INSIGHT

To conclude, GPI-APs are necessary for various biological functions. Advancement in oncology research has shown that GPI-anchored proteins play a critical role in cancer progression. Further studies demonstrated that GPI-anchored proteins have a unique expression pattern on neoplastic cells. Consequently, scientists are trying to use GPI-APs for early diagnosis and targeted therapy. Throughout this review, we focused on few GPI-anchored proteins (MSLN, Glypican-3, CEA, DAF, and MAC-i), with these proteins overexpressed in many cancers. When used as biomarkers, GPI-APs demonstrated high specificity. However, new assaying technologies are needed to enhance GPI-APs sensitivity. Another opportunity is investigating the expression level of GPI pathway members in different cancers. Surprisingly, our work showed that PIG-C expression is elevated in TNBC, while PIG-U expression was down regulated in KRAS mutant CRC (29, 30). This raises a critical question: why GPC-3 and CEA are over expressed in CRC? This opens the door for investigating whether other GPI pathway genes are elevated in CRC to compensate for PIG-U loss. Next, the status of immune-based therapies (antibodies, ADCs, CAR-T therapy, and tumor vaccine) was reviewed (see **Figure 5**). Encouragingly, many therapies advanced to clinical trials. Indeed, GPI-AP immunotherapies have improved response rate, overall survival and progression free survival when combined conventional chemotherapies. However, when testing GPI-AP immunotherapies alone, clinical trials results were controversial, where some studies showed significant improvement in response rate compared to control group (treated with standard chemotherapies), while other studies failed to show significant response rate improvement. These findings surely call for continuous research in this field, with the possibility of trying other therapies like genetic targeting with siRNAs and CRISPR/CAS, especially with expansion of non-coding RNAs targeting GPI-APs. As we mentioned; miR-219 targeted GPC-3, while miR-21, miR-611 and miR-877 targeted MSLN (100, 122, 123). In addition, our recent work showed that miR-2355 targeted PIG-C and MSLN mRNAs (121). PIG-C manipulation has also significantly impacted MSLN surface level (121). Another example is the success of CRISPR-Cas9-engineered mouse model for GPI anchor deficiency to resemble human phenotype (134). Additionally, PIG-V knock-out

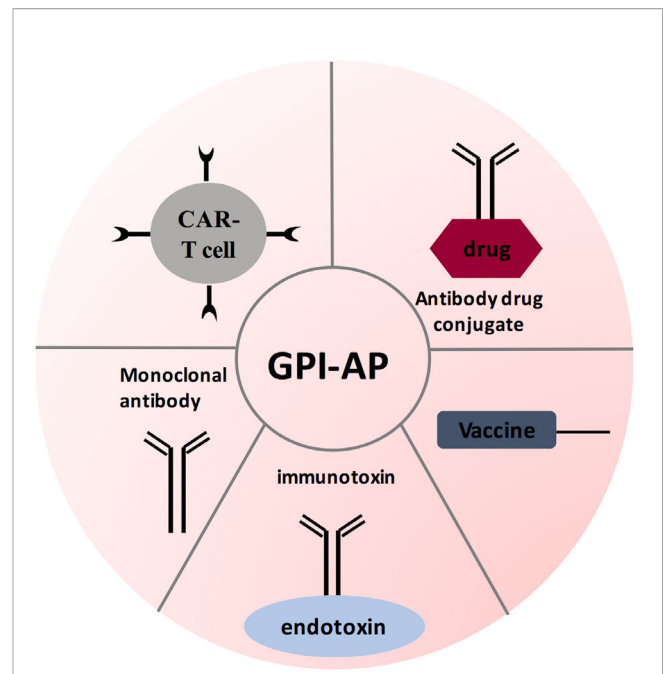


FIGURE 5 | GPI-AP-targeted immunotherapy strategies. Several therapeutic strategies have been designed for targeting GPI-AP on tumor cells: tumor vaccine strategy antibody-based therapies; and adoptive CAR T- cell therapy. These therapies are being evaluated in phase I and/or phase II clinical trials.

resulted in hippocampal synaptic dysfunctions (134). These findings inevitably prompt the utilization of RNA interference therapy to target GPI pathway genes as well as GPI-APs in cancer, whereby blocking GPI pathway can be a promising therapy as multiple signaling pathways will be cut off, causing death of cancer cells.

AUTHOR CONTRIBUTIONS

All authors contributed to the article and approved the submitted version.

ACKNOWLEDGMENTS

The authors wish to thank English Language Department, German University in Cairo for revising manuscript. Also, the authors would like to thank Esraa Atef Salama for her support in the figures.

SUPPLEMENTARY MATERIAL

The Supplementary Material for this article can be found online at: <https://www.frontiersin.org/articles/10.3389/fonc.2020.537311/full#supplementary-material>

REFERENCES

- International Agency for Research on Cancer (IARC) Cancer Fact sheet (2018). Available at: <https://www.who.int/en/news-room/fact-sheets/detail/cancer> [Retrieved November 08, 2019].
- National Cancer Institute. Risk Factors for Cancer (2015). Available from: <https://www.cancer.gov/about-cancer/causes-prevention/risk>.
- Hanahan D, Weinberg RA. The Hallmarks of Cancer Review. *Cell* (2000) 100:57–70. doi: 10.1016/S0092-8674(00)81683-9
- Hanahan D, Weinberg RA. Hallmarks of Cancer: The Next Generation. *Cell* (2011) 144:646–74. doi: 10.1016/j.cell.2011.02.013
- Lodig H, Berk A, Kaiser CA, Kreiger M, Scott MP, Bretcher A, et al. Chapter 13: Types of membrane proteins. In: *Molecular Cell Biology*, 6th ed. NY: W.H. Freeman and Company (2007). p. 100–50.
- Nelson DL, Cox MM. *Principles of Biochemistry*. 5th ed. New York, NY: W.H. Freeman and Company (2008). p. 377.
- Ott CM, Lingappa VR. Integral membrane protein biosynthesis : why topology is hard to predict. (2009) 115(10):2003–9.
- Dunn J, Rao S. Epigenetics and immunotherapy: The current state of play. *Mol Immunol* (2017) 87:227–39. doi: 10.1016/j.molimm.2017.04.012
- Kinoshita T. Biosynthesis and biology of mammalian GPI-anchored proteins. *Open Biol* (2020) 10190290:1–16. doi: 10.1098/rsob.190290
- Manea E. A step closer in defining glycosylphosphatidylinositol anchored proteins role in health and glycosylation disorders. *Mol Genet Metab Rep* (2018) 16:67–75. doi: 10.1016/j.ymgmr.2018.07.006
- Johnson B, Mahadevan D. Emerging role and targeting of carcinoembryonic antigen-related cell adhesion molecule 6 (CEACAM6) in human malignancies. *Clin Cancer Drugs* (2015) 2(2):100–11. doi: 10.2174/2212697X02666150602215823
- Ho M. Advances in Liver Cancer Antibody Therapies. *BioDrugs* (2011) 25 (5):275–84. doi: 10.2165/11595360-000000000-00000
- Ferguson MAJ, Hart GW, Kinoshita T. *Chapter 12 Glycosylphosphatidylinositol Anchors*. Cold Spring Harbor Laboratory Press (2017). pp. 1–19. doi: 10.1101/glycobiology.3e.012.
- Taylor DR, Hooper NM. GPI-Anchored Proteins in Health and Disease. In: *C. J. Vidal (Ed.), Post-Translational Modifications in Health and Disease* (pp. 39–55). New York, NY: Springer New York (2008). doi: 10.1007/978-1-4419-6382-6
- Guo Z, Bishop L. 7.4 Chemical Synthesis of Glycosylphosphatidylinositol (GPI) Anchors and GPI-Linked Structures. *Glycoscience* (2008) 1697. doi: 10.1007/978-3-540-30429-6_42
- Kinoshita T, Fujita M, Maeda Y. Biosynthesis, remodelling and functions of mammalian GPI-anchored proteins: recent progress. *J Biochem* (2008) 144 (3):287–94. doi: 10.1093/jb/mvn090
- Paulick MG, Bertozzi CR. The glycosylphosphatidylinositol anchor: a complex membrane-anchoring structure for proteins. *Biochemistry* (2008) 47(27):6991–7000. doi: 10.1021/bi8006324
- Lai JP, Oseini AM, Moser CD, Yu C, Elswa SF, Hu C, et al. The oncogenic effect of sulfatase 2 in human hepatocellular carcinoma is mediated in part by glypican 3-dependent Wnt activation. *Hepatology* (2010) 52(5):1680–9. doi: 10.1002/hep.23848
- Kinoshita T. Biosynthesis and deficiencies of glycosylphosphatidylinositol. *Proc Japan Academy Ser B* (2014) 90(4):130–43. doi: 10.2183/pjab.90.130
- Zhao P, Nairn AV, Hester S, Moremen KW, O'Regan RM, Oprea G, et al. Proteomic identification of glycosylphosphatidylinositol anchor-dependent membrane proteins elevated in breast carcinoma. *J Biol Chem* (2012) 287 (30):25230–40. doi: 10.1074/jbc.M112.339465
- Carmody LC, Blau H, Danis D, Zhang XA, Gouridine J-P, Vasilevsky N, et al. Significantly different clinical phenotypes associated with mutations in synthesis and transamidase+remodeling glycosylphosphatidylinositol (GPI)-anchor biosynthesis genes. *Orphanet J Rare Dis* (2020) 15:40. doi: 10.1186/s13023-020-1313-0
- Li Y, Yang L, Yang J, Shi J, Chai P, Ge S, et al. A novel variant in GPAA1, encoding a GPI transamidase complex protein, causes inherited vascular anomalies with various phenotypes. *Hum Genet* (2020) 139:1499–511. doi: 10.1007/s00439-020-02192-w
- Holtz AM, Harrington AW, McNamara ER, Kielian A, Soul JS, Martinez-Ojeda M, et al. Expanding the phenotypic spectrum of Mabry Syndrome with novel PIGO gene variants associated with hyperphosphatasia, intractable epilepsy, and complex gastrointestinal and urogenital malformations. *Eur J Med Genet* (2020) 63(4):103802. doi: 10.1016/j.jemg.2019.103802. ISSN 1769-7212.
- Zhang L, Mao X, Long H, Xiao B, Luo Z, Xiao W, et al. Compound Heterozygous PIGS Variants Associated With Infantile Spasm, Global Developmental Delay, Hearing Loss, Visual Impairment, and Hypotonia. *Front Genet* (2020) 11:564. doi: 10.3389/fgene.2020.00564
- Vetro A, Pisano T, Chiaro S, Procopio E, Guerra A, Parrini E, et al. Early infantile epileptic-dyskinetic encephalopathy due to biallelic PIGP mutations. *Neurol Genet* (2020) 6(1):e387. doi: 10.1212/NXG.0000000000000387. Simona.
- Johnstone DL, Nguyen TTM, Zamboni J, Kristin DK, Anik SD, Taila H, et al. Early infantile epileptic encephalopathy due to biallelic pathogenic variants in PIGQ: Report of seven new subjects and review of the literature. *J Inher Metab Dis* (2020) 1–12. doi: 10.1002/jimd.12278
- Li J, Lin Y, Chen L, Qin H, Tan J, Zou D, et al. Identification of acquired PIGA mutations and additional variants by next-generation sequencing in paroxysmal nocturnal hemoglobinuria. *Int J Lab Hematol* (2020) 42:473–81. doi: 10.1111/ijlh.13228
- Kesslering R, Thiel A, Pries R, Fichtner-Feigl S, Brunner S, Seidel P, et al. The complement receptors CD46, CD55 and CD59 are regulated by the tumour microenvironment of head and neck cancer to facilitate escape of complement attack. *Eur J Cancer* (2014) 50(12):2152–61. doi: 10.1016/j.ejca.2014.05.005
- Zhang M, Wang HZ, Li HO, Zhou YJ, Peng RY, Liu J, et al. Identification of PIGU as the Hub Gene Associated with KRAS Mutation in Colorectal Cancer by Coexpression Analysis. *DNA Cell Biol* (2020) 29(suppl 10):mdy487–035. doi: 10.1089/dna.2020.5574
- Armanios MM, Abdel Tawab R, El Tayebi HM. 104P PIG-C and SOCS3: Potential immunotargets regulated by non-coding RNAs in TNBC. *Ann Oncol* (2018) 29(suppl_10):mdy487–035. doi: 10.1093/annonc/mdy487.035
- Liu Y, Yang Z, Du F, Yang Q, Hou J, Yan X, et al. Molecular mechanisms of pathogenesis in hepatocellular carcinoma revealed by RNA sequencing. *Mol Med Rep* (2017) 16(5):6674–6682. doi: 10.3892/mmr.2017.7457
- Wu G, Guo Z, Chatterjee A, Huang X, Rubin E, Wu F, et al. Overexpression of glycosylphosphatidylinositol (GPI) transamidase subunits phosphatidylinositol glycan class T and/or GPI anchor attachment 1 induces tumorigenesis and contributes to invasion in human breast cancer. *Cancer Res* (2006) 66:9829–36. doi: 10.1158/0008-5472.CAN-06-0506
- Medof ME, Lublin DM, Holers VM, Ayers DJ, Getty RR, Leykam JF, et al. Cloning and characterization of cDNAs encoding the complete sequence of decay-accelerating factor of human complement. *Proc Natl Acad Sci U.S.A.* (1987) 84(7):2007–11. doi: 10.1073/pnas.84.7.2007
- Davies A, Simmons DL, Hale G, Harrison RA, Tighe H, Lachmann PJ, et al. CD59, an LY-6-like protein expressed in human lymphoid cells, regulates the action of the complement membrane attack complex on homologous cells. *J Exp Med* (1989) 170:637. doi: 10.1084/jem.170.3.637
- Spendlove III, Ramage J, Bradley R, Harris C, Durrant L. Complement decay accelerating factor (DAF)/CD55 in cancer. *Cancer Immunol Immunother CII* (2006) 55:987–95. doi: 10.1007/s00262-006-0136-8
- Li B, Lin H, Fan J, Lan J, Zhong Y, Yang Y, et al. CD59 is overexpressed in human lung cancer and regulates apoptosis of human lung cancer cells. *Int J Oncol* (2013) 43(3):850–8. doi: 10.3892/ijo.2013.2007
- Shang Y, Chai N, Gu Y, Ding L, Yang Y, Zhou J, et al. Systematic immunohistochemical analysis of the expression of CD46, CD55, and CD59 in colon cancer. *Arch Pathol Lab Med* (2014) 138(7):910–9. doi: 10.5858/arpa.2013-0064-OA
- Zhang Y, Zhang Z, Cao L, Lin J, Yang Z, Zhang X. A common CD55 rs2564978 variant is associated with the susceptibility of non-small cell lung cancer. *Oncotarget* (2017) 8(4):6216. doi: 10.18632/oncotarget.14053
- He Z, Wu H, Jiao Y, Zheng J. Expression and prognostic value of CD97 and its ligand CD55 in pancreatic cancer. *Oncol Lett* (2015) 9(2):793–7. doi: 10.3892/ol.2014.2751
- Ninomiya H, Sims PJ. The human complement regulatory protein CD59 binds to the alpha-chain of C8 and to the "b" domain of C9. *J Biol Chem* (1992) 267(19):13675–80.

41. Murray EW, Robbins SM. Antibody cross-linking of the glycosylphosphatidylinositol-linked protein CD59 on hematopoietic cells induces signaling pathways resembling activation by complement. *J Biol Chem* (1998) 273(39):25279–84. doi: 10.1074/jbc.273.39.25279
42. Bonfini L, Migliaccio E, Pelicci G, Lanfranccone L, Pelicci P. Not all Shc's roads lead to Ras. *Trends Biochem Sci* (1996) 21:257–61. doi: 10.1016/S0968-0004(96)10033-5
43. Damen JE, Lui L, Rosten P, Humphries RK, Jefferson AB, Majerus PW, et al. The 145-kDa protein induced to associate with Shc by multiple cytokines is an inositol tetrakisphosphate and phosphatidylinositol 3, 4, 5-trisphosphate 5-phosphatase. *Proc Natl Acad Sci USA* (1996) 93:1689–93. doi: 10.1073/pnas.93.4.1689
44. Liu L, Damen JE, Hughes MR, Babic I, Jirik FR, Krystal G. The Src homology 2 (SH2) domain of SH2-containing inositol phosphatase (SHIP) is essential for tyrosine phosphorylation of SHIP, its association with Shc, and its induction of apoptosis. *J Biol Chem* (1997) 272:8983–8. doi: 10.1074/jbc.272.14.8983
45. Song Q, Zhang Z, Liu Y, Han S, Zhang X. The tag SNP rs10746463 in decay-accelerating factor is associated with the susceptibility to gastric cancer. *Mol Immunol* (2015) 63(2):473–8. doi: 10.1016/j.molimm.2014.10.006
46. Shang Y, Chai N, Gu Y, Ding L, Yang Y, Zhou J, et al. Systematic immunohistochemical analysis of the expression of CD46, CD55, and CD59 in colon cancer. *Arch Pathol Lab Med* (2014) 138(7):910–9. doi: 10.5858/arpa.2013-0064-OA
47. Kapka-Skrzypczak L, Wolinska E, Szparek G, Wilczynski GM, Czajka M, Skrzypczak M. CD55, CD59, factor H and factor H-like 1 gene expression analysis in tumors of the ovary and corpus uteri origin. *Immunol Lett* (2015) 167(2):67–71. doi: 10.1016/j.imlet.2015.06.017
48. Mo X, Leung THY, Siu MKY, Ngan HYS. Elucidating the potential role of membrane complement regulatory proteins (CD46, CD55, CD59) in tumorigenesis of cervical cancer. (2020). doi: 10.1158/1538-7445.AM2020-3816
49. Ziller F, Macor P, Bulla R, Sblattero D, Marzari R, Tedesco F. Controlling complement resistance in cancer by using human monoclonal antibodies that neutralize complement-regulatory proteins CD55 and CD59. *Eur J Immunol* (2005) 35(7):2175–83. doi: 10.1002/eji.200425920
50. Macor P, Tripodo C, Zorzet S, Piovani E, Bossi F, Marzari R, et al. In vivo targeting of human neutralizing antibodies against CD55 and CD59 to lymphoma cells increases the antitumor activity of rituximab. *Cancer Res* (2007) 67(21):10556–63. doi: 10.1158/0008-5472.CAN-07-1811
51. Durrant LG. (2017), 363. U.S. Patent Application No. 15/404.
52. Heery C, Tesfaye A, Weinberg B, Marshall J. Chapter 3 Therapeutic Cancer Vaccines. In: *Immunotherapy for Gastrointestinal Cancer*. Cham: Springer (2017). doi: 10.1007/978-3-319-43063-8_3
53. Sivasankar B, Longhi MP, Gallagher KM, Betts GJ, Morgan BP, Godkin AJ, et al. CD59 blockade enhances antigen-specific CD4+ T cell responses in humans: a new target for cancer immunotherapy? *J Immunol* (2009) 182(9):5203–7. doi: 10.4049/jimmunol.0804243
54. Yin H, Li C, Wang S, Guo Q, Ren X, Jiang G. Silencing of CD59 enhanced the sensitivity of HT29 cells to 5-Fluorouracil and Oxaliplatin. *J Infect Chemother* (2015) 21(1):8–15. doi: 10.1016/j.jiac.2014.08.020
55. Macor P, Tripodo C, Zorzet S, Piovani E, Bossi F, Marzari R, et al. In vivo targeting of human neutralizing antibodies against CD55 and CD59 to lymphoma cells increases the antitumor activity of rituximab. *Cancer Res* (2007) 67(21):10556–63. doi: 10.1158/0008-5472.CAN-07-1811
56. Wang Y, Yang YJ, Wang Z, Liao J, Liu M, Zhong XR, et al. CD55 and CD59 expression protects HER2-overexpressing breast cancer cells from trastuzumab-induced complement-dependent cytotoxicity. *Oncol Lett* (2017) 14(3):2961–9. doi: 10.3892/ol.2017.6555
57. Holt DS, Botto M, Bygrave AE, Hanna SM, Walport MJ, Morgan BP. Targeted deletion of the CD59 gene causes spontaneous intravascular hemolysis and hemoglobinuria. *Blood J Am Soc Hematol* (2001) 98(2):442–9. doi: 10.1182/blood.V98.2.442
58. Chauhan D, Nohwal B, Pundir CS. An electrochemical CD59 targeted noninvasive immunosensor based on graphene oxide nanoparticles embodied pencil graphite for detection of lung cancer. *Microchem J* (2020) 156:104957. doi: 10.1016/j.microc.2020.104957
59. Richards SJ, Dickinson AJ, Cullen MJ, Griffin M, Munir T, McKinley C, et al. Presentation clinical, haematological and immunophenotypic features of 1081 patients with GPI-deficient (paroxysmal nocturnal haemoglobinuria) cells detected by flow cytometry. *Br J Haematol* (2020) 189:954–66. doi: 10.1111/bjh.16427
60. Miwa T, Zhou L, Hilliard B, Molina H, Song W-C. Crpy, but not CD59 and DAF, is indispensable for murine erythrocyte protection in vivo from spontaneous complement attack. *Blood* (2002) 99(10):3707–16. doi: 10.1182/blood.V99.10.3707
61. Mauro E, Gherlinzoni F. Efficacy and safety of Eculizumab in Paroxysmal Nocturnal Hemoglobinuria (PNH) after 15 years steroids treatment: A case report description. *International Journal of Medical Reviews and Case Reports* (2019) 3(11):773–6. doi: 10.5455/IJMRRC.Eculizumab-Paroxysmal-Nocturnal-Hemoglobinuria
62. Fattizzo B, Kulasekararaj AG. Second-Generation C5 Inhibitors for Paroxysmal Nocturnal Hemoglobinuria. *BioDrugs* (2020) 34:149–58. doi: 10.1007/s40259-019-00401-1
63. Thielen AJF, van Baarsen IM, Jongsma ML, Zeerleder S, Spaapen RM, Wouters D. CRISPR/Cas9 generated human CD46, CD55 and CD59 knockout cell lines as a tool for complement research. *J Immunol Methods* (2018) 456:15–22. doi: 10.1016/j.jim.2018.02.004. ISSN 0022-1759.
64. Hammarström S. The carcinoembryonic antigen (CEA) family: structures, suggested functions and expression in normal and malignant tissues. *Semin Cancer Biol* (1999) 9(2):67–81. doi: 10.1006/scbi.1998.0119
65. Xu J, Liu B, Ma S, Zhang J, Ji Y, Xu L, et al. Characterizing the tumor suppressor role of CEACAM1 in multiple myeloma. *Cell Physiol Biochem* (2018) 45(4):1631–40. doi: 10.1159/000487730
66. Eidelman FJ, Fuks A, DeMarte L, Taheri M, Stanners CP. Human carcinoembryonic antigen, an intercellular adhesion molecule, blocks fusion and differentiation of rat myoblasts. *J Cell Biol* (1993) 123(2):467–75. doi: 10.1083/jcb.123.2.467
67. Camacho-Leal P, Zhai AB, Stanners CP. A co-clustering model involving alpha5beta1 integrin for the biological effects of GPI- anchored human carcinoembryonic antigen (CEA). *J Cell Phys* (2007) 211(3):791–802. doi: 10.1002/jcp.20989
68. Duxbury MS, Ito H, Ashley SW, Whang EE. CEACAM6 crosslinking induces caveolin-1-dependent, Src-mediated focal adhesion kinase phosphorylation in BxPC3 pancreatic adenocarcinoma cells. *J Bio Chem* (2004) 279:23176–82. doi: 10.1074/jbc.M402051200
69. Takeuchi A, Yokoyama S, Nakamori M, Nakamura M, Ojima T, Yamaguchi S, et al. Loss of CEACAM1 is associated with poor prognosis and peritoneal dissemination of patients with gastric cancer. *Sci Rep* (2019) 9(1):1–9. doi: 10.1038/s41598-019-49230-w
70. Scholz S, Zimmermann W, Schwarzkopf G, Grunert F, Rogaczewski B, Thompson J. Carcinoembryonic antigen family members CEACAM6 and CEACAM7 are differentially expressed in normal tissues and oppositely deregulated in hyperplastic colorectal polyps and early adenomas. *Am J Pathol* (2000) 157:1051–2. doi: 10.1016/S0002-9440(10)64764-5
71. Blumenthal RD, Leon E, Hansen JH, Goldenberg DM. Expression patterns of CEACAM5 and CEACAM6 in primary and metastatic cancers. *BMC Cancer* (2007) 7:2. doi: 10.1186/1471-2407-7-2
72. Li L, He P, Zhou C, Jing L, Dong B, Chen S, et al. A novel bispecific antibody, S-Fab, induces potent cancer cell killing. *J Immunother* (2015) 38(9):350–6. doi: 10.1097/CJI.0000000000000099
73. Bacac M, Fauti T, Sam J, Colombetti S, Weinzierl T, Ouaret D, et al. A novel carcinoembryonic antigen T-cell bispecific antibody (CEA TCB) for the treatment of solid tumors. *Clin Cancer Res* (2016) 22(13):3286–97. doi: 10.1158/1078-0432.CCR-15-1696
74. Duxbury MS, Ito H, Ashley SW, Wang EE. CEACAM6 as a novel target for indirect type 1 immunotoxin-based therapy in pancreatic adenocarcinoma. *Biochem Biophys Res Commun* (2004) 317:837–43. doi: 10.1016/j.bbrc.2004.03.128
75. Shirasu N, Yamada H, Shibaguchi H, Kuroki M, Kuroki M. Potent and specific antitumor effect of CEA-targeted photoimmunotherapy. *Int J Cancer* (2014) 135(11):2697–710. doi: 10.1002/ijc.28907
76. Thistlethwaite FC, Gilham DE, Guest RD, Rothwell DG, Pillai M, Burt DJ, et al. The clinical efficacy of first-generation carcinoembryonic antigen (CEACAM5)-specific CAR T cells is limited by poor persistence and transient pre-conditioning-dependent respiratory toxicity. *Cancer*

- Immunol Immunother* (2017) 66(11):1425–36. doi: 10.1007/s00262-017-2034-7
77. Katz SC, Burga RA, McCormack E, Wang LJ, Mooring W, Point GR, et al. Phase I hepatic immunotherapy for metastases study of intra-arterial chimeric antigen receptor-modified T-cell therapy for CEA+ liver metastases. *Clin Cancer Res* (2015) 21(14):3149–59. doi: 10.1158/1078-0432.CCR-14-1421
 78. Tiernan JP, Ingram N, Marston G, Perry SL, Rushworth JV, Coletta PL, et al. CEA-targeted nanoparticles allow specific in vivo fluorescent imaging of colorectal cancer models. *Nanomedicine* (2015) 10(8):1223–31. doi: 10.2217/nnm.14.202
 79. Hasanzadeh M, Shadjou N, Lin Y, de la Guardia M. Nanomaterials for use in immunosensing of carcinoembryonic antigen (CEA): Recent advances. *TrAC Trends Anal Chem* (2017) 86:185–205. doi: 10.1016/j.trac.2016.11.003
 80. Wang W, Xu X, Tian B, Wang Y, Du L, Sun T, et al. The diagnostic value of serum tumor markers CEA, CA19-9, CA125, CA15-3, and TPS in metastatic breast cancer. *Clinica Chimica Acta* (2017) 470:51–5. doi: 10.1016/j.cca.2017.04.023
 81. Jain P, Mondal SK, Sinha SK, Mukhopadhyay M, Chakraborty I. Diagnostic and prognostic significance of different mucin expression, preoperative CEA, and CA-125 in colorectal carcinoma: A clinicopathological study. *J Natural Sci Biol Med* (2014) 5(2):404. doi: 10.4103/0976-9668.136207
 82. Primrose JN, Perera R, Gray A, Rose P, Fuller A, Corkhill A, et al. Effect of 3 to 5 years of scheduled CEA and CT follow-up to detect recurrence of colorectal cancer: the FACS randomized clinical trial. *Jama* (2014) 311(3):263–70. doi: 10.1001/jama.2013.285718
 83. Wu SG, He ZY, Ren HY, Yang LC, Sun JY, Li FY, et al. Use of CEA and CA15-3 to predict axillary lymph node metastasis in patients with breast cancer. *J Cancer* (2016) 7(1):37. doi: 10.7150/jca.13090
 84. Verberne CJ, Wiggers T, Grossmann I, Bock GH, Vermeulen KM. Cost-effectiveness of a carcinoembryonic antigen (CEA) based follow-up programme for colorectal cancer (the CEA Watch trial). *Colorectal Dis* (2016) 18(3):O91–6. doi: 10.1111/codi.13273
 85. Feng M, Ho M. Glypican-3 antibodies: a new therapeutic target for liver cancer. *FEBS Lett* (2014) 588(2):377–82. doi: 10.1016/j.febslet.2013.10.002
 86. Filmus J, Capurro M. Glypican-3: a marker and a therapeutic target in hepatocellular carcinoma. *FEBS J* (2013) 280(10):2471–6. doi: 10.1111/febs.12126
 87. Lai JP, Sandhu DS, Yu C, Han T, Moser CD, Jackson KK, et al. Sulfatase 2 up-regulates glypican 3, promotes fibroblast growth factor signaling, and decreases survival in hepatocellular carcinoma. *Hepatology* (2008) 47(4):1211–22. doi: 10.1002/hep.22202
 88. Kim H, Xu GL, Borczuk AC, Busch S, Filmus J, Capurro M, et al. The heparan sulfate proteoglycan GPC3 is a potential lung tumor suppressor. *Am J Respir Cell Mol Biol* (2003) 29(6):694–701. doi: 10.1165/rcmb.2003-0061OC
 89. Shirakawa H, Suzuki H, Shimomura M, Kojima M, Gotohda N, Takahashi S, et al. Glypican-3 expression is correlated with poor prognosis in hepatocellular carcinoma. *Cancer Sci* (2009) 100(8):1403–7. doi: 10.1111/j.1349-7006.2009.01206.x
 90. Luo JH, Ren B, Keryanov S, Tseng GC, Rao UN, Monga SP, et al. Transcriptomic and genomic analysis of human hepatocellular carcinomas and hepatoblastomas. *Hepatology* (2006) 44(4):1012–24. doi: 10.1002/hep.21328
 91. Azizpour S, Ezati R, Saidijam M, Razavi AE, Jalilian FA, Mahdavinizhad A, et al. The Expression of Glypican-3 in Colorectal Cancer. *Cytol Genet* (2019) 53(5):430–40. doi: 10.3103/S0095452719050037
 92. Umezu T, Shibata K, Kajiyama H, Yamamoto E, Nawa A, Kikkawa F. Glypican-3 expression predicts poor clinical outcome of patients with early-stage clear cell carcinoma of the ovary. *J Clin Pathol* (2010) 63:962–6. doi: 10.1136/jcp.2010.080234
 93. Andisheh-Tadbir A, Ranjbar MA. Glypican-3 Expression in Patients with Oral Squamous Cell Carcinoma. *J Dentist* (2020) 21(2):141. doi: 10.30476/DENTJODS.2019.84541.1089
 94. Murthy SS, Shen T, De Rienzo A, Lee WC, Ferriola PC, Jhanwar SC, et al. Expression of GPC3, an X-linked recessive overgrowth gene, is silenced in malignant mesothelioma. *Oncogene* (2000) 19(3):410–6. doi: 10.1038/sj.onc.1203322
 95. Boily G, Saikali Z, Sinnett D. Methylation analysis of the glypican 3 gene in embryonal tumours. *Br J Cancer* (2004) 90(8):1606–11. doi: 10.1038/sj.bjc.6601716
 96. Ishiguro T, Sugimoto M, Kinoshita Y, Miyazaki Y, Nakano K, Tsunoda H, et al. Anti-glypican 3 antibody as a potential antitumor agent for human liver cancer. *Cancer Res* (2008) 68(23):9832–8. doi: 10.1158/0008-5472.CAN-08-1973
 97. Nakano K, Orita T, Nezu J, Yoshino T, Ohizumi I, Sugimoto M, et al. Anti-glypican 3 antibodies cause ADCC against human hepatocellular carcinoma cells. *Biochem Biophys Res Commun* (2009) 378(2):279–84. doi: 10.1016/j.bbrc.2008.11.033
 98. Zhu AX, Gold PJ, El-khoueiry A, Abrams TA, Morikawa H, Ohishi N, et al. First-in-man phase I study of GC33, a novel recombinant humanized antibody against glypican-3, in patients with advanced hepatocellular carcinoma. *Clin Cancer Res* (2013) clincanres-2616. doi: 10.1158/1078-0432.CCR-12-2616
 99. Sawada Y, Yoshikawa T, Nobuoka D, Shirakawa H, Kurokawa T, Motomura Y, et al. Phase I trial of glypican-3-derived peptide vaccine for advanced hepatocellular carcinoma showed immunological evidence and potential for improving overall survival. *Clin Cancer Res* (2012) clincanres-3044. doi: 10.1158/1078-0432.CCR-11-3044
 100. Huang N, Lin J, Ruan J, Su N, Qing R, Liu F, et al. MiR-219-5p inhibits hepatocellular carcinoma cell proliferation by targeting glypican-3. *FEBS Lett* (2012) 586(6):884–91. doi: 10.1016/j.febslet.2012.02.017
 101. Haradwaj U, Marin-Muller C, Li M, Chen C, Yao Q. Mesothelin confers pancreatic cancer cell resistance to TNF- α -induced apoptosis through Akt/PI3K/NF- κ B activation and IL-6/Mcl-1 overexpression. *Mol Cancer* (2011) 10:106. doi: 10.1186/1476-4598-10-106
 102. Pastan I, Hassan R. Discovery of mesothelin and exploiting it as a target for immunotherapy. *Cancer Res* (2014) 74(11):2907–12. doi: 10.1158/0008-5472.CAN-14-0337
 103. Tang Z, Qian M, Ho M. The role of mesothelin in tumor progression and targeted therapy. *Anti Cancer Agents Medicinal Chem (Formerly Curr Medicinal Chemistry Anti Cancer Agents)* (2013) 13(2):276–80. doi: 10.2174/1871520611313020014
 104. Bharadwaj U, Marin-Muller C, Li M, Chen C, Yao Q. Mesothelin overexpression promotes autocrine IL-6/sIL-6R trans-signaling to stimulate pancreatic cancer cell proliferation. *Carcinogenesis* (2011) 32(7):1013–24. doi: 10.1093/carcin/bgr075
 105. Zhenjiang L, Rao M, Luo X, Sandberg E, Bartek J Jr, Schoutrop E, et al. Mesothelin-specific immune responses predict survival of patients with brain metastasis. *EBioMedicine* (2017) 23:20–4. doi: 10.1016/j.ebiom.2017.08.024
 106. Wang M, Li A, Sun G, Mbuagbaw L, Reid S, Lovrics PJ, et al. Association between mesothelin expression and survival outcomes in patients with triple-negative breast cancer: a protocol for a systematic review. *Systematic Rev* (2016) 5(1):133. doi: 10.1186/s13643-016-0313-6
 107. Parinyanitikul N, Blumenschein GR, Wu Y, Lei X, Chavez-MacGregor M, Smart M, et al. Mesothelin expression and survival outcomes in triple receptor negative breast cancer. *Clin Breast Cancer* (2013) 13(5):378–84. doi: 10.1016/j.clbc.2013.05.001
 108. Mizukami T, Kamachi H, Fujii Y, Matsuzawa F, Einama T, Kawamata F, et al. The anti-mesothelin monoclonal antibody amatuximab enhances the anti-tumor effect of gemcitabine against mesothelin-high expressing pancreatic cancer cells in a peritoneal metastasis mouse model. *Oncotarget* (2018) 9(73):33844–52. doi: 10.18632/oncotarget.26117
 109. Morello A, Sadelain M, Adusumilli PS. Mesothelin-targeted CARs: driving T cells to solid tumors. *Cancer Discovery* (2016) 6(2):133–46. doi: 10.1158/2159-8290.CD-15-0583
 110. Bendell J, Blumenschein G, Zinner R, Hong D, Jones S, Infante J, et al. First-in-human phase I dose escalation study of a novel anti-mesothelin antibody drug conjugate, BAY 94-9343. patients with advanced solid tumors. (2013) Washington, DC: American Association of Cancer Research.
 111. Liu W, Onda M, Lee B, Kreitman RJ, Hassan R, Xiang L, et al. Recombinant immunotoxin engineered for low immunogenicity and antigenicity by identifying and silencing human B-cell epitopes. *Proc Natl Acad Sci USA* (2012) 109:11782–7. doi: 10.1073/pnas.1209292109
 112. Mazon R, Vassall AN, Eberle JA, Beers R, Weldon JE, Venzon DJ, et al. Identification and elimination of an immunodominant T-cell epitope in

- recombinant immunotoxins based on *Pseudomonas* exotoxin A. *Proc Natl Acad Sci U.S.A.* (2012) 109:E3597–603. doi: 10.1073/pnas.1218138109
113. Hassan R, Jahan TM, Kindler HL, Bazhenova L, Reck M, Pastan I, et al. Amatuximab, a chimeric monoclonal antibody to mesothelin, in combination with pemetrexed and cisplatin in patients with unresectable pleural mesothelioma: results of a multicenter phase II clinical trial. *J Clin Oncol* (2012) suppl; abstr 7030:30. doi: 10.1200/jco.2012.30.15_suppl.7030
 114. ClinicalTrials.gov. Identifier: NCT00570713 An efficacy study of MORAB-009 in subjects with pancreatic cancer. Available at: <https://clinicaltrials.gov/ct2/show/results/NCT00570713>
 115. Hassan R, Cohen SJ, Phillips M, Pastan I, Sharon E, Kelly RJ, et al. Phase I clinical trial of the chimeric anti-mesothelin monoclonal anti- body MORAB-009 in patients with mesothelin-expressing cancers. *Clin Cancer Res* (2010) 16:6132–8. doi: 10.1158/1078-0432.CCR-10-2275
 116. Beatty GL, Haas AR, Maus MV, Torigian DA, Soulen MC, Plesa G, et al. Mesothelin-specific chimeric antigen receptor mRNA-engineered T cells induce anti-tumor activity in solid malignancies. *Cancer Immunol Res* (2014) 2:112–20. doi: 10.1158/2326-6066.CIR-13-0170
 117. ClinicalTrials.gov. Identifier: NCT01897415 Autologous redirected RNA meso CAR T cells for pancreatic cancer. Available at: <https://clinicaltrials.gov/ct2/show/record/NCT01897415>
 118. ClinicalTrials.gov. Identifier: NCT01583686 Treating cancer with anti-mesothelin modified lymphocytes. Available at: <https://clinicaltrials.gov/ct2/show/results/NCT01583686>
 119. Le DT, Brockstedt DG, Nir-Paz R, Hampl J, Mathur S, Nemunaitis J, et al. A live-attenuated *Listeria* vaccine (ANZ-100) and a live-attenuated *Listeria* vaccine expressing mesothelin (CRS-207) for advanced cancers: phase I studies of safety and immune induction. *Clin Cancer Res* (2012) 18:858–68. doi: 10.1158/1078-0432.CCR-11-2121
 120. Le DT, Wang-Gillam A, Picozzi V Jr, Gretten TF, Crocenzi TS, Springett GM, et al. A phase 2, randomized trial of GVAX pancreas and CRS-207 immunotherapy versus GVAX alone in patients with metastatic pancreatic adenocarcinoma: updated results. *J Clin Oncol* (2014) 32. (suppl 3; abstr 177):177–177. doi: 10.1200/jco.2014.32.3_suppl.177
 121. Hussein NH, El Tayebi HM, de Bruyn M. Neat-1: Culpit lncRNA tying PIG-C, MSLN, CD80 in TNBC. *Ann OF Oncol* (2019) 30:782–2. doi: 10.1093/annonc/mdz268.066
 122. De Santi C, Vencken S, Blake J, Haase B, Benes V, Gemignani F, et al. Identification of MiR-21-5p as a functional regulator of mesothelin expression using MicroRNA capture affinity coupled with next generation sequencing. *PloS One* (2017) 12(1):e0170999. doi: 10.1371/journal.pone.0170999
 123. Garritano S, De Santi C, Silvestri R, Melaiu O, Cipollini M, Barone E, et al. A common polymorphism within MSLN affects miR-611 binding site and soluble mesothelin levels in healthy people. *J Thoracic Oncol* (2014) 9 (11):1662–8. doi: 10.1097/JTO.0000000000000322
 124. Heider S, Dangerfield JA, Metzner C. Biomedical applications of glycosylphosphatidylinositol-anchored proteins. *J Lipid Res* (2016) 57 (10):1778–88. doi: 10.1194/jlr.R070201
 125. Zhao P, Nairn AV, Hester S, Moremen KW, O'Regan RM, Oprea G, et al. Proteomic identification of glycosylphosphatidylinositol anchor-dependent membrane proteins elevated in breast carcinoma. *J Biol Chem* (2012) 287 (30):25230–40. doi: 10.1074/jbc.M112.339465
 126. Pierce JM, Abbott KL. (2014). U.S. Patent Application No. 14/166,034.
 127. Dolezal S, Hester S, Kirby PS, Nairn A, Pierce M, Abbott KL. Elevated levels of glycosylphosphatidylinositol (GPI) anchored proteins in plasma from human cancers detected by C. septicum alpha toxin. *Cancer Biomarkers* (2014) 14(1):55–62. doi: 10.3233/CBM-130377
 128. Scholler N, Fu N, Yang Y, Ye Z, Goodman GE, Hellstroem KE, et al. Soluble member(s) of the mesothelin/megakaryocyte potentiating factor family are detectable in sera from patients with ovarian carcinoma. *Proc Natl Acad Sci U.S.A.* (1999) 96:11531–6. doi: 10.1073/pnas.96.20.11531
 129. Luo L, Shi HZ, Liang QL, Jiang J, Qin SM, Deng JM. Diagnostic value of soluble mesothelin-related peptides for malignant mesothelioma: a meta-analysis. *Respir Med* (2010) 104(1):149–56. doi: 10.1016/j.rmed.2009.05.017
 130. Bandiera E, Zanotti L, Fabricio AS, Bucca E, Squarcina E, Romani C, et al. Cancer antigen 125, human epididymis 4, kallikrein 6, osteopontin and soluble mesothelin-related peptide immunocomplexed with immunoglobulin M in epithelial ovarian cancer diagnosis. *Clin Chem Lab Med* (2013) 51(9):1815–24. doi: 10.1515/cclm-2013-0151
 131. Cui A, Jin XG, Zhai K, Tong ZH, Shi HZ. Diagnostic values of soluble mesothelin-related peptides for malignant pleural mesothelioma: updated meta-analysis. *BMJ Open* (2014) 4(2):e004145. doi: 10.1136/bmjopen-2013-004145
 132. Swarts BM, Guo Z. CHEMICALSYNTHESIS OF GLYCOSYL PHOSPHATIDYLINOSITOL ANCHORS. *Adv Carbohydr Chem Biochem* (2012) 67:137–219. doi: 10.1016/B978-0-12-396527-1.00004-8
 133. Roller RF, Malik A, Carillo MA, Garg M, Rella A, Raulf M-K, et al. Semisynthesis of Functional Glycosylphosphatidylinositol-Anchored Proteins. *Angew Chem Int Ed* (2020) 59:12035. doi: 10.1002/anie.202002479
 134. de los Santos MR, Rivalan M, David FS, Stumpf A, Velasquez LM, Voigt A, et al. A CRISPR-Cas9-engineered mouse model for GPI anchor deficiency mirrors human phenotype and shows hippocampal synaptic dysfunctions. (2020) *bioRxiv* 2020.04.20.050591. doi: 10.1101/2020.04.20.050591. bioRxiv 2020.04.20.050591.

Conflict of Interest: The authors declare that the research was conducted in the absence of any commercial or financial relationships that could be construed as a potential conflict of interest.

Copyright © 2020 Hussein, Amin and El Tayebi. This is an open-access article distributed under the terms of the Creative Commons Attribution License (CC BY). The use, distribution or reproduction in other forums is permitted, provided the original author(s) and the copyright owner(s) are credited and that the original publication in this journal is cited, in accordance with accepted academic practice. No use, distribution or reproduction is permitted which does not comply with these terms.



OPEN ACCESS

Edited by:

Cirino Botta,
Cosenza Hospital, Italy

Reviewed by:

Cristina Pérez Ruiz,
University of Navarra, Spain
Yuichi Iida,
Shimane University, Japan

*Correspondence:

Zhou Ye
yezhou126@126.com

Yang Lu
luyang@ihcams.ac.cn

Yan Jun Zhang
junjunfriend@126.com

Jianxiang Wang
wangjx@ihcams.ac.cn

Dongsheng Xiong
dsxiong@ihcams.ac.cn

†Permanent address:

Dongsheng Xiong,
State Key Laboratory of Experimental
Hematology, National Clinical
Research Center for Blood Diseases,
Institute of Hematology & Blood
Diseases Hospital, Chinese Academy
of Medical Sciences & Peking Union
Medical College, Tianjin, China

Specialty section:

This article was submitted to
Cancer Molecular Targets
and Therapeutics,
a section of the journal
Frontiers in Oncology

Received: 16 October 2020

Accepted: 12 November 2020

Published: 05 January 2021

Citation:

Lin F, Xiong M, Hao W, Song Y,
Liu R, Yang Y, Yuan X, Fan D, Zhang Y,
Hao M, Ye Z, Lu Y, Zhang Y, Wang J
and Xiong D (2021) A Novel
Blockade CD47 Antibody With
Therapeutic Potential for Cancer.
Front. Oncol. 10:615534.
doi: 10.3389/fonc.2020.615534

A Novel Blockade CD47 Antibody With Therapeutic Potential for Cancer

Fangzhen Lin¹, Mengshang Xiong¹, Wei Hao¹, Yuewen Song¹, Ruoqi Liu¹,
Yuanyuan Yang², Xiangfei Yuan³, Dongmei Fan¹, Yizi Zhang⁴, Mu Hao¹, Zhou Ye^{4*},
Yang Lu^{1*}, Yanjun Zhang^{1*}, Jianxiang Wang^{1*} and Dongsheng Xiong^{1*†}

¹ State Key Laboratory of Experimental Hematology, National Clinical Research Center for Blood Diseases, Institute of Hematology & Blood Diseases Hospital, Chinese Academy of Medical Sciences & Peking Union Medical College, Tianjin, China, ² Department of Pharmacy, Tianjin Medical University General Hospital, Tianjin, China, ³ Tianjin Institute of Integrative Medicine for Acute Abdominal Diseases, Tianjin Nankai Hospital, Tianjin, China, ⁴ Central Hospital of Karamay, Karamay, Xinjiang, China

Macrophages as components of the innate immune system play a critical role in antitumor responses. Strategies for targeting CD47 are becoming a hot spot for cancer therapy. The expression of CD47 is exercised by macrophages to make a distinction between “self” or “nonself.” Anti-CD47 antibodies block the interaction between macrophage signal regulatory protein- α (SIRP α) and tumor surface CD47. In this study, we report and assess a novel anti-CD47 blocking antibody named 2C8, which exhibits high affinity and tremendous anticancer effects. More concretely, 2C8 significantly induces macrophages, including protumorigenic subtype M2 macrophages killing tumor cells *in vitro*, and is revealed to be more effective than commercially available anti-CD47 mAb B6H12.2. *In vivo*, 2C8 controls tumor growth and extends survival of xenograft mice. The antitumor ability of 2C8 might be applicable to many other cancers. The generation of a novel CD47 antibody contributes to consolidating clinical interest in targeting macrophages for the treatment of malignancy and, moreover, as a supplement therapy when patients are resistant or refractory to other checkpoint therapies or relapse after such treatments.

Keywords: anti-CD47 mAb, CD47, cancer therapy, immunotherapy, phagocytosis

INTRODUCTION

Multiple lines of evidence indicate that immunotherapies, including checkpoint inhibitors such as programmed cell death protein 1 (PD-1) and cytotoxic T-lymphocyte-associated protein 4 (CTLA-4), are efficient strategies to shoot tumor cells (1). Unfortunately, only a minority of patients with certain tumor types can benefit from durable responses from immunotherapies. Particularly for

Abbreviations: AML, acute myeloid leukemia; ALL, acute lymphocytic leukemia; CART, chimeric antigen receptor T; CTLA-4, cytotoxic T-lymphocyte-associated protein 4; NHL, non-Hodgkin's Lymphoma; PD-1, death protein 1; SIRP α , signal regulatory protein- α ; SDS-PAGE, sodium dodecyl sulfate polyacrylamide gel electrophoresis; TAMs, tumor-associated macrophages.

non-Hodgkin's lymphoma (NHL) and the other solid malignancy patients, little progress has been observed. Poor cell infiltration and an immunosuppressive tumor milieu are important reasons (2).

Tumor-associated macrophages (TAMs) abundantly infiltrate most solid tumors and represent up to 50% of leukocytes in the tumor microenvironment. Generally, TAMs display an M2-like phenotype (anti-inflammatory function); however, macrophages are heterogeneous and can be modulated by the surrounding microenvironment from an M2- to an M1-like phenotype (pro-inflammatory function) (3). The rate of M2/M1 is associated with a poor prognosis in clinical outcomes, including with NHL (4–8). Given that macrophages are required for chemotherapy and immunotherapy (9, 10), targeting TAMs is designed to reprogram TAMs to a tumoricidal phenotype M1 rather than diminish TAMs directly so that it can reinvigorate antitumor immunity. There are multiple strategies for reorienting TAMs, including the CD47 antibody (11–14). One adequate approach that aims to activate TAMs is blocking CD47 (4, 15, 16).

As an integrin-associated protein, CD47 is ubiquitously expressed on the cell surface (17) and mediates immune escape from macrophage-mediated phagocytosis when it interacts with phagocyte-expressed signal regulatory protein alpha (SIRP α), a protein expressed in macrophages and dendritic cells (18). An increased expression of CD47 has been demonstrated in multiple solid and hematological malignancies compared with normal cells, including but not limited to breast (19), small-cell lung (20), colon (21), ovarian (22), acute myeloid leukemia (AML) (23), and acute lymphocytic leukemia (ALL) (24) malignancies. Targeting the CD47–SIRP α axis promotes macrophage migration into the tumor mass (14), leading to TAMs being functionally switched from a tumor-promoting M2-like phenotype to a tumoricidal M1-like phenotype and enabling TAMs to attack the tumor. In xenograft mouse models, blocking CD47 led to an increased presence of M1-like TAMs (12, 13).

We generated 2C8, a novel monoclonal antihuman CD47 antibody that has displayed high specificity and affinity for CD47 protein and stimulates M0, M1, and M2 macrophage-mediated phagocytosis more effectively in comparison to commercially available anti-CD47 mAb B6H12.2 *in vitro*, suppressing tumor growth *in vivo* and, thus, prolonging mouse survival. Above all, the 2C8 antibody, which harnesses the ability to induce macrophages to eliminate tumor cells, is a promising candidate for cancer therapy.

MATERIALS AND METHODS

Cell Culture

The murine fibroblast cell line 3T3; human embryonic kidney cell–derived 293T cell line; human acute T cell leukemia cell line Jurkat; human chronic myelogenous leukemia cell line K562; human colon cancer cell lines hCT116 and SW620; human leukemia cell line HL60; and human B cell lymphoma cell lines Raji, Daudi, and BJAB were obtained from the Institute

of Hematology and Blood Diseases Hospital, Chinese Academy of Medical Science and Peking Union Medical College, Tianjin, China.

Antibody Generation

293T cells were transfected with pCDH-CMV-MCS-EF1-copGFP-CD47 using X-tremeGENE DNA transfection reagents (Roche) for lentiviral production, and concentration was accomplished using standard protocols. Lentivirus was collected for 3T3 cell infection, and 6–8 h later, lentivirus was removed. After 48 h of infection, CD47 expressing 3T3 (3T3-CD47) cells were established as an immunogen. Six-week-old Balb/c mice were immunized with 3T3-CD47 cells at 2-week intervals for a total of 4 weeks. Blood was collected after immunization by tail bleeding for titer assessment. Hybridomas stably expressing CD47 were generated as standard protocols. In brief, the spleen cells were fused with SP2/0 cells. After the limiting dilution, hybridomas stably expressing CD47 were selected, and supernatants from the resulting clones were screened by flow cytometry analysis. The cDNA of the light (VL) and heavy (VH) variable regions of the 2C8 antibody were obtained by RT-PCR from RNA, which isolated it from the hybridoma.

Antibody Purification and Characterization

First, 3×10^6 hybridomas were collected and injected intraperitoneally into 6-week-old Balb/c mice, and 6–10 days later, soluble antibodies in the mouse ascites were purified by protein G HP columns (GE Healthcare) according to the manufacturer's instructions. Column were washed with PB buffer and eluted protein with the eluting buffer (0.1 M glycine-HCL buffer, pH 3.0). Collected fractions were neutralized with neutralizing buffer (1 M Tris-HCL buffer, pH 9.0). Finally, purified samples were dialyzed against PB buffer. The purity of the eluted antibody fraction was analyzed by sodium dodecyl sulfate polyacrylamide gel electrophoresis (SDS-PAGE) on 12% gels under nonreducing or reducing conditions. Bands were visualized by Coomassie brilliant blue staining. Antibody subtype was detected by Mouse Monoclonal Antibody Isotyping Kit (Roche).

Antigen Binding Analysis

The 2C8-PE anti-CD47 antibody was generated (China Resources Concord) and diluted into different concentrations to react with the 1×10^6 CD47 positive cell line Daudi. After 30 min incubation, cells were washed and analyzed by flow cytometry. Kd value was calculated using a nonlinear regression based on the MFI value of PE thereafter, which was performed by GraphPad Prism software.

Antibody Homology Modeling and Structural Analysis

To model 2C8, we input VH and VL into antibody homology modeling software Discovery Studio. Antibody sequences VH and VL were blasted separately to find the best templates in the protein data bank (PDB), which results in the creation of the homology model of an antibody. 2BRR (PDB ID number), which

exhibited 99.1% identity to the 2C8 VL amino acid sequence, and 2ZJS (PDB ID number), revealing 86.6% identity to 2C8 VH amino acid sequence, were chosen for the 2C8 modeling. After CDR loop optimization and energy minimization, the rationality of the modeling structure was assessed by Procheck, Profile-3D, and PROSA. The crystal structure of CD47-ECD (PDB ID: 5TZU) bound to B6H12.2 is publicly available. The binding mode between CD47-ECD and 2C8 was performed by a rigid body docking program ZDOCK. An optimized pose with high ZDOCK score (>12) was typed with the CHARMm Polar H force field and then refined using the RDOCK program. Finally, we chose the binding poses based on both RDOCK scores and protein binding interface.

Immunofluorescence Staining

Indicated Jurkat cells were fixed in 4% paraformaldehyde for 15 min and blocked with 1% BSA for 30 min at room temperature. Samples were incubated with primary antibodies 2C8 or B6H12.2 overnight at 4°C. Cells were washed three times in PBS and incubated with APC-conjugated antimouse IgG1 secondary antibodies (Bioscience) for 30 min at room temperature. Nuclei were stained with 1 µg/ml DAPI (Sigma) solution. Images were captured by a two-photon laser scanning confocal microscope (OLYMPUS, FV1200 MPE).

Preparation of BMDM or Human PBMC-Derived Macrophage

Human PBMC-derived macrophages were prepared from human peripheral blood using density gradient separation. PBMC was enriched by adherence to plates for 1 h at 37°C in FBS-free RPMI 1640 medium. Then, nonadherent cells were removed by extensive washing with PBS. Monocytes were cultured in complete RPMI 1640 medium containing 10 ng/ml recombinant human M-CSF (PeproTech) to induce macrophages. Human macrophages were harvested for phagocytosis assay on day 7.

To generate mouse M1 macrophages, peritoneal or bone marrow cells were isolated from female Balb/c mice and cultured with 5 ng/mL recombinant mouse GM-CSF (PeproTech) for 7 days. To generate M0 or M2 macrophages, bone marrow cells were isolated from female Balb/c mice and cultured with 25 ng/mL recombinant mouse M-CSF (PeproTech) for 7 days. On Day 5, M1 polarization was achieved with further treatment on day 5 by 20 ng/mL IFN- γ (PeproTech) stimulation for 1 h, followed by 100 ng/mL LPS (Sigma-Aldrich) for 48 h. M2 polarization was achieved by further treatment with 20 ng/mL IL-4 (PeproTech) and 20 ng/mL IL-13 (PeproTech) for 48 h. Macrophages were arrested for phagocytosis assay on day 7.

In Vitro Phagocytosis Assay

In vitro phagocytosis assays were performed as described previously. Briefly, different tumor cells were CFSE (ThermoFisher) labeled according to the manufacturer's instructions and incubated with human peripheral blood-derived macrophages or mouse macrophages in the presence of different concentrations of CD47 antibody 2C8 or control

antibody for 2 h at 37°C. Cells were washed with serum-free media repeatedly and resuspended in 200 µl media. Then, the cells were analyzed by a high-content screening system (PerkinElmer) to determine the phagocytic rate. The number of macrophages analyzed was more than 3000 per well.

In Vivo Antibody Treatment of Human AML Engrafted Mice

All animal studies were performed in accordance with the guidelines under the Animal Ethics Committee of the Institute of Hematology and Hospital of Blood Diseases, Chinese Academy of Medical Sciences and Peking Union Medical College. For the NHL xenograft model, 1×10^7 Raji or BJAB cells were suspended in PBS and injected subcutaneously into the axillary subcutaneous space of Nod/scid mice (female, 5–6 weeks of age, PUMC, China). After 7–10 days of growth, those tumor-bearing mice were given intravenous injection of indicating dose of 2C8 or PBS once every 3 days for three weeks. Mice were observed daily. Tumor volumes were calculated using $(\text{height} \times \text{weight} \times \text{weight})/2$, and the duration of survival was recorded.

RESULTS

Generation of CD47 Blocking Antibody

A cDNA fragment of human CD47 encoding the extracellular domain was used to establish CD47 positive cell line 3T3-CD47. Establishment was assessed by flow cytometry using commercially available anti-CD47 mAb B6H12.2 (**Figure 1A**). 3T3-CD47 was used to immunize mice to produce monoclonal mouse antihuman CD47 antibodies. Immunized mice spleen cells were fused with SP2/0 cells. Lentiviral shRNA vectors were used to generate CD47 knockout variants of Jurkat cells, and the efficiency was assessed by flow cytometry (**Figure 1B**). Furthermore, a pair of Jurkat cells were fixed on glass coverslips, incubated with CD47 antibody B6H12.2 overnight at 4°C, and photographed using a confocal microscope and immunofluorescence (**Figure 1C**).

Jurkat-WT cells and Jurkat-shCD47-GFP cells were mixed at a ratio of 1:1 to screen hybridomas that stably expressed CD47 antibodies by flow cytometry analysis. Hybridomas for which supernatants stably reacted with CD47 positive Jurkat cells instead of the CD47 negative Jurkat-shCD47 cell line were selected among three different kinds of hybridomas (**Figure 1D**). In antibody screening, some hybridomas did not produce antibodies (**Figure 1D** left) or produced nonspecific antibodies (**Figure 1D** middle), and we abandoned these hybridomas in subsequent experiments. Finally, nine clones stably producing antihuman CD47 antibodies, specifically binding to CD47 positive tumor cells were obtained. Immunofluorescence further determined clones binding CD47 in a specific manner (**Figure 1E**).

Characterization of CD47 Blocking Antibody 2C8

After indirect binding reaction screening based on mean fluorescence intensity (MFI) by flow cytometry (data not shown),

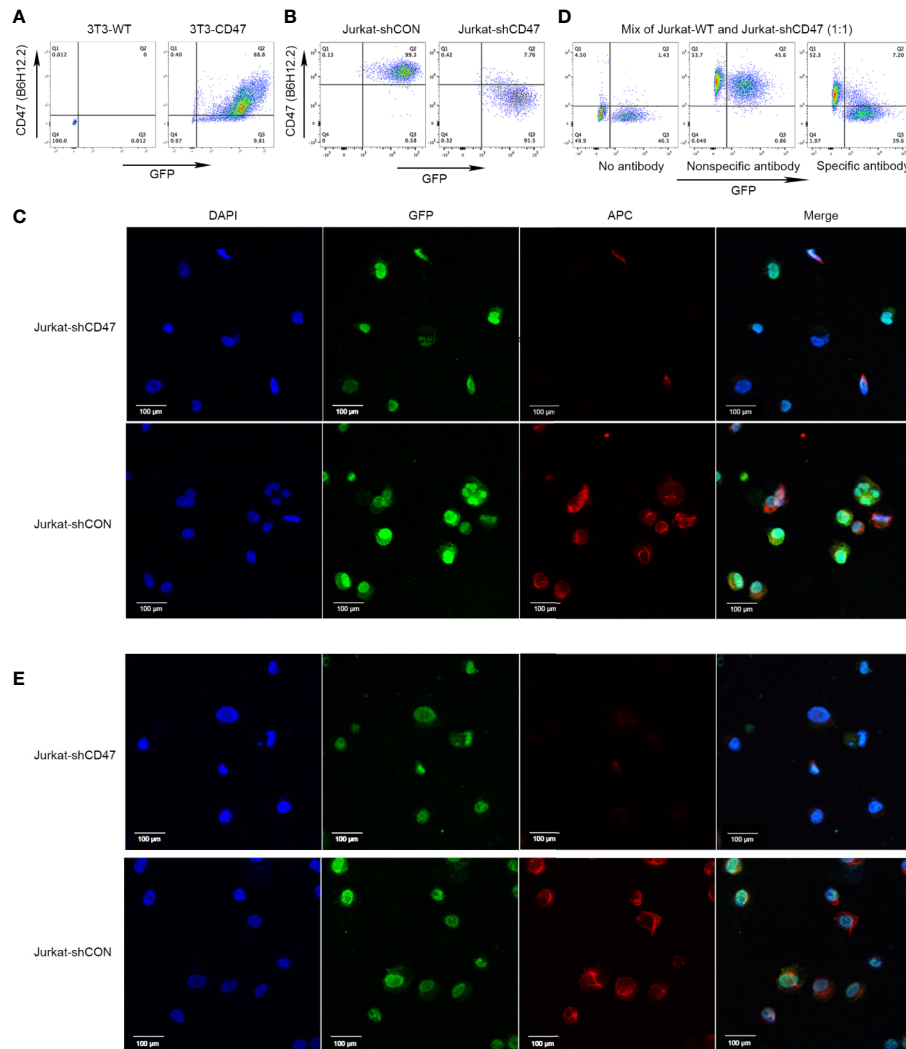


FIGURE 1 | Cloning of antihuman CD47 monoclonal antibodies. **(A)** Representative flow cytometry of 3T3-WT and 3T3-CD47 (GFP) cell line after staining with B6H12.2. **(B)** Representative flow cytometry of Jurkat-shCON (GFP) and Jurkat-shCD47 (GFP) cell line after staining with B6H12.2. **(C)** A pair of Jurkat-GFP cells were stained with B6H12.2 (red) and DAPI (blue) and observed under a two-photon confocal microscope. Scale bar, 100 μ m. The experiment was performed three times with similar results. **(D)** A mix of Jurkat-WT cells and Jurkat-shCD47-GFP cells were incubated with hybridoma supernatant and analyzed with flow cytometry. Hybridomas without antibody (left), hybridoma producing nonspecific antibody (middle), or hybridoma producing specific antibody (right). **(E)** A pair of Jurkat-GFP cells were stained with selected hybridoma supernatant (red) and DAPI (blue) and observed under a two-photon confocal microscope. Scale bar, 100 μ m. The experiment was performed three times with similar results.

a clone named 2C8 was chosen for further analysis. The 2C8 antibody subtype was detected by the indicated kit, brands showed that 2C8 was a mouse IgG1 subtype, and the light chain was a kappa chain (**Figure 2A**). RNA was isolated from the 2C8 hybridoma. The cDNA of the VL and VH variable regions of the 2C8 antibody was obtained by RT-PCR using universal antibody primers. VH and VL were successfully cloned, and the corresponding band sizes are shown in **Figure 2B** following purification with a protein G column (**Figure 2C**) and concentrated by centrifugal filters (3K). SDS-PAGE confirmed the purity of 2C8 (**Figure 2D**). The binding assay was carried out *via* flow cytometry analysis. The affinity constant of 2C8-PE was examined by GraphPad software based on MFI value of PE

(**Figure 2E**). As expected, 2C8 bound CD47 with a high affinity of 0.2991×10^{-9} M.

A fixed concentration of 2C8 antibodies was mixed with 0.28 nM APC labeled B6H12.2. Mixed antibodies were reactive with Daudi cells. As shown in **Figure 2F**, the MFI value of APC indicated that 2C8 dose-dependently disrupted the interaction between B6H12.2 and CD47. Then, we performed a structural analysis of 2C8 and B6H12.2 in complex with the CD47 extracellular domain. The homology modeling 3-D structure of 2C8 is shown in **Figure 2G**. We simulated the docking of antibodies and antigens and further compared the epitopes recognized by the two antibodies and the amino acid residues involved in antigen binding. As shown in **Figure 2H**,

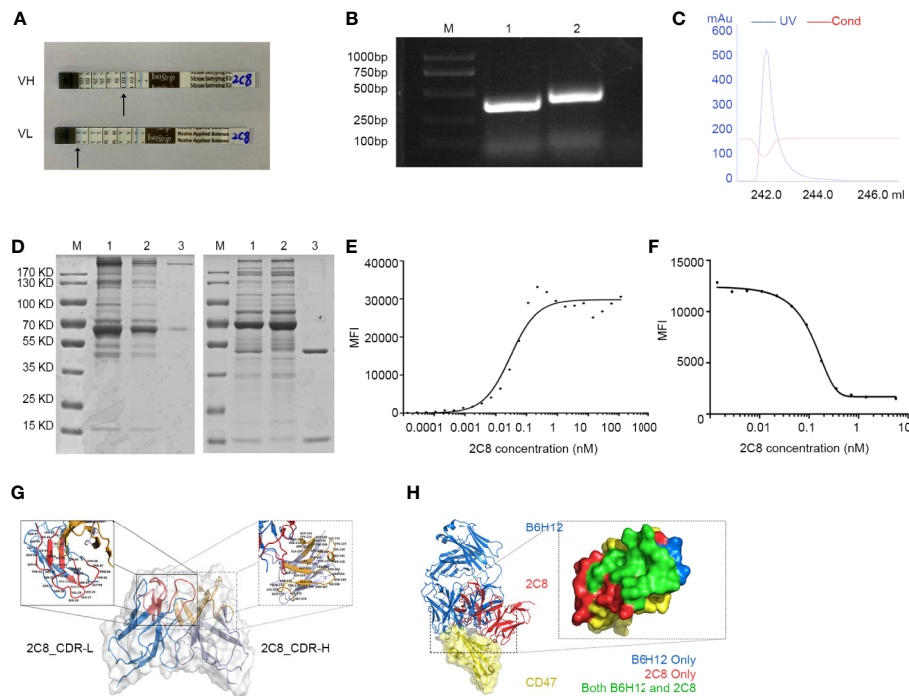


FIGURE 2 | Characterization of antihuman CD47 monoclonal antibody 2C8. **(A)** An antibody subtype was detected by the Mouse Monoclonal Antibody Isotyping Kit. **(B)** VH and VL regions amplified from hybridoma RNA/cDNA. M: marker; Lane 1: 2C8-VL region (330 bp); Lane 2: 2C8-VH region (351 bp). **(C)** UV spectrum of purified 2C8. **(D)** SDS-PAGE was used to show the purified 2C8 antibodies (M: marker, Lane 1, Mouse ascites before purification; Lane 2: purification flow through; Lane 3: purified 2C8). **(E)** Flow cytometry analysis shows that 2C8 shows a high affinity for CD47, which was 0.2991×10^{-9} M. **(F)** MFI demonstrates that 2C8 disrupts the binding of APC labeled B6H12.2 with Daudi cells. **(G)** Antibody homology modeling structure of 2C8. **(H)** Compound structure of B6H12.2/CD47-ECD superimposed on 2C8/CD47-ECD showing a shared molecular docking. Residues were interacting with only B6H12.2 (blue), only 2C8 (red), or both ligands (green).

obvious parallels between the 2C8/CD47D-ECD complex and B6H12.2/CD47-ECD complex indicate that 2C8 and B6H12.2 might compete for the same binding site on CD47.

2C8 Enables Macrophage-Mediated Phagocytosis

Next, we investigated whether 2C8 enabled phagocytosis. The Raji, HL60, Daudi, SW620, hCT116, BJAB, and K562 cell lines were labeled with CFSE (green) and used as target cells; human peripheral blood-derived and mouse macrophages (red) were applied as phagocytes. After 2 h incubation with control antibody CD19 (clone HI19a) or CD47 (2C8 or B6H12.2), phagocytic activity was captured and calculated by a high-content screening system to determine the phagocytic rates. The number of macrophages analyzed was more than 3000 per well. 2C8 treatment induced robust phagocytosis of Raji cells by both human (**Figure 3A**) and mouse macrophages (**Figure 3B** and **Supplementary Video 1**). 2C8 antibodies increased the phagocytosis rate by mouse macrophages in a concentration-dependent manner (**Figure 3C**). We further investigated the phagocytosis function of M1 and M2 subtypes with 2C8 or B6H12.2. The resulting M1 and M2 macrophage phagocytosis rates after 2C8 treatment were statistically significantly increased (**Figure 3D**). We checked the expression of CD47 in Raji, HL60, Daudi, SW620, hCT116, BJAB, and K562 cells (**S1 Fig**). They all

expressed a high level of CD47 on the cell surface. Our data indicates that 2C8 increased mouse macrophage-mediated phagocytosis of several types of CD47-positive tumor cells. The ceiling average of phagocytosis rate was more than 90% (**Figure 3E**). These results suggest that 2C8 is a feasible therapeutic agent to eliminate tumor cells. Importantly, 2C8 was more efficacious in comparison to B6H12.2 (**Figures 3C–E**).

In Vivo Antitumor Activity of the 2C8 Antibody

We evaluated the antitumor efficiency of 2C8 in NHL xenograft models using NOD/SCID mice to investigate its *in vivo* efficacy using NHL cell line Raji. Consistent with robust phagocytosis induction, as shown in **Figure 4A**, 2C8 was significantly efficacious in controlling Raji tumor growth with low (200 μ g/mouse) and high (400 μ g/mouse) doses. The final tumor growth inhibition (TGI) values were 91.4% and 86.5%, respectively. 2C8 treatment demonstrated a dramatic increase in survival (**Figure 4B**). We used another NHL cell line BJAB. The final TGI value was 82.0% in controlling BJAB tumor growth with 200 μ g/mouse doses. Mice in the control group died within 45 days after tumor cell inoculation, but mice treated with 2C8 demonstrated significantly increased survival (**Figures 4C, D**). These results confirm that 2C8 has potent antitumor activity in a mouse model.

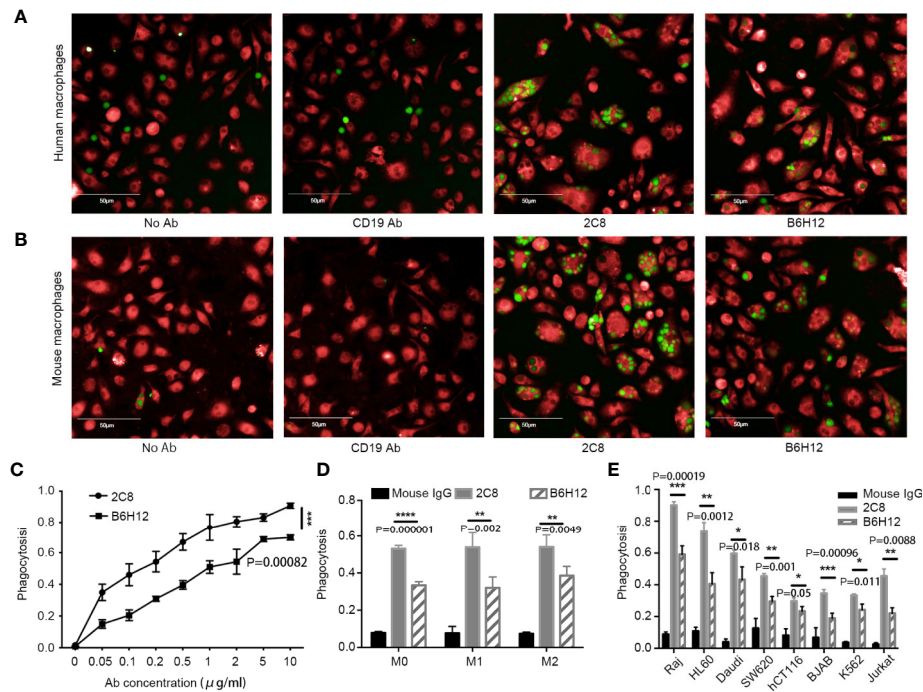


FIGURE 3 | 2C8 enables phagocytosis of tumor cells *in vitro*. **(A)** Representative images of human macrophages (red) phagocytosing Raji cells (green) following treatment with the 10 µg/ml indicated antibodies or not. Scale bar, 50 µm. **(B)** Representative images of mouse macrophages (red) phagocytosing Raji cells (green) following treatment with the 10 µg/ml indicated antibodies or not. Scale bar, 50 µm. **(C)** Mouse macrophages phagocytose Raji cells in the presence of 2C8 or B6H12.2 in a concentration-dependent manner. **(D)** Bar graph demonstrating the change of phagocytosis rates by mouse M0, M1, and M2 macrophages toward Raji cells in the presence of 10 µg/ml 2C8 or 10 µg/ml B6H12.2. **(E)** In vitro phagocytosis of multiple tumor cells by mouse macrophages in the presence of 10 µg/ml 2C8 or 10 µg/ml B6H12.2. The data are represented as mean ± SEM. (**** $p < 0.0001$; *** $p < 0.001$; ** $p < 0.01$; * $p < 0.05$, multiple t tests). The experiment was performed three times with similar results.

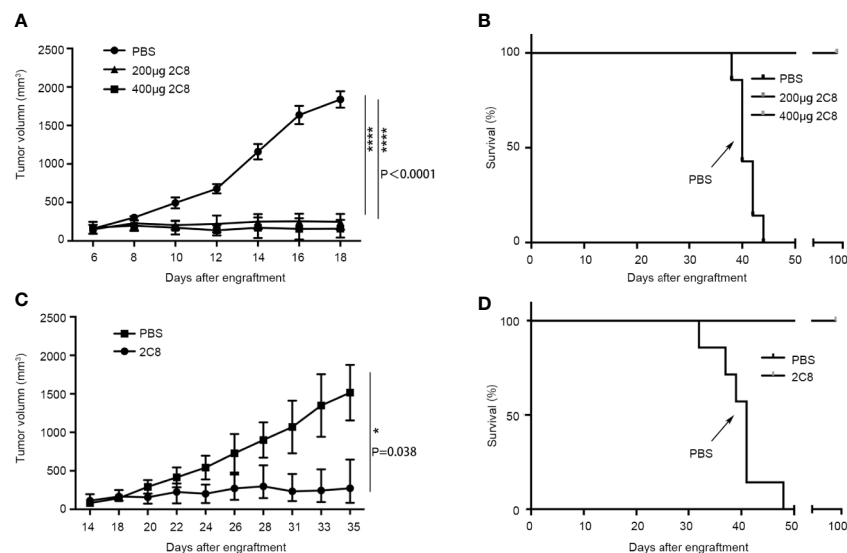


FIGURE 4 | 2C8 inhibits tumor growth in xenotransplantation models. **(A)** Raji xenografted mice treated with two different doses of 2C8 or PBS ($n = 7$). The tumor volume of Raji tumors per group ($n = 7$) is depicted over time. **(B)** Raji xenografted mouse survival after two different doses of 2C8 or PBS treatment ($n = 7$). **(C)** BJAB xenografted mice treated with 200 µg 2C8 or PBS ($n = 4$). The tumor volume of BJAB tumors per group ($n = 4$) is depicted over time. **(D)** BJAB xenografted mice survival after 200 µg 2C8 or PBS treatment ($n = 4$). The data are represented as mean ± SEM. (**** $p < 0.0001$; * $p < 0.05$, multiple t tests).

DISCUSSION

CD47 is highly expressed on multiple tumor cell surface membranes involved in regulating macrophage phagocytosis *via* binding SIRP α to protect host cells from being eliminated. CD47 blocking agents, such as monoclonal antibodies targeting CD47/SIRP α , could interrupt the interaction between cancer cells and macrophages and induce phagocytosis, potentially providing an effective method of cancer therapy. Antitumor mechanisms of the CD47 antibody can be divided into four groups: 1) Enabling phagocytic uptake of tumor cells by macrophages; 2) Promotion of adaptive immunity; 3) Induction of apoptosis; 4) NK cell-mediated ADCC and CDC (25).

The purpose of this study was to describe the generation of a novel blockade antibody 2C8 and assess its biological effects. We first constructed a 2C8 antibody based on the hybridoma technique. An antibody subtype was detected. An akta purification system was used to purify 2C8, and purification was confirmed by SDS-PAGE. Flow cytometry was further performed to assure the binding affinity of 2C8. The higher affinity of 2C8 means a better efficacy for the therapeutic antibodies. 2C8 inhibited APC conjecture B6H12.2 binding with the CD47 positive cell line. Three-dimensional molecular modeling analysis of 2C8 and B6H12.2 in complex with the CD47 extracellular domain suggests that 2C8 and B6H12.2 may partially bind a similar epitope on CD47.

Disruption of the CD47-SIRP α axis by blockade antibody results in enhanced phagocytosis of different kinds of tumor cells, including increased human and mouse macrophage phagocytosis of tumor cells significantly *in vitro* (26). To validate 2C8 as a genuine therapeutic agent, we next performed *in vitro* phagocytosis assays. The data strongly demonstrated that 2C8 was more efficacious than B6H12.2 in promoting phagocytosis. Additionally, the tumor inhibitory role of 2C8 *in vivo* was examined. 2C8 significantly inhibited tumor growth in both Raji and BJAB NHL carcinogenesis models with three times weekly treatment. In addition, 2C8 prolonged the survival of xenografted mice.

In conclusion, 2C8 was effectively generated and possessed ideal attributes. We prepared a CD47 blockade antibody 2C8 to blockade CD47 on tumor cells with high affinity selectively, and it embodied excellent antitumor capability both *in vitro* and *in vivo*. Our prophase results suggest that 2C8 is an efficacious therapeutic agent for human cancer and warrants further studies of 2C8 in different carcinoma diseases. It contributes to consolidate clinical interest in targeting macrophages for the treatment of malignancies and, moreover, as a supplement

therapy when patients are resistant or refractory to other checkpoint therapies or relapse after such treatments.

DATA AVAILABILITY STATEMENT

The original contributions presented in the study are included in the article/**Supplementary Material**. Further inquiries can be directed to the corresponding authors.

ETHICS STATEMENT

The animal study was reviewed and approved by Animal Ethics Committee of the Institute of Hematology & Hospital of Blood Diseases, Chinese Academy of Medical Sciences & Peking Union Medical College.

AUTHOR CONTRIBUTIONS

DX, FL, and MX have made substantial contributions to the conception or design of the work. FL, WH, YS, RL, and YY have made substantial contributions to the acquisition of the work. FL, XY, DF, YZZ, and MH have made substantial contributions to the analysis of the work. DX, ZYZ, YL, YJZ, and JW have drafted the work or revised it critically for important intellectual content. All authors contributed to the article and approved the submitted version.

FUNDING

This work was supported by the National Natural Science Foundation of China (Grant Nos.81773303, 81830005), Tianjin Municipal Science and Technology Commission Grant (Grant Nos.19JCZDJC65200, 19JCZDJC33100), CAMS Initiative for Innovative Medicine Sciences (CIFMS) (Grant Nos. 2016-I2M-1-007, 2016-I2M-3-013), and Scientific Research Project of Tianjin Education Commission (Grant Nos. 2019KJ196).

SUPPLEMENTARY MATERIAL

The Supplementary Material for this article can be found online at: <https://www.frontiersin.org/articles/10.3389/fonc.2020.615534/full#supplementary-material>

REFERENCES

1. Manson G, Houot R. Next-generation immunotherapies for lymphoma: one foot in the future. *Ann Oncol* (2018) 29(3):588–601. doi: 10.1093/annonc/mdy032
2. Li XL, Liu R, Su X, Pan YS, Han XF, Shao CS, et al. Harnessing tumor-associated macrophages as aids for cancer immunotherapy. *Mol Cancer* (2019) 18(1). doi: 10.1186/s12943-019-1102-3
3. Mantovani A, Sica A, Sozzani S, Allavena P, Vecchi A, Locati M. The chemokine system in diverse forms of macrophage activation and polarization. *Trends Immunol* (2004) 25(12):677–86. doi: 10.1016/j.it.2004.09.015
4. Zhang QW, Liu L, Gong CY, Shi HS, Zeng YH, Wang XZ, et al. Prognostic Significance of Tumor-Associated Macrophages in Solid Tumor: A Meta-Analysis of the Literature. *PloS One* (2012) 7:(12). doi: 10.1371/journal.pone.0050946

5. Marchesi F, Cirillo M, Bianchi A, Gately M, Olimpieri OM, Cerchiara E, et al. High density of CD68+/CD163+ tumour-associated macrophages (M2-TAM) at diagnosis is significantly correlated to unfavorable prognostic factors and to poor clinical outcomes in patients with diffuse large B-cell lymphoma. *Hematol Oncol* (2015) 33(2):110–2. doi: 10.1002/hon.2142
6. Jayasingam SD, Citartan M, Thang TH, Zin AAM, Ang KC, Ch'ng ES. Evaluating the Polarization of Tumor-Associated Macrophages Into M1 and M2 Phenotypes in Human Cancer Tissue: Technicalities and Challenges in Routine Clinical Practice. *Front Oncol* (2020) 9:1512. doi: 10.3389/fonc.2019.01512
7. Hasselblom S, Hansson U, Sigurdardottir M, Nilsson-Ehle H, Ridell B, Andersson PO. Expression of CD68+ tumor-associated macrophages in patients with diffuse large B-cell lymphoma and its relation to prognosis. *Pathol Int* (2008) 58(8):529–32. doi: 10.1111/j.1440-1827.2008.02268.x
8. Wada N, Zaki MAA, Hori Y, Hashimoto K, Tsukaguchi M, Tatsumi Y, et al. Tumour-associated macrophages in diffuse large B-cell lymphoma: a study of the Osaka Lymphoma Study Group. *Histopathology* (2012) 60(2):313–9. doi: 10.1111/j.1365-2559.2011.04096.x
9. Gul N, Babes L, Siegmund K, Korthouwer R, Bogels M, Braster R, et al. Macrophages eliminate circulating tumor cells after monoclonal antibody therapy. *J Clin Invest* (2014) 124(2):812–23. doi: 10.1172/jci66776
10. DeNardo DG, Ruffell B. Macrophages as regulators of tumour immunity and immunotherapy. *Nat Rev Immunol* (2019) 19(6):369–82. doi: 10.1038/s41577-019-0127-6
11. Mantovani A, Marchesi F, Malesci A, Laghi L, Allavena P. Tumour-associated macrophages as treatment targets in oncology. *Nat Rev Clin Oncol* (2017) 14(7):399–416. doi: 10.1038/nrclinonc.2016.217
12. Zhang M, Hutter G, Kahn SA, Azad TD, Gholamin S, Xu CY, et al. Anti-CD47 Treatment Stimulates Phagocytosis of Glioblastoma by M1 and M2 Polarized Macrophages and Promotes M1 Polarized Macrophages In Vivo. *PloS One* (2016) 11(4). doi: 10.1371/journal.pone.0153550
13. Willingham SB, Volkmer JP, Gentles AJ, Sahoo D, Dalerba P, Mitra SS, et al. The CD47-signal regulatory protein alpha (SIRPα) interaction is a therapeutic target for human solid tumors. *Proc Natl Acad Sci USA* (2012) 109(17):6662–7. doi: 10.1073/pnas.1121623109
14. Xiao Z, Chung H, Banan B, Manning PT, Ott KC, Lin S, et al. Antibody mediated therapy targeting CD47 inhibits tumor progression of hepatocellular carcinoma. *Cancer Lett* (2015) 360(2):302–9. doi: 10.1016/j.canlet.2015.02.036
15. Yang L, Zhang Y. Tumor-associated macrophages: from basic research to clinical application. *J Hematol Oncol* (2017) 10. doi: 10.1186/s13045-017-0430-2
16. Tang XQ. Tumor-associated macrophages as potential diagnostic and prognostic biomarkers in breast cancer. *Cancer Lett* (2013) 332(1):3–10. doi: 10.1016/j.canlet.2013.01.024
17. Brown EJ, Frazier WA. Integrin-associated protein (CD47) and its ligands. *Trends Cell Biol* (2001) 11(3):130–5. doi: 10.1016/s0962-8924(00)01906-1
18. Jaiswal S, Jamieson CHM, Pang WW, Park CY, Chao MP, Majeti R, et al. CD47 Is Upregulated on Circulating Hematopoietic Stem Cells and Leukemia Cells to Avoid Phagocytosis. *Cell* (2009) 138(2):271–85. doi: 10.1016/j.cell.2009.05.046
19. Betancur PA, Abraham BJ, Yiu YY, Willingham SB, Khameneh F, Zarnegar M, et al. A CD47-associated super-enhancer links pro-inflammatory signalling to CD47 upregulation in breast cancer. *Nat Commun* (2017) 8. doi: 10.1038/ncomms14802
20. Weiskopf K, Jahchan NS, Schnorr PJ, Cristea S, Ring AM, Maute RL, et al. CD47-blocking immunotherapies stimulate macrophage-mediated destruction of small-cell lung cancer. *J Clin Invest* (2016) 126(7):2610–20. doi: 10.1172/jci81603
21. Zhang Y, Sime W, Juhas M, Sjolander A. Crosstalk between colon cancer cells and macrophages via inflammatory mediators and CD47 promotes tumour cell migration. *Eur J Cancer* (2013) 49(15):3320–34. doi: 10.1016/j.ejca.2013.06.005
22. Liu R, Wei HT, Gao P, Yu H, Wang K, Fu Z, et al. CD47 promotes ovarian cancer progression by inhibiting macrophage phagocytosis. *Oncotarget* (2017) 8(24):39021–32. doi: 10.18632/oncotarget.16547
23. Majeti R, Chao MP, Alizadeh AA, Pang WW, Jaiswal S, Gibbs KD, et al. CD47 Is an Adverse Prognostic Factor and Therapeutic Antibody Target on Human Acute Myeloid Leukemia Stem Cells. *Cell* (2009) 138(2):286–99. doi: 10.1016/j.cell.2009.05.045
24. Chao MP, Alizadeh AA, Tang C, Jan M, Weissman-Tsukamoto R, Zhao FF, et al. Therapeutic Antibody Targeting of CD47 Eliminates Human Acute Lymphoblastic Leukemia. *Cancer Res* (2011) 71(4):1374–84. doi: 10.1158/0008-5472.Can-10-2238
25. Chao MP, Weissman IL, Majeti R. The CD47-SIRP alpha pathway in cancer immune evasion and potential therapeutic implications. *Curr Opin Immunol* (2012) 24(2):225–32. doi: 10.1016/j.coi.2012.01.010
26. Balzarotti F, Eilers Y, Gwosch KC, Gynnà AH, Westphal V, Stefani FD, et al. Nanometer resolution imaging and tracking of fluorescent molecules with minimal photon fluxes. *Science* (2017) 355(6325):606–12. doi: 10.1126/science.aak9913

Conflict of Interest: The authors declare that the research was conducted in the absence of any commercial or financial relationships that could be construed as a potential conflict of interest.

Copyright © 2021 Lin, Xiong, Hao, Song, Liu, Yang, Yuan, Fan, Zhang, Hao, Ye, Lu, Zhang, Wang and Xiong. This is an open-access article distributed under the terms of the Creative Commons Attribution License (CC BY). The use, distribution or reproduction in other forums is permitted, provided the original author(s) and the copyright owner(s) are credited and that the original publication in this journal is cited, in accordance with accepted academic practice. No use, distribution or reproduction is permitted which does not comply with these terms.



Targeting Adrenomedullin in Oncology: A Feasible Strategy With Potential as Much More Than an Alternative Anti-Angiogenic Therapy

Ramiro Vázquez^{1,2†}, Maria E. Riveiro^{1†}, Caroline Berenguer-Daizé³, Anthony O'Kane⁴, Julie Gormley⁴, Olivier Touzelet⁴, Keyvan Rezai⁵, Mohamed Bekradda¹ and L'Houcine Ouafik^{3,6*}

OPEN ACCESS

Edited by:

Marco Rossi,
University of Catanzaro, Italy

Reviewed by:

Kevin Xueying Sun,
Harbin Medical University, China
Alfredo Berruti,
University of Brescia, Italy

*Correspondence:

L'Houcine Ouafik
lhoucine.ouafik@univ-amu.fr

[†]These authors have contributed
equally to this work

Specialty section:

This article was submitted to
Cancer Molecular
Targets and Therapeutics,
a section of the journal
Frontiers in Oncology

Received: 30 July 2020

Accepted: 02 November 2020

Published: 06 January 2021

Citation:

Vázquez R, Riveiro ME,
Berenguer-Daizé C, O'Kane A,
Gormley J, Touzelet O, Rezai K,
Bekradda M and Ouafik L'H (2021)
Targeting Adrenomedullin in
Oncology: A Feasible Strategy With
Potential as Much More Than an
Alternative
Anti-Angiogenic Therapy.
Front. Oncol. 10:589218.
doi: 10.3389/fonc.2020.589218

¹ Preclinical Department, Early Drug Development Group (E2DG), Boulogne-Billancourt, France, ² Center for Genomic Science of IIT@SEMM, Fondazione Istituto Italiano di Tecnologia (IIT), Milan, Italy, ³ Aix Marseille University, CNRS, INP, Institute of NeuroPhysiopathology, Marseille, France, ⁴ Discovery and Scientific Affairs Department, Fusion Antibodies plc., Belfast, United Kingdom, ⁵ Department of Radio-Pharmacology, Institute Curie-René Huguenin Hospital, Saint-Cloud, France, ⁶ APHM, CHU Nord, Service de Transfert d'Oncologie Biologique, Marseille, France

The development, maintenance and metastasis of solid tumors are highly dependent on the formation of blood and lymphatic vessels from pre-existing ones through a series of processes that are respectively known as angiogenesis and lymphangiogenesis. Both are mediated by specific growth-stimulating molecules, such as the vascular endothelial growth factor (VEGF) and adrenomedullin (AM), secreted by diverse cell types which involve not only the cancerogenic ones, but also those constituting the tumor stroma (i.e., macrophages, pericytes, fibroblasts, and endothelial cells). In this sense, anti-angiogenic therapy represents a clinically-validated strategy in oncology. Current therapeutic approaches are mainly based on VEGF-targeting agents, which, unfortunately, are usually limited by toxicity and/or tumor-acquired resistance. AM is a ubiquitous peptide hormone mainly secreted in the endothelium with an important involvement in blood vessel development and cardiovascular homeostasis. In this review, we will introduce the state-of-the-art in terms of AM physiology, while putting a special focus on its pro-tumorigenic role, and discuss its potential as a therapeutic target in oncology. A large amount of research has evidenced AM overexpression in a vast majority of solid tumors and a correlation between AM levels and disease stage, progression and/or vascular density has been observed. The analysis presented here indicates that the involvement of AM in the pathogenesis of cancer arises from: 1) direct promotion of cell proliferation and survival; 2) increased vascularization and the subsequent supply of nutrients and oxygen to the tumor; 3) and/or alteration of the cell phenotype into a more aggressive one. Furthermore, we have performed a deep scrutiny of the pathophysiological prominence of each of the AM receptors (AM₁ and AM₂) in different cancers, highlighting their differential locations and functions, as well as regulatory mechanisms. From the therapeutic point of view, we summarize here an exhaustive series of preclinical studies showing a reduction of

tumor angiogenesis, metastasis and growth following treatment with AM-neutralizing antibodies, AM receptor antagonists, or AM receptor interference. Anti-AM therapy is a promising strategy to be explored in oncology, not only as an anti-angiogenic alternative in the context of acquired resistance to VEGF treatment, but also as a potential anti-metastatic approach.

Keywords: adrenomedullin, angiogenesis, cancer, metastasis, AM₁ and AM₂, RAMP1-3

INTRODUCTION

The term cancer comprises different types of pathologies characterized by uncontrolled proliferation of cells that, with the exception of those of hematological or lymphatic origin, give place to malignant tumor masses. Primary tumors grow supported by new vascularization resulting from pre-existing capillaries in a sequence of events that are collectively known as angiogenesis. This process is triggered in response to spontaneous or induced tissue hypoxia, a common phenomenon in solid tumors. These new vessels are also used by cancer cells to spread to other sites within the body after acquiring invasive potential, thereby causing metastasis and, without intervention, death. Surgery and radiotherapy constitute the first approaches in the treatment of localized tumors while systemic agents (chemotherapy, hormone and biological therapies) are the choice to confront the metastatic setting.

In this context, the discovery of tumor angiogenesis opened a new path in fighting cancer. Hypoxia-inducible factor-1 α (HIF-1 α) is the master switch of the cell machinery required to face O₂-lacking periods in physiological and pathological conditions. One of its target genes is that which encodes for the vascular endothelial growth factor (VEGF), the best characterized angiogenic promoter, involved in the modulation of vessel permeability and remodeling, and endothelial cell survival, proliferation and migration (1). The current angiogenesis-targeting approaches approved in clinical practice are: 1) VEGF-blocking monoclonal antibodies (bevacizumab/Avastin®); 2) decoy receptors, ‘VEGF-trap’ (aflibercept/Zaltrap®); 3) tyrosine kinase inhibitors (sunitinib/Sutent®, sorafenib/Nexavar®, axitinib/Inlyta®); and 4) monoclonal

antibodies targeting VEGF receptors (ramucirumab/Cyramza®) (2). These agents are being used in the treatment of breast, colorectal, hepatocellular, gastric, and lung among other cancers (2), increasing the effectiveness of conventional chemotherapy. However, a significant number of preclinical and clinical observations have shown that the process of angiogenesis is far from being clearly understood. Furthermore, this approach is not effective in all cancers and often has only limited impact on patient’s overall survival, which, added to the occurrence of frequent drug toxicity and the development of resistance, support the necessity to explore novel strategies aiming to influence alternative factors involved in tumor angiogenesis. In this regard, additional approaches are being tested in preclinical and clinical trials including: angiopoietins (Ang), epidermal growth factor (EGF), fibroblast growth factors (FGF1 and FGF2), hepatocyte growth factor (HGF), platelet-derived growth factor C (PDGF-C), or agents targeting angiogenesis indirectly by inhibiting oncogenic pathways (e.g., HER2, PI3k/Akt/mTOR, and mutated EGF receptor) or hormone signaling (3).

Adrenomedullin –onwards AM– is a regulatory peptide whose involvement in tumor progression and metastasis has become more evident in recent years. The whole literature supports the idea of AM as a survival factor for tumor cells, which can be produced either by the malignant cells themselves or by those located in adjacent/surrounding stroma. In general, AM expression is upregulated by hypoxia, and the excessive production of this peptide is associated with poorer prognosis in cancer patients (4, 5). Moreover, recent reports indicate that AM could be a master regulator upstream of the VEGF pathway and even induce HIF-1 α expression, therefore attracting much interest as a therapeutic strategy (6, 7).

Here, we review the physiological and pathological processes mediated by AM, analyzing the advantages that the employment of anti-AM therapy may offer in oncology.

AM IN PHYSIOLOGICAL CONTEXT

AM, Calcitonin-Like Peptides, and Their Physiological Roles

The isolation and characterization of AM was reported for the first time by Kitamura et al. in 1993 from human pheochromocytomas of adrenomedullary origin, identifying it as a potent vasodilator (8). The AM gene encodes for a 185-residue preprohormone composed of two bioactive peptides: AM

Abbreviations: ACTH, Adrenocorticotrophic hormone; AM, adrenomedullin; AM₁, adrenomedullin receptor type 1; AM₂, adrenomedullin receptor type 2; AM2, adrenomedullin 2 (intermedin); CAF, tumor-associated fibroblast. AMY, amylin; cAMP, cyclic-adenosine monophosphate; CGRP, calcitonin gene-related peptide; cGMP, cyclic guanosine monophosphate; CLR, calcitonin-receptor like receptor; CTR, calcitonin receptor; ECD, extracellular domain; ERK (1/2), extracellular signal regulated protein kinase (1/2); GPCR, G protein-coupled receptor; HIF-1 α , hypoxia-inducible factor-1 α ; LPS, Lipopolysaccharides; MAPK, mitogen activated protein kinase; MPM, malignant pleural mesothelioma; PAM, peptidylglycine α -amidating monooxygenase; PAMP, Proadrenomedullin N-terminal 20 peptide; PDAC, pancreatic ductal adenocarcinoma; PDPN, podoplanin; PDZ, PSD-95/DiscLarge/ZO-1; PKG, cGMP-dependent protein kinase or protein kinase G; RAMP, receptor-activity modifying protein; RCP, receptor-complement protein; SAR, structure-activity relationship; TAM, tumor-associated macrophage; VEGF, vascular endothelial growth factor.

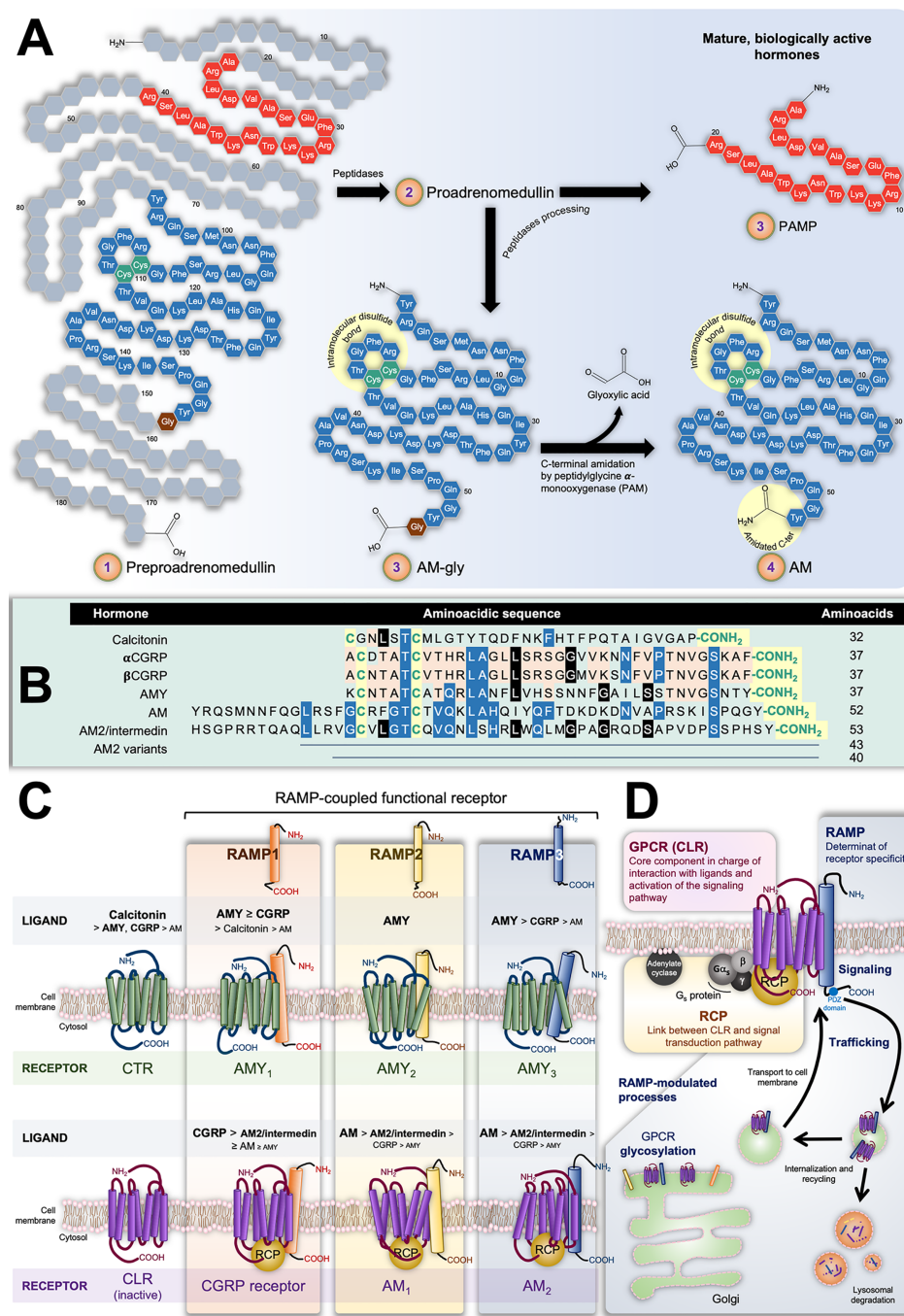


FIGURE 1 | (A) Scheme representing preproadrenomedullin processing to give rise to the mature biologically active peptides adrenomedullin (AM) and proadrenomedullin N-terminal 20 peptide (PAMP), a potent angiogenic agent. Common structural features of the calcitonin-like peptide family (i.e., disulfide bond and amidated C-terminal) are highlighted by yellow circles. **(B)** Sequences of human components of this family. As in **(A)**, conserved characteristic structures are highlighted in yellow. Different colors indicate position-shared amino acids amongst the AM (blue), AM2/Intermedin variants (black), calcitonin gene-related peptide CGRP, and amylin (AMY) (orange) peptides. **(C)** Receptors with their decreasing affinity for different ligands. The interaction of calcitonin receptor (CTR) and calcitonin-receptor like receptor (CLR) with receptor-activity modifying proteins (RAMPs) have been very well studied in terms of the ability of the former group to alter the GPCR specificity by acting on their ligand affinity. The CTR binds calcitonin whilst presenting low affinity for AMY and CGRP. In contrast, it forms three AMY-high-affinity and calcitonin-low-affinity receptors (AMY₁, AMY₂, and AMY₃) in the presence of RAMP1, RAMP2, or RAMP3, respectively. On the other hand, CLR itself is not able to bind any known ligand. Nonetheless, the CLR/RAMP1 dimer results in a high-affinity CGRP receptor, while its combination with RAMP2 or RAMP3 respectively produces the AM₁ and AM₂ subtypes of the AM receptor. Both CLR/RAMP1, AM₁ and AM₂ also show moderate affinity for AM2/intermedin. **(D)** Constituents of the AM₂ and their role in the tripartite complex.

and proadrenomedullin N-terminal 20-residue peptide (PAMP) (9, 10). The prehormone is firstly processed into proadrenomedullin, from which 20 amino acids at the N-terminus later form PAMP. The remaining AM precursor is successively converted into a C-terminal glycine extended intermediate of 53 amino acids (AM-gly) with scant activity $\sim 5\%$ of AM effect-, and further into the 52-amino acid biologically-active form by α -amidation of the tyrosine at the carboxy terminal by a peptidylglycine α -amidating monooxygenase (PAM; EC, 1.14.17.3 **Figure 1A**) (11). Together with the amidated C-terminus, an intramolecular disulfide bond in the N-terminus giving rise to a ring of six or seven residues represent the distinctive structural feature of the calcitonin-like peptide family, which, besides AM, includes calcitonin, the calcitonin gene-related peptide (CGRP), amylin (AMY), and intermedin (or AM2). It is interesting to note their limited sequence homology as evidenced in **Figure 1B**. Also, despite structural likeness and the fact they share some biological activities, their main physiological roles are diverse (12).

Calcitonin is a 32-amino acid peptide encoded by the *CALCA* gene secreted by parafollicular cells –also known as C cells– in the thyroid gland. It plays a key function in the physiological homeostasis of serum Ca^{2+} inducing its absorption by bone tissue, and hence, hypocalcemia. CGRP results as an alternative splicing of the *CALCA* gene mRNA transcript (α CGRP) in the nervous system (13, 14), or as the direct (only mature) product of the *CALCB* gene (β CGRP) (15). CGRP –both isoforms– is widely distributed along the gastrointestinal tract and the central and peripheral nervous systems (16, 17). It is synthesized and released by sensory nerves and has much prominence in afferent neurotransmission. It also induces potent and long-lasting dilation of microvasculature of the nervous system and is involved in nociceptive signaling in migraines (17, 18). It likewise induces hypocalcemia with moderate potency (19). AMY, also referred to as islet amyloid polypeptide (IAPP), possesses a significant level of homology with CGRP, sharing 16 of 37 amino acids (20). AMY was originally identified in the pancreas, where it is co-synthesized, co-packaged, and co-released with insulin from islet β cells (21, 22). Nevertheless, further studies also localized this hormone in areas of the central nervous systems implicated in metabolic control, such as the hypothalamus (23). AMY deposits in type II diabetes are associated with the illness progression (24). In all, AMY is involved in the regulation of energy metabolism by mainly activating and modulating the satiating effect and stomach emptying through the central nervous systems (23, 25, 26), and antagonizing anabolic activity of insulin (4, 27). It also has a potent hypocalcemic activity (28).

AM displays several biological effects, in part due to its almost ubiquitous tissue expression. Apart from malignant and normal adrenal medullary cells, Kitamura et al. detected significant immunoreactive amounts of AM in the lung and kidney (8). Subsequent investigations reported AM expression in neurons and glial cells, but also in blood vessels (endothelial and smooth muscle cells), cardiomyocytes, macrophages, retinal epithelium adipose tissue, and different cancer cells. In fact, it is thought that

all body tissues are able to secrete this peptide (29–31). In all cases, AM is not accumulated in vesicles, but its gene expression, synthesis, and subsequent secretion occur immediately in response to a vast series of biochemical (e.g., hormones and LPS) and physical (e.g., hypoxia and shear stress) cell type-dependent stimuli. In the context of this wide distribution of AM-secreting tissues, adrenal production is relative. Indeed, although present in lower concentrations (<1.5 fmol/mg), the total amount of AM in lung and kidney is higher than that produced by the adrenal medulla (≈ 150 fmol/mg) (8). Plasma concentration of total AM in humans (the sum of the less active, AM-gly and the mature active C-term amidated AM) varies from 2 to 20 fmol/ml (8, 32–35), being significantly increased in patients suffering from hypertension, chronic renal failure, heart failure, obesity, arteriosclerosis, and/or sepsis (30–37). However, it is worth noting that AM-gly is the main endogenous form of immunoreactive blood-circulating AM (38). In fact, the elevated concentration of total AM observed in hypertensive patients would be caused by AM-gly since plasmatic mature AM shows comparable levels between hypertensive and normotensive subjects (38). Kitamura et al. propound three non-mutually exclusive hypotheses to explain such paradoxical findings. 1) Most of the mature AM would act *in situ* by binding cell membrane receptors and thus a little fraction would be released to blood. 2) Alternatively, the scarce activity of AM-gly would not only facilitate its diffusion into peripheral vessels, but also extend its half-life. 3) Since the mature AM is thought to derive from AM-gly, both the location and activity of the PAM would therefore have a key role in regulating the AM/AM-gly ratio (38). In this sense, authors suggest that the misalignment in terms of PAM and AM expression amongst different tissues could explain the relatively high plasmatic levels of AM-gly. However, their hypothesis is based on the distribution of α -amidating enzymes in rat (39), which could differ in humans as observed in the case of the lung (40).

AM acts as a circulating hormone but it also elicits multiple biological activities in a paracrine and/or autocrine manner. Its effects are of importance for cardiovascular homeostasis, growth and development of cardiovascular tissues, modulation of the lymphatic flow, regulation of body fluids and diabetes mellitus (8–10, 41–48). Systemic AM administration has been demonstrated to reduce arterial pressure, decrease peripheral vascular resistance, and increase heart rate and cardiac output (8, 49). Moreover, AM and PAMP act as potent angiogenic agents, being necessary for the maintenance of functional membrane microvasculature integrity (45, 47), and regulate lymphatic edema drainage promoting a faster healing of epithelial wounds (50, 51).

In the context of body fluid volume and renal function, AM exerts a tight control of the hypothalamic-pituitary-adrenal axis at all levels (33, 52). AM and its receptors are abundantly expressed in the central nervous system and its cellular components (53). It plays an important role in the regulation of specific blood-brain barrier properties (54), it also increases preganglionic sympathetic discharges (55) and exerts several

neuroprotective actions against ischemic damage (56). Furthermore, relatively recent studies suggest that AM may be involved in the neuroendocrine response to stress and nociception (57).

In the digestive system, AM immunoreactivity is widely distributed in the mucosal and glandular epithelia of the stomach, esophagus, intestine, gallbladder, bile duct, and acini of the pancreas and salivary glands (58). It also regulates insulin secretion, directly acting on pancreatic cells (10), and is a potent inhibitor of basal gastrin-stimulated HCl secretion (59). Moreover, it has emerged as a novel and promising therapy for digestive pathologies related with inflammation such as gastric ulcers (60) and inflammatory bowel diseases (61). This is related to the local and systemic anti-inflammatory actions that AM is able to exert (62, 63). For example, it has been demonstrated that AM inhibits the secretion of pro-inflammatory cytokines into the medium by peripheral blood monocytes (64) and plays a role in the evolution of Th1/Th2 cytokine balance, decreasing pro-inflammatory cytokine levels (IL-6, IL-10, TNF- α , IFN- γ) (65–67). In addition to the regulatory role on immune cells, AM also decreases endothelial permeability, thus reducing the formation of inflammatory exudates (64). Likewise, it has been found in all epithelial surfaces that separate the external and internal environment and in all body secretions (68). This wide distribution suggests the possibility that AM has an immunity-related function. In this sense, it has been proven that AM displays potent antimicrobial action against Gram-positive and Gram-negative bacteria (69).

Despite other members of this family, AM possesses limited effect in bone tissue and therefore in calcemic regulation (12).

In 2004, two different groups independently reported the identification of an AM-high-homology peptide in humans. Takei et al., who had previously isolated this AM analog from pufferfish (70), called it AM2 (71); while Roh et al. employed the term intermedin (72). AM2/intermedin is a 53-amino acid peptide resulting from the cleavage of a (148-amino acid) pre-hormone (72, 73). Rho et al. also reported other two further alternative cuts able to generate 40- or 47-amino acid versions of the hormone (72). In mice, it is highly expressed in submaxillary gland, stomach, pancreas, intestines, kidney, lung, mesentery, thymus, spleen, ovary (but not in testis), and the immune system (71). Both Takei et al. and Rho et al. emphasize the relatively significant levels of the AM2/intermedin in the pituitary gland, which would regulate hormone secretion in an autocrine and/or paracrine manner (71, 72). Like AM, AM2/intermedin possesses a strong hypotensive effect in normal and in spontaneous hypertensive rats (72) as well as cardioprotective effects against myocardial ischemia/reperfusion injury in rats (73).

Particularities of the AM (and Calcitonin-Like Peptide) Receptors

At this point, it is clear that AM and the other hormones of this family exert a broad variety of physiological effects by acting on diverse tissues and systems. What is striking is the fact that all these processes arise from their interaction with only two closely related proteins: calcitonin and calcitonin-like receptors

(CTR and CLR, respectively). These are G protein-coupled receptors (GPCR) belonging to the B1 subfamily, which are linked with G_s and thereby signal through adenylate cyclase/cAMP (74). In principle, such apparent promiscuity could partially explain the superposition of biological activities displayed by some of these peptides. Nevertheless, the ligand affinity and thus pharmacological behavior of these GPCRs results from their additional heterodimerization with one of the three accessory receptor activity-modifying proteins (RAMP1, RAMP2 or RAMP3).

The three RAMPs share about 30% of homology in their \approx 160-amino acid sequence that gives place to a common structure including a large extracellular N-terminal domain, a single transmembrane domain, and a very short cytoplasmic C-terminal tail (C-tail) (75). RAMPs are well conserved amongst mammals. Indeed, mouse and human amino acid sequence identity for RAMP1, RAMP2, and RAMP3 are 70%, 68%, and 84%, respectively (76). In the endoplasmic reticulum, either, RAMP1, RAMP2, or RAMP3 can pair with CLR or CTR acting as chaperones that confer ligand specificity and binding affinity. Simultaneously, that assembly allows the transport of the receptor complex to the plasma membrane. It has been shown that only RAMP3 bears a PSD-95/Discs large/ZO-1 homology (PDZ) domain in the C-tail which allows its interaction with different factors responsible for further endocytic receptor trafficking and recycling (77). Although RAMPs are ubiquitous throughout the body, there are differences in their tissue distribution, and the abundance of each isoform depends on the tissue type (78–80).

The pharmacology of the CTR –mediator of calcitonin effects– switches differentially in presence of RAMP1, RAMP2 or RAMP3, giving rise to the AMY heterodimeric receptors AMY₁, AMY₂, and AMY₃, respectively. Analogously, the CGRP receptor results from dimerization of CLR with RAMP1, while AM receptors 1 (AM₁) and 2 (AM₂) correspondingly emerge from the assembly of CLR with RAMP2 or RAMP3. In parallel, AM2/intermedin exerts its effects through the CGRP receptor, AM₁ and AM₂, presenting the highest potency when binding the latter (72, 81). **Figure 1C** illustrates the CTR/RAMP- and CLR/RAMP-composed receptors and their respective affinity for the different ligands.

The modulating effect of RAMPs on the ligand affinity of CTR and CLR could be due to an allosteric change in the conformation of the GPCR, leading to the exposure of different binding epitopes; or to a direct contribution together with the GPCR with epitopes that interact with the hormones (82–85). As mentioned above, RAMPs do not only give rise to different AM-, CGRP-, and AM2/intermedin-preferring GPCRs, but also are involved in their trafficking from Golgi to the cell membrane, posttranslational modifications like glycosylation, signaling as well as recycling (82, 86, 87). Furthermore, it is worth mentioning that, although best studied and characterized, the modulating action of RAMPs is not exclusive to CTR and CLR. In this sense, RAMPs also operate as molecular chaperones and allosteric modulators of several GPCRs and their signaling pathways, including glucagon, growth hormone releasing

hormone (GHRH), parathyroid hormone and chemokine receptors among others (82, 88, 89).

In the case of the AM and the CGRP receptors, full functionality requires a third element: the receptor-complement protein (RCP) (90, 91). This cytosolic component, bound through ionic interactions to the cell membrane, couples CLR with the G_s -mediated signaling transduction pathway (92, 93). Different reports point out that RCP is not necessary for AM and CGRP receptors to recognize their respective ligands; however, they are not able to activate adenylate cyclase in its absence (91–93).

In all, **Figure 1D** illustrates the complex structure of AM receptors formed by the three aforementioned proteins: CLR acting as the ligand-recognizing component whose affinity and membrane location depends on the RAMP chaperone member, and the RCP as the transduction-coupling constituent.

Nowadays, it is well accepted that AM, as well as the remaining calcitonin-like peptides, exert their physiological and pathological activities through the complex receptors accordingly mentioned above and shown in **Figure 1C**. Nevertheless, as Hay et al. deeply reviewed and clearly explained, there have been some misunderstandings regarding the apparent capacity of two other particular proteins to act as AM receptors: RDC1 and GPR182 (also known as L1-R/G10D and, mistakenly, AMDR) (94). In the middle 1990s, both proteins were proposed as mediators of AM pharmacological effects (95, 96). Although further studies have not confirmed this (86, 97), the suggestion that RDC1 and GPR182 may be AM receptors persist to this day. Currently, RDC1 and GPR182 are not accepted to be genuine AM or CGRP receptors (94). RDC1 is considered an atypical chemokine receptor, also known as C-X-C motif receptor 7 (CXCR7) (98), while GPR182 has remained as an orphan GPCR so far (99).

Involvement of AM Receptors in Mediating Physiological and Pathological Processes

AM₂ and AM₁ present comparable affinity for AM (81), thereby making difficult the distinction of their individual involvement in the aforementioned AM-mediated physiological activities. In these circumstances, their tripartite structure and the fact that CLR and RAMPs seldom migrate to the cell surface separately make the RAMP2- and RAMP3-focussed studies a good approach to differentiate the roles of AM₁ and AM₂. Naturally, when drawing conclusions, it must be always considered that RAMPs do not interact exclusively with CLR (and CTR).

Several studies indicate that murine AM (AM^{-/-}), CLR (*Calcr1*^{-/-}) or RAMP2 (*Ramp2*^{-/-}) knockout embryos die at mid-gestation owing to severe edema as a consequence of altered angiogenesis and lymphatic vasculature (42, 45, 48, 100–104). Although there were divergences in terms of whether hemorrhage is present or not amongst the different models, which ultimately might be attributed to the employment of different mouse strains, the fact that the three knockout types resulted in a non-viable common phenotype not only suggests the importance of AM for embryonic development, but also evidences the necessity of the canonical AM₁-mediated signaling

in endothelial cells (105). In fact, this was confirmed by Kechele et al. achieving the survival of a *Ramp2*^{-/-} fetus by engineering mice with endothelial-specific expression of *Ramp2* under the control of the VE-cadherin promoter (104).

Nonetheless, it raised the question of whether AM₁ requirement was circumscribed to uterine growth. Concerning this, Koyama et al. further made use of interesting murine models enabling the study of AM^{-/-} and *Ramp2*^{-/-}-derived phenotypes in adulthood (47). Specifically, they developed endothelial cell-exclusive *Ramp2* and AM knockout mice (E-RAMP2^{-/-} and E-AM^{-/-}, respectively) as well as (tamoxifen) drug-inducible E-RAMP2^{-/-} mice (DI-E-RAMP2^{-/-}), for *Ramp2* deletion induction in adults. Contrary to conventional *Ramp2*^{-/-} mice, most (~95%) E-RAMP2^{-/-} and E-AM^{-/-} animals died during the peri-natal period, and not *in utero*. The surviving ones developed systemic and interstitial edema, vascular abnormalities and vasculitis throughout age. These effects were comparable in the DI-E-RAMP2^{-/-} model but less severe in E-AM^{-/-} mice, possibly given the fact that AM is produced by a wide range of tissues (47). Of note, *Ramp2*^{+/-} and DI-E-RAMP2^{-/-} animals presented a normal lymphatic system (48). In particular, *RAMP2*^{+/-} mice showed substantially reduced fertility and other endocrinological alterations, including basal and maternal hyperprolactinemia, enlarged pituitary gland, accelerated mammary gland development, and altered skeletal properties among others (45, 101, 106). Nevertheless, these phenotypes were not reproducible in the *Calcr1*^{+/-} genotype, implying they are not directly linked to AM/AM₁ but respond to CLR-independent physiological roles of RAMP2 in other systems (106).

Tam et al. carried out a series of experiments in RAMP2-overexpressing mice demonstrating a prominent physiological role of AM₁ in mediating the vasodilatory effects of AM in vascular smooth muscle cells (107). Likewise, their analysis indicates that AM would bind the CGRP receptor at high nanomolar-range concentrations once AM₁ has been blocked. Interestingly, Pawlak et al. more recently drew a fully opposing conclusion. In a study employing *Calcr1*^{+/-}, *Ramp2*^{+/-}, *Ramp1*^{-/-}, *Ramp3*^{-/-}, and *Ramp1*^{-/-}/*Ramp3*^{-/-} double-knockout mice, they demonstrated that the AM hypotensive effect would be mainly mediated by its action on CGRP receptor and secondarily on AM₁ (108). These discrepancies must be clarified in future investigations.

On the other hand, *Ramp3*^{-/-} mice presented normal fertility and angiogenesis in both embryos and as adults with no obvious phenotypic defects (48, 101). Postsurgical lymphoedema drainage was significantly delayed in these animals, pointing out AM₂ as principal AM mediator in the regulation of lymphatic functionality (48). In addition, Dackor et al. observed that this genotype failed in gaining body weight in adulthood (101); however, this was not further confirmed by other authors (48). Interestingly, Dackor et al. also reported that *Ramp3*^{-/-}, *Ramp2*^{+/-}, and wild type genotypes showed comparable blood pressure. Noteworthy, this was not due to any compensatory up-regulation of either *Ramp2* or *Ramp3* gene expression, supporting the lack of functional redundancy of AM₁

and AM₂ *in vivo* (45, 47, 109, 110). In contrast, Ichikawa-Shindo et al., showed that *Ramp2*^{+/-} mice displayed a slight but significant increase in blood pressure with respect to wild type animals accompanied by elevated compensatory levels of AM (45). Pawlak et al. also found elevated blood pressure in *Ramp3*^{-/-} mice with respect to wild type ones, particularly in males (108). In line with this, Barrick et al., have observed that, in the RenTgMK transgene mice model of angiotensin II-induced chronic hypertension, renal damage, cardiac hypertrophy and cardiac apoptosis were substantially exacerbated in males over females when animals presented the *Ramp3*^{-/-} genotype (109). The mechanistic reason that would explain these findings is not clear yet, but other RAMP3-regulated processes also seem to be influenced by gender (111). In fact, both AM and *Ramp3* may be induced by estrogens, RAMP3 even being associated with the origin of menopausal obesity, although independently of AM-signaling (111, 112). On the other hand, Zhao et al. have not observed estrogen-induced AM secretion in human endometrial primary cells (113).

Regardless of the apparent sexual dimorphism, *Ramp3* expression is consistently up-regulated in rodent models of cardiac hypertrophy, hypertension and heart failure, leading to the hypothesis that increased AM signaling through AM₂ may have a cardioprotective aim. In this sense, Cueille et al. also reported increased RAMP3 and (RAMP1) in atria and ventricles from rats in a non-ischemic model of chronic cardiac insufficiency due to pressure overload caused by aortic banding for six months (114). No variations were observed in CLR and AM at that time. In a further independent study, on the other hand, the left ventricle of rats with aortocaval shunt-induced cardiac hypertrophy presented up-regulated gene expressions of AM, *Calrl*, *Ramp2*, and *Ramp3* compared with controls five weeks after the surgery (115). In a similar work, Oie et al. found that basal *Ramp2* mRNA in rat ventricular cardiomyocytes and non-cardiomyocytes cells is significantly higher than *Ramp3* mRNA transcript. However, this pattern was drastically inverted one week after a congestive heart failure induced by left coronary artery ligation (116).

LPS-induced septic shock in mice resulted in a strong decrease of *Calrl* and *Ramp2* mRNA expression in lungs, accompanied by a substantial rise in the levels of RAMP3 in pulmonary tissue and the principal organs in immune system. This is thought to be a body response to dampen the inflammatory process (36, 110).

All these findings collectively suggest that AM₁ is essential for angiogenesis, vascular homeostasis and embryonic development while AM₂ is meaningfully involved in lymphatic system physiology and would be induced, under certain physiological or pathological conditions, to adjust the CLR signaling. It is also quite plausible that the particular PDZ domain-bearing C-tail of RAMP3, enabling its interaction with molecules involved in trafficking of GPCRs, could be of crucial importance in the precise and dynamic regulation of AM₂ availability in the cell membrane.

The signal transduction pathways activated by AM in order to regulate processes such as vasodilation, cell survival,

proliferation, migration, and vascular cord-like structure formation vary between species, organs, tissues, and cells. However, the main signaling pathways whereby AM exerts its actions involve cAMP, Akt, mitogen activated protein kinase (MAPK)-extracellular signal regulated protein kinase (ERK), and the tyrosine phosphorylation of focal adhesion kinase (P125^{FAK}) (117, 118).

AM ACTION IN MALIGNANT CONTEXT

Roles of AM in Cancer

Since its discovery from human pheochromocytoma extracts, cumulative clinical evidence has revealed the association between AM and a variety of tumor types, showing that it is expressed by malignant cells, endothelial cells, pro-angiogenic cancer-associated fibroblasts (CAFs) and tumor-associated macrophages (TAMs), immature monocytic cells including TIE2 + monocytes, VEGFR1+ hemangiocytes, and CD11b+ myeloid cells within the tumor microenvironment (119–122).

Elevated circulating AM has been reported in the plasma of patients with lung and gastrointestinal cancers (123), as well as in untreated Cushing's disease due to pituitary ACTH-producing adenoma, as compared with normal subjects (124). The increase in the former case seems related to ACTH production and immediately normalizes after surgical excision of the tumor. AM overexpression could be considered as a compensatory response to the elevated circulating cortisol. However, it is worth remarking that it was observed that AM concentration was about double on the side where the adenoma was localized, suggesting it may be directly produced by the tumor (124).

Patients with intraocular or orbital tumors presented significantly elevated AM mRNA levels in the malignant tissues in comparison with those having proliferative vitreoretinopathy, proliferative diabetic retinopathy, preretinal macular fibrosis, and acute retinal necrosis; indicating that AM may play a specific role in the pathogenesis of these cancers (125).

AM expression has been also described in human malignant pleural mesothelioma (MPM) and melanoma biopsies (119, 126). In colorectal cancer, the AM mRNA transcript level has been suggested as a useful marker for predicting high risk for relapse and cancer-related death in patients who undergo curative resection (127). Moreover, it has been found that plasma AM levels positively correlated with malignancy (120). Notably, increased expression levels of AM have been observed in samples harboring a mutation in *KRAS*. Instead, with the exception of scattered positive staining at the base of the glands in neuroendocrine cells, normal colon tissues were negative for AM expression (121, 122).

High expression of AM was found in human glioma samples, especially in the most aggressive form, namely, glioblastoma, whereas it was low in anaplastic astrocytoma and barely detectable in the low-grade astrocytoma and oligodendroglioma (128, 129).

Increased in AM mRNA expression was also reported in samples from those prostate cancer patients presenting the worse prognoses, as indicated by high Gleason's scores, while practically absent in tissues samples collected from benign pathologies (130). Similarly, different works indicate that elevated AM expression associates with higher incidence of metastasis, larger residual size of tumors after cytoreduction, and shorter disease-free and overall survival time in epithelial ovarian cancer patients (5, 131), and correlates with tumor grading and metastasis in osteosarcoma (4) and hepatocellular carcinoma (23, 132).

Analogously, elevated tissue AM mRNA is a distinguishing feature of clear-cell renal carcinomas compared with other kidney tumors, and it is associated with an increased risk of relapse after curative nephrectomy due to this type of carcinoma (133, 134). Actually, Michelsen et al. reported significantly increased plasma AM concentrations in patients with renal malignant disease compared with healthy controls (133). Nevertheless, as mentioned above, renal failure is associated with elevated blood levels of AM. Therefore, impaired function of the affected kidney may be partially responsible for AM up-regulation. For this reason, plasma AM may not be suited as a tumor marker for renal cancer (80, 134).

Quantification of plasmatic AM concentrations showed no substantial difference between breast cancer patients and healthy women (135). Nonetheless, a significant positive correlation between tumor diameter and plasma AM levels was observed, suggesting not only that the breast malignancies were actually the source of the circulating AM, but also that tumors require a critical size until a noteworthy increase of secreted AM is detectable in blood (120, 135).

The AM gene has been found markedly overexpressed in patients with pancreatic cancer when compared with controls with benign/cystic pancreatic diseases or pancreatitis (136, 137). Likewise, the expression of AM was higher in subjects with pancreatic cancer and diabetes mellitus as compared with those not suffering from the former. These increased levels were detected in malignant tissue, at both RNA and protein levels, and as circulating AM (137).

Preclinical research does not only support these findings, but also has made great efforts in order to explain them. In this regard, it is worth remarking upon the work carried out by Prof. Ouafik's group showing a correlation between AM expression and disease stage, progression or vascular density in the context of human glioblastoma (128), prostate (130, 138, 139), colon (121), MPM (126), pheochromocytomas (140), lung (141), and renal (134) cancers. In summary, these as well as studies from other laboratories indicate that AM itself does not cause cancer but can contribute to its pathogenesis in three main ways: 1) directly stimulating cell growth and inhibiting apoptosis (142–144); 2) inducing tumor angiogenesis and lymphangiogenesis, thereby supplying nutrients and oxygen to the tumor while boosting metastasis (45, 103, 126, 139, 145); 3) and/or changing the phenotype of cells, leading them to exhibit a more aggressive behavior (126, 138).

With respect to the first mechanism, several studies have demonstrated that AM exposure enhances cell growth and/or invasion in *in vitro* and/or *in vivo* models of breast (146), colon (121), prostate (139), renal (134), and glioblastoma (128) tumors, amongst others. The intrinsic processes behind these effects are not completely clear yet. Nevertheless, AM has proven to be able to inhibit apoptosis of tumor and endothelial cells by down-regulating pro-apoptotic factors such as fragmented PARP, Bax, and activated caspases (143, 144, 147).

In addition, AM protects malignant cells from hypoxia-induced cell death by up-regulation of Bcl-2 in an autocrine/paracrine manner in endometrial carcinoma and osteosarcoma cells (144, 148). In the former, the mechanism involves activation of the MEK/ERK1/2 signaling pathway (148). Similarly, AM was able to significantly increase proliferation and invasiveness of androgen-independent prostate cancer cell lines through stimulation of cAMP and the activation of the CRAF/MEK/ERK/MAPK pathway (139).

Furthermore, intraperitoneal injections of AM stimulated the growth of prostate androgen-dependent cell-derived tumors in castrated animals, suggesting that the peptide might be involved in tumor resurgence after testosterone ablation as in the case of patients treated with androgen-deprivation therapy (138).

Greillier et al. also reported increased activation of the CRAF/MEK/ERK/MAPK pathway in the AM-induced proliferation and invasiveness of the MPM-derived MSTO-211H and H2452 cell lines (126). In the case of hepatocellular carcinoma, the autocrine proliferative effect of AM in hypoxic conditions would be mediated by the PI3K signaling pathway (132). Likewise, the AM-activated PI3K/Akt pathway has been proved to protect endothelial cells from the apoptosis induced by hyperosmotic mannitol therapy for brain edema (149).

More interestingly, AM could also indirectly modulate MYC activity by regulating MYC-associated factor X (Max). This is based on the results of Shichiri et al. in quiescent rat endothelial cells, in which AM stimulated the expression of Max without affecting MYC, and so prevented apoptosis triggered by serum deprivation (150). AM-induced MYC/Max perturbation may result in favor of anti-apoptotic and proliferative effects of MYC.

On the other hand, tamoxifen is an anti-estrogen employed in the treatment of hormone-dependent breast cancer. A major concern of this therapy is its proliferative-inducing effect in endometrium, which significantly increases the risk of malignization with the long-term intake (151). The mitogenic and anti-apoptotic properties of AM point to this peptide as the principal intermediary of tamoxifen's adverse endometrial effects through non-canonical estrogen receptor-mediated mechanisms (113, 144, 152). Partial agonistic effects of tamoxifen on the estrogen receptor would be able to stimulate AM transcription *via* an activator protein-1 (AP-1)-directed pathway rather than estrogen signaling response elements in a cell type specific manner (113).

AM activity also appears to extend beyond the malignant cells, being able to act in the tumor environment. There, it may reduce the effectiveness of the immune system to destroy cancer cells by decreasing the expression of pro-inflammatory cytokines

and inhibiting the activation of the alternative complement pathway by binding to complement factor H (153, 154).

Infiltrations of myelomonocytic cells are common in the stroma of different tumors, such as pancreatic ductal adenocarcinoma (PDAC) and melanoma, and are related to poor prognosis (119, 120, 154). In their models of PDAC, Xu et al. demonstrated that AM promotes myelomonocytic cell migration and invasion and a pro-tumor phenotype through activation of the MAPK, PI3K/Akt, and NOS signaling pathways, as well as the expression and activity of the matrix metalloproteinase-2 (120). Comparable results were obtained by Chen et al. reporting not only that AM is involved in macrophage polarization –acquisition of a pro-tumor behavior–, but also that AM produced by TAMs is a central factor in macrophage-induced angiogenesis and melanoma growth (119).

More recently, CAFs have also been reported to play a key role in secreting and mediating AM pro-metastatic and angiogenic effects in melanoma (155), pancreatic (156), and breast (157) tumors.

The best-studied activity of AM in the tumor environment is the induction of neovascularization. In this regard, some works have shown that AM did not induce any direct mitogenic effect in the B16/F10 (melanoma), S180 (sarcoma), MDA-MB-231 (breast), A549 (lung), and pancreatic cancer cell lines; instead, when injected in mice, it would induce their growth as tumor masses by providing a suitable blood flow (119, 136, 141, 146, 158, 159).

Decreased O₂ partial pressure and the resulting increase of HIF-1 α have been implicated as one of the underlying pathways causing AM overexpression in human tumors (160). Hypoxia-stimulated AM expression has been observed in a broad variety of tumor cells, including endometrial (144), osteosarcoma (148), colorectal (121, 122), renal (161), hepatic (132), prostate and promyelocytic leukemia (162), pancreatic (136, 158), and so on. Actually, since tamoxifen has proven to induce hypoxia in xenografts, this has been proposed to be an alternative mechanism by which this anti-estrogen may induce AM in endometrium (144, 163). Thus, given the fact that localized hypoxia is an intrinsic hallmark of most solid tumors, it is not surprising that plasma AM is elevated in distinct common cancer types (133). It was described that AM expression correlates with both VEGF and HIF-1 α in colorectal cancer (127). Furthermore, It was observed that AM could be an upstream modulator of the HIF-1 α /VEGF pathway, suggesting that AM might induce angiogenesis through VEGF expression as consequence of JNK and AP-1 activation in epithelial ovarian cancer (6, 7). Analogously, several *in vitro* and *in vivo* studies have demonstrated the involvement of hypoxia, HIF-1 α , AM, and AM receptors in HCC development, and how anti-AM therapeutic approaches would be of great value to deal with this disease (164–166).

On the other hand, it must be considered that the major sources of AM are not only malignant cells themselves, but also the vascular endothelium. This was clearly demonstrated in a work by Iimuri et al. in which S180 sarcoma tumorigenic cells

presented more difficulty in developing tumors in AM-heterozygous knockout (AM+/-) mice –expressing \approx 50% of circulating AM– compared to wild type ones (159).

AM-producing tumors are characterized by an increased vascular density (163) that correlates with the probability of metastasis occurring (167). Indeed, once trapped in the lymphatic capillaries, the angiogenic potential of AM-overexpressing cancer cells would facilitate neovascularization and hence macroscopic metastatic growth (146). In line with this, the analysis of AM expression and the clinicopathologic features of breast cancer patients showed that axillary lymph node metastasis markedly correlated with the AM protein levels in tumors (135). In colorectal cancer, AM was one of the most selectively upregulated genes in cells with a mutant KRAS under hypoxic conditions (122). Silencing of K-ras drastically reduced AM expression levels in hypoxia compared to control, indicating that AM is a key target for the K-ras oncogenic action in poorly oxygenated tumors. In addition, knockdown of AM suppressed tumor growth and impaired angiogenesis in colon tumor xenografts (122). Studies in HUVEC indicate that AM-induced pro-angiogenic effects would be mediated by PI3K/Akt, ERK, and P125^{FAK} (118).

Besides modifying the nature of TAMs –inducing a M2 phenotype–, AM expression has proven to be associated with more aggressive forms of glioma (128), prostate (130, 138), ovarian (5, 131) and breast cancers, generally correlated with increased metastatic capacity (5, 146). In prostate cancer, AM promotes the appearance of a neuroendocrine-like phenotype –usually presented in the clinic as an aggressive and drug-resistant form– in an androgen-regulated manner in the testosterone-dependent LNCaP cell line (138). These cells normally express both AM as well as AM₁ and AM₂. However, AM production is significantly increased upon the removal of androgen both in culture and *in vivo* (when injected in immune-suppressed mice), suggesting that paracrine/autocrine AM secretion represents a survival mechanism that prostate malignant cells employ to regulate neuron-like differentiation when facing androgen deprivation conditions. Such a phenotypic effect would be mediated by AM-induced nuclear translocation of cGMP-dependent protein kinase (PKG), and subsequent regulation of gene expression.

In vitro studies with colon cancer cells have shown the capacity of AM to promote a more invasive phenotype (122).

In summary, **Figure 2** illustrates all the above-mentioned AM autocrine/paracrine pro-tumor actions on malignant cells and/or different components of the tumor stroma.

AM₁ and AM₂ in Cancer

Cancer cells employ circulating AM as well as that produced by themselves to promote tumor growth through the aforementioned mechanisms. In this section, we will review the role of key mediators of AM's pro-tumor activity: AM₁ and AM₂. The findings discussed below are summarized in **Table 1**.

Berenguer et al. observed that both AM₁ and AM₂ were responsible for mediating AM-induction of a neuroendocrine phenotype in the androgen-sensitive LNCaP cell line. Moreover,

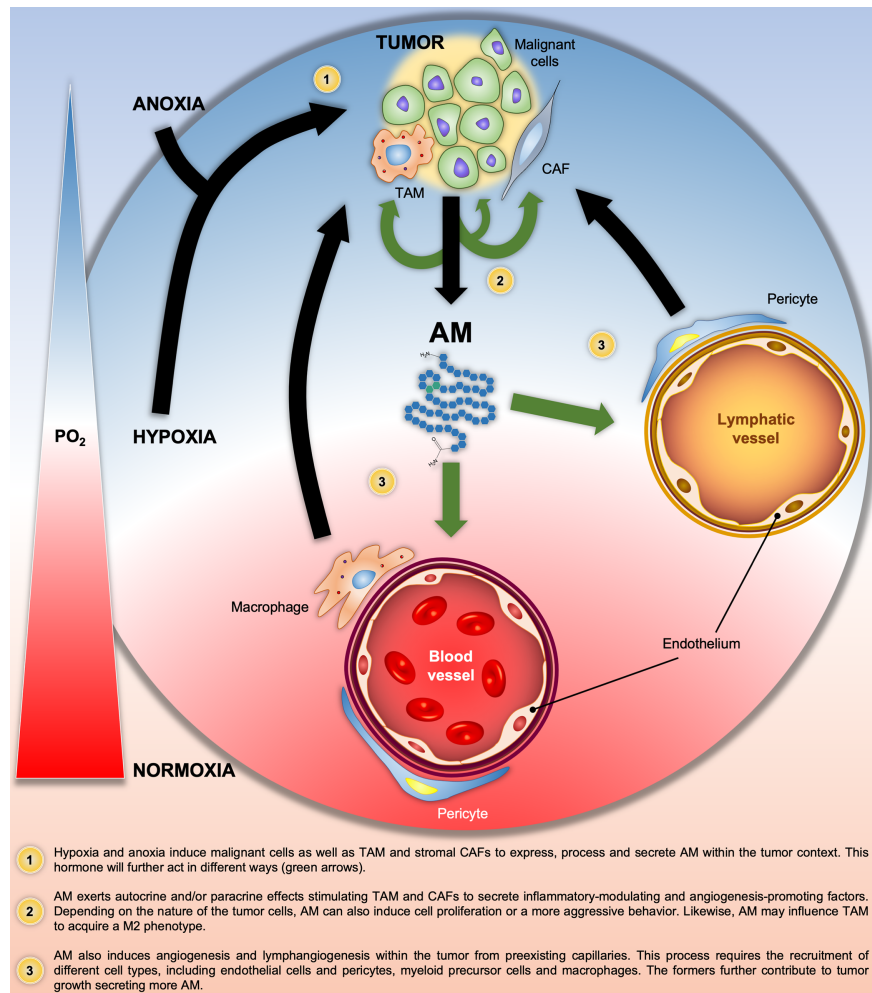


FIGURE 2 | Graphical summary of the Adrenomedullin (AM)-related pathologic processes in solid tumors. Black and green arrows indicate the progression of the pathologic processes and the AM target cells, respectively. PO_2 , O_2 partial pressure.

they described that, while the levels of CLR, RAMP2 and RAMP3 were not regulated by androgen status, levels of AM mRNA and immunoreactive AM increased 4- to 7-fold after androgen withdrawal *in vitro* and in LNCaP xenografts in animals after castration (138). Mazzocchi et al. did not find evidence of significant differences in the level of expression of either *Calclrl* or *Ramp1* and *Ramp2* mRNAs between prostate hyperplasia and cancer specimens. Nevertheless, they observed a clear higher expression of the *Ramp3* gene in the former group. Unfortunately, these authors did not specify the type and androgen dependency status of the cancers (172). Furthermore, these results were partially mirrored in *in vitro* studies with DU145 and PC3 androgen-independent prostate cancer cell lines. In this regard, *Calclrl*, *Ramp1* and *Ramp2* mRNA transcripts were detected in both cell types. In contrast, *Ramp3* expression was restricted to the DU145 cells, indicating that they resemble prostate cancer epithelial cells more closely than the PC3 cell line. Of note, AM showed proliferation-inducing and anti-apoptotic activities only in DU145 cells (130, 139, 172),

pointing at AM_2 as the mediator of such effects. This finding was supported by the fact that the AM antagonist CGRP8-37 was more effective than AM (22-52) inhibiting DU145 proliferation. It is well known the higher selectivity of CGRP8-37 for AM_2 with respect to AM_1 (172).

In clinical samples of renal cell carcinoma, RAMP3 has shown to be predominantly expressed in inflammatory cells associated with the tumor whereas RAMP2 was mainly localized in the malignant cells (134). On the other hand –and as part of the same study–, although authors suggest that the *in vitro* cell proliferation, invasion, and migration activated by exogenous AM would be mediated by both AM_1 and AM_2 , RAMP2 was barely detected in the renal cancer cell lines employed (786-O and BIZ) (134), indicating that they may not be representative models of that cancer.

Chen et al. observed that *in vivo* tumor growth is significantly attenuated by AM antagonists in the murine B16/F10 melanoma cell line, even when components of the AM receptors were not detected (119). In contrast, TAMs were found to express not only

TABLE 1 | Confirmed expression of AM, CLR, RAMP1, RAMP2, and RAMP3 in different tumors.

Cancer	Sample nature	AM	CLR	RAMP1	RAMP2	RAMP3	Report
Adrenocortical carcinoma	SW-13 cell line	+	+	NR	–	+	(168)
Aldosteronoma	Samples collected from patients	+	+	+	+	+	(142)
Breast	MDA-MB-231 cell line	+	+	NR	NR	+	(169)
	MCF-7 cell line	+	+	NR	+	+	(157, 170)
	CAFs collected from patient tumors	+	+	NR	+	+	(157)
Colorectal	Patient-derived tumors of clinical stages II, III, and IV	+	+	NR	+	+	(121, 122)
	HT-29	+	+	NR	+	+	(141)
	HCT116 cell line	NR	NR	NR	NR	+	(169)
Fibrosarcoma	HT1080 cell line	NR	NR	NR	NR	+	(169)
Glioblastoma	Patient-derived tumors	+	+	NR	+	+	(128)
	U87 cell line	+	+	NR	+	+	(128, 141)
	U373, U138, SW1783 and SW1088 cell lines	+	+	NR	+	SW1783	(128)
Kidney	Chromophobe and clear cell renal carcinomas	+	+	NR	+	+	(133, 134)
	786-O and BIZ cell lines	+	+	NR	–	+	(134)
Liver	Patient-derived hepatocellular carcinomas	+	NR	NR	+	+	(132)
	Huh-BAT and HepG2 cell lines	+	+	NR	+	+	
Lung	A549 cell line	NR	+	NR	+	+	(141, 146)
Melanoma	Patient samples	+	+	NR	+	+	(119)
	B16/F10 murine melanoma cell line	+	–	NR	–	–	
	B16/F10 xenograft TAMs	+	+	NR	+	+	(169)
	YU/PAC2 cell line	NR	NR	NR	NR	+	
	B16BL6 murine melanoma cell line	+	NR	NR	+	NR	(155)
MPM	Tumors collected from patients	+	+	NR	+	+	(126)
Osteosarcoma	F5M2 cell line	+	+	NR	+	+	(148)
Pancreas	Patient-derived PDAC	+	+	+	+	+	(136, 171)
	TAMs and PDAC-localized myelomonocytic cells	NR	+	NR	+	+	(120)
	Capan-1, Colo-357, T3M4, Mia-PaCa-2 and Panc-1 cell lines	+	+	+	+	T3M4	(136)
	BxPC-3 and PCI-35 cell lines	+	+	NR	+	NR	(158)
	PCI-10 and PCI-19 cell lines	+	–	NR	+	NR	
	PCI-43 cell line	+	–	NR	–	NR	
	PAN02 cell line	+	+	NR	+	+	(156)
	BxPC3, SU.86.86, Mia-PaCa-2, MPanc96, Aspc-1 and HPAC cell lines	+	–	+	+	–	(171)
	CFPAC-1 cell line	+	–	+	–	–	
	Panc-1 cell line	+	–	–	–	–	
	Mia-PaCa-2 cell line	+	–	–	+	–	
Pheochromocytoma	Clinical samples collected from benign and malignant tumors	+	+	+	+	+	(140, 142)
	Primary culture of tumor cells	+	+	+	+	+	(140)
Prostate	Prostate cancer of high-grade adenocarcinomas (Gleason's score > 7)	+	+	NR	+	+	(139)
	DU145 cell line	+	+	+	+	+	(130, 139, 162, 172)
	LNCaP cell line	+	+	NR	+	+	(138)
	PC3 cell line	+	+	+	+	–	(130, 146, 172)

The evaluation of the expression of AM, CLR, RAMP1, RAMP2, and RAMP3 was determined at mRNA transcription level (PCR), and/or at protein level by Western blot and/or immunohistochemistry. NR, not reported.

AM, but also CRLR, RAMP2, and RAMP3. These cells are thought to be the main producers of hypoxia-induced AM within the tumor masses and so the mediators of angiogenesis. Moreover, the peptide will act in a paracrine and autocrine way inducing the acquisition of an M2 phenotype.

In the clinic, most human melanoma tissues were positive for CRLR, RAMP2, and RAMP3 –apart from AM–, while their expression levels were much lower in control healthy samples (119). Nevertheless, it would be of great value to determine the distribution of these proteins amongst different tumor cell types.

Ishikawa et al. obtained similar results in a series of five pancreatic cancer cell lines. In this respect, although all of them presented AM, only two (BxPC-3 and PCI-35) showed CLR and RAMP2 proteins. PCI-10 and PCI-19 cells showed RAMP2, and the PCI-43 cell line neither CLR nor RAMP2 (158). Interestingly,

although anti-AM therapy had no effect in the *in vitro* proliferation of none the cell lines, it substantially abrogated PCI-43 cell-derived tumors *in vivo*, clearly implying that AM is acting on other components of the tumor environment.

A subsequent independent series of experiments performed by Keleg et al. in five other pancreatic cancer cell lines (Capan-1, Colo-357, T3M4, Mia-PaCa-2, and Panc-1) were partially in agreement with the previous results (136). The five assessed cell lines expressed AM, CLR, RAMP1, and RAMP2, whereas RAMP3 was detected in only one of them. Studies with patient samples showed increases in median *Calcr1* mRNA expression in PDAC in comparison to normal pancreatic tissues. In contrast, they observed >2- and >7-fold reduction in the median transcripts of *Ramp1* and *Ramp3*, respectively, in PDAC tissues compared to normal pancreas samples while no

differences were detected in the expression of *Ramp2* between healthy and malignant tissues. Immunohistochemical analysis of CLR and RAMP1, RAMP2 and RAMP3 demonstrated moderate to strong staining in islets in the normal pancreas. In PDAC tissue, however, CLR colocalized with RAMP1 and RAMP2, and they were prominently expressed in malignant cells while RAMP3 was not detected. More recently, Xu et al. reported CLR, RAMP2, and RAMP3 in the pro-tumorigenic myelocytic cells associated with PDAC (120), which is in line with the capacity of AM to recruit different cell types reported by Kaafarani et al. (141).

Considering the AM pro-tumor effect, as well as RAMP1, RAMP2 and RAMP3 expression levels, it could be said that the results published by Ramachandran et al. in pancreatic cancer are partially in agreement with the previous ones. More specifically, none of the assayed cell lines (BxPC3, MiaPaCa-2, CFPAC-1, HPAC, MPanc96, Panc-1, Aspc-1, and SU.86.86) presented *Ramp3* or *CLR* expression. However, there are discrepancies in terms of *Ramp1* and *Ramp2* expression in BxPC-3, Panc-1, and Mia-PaCa-2 cells (171). Instead, authors attributed the AM-mediated pro-tumoral activity to the GPR182 receptor. They observed that by silencing GPR182 the basal growth was reduced as well as the AM-stimulated growth and invasive capacity of the malignant cells when compared with control shRNA (171). As in the case of the first report proposing GPR182 as an AM receptor, these findings have not been yet confirmed. Indeed, as concluded some paragraphs above, most of the cumulative evidence suggests that AM-induced tumor development in pancreatic cancer is mediated by AM₁ and AM₂. It is also noteworthy that they evaluated RCP expression, finding it in all the cell lines except CFPAC-1.

In all, these findings indicate that AM₁ would be more relevant than AM₂ in the pro-tumor action of AM in PDAC. Likewise, *in vitro* and *in vivo* evidence strongly suggest that AM induced tumor growth by mainly acting on tumor stroma components (120, 136, 158), proposing that the focus should not be on the malignant cells *per se* but in the peripheral stroma. In line with this, very recent experiments carried out by Dai et al. inoculating PAN02 tumor cells in the spleen of *Ramp3*^{-/-} and DI-E-RAMP2^{-/-} mice not only demonstrated the active involvement of CAFs in the tumorigenic and metastatic capacity of these pancreatic cells, but also the different roles played by AM₁ and AM₂ (156). In this sense, when injected in DI-E-RAMP2^{-/-} animals, despite the tumor masses being significantly reduced and accompanied by defective angiogenesis, metastases to the liver were notably increased. In them, CAFs presented elevated RAMP3 and podoplanin (PDPN), a marker of lymphatic endothelial cells and lymphangiogenesis associated with a poor prognosis in various types of cancers. On the other hand, in *Ramp3*^{-/-} mice, although tumor growth and angiogenesis were not affected (with respect to *Ramp3*^{+/+} animals), tumors presented a less aggressive phenotype as indicated by the marked reduction in liver metastases as well as the number of PDPN-positive CAFs. In summary, in pancreatic cancer AM₁ would be essential in promoting tumor growth and angiogenesis while antagonizing an AM₂-mediated pro-metastatic effect (156).

This group had previously observed an increased propensity to lung metastasis in DI-E-RAMP2^{-/-} mice by generating B16BL6 melanoma cell line-derived tumors (155). Most tellingly, endothelial cell-specific RAMP2 overexpression in E-RAMP2 Tg mice strongly reduced lung metastasis and promoted survival. The authors hypothesized that the irregularly shaped, tortuous, and hyperpermeable vessels resulting from deficient angiogenesis (consequent of the DI-E-RAMP2^{-/-} phenotype) would be suitable substrate for the formation of pre-metastatic niches in distant organs (155). The sum of these findings suggests that a physiologically active AM/AM₁ signaling system may be crucial to reduce the likelihood of metastasis in at least pancreatic and melanoma tumors.

Benyahia et al. more recently also demonstrated that CAFs extracted from invasive human breast adenocarcinomas are more competent than normal fibroblasts in enhancing MCF-7 cell growth by induction of stable vascularization when injected into immunocompromised mice (157). The authors demonstrated that AM is one of the CAF-derived factors responsible for endothelial cell-like and pericyte recruitment.

CLR, RAMP2 and RAMP3 have been also detected in glioblastoma tumors –both patient-collected samples and in immortalized malignant cell lines (128)– and in MPM (126). Indeed, expression levels in the former have shown to be much higher than in normal adjacent (pleural) tissue (126). Analogously, CLR, RAMP2, and RAMP3 immunostaining was scarcely detectable in the colonic epithelia of the crypts in normal tissue whereas the epithelial compartment in the well-differentiated adenocarcinoma samples showed strong staining for all these proteins (121). Evidence suggests that AM would act in a paracrine and autocrine manner in colorectal tumors; however, it is not yet clear the individual roles of AM₁ and AM₂ in the physio-pathology of the disease (121, 141). This is also applicable in hepatocellular carcinoma cell lines (132).

In vitro studies determined that the human SW-13 adrenocortical carcinoma-derived cell line only expressed *Calcr1* and *Ramp3*, while normal adrenocortical cells presented *Ramp1*, *Ramp2* and *Ramp3* mRNA transcripts, suggesting that the AM proliferative effects in the malignant cells are mediated by AM₂ stimulation (168).

Clinical aldosteronoma samples were shown to express CLR, RAMP1, RAMP2, and RAMP3 mRNA, the levels of the two former being much higher than those of RAMP1 (142).

Studies with clinical samples and in primary culture of tumor cells have shown that, although benign pheochromocytomas secrete more AM than malignant ones, both share comparable expression levels of AM and (and CGRP) receptor components (CLR and RAMPs), RAMP1 being markedly abundant (up to 12-fold) with respect to RAMP2 and RAMP3 (140). Nevertheless, Thouënnon et al. suggest that RDC1 could be the predominant receptor for the autocrine effect of AM in this type of tumor basing their hypothesis on three pillars: 1) the elevated rate of expression of RDC1 over AM receptors components; 2) the fact that, among all genes examined in benign and malignant pheochromocytomas, *RDC1* was the only one that exhibited a significant differential expression between the two tumor

subtypes, suggesting that it could be involved in malignant transformation; and 3) the assumption that AM is not pharmacologically active on the CGRP receptor. Considering the aforementioned strongly increased levels of RAMP1 over RAMP2 and RAMP3, authors presume that the competition for CLR would leave scarce possibility for the assembly of AM₁ and AM₂. If this is combined with the third pillar, there would not be a place for AM action in these cells. However, at this point it may be of particular interest to reconsider the, already mentioned, articles of Tam et al. (107) and Pawlak et al. (108) describing AM cardiovascular effects mediated through the CLR/RAMP1 complex. Considering that Thouënnon et al. do not give any proof of RDC1-activated signaling specifically in response to AM, the CGRP receptor seems more plausible as the AM target in pheochromocytoma. This is indeed supported by results obtained in the *RDC1*-downmodulated rat pheochromocytoma-derived PC12 cell lines suggesting that, although RDC1 may be involved in cell survival in serum deprivation conditions, it does not appear to be implicated in the AM-induced proliferative effect (140).

In line with the idea of alternative receptors, Zudaire et al. have reported that, in the tumor context, AM is able to induce mast cells to secrete different inflammation and angiogenesis mediators such as histamine and β -hexosaminidase by way of a process that would not be mediated by AM classical receptors, but, instead, by its interaction with other cell membrane proteins through electric charges. This effect is of particular pharmacological interest given the fact that it would escape from the action of AM₁ or AM₂ antagonists (160).

In all, except in the work of Ramachandran et al., AM pro-tumor effects always correlate with the occurrence of the necessary subunits to assemble functional AM₁ and/or AM₂, whether directly in cancer cells or in diverse stroma cell components (e.g., TAMs, CAFs, endothelium, etc.) (173). Likewise, there appears to be a differential predominance by one type of receptor depending on the type of cancer, which is of much importance in the eventual development of therapeutic approaches. In this sense, specific anti-AM₂ agents would be more efficient in prostate cancers than in PDACs.

AM-Targeting Agents and Potential Employment in Oncology

Several strategies have been proposed to inhibit AM-mediated processes with potential application in oncology, including impediment of the AM-receptor interaction by antagonistic ligands, direct targeting of AM by specific blocking antibodies, and even regulation of the AM mRNA transcript. All these potential therapeutic approaches are discussed in the following paragraphs and summarized in **Figure 3**.

The first AM antagonists arose as result of structure-activity relationship (SAR) studies indicating that both the ring formed between amino acids 16 and 21 and the C-terminal amide are essential for the full demonstration of the AM hypotensive effect (174). On this basis, different laboratories undertook the search for truncated, pharmacologically inactive versions of AM able to antagonize it by competing for receptors. These

investigations gave place to different types of derivatives: 1) AM (16-52)CONH₂, AM (13-52)CONH₂ (174), and AM (15-52)CONH₂ (175) peptides with hypotensive and vasodilatory activity comparable to that shown by AM; 2) AM (22-52)CONH₂ –also known as AM antagonist (AMA) and weakly selective for AM₁ over AM₂–, AM (1-52)COOH (176, 177), and AM (37-52)CONH₂ (178), showing significantly lower receptor binding and pharmacological response; 3) AM (16-21), AM (16-31), AM (1-25) (179), and AM (11-26) (176), as inducers of increased systemic arterial pressure in rat; and 4) AM (33-52)CONH₂ and AM (1-10)COOH, not able to bind AM receptors (174).

Together with the CGRP derivative CGPR (8-37), some molecules belonging to group 2 have been commonly employed as AM antagonists (172, 180), shown to reduce AM-mediated endothelial cell proliferation, migration, angiogenesis, tumor growth, and vascularization (5, 121, 157–159). However, whatever the pharmacological use the aforementioned peptides may have, their short half-life, low potency, and lack of selectivity circumscribe them only into the research field (175, 177, 180, 181).

It is worth mentioning that, at the moment at which most of those ligands were identified, the structures of the AM receptors were still unknown. Indeed, in many cases the evaluation of their antagonistic potency was determined by measuring their capacity to displace ¹²⁵I-AM from the cell surface (174). Much effort has been made since then in order to get a molecular comprehension of the interaction of AM with its receptors for the further design and development of more selective and potent antagonists. In point of fact, nowadays it is accepted that while the C-terminal half of the AM binds the complex extracellular domain (ECD) formed by the N-terminals of CLR and RAMPs, the AM N-terminal portion –more precisely, residues 16–30–interacts with the CLR 7-transmembrane domain of the receptor, so stabilizing the conformation that will induce cytoplasmic signaling (83, 84, 182). In this context, Moad, and Pioszak identified the AM (37-52)CONH₂ fragment as the minimal structure required to interact with the binding region of the ECD complex (178).

Robinson et al. carried out a series of studies with a number of peptide chimeras formed with AM, intermedin/AM2 and CGRP fragments, identifying several molecules with increased affinity compared to AM (22-52)CONH₂ for AM receptors. Interestingly, the peptide called ‘C7’ [AM (22-36)-AM2 (23-30)-AM (37-52)] presented significantly higher selectivity for AM₂ with respect to AM₁ and the CGRP receptor, which is of great value from the pharmacological point of view in discriminating the individual role of each receptor in AM activity (183). In addition, these, and other authors, have demonstrated that selectivity is strongly established by the interaction of residue 74 in RAMPs with a series of a few amino acids in the C-terminal of AM (181, 183). More recently, Booe et al. identified that AM residues at position 45 and 50 are crucial in determining the affinity of AM for its receptors, as demonstrated by the significantly increased antagonistic capacity of AM (37-52)CONH₂ after A45W and Q50W substitutions (84). Complementing this finding, Fischer

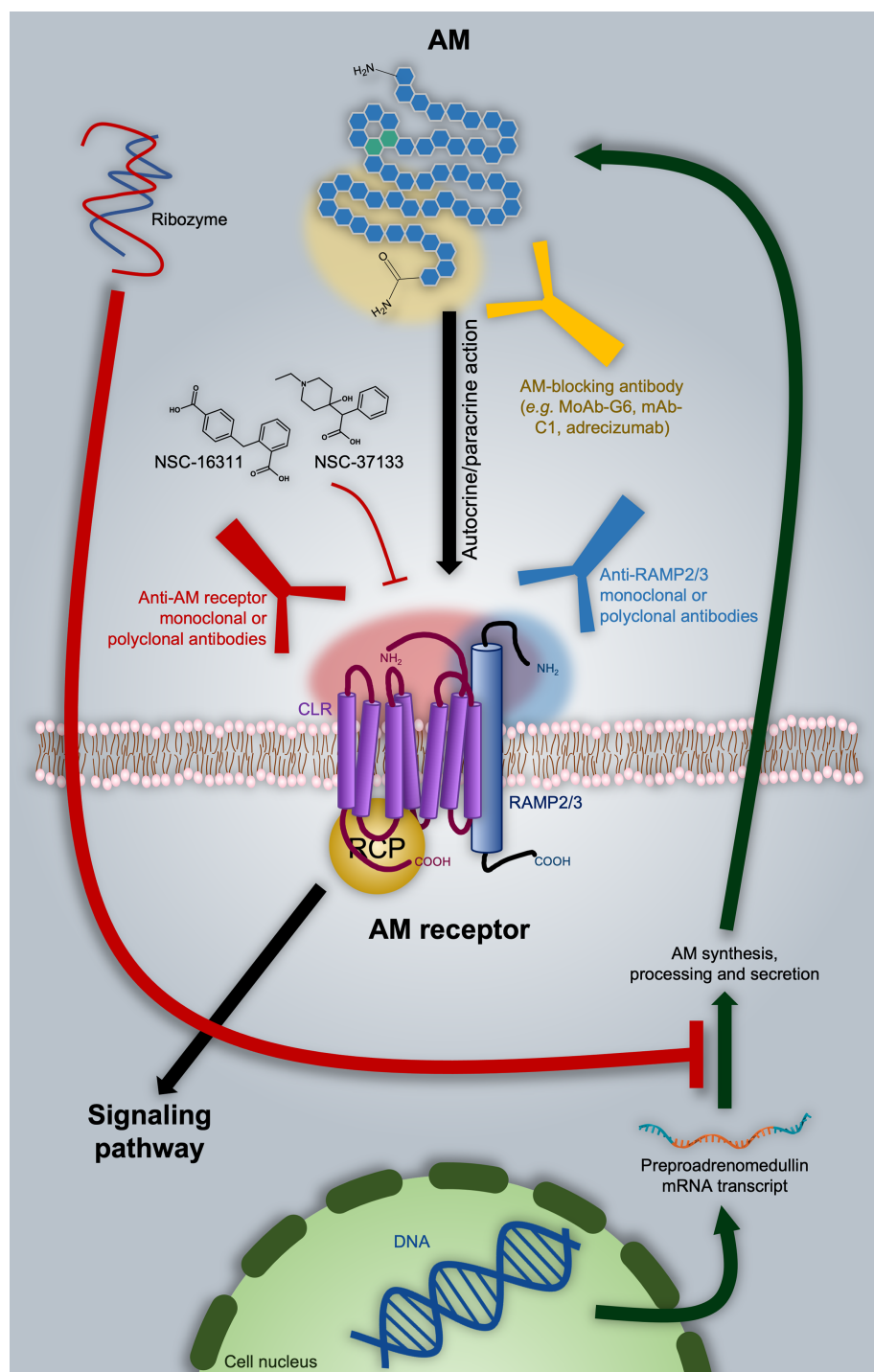


FIGURE 3 | Adrenomedullin (AM)-based therapeutic approaches in oncology. As discussed in the text, one of the options is directly targeting AM with blocking antibodies, as in the case of the MoAb-G6, mAb-C1, and adrelezumab. A ribozyme has proven to be effective in diminishing AM expression. Nevertheless, it still presents significant disadvantages from the pharmacokinetic point of view. AM-receptor antagonists are represented by NSC-16311 and NSC-37133. These compounds have more favorable pharmacokinetic features with respect to peptides like AM (22–52)CONH₂ (not shown). The binding of AM to its receptors can be also impeded by targeting the former with specific antibodies. In this respect, we introduce the possibility of employing anti-RAMP2 or anti-RAMP3 antibodies in order to get selective inhibition of AM₁ or AM₂ respectively. Potential epitope domains on AM and AM receptor components are indicated as shaded areas with the respective color of the targeting antibody.

et al. proved that the conformation of the ring 16-21 in AM is not only determined by the amino acid at position 22 (Thr), but also has a strong influence on the selectivity within the receptor system (182).

Unfortunately, so far, there are no further reports regarding the potential application in oncology of AM antagonists derived from these more recent studies. On the other hand, even if they resulted in more potent and selective molecules, the issue regarding their high metabolism rate would still not be solved.

The development of efficient, druggable small molecules is an alternative strategy to overcome the limiting poor selectivity and potency as well as short half-life often presented by peptide ligands. In this sense, Martínez et al. developed an elegant antibody-mediated method to screen for potential AM-antagonists in chemical libraries (180). Amongst the compounds identified, the piperidine derivative of phenylacetic acid, 16311 (also known as NSC-16311), elevated blood pressure when administered to normotensive (anesthetized) rats. On the other hand, the benzoic acid derivative, 37133 (also referred as NSC-37133), had no hemodynamic effects (180). In a later publication, the same group reported that both NSC-16311 and NSC-37133 as well as several other analogs exerted anti-proliferative effects in the human breast cancer cell line T47D, probably related to their AM-antagonistic behavior. In line with this, the AM-antagonistic action of NSC-16311 was further employed by Portal-Núñez et al. to demonstrate the AM contribution to the carcinogenic effect of tobacco combustion products in pulmonary tissue (184). More recently, Siclari et al. proved that NSC-16311 and NSC-37133 may be effective against breast cancer bone metastases due to their selective blockade of the osteolytic and pro-tumor-invasive actions of AM (146).

Taking advantage of the screening assay developed by Martínez et al. and complementing it by 3D quantitative SAR (3D-QSAR) and cell signaling studies, Roldós et al. further identified critical functional groups to be considered for the design of this type of ligands (185). Specifically, an aromatic ring, a hydrogen bond donor and a free carboxylic group seems to be essential to get AM-negative modulators to be eventually assessed as antiangiogenic and anti-cancer agents (185). However, it is notable that to date there are no clinical trials involving small-molecule AM antagonists.

In contrary, different selective small-molecule CGRP antagonists achieved clinical status for the treatment of migraine, including BIBN4096BS/olcegepant (186) (NCT02194777, NCT02194322, etc.), MK-0974/telcagepant (187) (NCT01294709, NCT00432237, etc.), MK-3207 (188) (NCT00712725, NCT00548353), and the very recently Food and Drug Administration (FDA)-approved MK-1602/ubrogepant (Ubrovelvy®) (189) (NCT04179474, NCT02867709, etc.). This indicates the potential for developing selective antagonists for other CLR/RAMP heterodimers by exploiting key residue differences amongst RAMPs. In line with the aforementioned relevance of residue 74 in determining the selective interaction of RAMPs with their respective ligands, the tryptophan located in this position is crucial in mediating the binding of these compounds to RAMP1 (188). Instead, RAMP2 and RAMP3 share a glutamic acid residue at this position, indicating

that such a class of anti-CGRP compounds may not be suitable scaffolds for the development of AM antagonists with oncological value. Even more so when taking into account that they were abandoned after some trial participants showed signs of hepatotoxicity (81).

On the other hand, the list of anti-CGRP agents with therapeutic action in migraine is not limited only to antagonists of the CLR/RAMP1 receptor, but also contains the commercially available, CGRP-neutralizing antibody fremanezumab (Ajovy®) (190) (NCT03308968, NCT04041284, etc.). Both mono- and polyclonal AM-blocking antibodies have been preclinically employed to inhibit AM pro-tumor and/or pro-angiogenic activity in glioblastoma (128), melanoma (119), lung (170), prostate (138, 139), ovarian, breast, and colon (121, 170) cancer models. Just to give examples, MoAb-G6 (170) and [anti-AM-(46–52)] mAb-C1 (191) are some of the monoclonal antibodies tested in these studies. Of note, no sign of toxicity was observed with this therapy (139). Nevertheless, the most relevant AM-blocking antibody is adrecizumab, currently under evaluation in cardiogenic and septic shock patients (NCT03083171, NCT04252937, etc.) (192). Results from these trials will be of great value given the fact that they will provide information on eventual side effects. Another question raised by the application of this approach concerns the impact competition with the AM-gly fraction –the most abundant circulating form of the hormone– may have on the bioavailability of the AM-neutralizing antibodies. To our knowledge, there are no reports in this respect.

Around 30% of all pharmaceutical products currently employed exert their therapeutic actions by modulating GPCRs (45, 75). The vast majority is represented by small molecules, then there is a minimal proportion composed by peptides, and, interestingly, the list is completed with only two FDA-approved monoclonal antibodies: mogamulizumab/Poteligeo®, employed in the treatment of mycosis fungoides or Sézary syndrome by targeting the CC chemokine receptor 4 (CCR4); and AMG 334/erenumab/Aimovig®, targeting CGRP receptor and prescribed for migraine prophylaxis (193–195). The approval of these two monoclonal antibodies gives promise to the potential of the currently available AM₁-, AM₂-, and CLR-targeting antibodies with proved tumor growth-inhibitory activity in preclinical models of colon, glioblastoma, PDAC, lung and breast cancer (120, 141, 157, 196). The anti-tumor effects of these antibodies are a direct consequence of their anti-angiogenic capacity. Indeed, treated tumor have been reported to appear pale or translucent, with diminished vasculature, permeability and recruitment of pericytes and macrophages and other myeloid cells (120, 141, 157, 196). Most tellingly, it must be noted that Kaafarani et al. did not observe signs of toxicity associated with long-term therapy (60 days). Histological analysis revealed no abnormalities of physiological vasculature in heart, liver, kidney, lung, and spleen. This could be partially explained by the specificity of the antibodies. In addition, it may mean that tumor angiogenic cells overexpressing AM₁ and AM₂ would become more susceptible to AM signaling blockade than the quiescent vasculature-associated cell components (141).

Over the years, several process-intrinsic challenges have limited the interest of the pharmaceutical industry in developing monoclonal antibodies against membrane proteins (195). However, the theory suggests that the complex structure of AM (and CGPR) receptors may compensate such restrictions, simultaneously offering encouraging advantages. A key factor in the development of such agents is to get antigens as close to the native conformation as possible, which is not a simple task for those proteins constantly moving immersed in a liquid film of phospholipids, as in the case of GPCRs. In this regard, it is thought that the mutual stabilization of the proteins (CLR and RAMPs) within the heterodimeric structure of AM₁ and AM₂ could allow them to remain longer in a physiologically relevant conformation. Moreover, the bipartite ECD creates a larger antigenic surface that increases the range of epitopes available to the antibodies, and so the chances of obtaining an appropriate therapeutic candidate (195). In contrast, the individual RAMP accessory proteins are more conventional single-pass receptors, and taken in isolation, represent more attractive targets, as recombinant expression of the extracellular domain is much less technically challenging. The RAMP components themselves represent individual therapeutic targets since they constitute strategic tools to define the pharmacological selectivity. In this sense, although its deficiency affects tumor vasculature and growth, RAMP2 does not appear to be a logical candidate for targeting given its role in preventing metastasis. In contrast, RAMP3 blockade in the context of a healthy AM/AM₁ signaling is expected to considerably suppress tumor metastatic capacity (155, 156). Moreover, even when partial, RAMP2 deletion resulted in abnormalities in various vascular endothelial cells, which suggests attention must be paid regarding side effects when considering RAMP2 as the therapeutic target (155). On the other hand, *Ramp3*^{-/-} mice did not show major phenotypic alterations (48, 110). Therefore, the incorporation of anti-RAMP3 agents in current therapeutic protocols in oncology may represent a promising anti-metastatic approach.

Lastly, a less conventional approach was proposed by Taylor and Samson, which consisted in the design of a catalytically active ribozyme that specifically recognizes and cleaves the preproadrenomedullin mRNA transcript (197). This molecule showed a good enough half-life to observe physiological variations both *in vitro*, decreasing AM content in cultured vascular smooth muscle cells, and *in vivo*, where reduction of AM resulted in exaggerated water drinking by rats after overnight water restriction or central administration of angiotensin II. Nevertheless, as an RNA-based molecule, stability, and route of administration are still drawbacks to consider in this strategy.

DISCUSSION

AM and VEGF share common features in that they are both hypoxically regulated, increase vascular permeability and are key pro-angiogenic factors. Indeed, their deficiency causes dysfunctional vascularization, even leading to embryonic

lethality in mice when absolute (198, 199). It has been observed that both molecules can interact in an alternate complementary fashion in angiogenesis-involving processes. VE-cadherin is a protein component of endothelial cell-to-cell adherent junctions with a key role in the maintenance of vascular integrity, neovessel assembly and remodeling of pericyte-endothelial cell association. Dr. Ouafik and collaborators have demonstrated that AM blockade, using anti-AM or anti-AM receptor antibodies, increases endothelial cell permeability by inhibiting cell-cell contacts predominantly through disruption of the VE-cadherin/β-catenin/Akt signaling pathway (200). At a molecular level, AM blockade induces phosphorylation of VE-cadherin at the critical residue Tyr731, preventing binding of its cytoplasmic tail with β-catenin and thus disrupting vasculature structure. In contrast, the activation of the VEGF receptor 2 increases the phosphorylation of VE-cadherin VE at Tyr731 inducing loss of cell polarity and lumen formation, consequently allowing VEGF to stimulate endothelial cell proliferation (201). They also interact at the cell signaling level since VEGF activates a number of different intracellular signaling pathways, including ERK's and PI3K/Akt to ensure endothelial cell survival and proliferation (202), which can be inhibited by AM blockade leading to endothelial cell death by apoptosis (personal communication of Prof. Ouafik's group).

The general outcome of anti-angiogenesis therapy is still unsatisfactory, principally due to low efficacy and the development of tumor-acquired resistance and adverse effects. Although the causes are not clear, several hypotheses have been posed in order to explain the discrepancy observed in terms of the effectiveness of anti-VEGF treatments amongst (in-mice) preclinical studies and the clinic. One reason may be in the administration of higher doses in animals, that in general are younger and relatively healthier than patients, and for which therapy-related toxic reactions are often omitted (203).

Also, attention must be paid to the fact that anti-VEGF agents do not act directly on tumor cells, but on their supply of nutrients and O₂. In this sense, residual hypoxia-resistant cells –usually associated with the cancer stem cell-like subpopulation– would act as a remnant source of VEGF and other factors that combined, would overcome the VEGF signaling blockade (203).

AM meets all the requirements to alternatively bypass VEGF inhibition, including a direct mitogen activity on malignant cells. Indeed, Gao et al. have demonstrated not only that AM expression was significantly (4-fold) increased in sunitinib-resistant renal carcinoma cells, but also that the treatment with AM (22-52) CONH₂ markedly reduced the growth of tumors derived from those cells (204). In all, evidence points to AM as an alternative target in tumors resistant to anti-VEGF agents. In this respect, AM also offers a broader front of action within the milieu of solid tumors, being able to act as modulator of endothelial cell interactions with other endothelial cells and/or pericytes, recruiter of different cell types into hypoxic areas and stimulator of cancer cell proliferation. On the other hand, the mitogenic activity of VEGF is mainly restricted to endothelial cells.

However, such multitasking role carries increased risk of adverse effects. In this regard, hypertension and its associated

secondary events (i.e., myocardial infarction and stroke) may be the main complication in anti-AM therapy, which is indeed an adverse effect observed in patients undergoing VEGF-inhibiting treatments. In general, however, anti-VEGF agents are well tolerated, especially when compared with chemotherapy; although, undesirable effects can limit their administration in some cases. These include venous and arterial thromboembolism, proteinuria, hemorrhage, gastrointestinal perforation and impaired wound healing (203, 205, 206). Actually, the former has been already reported in anti-AM therapy preclinical models. Mice-based studies indicate that the major adverse effects related to AM-inhibitory treatments may involve development of secondary lymphoedema (207, 208) and altered wound healing capacity (50). Both are of importance for those patients who undergo surgery and/or radiotherapy or might present a genetic susceptibility to the risk of developing secondary lymphoedema (208). However, they are manageable and usually pose a significantly lower risk than the tumors being treated.

One aspect to consider in any therapy is the capacity of identifying prognostic factors. Although in anti-VEGF regimens these types of molecules have remained elusive, VEGF itself has been postulated as general biomarker of angiogenic activity and tumor progression in cancer patients (129, 209). In this respect, increased circulating values of VEGF generally correlate with worse outcome (206, 209). In the case of anti-AM therapy, VEGF should be thought, at least, as the starting prognostic parameter to be evaluated.

We are of the opinion that there is mounting evidence of the potential of anti-AM strategies in oncology, representing more than just an anti-angiogenesis therapy, to merit further investigation. The efforts should be onwards focused on the discussion and development of efficient therapeutic approaches, taking also into account the feasibility of combination therapy with conventional chemotherapy. For example, Li et al. observed a significant potentiation of the tumor growth-inhibitory effect of cisplatin in AM-deficient liver cancer cells (210).

Considering the already described involvement of AM in different physiological activities, the extrapolation of a bevacizumab/Avastin®-like approach (directly targeting the ligand) may, in principle, not be a first option as a therapeutic strategy for AM. Another point to take into account in this respect is the fact that the AM-gly is the major circulating form of this protein. Thus, a potential antibody should be able to discern the AM mature variant in order to avoid the bioavailability-reducing competition with the inactive one, highlighting the AM amidated C-terminal as the antigenic epitope of choice.

As pointed out above, current clinical trials with adrecizumab will be more than interesting in addressing the feasibility of this strategy in oncology. Nevertheless, the blockade of AM receptors might represent a more suitable alternative. Moreover, the recent FDA approval of the CGRP receptor-targeting erenumab/Aimovig® antibody encourages the application of the anti-AM receptors strategy in oncology. One of the key challenges regarding this approach is the ability to selectively target individual components.

Collectively, data discussed in the previous sections suggests that both AM₁ and AM₂ possess crucial roles within the tumor structure regulating diverse functional aspects of the cell components. In this context, RAMP2 and RAMP3 themselves represent target candidates. However, AM₂ blockade could be presented as more advantageous by decreasing the chances of metastasis and having less impact on the physiological angiogenic processes. Furthermore, although it can be said it is a general feature of the AM system, the AM₂ signaling pathway in particular appears to be in a physiological dormant state ready to assemble and operate in response to diverse pathological conditions. This could explain the low incidence of adverse effects observed when targeting this receptor in preclinical models.

In the light of the current evidence, AM inhibition is a promising first-in-class therapeutic strategy in oncology and its potential needs to be further explored for the development of selective pharmacological options in cancer patients.

AUTHOR CONTRIBUTIONS

RV: As primary author, conceived the original idea of the article, drafting and writing the paper, and made the figures. MR: primary author conceived the original idea of the article, and drafting and writing most of the paper. CB-D, AO'K, JG, OT, and KR: Participated in revisions to scientific content of specific sections of the manuscript. MB: Participated in the critical revision, editing, and writing of the manuscript. Provided revisions to scientific content of the manuscript. L'HO: Conceived the original idea and provided critical revision of the manuscript as well as the final approval of the version to publish. All authors contributed to the article and approved the submitted version.

ACKNOWLEDGMENTS

This work is dedicated to the memory of Iva Ricchi, Tata.

REFERENCES

1. Cross MJ, Claesson-Welsh L. FGF and VEGF function in angiogenesis: signalling pathways, biological responses and therapeutic inhibition. *Trends Pharmacol Sci* (2001) 224:201–7. doi: 10.1016/S0165-6147(00)01676-X
2. Qin S, Li A, Yi M, Yu S, Zhang M, Wu K. Recent advances on anti-angiogenesis receptor tyrosine kinase inhibitors in cancer therapy. *J Hematol Oncol* (2019) 121:27. doi: 10.1186/s13045-019-0718-5
3. Fallah A, Sadeghinia A, Kahroba H, Samadi A, Heidari HR, Bradaran B, et al. Therapeutic targeting of angiogenesis molecular pathways in angiogenesis-dependent diseases. *BioMed Pharmacother* (2019) 110:775–85. doi: 10.1016/j.biopha.2018.12.022
4. Dai X, Ma W, He XJ, Jha RK. Elevated expression of adrenomedullin is correlated with prognosis and disease severity in osteosarcoma. *Med Oncol* (2013) 301:347. doi: 10.1007/s12032-012-0347-0
5. Deng B, Zhang S, Miao Y, Han Z, Zhang X, Wen F, et al. Adrenomedullin expression in epithelial ovarian cancers and promotes HO8910 cell migration associated with upregulating integrin alpha5beta1 and phosphorylating FAK and paxillin. *J Exp Clin Cancer Res* (2012) 31:19. doi: 10.1186/1756-9966-31-19

6. Chen Q, Chen P, Pang X, Hu Y, Zhang Y. Adrenomedullin Up-regulates the Expression of Vascular Endothelial Growth Factor in Epithelial Ovarian Carcinoma Cells via JNK/AP-1 Pathway. *Int J Gynecol Cancer* (2015) 256:953–60. doi: 10.1097/IGC.0000000000000465
7. Zhang Y, Xu Y, Ma J, Pang X, Dong M. Adrenomedullin promotes angiogenesis in epithelial ovarian cancer through upregulating hypoxia-inducible factor-1 α and vascular endothelial growth factor. *Sci Rep* (2017) 7:40524. doi: 10.1038/srep40524
8. Kitamura K, Kangawa K, Kawamoto M, Ichiki Y, Nakamura S, Matsuo H, et al. Adrenomedullin: a novel hypotensive peptide isolated from human pheochromocytoma. *Biochem Biophys Res Commun* (1993) 192:553–60. doi: 10.1006/bbrc.1993.1451
9. Eto T. A review of the biological properties and clinical implications of adrenomedullin and proadrenomedullin N-terminal 20 peptide (PAMP), hypotensive and vasodilating peptides. *Peptides* (2001) 221:1693–711. doi: 10.1016/S0196-9781(01)00513-7
10. Zudaire E, Cuttitta F, Martinez A. Regulation of pancreatic physiology by adrenomedullin and its binding protein. *Regul Pept* (2003) 1121-3:121–30. doi: 10.1016/S0167-0115(03)00030-2
11. Kitamura K, Sakata J, Kangawa K, Kojima M, Matsuo H, Eto T. Cloning and characterization of cDNA encoding a precursor for human adrenomedullin. *Biochem Biophys Res Commun* (1993) 194:720–5. doi: 10.1006/bbrc.1993.1881
12. Naot D, Musson DS, Cornish J. The Activity of Peptides of the Calcitonin Family in Bone. *Physiol Rev* (2019) 99:1781–805. doi: 10.1152/physrev.00066.2017
13. Amara SG, Jonas V, Rosenfeld MG, Ong ES, Evans RM. Alternative RNA processing in calcitonin gene expression generates mRNAs encoding different polypeptide products. *Nature* (1982) 298:5871:240–4. doi: 10.1038/298240a0
14. Rosenfeld MG, Mermod JJ, Amara SG, Swanson LW, Sawchenko PE, Rivier J, et al. Production of a novel neuropeptide encoded by the calcitonin gene via tissue-specific RNA processing. *Nature* (1983) 304:5922:129–35. doi: 10.1038/304129a0
15. Hoppener JW, Steenbergh PH, Zandberg J, Geurts van Kessel AH, Baylin SB, Nelkin BD, et al. The second human calcitonin/CGRP gene is located on chromosome 11. *Hum Genet* (1985) 70:3259–63. doi: 10.1007/BF00273453
16. Glowka TR, Steinebach A, Stein K, Schwandt T, Lysson M, Holzmänn B, et al. The novel CGRP receptor antagonist BIBN4096BS alleviates a postoperative intestinal inflammation and prevents postoperative ileus. *Neurogastroenterol Motil* (2015) 277:1038–49. doi: 10.1111/nmo.12584
17. Edvinsson L. Role of CGRP in Migraine. *Handb Exp Pharmacol* (2019) 255:121–30. doi: 10.1007/164_2018_201
18. Goadsby PJ, Edvinsson L, Ekman R. Vasoactive peptide release in the extracerebral circulation of humans during migraine headache. *Ann Neurol* (1990) 282:183–7. doi: 10.1002/ana.410280213
19. Roos BA, Fischer JA, Pignat V, Alander CB, Raisz LG. Evaluation of the in vivo and in vitro calcium-regulating actions of noncalcitonin peptides produced via calcitonin gene expression. *Endocrinology* (1986) 1181:46–51. doi: 10.1210/endo-118-1-46
20. Hay DL. Amylin. *Headache* (2017) 57 Suppl 2:89–96. doi: 10.1111/head.13077
21. Hartter E, Svoboda T, Ludvik B, Schuller M, Lell B, Kuenburg E, et al. Basal and stimulated plasma levels of pancreatic amylin indicate its co-secretion with insulin in humans. *Diabetologia* (1991) 341:52–4. doi: 10.1007/BF00404025
22. Cooper GJ. Amylin compared with calcitonin gene-related peptide: structure, biology, and relevance to metabolic disease. *Endocr Rev* (1994) 152:163–201. doi: 10.1210/edrv-15-2-163
23. Li Z, Kelly L, Heiman M, Greengard P, Friedman JM. Hypothalamic Amylin Acts in Concert with Leptin to Regulate Food Intake. *Cell Metab* (2015) 226:1059–67. doi: 10.1016/j.cmet.2015.10.012
24. Kahn SE, Andrikopoulos S, Verchere CB. Islet amyloid: a long-recognized but underappreciated pathological feature of type 2 diabetes. *Diabetes* (1999) 482:241–53. doi: 10.2337/diabetes.48.2.241
25. Boyle CN, Lutz TA, Le Foll C. Amylin - Its role in the homeostatic and hedonic control of eating and recent developments of amylin analogs to treat obesity. *Mol Metab* (2018) 8:203–10. doi: 10.1016/j.molmet.2017.11.009
26. Asthana S, Mallick B, Alexandrescu AT, Jha S. IAPP in type II diabetes: Basic research on structure, molecular interactions, and disease mechanisms suggests potential intervention strategies. *Biochim Biophys Acta Biomembr* (2018) 6:S0005-2736(18)30061-0. doi: 10.1016/j.bbmem.2018.02.020
27. Castle AL, Kuo CH, Han DH, Ivy JL. Amylin-mediated inhibition of insulin-stimulated glucose transport in skeletal muscle. *Am J Physiol* (1998) 275:3:E531–6. doi: 10.1152/ajpendo.1998.275.3.E531
28. Datta HK, Zaidi M, Wimalawansa SJ, Ghatei MA, Beacham JL, Bloom SR, et al. In vivo and in vitro effects of amylin and amylin-amide on calcium metabolism in the rat and rabbit. *Biochem Biophys Res Commun* (1989) 1622:876–81. doi: 10.1016/0006-291X(89)92391-7
29. Minamino N, Kikumoto K, Isumi Y. Regulation of adrenomedullin expression and release. *Microsc Res Tech* (2002) 571:28–39. doi: 10.1002/jemt.10048
30. Nomura I, Kato J, Tokashiki M, Kitamura K. Increased plasma levels of the mature and intermediate forms of adrenomedullin in obesity. *Regul Pept* (2009) 1581-3:127–31. doi: 10.1016/j.regpep.2009.08.003
31. Kawano S, Kawagoe Y, Kuwasako K, Shimamoto S, Igarashi K, Tokashiki M, et al. Gender-related alterations in plasma adrenomedullin level and its correlation with body weight gain. *Endocr Connect* (2015) 41:43–9. doi: 10.1530/EC-14-0131
32. Ishimitsu T, Nishikimi T, Saito Y, Kitamura K, Eto T, Kangawa K, et al. Plasma levels of adrenomedullin, a newly identified hypotensive peptide, in patients with hypertension and renal failure. *J Clin Invest* (1994) 945:2158–61. doi: 10.1172/JCI117573
33. Jougasaki M, Wei CM, Aarhus LL, Heublein DM, Sandberg SM, Burnett JC Jr. Renal localization and actions of adrenomedullin: a natriuretic peptide. *Am J Physiol* (1995) 268(4 Pt 2):F657–63. doi: 10.1152/ajprenal.1995.268.4.F657
34. Suzuki Y, Horio T, Hayashi T, Nonogi H, Kitamura K, Eto T, et al. Plasma adrenomedullin concentration is increased in patients with peripheral arterial occlusive disease associated with vascular inflammation. *Regul Pept* (2004) 1181-2:99–104. doi: 10.1016/j.regpep.2003.11.001
35. Kato J, Kitamura K, Eto T. Plasma adrenomedullin level and development of hypertension. *J Hum Hypertens* (2006) 208:566–70. doi: 10.1038/sj.jhh.1002033
36. Ono Y, Okano I, Kojima M, Okada K, Kangawa K. Decreased gene expression of adrenomedullin receptor in mouse lungs during sepsis. *Biochem Biophys Res Commun* (2000) 2711:197–202. doi: 10.1006/bbrc.2000.2606
37. Voors AA, Kremer D, Geven C, Ter Maaten JM, Struck J, Bergmann A, et al. Adrenomedullin in heart failure: pathophysiology and therapeutic application. *Eur J Heart Fail* (2019) 212:163–71. doi: 10.1002/ehf.1366
38. Kitamura K, Kato J, Kawamoto M, Tanaka M, Chino N, Kangawa K, et al. The intermediate form of glycine-extended adrenomedullin is the major circulating molecular form in human plasma. *Biochem Biophys Res Commun* (1998) 2442:551–5. doi: 10.1006/bbrc.1998.8310
39. Sakata J, Mizuno K, Matsuo H. Tissue distribution and characterization of peptide C-terminal alpha-amidating activity in rat. *Biochem Biophys Res Commun* (1986) 1401:230–6. doi: 10.1016/0006-291X(86)91080-6
40. Saldise L, Martinez A, Montuenga LM, Treston A, Springall DR, Polak JM, et al. Distribution of peptidyl-glycine alpha-amidating mono-oxygenase (PAM) enzymes in normal human lung and in lung epithelial tumors. *J Histochem Cytochem* (1996) 441:3–12. doi: 10.1177/44.1.8543779
41. Samson WK. Adrenomedullin and the control of fluid and electrolyte homeostasis. *Annu Rev Physiol* (1999) 61:363–89. doi: 10.1146/annurev.physiol.61.1.363
42. Caron KM, Smithies O. Extreme hydrops fetalis and cardiovascular abnormalities in mice lacking a functional Adrenomedullin gene. *Proc Natl Acad Sci USA* (2001) 982:615–9. doi: 10.1073/pnas.98.2.615
43. Wang C, Dobrzynski E, Chao J, Chao L. Adrenomedullin gene delivery attenuates renal damage and cardiac hypertrophy in Goldblatt hypertensive rats. *Am J Physiol Renal Physiol* (2001) 2806:F964–71. doi: 10.1152/ajprenal.2001.280.6.F964
44. Nicholls MG. Hemodynamic and hormonal actions of adrenomedullin. *Braz J Med Biol Res* (2004) 378:1247–53. doi: 10.1590/S0100-879X2004000800016
45. Ichikawa-Shindo Y, Sakurai T, Kamiyoshi A, Kawate H, Iinuma N, Yoshizawa T, et al. The GPCR modulator protein RAMP2 is essential for angiogenesis and vascular integrity. *J Clin Invest* (2008) 1181:29–39. doi: 10.1172/JCI33022
46. Cam-Etoz B, Isbil-Buyukcoskun N, Ozluk K. Cardiovascular effects of the intracerebroventricular injection of adrenomedullin: roles of the peripheral

- vasopressin and central cholinergic systems. *Braz J Med Biol Res* (2012) 453:250–5. doi: 10.1590/S0100-879X2012007500027
47. Koyama T, Ochoa-Callejero L, Sakurai T, Kamiyoshi A, Ichikawa-Shindo Y, Iinuma N, et al. Vascular endothelial adrenomedullin-RAMP2 system is essential for vascular integrity and organ homeostasis. *Circulation* (2013) 127:842–53. doi: 10.1161/CIRCULATIONAHA.112.000756
 48. Yamauchi A, Sakurai T, Kamiyoshi A, Ichikawa-Shindo Y, Kawate H, Igarashi K, et al. Functional differentiation of RAMP2 and RAMP3 in their regulation of the vascular system. *J Mol Cell Cardiol* (2014) 77:73–85. doi: 10.1016/j.yjmcc.2014.09.017
 49. Kataoka Y, Miyazaki S, Yasuda S, Nagaya N, Noguchi T, Yamada N, et al. The first clinical pilot study of intravenous adrenomedullin administration in patients with acute myocardial infarction. *J Cardiovasc Pharmacol* (2010) 56:413–9. doi: 10.1097/FJC.0b013e3181f15b45
 50. Harada K, Yamahara K, Ohnishi S, Otani K, Kanoh H, Ishibashi-Ueda H, et al. Sustained-release adrenomedullin ointment accelerates wound healing of pressure ulcers. *Regul Pept* (2011) 168:3:21–6. doi: 10.1016/j.regpep.2011.02.014
 51. Garcia-Hondurilla N, Cifuentes A, Bellon JM, Bujan J, Martinez A. The angiogenesis promoter, proadrenomedullin N-terminal 20 peptide (PAMP), improves healing in both normoxic and ischemic wounds either alone or in combination with autologous stem/progenitor cells. *Histol Histopathol* (2013) 28:115–25. doi: 10.14670/HH-28.115
 52. Nishikimi T. Adrenomedullin in the kidney-renal physiological and pathophysiological roles. *Curr Med Chem* (2007) 14:15:1689–99. doi: 10.2174/092986707780830943
 53. Serrano J, Alonso D, Fernandez AP, Encinas JM, Lopez JC, Castro-Blanco S, et al. Adrenomedullin in the central nervous system. *Microsc Res Tech* (2002) 57:76–90. doi: 10.1002/jemt.10053
 54. Kis B, Abraham CS, Deli MA, Kobayashi H, Niwa M, Yamashita H, et al. Adrenomedullin, an autocrine mediator of blood-brain barrier function. *Hypertens Res* (2003) 26 Suppl:S61–70. doi: 10.1291/hypres.26.S61
 55. Saita M, Shimokawa A, Kunitake T, Kato K, Hanamori T, Kitamura K, et al. Central actions of adrenomedullin on cardiovascular parameters and sympathetic outflow in conscious rats. *Am J Physiol* (1998) 274:R979–84. doi: 10.1152/ajpregu.1998.274.4.R979
 56. Miyashita K, Itoh H, Arai H, Suganami T, Sawada N, Fukunaga Y, et al. The neuroprotective and vasculo-neuro-regenerative roles of adrenomedullin in ischemic brain and its therapeutic potential. *Endocrinology* (2006) 147:1642–53. doi: 10.1210/en.2005-1038
 57. Fernandez AP, Serrano J, Tessarollo L, Cuttitta F, Martinez A. Lack of adrenomedullin in the mouse brain results in behavioral changes, anxiety, and lower survival under stress conditions. *Proc Natl Acad Sci USA* (2008) 105:12581–6. doi: 10.1073/pnas.0803174105
 58. Marutsuka K, Hatakeyama K, Sato Y, Yamashita A, Sumiyoshi A, Asada Y. Immunohistological localization and possible functions of adrenomedullin. *Hypertens Res* (2003) 26 Suppl:S33–40. doi: 10.1291/hypres.26.S33
 59. Rossowski WJ, Cheng BL, Jiang NY, Coy DH. Examination of somatostatin involvement in the inhibitory action of GIP, GLP-1, amylin and adrenomedullin on gastric acid release using a new SRIF antagonist analogue. *Br J Pharmacol* (1998) 125:1081–7. doi: 10.1038/sj.bjp.0702160
 60. Fukuda K, Tsukada H, Onomura M, Saito T, Kodama M, Nakamura H, et al. Effect of adrenomedullin on ion transport and muscle contraction in rat distal colon. *Peptides* (1998) 19:1043–7. doi: 10.1016/S0196-9781(98)00043-6
 61. Ashizuka S, Kita T, Inatsu H, Kitamura K. Adrenomedullin: a novel therapy for intractable ulcerative colitis. *Inflammation Bowel Dis* (2013) 19:2:E26–7. doi: 10.1002/ibd.22891
 62. Rulle S, Ah Koon MD, Asensio C, Mussard J, Ea HK, Boissier MC, et al. Adrenomedullin, a neuropeptide with immunoregulatory properties induces semi-mature tolerogenic dendritic cells. *Immunology* (2012) 136:252–64. doi: 10.1111/j.1365-2567.2012.03577.x
 63. Talero E, Di Paola R, Mazzon E, Esposito E, Motilva V, Cuzzocrea S. Anti-inflammatory effects of adrenomedullin on acute lung injury induced by Carrageenan in mice. *Mediators Inflamm* (2012) 2012:717851. doi: 10.1155/2012/717851
 64. Hippenstiel S, Witzernath M, Schmeck B, Hocke A, Krisp M, Krull M, et al. Adrenomedullin reduces endothelial hyperpermeability. *Circ Res* (2002) 91:7:618–25. doi: 10.1161/01.RES.0000036603.61868.F9
 65. Ashizuka S, Ishikawa N, Kato J, Yamaga J, Inatsu H, Eto T, et al. Effect of adrenomedullin administration on acetic acid-induced colitis in rats. *Peptides* (2005) 26:2610–5. doi: 10.1016/j.peptides.2005.05.007
 66. Talero E, Sanchez-Fidalgo S, de la Lastra CA, Illanes M, Calvo JR, Motilva V. Acute and chronic responses associated with adrenomedullin administration in experimental colitis. *Peptides* (2008) 29:11:2001–12. doi: 10.1016/j.peptides.2008.07.013
 67. Ashizuka S, Inagaki-Ohara K, Kuwasako K, Kato J, Inatsu H, Kitamura K. Adrenomedullin treatment reduces intestinal inflammation and maintains epithelial barrier function in mice administered dextran sulphate sodium. *Microbiol Immunol* (2009) 53:573–81. doi: 10.1111/j.1348-0421.2009.00159.x
 68. Martinez A, Elsasser TH, Muro-Cacho C, Moody TW, Miller MJ, Macri CJ, et al. Expression of adrenomedullin and its receptor in normal and malignant human skin: a potential pluripotent role in the integument. *Endocrinology* (1997) 138:25597–604. doi: 10.1210/endo.138.12.5622
 69. Allaker RP, Zihni C, Kapas S. An investigation into the antimicrobial effects of adrenomedullin on members of the skin, oral, respiratory tract and gut microflora. *FEMS Immunol Med Microbiol* (1999) 234:289–93. doi: 10.1111/j.1574-695X.1999.tb01250.x
 70. Ogoshi M, Inoue K, Takei Y. Identification of a novel adrenomedullin gene family in teleost fish. *Biochem Biophys Res Commun* (2003) 311:4:1072–7. doi: 10.1016/j.bbrc.2003.10.111
 71. Takei Y, Inoue K, Ogoshi M, Kawahara T, Bannai H, Miyano S. Identification of novel adrenomedullin in mammals: a potent cardiovascular and renal regulator. *FEBS Lett* (2004) 556:1:353–8. doi: 10.1016/S0014-5793(03)01368-1
 72. Roh J, Chang CL, Bhalla A, Klein C, Hsu SY. Intermedin is a calcitonin/calcitonin gene-related peptide family peptide acting through the calcitonin receptor-like receptor/receptor activity-modifying protein receptor complexes. *J Biol Chem* (2004) 279:7264–74. doi: 10.1074/jbc.M305332200
 73. Yang JH, Jia YX, Pan CS, Zhao J, Ouyang M, Yang J, et al. Effects of intermedin-1-53 on cardiac function and ischemia/reperfusion injury in isolated rat hearts. *Biochem Biophys Res Commun* (2005) 327:713–9. doi: 10.1016/j.bbrc.2004.12.071
 74. Harmar AJ. Family-B G-protein-coupled receptors. *Genome Biol* (2001) 2:12. REVIEWS3013. doi: 10.1186/gb-2001-2-12-reviews3013
 75. Hay DL, Pioszak AA. Receptor Activity-Modifying Proteins (RAMPs): New Insights and Roles. *Annu Rev Pharmacol Toxicol* (2016) 56:469–87. doi: 10.1146/annurev-pharmtox-010715-103120
 76. Husmann K, Sexton PM, Fischer JA, Born W. Mouse receptor-activity-modifying proteins 1, -2 and -3: amino acid sequence, expression and function. *Mol Cell Endocrinol* (2000) 162:1:235–43. doi: 10.1016/S0303-7207(00)00212-4
 77. Bomberger JM, Parameswaran N, Hall CS, Aiyar N, Spielman WS. Novel function for receptor activity-modifying proteins (RAMPs) in post-endocytic receptor trafficking. *J Biol Chem* (2005) 280:10:9297–307. doi: 10.1074/jbc.M413786200
 78. Oliver KR, Kane SA, Salvatore CA, Mallee JJ, Kinsey AM, Koblan KS, et al. Cloning, characterization and central nervous system distribution of receptor activity modifying proteins in the rat. *Eur J Neurosci* (2001) 14:4:618–28. doi: 10.1046/j.0953-816x.2001.01688.x
 79. Parameswaran N, Spielman WS. RAMPs: The past, present and future. *Trends Biochem Sci* (2006) 31:11:631–8. doi: 10.1016/j.tibs.2006.09.006
 80. Wunder F, Rebmann A, Geerts A, Kalthof B. Pharmacological and kinetic characterization of adrenomedullin 1 and calcitonin gene-related peptide 1 receptor reporter cell lines. *Mol Pharmacol* (2008) 73:4:1235–43. doi: 10.1124/mol.107.042283
 81. Hay DL, Gareja ML, Poyner DR, Walker CS. Update on the pharmacology of calcitonin/CGRP family of peptides: IUPHAR Review 25. *Br J Pharmacol* (2018) 175:1:3–17. doi: 10.1111/bph.14075
 82. Wooten DL, Simms J, Hay DL, Christopoulos A, Sexton PM. Receptor activity modifying proteins and their potential as drug targets. *Prog Mol Biol Transl Sci* (2010) 91:53–79. doi: 10.1016/S1877-1173(10)91003-X
 83. Booe JM, Walker CS, Barwell J, Kuteyi G, Simms J, Jamaluddin MA, et al. Structural Basis for Receptor Activity-Modifying Protein-Dependent Selective Peptide Recognition by a G Protein-Coupled Receptor. *Mol Cell* (2015) 58:6:1040–52. doi: 10.1016/j.molcel.2015.04.018

84. Booe JM, Warner ML, Roehrke AM, Hay DL, Pioszak AA. Probing the Mechanism of Receptor Activity-Modifying Protein Modulation of GPCR Ligand Selectivity through Rational Design of Potent Adrenomedullin and Calcitonin Gene-Related Peptide Antagonists. *Mol Pharmacol* (2018) 934:355–67. doi: 10.1124/mol.117.110916
85. Watkins HA, Chakravarthy M, Abhayawardana RS, Gingell JJ, Garelja M, Pardamwar M, et al. Receptor Activity-modifying Proteins 2 and 3 Generate Adrenomedullin Receptor Subtypes with Distinct Molecular Properties. *J Biol Chem* (2016) 29122:11657–75. doi: 10.1074/jbc.M115.688218
86. McLatchie LM, Fraser NJ, Main MJ, Wise A, Brown J, Thompson N, et al. RAMPs regulate the transport and ligand specificity of the calcitonin-receptor-like receptor. *Nature* (1998) 393:6683:333–9. doi: 10.1038/30666
87. Nag K, Sultana N, Kato A, Dranik A, Nakamura N, Kutsuzawa K, et al. Ligand-induced internalization, recycling, and resensitization of adrenomedullin receptors depend not on CLR or RAMP alone but on the receptor complex as a whole. *Gen Comp Endocrinol* (2015) 212:156–62. doi: 10.1016/j.ygcen.2014.04.029
88. Weston C, Lu J, Li N, Barkan K, Richards GO, Roberts DJ, et al. Modulation of Glucagon Receptor Pharmacology by Receptor Activity-modifying Protein-2 (RAMP2). *J Biol Chem* (2015) 29038:23009–22. doi: 10.1074/jbc.M114.624601
89. Mackie DI, Nielsen NR, Harris M, Singh S, Davis RB, Dy D, et al. RAMP3 determines rapid recycling of atypical chemokine receptor-3 for guided angiogenesis. *Proc Natl Acad Sci USA* (2019) 11648:24093–9. doi: 10.1073/pnas.1905561116
90. Egea SC, Dickerson IM. Direct interactions between calcitonin-like receptor (CLR) and CGRP-receptor component protein (RCP) regulate CGRP receptor signaling. *Endocrinology* (2012) 1534:1850–60. doi: 10.1210/en.2011-1459
91. Dickerson IM. Role of CGRP-receptor component protein (RCP) in CLR/RAMP function. *Curr Protein Pept Sci* (2013) 145:407–15. doi: 10.2174/13892037113149990057
92. Evans BN, Rosenblatt MI, Mnayer LO, Oliver KR, Dickerson IM. CGRP-RCP, a novel protein required for signal transduction at calcitonin gene-related peptide and adrenomedullin receptors. *J Biol Chem* (2000) 27540:31438–43. doi: 10.1074/jbc.M005604200
93. Prado MA, Evans-Bain B, Oliver KR, Dickerson IM. The role of the CGRP-receptor component protein (RCP) in adrenomedullin receptor signal transduction. *Peptides* (2001) 2211:1773–81. doi: 10.1016/S0196-9781(01)00517-4
94. Hay DL, Walker CS, Poyner DR. Adrenomedullin and calcitonin gene-related peptide receptors in endocrine-related cancers: opportunities and challenges. *Endocr Relat Cancer* (2011) 181:C1–14. doi: 10.1677/ERC-10-0244
95. Kapas S, Catt KJ, Clark AJ. Cloning and expression of cDNA encoding a rat adrenomedullin receptor. *J Biol Chem* (1995) 27043:25344–7. doi: 10.1074/jbc.270.43.25344
96. Kapas S, Clark AJ. Identification of an orphan receptor gene as a type 1 calcitonin gene-related peptide receptor. *Biochem Biophys Res Commun* (1995) 2173:832–8. doi: 10.1006/bbrc.1995.2847
97. Kennedy SP, Sun D, Oleynek JJ, Hoth CF, Kong J, Hill RJ. Expression of the rat adrenomedullin receptor or a putative human adrenomedullin receptor does not correlate with adrenomedullin binding or functional response. *Biochem Biophys Res Commun* (1998) 2443:832–7. doi: 10.1006/bbrc.1998.8349
98. Yun HJ, Ryu H, Choi YS, Song IC, Jo DY, Kim S, et al. C-X-C motif receptor 7 in gastrointestinal cancer. *Oncol Lett* (2015) 103:1227–32. doi: 10.3892/ol.2015.3407
99. Schmid CD, Schledzewski K, Mogler C, Waldburger N, Kalna V, Marx A, et al. GPR182 is a novel marker for sinusoidal endothelial differentiation with distinct GPCR signaling activity in vitro. *Biochem Biophys Res Commun* (2018) 4971:32–8. doi: 10.1016/j.bbrc.2018.01.185
100. Shimomura T, Shibagaki Y, Ishibashi K, Kitamura K, Kangawa K, Kato S, et al. Adrenomedullin, an endogenous peptide, counteracts cardiovascular damage. *Circulation* (2002) 1051:106–11. doi: 10.1161/hc0102.101399
101. Dackor RT, Fritz-Six K, Dunworth WP, Gibbons CL, Smithies O, Caron KM. Hydrops fetalis, cardiovascular defects, and embryonic lethality in mice lacking the calcitonin receptor-like receptor gene. *Mol Cell Biol* (2006) 267:2511–8. doi: 10.1128/MCB.26.7.2511-2518.2006
102. Imai Y, Shiindo T, Maemura K, Kurihara Y, Nagai R, Kurihara H. Evidence for the physiological and pathological roles of adrenomedullin from genetic engineering in mice. *Ann N Y Acad Sci* (2001) 947:26–33; discussion –4. doi: 10.1111/j.1749-6632.2001.tb03927.x
103. Fritz-Six KL, Dunworth WP, Li M, Caron KM. Adrenomedullin signaling is necessary for murine lymphatic vascular development. *J Clin Invest* (2008) 1181:40–50. doi: 10.1172/JCI33302
104. Kechele DO, Dunworth WP, Trincot CE, Wetzel-Strong SE, Li M, Ma H, et al. Endothelial Restoration of Receptor Activity-Modifying Protein 2 Is Sufficient to Rescue Lethality, but Survivors Develop Dilated Cardiomyopathy. *Hypertension* (2016) 683:667–77. doi: 10.1161/HYPERTENSIONAHA.116.07191
105. Kadmiel M, Fritz-Six KL, Caron KM. Understanding RAMPs through genetically engineered mouse models. *Adv Exp Med Biol* (2012) 744:49–60. doi: 10.1007/978-1-4614-2364-5_5
106. Kadmiel M, Fritz-Six K, Pacharne S, Richards GO, Li M, Skerry TM, et al. Research resource: Haploinsufficiency of receptor activity-modifying protein-2 (RAMP2) causes reduced fertility, hyperprolactinemia, skeletal abnormalities, and endocrine dysfunction in mice. *Mol Endocrinol* (2011) 257:1244–53. doi: 10.1210/me.2010-0400
107. Tam CW, Husmann K, Clark NC, Clark JE, Lazar Z, Ittner LM, et al. Enhanced vascular responses to adrenomedullin in mice overexpressing receptor-activity-modifying protein 2. *Circ Res* (2006) 982:262–70. doi: 10.1161/01.RES.0000200737.63865.58
108. Pawlak JB, Wetzel-Strong SE, Dunn MK, Caron KM. Cardiovascular effects of exogenous adrenomedullin and CGRP in Ramp and Calcr1 deficient mice. *Peptides* (2017) 88:1–7. doi: 10.1016/j.peptides.2016.12.002
109. Barrick CJ, Lenhart PM, Dackor RT, Nagle E, Caron KM. Loss of receptor activity-modifying protein 3 exacerbates cardiac hypertrophy and transition to heart failure in a sex-dependent manner. *J Mol Cell Cardiol* (2012) 521:165–74. doi: 10.1016/j.jmcc.2011.10.021
110. Dackor R, Caron K. Mice heterozygous for adrenomedullin exhibit a more extreme inflammatory response to endotoxin-induced septic shock. *Peptides* (2007) 2811:2164–70. doi: 10.1016/j.peptides.2007.08.012
111. Liu T, Kamiyoshi A, Tanaka M, Iida S, Sakurai T, Ichikawa-Shindo Y, et al. RAMP3 deficiency enhances postmenopausal obesity and metabolic disorders. *Peptides* (2018) 110:10–8. doi: 10.1016/j.peptides.2018.10.006
112. Watanabe H, Takahashi E, Kobayashi M, Goto M, Krust A, Chambon P, et al. The estrogen-responsive adrenomedullin and receptor-modifying protein 3 gene identified by DNA microarray analysis are directly regulated by estrogen receptor. *J Mol Endocrinol* (2006) 361:81–9. doi: 10.1677/jme.1.01825
113. Zhao Y, Hague S, Manek S, Zhang L, Bicknell R, Rees MC. PCR display identifies tamoxifen induction of the novel angiogenic factor adrenomedullin by a non estrogenic mechanism in the human endometrium. *Oncogene* (1998) 163:409–15. doi: 10.1038/sj.onc.1201768
114. Cueille C, Pidoux E, de Vernejoul MC, Ventura-Clapier R, Garel JM. Increased myocardial expression of RAMP1 and RAMP3 in rats with chronic heart failure. *Biochem Biophys Res Commun* (2002) 2942:340–6. doi: 10.1016/S0006-291X(02)00487-4
115. Yoshihara F, Nishikimi T, Okano I, Hino J, Horio T, Tokudome T, et al. Upregulation of intracardiac adrenomedullin and its receptor system in rats with volume overload-induced cardiac hypertrophy. *Regul Pept* (2005) 1271:3:239–44. doi: 10.1016/j.regpep.2004.12.017
116. Oie E, Vinge LE, Andersen GO, Yndestad A, Krobert KA, Sandberg C, et al. RAMP2 and RAMP3 mRNA levels are increased in failing rat cardiomyocytes and associated with increased responsiveness to adrenomedullin. *J Mol Cell Cardiol* (2005) 381:145–51. doi: 10.1016/j.jmcc.2004.10.009
117. Nishimatsu H, Suzuki E, Nagata D, Moriyama N, Satonaka H, Walsh K, et al. Adrenomedullin induces endothelium-dependent vasorelaxation via the phosphatidylinositol 3-kinase/Akt-dependent pathway in rat aorta. *Circ Res* (2001) 891:63–70. doi: 10.1161/hh1301.092498
118. Kim W, Moon SO, Sung MJ, Kim SH, Lee S, So JN, et al. Angiogenic role of adrenomedullin through activation of Akt, mitogen-activated protein kinase, and focal adhesion kinase in endothelial cells. *FASEB J* (2003) 1713:1937–9. doi: 10.1096/fj.02-1209fje

119. Chen P, Huang Y, Bong R, Ding Y, Song N, Wang X, et al. Tumor-associated macrophages promote angiogenesis and melanoma growth via adrenomedullin in a paracrine and autocrine manner. *Clin Cancer Res* (2011) 1723:7230–9. doi: 10.1158/1078-0432.CCR-11-1354
120. Xu M, Qi F, Zhang S, Ma X, Wang S, Wang C, et al. Adrenomedullin promotes the growth of pancreatic ductal adenocarcinoma through recruitment of myelomonocytic cells. *Oncotarget* (2016) 734:55043–56. doi: 10.18632/oncotarget.10393
121. Nouguerede E, Berenguer C, Garcia S, Bennani B, Delfino C, Nanni I, et al. Expression of adrenomedullin in human colorectal tumors and its role in cell growth and invasion in vitro and in xenograft growth in vivo. *Cancer Med* (2013) 22:196–207. doi: 10.1002/cam4.51
122. Wang L, Gala M, Yamamoto M, Pino MS, Kikuchi H, Shue DS, et al. Adrenomedullin is a therapeutic target in colorectal cancer. *Int J Cancer* (2014) 1349:2041–50. doi: 10.1002/ijc.28542
123. Ehlenz K, Koch B, Preuss P, Simon B, Koop I, Lang RE. High levels of circulating adrenomedullin in severe illness: correlation with C-reactive protein and evidence against the adrenal medulla as site of origin. *Exp Clin Endocrinol Diabetes* (1997) 1053:156–62. doi: 10.1055/s-0029-1211745
124. Letizia C, Di Iorio R, De Toma G, Marinoni E, Cerci S, Celi M, et al. Circulating adrenomedullin is increased in patients with corticotropin-dependent Cushing's syndrome due to pituitary adenoma. *Metabolism* (2000) 496:760–3. doi: 10.1053/meta.2000.6241
125. Uono T, Totsune K, Takahashi K, Abe T, Sato M, Shibahara S, et al. Increased expression of adrenomedullin mRNA in the tissues of intraocular and orbital tumors. *Am J Ophthalmol* (2000) 1294:555–6. doi: 10.1016/S0002-9394(99)00442-0
126. Greillier L, Tounsi A, Berenguer-Daize C, Dussault N, Delfino C, Benyahia Z, et al. Functional Analysis of the Adrenomedullin Pathway in Malignant Pleural Mesothelioma. *J Thorac Oncol* (2016) 111:94–107. doi: 10.1016/j.jtho.2015.09.004
127. Uemura M, Yamamoto H, Takemasa I, Mimori K, Mizushima T, Ikeda M, et al. Hypoxia-inducible adrenomedullin in colorectal cancer. *Anticancer Res* (2011) 312:507–14.
128. Ouafik L, Sauze S, Boudouresque F, Chinot O, Delfino C, Fina F, et al. Neutralization of adrenomedullin inhibits the growth of human glioblastoma cell lines in vitro and suppresses tumor xenograft growth in vivo. *Am J Pathol* (2002) 1604:1279–92. doi: 10.1016/S0002-9440(10)62555-2
129. Takahashi K, Satoh F, Hara E, Murakami O, Kumabe T, Tominaga T, et al. Production and secretion of adrenomedullin by cultured choroid plexus carcinoma cells. *J Neurochem* (1997) 682:726–31. doi: 10.1046/j.1471-4159.1997.68020726.x
130. Rocchi P, Boudouresque F, Zamora AJ, Muracciole X, Lechevallier E, Martin PM, et al. Expression of adrenomedullin and peptide amidation activity in human prostate cancer and in human prostate cancer cell lines. *Cancer Res* (2001) 613:1196–206.
131. Hata K, Takebayashi Y, Akiba S, Fujiwaki R, Iida K, Nakayama K, et al. Expression of the adrenomedullin gene in epithelial ovarian cancer. *Mol Hum Reprod* (2000) 610:867–72. doi: 10.1093/molehr/6.10.867
132. Park SC, Yoon JH, Lee JH, Yu SJ, Myung SJ, Kim W, et al. Hypoxia-inducible adrenomedullin accelerates hepatocellular carcinoma cell growth. *Cancer Lett* (2008) 2712:314–22. doi: 10.1016/j.canlet.2008.06.019
133. Michelsen J, Thieson H, Walter S, Ottosen PD, Skott O, Jensen BL. Tissue expression and plasma levels of adrenomedullin in renal cancer patients. *Clin Sci (Lond)* (2006) 1111:61–70. doi: 10.1042/CS20060030
134. Deville JL, Bartoli C, Berenguer C, Fernandez-Sauze S, Kaafarani I, Delfino C, et al. Expression and role of adrenomedullin in renal tumors and value of its mRNA levels as prognostic factor in clear-cell renal carcinoma. *Int J Cancer* (2009) 12510:2307–15. doi: 10.1002/ijc.24568
135. Oehler MK, Fischer DC, Orlowska-Volk M, Herrle F, Kieback DG, Rees MC, et al. Tissue and plasma expression of the angiogenic peptide adrenomedullin in breast cancer. *Br J Cancer* (2003) 8910:1927–33. doi: 10.1038/sj.bjc.6601397
136. Keleg S, Kaye H, Jiang X, Penzel R, Giese T, Buchler MW, et al. Adrenomedullin is induced by hypoxia and enhances pancreatic cancer cell invasion. *Int J Cancer* (2007) 1211:21–32. doi: 10.1002/ijc.22596
137. Aggarwal G, Ramachandran V, Javed N, Arumugam T, Dutta S, Klee GG, et al. Adrenomedullin is up-regulated in patients with pancreatic cancer and causes insulin resistance in beta cells and mice. *Gastroenterology* (2012) 1436:1510–7. doi: 10.1053/j.gastro.2012.08.044
138. Berenguer C, Boudouresque F, Dussert C, Daniel L, Muracciole X, Grino M, et al. Adrenomedullin, an autocrine/paracrine factor induced by androgen withdrawal, stimulates 'neuroendocrine phenotype' in LNCaP prostate tumor cells. *Oncogene* (2008) 274:506–18. doi: 10.1038/sj.onc.1210656
139. Berenguer-Daize C, Boudouresque F, Bastide C, Tounsi A, Benyahia Z, Acunzo J, et al. Adrenomedullin blockade suppresses growth of human hormone-independent prostate tumor xenograft in mice. *Clin Cancer Res* (2013) 1922:6138–50. doi: 10.1158/1078-0432.CCR-13-0691
140. Thouennon E, Pierre A, Tanguy Y, Guillemot J, Manecka DL, Guerin M, et al. Expression of trophic amidated peptides and their receptors in benign and malignant pheochromocytomas: high expression of adrenomedullin RDC1 receptor and implication in tumoral cell survival. *Endocr Relat Cancer* (2010) 173:637–51. doi: 10.1677/ERC-10-0109
141. Kaafarani I, Fernandez-Sauze S, Berenguer C, Chinot O, Delfino C, Dussert C, et al. Targeting adrenomedullin receptors with systemic delivery of neutralizing antibodies inhibits tumor angiogenesis and suppresses growth of human tumor xenografts in mice. *FASEB J* (2009) 2310:3424–35. doi: 10.1096/fj.08-127852
142. Forneris M, Gottardo L, Albertin G, Malendowicz LK, Nussdorfer GG. Expression and function of adrenomedullin and its receptors in Conn's adenoma cells. *Int J Mol Med* (2001) 86:675–9. doi: 10.3892/ijmm.8.6.675
143. Martinez A, Vos M, Guede L, Kaur G, Chen Z, Garayoa M, et al. The effects of adrenomedullin overexpression in breast tumor cells. *J Natl Cancer Inst* (2002) 9416:1226–37. doi: 10.1093/jnci/94.16.1226
144. Oehler MK, Norbury C, Hague S, Rees MC, Bicknell R. Adrenomedullin inhibits hypoxic cell death by upregulation of Bcl-2 in endometrial cancer cells: a possible promotion mechanism for tumour growth. *Oncogene* (2001) 2023:2937–45. doi: 10.1038/sj.onc.1204422
145. Hague S, Zhang L, Oehler MK, Manek S, MacKenzie IZ, Bicknell R, et al. Expression of the hypoxically regulated angiogenic factor adrenomedullin correlates with uterine leiomyoma vascular density. *Clin Cancer Res* (2000) 67:2808–14.
146. Siclari VA, Mohammad KS, Tompkins DR, Davis H, McKenna CR, Peng X, et al. Tumor-expressed adrenomedullin accelerates breast cancer bone metastasis. *Breast Cancer Res* (2014) 166:458. doi: 10.1186/s13058-014-0458-y
147. Abasolo I, Montuenga LM, Calvo A. Adrenomedullin prevents apoptosis in prostate cancer cells. *Regul Pept* (2006) 1331-3:115–22. doi: 10.1016/j.regpep.2005.09.026
148. Wu XY, Hao CP, Ling M, Guo CH, Ma W. Hypoxia-induced apoptosis is blocked by adrenomedullin via upregulation of Bcl-2 in human osteosarcoma cells. *Oncol Rep* (2015) 342:787–94. doi: 10.3892/or.2015.4011
149. Kim W, Moon SO, Sung MJ, Kim SH, Lee S, Kim HJ, et al. Protective effect of adrenomedullin in mannitol-induced apoptosis. *Apoptosis* (2002) 76:527–36. doi: 10.1023/A:1020695110648
150. Shichiri M, Kato H, Doi M, Marumo F, Hirata Y. Induction of max by adrenomedullin and calcitonin gene-related peptide antagonizes endothelial apoptosis. *Mol Endocrinol* (1999) 138:1353–63. doi: 10.1210/mend.13.8.0324
151. Carthew P, Edwards RE, Nolan BM, Martin EA, Heydon RT, White IN, et al. Tamoxifen induces endometrial and vaginal cancer in rats in the absence of endometrial hyperplasia. *Carcinogenesis* (2000) 214:793–7. doi: 10.1093/carcin/21.4.793
152. Withers DJ, Coppock HA, Seufferlein T, Smith DM, Bloom SR, Rozengurt E. Adrenomedullin stimulates DNA synthesis and cell proliferation via elevation of cAMP in Swiss 3T3 cells. *FEBS Lett* (1996) 3781:83–7. doi: 10.1016/0014-5793(95)01427-6
153. Zudaire E, Portal-Nunez S, Cuttitta F. The central role of adrenomedullin in host defense. *J Leukoc Biol* (2006) 802:237–44. doi: 10.1189/jlb.0206123
154. Larrayoz IM, Martinez-Herrero S, Garcia-Sanmartin J, Ochoa-Callejero L, Martinez A. Adrenomedullin and tumour microenvironment. *J Transl Med* (2014) 12:339. doi: 10.1186/s12967-014-0339-2
155. Tanaka M, Koyama T, Sakurai T, Kamiyoshi A, Ichikawa-Shindo Y, Kawate H, et al. The endothelial adrenomedullin-RAMP2 system regulates vascular integrity and suppresses tumour metastasis. *Cardiovasc Res* (2016) 1114:398–409. doi: 10.1093/cvr/cvw166
156. Dai K, Tanaka M, Kamiyoshi A, Sakurai T, Ichikawa-Shindo Y, Kawate H, et al. Deficiency of the adrenomedullin-RAMP3 system suppresses

- metastasis through the modification of cancer-associated fibroblasts. *Oncogene* (2020) 399:1914–30. doi: 10.1038/s41388-019-1112-z
157. Benyahia Z, Dussault N, Cayol M, Sigaud R, Berenguer-Daize C, Delfino C, et al. Stromal fibroblasts present in breast carcinomas promote tumor growth and angiogenesis through adrenomedullin secretion. *Oncotarget* (2017) 89:15744–62. doi: 10.18632/oncotarget.14999
 158. Ishikawa T, Chen J, Wang J, Okada F, Sugiyama T, Kobayashi T, et al. Adrenomedullin antagonist suppresses in vivo growth of human pancreatic cancer cells in SCID mice by suppressing angiogenesis. *Oncogene* (2003) 228:1238–42. doi: 10.1038/sj.onc.1206207
 159. Iimuro S, Shindo T, Moriyama N, Amaki T, Niu P, Takeda N, et al. Angiogenic effects of adrenomedullin in ischemia and tumor growth. *Circ Res* (2004) 95:415–23. doi: 10.1161/01.RES.0000138018.61065.d1
 160. Zudaire E, Martinez A, Garayoa M, Pio R, Kaur G, Woolhiser MR, et al. Adrenomedullin is a cross-talk molecule that regulates tumor and mast cell function during human carcinogenesis. *Am J Pathol* (2006) 168:1280–91. doi: 10.2353/ajpath.2006.050291
 161. Fujita Y, Mimata H, Nasu N, Nomura T, Nomura Y, Nakagawa M. Involvement of adrenomedullin induced by hypoxia in angiogenesis in human renal cell carcinoma. *Int J Urol* (2002) 96:285–95. doi: 10.1046/j.1442-2042.2002.00469.x
 162. Garayoa M, Martinez A, Lee S, Pio R, An WG, Neckers L, et al. Hypoxia-inducible factor-1 (HIF-1) up-regulates adrenomedullin expression in human tumor cell lines during oxygen deprivation: a possible promotion mechanism of carcinogenesis. *Mol Endocrinol* (2000) 146:848–62. doi: 10.1210/mend.14.6.0473
 163. Oehler MK, Hague S, Rees MC, Bicknell R. Adrenomedullin promotes formation of xenografted endometrial tumors by stimulation of autocrine growth and angiogenesis. *Oncogene* (2002) 2118:2815–21. doi: 10.1038/sj.onc.1205374
 164. Li F, Yang R, Zhang X, Liu A, Zhao Y, Guo Y. Silencing of hypoxia-inducible adrenomedullin using RNA interference attenuates hepatocellular carcinoma cell growth in vivo. *Mol Med Rep* (2014) 103:1295–302. doi: 10.3892/mmr.2014.2320
 165. Park SJ, Kim JG, Son TG, Yi JM, Kim ND, Yang K, et al. The histone demethylase JMJD1A regulates adrenomedullin-mediated cell proliferation in hepatocellular carcinoma under hypoxia. *Biochem Biophys Res Commun* (2013) 434:722–7. doi: 10.1016/j.bbrc.2013.03.091
 166. Drimal J, Faberova V, Schmidtova L, Bednarikova M, Drimal JJr., Drimal D. The ACAT inhibitor VULM1457 significantly reduced production and secretion of adrenomedullin (AM) and down-regulated AM receptors on human hepatoblastic cells. *Gen Physiol Biophys* (2005) 244:397–409.
 167. Fidler IJ, Kripke ML. The challenge of targeting metastasis. *Cancer Metastasis Rev* (2015) 344:635–41. doi: 10.1007/s10555-015-9586-9
 168. Albertin G, Rucinski M, Carraro G, Forneris M, Andreis P, Malendowicz LK, et al. Adrenomedullin and vascular endothelium growth factor genes are overexpressed in the regenerating rat adrenal cortex, and AM and VEGF reciprocally enhance their mRNA expression in cultured rat adrenocortical cells. *Int J Mol Med* (2005) 163:431–5. doi: 10.3892/ijmm.16.3.431
 169. Brekhman V, Lugassie J, Zaffryar-Eilol S, Sabo E, Kessler O, Smith V, et al. Receptor activity modifying protein-3 mediates the protumorigenic activity of lysyl oxidase-like protein-2. *FASEB J* (2011) 251:55–65. doi: 10.1096/fj.10-162677
 170. Miller MJ, Martinez A, Unsworth EJ, Thiele CJ, Moody TW, Elsasser T, et al. Adrenomedullin expression in human tumor cell lines. Its potential role as an autocrine growth factor. *J Biol Chem* (1996) 27138:23345–51. doi: 10.1074/jbc.271.38.23345
 171. Ramachandran V, Arumugam T, Hwang RF, Greenon JK, Simeone DM, Logsdon CD. Adrenomedullin is expressed in pancreatic cancer and stimulates cell proliferation and invasion in an autocrine manner via the adrenomedullin receptor, ADMR. *Cancer Res* (2007) 676:2666–75. doi: 10.1158/0008-5472.CAN-06-3362
 172. Mazzocchi G, Malendowicz LK, Ziolkowska A, Spinazzi R, Rebuffat P, Aragona F, et al. Adrenomedullin (AM) and AM receptor type 2 expression is up-regulated in prostate carcinomas (PC), and AM stimulates in vitro growth of a PC-derived cell line by enhancing proliferation and decreasing apoptosis rates. *Int J Oncol* (2004) 256:1781–7. doi: 10.3892/ijo.25.6.1781
 173. Albertin G, Sorato E, Oselladore B, Mascarin A, Tortorella C, Guidolin D. Involvement of vascular endothelial growth factor signaling in CLR/RAMP1 and CLR/RAMP2-mediated pro-angiogenic effect of intermedin on human vascular endothelial cells. *Int J Mol Med* (2010) 262:289–94. doi: 10.3892/ijmm.00000464
 174. Eguchi S, Hirata Y, Iwasaki H, Sato K, Watanabe TX, Inui T, et al. Structure-activity relationship of adrenomedullin, a novel vasodilatory peptide, in cultured rat vascular smooth muscle cells. *Endocrinology* (1994) 1356:2454–8. doi: 10.1210/endo.135.6.7988431
 175. Santiago JA, Garrison EA, Ventura VL, Coy DH, Bitar K, Murphy WA, et al. Synthetic human adrenomedullin and adrenomedullin 15–52 have potent short-lived vasodilator activity in the hindlimb vascular bed of the cat. *Life Sci* (1994) 555:PL85–90. doi: 10.1016/0024-3205(94)00652-0
 176. Kitamura K, Matsui E, Kato J, Katoh F, Kita T, Tsuji T, et al. Adrenomedullin 11–26: a novel endogenous hypertensive peptide isolated from bovine adrenal medulla. *Peptides* (2001) 2211:1713–8. doi: 10.1016/S0196-9781(01)00529-0
 177. Hay DL, Howitt SG, Conner AC, Schindler M, Smith DM, Poyner DR. CL/RAMP2 and CL/RAMP3 produce pharmacologically distinct adrenomedullin receptors: a comparison of effects of adrenomedullin22–52, CGRP8–37 and BIBN4096BS. *Br J Pharmacol* (2003) 1403:477–86. doi: 10.1038/sj.bjp.0705472
 178. Moad HE, Pioszak AA, Selective CGRP. and adrenomedullin peptide binding by tethered RAMP-calcitonin receptor-like receptor extracellular domain fusion proteins. *Protein Sci* (2013) 2212:1775–85. doi: 10.1002/pro.2377
 179. Champion HC, Friedman DE, Lambert DG, Murphy WA, Coy DH, Kadowitz PJ. Adrenomedullin 16–31 has pressor activity in the rat but not the cat. *Peptides* (1997) 181:133–6. doi: 10.1016/S0196-9781(96)00251-3
 180. Martinez A, Julian M, Bregonzio C, Notari L, Moody TW, Cuttitta F. Identification of vasoactive nonpeptidic positive and negative modulators of adrenomedullin using a neutralizing antibody-based screening strategy. *Endocrinology* (2004) 1458:3858–65. doi: 10.1210/en.2003-1251
 181. Qi T, Christopoulos G, Bailey RJ, Christopoulos A, Sexton PM, Hay DL. Identification of N-terminal receptor activity-modifying protein residues important for calcitonin gene-related peptide, adrenomedullin, and amylin receptor function. *Mol Pharmacol* (2008) 744:1059–71. doi: 10.1124/mol.108.047142
 182. Fischer JP, Els-Heindl S, Schonauer R, Bierer D, Kobberling J, Riedl B, et al. The Impact of Adrenomedullin Thr22 on Selectivity within the Calcitonin Receptor-like Receptor/Receptor Activity-Modifying Protein System. *ChemMedChem* (2018) 1317:1797–805. doi: 10.1002/cmdc.201800329
 183. Robinson SD, Aitken JF, Bailey RJ, Poyner DR, Hay DL. Novel peptide antagonists of adrenomedullin and calcitonin gene-related peptide receptors: identification, pharmacological characterization, and interactions with position 74 in receptor activity-modifying protein 1/3. *J Pharmacol Exp Ther* (2009) 3312:513–21. doi: 10.1124/jpet.109.156448
 184. Portal-Nunez S, Shankavaram UT, Rao M, Datrice N, Atay S, Aparicio M, et al. Aryl hydrocarbon receptor-induced adrenomedullin mediates cigarette smoke carcinogenicity in humans and mice. *Cancer Res* (2012) 7222:5790–800. doi: 10.1158/0008-5472.CAN-12-0818
 185. Roldos V, Martin-Santamaria S, Julian M, Martinez A, Choulier L, Altschuh D, et al. Small-molecule negative modulators of adrenomedullin: design, synthesis, and 3D-QSAR study. *ChemMedChem* (2008) 39:1345–55. doi: 10.1002/cmdc.200800066
 186. Olesen J, Diener HC, Husstedt IW, Goadsby PJ, Hall D, Meier U, et al. Calcitonin gene-related peptide receptor antagonist BIBN 4096 BS for the acute treatment of migraine. *N Engl J Med* (2004) 35011:1104–10. doi: 10.1056/NEJMoa030505
 187. Salvatore CA, Hershey JC, Corcoran HA, Fay JF, Johnston VK, Moore EL, et al. Pharmacological characterization of MK-0974 [N-[(3R,6S)-6-(2,3-difluorophenyl)-2-oxo-1-(2,2,2-trifluoroethyl)azepan-3-yl]-4-(2-oxo-2,3-dihydro-1H-imidazo[4,5-b]pyridin-1-yl)piperidine-1-carboxamide], a potent and orally active calcitonin gene-related peptide receptor antagonist for the treatment of migraine. *J Pharmacol Exp Ther* (2008) 3242:416–21. doi: 10.1124/jpet.107.130344
 188. Salvatore CA, Moore EL, Calamari A, Cook JJ, Michener MS, O'Malley S, et al. Pharmacological properties of MK-3207, a potent and orally active calcitonin gene-related peptide receptor antagonist. *J Pharmacol Exp Ther* (2010) 3331:152–60. doi: 10.1124/jpet.109.163816

189. Dodick DW, Lipton RB, Ailani J, Halker Singh RB, Shewale AR, Zhao S, et al. Ubrogapant, an Acute Treatment for Migraine, Improved Patient-Reported Functional Disability and Satisfaction in 2 Single-Attack Phase 3 Randomized Trials, ACHIEVE I and II. *Headache* (2020) 604:686–700. doi: 10.1111/head.13766
190. Silberstein SD, Dodick DW, Bigal ME, Yeung PP, Goadsby PJ, Blankenbiller T, et al. Fremanezumab for the Preventive Treatment of Chronic Migraine. *N Engl J Med* (2017) 37722:2113–22. doi: 10.1056/NEJMoa1709038
191. Isumi Y, Minamino N, Katafuchi T, Yoshioka M, Tsuji T, Kangawa K, et al. Adrenomedullin production in fibroblasts: its possible function as a growth regulator of Swiss 3T3 cells. *Endocrinology* (1998) 1395:2552–63. doi: 10.1210/endo.139.5.6004
192. Blet A, Deniau B, Geven C, Sadoune M, Caillard A, Kounde PR, et al. Adrecrezumab, a non-neutralizing anti-adrenomedullin antibody, improves haemodynamics and attenuates myocardial oxidative stress in septic rats. *Intensive Care Med Exp* (2019) 71:25. doi: 10.1186/s40635-019-0255-0
193. Shi L, Lehto SG, Zhu DX, Sun H, Zhang J, Smith BP, et al. Pharmacologic Characterization of AMG 334, a Potent and Selective Human Monoclonal Antibody against the Calcitonin Gene-Related Peptide Receptor. *J Pharmacol Exp Ther* (2016) 3561:223–31. doi: 10.1124/jpet.115.227793
194. Goadsby PJ, Reuter U, Hallstrom Y, Broessner G, Bonner JH, Zhang F, et al. A Controlled Trial of Erenumab for Episodic Migraine. *N Engl J Med* (2017) 37722:2123–32. doi: 10.1056/NEJMoa1705848
195. Dolgin E. First GPCR-directed antibody passes approval milestone. *Nat Rev Drug Discovery* (2018) 177:457–9. doi: 10.1038/nrd.2018.103
196. Fernandez-Sauze S, Delfino C, Mabrouk K, Dussert C, Chinot O, Martin PM, et al. Effects of adrenomedullin on endothelial cells in the multistep process of angiogenesis: involvement of CRLR/RAMP2 and CRLR/RAMP3 receptors. *Int J Cancer* (2004) 1086:797–804. doi: 10.1002/ijc.11663
197. Taylor MM, Samson WK. Ribozyme compromise of adrenomedullin mRNA reveals a physiological role in the regulation of water intake. *Am J Physiol Regul Integr Comp Physiol* (2002) 2826:R1739–45. doi: 10.1152/ajpregu.00696.2001
198. Dackor R, Fritz-Six K, Smithies O, Caron K. Receptor activity-modifying proteins 2 and 3 have distinct physiological functions from embryogenesis to old age. *J Biol Chem* (2007) 28225:18094–9. doi: 10.1074/jbc.M703544200
199. Kotch LE, Iyer NV, Laughner E, Semenza GL. Defective vascularization of HIF-1 α -null embryos is not associated with VEGF deficiency but with mesenchymal cell death. *Dev Biol* (1999) 2092:254–67. doi: 10.1006/dbio.1999.9253
200. Khalfaoui-Bendris G, Dussault N, Fernandez-Sauze S, Berenguer-Daizé C, Sigaud R, Delfino C, et al. Adrenomedullin blockade induces regression of tumor neovessels through interference with vascular endothelial-cadherin signalling. *Oncotarget* (2015) 610:7536–53. doi: 10.18632/oncotarget.3167
201. Hayashi M, Majumdar A, Li X, Adler J, Sun Z, Vertuani S, et al. VE-PTP regulates VEGFR2 activity in stalk cells to establish endothelial cell polarity and lumen formation. *Nat Commun* (2013) 4:1672. doi: 10.1038/ncomms2683
202. Fujio Y, Walsh K. Akt mediates cytoprotection of endothelial cells by vascular endothelial growth factor in an anchorage-dependent manner. *J Biol Chem* (1999) 27423:16349–54. doi: 10.1074/jbc.274.23.16349
203. Sitohy B, Nagy JA, Dvorak HF. Anti-VEGF/VEGFR therapy for cancer: reassessing the target. *Cancer Res* (2012) 728:1909–14. doi: 10.1158/0008-5472.CAN-11-3406
204. Gao Y, Li J, Qiao N, Meng Q, Zhang M, Wang X, et al. Adrenomedullin blockade suppresses sunitinib-resistant renal cell carcinoma growth by targeting the ERK/MAPK pathway. *Oncotarget* (2016) 739:63374–87. doi: 10.18632/oncotarget.11463
205. Kamba T, McDonald DM. Mechanisms of adverse effects of anti-VEGF therapy for cancer. *Br J Cancer* (2007) 9612:1788–95. doi: 10.1038/sj.bjc.6603813
206. Meadows KL, Hurwitz HI. Anti-VEGF therapies in the clinic. *Cold Spring Harb Perspect Med* (2012) 210. doi: 10.1101/cshperspect.a006577
207. Jin D, Harada K, Ohnishi S, Yamahara K, Kangawa K, Nagaya N. Adrenomedullin induces lymphangiogenesis and ameliorates secondary lymphoedema. *Cardiovasc Res* (2008) 803:339–45. doi: 10.1093/cvr/cvn228
208. Nikitenko LL, Shimosawa T, Henderson S, Makinen T, Shimosawa H, Qureshi U, et al. Adrenomedullin haploinsufficiency predisposes to secondary lymphedema. *J Invest Dermatol* (2013) 1337:1768–76. doi: 10.1038/jid.2013.47
209. Poon RT, Fan ST, Wong J. Clinical implications of circulating angiogenic factors in cancer patients. *J Clin Oncol* (2001) 194:1207–25. doi: 10.1200/JCO.2001.19.4.1207
210. Qiao G, Xu H, Li C, Li X, Farooqi AA, Zhao Y, et al. Granulin A Synergizes with Cisplatin to Inhibit the Growth of Human Hepatocellular Carcinoma. *Int J Mol Sci* (2018) 19(10):3060. doi: 10.3390/ijms19103060

Conflict of Interest: Authors AO’K, JG, and OT are employed by the company Fusion Antibodies. RV, MR, and MB are stockholders of Early Drug Development Group.

The remaining authors declare that the research was conducted in the absence of any commercial or financial relationships that could be construed as a potential conflict of interest.

Copyright © 2021 Vázquez, Riveiro, Berenguer-Daizé, O’Kane, Gormley, Touzelet, Rezai, Bekradda and Ouafik. This is an open-access article distributed under the terms of the Creative Commons Attribution License (CC BY). The use, distribution or reproduction in other forums is permitted, provided the original author(s) and the copyright owner(s) are credited and that the original publication in this journal is cited, in accordance with accepted academic practice. No use, distribution or reproduction is permitted which does not comply with these terms.



P. aeruginosa Mediated Necroptosis in Mouse Tumor Cells Induces Long-Lasting Systemic Antitumor Immunity

Jia-long Qi^{1†}, Jin-rong He^{1,2†}, Shu-mei Jin^{3†}, Xu Yang¹, Hong-mei Bai¹, Cun-bao Liu¹ and Yan-bing Ma^{1*}

OPEN ACCESS

Edited by:

Cirino Botta,
Cosenza Hospital, Italy

Reviewed by:

Joanne Hildebrand,
Walter and Eliza Hall Institute of
Medical Research, Australia
Yuichi Iida,
Shimane University, Japan

*Correspondence:

Yan-bing Ma
yanbingma@126.com

[†]These authors share first authorship

Specialty section:

This article was submitted to
Cancer Molecular Targets
and Therapeutics,
a section of the journal
Frontiers in Oncology

Received: 26 September 2020

Accepted: 21 December 2020

Published: 12 February 2021

Citation:

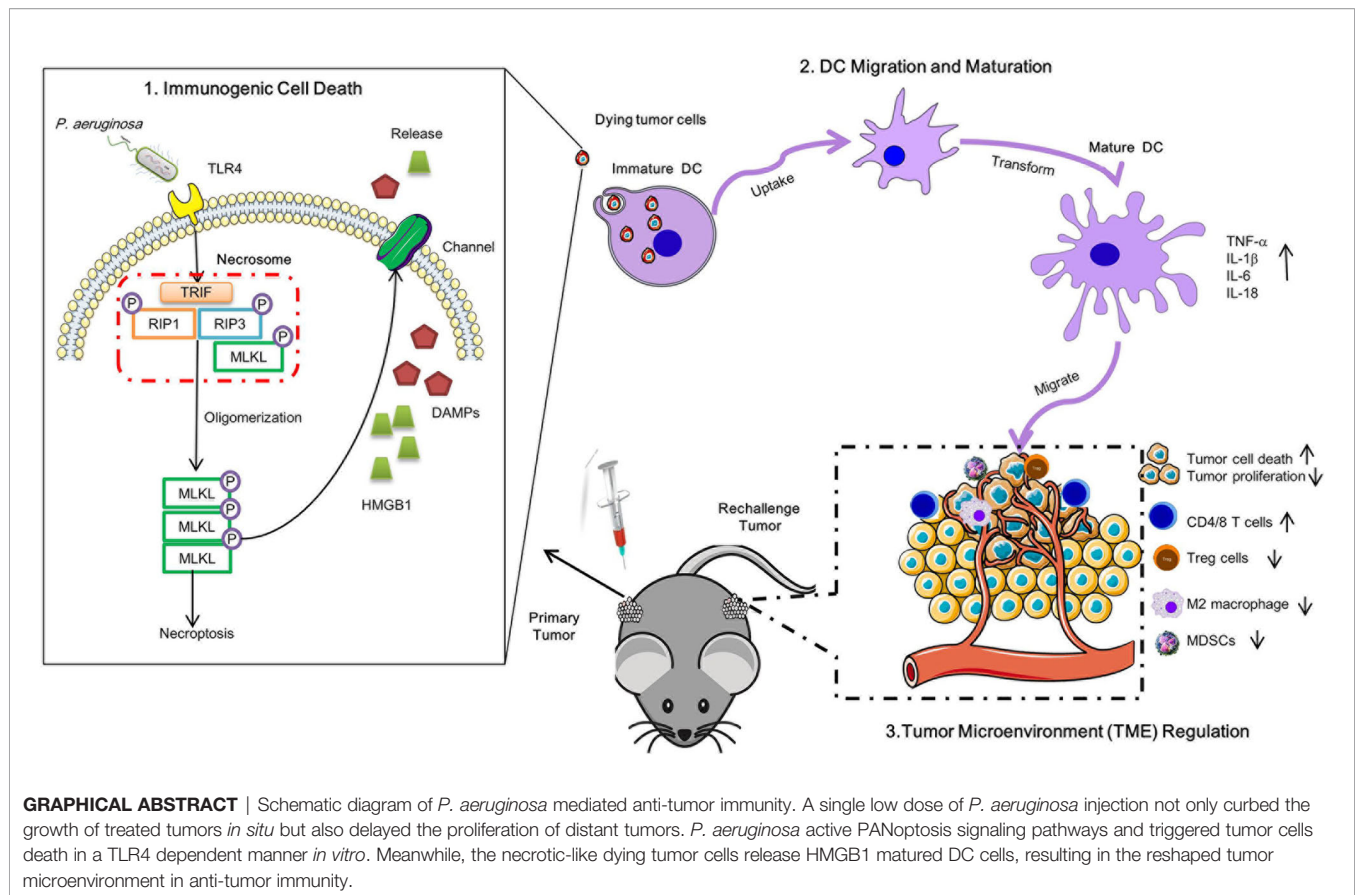
Qi J-l, He J-r, Jin S-m, Yang X,
Bai H-m, Liu C-b and Ma Y-b (2021)
P. aeruginosa Mediated Necroptosis
in Mouse Tumor Cells Induces Long-
Lasting Systemic Antitumor Immunity.
Front. Oncol. 10:610651.
doi: 10.3389/fonc.2020.610651

¹ Institute of Medical Biology, Chinese Academy of Medical Sciences and Peking Union Medical College, Kunming, China,
² Institute of Medical Biology, Kunming Medical University, Kunming, China, ³ Department of Pathology, Yunnan Institute of
Materia, Kunming, China

Necroptosis is a form of programmed cell death (PCD) characterized by RIP3 mediated MLKL activation and increased membrane permeability via MLKL oligomerization. Tumor cell immunogenic cell death (ICD) has been considered to be essential for the anti-tumor response, which is associated with DC recruitment, activation, and maturation. In this study, we found that *P. aeruginosa* showed its potential to suppress tumor growth and enable long-lasting anti-tumor immunity *in vivo*. What's more, phosphorylation- RIP3 and MLKL activation induced by *P. aeruginosa* infection resulted in tumor cell necrotic cell death and HMGB1 production, indicating that *P. aeruginosa* can cause immunogenic cell death. The necrotic cell death can further drive a robust anti-tumor response via promoting tumor cell death, inhibiting tumor cell proliferation, and modulating systemic immune responses and local immune microenvironment in tumor. Moreover, dying tumor cells killed by *P. aeruginosa* can catalyze DC maturation, which enhanced the antigen-presenting ability of DC cells. These findings demonstrate that *P. aeruginosa* can induce immunogenic cell death and trigger a robust long-lasting anti-tumor response along with reshaping tumor microenvironment.

Keywords: dying tumor cell, tumor microenvironment, antitumor immunity, necroptosis, *P. aeruginosa*

Abbreviations: TME, Tumor microenvironment; RIP3, Receptor Interacting Serine/Threonine Kinase 3; MLKL, Mixed Lineage Kinase Domain Like Pseudokinase; HMGB1, High Mobility Group Box 1; PA-MSHA, *Pseudomonas aeruginosa*-mannose-sensitive hemagglutinin; CB-CIK, Cord-blood cytokine-induced killer; TLR, Toll-like receptor; DC, Dendritic cells; NK, Nature killer cells; NKT, Nature killer T cells; TAM, Tumor associated macrophages; MDSC, Myeloid-derived suppressor cells; PDA, Pancreatic ductal adenocarcinoma; CAC, Colitis-associated cancer; ICD, Immunogenic cell death; DAMPs, Danger-associated molecular patterns; LDH, Lactate dehydrogenase; MPO, Myeloperoxidase; FCM, Flow cytometry; OMVs, outer membrane vesicles; VLP, virus-like particles; TAAs, Tumor associated-antigens.



HIGHLIGHTS

1. *P. aeruginosa* infection triggered necrotic tumor cell death to enhance long-lasting anti-tumor response *in vivo*.
2. *P. aeruginosa*-induced robust antitumor immunity modulated tumor microenvironment (TME) immune cells infiltration and cytokines production.
3. Dying tumor cells orchestrated DC recruitment, activation, and maturation.

INTRODUCTION

In the last decades, more research has revealed the potential connection between specific microorganisms and different types of cancer, which was observed by investigation microbiome in cancer patients (1). Microbiota can not only promote tumor cell death but also reshape tumor microenvironment (TME) to turn “cold” tumor into “hot” tumor by increasing the number of immune-effective cells and enhancing the anti-tumor ability, while decreasing the number of immune-suppressive cells and suppressing their tumor-suppressive function (2). Alternatively, bacteria-derived metabolites cause cancer cell autophagy and

facilitate anti-tumor immune-surveillance (3). To this end, the bacteria-mediated anti-cancer effects can prominently affect the outcomes of immunotherapy.

The first immunotherapeutic bacteria applied to cancer immunotherapy can be dated back to the late 19th century (4). Up to now, numerous types of bacteria have been identified with robust ability to inhibit tumor growth with low toxicity (5). Although the most well-established studies of the relationship between the microbiota, tumorigenesis, and tumor drug-resistance have been focused on the gut microbiome, the acquisition of the human upper respiratory tract, especially lung microbiome, also plays a crucial role in protecting the host from infection, inflammation, and anti-tumor response (6, 7). The migration, maturation, and activation of innate immune cells in lung tissues require commensal host-microbial interaction.

Pseudomonas aeruginosa parasitized on the skin is an opportunistic Gram-negative pathogen that can also cause diverse infections in the lungs (8). Previous studies have demonstrated that the lipopolysaccharide of *P. aeruginosa* is essential to inhibit tumor growth as an adjuvant and promote interferon cytokines production (9). In addition, *P. aeruginosa*-mannose-sensitive hemagglutinin (PA-MSHA) enhances anti-tumor immunity of cord-blood cytokine-induced killer (CB-CIK) cells *via* IFN- γ release and Toll-like receptor (TLR) activation (10). What's more, PA-MSHA directly stimulates

T cell, migration, and maturation of dendritic cells (DC) *via* TLR4-dependent manner that elicits antitumor immunity (11). PA-MSHA also directly triggers tumor cell apoptosis, arrests cell cycle, as well as inhibits autophagy *via* EGFR pathway and/or p62 regulating (12–15). However, other types of cell death that can be triggered by *P. aeruginosa*, like necroptosis, in antitumor responses have not been comprehensively evaluated. Here, we employed a TC-1 solid tumor model to evaluate the role of *P. aeruginosa* triggered necroptosis in antitumor response.

Necroptosis is a form of programmed cell death that is characterized by RIP3 mediated MLKL activation and can increase cell membrane permeability by MLKL oligomerization (16). Necroptosis also participates in cardiovascular diseases (17), anti-bacteria (18), anti-viral infection (19), and even anti-tumor response (20). It has been reported that Gram-positive bacteria *S. aureus*-induce lung cancer cell A549 cell death is enhanced by TNF- α , which is associated by RIP3-dependent necroptosis (21). RIP3-mediated CXCL1 promote tumor associated macrophages (TAM)-induced adaptive immune suppression and myeloid-derived suppressor cells (MDSC)-induced adaptive immune suppression in pancreatic ductal adenocarcinoma (PDA) and colitis-associated cancer (CAC) (22, 23). Similarly, MLKL suppresses colon inflammation and tumorigenesis *via* MEK/ERK activation in DC (24). Intra-tumor therapy with an MLKL-mRNA-based vaccine inhibit CAC growth reshaped the tumor microenvironment inducing systemic antitumor response directed against neo-epitopes (25, 26). In addition, tumor cell immunogenic cell death (ICD) has been considered to be essential for anti-tumor response associated with DC recruitment, activation, and maturation (27, 28). Although chemotherapeutics normally trigger cell death in RIP3-/- or MLKL-/- tumor cell death *via* caspase-3-dependent apoptosis, it is unable to induce systemic anti-tumor response and inhibit tumor growth *in vivo*, which indicates necroptosis pathway plays a potential role in ICD (29). Notably, the danger-associated molecular patterns (DAMPs) released by necrotic cell death contribute to hosting immune system activation, particularly HMGB-1 released by the dying cell, which can stimulate DC maturation through TLR4-myD88 pathway (30). However, it is not clear whether bacteria-mediated necrotic cell death is a form of ICD and whether these bacteria-triggered dying cells can induce systemic anti-tumor immunity.

Herein, we identify a beneficial immunotherapeutic role of *P. aeruginosa* that mediates necrotic tumor cell death *in vitro* and *in vivo*, which provides a long-lasting anti-tumor immunity by reshaping systemic and tumor microenvironment. Surprisingly, *P. aeruginosa* not only inhibited tumor growth *in vivo* but also activated functions of DC cells, therefore indicating a strategy for designing bacteria-based immunotherapy against the tumor. These beneficial effects occur after co-administration of bacteria in tumor cells simultaneously, indicating that the protective effects are due to bacteria triggered RIP3-MLKL-dependent necroptosis. In conclusion, our findings demonstrate that *P. aeruginosa* triggers tumor necrotic cell death to promote robust antitumor immunity.

MATERIALS AND METHODS

Ethics Statement

The Ethics Committee of Animal Care and Welfare of IMBCAMS and PUMC (Permit Number: SYXK (dian)2010-0007) approved all of the animal experiments according to the guidelines of the Institute of the Medical Biology Chinese Academy of Medical Sciences (IMBCAMS) & Perking Union Medical College (PUMC). All efforts were made to minimize animal suffering.

Mice

All mice, six- to eight-week-old female C57BL/6N were purchased from Beijing Vital River Laboratory Animal Technology Co., Ltd. (Beijing, People's Republic of China), maintained under specific pathogen-free (SPF) conditions and raised in the central animal care services of IMBCAMS. Before bacterial infection or tumor injection, mice were anesthetized with 3% isoflurane in oxygen for 2–5 min until immobile. At the experiment endpoints, mice were first anesthetized and then sacrificed by an increasing CO₂ concentration for 5–10 min in a closed chamber until mice pupil dilation, stopped breathing, and stopped heartbeat.

Bacteria Culture and Mice Infection

The clinical isolate *P. aeruginosa* 1409, which was identified and stored by our own lab, was grown overnight with shaking Luria-Bertani (LB) medium under 37°C. The next day, the bacteria were sub-cultured with fresh LB medium for 4 h. Until the bacterial concentration corresponding to an OD value reaches 0.5, the culture was collected with a centrifuge at 7000 \times g for 10 min and washed the bacterial twice with sterile phosphate-buffered saline (PBS). The murine bacteremia model was established with a subcutaneous injection with a 50 μ l per mouse total volume solution containing 3×10^6 CFU to 3×10^8 CFU bacterial in Basement Membrane Matrix (BD Bioscience, San Jose, CA, USA). Each group contains 8 mice and continuous monitoring of the bacterial challenged mice survival rate for seven days, considered as the endpoint.

Tumor Model

To establish the tumor cell-grafted model, indicated 1×10^6 cells incubated with- or without- 3×10^6 CFU bacteria were mixed with Basement Membrane Matrix (BD Bioscience, San Jose, CA, USA) and subcutaneously implanted in the left dorsal flank of C57BL/6N mice for the primary tumor model construction. The mice were monitored three times per week for tumor growth using a slide caliper as described previously. Body weight changes were monitored every two days of tumor-bearing mice to identify the bacteria infection induced disadvantages for 15 days, and the survival rates were monitored until all mice were dead in the control group, and then the experimental group were euthanized. After the primary tumor established, tumor-free mice were rechallenged with TC-1 tumor cells in the other side flank of mice (n=5–6). Secondary tumor growth curve was monitored. All tumor volumes were measured with a caliper and calculated as (length \times width²)/2.

Indirect Immunofluorescence and H & E Staining

At the experiment endpoint, the mice were anesthetized and sacrificed. Tumor tissues were stripped and obtained, frozen in liquid nitrogen, embedded in optimal cutting temperature compound (OCT), and sectioned in 5 μ m thickness pieces. The sections were performed for indirect immunofluorescence staining assay. Briefly, the cryo-sections were fixed in 95% alcohol and permeabilized with 2% BSA in 0.1% TritonX-100/PBS overnight at 4°C for 30 min, and then blocked with 5% bovine serum albumin (BSA) for 1 h. After blocking, the sections were incubated with Caspase-3, MLKL, MPO, and Ki67 primary antibody overnight at 4°C, respectively. The bound antibodies were labeled with FITC fluorescent secondary antibodies for 1 h at room temperature. After washing, all cryo-sections were stained with 4',6-diamidino-2-phenylindole (DAPI) for 15 min at room temperature, and then photographed under a fluorescence microscope. Tumor tissues frozen sections were also stained for histologic examination by staining with hematoxylin and eosin (H & E) kit, according to the manufacturer's protocol. Areas of positive were measured with software Image J.

Flow Cytometry Assay (FCM)

Lymphocytes cells isolated from the spleen and tumor tissues of tumor-bearing mice were plated into a 96-microwells plate for immune cell profiles assay. Cell surface staining was performed by incubating cells with corresponding antibodies for 20 min on ice. Cells were stained with APC labeled anti mouse CD3 and FITC labeled anti mouse CD4 for CD4 positive T cells; APC labeled anti mouse CD3 and FITC labeled anti mouse CD8 for CD8 positive T cells; APC labeled anti mouse CD3 and PE labeled anti mouse NK1.1 for NK and NKT cells; APC labeled anti mouse CD11b and FITC labeled F4/80 for macrophages; APC labeled anti mouse CD11b and PE labeled Gr-1 for MDSC cells; FITC labeled anti mouse CD4, PE labeled anti mouse CD25 and APC labeled anti mouse Foxp3 for Treg cells. All FCM reagents were purchased from Biolegend, San Diego, CA, USA. After washing, the cells were resuspended in 200 μ l staining buffer and analyzed by flow cytometry (CytoFLEX LX, Beckman, USA), and the data were analyzed using CytExpert 2.0 software.

Enzyme-Linked Immunospot Assay (ELISPOT)

For ELISPOT assay, the protocol was the same as previously reported. In brief, splenic lymphocytes and tumor-infiltrating lymphocytes were harvested and extracted by mouse lymphocytes separation kit (BioLedgen, USA), and then washed with fresh RPMI 1640 medium. Next, 1×10^5 cells were seeded into a 96-microwells plate, which was pre-coated with IFN- γ - and IL-2-specific coated antibodies, and then 2 μ g/ml HPV 16 E7₄₉₋₅₇ specific peptides was added into the plates. After 18 h stimulation, the culture medium was gently discarded and fresh pre-cooled water was added for rupturing lymphocytes. Then, incubating IFN- γ - and IL-2- capture secondary antibodies that were labeled with biotin for 1 h at room temperature, followed by avidin-conjugated HRP. After

immuno-imaging, spots representing activated lymphocytes were counted by an ELISPOT reader system (AID Diagnostika GmbH, Strabberg, Germany).

LDH Release Assay

Tumor cells were stimulated with 10 MOI *P. aeruginosa* 1409 for 12 h, cell culture supernatants were gently discarded and incubated with LDH release reagent for 1 h, all supernatants were removed to a new cell culture plate and 60 μ l LDH working solution was added and then slowly shaking at room temperature for 30 min in the dark environment. Absorbance [A490nm-A620 nm] stands for the quantification of LDH release.

Immunoblotting Assay

For immunoblot assay, TC-1 cells were seeded into 12-well plates, 10^6 cells per well; the next day before infection, cells were washed with PBS three times and then 500 μ l FBS- and antibiotics-free RPMI1640 medium added to each well. To evaluate bacterial infection on TC-1, 10 MOI *P. aeruginosa* 1409 were added into cell culture for 1 h, 4 h, and 12 h at 37°C in 5% CO₂ atmosphere. All cells were washed with PBS three times and lysed in 100 μ l RIPA (Tris pH 7.4 50 mmol/L, NaCl 150 mmol/L, NP-40 1%, SDS 0.1%, EDTA 2 mmol/L) buffer containing proteinase and phosphatase cocktail inhibitor. All samples were separated by 12% SDS-PAGE and transferred to polyvinylidene fluoride membranes (PVDF), which were blocked by 5% BSA blocking reagent at room temperature for 2 h. The primary antibodies used: anti-MLKL (CST, 37705), anti-pMLKL (CST, 37333S), anti-RIP3 (CST, 95702), anti-pRIP3 (CST, 57220), anti-LC3B (Abcam; ab51520), anti-HMGB1 (Abcam; ab 18256), anti- β -actin (Abcam; ab6276), anti-GAPDH. The secondary antibodies used HRP-labeled anti-rabbit or mouse antibodies (Abcam). At last, the blotting was developed by the ECL chemiluminescence substrate. Image J software was used to quantify the Western Blot bands grayscale value.

ELISA

The DCs were incubated with bacteria-treated dying tumor cells for 24 h. The cell culture mediums were collected for cytokines quantitation. The IL-1 β , IL-6, TNF- α , and MCP-1 were measured by mouse IL-1 β , IL-6, TNF- α , and MCP-1 quantikine ELISA kits (R&D systems), respectively, according to the manufacturer's protocol.

Real-Time Quantitative PCR

Indicated 1×10^6 TC-1 tumor cells were seeded into a 12-well cell culture plates. The next day, 1×10^7 CFU bacteria were added into the cell culture for stimulation for 1 h and 4 h, the medium were discarded, and the dying tumor cells were harvest. Total RNA was isolated using TRIzol (RNAiso, Takara) and purified by the chloroform-phenol extraction kits. cDNA was reverse transcribed with the SureScript First-stand cDNA Synthesis Kit (GeneCopoeia) and then detected by the All-in-OneTM miRNA qRT-PCR Detection Kit (GeneCopoeia). Real-time quantitative PCR (RT-qPCR) was performed on a Bio-Rad CFX-96 Touch

Real-Time Detection system. Primer sequences are listed in supplemental **Table S1**.

Statistical Analysis

Graphpad Prism 8.2.1 (Graphpad Software, Inc., La Jolla, CA, USA) was employed for data statistical analysis, which was all presented as mean \pm standard error of mean (SEM). Tumor growth curve was performed with two-way ANOVA after Bonferroni correction. One-Way ANOVA and Student's paired *t*-test analysis were performed for three or two groups' comparisons, respectively, and non-parametric log-rank tests were used for survival rates. * indicate *P*-values ≤ 0.05 was considered significant, ** indicate *P*-values ≤ 0.01 , *** indicate *P*-values ≤ 0.001 , **** indicate *P*-values ≤ 0.0001 , ns indicate non-significance.

RESULTS

P. aeruginosa Stimulation Significantly Inhibited TC-1 Growth *In Vivo*

A mouse lung epithelial cell line, TC-1, which was co-transfected with HPV16 E6, E7, and Ras into C57BL/c (H-2b) cell that was

broadly used as an HPV tumor model, was performed to establish a subcutaneous solid tumor model to evaluate *P. aeruginosa*-mediated anti-tumor response *in vivo*. First, the mouse sepsis model was established by subcutaneous administration with a dose-dependent bacteria injection and the mice survival rate was monitored in a week, and the survival curves indicated that none of the mice in the lowest-dose group was dead (**Figure 1A**). We chose the lowest dose of 3×10^6 CFU per mouse for further analysis. TC-1 cells were co-injected with bacteria subcutaneously in the right side of the mouse, and tumor growth curve was continuously monitored (**Figure 1B**). The results of tumor volume in mice showed that the bacteria co-injection group suppressed tumor growth more significantly than that in the control group. Obviously, all tumors were growing well in the control group and only one tumor in bacteria group has a volume less than 100 mm^3 at the observation endpoint (**Figure 1C**). These results demonstrated the robust anti-tumor response resulted from bacteria co-injection that 80% of mice in the bacteria group were tumor-free mice (**Figure 1D**). Meanwhile, we also monitored the weight of mice after tumor inoculation. After bacteria co-injection, mouse weights recovered after a slight loss of body weight (**Figure 1E**). All the mice in the bacteria co-injection group

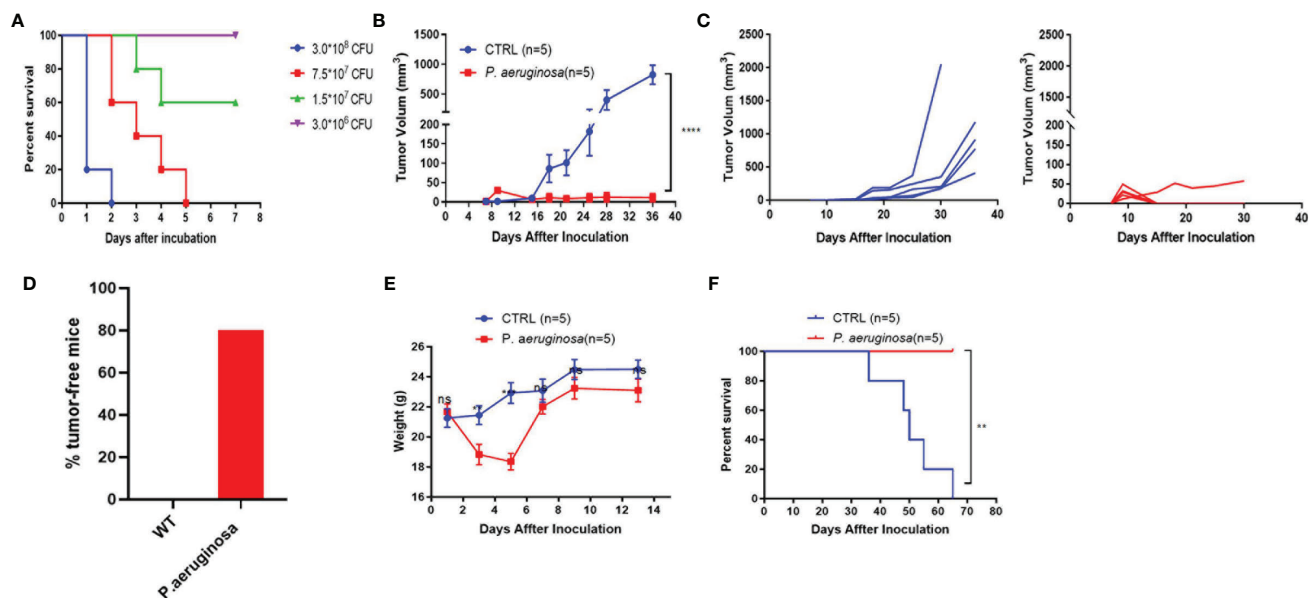


FIGURE 1 | The low sublethal dose of *P. aeruginosa* co-injection inhibits tumor growth in the mouse TC-1 model. **(A)** Survival rate of mice subcutaneously challenged by a gradient of *P. aeruginosa* concentrations (n=8). Mice were continuously monitored for 7 days, which was considered the endpoint. **(B)** Tumor growth curve shown as average tumor volumes and standard error of the mean per group (n=5). **(C)** Tumor growth curve of individual mice are shown for control (n=5) and *P. aeruginosa* (n=5) co-injected groups. Numbers in the panel demonstrated tumor size and the number of mice are still alive at day 40. This experiment was repeated twice. **(D)** Tumor-free mice percentage. Tumors were grown at early stage in both group, but only one tumor-bearing in *P. aeruginosa* co-injected group to the endpoint and all mice in control group were tumor-bearing mice. **(E)** The mice body weight monitor curve. After bacteria-tumor mix injection, all mice weight was continuously monitored for 14 days. The weight of mice in *P. aeruginosa* co-injected group dropped down at early stage and recovered at day 7. **(F)** Survival curves of tumor bearing mice (n=5). All mice in control group were dead before day 70 after tumor cells incubation while none of the dead mice appeared in the *P. aeruginosa* co-injected group. Data are means \pm SEM. Paired Student's *t*-test was performed for mice body weight comparisons, Two-way ANOVA for tumor growth curve comparisons, and survival curve analysis by Log Rank (Mantel-cox) test. ** indicate *P*-values ≤ 0.01 , *** indicate *P*-values ≤ 0.001 , **** indicate *P*-values ≤ 0.0001 , and ns indicates non-significance.

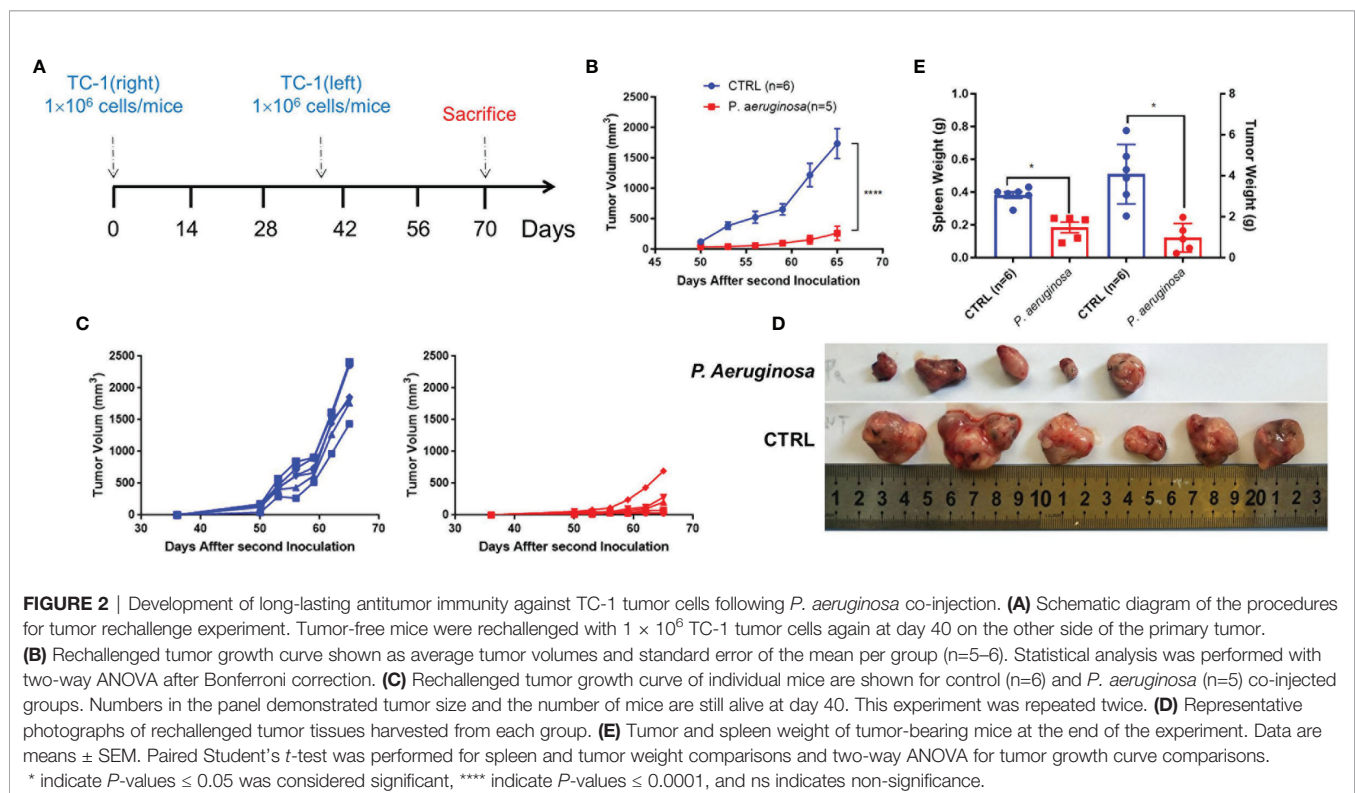
survived to the end of the experimental period, demonstrating a 100% protective efficacy, and all mice in the control group were dead in two months (Figure 1F). Altogether, we showed that *P. aeruginosa* co-injection suppresses tumor growth and prolongs survival *in vivo*.

Rechallenge Tumor Cells Indicated *P. aeruginosa*-Mediated Long-Lasting Antitumor Immunity

We hypothesized that *P. aeruginosa*-mediated anti-tumor response could exist in a long-lasting function *in vivo*. To verify the thought, we rechallenged mice with 1×10^6 TC-1 tumor cells at day 40 in the left side and monitored continuously (Figure 2A). The tumor growth curve showed that the rechallenged tumor growth in bacteria-treated group was significantly suppressed (Figure 2B). Rechallenged tumor growth curve of individual mice suggested that although tumors kept growing in both groups, the tumor growth in the bacteria-treated group was much slower than that in the control group (Figure 2C). At the endpoint of the experiment, all tumor-bearing mice were sacrificed, and tumors and spleen tissues were harvested. Photographs of rechallenged tumor tissues that were stripped from sacrificed mouse indicated that the rechallenged tumor volumes were smaller in the bacteria injection group than that in the control group (Figure 2D). In addition, the weights of tumors and spleen were also significantly lower in the bacteria group (Figure 2E). Consistently, these results suggested that *P. aeruginosa* mediated a robust long-lasting anti-tumor response *in vivo*.

Immunotherapeutic Bacteria *P. aeruginosa* Activate Multiple Cell Death *In Vitro*

To explore the molecular mechanisms of *P. aeruginosa* induced anti-tumor response, we co-cultured *P. aeruginosa* and TC-1 tumor cells *in vitro*. As expected, tumor cells were dead after incubating with bacteria (Figure 3A), which was also confirmed by LDH release (Figure 3B). To examine if necrotic cell death occurred with *P. aeruginosa* incubation, we performed TC-1 cells infected with *P. aeruginosa* and examined the cell death pathways. We detected the active, phosphorylated form of RIP3 and MLKL in the lysate cell supernatants of bacteria treated tumor cells, indicating that bacteria were able to induce necrotic cell death activation. Furthermore, we observed that p-RIP3 and p-MLKL were upregulated with bacteria incubation, as well as naive RIP3 and MLKL (Figures 3C, D). In addition, we also detected the active LC3B in treated cell lysate and the ratio of LC3B II/GAPDH were increased, conforming that autophagic cell death is activated in response to bacterial infection (Figures 3C, D). To determine whether *P. aeruginosa* infection can induce apoptosis, we performed a FCM analysis by 7AAD-Annexin V-PE apoptosis kit. Notably, after bacterial incubation, the percent of apoptotic TC-1 cells was increased and the freeze-thaw tumor cells as a positive control (Figures 3E, F). To understand whether *P. aeruginosa* induced necrotic cell death drives immunogenic cell death (ICD) *in vitro*, we tested the release of the ICD marker HMGB1 with or without *P. aeruginosa* incubation (Figures 3G, H). We also found that TLR4 expression was increased in a time-dependent manner, indicating bacterial-triggered cell death *via* activated TLR4 signaling pathway (Figure 3I). Taken together,



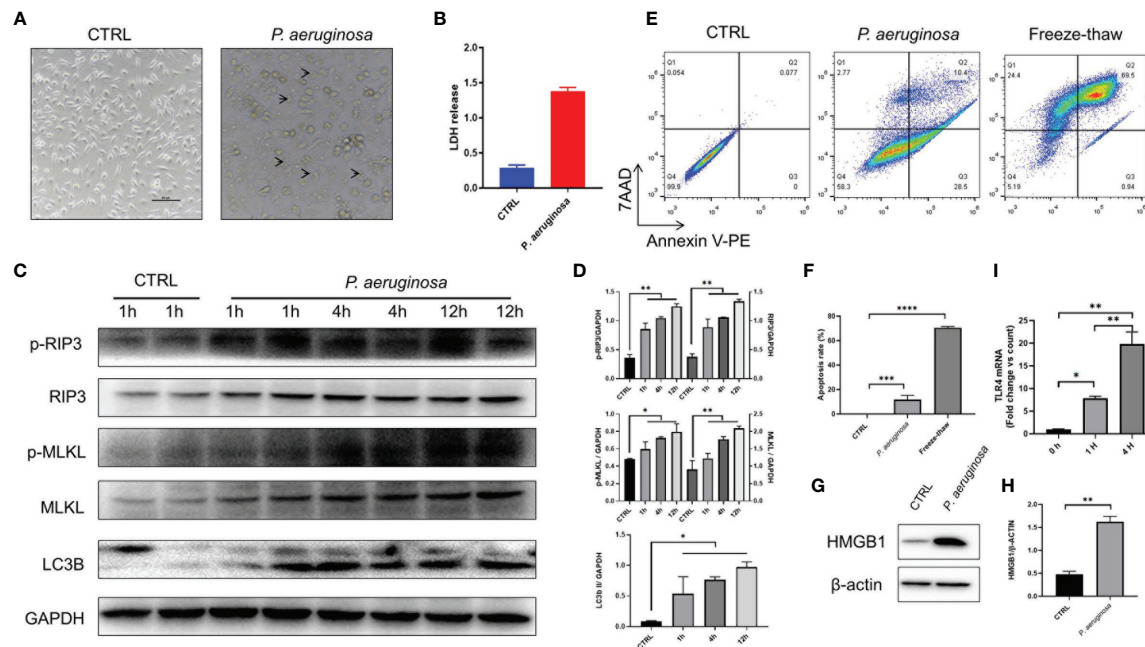


FIGURE 3 | *P. aeruginosa* incubation triggered PANoptosis in TC-1 tumor cells. 1×10^6 tumor cells were infected with 10 MOI *P. aeruginosa* for 1 h, 4 h, and 12 h, cell culture supernatants were gently removed and tumor cells were photographed and harvested for immunoassay. **(A)** Representative photographs of tumor cells treated with or without *P. aeruginosa*. After incubation, tumor cells were swollen and lysed under the microscope. Arrow represented dying cells. **(B)** Histogram analysis of lactate dehydrogenase (LDH) release. LDH releasements are represented for tumor cell death *in vitro*. **(C)** Western blots of RIP3/pRIP3/MLKL/pMLKL and LC3B in TC-1 cells treated with *P. aeruginosa*. The WB bands intensity was quantified by image J software. **(D)** Histogram analysis of the ratio of pRIP3/GAPDH, pMLKL/GAPDH, RIP3/GAPDH, MLKL/GAPDH, LC3B II/GAPDH. **(E)** Represent FCM images of 7AAD-Annexin V-PE assay. Freeze-thawed TC-1 cells were performed as positive control. **(F)** The results of cell apoptosis assay. **(G)** Western blots of HMGB1. **(H)** Histogram analysis of HMGB1 expression. **(I)** Histogram analysis of TLR4 expression by RT-PCR in a time-dependent manner. Data are means \pm SEM. Paired Student's *t*-test was performed for two group comparisons and one-way ANOVA for three groups. * indicate *P*-values ≤ 0.05 was considered significant, ** indicate *P*-values ≤ 0.01 , *** indicate *P*-values ≤ 0.001 , **** indicate *P*-values ≤ 0.0001 , and ns indicates non-significance.

the results indicated *P. aeruginosa* infection triggered PANoptosis *in vitro*, including necroptosis, apoptosis, and autophagy. Furthermore, bacteria-mediated necrotic cell death is also a form of ICD *in vitro*.

P. aeruginosa Co-Injection Induced Tumor Tissues Cell Death and Inhibited Proliferation

P. aeruginosa co-injection caused long-lasting tumor suppression in mice and induced tumor cell death *in vitro*. In line with these findings, we observed the hallmarks of cell death expression in tumor tissues; compared to the control group, the immunofluorescence results show that caspase-3, MPO, and MLKL expression in tumor tissues after bacteria treatment were significantly increased (**Figure 4A**). Quantification analysis confirmed that bacteria co-injection also induced tumor cell death in tissues (**Figure 4B**). Consistent with this data, we also detected Ki-67 expression levels in tumor tissues, which was considered as a hallmark of cell proliferation. The immunofluorescence results show that Ki-67 was reduced in the bacteria group (**Figure 4A**). Statistical analysis confirmed that bacterial infection induced antitumor response results in inhibition of tumor cell proliferation (**Figure 4B**). Additionally,

H & E staining analysis shows that more necrotic areas were observed and more inflammatory cells were infiltrated, respectively (**Figure 4C**). Taken together, our results indicated that *P. aeruginosa* infection induced anti-tumor response can promote tumor tissues cell death and suppress tumor cells proliferation.

Pre-Injection With *P. aeruginosa*-Tumor Cell Mixture Reshape the Tumor Microenvironment

To better understand the function of systemic and tumor microenvironment for antitumor immunity, we assessed the immune cell composition in tumor and splenic lymphocytes. Herein, we used the HPV 16 E7₄₉₋₅₇ peptide as tumor specific antigen for stimulation, and the immunocytes profiles of tumor-infiltrating and splenic lymphocytes were analyzed *via* flow cytometry (FCM) assay (**Figures 5A, B**). FCM analysis showed that percentages of CD4 and CD8 positive T cells were increased in the splenic and tumor lymphocytes. In line with this result, we found that tumor infiltrated CD3⁺NK1.1⁺ nature killer cells (NK) exhibited an identical tendency but there was no significant difference in the number of tumor infiltrated CD3⁺NK1.1⁺ nature killer T cells (NKT) in microenvironment. In addition,

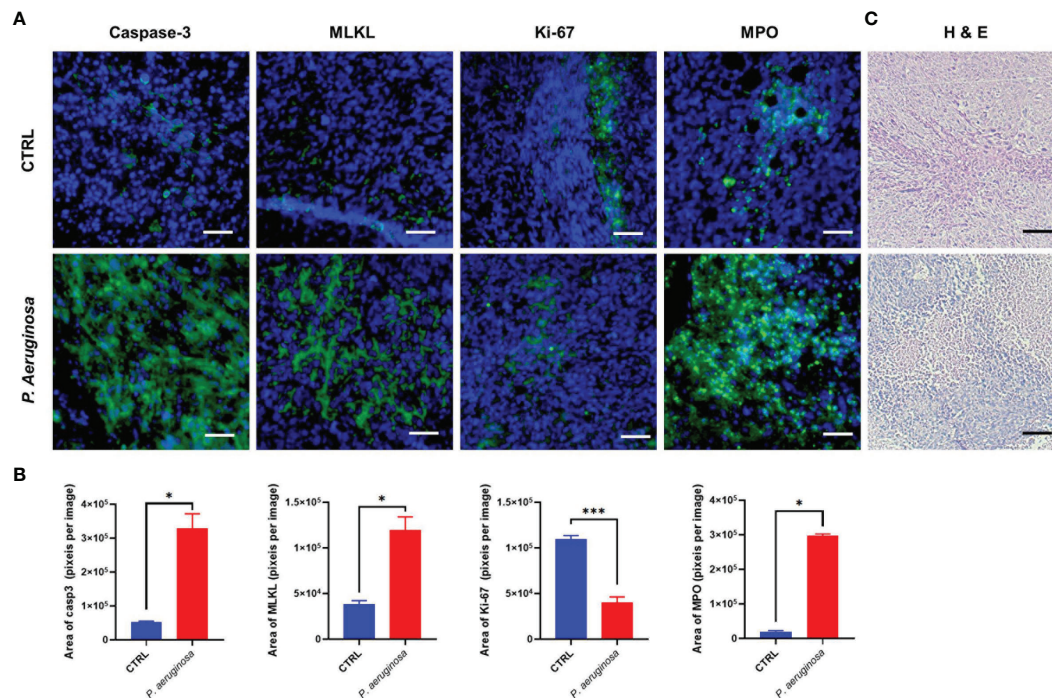


FIGURE 4 | Immunofluorescence assay for the detection of cell death and proliferation in tumor tissues. **(A)** Representative images of the immunofluorescence assay for tumor tissue sections. Caspase-3 staining was identified as cell apoptosis; MLKL staining was identified as cell necroptosis; MPO staining was identified as Neutrophils (31); Ki-67 staining was identified as cell proliferation. Cell nuclei were stained with DAPI. **(B)** Quantitative analysis of FITC positive cells in tumor tissues. All experiments were repeated three times. The area of immunofluorescence intensity was quantified by image J software. **(C)** H & E staining for tumor tissue sections collected at the experimental end point. Data are means \pm SEM. Paired Student's *t*-test was performed for comparisons. * indicate *P*-values \leq 0.05 was considered significant, *** indicate *P*-values \leq 0.001, and ns indicates non-significance.

the percentage of CD4⁺CD25⁺FoxP3⁺ labeled Treg cells were decreased in the bacteria-treated group. Analysis of the myeloid compartment showed decreased fractions of CD11b⁺Gr-1⁺ labeled MDSCs and CD11b⁺F4/80⁺ M2 macrophages (Mar) in the control group than that in the bacteria group. Meanwhile, the ELISPOT results indicated that IFN- γ and IL-2 produced splenic and tumor infiltrating lymphocytes were significantly increased (Figure 5C). Quantification results showed that the number of plots was increased and tumor antigen-specific cellular immune response in tumor-bearing mice were promoted (Figure 5D). In summary, our results suggest that *P. aeruginosa* infection increased antitumor lymphocytes accumulation and reduced immune-suppressive myeloid cell frequencies during tumor progression, thus inducing remarkable anti-tumor response and promoting antitumor cytokine-producing lymphocytes.

P. aeruginosa-Mediated Immunogenic Cell Death Promotes DC Maturation

To investigate whether bacteria-mediated tumor cell immunogenic cell death can active DCs' function, we incubated DCs with bacteria treated- and none-treated tumor cells *in vitro*, respectively, and then the DC maturation and cytokines was assessed. We detected the cytokines release for the identification of DCs functional maturation. As expected, DCs responded to bacteria treated tumor cells with significant increase in cytokines

secretion, including IL-1 β , IL-6, MCP-1, and TNF- α (Figure 6). In line with these results, we also detected the ATP release of TC-1 cells under bacterial treatment. We found that ATP were sharply increased in the first one hour and then maintained a high level after a slight decrease (Figure 1C). Collectively, these results indicate bacteria treated tumor cells induced immunogenic cell death that triggered migration and maturation of DCs.

DISCUSSION

Herein, we have applied the immunotherapeutic role of bacteria *P. aeruginosa* in cancer therapy in a TC-1 grafted tumor model, which empowered local therapeutic and promoted a long-lasting anti-tumor immunity. Furthermore, we characterized a single, extremely low dose of bacteria incubation that triggered tumor cell PANoptosis not only in primary tumor sites but also suppressed distant untreated tumors. Our data suggest that treating with bacteria *P. aeruginosa* reshaped the systemic- and tumor-microenvironment, matured DCs, which result in a robust, durable anti-tumor immune response.

Bacteria has shown its anti-tumor propensity in the long history of cancer immunotherapy on the basis of these demonstrated theories: (1) The colonization and growth of bacteria consume oxygen and nutrition in tumor tissues;

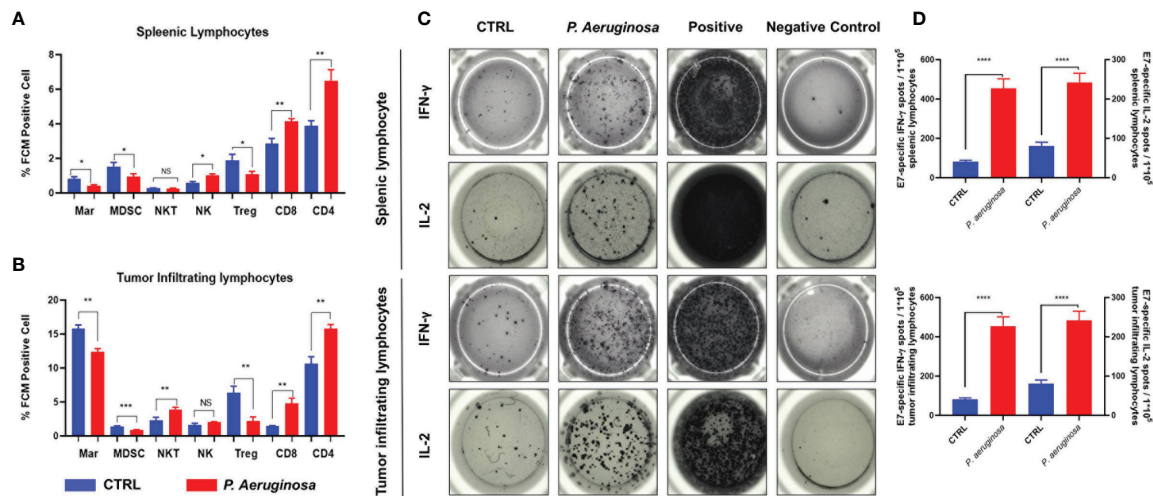


FIGURE 5 | *P. aeruginosa* mediated anti-tumor response remodeled systematic and tumor microenvironment immune cell profiles and promoted lymphocytes activation. Histogram analysis of immune cell profiles in (A) spleen lymphocytes and (B) tumor infiltrating lymphocytes by FCM. CD3⁺CD4⁺ staining cells were identified as CD4 T cells; CD3⁺CD8⁺ staining cells were identified as CD8 T cells; CD4⁺CD25⁺ Foxp3⁺ staining cells were identified as Treg cells; CD3⁺NK1.1⁺ staining cells were identified as NK cells; CD3⁺NK1.1⁺ staining cells were identified as NK T cells; CD11b⁺F4/80⁺ staining cells were identified as macrophages cells; (C) representative images of ELISPOT assay. Indicated 1×10^5 splenic lymphocytes and tumor infiltrating lymphocytes were stimulated with 2 ug/ml E7 specific peptides. Spots were represented as activated lymphocytes, PMA was performed as positive control. (D) Quantitative analysis of antigen specific IFN- γ - and IL-2-expressing lymphocytes detected by ELISPOT. Data are means \pm SEM. Paired Student's *t*-test was performed for comparisons. * indicate *P*-values ≤ 0.05 was considered significant, ** indicate *P*-values ≤ 0.01 , *** indicate *P*-values ≤ 0.001 , **** indicate *P*-values ≤ 0.0001 , and ns indicates non-significance.

(2) Bacteria and their metabolites directly promote cell death; (3) The reconstructed tumor microenvironment enhances the capability to kill tumor cells and suppress tumor growth by immune cells. Although surgery is the most used clinical treatment, radiotherapy, chemotherapy, and immune checkpoint therapy also become prevailing for cancer treatment today. However, the high cost, drug resistance, and side-effects of these treatments narrow the clinical therapeutic applicability. Here, we used a single, extremely low dose of bacteria *P. aeruginosa* as a novel “oncolytic bacteria” to induce tumor necrotic cell death, and thus promote tumor regression at the primary sites and also inhibiting rechallenged tumor growth in the distant sites (Figures 1 and 2). Meanwhile, the theory of oncolytic bacteria has already been proved by other groups (32, 33). Recently, the SLC delivery system in the safe and widely applied programmed probiotics Ecoil Niddle 1917 that constitute produced nanobody antagonist of PD-L1, CTLA-4 (33), or CD47⁵ combined with a controllable lysing mechanism, a minimized of toxicities in tumor tissues. The application of oncolytic bacteria successfully stimulated antitumor immunity, promoted tumor regression directly within the tumor microenvironment in multiple syngeneic mouse models for inhibiting primary tumor growth and distant metastasis colonization, indicating the application prospect of oncolytic bacteria in the further treatment.

Oncolytic bacteria is first identified by Danino T^o group, which possesses some natural advantages for cancer immunotherapeutic: (1) targeting effects, with the growth of tumor tissues, the immune-suppressed, and hypoxia TME provides the hotbed for facultative anaerobic bacteria and

anaerobic bacteria colonization; (2) modifiable genome, the bacteria hold a huge genome that could be easily and widely applied for gene editing; (3) easy to grow, multiple cell culture powders have been developed for bacteria growth; (4) cheap, the costs for bacteria growth are cheap; (5) natural adjuvant effects, numerous evidence demonstrate that the bacteria ghosts, flagella, CPG, RNA, and DNA are ligands for TLR or NLR, which activate a natural immune pathway.

We employed *P. aeruginosa* to identify its potential role in antitumor response as a novel oncolytic bacterial. First, we defined that *P. aeruginosa* directly trigger tumor cell death in a necrotic-like death by increasing the activate form of phosphorylation- RIP3 and MLKL expression in tumor cells (Figure 3). Pervious works identified that expression of RIP1/3 and MLKL was not only necessary to the necroptosis pathway but also contributes to the immunogenic cell death in TC-1 tumor cells (29). The expression of RIP3 was found down-regulated over half of the test cancer cell lines, suggesting tumor cells evade necrotic cell death, which is an important immune escape mechanism (34, 35). Moreover, the hypoxia TME and promoted methylation also contribute in RIP3 regulation for antitumor response (34). In addition, the expression of MLKL was also found decreased in multiple tumor tissues including ovarian carcinoma, gastric cancer, colon cancers, and so on (36–38). Then, we found that bacteria also triggered high levels of caspase-3-dependent apoptosis and other cell death like necroptosis and NETosis in tumor tissues; in the meantime, cell proliferation was also decreased according to Ki67 detection (Figure 4). Our previous works indicated that no

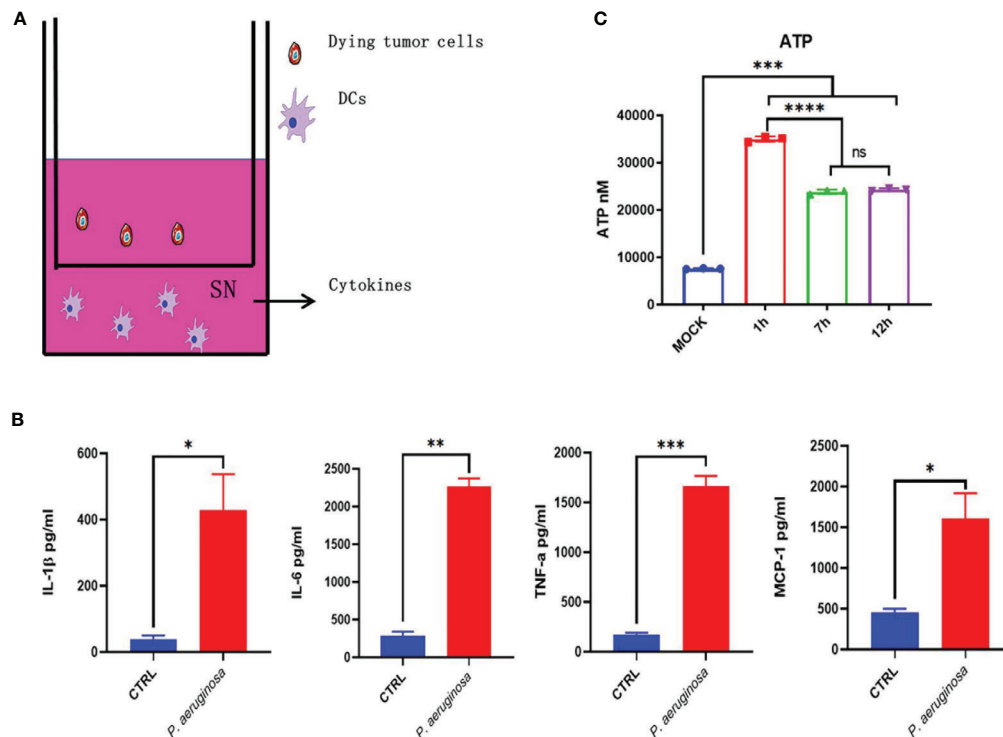


FIGURE 6 | Dying tumor cells trigger DC maturation. **(A)** Schematic diagram of incubation of DC2.4 with dying tumor cells. **(B)** The concentration of cytokines with IL-1 β , IL-6, TNF- α , and MCP-1 in DC supernatant after treatment. **(C)** Histogram analysis of ATP release. One-way ANOVA and paired Student's *t*-test was performed for comparisons. * indicate *P*-values ≤ 0.05 was considered significant, ** indicate *P*-values ≤ 0.01 , and *** indicate *P*-values ≤ 0.001 , **** indicate *P*-value ≤ 0.0001 .

matter HBV virus-like particles- (VLPs) or bacterial outer membrane vesicles (OMVs)-based tumor vaccines, which directly deliver cytokines or tumor associated-antigens (TAAs), can suppress tumor growth and reconstituted the immune-suppressed tumor microenvironment (39–44). At last, our results also indicated oncolytic bacteria *P. aeruginosa* produced durable tumor regression and reshaped the systemic and tumor-infiltrating immune cells profile changes, especially IFN- γ - and IL-2-producing lymphocytes (**Figure 5**). More importantly, we found that NK and/or NKT cells were also remodeled by bacteria treatment. In summary, *P. aeruginosa* is proved to induce TC-1 tumor cell death efficiently as well as educate the host immune system *in vitro* and *in vivo*. Future modified and attenuated *P. aeruginosa* could be used in combination therapy such as surgery, chemotherapy, or radiotherapy for treatment of multiple-malignant tumors. For these tumor tissues that are difficult to remove surgically or have to undergo palliative resection, *P. aeruginosa* has potential to effectively suppress metastasis *via* direct intra-tumor injection (45) or spray-on metastases and lymphatic areas.

As one of the most important specific antigen presentation cells in the immune system, DCs perform robust antigen presentation capability. There are many advantages for DCs acting as APCs: (1) overexpression of MHC-II on the cell surface; (2) upregulated expression of antigen uptake and

specific transport receptors; (3) effective antigen uptake, processing, and migration to T cell niches; (4) activate naïve T cells and promote T cell proliferation and differentiation; (5) enhance antigen presentation efficiency and activate T cell function. Notably, the expression of chemokine profile change is related to DCs differentiation, maturation, and realization of antigen presentation, which is the most important feature of DCs. It has been reported that chemokine CCR1, CCR2, CCR5, CXCR1, and CXCR2 are expressed on immature DCs, while CCR7 and CXCR4 are expressed on mature DCs. Excessive bacterial infection will definitely cause macrophages and/or DC cell death, but a moderate amount of bacterial infection can effectively activate DCs and help antigens presentation. So in **Figure 1** we first evaluated the dose of *P. aeruginosa* *in vivo*, and we choose the lowest infection dose that causes minimal damage. Herein, oncolytic *P. aeruginosa* mediated dying tumor cell co-cultured with DC2.4 enhance cytokines release, representing the maturation of DC cells. The expression of MCP-1, which is a ligand of CCR2, located on DC membranes was upregulated in epithelial cell-derived tumor cells. Mature DCs may be caused by calcium influx and/or PI3K-MAPK single pathway activating, which needs be examined further. After stimulating with E7 peptides, IL-2-producing lymphocytes were increased (**Figure 5B**), which also could promote DC differentiation and regulate the transition of Th0 cells to Th1 cells. IFN- γ -producing

lymphocytes (**Figure 5B**) from CTL, Th1, and/or NK cells can also directly promote tumor cell death in TME. The dying tumor cells can release HMGB1 (**Figures 3G, H**) that matured DCs through TLR-4-dependent manner. After matured DCs migrate to regional lymph nodes, tumor associated-antigens will be presented for stimulating T cell immune response. Overall, in our study, we found that the dying tumor cells significantly activated DC maturation.

CONCLUSION

In this study, we demonstrated *P. aeruginosa* was utilized as an efficient oncolytic bacterial anticancer therapy, which can modulate TME through activating tumor cell PANoptosis and DC maturation. Given the potency and excellent safety at the clinical level, our study further suggested a promising bacteria treatment within the anti-tumor immunotherapy strategies.

DATA AVAILABILITY STATEMENT

The original contributions presented in the study are included in the article/supplementary material. Further inquiries can be directed to the corresponding author.

ETHICS STATEMENT

The animal study was reviewed and approved by The Ethics Committee of Animal Care and Welfare of IMBCAMS and PUMC (Permit Number: SYXK(dian)2010-0007).

REFERENCES

- Elinav E, Garrett WS, Trinchieri G. The cancer microbiome. *Nat Rev Cancer* (2019) 19:371–6. doi: 10.1038/s41568-019-0155-3
- Zitvogel L, Ayyoub M, Routy B, Kroemer G. Microbiome and Anticancer Immunosurveillance. *Cell* (2016) 165:276–87. doi: 10.1016/j.cell.2016.03.001
- Pope JL, Tomkovich S, Yang Y, Jobin C. Microbiota as a mediator of cancer progression and therapy. *Trans Res J Lab Clin Med* (2017) 179:139–54. doi: 10.1016/j.trsl.2016.07.021
- Decker WK, da Silva RF, Sanabria MH, Angelo LS, Guimarães F, Burt BM, et al. Cancer Immunotherapy: Historical Perspective of a Clinical Revolution and Emerging Preclinical Animal Models. *Front Immunol* (2017) 8:829. doi: 10.3389/fimmu.2017.00829
- Chowdhury S, Castro S, Coker C, Hinchliffe TE, Arpaia N. Programmable bacteria induce durable tumor regression and systemic antitumor immunity. *Nat Med* (2019) 25:1057–63. doi: 10.1038/s41591-019-0498-z
- Sommariva M, Le Noci V. The lung microbiota: role in maintaining pulmonary immune homeostasis and its implications in cancer development and therapy. *Cell Mol Life Sci* (2020) 77:2739–49. doi: 10.1007/s00018-020-03452-8
- Carbone C, Piro G, Di Noia V, D'Argento E, Vita E, Ferrera MG, et al. Lung and Gut Microbiota as Potential Hidden Driver of Immunotherapy Efficacy in Lung Cancer. *Mediators Inflamm* (2019) 2019:7652014. doi: 10.1155/2019/7652014
- Liu C, Qi J, Shan B, Gao R, Gao F, Xie H, et al. Pretreatment with cathelicidin-BF ameliorates *Pseudomonas aeruginosa* pneumonia in mice by enhancing

AUTHOR CONTRIBUTIONS

J-LQ and Y-BM conceptualized, designed, and supervised this study and take responsibility for data integrity and accuracy of analysis. J-RH and J-LQ acquired, analyzed, and interpreted the data. S-MJ, XY, and CL provided materials and technical support. J-RH, S-MJ, and J-LQ wrote this manuscript. Y-BM revised and edited the manuscript. All authors contributed to the article and approved the submitted version.

FUNDING

This work was financially supported by the CAMS initiative for innovative medicine (grant number 2016-12M-1-019), the Fundamental Research Funds for the Central Universities of China (grant number 3332019162), and the funds for IMBCAMS PhD Innovation (grant number 2018018001) and the Foundation for Studying Abroad from the China Scholarship Council (grant number 201906210477 and 201808110121).

ACKNOWLEDGMENTS

We thank Professor Bin Shan from the First Affiliated Hospital of Kunming Medical University for supplying the *P. aeruginosa*.

SUPPLEMENTARY MATERIAL

The Supplementary Material for this article can be found online at: <https://www.frontiersin.org/articles/10.3389/fonc.2020.610651/full#supplementary-material>

- NETosis and the autophagy of recruited neutrophils and macrophages. *Int Immunopharmacol* (2018) 65:382–91. doi: 10.1016/j.intimp.2018.10.030
- Tanamoto K, Abe C, Homma JY, Kojima Y. Regions of the lipopolysaccharide of *Pseudomonas aeruginosa* essential for antitumor and interferon-inducing activities. *Eur J Biochem* (1979) 97:623–9. doi: 10.1111/j.1432-1033.1979.tb13152.x
- Zhang Z, Wang LP, Zhao XL, Wang F, Huang L, Wang M, et al. *Pseudomonas aeruginosa* injection enhanced antitumor cytotoxicity of cytokine-induced killer cells derived from cord blood. *Biomed Pharmacother = Biomed Pharmacother* (2014) 68:1057–63. doi: 10.1016/j.biopha.2014.10.024
- Zhang M, Luo F, Zhang Y, Wang L, Lin W, Yang M, et al. *Pseudomonas aeruginosa* mannose-sensitive hemagglutinin promotes T-cell response via toll-like receptor 4-mediated dendritic cells to slow tumor progression in mice. *J Pharmacol Exp Ther* (2014) 349:279–87. doi: 10.1124/jpet.113.212316
- Wei Y, Liu D, Jin X, Gao P, Wang Q, Zhang J, et al. PA-MSHA inhibits the growth of doxorubicin-resistant MCF-7/ADR human breast cancer cells by downregulating Nrf2/p62. *Cancer Med* (2016) 5:3520–31. doi: 10.1002/cam4.938
- Li T, Dong ZR, Guo ZY, Wang CH, Zhi XT, Zhou JW, et al. Mannose-mediated inhibitory effects of PA-MSHA on invasion and metastasis of hepatocellular carcinoma via EGFR/Akt/IkappaBbeta/NF-kappaB pathway. *Liver Int Off J Int Assoc Study Liver* (2015) 35:1416–29. doi: 10.1111/liv.12644
- Xu WH, Liu ZB, Hou YF, Hong Q, Hu DL, Shao ZM. Inhibition of autophagy enhances the cytotoxic effect of PA-MSHA in breast cancer. *BMC Cancer* (2014) 14:273. doi: 10.1186/1471-2407-14-273

15. Cheng X, Wang B, Jin Z, Ma D, Yang W, Zhao R, et al. Pseudomonas aeruginosa-mannose-sensitive hemagglutinin inhibits pancreatic cancer cell proliferation and induces apoptosis via the EGFR pathway and caspase signaling. *Oncotarget* (2016) 7:77916–25. doi: 10.18632/oncotarget.12844
16. Sun L, Wang H, Wang Z, He S, Chen S, Liao D, et al. Mixed lineage kinase domain-like protein mediates necrosis signaling downstream of RIP3 kinase. *Cell* (2012) 148:213–27. doi: 10.1016/j.cell.2011.11.031
17. Ruan ZH, Xu ZX, Zhou XY, Zhang X, Shang L. Implications of Necroptosis for Cardiovascular Diseases. *Curr Med Sci* (2019) 39:513–22. doi: 10.1007/s11596-019-2067-6
18. Kitur K, Parker D, Nieto P, Ahn DS, Cohen TS, Chung S, et al. Toxin-induced necroptosis is a major mechanism of Staphylococcus aureus lung damage. *PLoS Pathog* (2015) 11:e1004820. doi: 10.1371/journal.ppat.1004820
19. Huang Z, Wu SQ, Liang Y, Zhou X, Chen W, Li L, et al. RIP1/RIP3 binding to HSV-1 ICP6 initiates necroptosis to restrict virus propagation in mice. *Cell Host Microbe* (2015) 17:229–42. doi: 10.1016/j.chom.2015.01.002
20. Wang Y, Zhao M, He S, Luo Y, Zhao Y, Cheng J, et al. Necroptosis regulates tumor repopulation after radiotherapy via RIP1/RIP3/MLKL/JNK/IL8 pathway. *J Exp Clin Cancer Res* (2019) 38:461. doi: 10.1186/s13046-019-1423-5
21. Wen SH, Lin LN, Wu HJ, Yu L, Lin L, Zhu LL, et al. TNF- α increases Staphylococcus aureus-induced death of human alveolar epithelial cell line A549 associated with RIP3-mediated necroptosis. *Life Sci* (2018) 195:81–6. doi: 10.1016/j.lfs.2018.01.008
22. Seifert L, Werba G, Tiwari S, Gao LY, Allothman S, Alqunaibit D, et al. The necrosome promotes pancreatic oncogenesis via CXCL1 and Mincle-induced immune suppression. *Nature* (2016) 532:245–9. doi: 10.1038/nature17403
23. Liu ZY, Zheng M, Li YM, Fan XY, Wang JC, Li ZC, et al. RIP3 promotes colitis-associated colorectal cancer by controlling tumor cell proliferation and CXCL1-induced immune suppression. *Theranostics* (2019) 9:3659–73. doi: 10.7150/thno.32126
24. Zhao Q, Yu X, Li M, Liu Y, Han Y, Zhang X, et al. MLKL attenuates colon inflammation and colitis-tumorigenesis via suppression of inflammatory responses. *Cancer Lett* (2019) 459:100–11. doi: 10.1016/j.canlet.2019.05.034
25. Van Hoecke L, Van Lint S. Treatment with mRNA coding for the necroptosis mediator MLKL induces antitumor immunity directed against neo-epitopes. *Nat Commun* (2018) 9:3417. doi: 10.1038/s41467-018-05979-8
26. Van Hoecke L, Saelens X. Therapeutic anti-tumor immunity directed against neo-epitopes by intratumor delivery of mRNA encoding MLKL. *Cell Stress* (2018) 2:279–81. doi: 10.15698/cst2018.10.160
27. Obeid M, Tesniere A, Ghiringhelli F, Fimia GM, Apetoh L, Perfettini JL, et al. Calreticulin exposure dictates the immunogenicity of cancer cell death. *Nat Med* (2007) 13:54–61. doi: 10.1038/nm1523
28. Kawano M, Tanaka K, Itonaga I, Iwasaki T, Miyazaki M, Ikeda S, et al. Dendritic cells combined with doxorubicin induces immunogenic cell death and exhibits antitumor effects for osteosarcoma. *Oncol Lett* (2016) 11:2169–75. doi: 10.3892/ol.2016.4175
29. Yang H, Ma Y, Chen G, Zhou H, Yamazaki T, Klein C, et al. Contribution of RIP3 and MLKL to immunogenic cell death signaling in cancer chemotherapy. *Oncoimmunology* (2016) 5:e1149673. doi: 10.1080/2162402x.2016.1149673
30. Apetoh L, Ghiringhelli F, Tesniere A, Obeid M, Ortiz C, Criollo A, et al. Toll-like receptor 4-dependent contribution of the immune system to anticancer chemotherapy and radiotherapy. *Nat Med* (2007) 13:1050–9. doi: 10.1038/nm1622
31. Azzouz D, Khan MA, Sweezey N, Palaniyar N. Two-in-one: UV radiation simultaneously induces apoptosis and NETosis. *Cell Death Discovery* (2018) 4:51. doi: 10.1038/s41420-018-0048-3
32. Chen J, Danino T, Prindle A, Skalak M, Selimkhanov J, Allen K, et al. Modulation of Salmonella Tumor-Colonization and Intratumoral Anti-angiogenesis by Triptolide and Its Mechanism. *Theranostics* (2017) 7:2250–60. doi: 10.7150/thno.18816
33. Din MO, Morgan MJ, Lee DG, Kim WJ, Yoon JH, et al. Synchronized cycles of bacterial lysis for in vivo delivery. *Nature* (2016) 536:81–5. doi: 10.1038/nature18930
34. Koo GB, Wang J, Schilling R, Horn S, Harris PA, Bertin J, et al. Methylation-dependent loss of RIP3 expression in cancer represses programmed necrosis in response to chemotherapeutics. *Cell Res* (2015) 25:707–25. doi: 10.1038/cr.2015.56
35. Geserick P, Yu W, Shen L, Huang T. Absence of RIPK3 predicts necroptosis resistance in malignant melanoma. *Cell Death Dis* (2015) 6:e1884. doi: 10.1038/cddis.2015.240
36. Sun W, Yu W, Shen L, Huang T. MLKL is a potential prognostic marker in gastric cancer. *Oncol Lett* (2019) 18:3830–6. doi: 10.3892/ol.2019.10687
37. He L, Peng K, Liu Y, Xiong J, Zhu FF. Low expression of mixed lineage kinase domain-like protein is associated with poor prognosis in ovarian cancer patients. *OncoTargets Ther* (2013) 6:1539–43. doi: 10.2147/ott.s52805
38. Li X, Sun P, Xie H, Huang W, Qi J, Ma J. Association of Mixed Lineage Kinase Domain-Like Protein Expression With Prognosis in Patients With Colon Cancer. *Technol Cancer Res Treat* (2017) 16:428–34. doi: 10.1177/1533034616655909
39. Shu C, Shu C, Hua L, Zhao Y, Xie H, Qi J, et al. Virus-Like Particles Presenting the FGF-2 Protein or Identified Antigenic Peptides Promoted Antitumor Immune Responses in Mice. *Int J Nanomed* (2020) 15:1983–96. doi: 10.2147/ijn.s237182
40. Huang W, Liu H, Chu X, Sun P, Huang W, Liu C, et al. Modified bacterial outer membrane vesicles induce autoantibodies for tumor therapy. *Acta Biomater* (2020) 100:316–25. doi: 10.1016/j.actbio.2020.03.030
41. Feng X, Li Y, Huang W, Feng X, Sun P, Yao Y, et al. Recombinant virus-like particles presenting IL-33 successfully modify the tumor microenvironment and facilitate antitumor immunity in a model of breast cancer. *Acta Biomater* (2019) 100:316–25. doi: 10.1016/j.actbio.2019.09.024
42. Chu X, Li Y, Long Q, Xia Y, Yao Y, Sun W, et al. Combined immunization against TGF- β 1 enhances HPV16 E7-specific vaccine-elicited antitumor immunity in mice with grafted TC-1 tumours. *Artif Cells Nanomed Biotechnol* (2018) 46:1199–209. doi: 10.1080/21691401.2018.1482306
43. Chu X, Huang W, Li K, Yao Y, Yang X, Bai H, et al. Chimeric HBcAg virus-like particles presenting a HPV 16 E7 epitope significantly suppressed tumor progression through preventive or therapeutic immunization in a TC-1-grafted mouse model. *Int J Nanomed* (2016) 11:2417–29. doi: 10.2147/ijn.s102467
44. Wang S, Zhang L, Janku F, Collins A, Bai RY, Staedtke V, et al. Engineered outer membrane vesicle is potent to elicit HPV16E7-specific cellular immunity in a mouse model of TC-1 graft tumor. *Int J Nanomed* (2017) 12:6813–25. doi: 10.2147/ijn.s143264
45. Roberts NJ, Khan MA, Sweezey N, Palaniyar N. Intratumoral injection of Clostridium novyi-NT spores induces antitumor responses. (2018) 4(1):51. doi: 10.1038/s41420-018-0048-3

Conflict of Interest: The authors declare that the research was conducted in the absence of any commercial or financial relationships that could be construed as a potential conflict of interest.

Copyright © 2021 Qi, He, Jin, Yang, Bai, Liu and Ma. This is an open-access article distributed under the terms of the Creative Commons Attribution License (CC BY). The use, distribution or reproduction in other forums is permitted, provided the original author(s) and the copyright owner(s) are credited and that the original publication in this journal is cited, in accordance with accepted academic practice. No use, distribution or reproduction is permitted which does not comply with these terms.



Pictilisib Enhances the Antitumor Effect of Doxorubicin and Prevents Tumor-Mediated Bone Destruction by Blockade of PI3K/AKT Pathway

Chao Liang^{1†}, Xijiao Yu^{2†}, Naping Xiong^{3†}, Zhichang Zhang¹, Zhenyu Sun^{1*} and Yang Dong^{1*}

¹ Department of Orthopedics, Shanghai Jiao Tong University Affiliated Sixth People's Hospital, Shanghai, China, ² Department of Endodontics, Jinan Stomatological Hospital, Jinan, China, ³ School of Life Science and Technology, ShanghaiTech University, Shanghai, China

OPEN ACCESS

Edited by:

Niels Weinhold,
Heidelberg University, Germany

Reviewed by:

Azhar Ali,
National University of Singapore,
Singapore
Zhifang Zhang,
Beckman Research Institute,
City of Hope, United States

*Correspondence:

Yang Dong
dongyang6405@163.com
Zhenyu Sun
AaronSun616@163.com

[†]These authors have contributed
equally to this work

Specialty section:

This article was submitted to
Cancer Molecular Targets and
Therapeutics,
a section of the journal
Frontiers in Oncology

Received: 08 October 2020

Accepted: 16 December 2020

Published: 15 February 2021

Citation:

Liang C, Yu X, Xiong N, Zhang Z, Sun Z
and Dong Y (2021) Pictilisib Enhances
the Antitumor Effect of Doxorubicin
and Prevents Tumor-Mediated Bone
Destruction by Blockade of
PI3K/AKT Pathway.
Front. Oncol. 10:615146.
doi: 10.3389/fonc.2020.615146

Despite advances in neoadjuvant chemotherapy, outcomes for patients with osteosarcoma resistant to first-line chemotherapy have been dismal for decades. There is thus an urgent need to develop novel targeted drugs to effectively treat refractory osteosarcoma. Dysregulation in the PI3K/AKT pathway has been observed during the development of osteosarcoma. Herein, we first evaluated p-AKT (Ser473) expression levels in osteosarcoma tissue using high-throughput tissue microarrays. Then, we demonstrated the role of pictilisib, a novel potent PI3K inhibitor, in osteosarcoma and related osteolysis. Functional studies of pictilisib in osteosarcoma cell lines and bone marrow-derived macrophages were performed *in vitro*. Patient-derived xenografts and orthotopic mouse models were used to assess the effects of pictilisib *in vivo*. The results showed that positive p-AKT expression levels after neoadjuvant chemotherapy were significantly associated with tumor cell necrosis rate. Pictilisib effectively inhibited the proliferation of osteosarcoma through G0/G1-S phase cell cycle arrest, and enhanced the sensitivity of osteosarcoma to doxorubicin, although it failed to induce cell apoptosis alone. In addition, pictilisib inhibited differentiation of osteoclasts and bone resorption *in vitro* and tumor-related osteolysis *in vivo* via inhibition of the PI3K/AKT/GSK3 β and NF- κ B pathways. Pictilisib combined with conventional chemotherapy drugs represents a potential treatment strategy to suppress tumor growth and bone destruction in p-AKT-positive patients.

Keywords: pictilisib, osteosarcoma, osteoclasts, targeted therapy, PI3K inhibitor

INTRODUCTION

Osteosarcoma (OS) is the most frequent primary malignant bone tumor and occurs mainly in the young (1, 2). Currently, the standard therapy for newly diagnosed OS consists of four to six cycles of neoadjuvant chemotherapy with cisplatin, doxorubicin (DOX), methotrexate, and ifosfamide after biopsy. With this combination of drugs, the 5-year survival rate in non-metastatic OS patients has increased to 50–70%. However, the survival rate has not improved since the mid-1980s owing to a

lack of targeted drugs (3, 4). Accumulating evidence indicates that activation of the PI3K/AKT pathway has a critical oncogenic role in the initiation and progression of OS (5). Enrichment of mutated genes in the PI3K/AKT pathway in the early and late stages of OS has been demonstrated by next-generation sequencing (6); alterations of genes in this pathway were detected in 24% of OS patients (7). Activation of the PI3K/AKT pathway has also been observed in the majority of OS cell lines by detecting kinome and mRNA expression profiling (8). Moreover, research suggests that the PI3K/AKT pathway contributes to multiple pathological processes of OS, including tumorigenesis, proliferation, invasion, cell cycle progression, lung metastasis, and chemoresistance (5). Ji et al. found that the expression of p-AKT (Ser473) was negatively correlated with tumor cell necrosis rate (TCNR) after chemotherapy (9). Thus, the PI3K/AKT signaling pathway is a potential source of therapeutic targets.

OS is an osteoblastic tumor, but many studies have shown that osteoclasts have a vital role in its progression (10–12). OS tumor cells originating from osteoblasts produce receptor activator of nuclear factor kappa B ligand (RANKL), which regulates the differentiation of bone marrow-derived macrophages (BMMs) into bone-resorbing osteoclasts expressing activator of nuclear factor kappa B (RANK). OS-activated osteoclasts continuously destroy mineralized bone matrix, resulting in the release of growth factors including transforming growth factor- β (TGF- β), insulin like growth factor-1 (IGF-1), fibroblast growth factor (FGF), and bone morphogenetic protein (BMP), and providing a niche microenvironment for OS cells (11). Based on evidence from bone metastasis, a “vicious cycle” involving osteoclasts, osteoblasts, and sarcoma cells has been hypothesized to occur during the development of OS. In a recent study by Francois et al., overexpression of osteoprotegerin, a soluble decoy receptor, in a mouse model of OS did not directly affect proliferation of tumor cells but indirectly decreased tumor growth by blocking the vicious cycle of tumor cell proliferation and bone resorption (13). The formation of osteoclasts is mainly regulated by RANKL and macrophage-colony stimulating factor (M-CSF), both of which initiate the activation of various downstream pathways including the PI3K/AKT and NF- κ B signaling pathways. Thus, osteoclasts could be exploited as therapeutic targets (14).

With a greater understanding of the pathogenesis, progression, and microenvironment of OS at a molecular level, targeting the PI3K/AKT pathway may be a promising therapy for OS. The most direct approach to blocking the PI3K/AKT pathway is to target PI3K itself. The catalytic PI3K family consists of three classes (I–III), of which class I PI3Ks are the most relevant to cancers owing to their role in regulating cell proliferation and tumorigenesis (15). Inactivated PI3K cannot convert its substrate phosphatidylinositol 4,5-bisphosphate into phosphatidylinositol 3,4,5-triphosphate. Thus, the downstream effector AKT is not phosphorylated. Pictilisib, also known as GDC-0941, inhibits all four class I PI3K p110 isoforms (16, 17) and has been shown to have significant efficacy in preclinical breast cancer and advanced solid tumors, with tolerable side effects (18–20).

In the present study, we investigated the ability of pictilisib to decrease proliferation and related osteolysis in OS cell lines *in vitro* and in two mouse models *in vivo*.

MATERIALS AND METHODS

Human Osteosarcoma Tissue Microarray

A total of 60 tumor samples from 31 individual OS patients at Shanghai Sixth People's Hospital between 2014 and 2018 were used to construct a high-throughput tissue microarray. These tissue blocks consisted of 29 biopsy samples, 31 resection samples obtained after chemotherapy, and five normal bone marrow tissue samples from patients with OS. Related clinical information was collected for all participants, including sex, age, location, Enneking stage, and chemotherapy response. Five-millimeter paraffin-embedded tissue section slides for tissue microarray were baked for 2 h at 60°C, deparaffinized in xylene, and then transferred through graded ethanol for rehydration. After heat-induced epitope retrieval, the endogenous peroxidase was quenched with 3% hydrogen peroxide. Proteins were incubated with rabbit anti-human p-AKT (Ser473) antibody (#4060, 1:100, Cell Signaling Technology, USA) at 4°C overnight. We next evaluated the expression of p-AKT (Ser473) using immunohistochemistry (IHC). The immunostaining density of p-AKT was classified as follows: 0, no staining; 1+, weak staining; 2+, moderate staining; and 3+, intense staining. No specific staining with p-AKT was observed in ordinary bone tissue. The project was approved by the ethics committee of Shanghai Sixth People's Hospital.

Drugs, Cell Lines, and Culture Conditions

Pictilisib ($C_{23}H_{27}N_7O_3S_2$; MW, 513.64; purity, $\geq 99\%$) Doxorubicin hydrochloride ($C_{27}H_{29}NO_{11} \cdot HCl$; MW, 579.99; purity, 99.37%), and dimethyl sulfoxide (DMSO) were purchased from TargetMol (Shanghai, China) and stored at -20°C . Four OS cell lines (MG-63, U2OS, Saos2, and 143B) were cultured in Dulbecco's modified Eagle's medium (DMEM) supplemented with 10% fetal bovine serum (FBS) and 1% penicillin/streptomycin. Primary BMMs were isolated from C57BL/6 mice and cultured in α -modified Eagle's medium supplemented with 1% penicillin/streptomycin, 10% FBS, and 30 ng/ml M-CSF at 37°C and 5% CO_2 (21). Recombinant murine M-CSF and RANKL were obtained from R&D Systems (Minneapolis, MN, USA).

Cell Viability Assay

The cell viability assay was performed as previously described (22). BMMs and OS cells were seeded in 96-well plates in DMEM (1×10^3 cells/well) in triplicate. Half-maximal inhibitory concentration (IC_{50}) values were determined using a Cell Counting Kit-8 (Dojindo, Japan) on OS cell lines after treatment with escalating doses of pictilisib (from 0 to 10 μM) at time points from 24 to 72 h. Absorbance was measured at 450 nm on an ELx800 microplate reader (Bio-Tek Instruments, USA). The IC_{50} of pictilisib was calculated using the Prism v.5.0c software (GraphPad, San Diego, CA).

Cell Cycle Analysis

Tumor cells were seeded in six-well dishes and incubated with a range of concentrations of pictilisib (from 0 to 5 μM) for 24 h. Floating and adherent cells were collected by trypsinization and washed with phosphate-buffered saline (PBS). Cells were incubated in 70% ethanol at -4°C overnight, treated with RNase A, then stained with propidium iodide (PI). Cell cycle distribution was determined using flow cytometry (CytoFLEX, Beckman Coulter, USA) and DNA cell cycle analysis software (ModFit LT, USA).

Detection of Apoptotic Cells

Apoptosis of MG-63 and U2OS cells treated with pictilisib and/or DOX at various concentrations was assessed using a FITC Annexin V Apoptosis Detection Kit I (Becton Dickinson, USA) according to the manufacturer's instructions. Treated cells were resuspended at a density of 1×10^6 cells/ml in 100 μl binding buffer, then incubated with 5 μl PI and 5 μl Annexin V-FITC for 15 min at room temperature. Detection of apoptotic cells was performed using a flow cytometer (CytoFLEX, Beckman Coulter, USA).

Osteoclast Differentiation and Resorptive Function Assay *In Vitro*

To assess osteoclast differentiation, BMMs were seeded at a density of 1×10^4 cells/well in 96-well plates, stimulated with 30 ng/ml M-CSF and 50 ng/ml RANKL, and treated with the appropriate concentrations of pictilisib for approximately 7 days. Fresh media containing these two factors were changed every other day until multinucleated osteoclasts had formed in the RANKL-only control wells. After fixed with 4% paraformaldehyde for 30 min, cells were stained using a tartrate-resistant acid phosphatase (TRAP) kit. Digital images were captured with an optical light microscope (Olympus, Tokyo, Japan). The ImageJ software (NIH, Bethesda, MD, USA) was used to analyze the numbers and area of TRAP-positive osteoclasts with at least three nuclei.

For the bone resorption assay, BMMs were seeded in six-well plates and cultured with 30 ng/ml M-CSF and 50 ng/ml RANKL until small osteoclasts were observed. Then, the cells were reseeded in phosphate-coated Osteo Assay Stripwell Plates (Corning, NY, USA) in triplicate. Cells were incubated in media containing various concentrations of pictilisib (0, 0.5, 1, 2 μM) together with 30 ng/ml M-CSF and 50 ng/ml RANKL until day 7, when mature osteoclasts were observed. Osteoclasts were removed using 10% sodium hypochlorite solution. Subsequently, resorption pits were imaged under a light microscope (Leica, Wetzlar, Germany). The resorption pit area was analyzed with ImageJ software (NIH, Bethesda, MD, USA).

Western Blotting

Treated cells were lysed with radio-immunoprecipitation assay and a phosphatase inhibitor (Sigma, MO, USA). Total protein extracts were separated by sodium dodecyl polyacrylamide gel electrophoresis and then transferred to polyvinylidene fluoride membranes for western blotting. The membranes were blocked

with 5% skimmed milk for 1 h at room temperature, incubated with primary antibody (1:1,000) overnight at 4°C , and then with secondary antibodies (1:5,000) for 1 h. Finally, membranes were developed using an enhanced chemiluminescence substrate. Detailed information about antibodies is available in the supplemental files.

Establishment of Patient-Derived Xenograft Model

Four-week-old female BALB/c nude mice were purchased from Shanghai Laboratory Animal Research Center (Shanghai, China). Three fresh surgical specimens with p-AKT-positive staining were obtained from different individuals with OS and cut into 1–3 mm³ fragments under sterile conditions. Subsequently, they were implanted subcutaneously into three nude mice within 2 h. Only one tumor specimen, from a 15 year-old girl with chemotherapy-resistant OS, was successfully used to generate an experimental patient-derived xenograft (PDX) model. When the subcutaneously implanted tumors grew to approximately 1,000 mm³, they were dissected and passed to other mice in preparation for subsequent studies. When tumors grew to approximately 100 mm³, they were randomly separated into four groups ($n = 5$) and treated with PBS [intragastric (i.g.) administration, every other day]; 50 mg/kg pictilisib (i.g. administration, every other day); 2 mg/kg DOX [2-day continuous intraperitoneal (i.p.) injection per week]; or 50 mg/kg pictilisib and 2 mg/kg DOX (i.g. administration, every other day and 2-day continuous i.p. injection per week). Tumor volumes were calculated every 7 days by the following standard formula: $(\text{length} \times \text{width}^2)/2$. After 28 days of treatment, all the mice were sacrificed, and the tumors were harvested and weighed. The animal study was approved by the Animal Ethics Committee of Shanghai Sixth People's Hospital (Shanghai, China).

Cell-Derived Orthotopic Mouse Model

An orthotopic mouse model was established using 143B-luc to evaluate the effects of pictilisib on tumor progression and bone absorption *in vivo*. Initially, 1×10^6 cells were suspended in 100 μl BD Matrigel TM Matrix (Becton, USA) and subcutaneously injected into the back of one mouse. Three weeks later, the tumor sample was cut into $1 \times 1 \times 1$ mm³ pieces. The left posterior limb of each nude mouse, anesthetized by chloral hydrate, was cut in the proximal part of the tibia, and one tumor fragment was inserted on the surface of tibia. After 2 weeks, the mice were randomly divided into four groups ($n = 5$) and treated as follows: 143B with PBS (i.g. administration), 143B with pictilisib (50 mg/kg, i.g. administration, every other day), 143B with pictilisib (100 mg/kg, i.g. administration, every other day), or 143B with pictilisib (50 mg/kg, i.g. administration, every other day) and DOX (2 mg/kg, 2-day continuous i.p. injection per week). Body weight of mice was measured at 1-week intervals for 4 weeks. *In vivo* bioluminescence imaging was performed to observe the progression of tumors at days 0, 14, and 28. After sacrifice, the left posterior limb of each nude mouse in each group was weighed.

Micro-Scanning and Radiological Analyses

Destruction of fixed tibiae mediated by tumors was analyzed using a high-resolution micro-CT scanner (μ CT-100; SCANCO, Bröttisellen, Switzerland). Parameters were set to an isometric resolution of 1–10 mm and X-ray energy settings of 70 kV and 200 μ A. After reconstruction, the bone volume to total volume (BV/TV) ratio was measured in the region of interest.

Immunohistochemistry, Ki67, and Hematoxylin and Eosin Staining

Fresh tumor samples and primary organs were fixed in 10% formalin and embedded in paraffin before sectioning and staining. Tumor specimens were stained with anti-human p-AKT (Ser473) antibody (#4060, 1:100, Cell Signaling Technology, USA) and anti-human cleaved caspase-3 (Asp175) (#9661, 1:400, Cell Signaling Technology, USA) antibody. Ki67 staining was performed to evaluate the proliferation of tumors with anti-ki-67 antibody (1 μ g/ml, Abcam, Cambridge, MA). H&E staining was performed to assess the toxic effects of pictilisib on the heart, lung, liver, and kidney.

Statistical Analysis

Statistical analysis was performed using SPSS version 18.0 software (IBM Corporation, Chicago). Data are shown as the mean \pm SD of three independent experiments. Differences between experimental and control groups were calculated by two-tailed student's t-tests. Correlations between p-AKT (Ser473) and expression levels and pathological features of patients with OS were analyzed by both χ^2 -test and student's t-test. $P < 0.05$ was regarded as significant for all statistical analyses.

RESULTS

p-AKT Is Partly Positive in Human Osteosarcoma Tissues and Negatively Correlated With Tumor Cell Necrosis Rate After Chemotherapy

Tissue microarray analysis with 60 OS samples and five normal bone marrow samples was conducted to assess the expression levels of p-AKT (Ser473) using IHC. Clinical information of OS patients is shown in **Table 1**. Positive staining for p-AKT proteins manifested as purple particles in the cytoplasm, ranging from no staining (0, 28/60, 46.7%), weak staining (1+, 17/60, 28.3%), and moderate staining (2+, 10/60, 16.7%) to intense staining (3+, 5/60, 8.3%). Normal bone marrow tissue was used as a negative control group with no staining (**Figure 1A**). Subsequently, the correlations between p-AKT (Ser473) expression levels in biopsy samples and specimens after chemotherapy were analyzed. The p-AKT-positive rate in biopsy samples was significantly higher than that in specimens after chemotherapy (75.9 vs 32.2%, $P = 0.002$) (**Figure 1B**). Our results also confirmed that p-AKT (Ser473) had a significant correlation with TCNR after chemotherapy ($\chi^2 = 11.487$, $P = 0.002$) (**Figure 1D**), that is, positive p-AKT after chemotherapy was considered to be a sign of poor response to chemotherapy (TCNR <90%). By

TABLE 1 | Demographic data for patients with OS.

Variable	Number
Average age at diagnosis (years)	13.56 \pm 3.54
Gender	
Male	17
Female	14
Location	
Upper limb	11
Lower limb	18
Pelvis	2
Enneking stage	
II A	2
II B	25
III	4
Chemotherapy response	
Good response ^a	22
Poor response ^b	9

^aGood response: TCNR \geq 90%; ^bPoor response: TCNR < 90%.

contrast, there was no significant difference between expression levels of p-AKT in biopsy samples and TCNR ($\chi^2 = 0.758$, $P = 0.954$) (**Figure 1C**) (**Table 2**).

Inhibitory Effect of Pictilisib Against Osteosarcoma Depends on the Induction of Cell Cycle Arrest, and Pictilisib Enhances the Sensitivity to Chemotherapy

To determine the effects of pictilisib (**Figure 2A**) on cultured OS cells, a CCK8 assay was performed on a panel of OS cell lines (MG-63, U2OS, Saos2, and 143B). The results showed that pictilisib dose-dependently inhibited OS cell proliferation for 24, 48, and 72 h (**Figure 2B**). At least 48 h was required for pictilisib to exert a significant inhibitory effect on OS cells, and MG-63 cells showed a strong response with the lowest IC₅₀. Among the four OS cell lines, 143B was the least sensitive to pictilisib (**Figure 2C**). Next, cell cycle and apoptosis assays were performed to investigate how pictilisib inhibited proliferation of OS cells. We found that the majority of tumor cells were arrested in G0/G1-S phase by stepwise concentrations of pictilisib, in contrast to untreated cells (**Figures 2D, E**). The apoptosis assays revealed no significant difference over a range of concentrations of pictilisib (0–2 μ M) (**Supplemental Figures 1A, B**). Thus, pictilisib exerted its inhibitory effect against OS *via* cell cycle arrest rather than induction of apoptosis. Considering the correlation between p-AKT expression levels and chemotherapy resistance in OS, we investigated whether pictilisib sensitized OS cells to chemotherapy. The results of the CCK8 assays indicated that pictilisib at a low concentration (1 μ M) failed to affect the viability of more than 90% of OS cells. However, this low concentration increased the rate of inhibition of OS cell proliferation by DOX (0.5 μ g/ml) by approximately 20% (**Figure 3A**). In addition, flow cytometry showed that pictilisib alone had no effect on apoptosis of OS cells on concentrations ranging from 0 to 2 μ M (**Supplemental Figure 1A**). However, we found 1 μ M pictilisib increased DOX-mediated apoptosis by at least ten percentage points although it did not induce apoptosis of tumor cells over 24 h alone (**Figures 3B, C**).

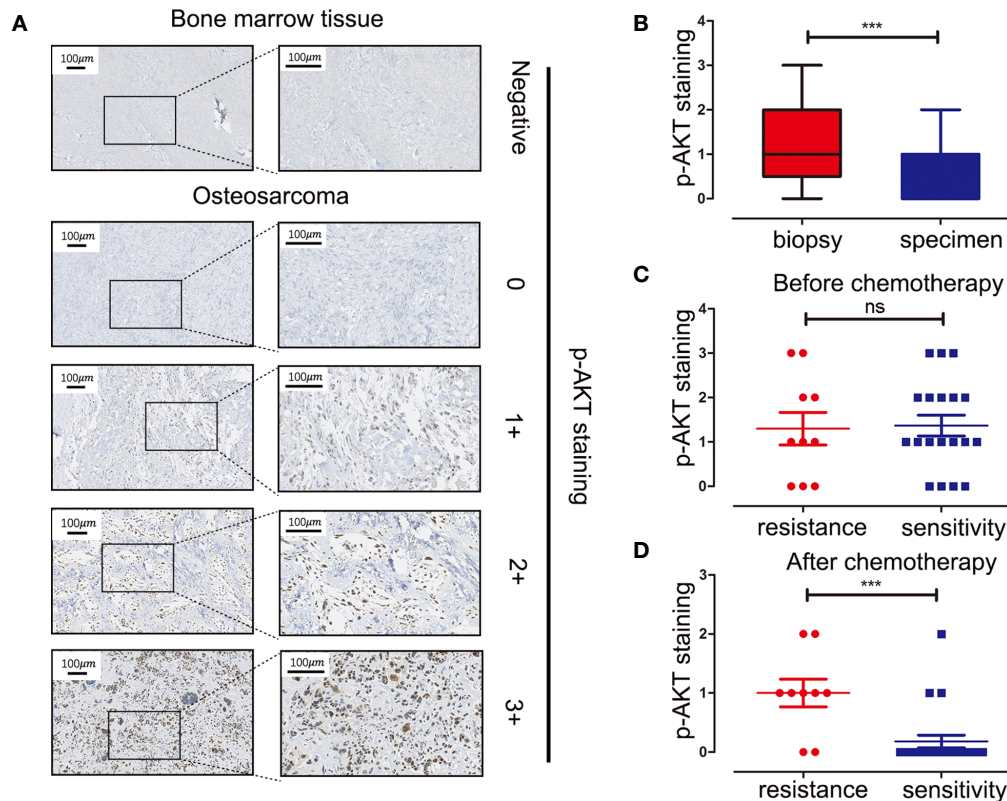


TABLE 2 | Correlations between p-AKT (Ser473) expression level and chemotherapy response.

Cases			p-AKT (Ser473) staining intensity score				χ^2 -value	P-value
			0	1+	2+	3+		
Stage	Biopsy ^a	29	7	10	7	5	16.368	0.002
	Specimen ^a	31	21	7	3	0		
Biopsy	Sensitivity ^b	19	4	7	5	3	0.758	0.954
	Resistance ^b	10	3	3	2	2		
Specimen	Sensitivity	22	19	2	1	0	11.487	0.002
	Resistance	9	2	5	2	0		

^aBiopsy: OS tissue before chemotherapy; ^aSpecimen: OS tissue after chemotherapy; ^bSensitivity: good response or TCNR $\geq 90\%$; ^bResistance: poor response or TCNR $< 90\%$.

Pictilisib Impairs Receptor Activator Of Nuclear Factor Kappa B Ligand-Induced Osteoclast Differentiation and Osteoclastic Bone Resorption *In Vitro*

To examine the effects of pictilisib on osteoclast differentiation, BMMs were induced by 30 ng/ml M-CSF and 50 ng/ml RANKL with various doses of pictilisib (0, 0.5, 1, and 2 μ M). The cellular morphology of BMMs was captured under a microscope after TRAP staining on day 7. The control group formed typical well-

spread “pancake-shaped” multinucleated osteoclasts with positive TRAP staining. The inhibitory effect of pictilisib was enhanced with increasing concentration. The progression from RANKL-dependent BMMs to mature osteoclasts was totally blocked by 2 μ M pictilisib (**Figure 4A**). TRAP-positive cell numbers and areas of osteoclasts per well were calculated and analyzed (**Figure 4B**). Next, a phosphate-coated bone plate was prepared to examine osteoclastic bone resorption. In the control groups without pictilisib, osteoclasts extensively eroded the calcium coating of

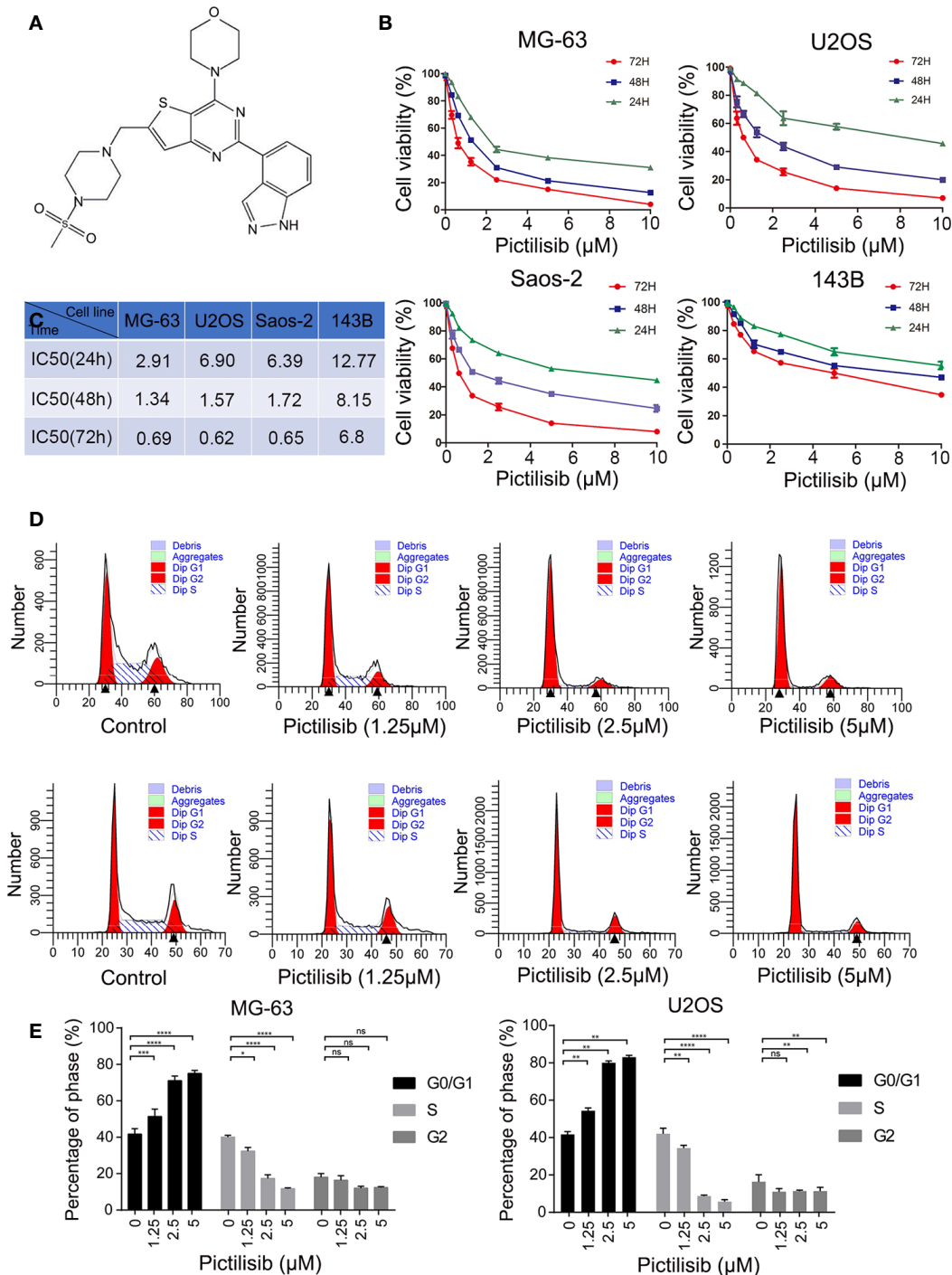


FIGURE 2 | Pictilisib inhibited cell proliferation by inducing cell cycle arrest. **(A)** Chemical structure of pictilisib. **(B, C)** OS cell lines were treated with pictilisib at the indicated concentrations for 24, 48, and 72 h. IC₅₀ values for the four OS cell lines were determined by CCK8 assays and are reported in the table. **(D, E)** Cells treated with pictilisib at the indicated concentrations for 24 h were stained with PI for flow cytometric analysis and analyzed by ModFit. Percentages of G0/G1, S, and G2 phase cells after treatment with the indicated concentrations of pictilisib. **P* < 0.05, ***P* < 0.01, ****P* < 0.001, *****P* < 0.0001, ns, no significance.

the bone-mimicking plates. However, the bone absorption function was attenuated by pictilisib in a dose-dependent manner. With 2 μM pictilisib, bone resorption was almost completely abolished in osteoclasts (**Figures 4C, D**). Overall, the

results demonstrated that pictilisib could inhibit RANKL-induced osteoclast differentiation and osteoclastic bone resorption *in vitro*. In addition, a CCK-8 assay was performed to evaluate the cell viability of BMMs cultured with pictilisib at a range of

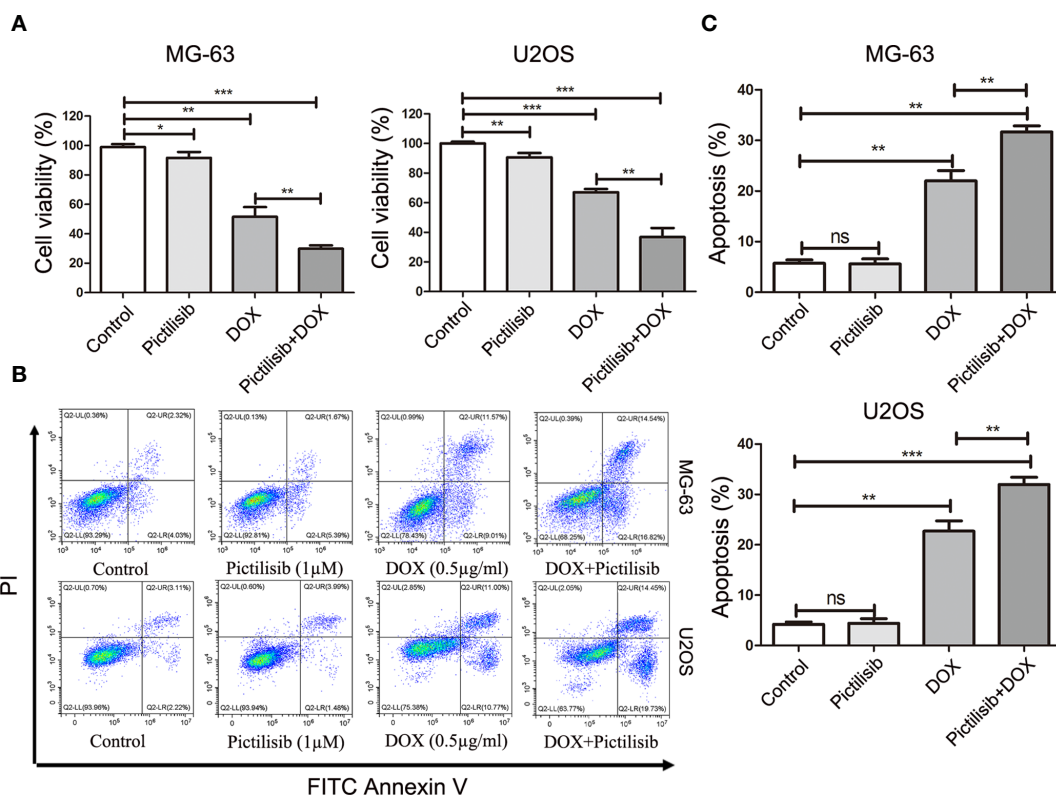


FIGURE 3 | Low-dose pictilisib failed to induce cell apoptosis but enhanced sensitivity of OS cells to DOX. **(A)** Cells were treated with 1 μ M pictilisib with or without 0.5 μ g/ml DOX, and CCK8 assays were performed to evaluate cell viability. **(B, C)** Percentages of apoptotic cells treated with 1 μ M pictilisib with or without 0.5 μ g/ml DOX for 24 h were detected by using a flow cytometry. * $P < 0.05$, ** $P < 0.01$, *** $P < 0.001$, ns: no significance.

concentrations. Pictilisib exhibited no cytotoxicity to BMMs at concentrations below 10 μ M for 48, 72, and 96 h (**Figure 4E**).

Pictilisib Inhibits AKT Phosphorylation and Its Downstream Effectors

Initially, pictilisib was designed to suppress tumor proliferation and overcome resistance to antiestrogen therapy in breast cancer *via* inhibition of all four class I PI3K isoforms (20). The most important downstream effector of PI3K activation is thought to be AKT. Thus, we detected p-AKT expression levels in OS cell lines after treatment with pictilisib. The western blotting results indicated that AKT activation, as evidenced by a reduction in phosphorylation at Ser-473, was inhibited by pictilisib in a dose- and time-dependent manner. Next, we analyzed the expression of downstream genes related to the cell cycle and apoptosis. cyclin D1, cyclin E, and CDK4 were significantly down-regulated in the pictilisib groups compared with the negative control groups (**Figures 5A, B**). These genes encode key proteins involved in the G0/G1-S transition of the cell cycle. There were no significant changes in the expression of cleaved poly(ADP ribose) polymerase (PARP) and cleaved caspase-3 over a range of concentrations of pictilisib (**Supplemental Figure 1C**), but the addition of pictilisib enhanced their expression (**Figures 5C, D**). Together, these results demonstrate that pictilisib inhibited the

proliferation of OS cell lines *via* inducing cell cycle arrest at G0/G1 phase and increased their sensitivity to DOX.

The AKT/GSK3 β pathway is known to be associated with regulation of NFATc1 during osteoclast differentiation (23). Our results showed that pictilisib effectively inhibited the expression of p-AKT (Ser473) and p-GSK3 β (Ser9) compared with their total protein contents in BMMs (**Figures 6A, C**). To confirm that the downstream NF- κ B pathway was also inhibited by pictilisib, the expression levels of p65 and p-p65 (Ser563) were measured by western blotting. In control groups, we observed that NF- κ B p-65 (Ser563) was rapidly phosphorylated by RANKL stimulation (**Figures 6A, C**). Therefore, the target genes NFATc1 and c-fos were upregulated; these genes encode key transcription factors required for osteoclast differentiation. However, this process was attenuated by the addition of pictilisib (**Figures 6B, D**). Thus, the inhibitory effect of pictilisib on osteoclast differentiation may involve modulation of the AKT/GSK3 β and NF- κ B signaling pathways.

Pictilisib Enhances the Sensitivity of Osteosarcoma to Doxorubicin in Patient-Derived Xenograft Models

In recent years, PDX technology has offered more accurate and reliable preclinical models of cancer. Tumor fragments

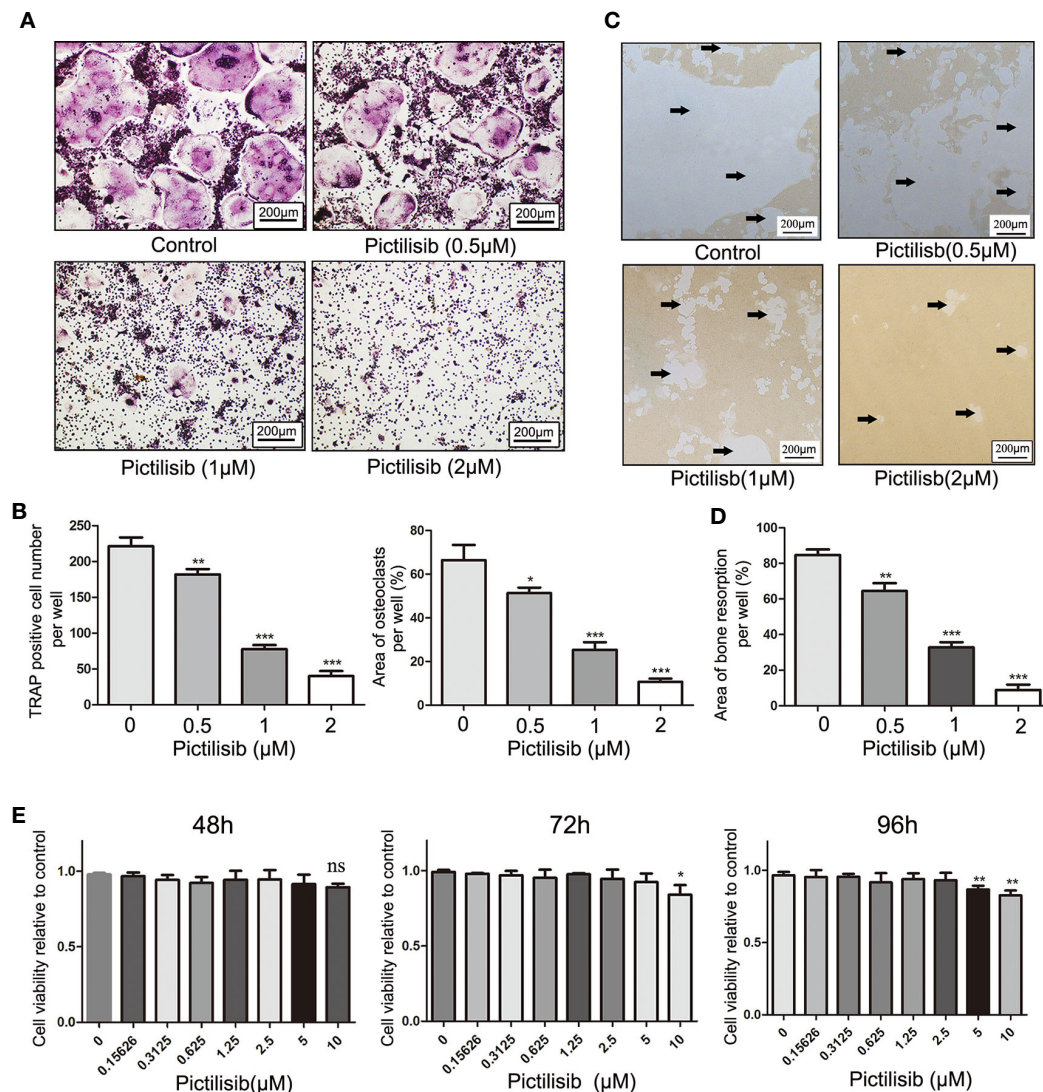


FIGURE 4 | Pictilisib inhibited formation and bone absorption of RANKL-induced osteoclasts *in vitro*. **(A)** Representative images of TRAP-stained multinucleated osteoclasts following treatment with a range of concentrations of pictilisib, 30 ng/ml M-CSF, and 50 ng/ml RANKL for 6 days. **(B)** The number and area of TRAP-positive osteoclasts with at least three nuclei were measured. **(C, D)** BMMs were seeded on a phosphate-coated bone plate in the presence of pictilisib at various concentrations, 30 ng/ml M-CSF, and 50 ng/ml RANKL. At day 7, the resorption pit area was analyzed with ImageJ. **(E)** The proliferation and viability of BMMs treated with a range of concentrations of pictilisib were measured by CCK-8 assay at 48, 72, and 96 h. * $P < 0.05$, ** $P < 0.01$, *** $P < 0.001$, ns: no significance.

from established models were subcutaneously implanted in the dorsal flanks of BALB/c nude mice. A low dose of pictilisib (50 mg/kg) alone failed to significantly suppress tumor growth compared with the control, but 50 mg/kg pictilisib combined with 2 mg/kg DOX effectively reduced tumor volumes to the size smaller than the initial one over a period of 28 days (**Figures 7A, B**). Tumor weight following treatment with the combination of drugs were lower than those following treatment with either pictilisib or DOX alone (**Figure 7C**). Next, we determined the protein levels of p-AKT (Ser475) and cleaved caspase-3 (Asp175) to test whether pictilisib could enhance the antitumor effects of DOX by downregulating

phosphorylation of AKT and upregulating cleaved caspase-3 (Asp175). The results from the PDX model showed that 50 mg/kg pictilisib combined with 2 mg/kg DOX inhibited almost phosphorylation of AKT and significantly elevated the expression of cleaved caspase-3 protein. In addition, Ki-67 staining demonstrated that this combination of pictilisib and DOX reduced the cell population in the proliferative phase compared with single drug treatment (**Figure 7D**). Finally, sections of organs including heart, liver, and kidney were stained with H&E to examine their morphology and assess the toxic effects of treatment (**Supplemental Figure 2A**).

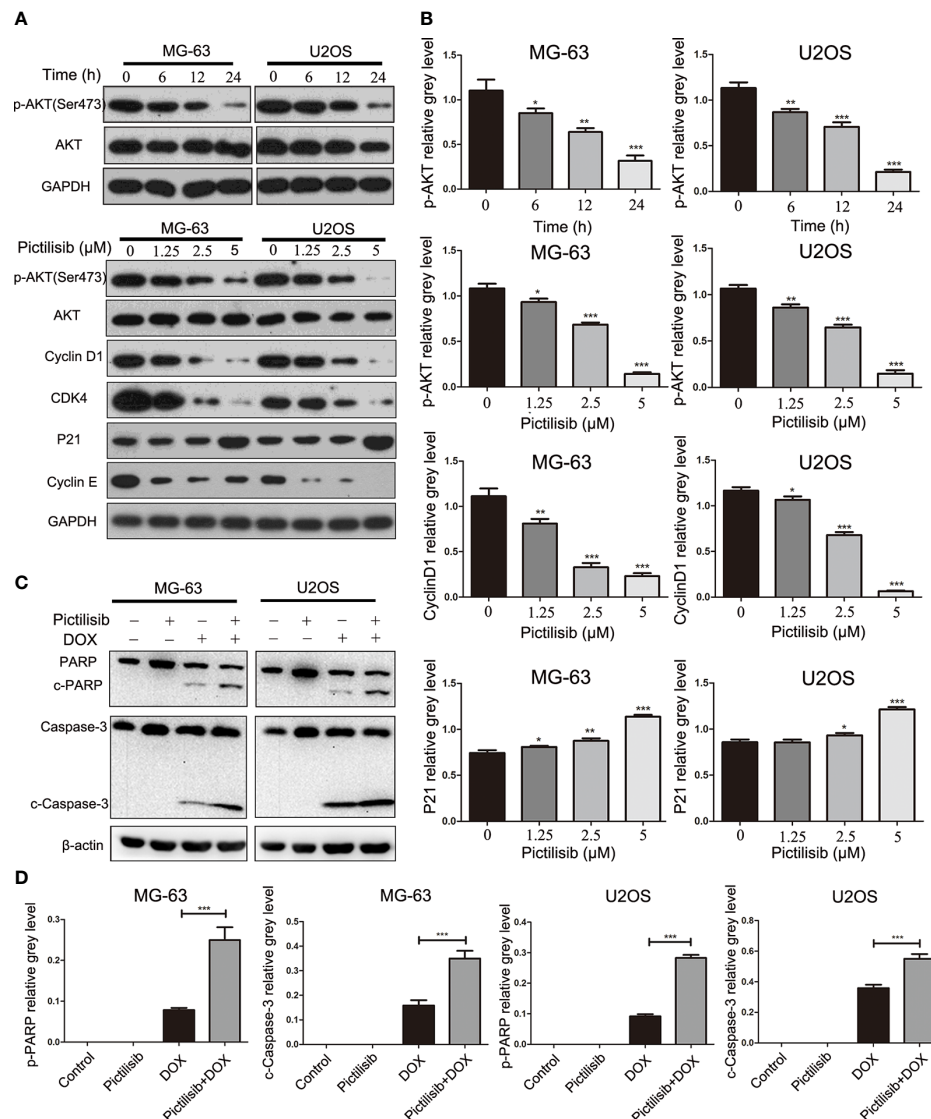


FIGURE 5 | Pictilisib inhibited the phosphorylation of AKT and downstream signaling pathways. **(A)** Western blot analysis was performed to detect total AKT and phosphorylation of AKT in OS cells treated with 2.5 μM pictilisib at 0, 6, 12, and 24 h, and with different pictilisib concentrations (0, 1.25, 2.5, and 5 μM) over 24 h. Proteins related to regulation of the cell cycle were detected by western blotting; these included cyclin D1, CDK4, P21, and cyclin E1. **(B)** Quantitative densitometric analysis of p-AKT compared with t-AKT; cyclin D1 and P21 were normalized to GAPDH. **(C)** Total protein extracted from cells treated with 1 μM pictilisib with or without 0.5 μg/ml DOX for 24 h. Apoptosis was evaluated by detection of cleaved PARP and caspase-3 by western blotting. **(D)** Quantitative densitometric analysis of p-AKT compared with t-AKT; cyclin D1 and P21 were normalized to β-actin *P < 0.05, **P < 0.01, ***P < 0.001.

Pictilisib Slows Tumor Growth in an Orthotopic Model and Reduces Tumor-Induced Osteolysis

The therapeutic value of pictilisib was studied in an orthotopic mouse model of OS using the 143B-luc cell line. Tumors of $1 \times 1 \times 1 \text{ mm}^3$ in size were implanted on the surfaces of the left tibiae of mice. The mice received treatment of 50 or 100 mg/kg pictilisib and/or 2 mg/kg DOX for 4 weeks. Mice treated with the low or high dose of pictilisib showed slower tumor growth compared with control mice. Besides, the combination treatment with

pictilisib and DOX significantly reduced tumor sizes (**Figures 8A, B**). Nevertheless, weight of mice was not significantly affected by pictilisib (**Figure 8C**). Luciferase imaging was performed on days 0, 14, and 28 to observe changes in tumor size (**Figure 8D**). Next, the role of pictilisib in tumor-induced osteolysis was assessed by X-ray analysis and high-resolution micro-CT. In control groups, pathological fracture was induced by severe osteolysis. Treatment with pictilisib at a dose of 100mg/kg reduced OS-mediated bone destruction (**Figure 8E**). Quantitative analyses of bone morphometric parameters

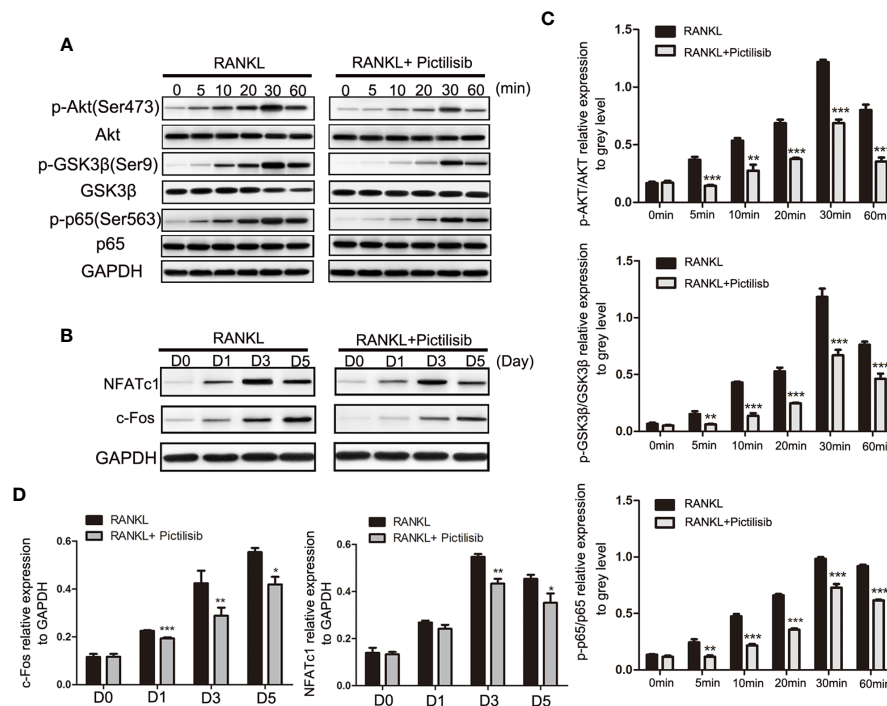


FIGURE 6 | Pictilisib treatment impaired RANKL-induced activation of AKT/GSK3 β and NF- κ B signaling pathways, leading to down-regulation of NFATc1 and c-Fos expression. **(A)** Total cellular proteins were extracted from BMMs stimulated with 50 ng/ml RANKL with or without 2 μ M pictilisib for 0, 5, 10, 20, 30, and 60 min and subjected to immunoblotting analysis against total and phosphorylated forms of Akt, GSK3 β , and NF- κ B p65. **(B)** Quantitative densitometric analysis of p-Akt, p-GSK3 β , and p-p65 compared with total protein, respectively. **(C)** BMMs were cultured with 30 ng/ml M-CSF and 50 ng/ml RANKL with or without 2 μ M pictilisib for 0, 1, 3, and 5 days, and protein levels of c-Fos and NFATc1 normalized to that of GAPDH were measured. **(D)** Quantitative densitometric analysis of c-Fos and NFATc1 normalized to GAPDH. * $P < 0.05$, ** $P < 0.01$, *** $P < 0.001$.

demonstrated that pictilisib markedly increased BV/TV in the region of interest (**Figure 8F**).

DISCUSSION

OS is the most common primary malignant bone tumor and occurs mainly in children and adolescents. The introduction of neoadjuvant chemotherapy in the 1970s led to a dramatic increase in overall survival rates from 20 to 50–70%, but many novel therapeutic approaches developed over the past 40 years have failed to achieve higher cure rates (3). Targeted therapies have achieved great success in some malignant bone and soft-tissue sarcomas (24–26), there is now a critical need to develop new targeted drugs to improve clinical outcomes in OS. Targeting PI3K represents a potential strategy to treat OS (27). Here, we found that 75.9% patients who provided biopsy samples were p-AKT positive; this was significantly higher than the 32.2% of patients after multi-drug chemotherapy. Our findings confirmed that positive expression of p-AKT after chemotherapy was associated with lower TCNR (<90%). This indicated that neoadjuvant chemotherapy effectively eliminated the majority of tumor cells owing to strong proliferation signals

in most patients. The remaining p-AKT-positive patients showed a poor response to chemotherapy. TCNR following chemotherapy is well known to have a strong influence on patient survival and prognosis. Thus, molecular inhibition of the PI3K/AKT pathway may be an alternative strategy for treatment of patients with positive expression of p-AKT before or after surgery.

Pictilisib, a selective and potent oral inhibitor of class I PI3K, was initially developed for the treatment of advanced breast cancer in combination with bevacizumab, trastuzumab, or letrozole (20). Here, we found that the proliferation of several different OS cell lines could be inhibited by pictilisib to varying degrees; it had the most powerful effect on MG-63 cells, whereas 143B cells were slightly inhibited. In another study, 143B cells harboring an oncogenic KRAS transformation did not show any response to MK-2206, an AKT inhibitor, at concentrations below 5 μ M. Kuijjer proposed that insensitivity to inhibition of the AKT pathway was mainly caused by activation of the Ras/Raf/ERK pathway, based on differences in kinome profiles of 143B cells treated with or without MK-2206 (8). Next, we demonstrated that the inhibition of OS depended on cell cycle arrest in G0/G phase *in vitro*. Cyclin D1 is known to have a key role in G1 to S phase

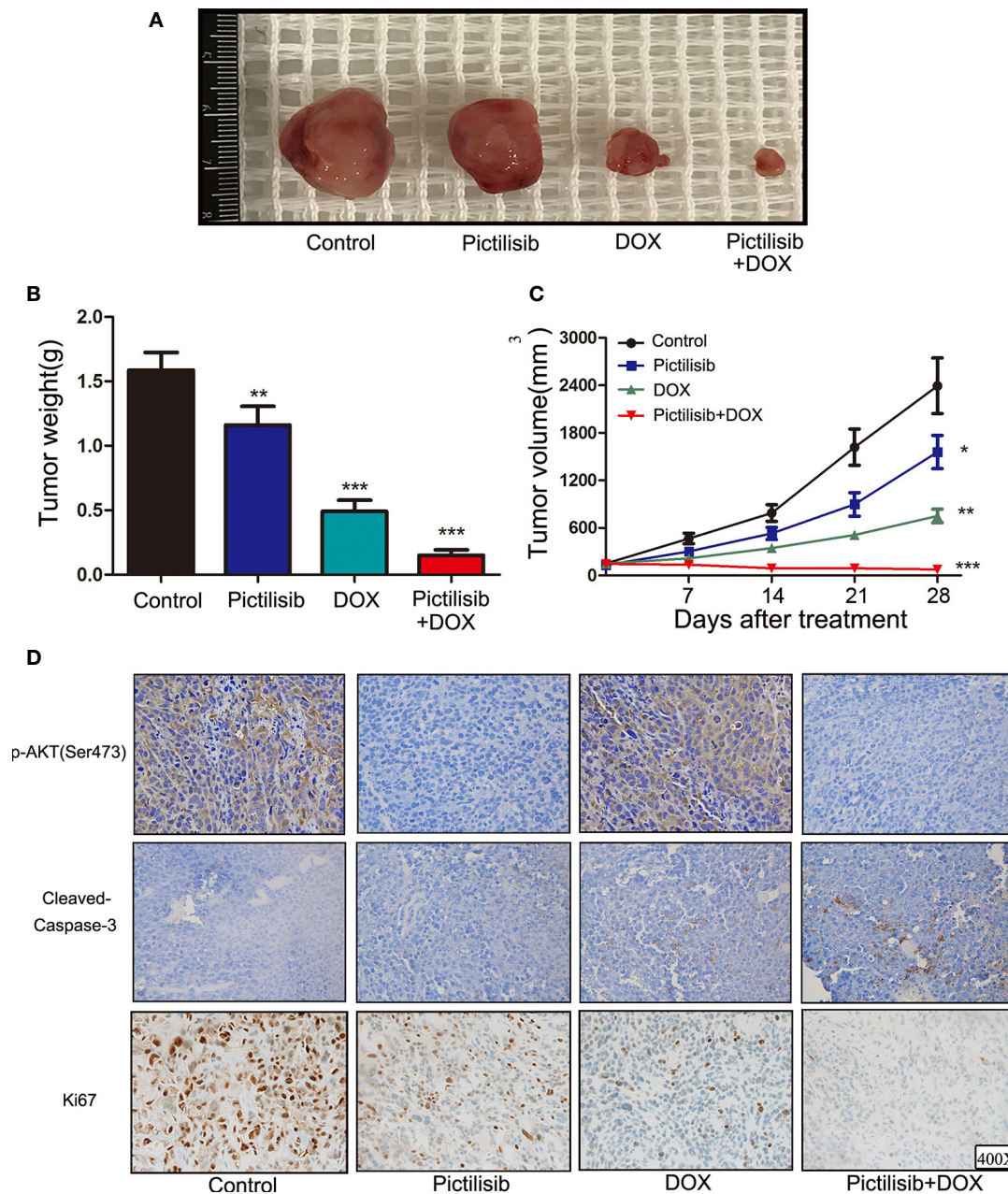


FIGURE 7 | Pictilisib suppressed tumor growth and enhanced sensitivity of chemotherapy in PDX animals. Surgical specimens from a girl with OS were subcutaneously implanted in the abdominal walls of BALB/c-nu mice ($n = 5$ per group). After 3 weeks, mice were treated with 50 mg/kg pictilisib and/or 2 mg/kg DOX. **(A)** Gross view of tumor specimens from different treatment groups. **(B)** Tumor volumes were calculated once a week following a standard formula: $(\text{length} \times \text{width}^2)/2$. **(C)** Tumor sections were weighed on day 28. **(D)** IHC and ki-67 staining were used to measure p-AKT (Ser473) and cleaved-caspase3 (c-caspase3) expression and the degree of proliferation in samples from different groups. * $P < 0.05$, ** $P < 0.01$, *** $P < 0.001$.

transition and to act as a downstream target of p-AKT. In addition, overexpression and amplification of cyclin D1 have been detected in 22 and 4% of OS samples, respectively (28). However, according to the flow cytometry and western blotting analyses, pictilisib did not affect apoptosis rates in OS cell lines. Another study showed that NVP-BEZ235, a dual PI3K/mTOR

inhibitor, was also unable to induce apoptosis of OC cell lines (29). This may have been because of the activation of the MEK/Erk pathway (30). Pictilisib showed a stronger inhibitory effect when combined with DOX, indicating that pictilisib may improve sensitivity to chemotherapy by reducing the occurrence of drug-resistant cells.

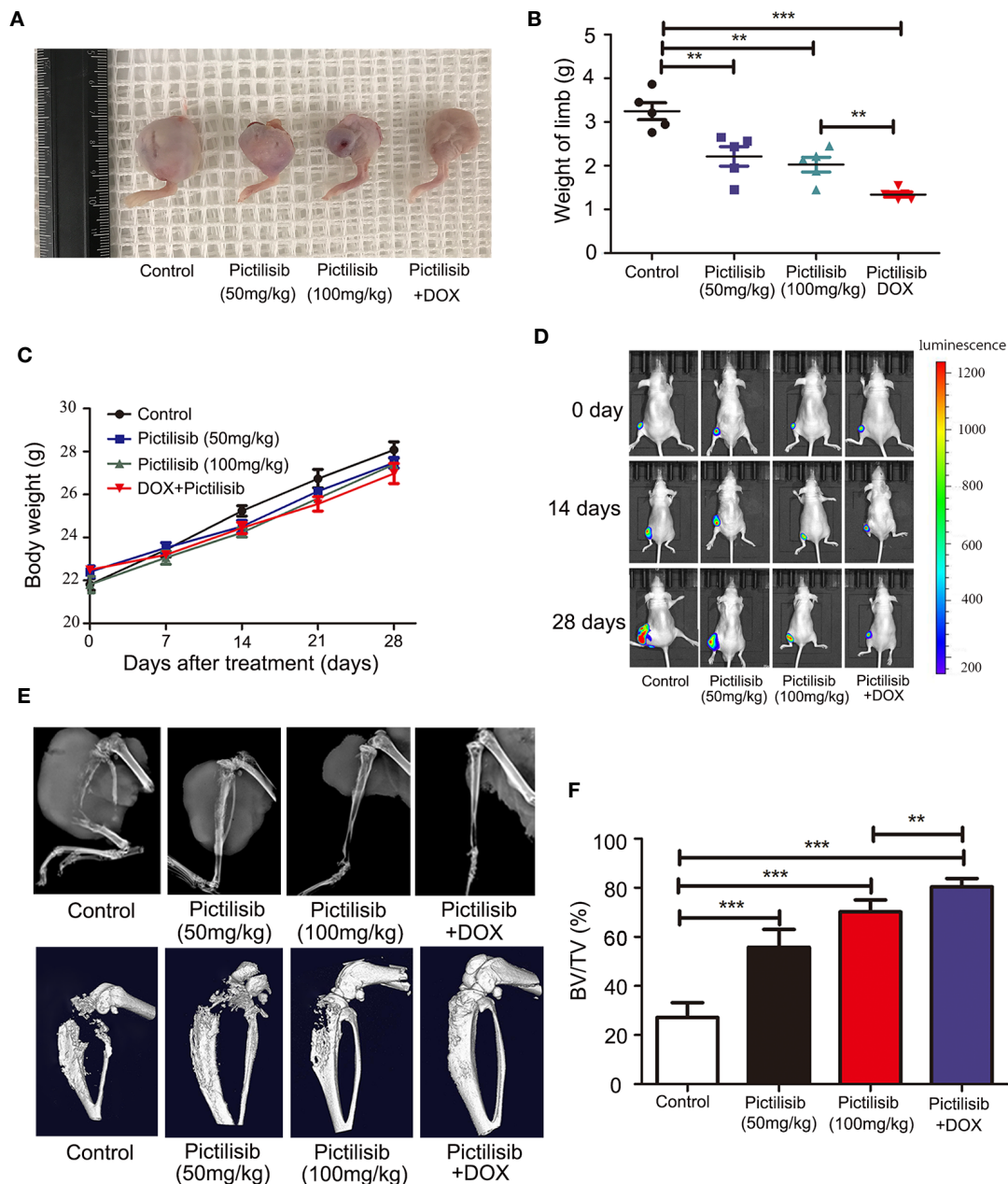


FIGURE 8 | Pictilisib inhibited the growth of tumors and OS-induced osteolysis in orthotopic mouse models. 143B cells expressing luciferase were injected into the backs of mice, then 1×1 mm pieces from tumors were embedded into a site adjacent to the left proximal tibia. Mice were treated with PBS, 50 mg/kg pictilisib, 100 mg/kg pictilisib, or 50 mg/kg pictilisib + 2 mg/kg DOX for 28 days. **(A)** Representative photos of left posterior limb from each group after sacrifice. **(B)** The weights of left legs with tumors were measured on day 28. **(C)** Changes in weight of each group on average after treatment. **(D)** Tumor growth was monitored by measuring luciferase activity in tumor-bearing mice after treatment on days 0, 14 and 28. **(E)** Tumor-induced osteolysis was measured by X-ray and micro-CT on day 28. Typical X-ray and three-dimensional reconstructed images are shown. **(F)** Quantitative analyses of BV/TV in the region of interest. ** $P < 0.01$, *** $P < 0.001$.

Further, the “seed and soil” theory of cancer is widely accepted, and the OS microenvironment is composed of bone matrix including osteoclasts, osteoblastomas, fibrocytes, and endothelial cells. Previous studies have suggested that osteoclasts provide “nutrition” for OS but increase the risk of

lung metastasis if they are inhibited at a late stage (31). In our research, TRAP-positive osteoclasts were efficiently inhibited by pictilisib *in vitro* via down-regulation of the AKT/GSK3 β /NFATc1 and NF- κ B pathways. We tested the efficiency of pictilisib in inhibition of tumor growth and tumor-induced

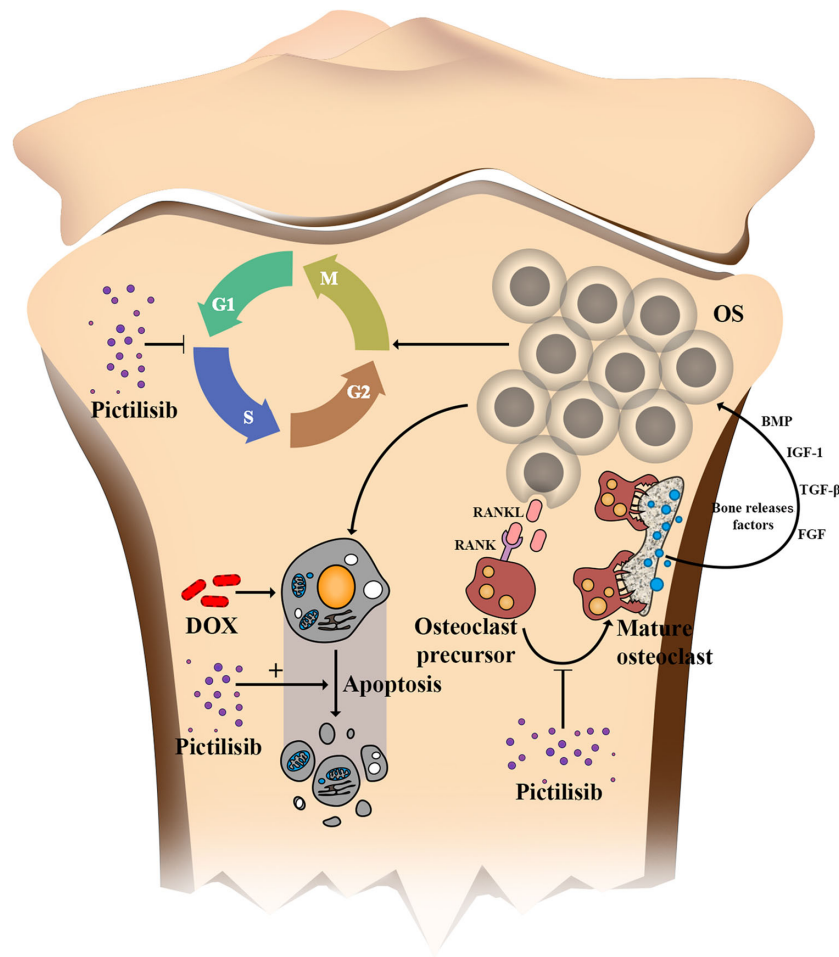


FIGURE 9 | Schematic of the effects of pictilisib on OS cells and osteoclasts in the tumor microenvironment. In brief, pictilisib inhibited proliferation of OS via cell cycle arrest rather than induction of cell apoptosis. In addition, pictilisib enhanced the sensitivity of OS cells to DOX. Further, tumor-induced osteolysis was effectively prevented by pictilisib.

osteolysis in orthotopic mice models. In other studies, zoledronic acid alone or combined with ifosfamide showed good results (32, 33). However, we failed to observe lung metastasis in any group, so it was unclear whether pictilisib had an effect on lung metastasis (**Supplemental Figure 2B**). In our study, lipopolysaccharide (LPS)-induced osteolysis was also inhibited by pictilisib in a mouse calvaria model (**Supplemental Figures 3A–F**). Inflammation-induced osteolysis and tumor-mediated bone destruction have shared downstream pathways involving interaction between RANKL and RANK in activation of osteoclasts (**Figure 9**). These include the AKT/GSK3 β /NFATc1 and NF- κ B pathways, which are the main regulators of differentiation and activation of osteoclasts (34, 35). A limitation of pictilisib is its lack of a cytotoxic effect; thus, it is necessary to combine it with other cytotoxic drugs.

Overall, our findings indicate that pictilisib combined with standard chemotherapy may be an efficient treatment for patients with positive p-AKT (Ser473) expression.

DATA AVAILABILITY STATEMENT

The original contributions presented in the study are included in the article/**Supplementary Material**; further inquiries can be directed to the corresponding authors.

ETHICS STATEMENT

The studies involving human participants were reviewed and approved by the Ethics Committee of Shanghai Sixth People's Hospital. Written informed consent to participate in this study was provided by the participants' legal guardian/next of kin.

AUTHOR CONTRIBUTIONS

YD and ZS designed and conceptualized the project. CL, XY, and NX performed the research and collected the data. ZZ performed

the data statistical analysis. CL drafted the manuscript. All authors contributed to the article and approved the submitted version.

FUNDING

This research was supported by grants from the Interdisciplinary Research Fund of Translational Medicine from Shanghai Jiao Tong University (ZH2018QNB06).

SUPPLEMENTARY MATERIAL

The Supplementary Material for this article can be found online at: <https://www.frontiersin.org/articles/10.3389/fonc.2020.615146/full#supplementary-material>

REFERENCES

- Mirabello L, Troisi RJ, Savage SA. Osteosarcoma incidence and survival rates from 1973 to 2004: data from the Surveillance, Epidemiology, and End Results Program. *Cancer* (2009) 115(7):1531–43. doi: 10.1002/cncr.24121
- Ottaviani G, Jaffe N. The epidemiology of osteosarcoma. *Cancer Treat Res* (2009) 152:3–13. doi: 10.1007/978-1-4419-0284-9_1
- Lilienthal I, Herold N. Targeting Molecular Mechanisms Underlying Treatment Efficacy and Resistance in Osteosarcoma: A Review of Current and Future Strategies. *Int J Mol Sci* (2020) 21(18):6885. doi: 10.3390/ijms21186885
- Chou AJ, Geller DS, Gorlick R. Therapy for osteosarcoma: where do we go from here? *Paediatr Drugs* (2008) 10(5):315–27. doi: 10.2165/00148581-200810050-00005
- Zhang J, Yu X, Yan Y, Wang C, Wang W. Clinica Chimica Acta PI3K / Akt signaling in osteosarcoma. *Clin Chim Acta* (2015) 444:182–92. doi: 10.1016/j.cca.2014.12.041
- Wang D, Niu X, Wang Z, Song C-L, Huang Z, Chen K-N, et al. Multiregion Sequencing Reveals the Genetic Heterogeneity and Evolutionary History of Osteosarcoma and Matched Pulmonary Metastases. *Cancer Res* (2019) 79(1):7–20. doi: 10.1158/0008-5472.CAN-18-1086
- Perry JA, Kiezun A, Tonzi P, Van Allen EM, Carter SL, Baca SC, et al. Complementary genomic approaches highlight the PI3K/mTOR pathway as a common vulnerability in osteosarcoma. *Proc Natl Acad Sci U S A* (2014) 111(51):E5564–73. doi: 10.1073/pnas.1419260111
- Kuijjer ML, Akker BEWM, Van Den, Hilhorst R, Mommersteeg M, Buddingh EP, Serra M, et al. Kinome and mRNA expression profiling of high-grade osteosarcoma cell lines implies Akt signaling as possible target for therapy. *BMC Med Genomics* (2014) 7:4. doi: 10.1186/1755-8794-7-4
- Ji F, Lv RAN, Zhao T. A correlation analysis between tumor imaging changes and p-AKT and HSP70 expression in tumor cells after osteosarcoma chemotherapy. *Oncol Lett* (2017) 14(6):6749–53. doi: 10.3892/ol.2017.7005
- Alfranca A, Juan LM, Ander T, Amaral T, Tumor O, Microenvironment Á. Bone microenvironment signals in osteosarcoma development. *Cell Mol Life Sci* (2015) 72(16):3097–113. doi: 10.1007/s00018-015-1918-y
- Kelleher FC, O'Sullivan H. Monocytes, Macrophages, and Osteoclasts in Osteosarcoma. *J Adolesc Young Adult Oncol* (2017) 6(3):396–405. doi: 10.1089/jayao.2016.0078
- Avnet S, Longhi A, Salerno M, Hallett JM, Perut F, Granchi D, et al. Increased osteoclast activity is associated with aggressiveness of osteosarcoma. *Int J Oncol* (2008) 33(6):1231–8. doi: 10.3892/ijo_00000113
- Lamoureux F, Richard P, Wittrant Y, Battaglia S, Pilet P, Trichet V, et al. Therapeutic relevance of osteoprotegerin gene therapy in osteosarcoma: blockade of the vicious cycle between tumor cell proliferation and bone resorption. *Cancer Res* (2007) 67(15):7308–18. doi: 10.1158/0008-5472.CAN-06-4130
- Supplementary Figure 1 | Low-dose pictilisib failed to induce apoptosis of OS cells (MG-63, U2OS). (A, B) Apoptotic cells induced with a range of concentrations of pictilisib were detected by flow cytometry. Proportions of apoptotic cells were compared among the four groups. (C) Expression of cleaved PARP and caspase-3 was evaluated by western blotting. *P < 0.05. ns, no significance.
- Supplementary Figure 2 | H&E staining of organs was performed to assess the toxicity of pictilisib in PDX models and lung metastasis in orthotopic models. (A) H&E staining of sections of heart, lung and kidney in the four groups. (B) H&E staining of sections of lung samples from orthotopic models.
- Supplementary Figure 3 | Pictilisib reduced osteolysis caused by LPS-induced inflammation *in vivo*. Collagen sponges soaked with PBS (control) or 10 mg/kg LPS were implanted over murine calvarias, and mice received subcutaneous injection of PBS or pictilisib (20 nM or 2 µM) over the sagittal middle suture of the calvaria for 10 days. (A) Representative three-dimensional micro-CT reconstructed images of mice calvaria. (B–E) Quantitative morphometric analyses of BV/TV (%), number of pores, bone mineral density(BMD) (mg/cc), and porosity as a percentage. (F) Representative images of H&E (x50 and x100) and TRAP (x100 and x200) staining in control and treatment groups. *P < 0.05, **P < 0.01, ***P < 0.001.
- Sharma A, Sharma L, Goyal R. Molecular Signaling Pathways and Essential Metabolic Elements in Bone Remodeling: An Implication of Therapeutic Targets for Bone Diseases. *Curr Drug Targets* (2020) 22(1):77–104. doi: 10.2174/1389450121666200910160404
- Edgar KA, Wallin JJ, Berry M, Lee LB, Prior WW, Sampath D, et al. Isoform-specific phosphoinositide 3-kinase inhibitors exert distinct effects in solid tumors. *Cancer Res* (2010) 70(3):1164–72. doi: 10.1158/0008-5472.CAN-09-2525
- Folkes AJ, Ahmadi K, Alderton WK, Alix S, Baker SJ, Box G, et al. The identification of 2-(1H-indazol-4-yl)-6-(4-methanesulfonyl-piperazin-1-ylmethyl)-4-morpholin-4-yl-thieno[3,2-d]pyrimidine (GDC-0941) as a potent, selective, orally bioavailable inhibitor of class I PI3 kinase for the treatment of cancer. *J Med Chem* (2008) 51(18):5522–32. doi: 10.1021/jm800295d
- Foukas LC, Claret M, Pearce W, Okkenhaug K, Meek S, Peskett E, et al. Critical role for the p110alpha phosphoinositide-3-OH kinase in growth and metabolic regulation. *Nature* (2006) 441(7091):366–70. doi: 10.1038/nature04694
- Sarker D, Ang JE, Baird R, Kristeleit R, Shah K, Moreno V, et al. First-in-human phase I study of pictilisib (GDC-0941), a potent pan-class I phosphatidylinositol-3-kinase (PI3K) inhibitor, in patients with advanced solid tumors. *Clin Cancer Res* (2015) 21(1):77–86. doi: 10.1158/1078-0432.CCR-14-0947
- Zeng S-X, Zhu Y, Ma A-H, Yu W, Zhang H, Lin T-Y, et al. The Phosphatidylinositol 3-Kinase Pathway as a Potential Therapeutic Target in Bladder Cancer. *Clin Cancer Res* (2017) 23(21):6580–91. doi: 10.1158/1078-0432.CCR-17-0033
- Schöffski P, Cresta S, Mayer IA, Wildiers H, Damian S, Gendreau S, et al. A phase Ib study of pictilisib (GDC-0941) in combination with paclitaxel, with and without bevacizumab or trastuzumab, and with letrozole in advanced breast cancer. *Breast Cancer Res* (2018) 20(1):109. doi: 10.1186/s13058-018-1015-x
- Sun Z, Zeng J, Wang W, Jia X, Wu Q, Yu D, et al. Magnoflorine Suppresses MAPK and NF-κB Signaling to Prevent Inflammatory Osteolysis Induced by Titanium Particles *In Vivo* and Osteoclastogenesis via RANKL *In Vitro*. *Front Pharmacol* (2020) 11:389. doi: 10.3389/fphar.2020.00389
- Wang Y, Zeng L, Liang C, Zan R, Ji W, Zhang Z, et al. Integrated analysis of transcriptome-wide m(6)A methylome of osteosarcoma stem cells enriched by chemotherapy. *Epigenomics* (2019) 11(15):1693–715. doi: 10.2217/epi-2019-0262
- Moon JB, Kim JH, Kim K, Youn BU, Ko A, Lee SY, et al. Akt induces osteoclast differentiation through regulating the GSK3β/NFATc1 signaling cascade. *J Immunol* (2012) 188(1):163–9. doi: 10.4049/jimmunol.1101254
- Lee YT, Tan YJ, Oon CE. Molecular targeted therapy: Treating cancer with specificity. *Eur J Pharmacol* (2018) 834:188–96. doi: 10.1016/j.ejphar.2018.07.034

25. Gao Y, Liu P, Shi R. Anlotinib as a molecular targeted therapy for tumors. *Oncol Lett* (2020) 20(2):1001–14. doi: 10.3892/ol.2020.11685
26. Chawla S, Blay J-Y, Rutkowski P, Le Cesne A, Reichardt P, Gelderblom H, et al. Denosumab in patients with giant-cell tumour of bone: a multicentre, open-label, phase 2 study. *Lancet Oncol* (2019) 20(12):1719–29. doi: 10.1016/S1470-2045(19)30663-1
27. Heymann D, Rédini F. Targeted therapies for bone sarcomas. *Bonekey Rep* (2013) Jul2:378. doi: 10.1038/bonekey.2013.112
28. Tang N, Song W-X, Luo J, Haydon RC, He T-C. Osteosarcoma development and stem cell differentiation. *Clin Orthop Relat Res* (2008) 466(9):2114–30. doi: 10.1007/s11999-008-0335-z
29. Gobin B, Battaglia S, Lanel R, Chesneau J, Amiaud J, Rédini F, et al. NVP-BEZ235, a dual PI3K/mTOR inhibitor, inhibits osteosarcoma cell proliferation and tumor development in vivo with an improved survival rate. *Cancer Lett* (2014) 344(2):291–8. doi: 10.1016/j.canlet.2013.11.017
30. Zhu Y-R, Min H, Fang J-F, Zhou F, Deng X-W, Zhang Y-Q. Activity of the novel dual phosphatidylinositol 3-kinase/mammalian target of rapamycin inhibitor NVP-BEZ235 against osteosarcoma. *Cancer Biol Ther* (2015) 16(4):602–9. doi: 10.1080/15384047.2015.1017155
31. Endo-Munoz L, Evdokiou A, Saunders NA. The role of osteoclasts and tumour-associated macrophages in osteosarcoma metastasis. *Biochim Biophys Acta* (2012) 1826(2):434–42. doi: 10.1016/j.bbcan.2012.07.003
32. Moriceau G, Ory B, Gobin B, Verrecchia F, Gouin F, Blanchard F, et al. Therapeutic approach of primary bone tumours by bisphosphonates. *Curr Pharm Des* (2010) 16(27):2981–7. doi: 10.2174/138161210793563554
33. Heymann D, Ory B, Blanchard F, Heymann M-F, Coipeau P, Charrier C, et al. Enhanced tumor regression and tissue repair when zoledronic acid is combined with ifosfamide in rat osteosarcoma. *Bone* (2005) 37(1):74–86. doi: 10.1016/j.bone.2005.02.020
34. Xi J-C, Zang H-Y, Guo L-X, Xue H-B, Liu X-D, Bai Y-B, et al. The PI3K/AKT cell signaling pathway is involved in regulation of osteoporosis. *J Recept Signal Transduct Res* (2015) 35(6):640–5. doi: 10.3109/10799893.2015.1041647
35. Nakashima T, Hayashi M, Takayanagi H. New insights into osteoclastogenic signaling mechanisms. *Trends Endocrinol Metab* (2012) 23(11):582–90. doi: 10.1016/j.tem.2012.05.005

Conflict of Interest: The authors declare that the research was conducted in the absence of any commercial or financial relationships that could be construed as a potential conflict of interest.

Copyright © 2021 Liang, Yu, Xiong, Zhang, Sun and Dong. This is an open-access article distributed under the terms of the Creative Commons Attribution License (CC BY). The use, distribution or reproduction in other forums is permitted, provided the original author(s) and the copyright owner(s) are credited and that the original publication in this journal is cited, in accordance with accepted academic practice. No use, distribution or reproduction is permitted which does not comply with these terms.



Potential Roles of Acute Phase Proteins in Cancer: Why Do Cancer Cells Produce or Take Up Exogenous Acute Phase Protein Alpha1-Antitrypsin?

Sabina Janciauskiene*, Sabine Wrenger, Steffen Günzel, Anna Ricarda Gründing, Heiko Golpon and Tobias Welte

Biomedical Research in Endstage and Obstructive Lung Disease Hannover (BREATH), Member of the German Center for Lung Research (DZL), Department of Respiratory Medicine, Hannover Medical School, Hannover, Germany

OPEN ACCESS

Edited by:

Niels Weinhold,
Heidelberg University, Germany

Reviewed by:

Yun Dai,
First Affiliated Hospital of Jilin
University, China
Kamini Singh,
Memorial Sloan Kettering Cancer
Center, United States

*Correspondence:

Sabina Janciauskiene
Janciauskiene.Sabina@mh-
hannover.de

Specialty section:

This article was submitted to
Cancer Molecular Targets
and Therapeutics,
a section of the journal
Frontiers in Oncology

Received: 27 October 2020

Accepted: 06 January 2021

Published: 19 February 2021

Citation:

Janciauskiene S, Wrenger S, Günzel S,
Gründing AR, Golpon H and Welte T
(2021) Potential Roles of Acute
Phase Proteins in Cancer: Why Do
Cancer Cells Produce or Take Up
Exogenous Acute Phase Protein
Alpha1-Antitrypsin?
Front. Oncol. 11:622076.
doi: 10.3389/fonc.2021.622076

An association between acute-phase proteins (APPs) and cancer has long been established and there are numerous reports correlating altered levels and/or molecular forms of APPs with different types of cancers. Many authors have shown a positive correlation between high levels of APPs, like alpha1-antitrypsin (AAT), and unfavorable clinical outcome in cancers. Conversely, others proposed that high levels of APPs are probably just a part of nonspecific inflammatory response to cancer development. However, this might not be always true, because many cancerous cells produce or take up exogenous APPs. What is the biological significance of this and what benefit do cancer cells have from these proteins remains largely unknown. Recent data revealed that some APPs, including AAT, are able to enhance cancer cell resistance against anticancer drug-induced apoptosis and autophagy. In this review, we specifically discuss our own findings and controversies in the literature regarding the role of AAT in cancer.

Keywords: cancer cells, alpha1-antitrypsin, acute phase proteins, apoptosis, autophagy, cancer microenvironment

INTRODUCTION

The relationship between inflammation, immunity and cancer is widely accepted. The cancer-related inflammatory responses can occur due to the chemotherapy as well as due to the tumor cell migration, invasion, activation of anti-apoptotic signaling pathways, and metastasis (1). Cancer-caused inflammation may result in the activation of transcription factors like nuclear factor- κ B, signal transducer and activator of transcription 3, and hypoxia-inducible factor 1 α , which further enhances inflammatory response. Accordingly, markers of systemic inflammation, including C-reactive protein (CRP), albumin, neutrophils, lymphocytes, neutrophil-to-lymphocyte ratio, platelet-to-lymphocyte ratio, and cytokines have been shown to be altered in patients with various cancers (2). These changes in local and systemic inflammatory mediators can induce epigenetic changes that favor tumor initiation, and create a milieu to either enhance or suppress cancer development (3).

The hallmarks of cancer-related environment include immune cells, stromal cells (including myofibroblasts), and inflammatory mediators, tissue remodeling and angiogenesis factors, similar like those seen in chronic inflammatory conditions or in tissue repair. Under the influence of cytokines and chemokines, liver but also other cells, like endothelial and epithelial cells, produce acute phase proteins (APPs). Experimental observations suggest that various cytokine combinations may have additive, synergistic, or inhibitory effects on the production of individual APPs (4). On the other hand, APPs *per se* modulate inflammatory reaction, as can be illustrated by the CRP example. First, pro-inflammatory cytokines/chemokines, like IL-6, TNF α , and IL-8 induce the production and release of CRP (5), but thereafter CRP itself increases the release of these pro-inflammatory mediators. In line, the infusion of recombinant human CRP into healthy volunteers was found to result in a significant induction of serum levels of the IL-6 and IL-8 as well as amyloid A, phospholipase A, and coagulation markers (6). These observations support a notion that CRP, but also other APPs, are not only markers of inflammation. The functions of APPs are important in trapping of microorganisms and their products, in activating the complement system, in neutralizing enzymes, scavenging free hemoglobin and radicals, and in modulating the host's immune response. Thus, APPs actively participate in the development and resolution of inflammation, and the overall profiles of APPs seem to depend on the nature of the initial inflammatory event, and how this event induces a systemic protein/cytokine response.

Elevated levels of APPs in patients with a variety of cancers were suggested to serve as prognostic or diagnostic markers in the context of clinical examinations. Interestingly, many types of cancer can express but also take up exogenous APPs, which may influence drug resistance, cancer progression and metastasis (7). For example, recent data have shown that the property of cancer cells to produce serum amyloid A enhances their resistance to T-cell immunity due to the activation of immunosuppressive granulocytes (8, 9).

The relationship between tumorigenesis and altered levels of circulating or tumor-associated APPs, such as haptoglobin, ceruloplasmin, CRP, alpha-2 macroglobulin, alpha-1-acid glycoprotein, plasminogen activator inhibitor-1 and alpha-1-antitrypsin has been reported (Table 1).

Single APPs are used as biomarkers, especially for cancer prognosis and diagnosis of complications to anticancer treatments. However, clinical studies show that the inflammatory phenotype (i.e., the APPs/cytokine profile) differs between patients not only with different malignancies but also with the same malignant disease (53). Therefore, we and other scientists think that APPs may become more valuable biomarkers if used in combinations or used with other acute phase markers, as a part of an acute phase profile. So far, the most commonly investigated prognostic markers were CRP, albumin, and the CRP: albumin ratio.

Regarding single APPs, an extensive literature supports the pro-tumorigenic activity of plasminogen activator inhibitor 1

(PAI-1, Serpin E1) (54). Clinical studies have shown that higher expression of PAI-1 positively correlates with a poor clinical outcome in patients with breast, ovarian, bladder, colon and non-small cell lung cancers (NSCLC) (26). A number of experimental studies described PAI-1 as an anti-apoptotic protein and a stimulator of angiogenesis (27, 28). On the other hand, employment of small molecule or antibody inhibitors of PAI-1 so far provided no evidence that inhibition of PAI-1 could have any therapeutic effect in cancer patients (29, 30). Likewise, another protease inhibitor, alpha1-antitrypsin (AAT, Serpin A1) has been identified as a prognostic marker of tumor recurrence and prognosis. Our recent results obtained from more than 300 patients with NSCLC revealed that higher serum levels of AAT are prognostic for the patient's worse outcome (36). Nevertheless, studies regarding the role of AAT in lung cancer are contradictory. Some demonstrate a direct relationship between high levels of AAT and the risk of lung cancer (36, 37) while opposite, others associate genetic AAT deficiency with an increased risk of lung cancer development (55). In this review, we specifically discuss our own findings and controversies in the literature regarding the role of AAT in lung cancer. Insights gained into the action of AAT towards lung cancer cells could be exploited for the future understanding of APPs' role in tumorigenesis.

OVEREXPRESSION OR DEFICIENCY OF HUMAN AAT, WHICH ONE IS RELATED TO TUMORIGENESIS

AAT Functions Beyond Serine Protease Inhibition

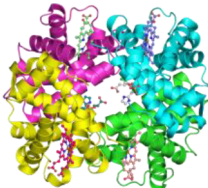
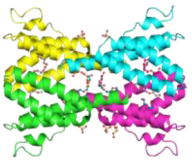
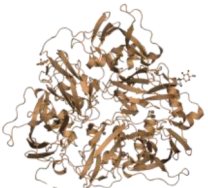
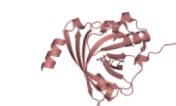
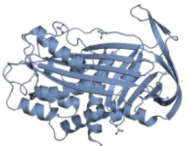
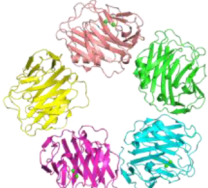

Human alpha1-antitrypsin (AAT), a member of the serpin (serine protease inhibitor) superfamily, is an acute phase glycoprotein and the best recognized inhibitor of neutrophil elastase. Various studies show that AAT also inhibits the activity of metalloproteases and caspases that play an essential role in cell apoptosis. AAT is a product of *SERPINA1* gene mainly expressed by hepatocytes and monocytes/macrophages. Its expression is regulated by interleukin 6-type cytokines. Both genetic and environmental factors influence an individual's basal level of AAT, and thus circulating AAT in apparently healthy people can vary from 1 to 2 g/L (56).

Experimental and clinical studies provide evidence that AAT expresses broad anti-inflammatory and immunomodulatory properties, some of which unrelated to protease inhibition. For example, AAT interacts and builds complexes with various inflammation-related ligands including chemokines IL-8 and LTB₄, complement factors, and heat-shock proteins (57–60). Moreover, AAT regulates cellular adhesion, chemotaxis, and wound healing and modulates signaling pathways to promote cell proliferation and angiogenesis (61).

AAT Favors Cancer Development

During chronic inflammation, which is a driving force in cancer development, increased levels and functional activity of AAT can

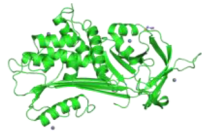
TABLE 1 | Acute phase proteins in cancer.

Acute phase protein	Function	Cancer type	Reference
Haptoglobin (Hp) 	<ul style="list-style-type: none"> – Iron-containing oxygen-transport metalloprotein – Scavenger for free hemoglobin – Inhibitor of prostaglandin production – Regulator of leukocyte recruitment and cytokine release – Prognostic biomarker for NSCLC 	Increased in ovarian, colorectal, pancreatic, breast and lung cancer	(10–14)
Serum amyloid A (SAA) 	<ul style="list-style-type: none"> – Apolipoprotein associated with high-density lipoprotein – Regulator of cell-cell communication, inflammatory, immunologic, neoplastic and protective pathways – Prognostic biomarker for solid tumors 	Increased in gastric cancer, colorectal cancer, NSCLC, melanoma, renal cancer, neuroblastoma	(15–20)
Ceruloplasmin (Cp) 	<ul style="list-style-type: none"> – Major copper transport protein, oxidase – Protector against oxidative stress – Potential cancer biomarker 	Increased in hepatocellular carcinoma, breast cancer, cervical cancer, bile duct cancer	(21–24)
Alpha-1-acid glycoprotein (AGP, orosomucoid) 	<ul style="list-style-type: none"> – Carrier of basic and neutrally charged lipophilic compounds – Potential biomarker in breast cancer 	Increased in plasma and ascites of cancer patients with peritoneal carcinomatosis, breast cancer	(7, 25)
Plasminogen activator inhibitor 1 (PAI-1) 	<ul style="list-style-type: none"> – Serine protease inhibitor – Inhibitor of tissue plasminogen activator and urokinase, – Pro-tumorigenic and anti-apoptotic – Stimulator of angiogenesis 	Increased in breast, ovarian, bladder, colon cancer and NSCLC	(26–30)
C-reactive protein (CRP) 	<ul style="list-style-type: none"> – Modulator of inflammatory processes and host responses to infection including complement pathway, apoptosis, phagocytosis, nitric oxide release, and production of cytokines – Prognostic marker for solid tumors including NSCLC 	Increased in stomach, pancreas, colorectal, esophageal, ovarian, renal, breast cancer and NSCLC, melanoma, neuroblastoma	(5, 31, 32)
Alpha-2-macroglobulin (AMG) 	<ul style="list-style-type: none"> – Broad spectrum protease inhibitor – Carrier of growth factors and cytokines – Antioxidant, anti-fibrotic and anti-inflammatory – Protects against radiation induced cell damage – Suggested biomarker for the diagnosis of B-cell acute lymphoblastic leukemia 	Decreased levels in more progressed prostate cancer; Increased levels in acute lymphoblastic leukemia	(33–35)

(Continued)

TABLE 1 | Continued

Acute phase protein	Function	Cancer type	Reference
Alpha1-Antitrypsin (AAT)	<ul style="list-style-type: none"> – Broad spectrum protease inhibitor – Anti-inflammatory and immunomodulatory – Regulator of cell adhesion, migration, invasion, proliferation and angiogenesis – Anti-apoptotic – Prognostic marker 	Increased serum levels in NSCLC, pancreas, prostate, cervix, ovary, breast, larynx and other carcinomas	(36–52)



NSCLC, non-small cell lung cancer.

rescue not only normal but also cancer cells. Indeed, AAT seems to be involved in the metastatic outgrowth of various cancer types including ovarian, cervical, colorectal, breast, and lung adenocarcinomas (38–42). Elevated plasma levels of AAT have been reported in patients with Hodgkin's lymphoma, pancreas, prostate, cervix, ovary, breast, larynx, colorectal, and other carcinomas, and proposed to be useful as prognostic factors (43–52). In breast cancer a high level of AAT has been associated with poor clinical prognosis (62). Furthermore, AAT seems to be directly involved in metastasis of ovarian, cervical, colorectal, breast, and lung adenocarcinomas (39, 40). Given an increasing body of research in this area, with pro-tumorigenic claims about AAT, we and others raised the hypothesis that individuals with inherited AAT deficiency might have a lower risk of developing cancer.

AAT Deficiency—Protects or Predisposes to Cancer Development

The deficiency, defined as an AAT blood level less than 35% of the mean expected value, is usually associated with Z allele (point mutation Lys342Glu), and less frequently with combinations of S (Lys264Val) or null alleles (63). Severe AAT deficiency predisposes to early onset of chronic obstructive pulmonary disease with emphysema, to liver cirrhosis at any age, neutrophilic panniculitis, systemic vasculitis, and possibly other inflammatory disease risks (64, 65). Severe AAT deficiency is a risk factor of developing hepatocellular carcinomas because of the damage of hepatocytes caused by retained intracellular polymers of mutant AAT protein, and an inappropriate hepatocellular regeneration. Data from the Swedish National AAT Deficiency Register revealed hepatocellular cancer diagnosis in 32 (2%) out of 1,595 individuals with ZZ AAT deficiency (66). Nevertheless, a risk of hepatocellular carcinoma in AAT deficiency is difficult to quantify because of a global variation in AAT genetics and the incidences of liver cancer (67).

In contrast, there are other reports showing that AAT deficiency people have lower or no increase in risk of developing lung and probably other types of cancers. For example, results from a cross-sectional survey study conducted among 720 AAT deficient people of the Alpha-1 Foundation Research Registry at the Medical University of South Carolina have shown that only 8 (1.1%) of participants have a diagnosis of lung cancer. In line, the comparison of 1585 ZZ AAT deficient subjects from Swedish AAT Deficiency Register and 5,999 population-based controls showed that death due to cancer in general was lower among ZZ individuals compared

to the controls, i.e. 11% versus 33%. Pulmonary carcinoma accounted for 1% of the causes of death in ZZ individuals and 4% in the controls (68). There are ongoing clinical studies designed to downregulate endogenous AAT expression within hepatocytes by using small-interfering RNA (siRNA) based drugs (69–71). These studies aim to cure/prevent liver disease in individuals with inherited AAT deficiency caused by intrahepatic accumulation of mutant AAT (63). Hypothetically, this approach of a temporal elimination of AAT protein synthesis might be helpful in the field of cancer and warrants further investigations.

Therapy With Human Plasma AAT Shows No Risk for Cancer Development

It is important to point out that the therapy with human plasma AAT used for over three decades to treat patients with inherited AAT deficiency-related emphysema does not rise tumor development rates. In fact, if untreated, individuals with inherited AAT deficiency seem to have higher risk of developing lung (72), gastrointestinal (73), and liver cancers (74). Likewise, few studies in patients with colorectal and gastric cancer found less AAT in both tissues and serum than in normal counterparts (75, 76). Therefore, one needs carefully consider differences between non-tumor and tumor-related environmental settings. The involvement of AAT in tumorigenesis may strongly depend on cancer cell properties as well as on the concentration and molecular forms of AAT, which are influenced by genetic and microenvironmental factors. For example in the B16-F10 lung metastasis mice model, Guttman and co-authors provided experimental evidence that NK cell-sensitive tumors are unaffected whereas CD8⁺ T cell-sensitive tumors can be significantly inhibited by the treatment with human AAT (77). It is also important to notify, that during inflammatory conditions AAT can undergo post-translational modifications like S-nitrosylation on its single surface cysteine residue, forming S-NO-AAT, a reducer of tumor cell viability (78).

Role of AAT in Non-Small Cell Lung Cancer

Non-small cell lung cancer (NSCLC) is one of the most common lung cancers worldwide, and about 70% of patients with this cancer present with advanced or metastatic disease at the time of diagnosis (79). Hitherto, there are only limited studies addressing the role of AAT in lung cancer (36, 37, 55). Therefore, to gain further insights into this matter, Schwarz et al. investigated the effects of extracellular AAT on NSCLC cell

behavior, *in vitro* (80). By comparing cancer cells grown in a regular medium versus medium supplemented with AAT, authors found that in the presence of physiological concentrations (0.5–1 mg/ml) of AAT cells acquire better pro-tumorigenic properties, and second that AAT strongly enhances cancer cell resistance against staurosporine-induced toxicity (80).

Staurosporine is a nonspecific protein kinase inhibitor derived from *Streptomyces staurosporeus* that can trigger cancer cell death through activation of both, apoptosis and autophagy pathways. Several lines of evidence indicate a cross-talk or mutual function between autophagy and apoptosis (81). As an inducer of apoptosis, staurosporine specifically acts through the activation of the mitochondrial apoptotic pathway, which is mainly controlled by Bak and Bax proteins (82, 83). When activated, these proteins can form pores on the mitochondrial outer membrane causing cytochrome c release that binds to apoptotic protease activating factor 1 (Apaf-1) and induces its oligomerization, known as the apoptosome formation. The apoptosome promotes cleavage of procaspase-9 into active caspase-9 which in turn activates caspases-3 and -7 to execute the final steps of apoptosis (84) (**Figure 1**).

AAT INHIBITS STAUROSPORINE-INDUCED NSCLC CELL APOPTOSIS

According to the results from Schwarz et al., staurosporine-induced NSCLC cell apoptosis was completely hampered in the presence of AAT. More detailed investigations revealed that AAT prevented the cleavage of procaspase-3, a precursor of caspase-3 which is one of the most deleterious executioner caspases in apoptosis pathway (80). As yet, the anti-apoptotic effects of AAT have been mostly attributed to the direct inhibition of caspase-3 activity. Investigators reported that exogenous AAT reduces the activity of caspase-3 in β -cells, lung endothelial and epithelial cells, cardiomyocytes and neutrophils (85–88), and that AAT inhibits active caspase-3 by forming an AAT-caspase-3-complex (89). In cell-free assays, AAT was also demonstrated to inhibit other executioner caspases, especially caspases-6 and -7, but not the initiator caspases, like caspase-9 (90). However, the results presented by Schwarz et al., indicate that protective effects of AAT against staurosporine-induced NSCLC cells apoptosis might be earlier in the apoptosis pathway than the inhibition of executioner caspases. In concordance, a recent study has shown that AAT significantly suppresses cytokine-induced cleavage of procaspase-9 in human islets (91).

CROSSTALK BETWEEN APOPTOSIS AND AUTOPHAGY

Several autophagy proteins are substrates for caspase-induced apoptosis. For example, caspase-3 and -9-mediated cleavage of Atg5 (E2-like enzyme is required for the formation of autophagosomes) and beclin-1 (implicated in the autophagic programmed cell death) switches autophagy to apoptosis (92).

Atg5 has also been found to be cleaved by calpain and translocate to the mitochondria to contribute to the release of cytochrome c. Previous finding that AAT inhibits calpain activity in human neutrophils (93) allows speculating that AAT may protect cancer cells *via* inhibition of other proteases than caspases.

AAT INHIBITS STAUROSPORINE-INDUCED AUTOPHAGY IN NSCLC CELLS

The mechanism(s) by which AAT helps lung cancer cells to acquire resistance towards staurosporine-induced apoptosis can also involve a shift of the balance towards anti-apoptotic proteins. As a matter of fact, the overexpression of AAT protein in lung cancer cell lines resulted in increased Bcl-2 and decreased beclin-1 levels (94). Thus, AAT may promote cancer cell survival by increasing Bcl-2, an anti-apoptotic, membrane associated protein (95) and by inhibiting beclin-1-dependent autophagy and apoptosis (96–99).

As already mentioned above, similarly to other anticancer agents, staurosporine can induce cancer cell death by simultaneous activation of apoptosis and autophagy (100). Autophagy may serve as a backup process for apoptosis—to enhance and/or contribute to the apoptosis (101–103). Autophagy involves the formation of double-membraned structures known as autophagosomes responsible for the engulfment of cargoes that are subsequently degraded after fusion with lysosomes (104). Autophagosome formation involves a set of proteins named Atg (autophagy-related) that orchestrate autophagosome initiation and biogenesis. Currently, the light chain 3 (LC3) is considered as one of the best autophagosome markers because the amount of LC3-II reflects the number of autophagosomes (105). Again, the LC3-II amount as well as LC3-II/LC3-I ratio not necessarily mirrors the autophagic activity, since the amount of LC3-II might increase not only due to autophagy activation but also due to the inhibition of autophagosome degradation. Therefore, for monitoring autophagic activity is used p62 (known as sequestosome-1), autophagic substrate receptor that is constantly being degraded by autophagy (106, 107). The reduced phosphorylation of mTOR is one more factor well reflecting the activation of autophagic flux (108). Results by Schwarz et al. confirmed that staurosporine added to NSCLC cells activates autophagy as measured by increase in LC3-II/LC3-I ratio, reduced mTOR activity as shown by dephosphorylated/less phosphorylated ribosomal protein S6 (RP-S6), degradation of p62 and downregulation of Flightless I, controlling the binding activity of p62 to LC3 (80). Clearly, in the presence of AAT all above mentioned markers of autophagy activation were unaffected by staurosporine.

POTENTIAL PRO-TUMORIGENIC FUNCTIONS OF AAT

Because autophagy can promote caspase-independent or caspase-dependent cell death (109–112), a major remaining

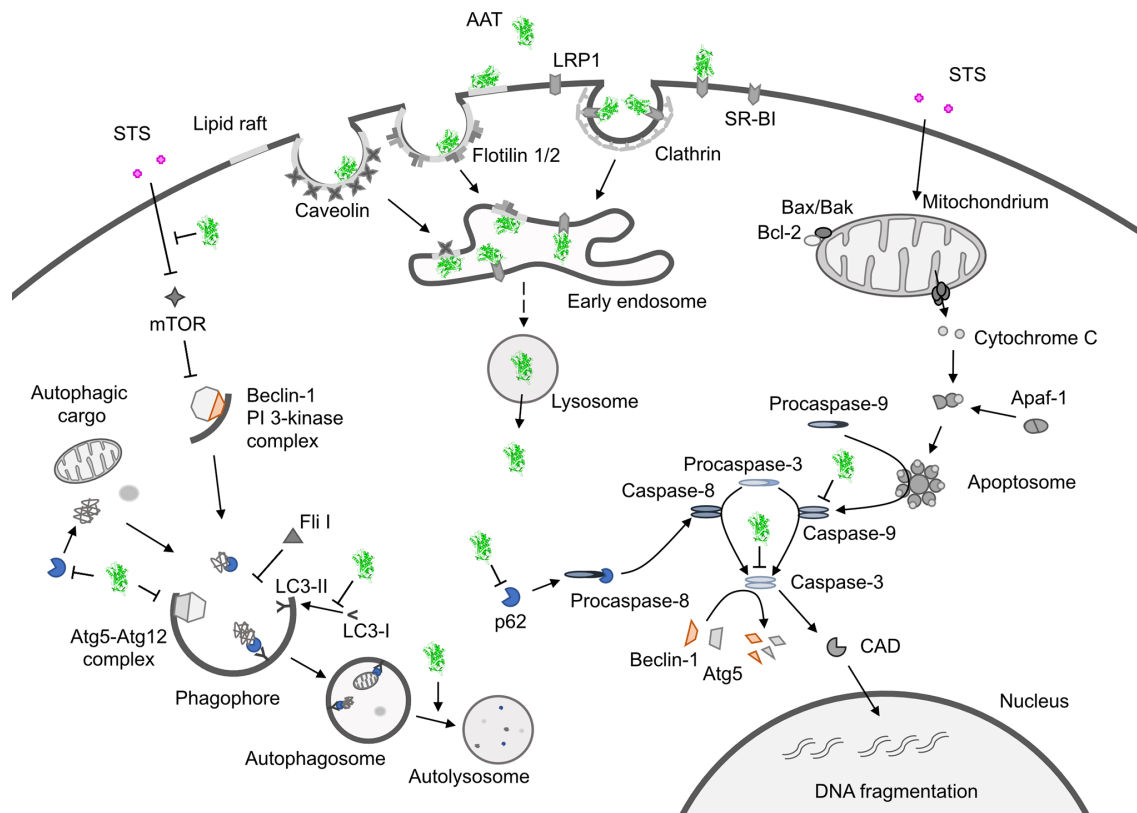


FIGURE 1 | Hypothetical model showing how alpha1-antitrypsin (AAT) may affect staurosporine (STS)-induced apoptosis and autophagy in NSCLC cells.

Intracellular entry of AAT occurs constitutively based on lipid raft independent pathways, namely clathrin-mediated, or lipid rafts-dependent, which include caveolae- and flotilin-dependent endocytosis. The AAT could be sequestered into clathrin-coated pits by binding to LRP1 (low-density lipoprotein receptor related protein 1) and SR-BI (scavenger receptor class b type I). Alternatively, AAT can associate with caveolin or flotilin 1/2-positive lipid rafts. All entry pathways might generate AAT-containing vesicles fusing with early endosomes and lysosomes from which—by unknown mechanisms - AAT escapes into the cytoplasm (green structure). There, AAT could affect cancer cell responses to cytotoxic drugs, like STS (staurosporine). STS activates autophagy by inhibiting mTOR (mammalian target of rapamycin), which allows Beclin-1/PI 3-kinase complex formation, increases LC3-II/LC3-I ratio, p62 degradation in autolysosomes and downregulation of Fli I (Flightless I), a controller of p62-LC3 interaction. Indeed, AAT seems to block different steps required for STS to induce autophagy. Potentially, AAT may also interfere with Atg5-Atg12 complex required for the formation of autophagosomes or recruitment of LC-3 to autophagosomes (green structures). As an inducer of apoptosis, STS acts through the activation of the mitochondrial apoptotic pathway. STS causes the aggregation of Bax/Bak and the release of cytochrome c that binds to Apaf-1 (apoptotic protease-activating factor 1) allowing apoptosome assembly and the recruitment of procaspase-9 to the apoptosome. In this scenario AAT might inhibit activation of procaspases-8, -9, -3 preventing Beclin-1/Atg5 degradation and activation of CAD (caspase-activated DNase). A crosstalk between STS-induced autophagy and apoptosis is in part mediated by p62 and beclin-1. Finding that AAT by itself strongly reduces p62 levels but prevents p62 reduction in STS-treated cells suggests that cancer cells utilize AAT to regulate apoptosis and autophagy dependent on the situation. Under basal conditions, AAT as a reducer of p62 protein levels (also important for the activation of procaspase-8), might activate autophagy as a cytoprotective pathway. In the setting when cancer cells face pro-apoptotic activation, autophagy inhibition may become a strategy to escape apoptosis.

question is whether effect of AAT on autophagy is independent or dependent of apoptosis. We would like to pay particular attention to the finding that, although AAT significantly prevented the reduction in p62 levels in staurosporine-treated NSCLC cancer cells, AAT by itself strongly reduced p62 protein levels as compared to non-treated controls. p62 is a regulator of selective autophagy (113) and recruiter of caspase-8 on autophagic membranes, which establishes a crosstalk between autophagy and apoptosis (114). Thus, the way by which cancer cells utilize AAT to regulate apoptosis and autophagy, probably is a context dependent. Under basal conditions, autophagy as a cyto-protective pathway can be activated by exogenous AAT whereas in the setting when cancer cells face pro-apoptotic

activation, autophagy inhibition by AAT may become a strategy to enhance survival. In fact, earlier Shapira et al. reported that intracellularly synthesized AAT prevents autophagic cell death and that exogenous AAT added to the cells prior to the induction of autophagy by tamoxifen reduces autophagy and cell death (115).

One cannot exclude that AAT may also facilitate cell survival through other mechanisms than modulation of autophagy. For example, study by Seung-Hee Chang et al., found that in AAT-overexpressing L132 cancer cells, the expression of manganese superoxide dismutase (SOD2), a tumor suppressive protein acting *via* inhibition of cell proliferation and induction of apoptosis (116), was markedly reduced.

DISCUSSION

Taken together, current findings promote a notion that higher levels of AAT either due to the increased intracellular expression or external entry can prevent cancer cell death. In fact, intracellular entry of AAT occurs constitutively in all mammalian cells, including cancer cells. The intracellular endocytosis of AAT may depend on the pathways non-involving lipid rafts, namely clathrin-mediated endocytosis, or pathways that take place in lipid rafts, which include caveolae-mediated endocytosis and flotillin-dependent endocytosis (91, 117, 118) (**Figure 1**). We and other investigators have previously found that cellular uptake of AAT takes place in lipid rafts (108, 118). We hypothesize that the uptake and subcellular trafficking of AAT might strongly depend on its concentration and the activation status of the cells. The uptake of high concentrations of AAT may involve clathrin-mediated endocytosis whereas lower concentrations of AAT may enter *via* caveolae pathway. Caveolae, in contrast to clathrin-coated pits, are very heterogeneous and the alterations in caveolae are not only important in tumor heterogeneity but also have a prognostic value (119). Hence, to better understand the role of AAT in tumorigenesis, intracellular entry and processing of AAT, but also other APPs, by cancer cells cannot be denied and warrants more detailed investigations.

Finally, it is important to keep in mind that AAT can modulate activities of different cells acting within tumor microenvironment. For example, fibroblasts are one of the important components of the tumor microenvironment, which participate in remodeling and a crosstalk between cancer cells and infiltrating leukocytes (120). Previously, it has been reported that AAT stimulates fibroblast proliferation and extracellular matrix production (120, 121). Remarkably, decreased p62 expression seems to be crucial for myofibroblast differentiation to support fibrosis and tumor

growth (122–124). In line, findings by Schwarz and co-authors show that AAT suppresses p62 levels in lung cancer cells. AAT is also reported to affect leukocyte profiles associated with inflammatory resolution and tissue regeneration (125, 126) and to promote macrophage polarization towards the pro-tumorigenic M2-like profile (126, 127). Unfortunately, the possible influence of AAT on the interactions between tumor and tumor-associated cells, which are of critical importance in tumorigenesis, has been only minimally addressed.

Based on the current knowledge, one can conclude that the involvement of AAT as well as other APPs in cancers can be direct (on cancer cells) or indirect (*via* cancer associated cells), and dependent on protein concentration, molecular form and tumor microenvironment. APPs may form pro- or anti-cancer host defense response, which needs to be taken into consideration for designing cancer treatments. Future work will have to determine whether some of the APPs contribute to and/or reflect cancer development, therefore representing potential therapeutic targets and/or biomarkers in tumorigenesis.

AUTHOR CONTRIBUTIONS

SJ and SG wrote the first draft. SW prepared figure and table and helped with manuscript preparation. AG, HG, and TW added comments. All authors contributed to the article and approved the submitted version.

FUNDING

This work has been supported by funding from the German Center for Lung Research (grant 82DZL002A1).

REFERENCES

- Nickoloff BJ, Ben-Neriah Y, Pikarsky E. Inflammation and cancer: is the link as simple as we think? *J Invest Dermatol* (2005) 124:x–xiv. doi: 10.1111/j.0022-202X.2005.23724.x
- Guthrie GJ, Charles KA, Roxburgh CS, Horgan PG, McMillan DC, Clarke SJ. The systemic inflammation-based neutrophil-lymphocyte ratio: experience in patients with cancer. *Crit Rev Oncol Hematol* (2013) 88:218–30. doi: 10.1016/j.critrevonc.2013.03.010
- Liotta LA, Kohn EC. The microenvironment of the tumour-host interface. *Nature* (2001) 411:375–9. doi: 10.1038/35077241
- Gabay C, Kushner I. Acute-phase proteins and other systemic responses to inflammation. *N Engl J Med* (1999) 340:448–54. doi: 10.1056/NEJM199902113400607
- Sproston NR, Ashworth JJ. Role of C-Reactive Protein at Sites of Inflammation and Infection. *Front Immunol* (2018) 9:754. doi: 10.3389/fimmu.2018.00754
- Bisoendial RJ, Kastelein JJ, Levels JH, Zwaginga JJ, van den Bogaard B, Reitsma PH, et al. Activation of inflammation and coagulation after infusion of C-reactive protein in humans. *Circ Res* (2005) 96:714–6. doi: 10.1161/01.RES.0000163015.67711.AB
- Orr WS, Malkas LH, Hickey RJ, Sandoval JA, Veas F. Acute Phase Proteins as Cancer Biomarkers. In: *Acute Phase Proteins as Early Non-Specific Biomarkers of Human and Veterinary Diseases*. Edn ed. Rijeka, Croatia, Intech: London, UK (2011). p. 408.
- De Santo C, Arscott R, Booth S, Karydis I, Jones M, Asher R, et al. Invariant NKT cells modulate the suppressive activity of IL-10-secreting neutrophils differentiated with serum amyloid A. *Nat Immunol* (2010) 11:1039–46. doi: 10.1038/ni.1942
- Greten TF, Manns MP, Korangy F. Myeloid derived suppressor cells in human diseases. *Int Immunopharmacol* (2011) 11:802–7. doi: 10.1016/j.intimp.2011.01.003
- Arredouani M, Matthijs P, Van Hoeyveld E, Kasran A, Baumann H, Ceuppens JL, et al. Haptoglobin directly affects T cells and suppresses T helper cell type 2 cytokine release. *Immunology* (2003) 108:144–51. doi: 10.1046/j.1365-2567.2003.01569.x
- Lu J, Wang Y, Yan M, Feng P, Yuan L, Cai Y, et al. High serum haptoglobin level is associated with tumor progression and predicts poor prognosis in non-small cell lung cancer. *Oncotarget* (2016) 7:41758–66. doi: 10.18632/oncotarget.9676
- Maffei M, Funicello M, Vottari T, Gamucci O, Costa M, Lisi S, et al. The obesity and inflammatory marker haptoglobin attracts monocytes via interaction with chemokine (C-C motif) receptor 2 (CCR2). *BMC Biol* (2009) 7:87. doi: 10.1186/1741-7007-7-87
- Saeed SA, Denning-Kendall PA, McDonald-Gibson WJ, Collier HOJ. Human haptoglobin: an endogenous inhibitor of prostaglandin synthase. In: DA Willoughby, JP Giroud, editors. *Inflammation: Mechanisms and*

- Treatment*, 4. Edn ed. Cham, Switzerland: Springer Netherlands (1980). p. 873.
14. Tai CS, Lin YR, Teng TH, Lin PY, Tu SJ, Chou CH, et al. Haptoglobin expression correlates with tumor differentiation and five-year overall survival rate in hepatocellular carcinoma. *PLoS One* (2017) 12:e0171269. doi: 10.1371/journal.pone.0171269
 15. Cho WC, Yip TT, Cheng WW, Au JS. Serum amyloid A is elevated in the serum of lung cancer patients with poor prognosis. *Br J Cancer* (2010) 102:1731–5. doi: 10.1038/sj.bjc.6605700
 16. Cocco E, Bellone S, El-Sahwi K, Cargnelli M, Buza N, Tavassoli FA, et al. Serum amyloid A: a novel biomarker for endometrial cancer. *Cancer* (2010) 116:843–51. doi: 10.1002/cncr.24838
 17. Gutfeld O, Prus D, Ackerman Z, Dishon S, Linke RP, Levin M, et al. Expression of serum amyloid A, in normal, dysplastic, and neoplastic human colonic mucosa: implication for a role in colonic tumorigenesis. *J Histochem Cytochem* (2006) 54:63–73. doi: 10.1369/jhc.5A6645.2005
 18. Sack GH Jr. Serum amyloid A - a review. *Mol Med* (2018) 24:46. doi: 10.1186/s10020-018-0047-0
 19. Sung HJ, Ahn JM, Yoon YH, Rhim TY, Park CS, Park JY, et al. Identification and validation of SAA as a potential lung cancer biomarker and its involvement in metastatic pathogenesis of lung cancer. *J Proteome Res* (2011) 10:1383–95. doi: 10.1021/pr101154j
 20. Urieli-Shoval S, Finci-Yeheskel Z, Dishon S, Galinsky D, Linke RP, Ariel I, et al. Expression of serum amyloid A in human ovarian epithelial tumors: implication for a role in ovarian tumorigenesis. *J Histochem Cytochem* (2010) 58:1015–23. doi: 10.1369/jhc.2010.956821
 21. Ferrin G, Rodriguez-Peralvarez M, Aguilar-Melero P, Ranchal I, Llamaza C, Linares CI, et al. Plasma protein biomarkers of hepatocellular carcinoma in HCV-infected alcoholic patients with cirrhosis. *PLoS One* (2015) 10:e0118527. doi: 10.1371/journal.pone.0118527
 22. Pan Q, Kleer CG, van Golen KL, Irani J, Bottema KM, Bias C, et al. Copper deficiency induced by tetrathiomolybdate suppresses tumor growth and angiogenesis. *Cancer Res* (2002) 62:4854–9.
 23. Arumanayagam M, Wong FW, Rogers M, Swaminathan R. Serum ceruloplasmin, plasma copper concentration and copper to ceruloplasmin ratio in cervical carcinoma. *Gynecol Obstet Invest* (1993) 35:175–8. doi: 10.1159/000292694
 24. Han IW, Jang JY, Kwon W, Park T, Kim Y, Lee KB, et al. Ceruloplasmin as a prognostic marker in patients with bile duct cancer. *Oncotarget* (2017) 8:29028–37. doi: 10.18632/oncotarget.15995
 25. Ohbatake Y, Fushida S, Tsukada T, Kinoshita J, Oyama K, Hayashi H, et al. Elevated alpha1-acid glycoprotein in gastric cancer patients inhibits the anticancer effects of paclitaxel, effects restored by co-administration of erythromycin. *Clin Exp Med* (2016) 16:585–92. doi: 10.1007/s10238-015-0387-9
 26. Schmitt M, Harbeck N, Brunner N, Janicke F, Meisner C, Muhlenweg B, et al. Cancer therapy trials employing level-of-evidence-1 disease forecast cancer biomarkers uPA and its inhibitor PAI-1. *Expert Rev Mol Diagn* (2011) 11:617–34. doi: 10.1586/erm.11.47
 27. Bajou K, Masson V, Gerard RD, Schmitt PM, Albert V, Praus M, et al. The plasminogen activator inhibitor PAI-1 controls in vivo tumor vascularization by interaction with proteases, not vitronectin. Implications for antiangiogenic strategies. *J Cell Biol* (2001) 152:777–84. doi: 10.1083/jcb.152.4.777
 28. Schneider DJ, Chen Y, Sobel BE. The effect of plasminogen activator inhibitor type 1 on apoptosis. *Thromb Haemost* (2008) 100:1037–40. doi: 10.1160/TH08-04-0234
 29. Li S, Wei X, He J, Tian X, Yuan S, Sun L. Plasminogen activator inhibitor-1 in cancer research. *Biomed Pharmacother* (2018) 105:83–94. doi: 10.1016/j.biopha.2018.05.119
 30. Rouch A, Vanucci-Bacque C, Bedos-Belval F, Baltas M. Small molecules inhibitors of plasminogen activator inhibitor-1 - an overview. *Eur J Med Chem* (2015) 92:619–36. doi: 10.1016/j.ejmech.2015.01.010
 31. Shrotriya S, Walsh D, Nowacki AS, Lorton C, Aktas A, Hullihen B, et al. Serum C-reactive protein is an important and powerful prognostic biomarker in most adult solid tumors. *PLoS One* (2018) 13:e0202555. doi: 10.1371/journal.pone.0202555
 32. Yang JR, Xu JY, Chen GC, Yu N, Yang J, Zeng DX, et al. Post-diagnostic C-reactive protein and albumin predict survival in Chinese patients with non-small cell lung cancer: a prospective cohort study. *Sci Rep* (2019) 9:8143. doi: 10.1038/s41598-019-44653-x
 33. Chen X, Kong X, Zhang Z, Chen W, Chen J, Li H, et al. Alpha-2-macroglobulin as a radioprotective agent: a review. *Chin J Cancer Res* (2014) 26:611–21. doi: 10.3978/j.issn.1000-9604.2014.09.04
 34. Guo L, Ren H, Zeng H, Gong Y, Ma X. Proteomic analysis of cerebrospinal fluid in pediatric acute lymphoblastic leukemia patients: a pilot study. *Oncotargets Ther* (2019) 12:3859–68. doi: 10.2147/OTT.S193616
 35. Kano H, Ohara T, Egawa S, Baba S, Akahoshi T. Prognostic potential of a PSA complex in sera of prostate cancer patients with alpha2-macroglobulin deficiency. *J Clin Lab Anal* (2008) 22:302–6. doi: 10.1002/jcla.20260
 36. Erceetin E, Richtmann S, Delgado BM, Gomez-Mariano G, Wrenger S, Korenbaum E, et al. Clinical Significance of SERPINA1 Gene and Its Encoded Alpha1-antitrypsin Protein in NSCLC. *Cancers (Basel)* (2019) 11:1306. doi: 10.3390/cancers11091306
 37. El-Akawi ZJ, Abu-Awad AM, Sharara AM, Khader Y. The importance of alpha-1 antitrypsin (alpha1-AT) and neopterin serum levels in the evaluation of non-small cell lung and prostate cancer patients. *Neuroendocrinol Lett* (2010) 31:113–6.
 38. Mbeunkui F, Metge BJ, Shevde LA, Pannell LK. Identification of differentially secreted biomarkers using LC-MS/MS in isogenic cell lines representing a progression of breast cancer. *J Proteome Res* (2007) 6:2993–3002. doi: 10.1021/pr060629m
 39. Normandin K, Peant B, Le Page C, de Ladurantaye M, Ouellet V, Tonin PN, et al. Protease inhibitor SERPINA1 expression in epithelial ovarian cancer. *Clin Exp Metastasis* (2010) 27:55–69. doi: 10.1007/s10585-009-9303-6
 40. Scamuffa N, Siegfried G, Bontemps Y, Ma L, Basak A, Cherel G, et al. Selective inhibition of proprotein convertases represses the metastatic potential of human colorectal tumor cells. *J Clin Invest* (2008) 118:352–63. doi: 10.1172/JCI32040
 41. Wozniak B, Mila-Kierzenkowska C, Wozniak A, Drewa G, Soponska M, Drewa T, et al. The effect of combined therapy on activity of cathepsin D and alpha-1-antitrypsin in the blood serum of women with cervical cancer. *Eur J Gynaecol Oncol* (2008) 29:617–9.
 42. Zelyte I, Wallmark A, Piitulainen E, Westin U, Janciauskiene S. Increased plasma levels of serine proteinase inhibitors in lung cancer patients. *Anticancer Res* (2004) 24:241–7.
 43. Brkic S, Salkic A, Nuhbegovic S, Brkic F, Umihanic S. Influence of surgical therapy on serum values of alpha 1-antitrypsin in patients with head and neck tumors. *Med Arh* (2011) 65:99–101.
 44. Dabrowska M, Kemona H, Prokopowicz J, Kiluk S. Serum concentration of alpha-2-macroglobulin, alpha-1-antitrypsin and alpha-1-antichymotrypsin [correction of alpha-2-antichymotrypsin] in patients with Hodgkin's disease. *Mater Med Pol* (1992) 24:28–30.
 45. Krecicki T, Leluk M. Acute phase reactant proteins—an aid to monitoring surgical treatment of laryngeal carcinoma. *J Laryngol Otol* (1992) 106:613–5. doi: 10.1017/s002221510012033x
 46. Latner AL, Turner GA, Lamin MM. Plasma alpha-1-antitrypsin levels in early and late carcinoma of the cervix. *Oncology* (1976) 33:12–4. doi: 10.1159/000225093
 47. Perez-Holanda S, Blanco I, Menendez M, Rodrigo L. Serum concentration of alpha-1 antitrypsin is significantly higher in colorectal cancer patients than in healthy controls. *BMC Cancer* (2014) 14:355. doi: 10.1186/1471-2407-14-355
 48. Tountas Y, Sparos L, Theodoropoulos C, Trichopoulos D. Alpha 1-antitrypsin and cancer of the pancreas. *Digestion* (1985) 31:37–40. doi: 10.1159/000199175
 49. Vasishta A, Baker PR, Preece PE, Wood RA, Cuschieri A. Serum proteinase-like peptidase activities and proteinase inhibitors in women with breast disease. *Eur J Cancer Clin Oncol* (1984) 20:197–202. doi: 10.1016/0277-5379(84)90184-6
 50. Ward AM, Cooper EH, Houghton AL. Acute phase reactant proteins in prostatic cancer. *Br J Urol* (1977) 49:411–8. doi: 10.1111/j.1464-410x.1977.tb04168.x
 51. Warwas M, Gerber J, Pietkiewicz A. Haptoglobin and proteinase inhibitors in the blood serum of women with inflammatory, benign and neoplastic lesions of the ovary. *Neoplasma* (1986) 33:79–84.
 52. Zbroja-Sontag W. Defense proteins and immune complexes in the blood serum of women with inflammatory and neoplastic lesions of the ovary. *Am J Reprod Immunol* (1983) 4:11–20. doi: 10.1111/j.1600-0897.1983.tb00247.x

53. Bruserud O, Aarstad HH, Tvedt THA. Combined C-Reactive Protein and Novel Inflammatory Parameters as a Predictor in Cancer-What Can We Learn from the Hematological Experience? *Cancers (Basel)* (2020) 12:1966. doi: 10.3390/cancers12071966
54. Kubala MH, DeClerck YA. The plasminogen activator inhibitor-1 paradox in cancer: a mechanistic understanding. *Cancer Metastasis Rev* (2019) 38:483–92. doi: 10.1007/s10555-019-09806-4
55. Torres-Duran M, Ruano-Ravina A, Parente-Lamelas I, Abal-Arca J, Leiro-Fernandez V, Montero-Martinez C, et al. Alpha-1 Antitrypsin Deficiency and Lung Cancer Risk: A Case-Control Study in Never-Smokers. *J Thoracic Oncol* (2015) 10:1279–84. doi: 10.1097/JTO.0000000000000609
56. Ferrarotti I, Poplowska-Wisniewska B, Trevisan MT, Koepke J, Dresel M, Koczulla R, et al. How Can We Improve the Detection of Alpha1-Antitrypsin Deficiency? *PloS One* (2015) 10:e0135316. doi: 10.1371/journal.pone.0135316
57. O'Brien ME, Fee L, Browne N, Carroll TP, Meleady P, Henry M, et al. Activation of complement component 3 is associated with airways disease and pulmonary emphysema in alpha-1 antitrypsin deficiency. *Thorax* (2020) 75:321–30. doi: 10.1136/thoraxjnl-2019-214076
58. Finotti P, Pagetta A. A heat shock protein70 fusion protein with alpha1-antitrypsin in plasma of type 1 diabetic subjects. *Biochem Biophys Res Commun* (2004) 315:297–305. doi: 10.1016/j.bbrc.2004.01.058
59. Bergin DA, Reeves EP, Meleady P, Henry M, McElvaney OJ, Carroll TP, et al. alpha-1 Antitrypsin regulates human neutrophil chemotaxis induced by soluble immune complexes and IL-8. *J Clin Invest* (2010) 120:4236–50. doi: 10.1172/JCI41196
60. O'Dwyer CA, O'Brien ME, Wormald MR, White MM, Banville N, Hurley K, et al. The BLT1 Inhibitory Function of alpha-1 Antitrypsin Augmentation Therapy Disrupts Leukotriene B4 Neutrophil Signaling. *J Immunol* (2015) 195:3628–41. doi: 10.4049/jimmunol.1500038
61. Janciauskiene S, Wrenger S, Immenschuh S, Olejnicka B, Greulich T, Welte T, et al. The Multifaceted Effects of Alpha1-Antitrypsin on Neutrophil Functions. *Front Pharmacol* (2018) 9:341. doi: 10.3389/fphar.2018.00341
62. Zhao Z, Ma J, Mao Y, Dong L, Li S, Zhang Y. Silence of alpha1-Antitrypsin Inhibits Migration and Proliferation of Triple Negative Breast Cancer Cells. *Med Sci Monit* (2018) 24:6851–60. doi: 10.12659/MSM.910665
63. Janciauskiene SM, Bals R, Koczulla R, Vogelmeier C, Kohnlein T, Welte T. The discovery of alpha1-antitrypsin and its role in health and disease. *Respir Med* (2011) 105:1129–39. doi: 10.1016/j.rmed.2011.02.002
64. de Serres F, Blanco I. Role of alpha-1 antitrypsin in human health and disease. *J Intern Med* (2014) 276:311–35. doi: 10.1111/joim.12239
65. Janciauskiene S, Welte T. Well-Known and Less Well-Known Functions of Alpha-1 Antitrypsin. Its Role in Chronic Obstructive Pulmonary Disease and Other Disease Developments. *Ann Am Thorac Soc* (2016) 13(Suppl 4):S280–8. doi: 10.1513/AnnalsATS.201507-468KV
66. Tanash HA, Piitulainen E. Liver disease in adults with severe alpha-1-antitrypsin deficiency. *J Gastroenterol* (2019) 54:541–48. doi: 10.1007/s00535-019-01548-y
67. Yang JD, Hainaut P, Gores GJ, Amadou A, Plymoth A, Roberts LR. A global view of hepatocellular carcinoma: trends, risk, prevention and management. *Nat Rev Gastroenterol Hepatol* (2019) 16:589–604. doi: 10.1038/s41575-019-0186-y
68. Tanash HA, Ekstrom M, Ronmark E, Lindberg A, Piitulainen E. Survival in individuals with severe alpha 1-antitrypsin deficiency (PiZZ) in comparison to a general population with known smoking habits. *Eur Respir J* (2017) 50:1700198. doi: 10.1183/13993003.00198-2017
69. Hu B, Weng Y, Xia X-H, Liang X-j, Huang Y. Clinical advances of siRNA therapeutics. *J Gene Med* (2019) 21:e3097. doi: 10.1002/jgm.3097
70. Hu B, Zhong L, Weng Y, Peng L, Huang Y, Zhao Y, et al. Therapeutic siRNA: state of the art. *Signal Transduct Targeted Ther* (2020) 5:101. doi: 10.1038/s41392-020-0207-x
71. Chakraborty C, Sharma AR, Sharma G, Doss CGP, Lee SS. Therapeutic miRNA and siRNA: Moving from Bench to Clinic as Next Generation Medicine. *Mol Ther Nucleic Acids* (2017) 8:132–43. doi: 10.1016/j.omtn.2017.06.005
72. Yang P, Sun Z, Krowka MJ, Aubry MC, Bamlet WR, Wampfler JA, et al. Alpha1-antitrypsin deficiency carriers, tobacco smoke, chronic obstructive pulmonary disease, and lung cancer risk. *Arch Internal Med* (2008) 168:1097–103. doi: 10.1001/archinte.168.10.1097
73. Sun Z, Yang P. Role of imbalance between neutrophil elastase and alpha 1-antitrypsin in cancer development and progression. *Lancet Oncol* (2004) 5:182–90. doi: 10.1016/S1470-2045(04)01414-7
74. Rudnick DA, Perlmutter DH. Alpha-1-antitrypsin deficiency: a new paradigm for hepatocellular carcinoma in genetic liver disease. *Hepatology* (2005) 42:514–21. doi: 10.1002/hep.20815
75. Wu JY, Cheng CC, Wang JY, Wu DC, Hsieh JS, Lee SC, et al. Discovery of tumor markers for gastric cancer by proteomics. *PloS One* (2014) 9:e84158. doi: 10.1371/journal.pone.0084158
76. Xie LQ, Zhao C, Cai SJ, Xu Y, Huang LY, Bian JS, et al. Novel proteomic strategy reveal combined alpha1 antitrypsin and cathepsin D as biomarkers for colorectal cancer early screening. *J Proteome Res* (2010) 9:4701–9. doi: 10.1021/pr100406z
77. Guttman O, Freixo-Lima GS, Kaner Z, Lior Y, Rider P, Lewis EC. Context-Specific and Immune Cell-Dependent Antitumor Activities of alpha1-Antitrypsin. *Front Immunol* (2016) 7:559. doi: 10.3389/fimmu.2016.00559
78. Miyamoto Y, Akaike T, Maeda H. S-nitrosylated human alpha(1)-protease inhibitor. *Biochim Biophys Acta* (2000) 1477:90–7. doi: 10.1016/s0167-4838(99)00264-2
79. Dela Cruz CS, Tanoue LT, Matthay RA. Lung cancer: epidemiology, etiology, and prevention. *Clinics Chest Med* (2011) 32:605–44. doi: 10.1016/j.ccm.2011.09.001
80. Schwarz N, Tumpara S, Wrenger S, Ercetin E, Hamacher J, Welte T, et al. Alpha1-antitrypsin protects lung cancer cells from staurosporine-induced apoptosis: the role of bacterial lipopolysaccharide. *Sci Rep* (2020) 10:9563. doi: 10.1038/s41598-020-66825-w
81. Chang SH, Lee HJ, Kang B, Yu KN, Minai-Tehrani A, Lee S, et al. Methylmercury induces caspase-dependent apoptosis and autophagy in human neural stem cells. *J Toxicol Sci* (2013) 38:823–31. doi: 10.2131/jts.38.823
82. Delbridge AR, Grabow S, Strasser A, Vaux DL. Thirty years of BCL-2: translating cell death discoveries into novel cancer therapies. *Nat Rev Cancer* (2016) 16:99–109. doi: 10.1038/nrc.2015.17
83. Vince JE, De Nardo D, Gao W, Vince AJ, Hall C, McArthur K, et al. The Mitochondrial Apoptotic Effectors BAX/BAK Activate Caspase-3 and -7 to Trigger NLRP3 Inflammasome and Caspase-8 Driven IL-1beta Activation. *Cell Rep* (2018) 25:2339–53 e4. doi: 10.1016/j.celrep.2018.10.103
84. Wu CC, Lee S, Malladi S, Chen MD, Mastrandrea NJ, Zhang Z, et al. The Apaf-1 apoptosome induces formation of caspase-9 homo- and heterodimers with distinct activities. *Nat Commun* (2016) 7:13565. doi: 10.1038/ncomms13565
85. Gao W, Zhao J, Kim H, Xu S, Chen M, Bai X, et al. alpha1-Antitrypsin inhibits ischemia reperfusion-induced lung injury by reducing inflammatory response and cell death. *J Heart Lung Transplant* (2014) 33:309–15. doi: 10.1016/j.healun.2013.10.031
86. Hurley K, Lacey N, O'Dwyer CA, Bergin DA, McElvaney OJ, O'Brien ME, et al. Alpha-1 antitrypsin augmentation therapy corrects accelerated neutrophil apoptosis in deficient individuals. *J Immunol* (2014) 193:3978–91. doi: 10.4049/jimmunol.1400132
87. Toldo S, Seropian IM, Mezzaroma E, Van Tassell BW, Salloum FN, Lewis EC, et al. Alpha-1 antitrypsin inhibits caspase-1 and protects from acute myocardial ischemia-reperfusion injury. *J Mol Cell Cardiol* (2011) 51:244–51. doi: 10.1016/j.yjmcc.2011.05.003
88. Zhang B, Lu Y, Campbell-Thompson M, Spencer T, Wasserfall C, Atkinson M, et al. Alpha1-antitrypsin protects beta-cells from apoptosis. *Diabetes* (2007) 56:1316–23. doi: 10.2337/db06-1273
89. Petrache I, Fijalkowska I, Medler TR, Skirball J, Cruz P, Zhen L, et al. alpha-1 antitrypsin inhibits caspase-3 activity, preventing lung endothelial cell apoptosis. *Am J Pathol* (2006) 169:1155–66. doi: 10.2353/ajpath.2006.060058
90. Lockett AD, Van Demark M, Gu Y, Schweitzer KS, Sigua N, Kamocki K, et al. Effect of cigarette smoke exposure and structural modifications on the alpha-1 Antitrypsin interaction with caspases. *Mol Med* (2012) 18:445–54. doi: 10.2119/molmed.2011.00207
91. Wang J, Gou W, Kim DS, Strange C, Wang H. Clathrin-mediated Endocytosis of Alpha-1 Antitrypsin is Essential for its Protective Function

- in Islet Cell Survival. *Theranostics* (2019) 9:3940–51. doi: 10.7150/thno.31647
92. Nikolettoupolou V, Markaki M, Palikaras K, Tavernarakis N. Crosstalk between apoptosis, necrosis and autophagy. *Biochim Biophys Acta* (2013) 1833:3448–59. doi: 10.1016/j.bbamcr.2013.06.001
 93. Al-Omari M, Korenbaum E, Ballmaier M, Lehmann U, Jonigk D, Manstein DJ, et al. Acute-phase protein alpha1-antitrypsin inhibits neutrophil calpain I and induces random migration. *Mol Med* (2011) 17:865–74. doi: 10.2119/molmed.2011.00089
 94. Chang S-H, Cho K-C, Yu K-N, Hong S-H, Park S, Lee AY, et al. Alpha 1-antitrypsin activates lung cancer cell survival by acting on cap-dependent protein translation, vesicle-mediated transport, and metastasis. *Oncotarget* (2016). doi: 10.18632/oncotarget.10695
 95. Yang J, Liu X, Bhalla K, Kim CN, Ibrado AM, Cai J, et al. Prevention of apoptosis by Bcl-2: release of cytochrome c from mitochondria blocked. *Science* (1997) 275:1129–32. doi: 10.1126/science.275.5303.1129
 96. Fox JL, MacFarlane M. Targeting cell death signalling in cancer: minimising 'Collateral damage'. *Br J Cancer* (2016) 115:5–11. doi: 10.1038/bjc.2016.111
 97. Kihara A, Kabeya Y, Ohsumi Y, Yoshimori T. Beclin-phosphatidylinositol 3-kinase complex functions at the trans-Golgi network. *EMBO Rep* (2001) 2:330–5. doi: 10.1093/embo-reports/kve061
 98. Pattingre S, Tassa A, Qu X, Garuti R, Liang XH, Mizushima N, et al. Bcl-2 antiapoptotic proteins inhibit Beclin 1-dependent autophagy. *Cell* (2005) 122:927–39. doi: 10.1016/j.cell.2005.07.002
 99. Shin JY, Hong SH, Kang B, Minai-Tehrani A, Cho MH. Overexpression of beclin1 induced autophagy and apoptosis in lungs of K-rasLA1 mice. *Lung Cancer* (2013) 81:362–70. doi: 10.1016/j.lungcan.2013.05.009
 100. Bampton ET, Goemans CG, Niranjani D, Mizushima N, Tolkovsky AM. The dynamics of autophagy visualized in live cells: from autophagosome formation to fusion with endo/lysosomes. *Autophagy* (2005) 1:23–36. doi: 10.4161/auto.1.1.1495
 101. Kumar D, Shankar S, Srivastava RK. Rottlerin-induced autophagy leads to the apoptosis in breast cancer stem cells: molecular mechanisms. *Mol Cancer* (2013) 12:171. doi: 10.1186/1476-4598-12-171
 102. Laussmann MA, Passante E, Dussmann H, Rauen JA, Wurstle ML, Delgado ME, et al. Proteasome inhibition can induce an autophagy-dependent apical activation of caspase-8. *Cell Death Differ* (2011) 18:1584–97. doi: 10.1038/cdd.2011.27
 103. Liao A, Hu R, Zhao Q, Li J, Li Y, Yao K, et al. Autophagy induced by FTY720 promotes apoptosis in U266 cells. *Eur J Pharm Sci* (2012) 45:600–5. doi: 10.1016/j.ejps.2011.12.014
 104. Bento CF, Renna M, Ghislat G, Puri C, Ashkenazi A, Vicinanza M, et al. Mammalian Autophagy: How Does It Work? *Annu Rev Biochem* (2016) 85:685–713. doi: 10.1146/annurev-biochem-060815-014556
 105. Wild P, McEwan DG, Dikic I. The LC3 interactome at a glance. *J Cell Sci* (2014) 127:3–9. doi: 10.1242/jcs.140426
 106. Bjorkoy G, Lamark T, Brech A, Outen Z, Perander M, Overvatn A, et al. p62/SQSTM1 forms protein aggregates degraded by autophagy and has a protective effect on huntingtin-induced cell death. *J Cell Biol* (2005) 171:603–14. doi: 10.1083/jcb.200507002
 107. Sanchez-Martin P, Komatsu M. p62/SQSTM1 - steering the cell through health and disease. *J Cell Sci* (2018) 131:jcs222836. doi: 10.1242/jcs.222836
 108. Jung CH, Ro SH, Cao J, Otto NM, Kim DH. mTOR regulation of autophagy. *FEBS Lett* (2010) 584:1287–95. doi: 10.1016/j.febslet.2010.01.017
 109. Chen Y, McMillan-Ward E, Kong J, Israels SJ, Gibson SB. Oxidative stress induces autophagic cell death independent of apoptosis in transformed and cancer cells. *Cell Death Differ* (2008) 15:171–82. doi: 10.1038/sj.cdd.4402233
 110. Maiuri MC, Zalckvar E, Kimchi A, Kroemer G. Self-eating and self-killing: crosstalk between autophagy and apoptosis. *Nat Rev Mol Cell Biol* (2007) 8:741–52. doi: 10.1038/nrm2239
 111. Shimizu S, Kanaseki T, Mizushima N, Mizuta T, Arakawa-Kobayashi S, Thompson CB, et al. Role of Bcl-2 family proteins in a non-apoptotic programmed cell death dependent on autophagy genes. *Nat Cell Biol* (2004) 6:1221–8. doi: 10.1038/ncb1192
 112. Wang Y, Han R, Liang ZQ, Wu JC, Zhang XD, Gu ZL, et al. An autophagic mechanism is involved in apoptotic death of rat striatal neurons induced by the non-N-methyl-D-aspartate receptor agonist kainic acid. *Autophagy* (2008) 4:214–26. doi: 10.4161/auto.5369
 113. Cha-Molstad H, Yu JE, Feng Z, Lee SH, Kim JG, Yang P, et al. p62/SQSTM1/Sequestosome-1 is an N-recognition of the N-end rule pathway which modulates autophagosome biogenesis. *Nat Commun* (2017) 8:102. doi: 10.1038/s41467-017-00085-7
 114. Yan XY, Zhong XR, Yu SH, Zhang LC, Liu YN, Zhang Y, et al. p62 aggregates mediated Caspase 8 activation is responsible for progression of ovarian cancer. *J Cell Mol Med* (2019) 23:4030–42. doi: 10.1111/jcmm.14288
 115. Shapira MG, Khalif B, Lewis EC, Parola AH, Nathan I. Regulation of autophagy by alpha1-antitrypsin: "a foe of a foe is a friend". *Mol Med* (2014) 20:417–26. doi: 10.2119/molmed.2014.00054
 116. Oberley LW. Mechanism of the tumor suppressive effect of MnSOD overexpression. *Biomed Pharmacother* (2005) 59:143–8. doi: 10.1016/j.biopha.2005.03.006
 117. Sohrab S, Petrusca DN, Lockett AD, Schweitzer KS, Rush NI, Gu Y, et al. Mechanism of alpha-1 antitrypsin endocytosis by lung endothelium. *FASEB J* (2009) 23:3149–58. doi: 10.1096/fj.09-129304
 118. Subramaniam D, Zhou H, Liang M, Welte T, Mahadeva R, Janciauskiene S. Cholesterol rich lipid raft microdomains are gateway for acute phase protein, SERPINA1. *Int J Biochem Cell Biol* (2010) 42:1562–70. doi: 10.1016/j.biocel.2010.06.009
 119. Martinez-Outschoorn UE, Sotgia F, Lisanti MP. Caveolae and signalling in cancer. *Nat Rev Cancer* (2015) 15:225–37. doi: 10.1038/nrc3915
 120. Sahai E, Axtsurov I, Cukierman E, DeNardo DG, Egeblad M, Evans RM, et al. A framework for advancing our understanding of cancer-associated fibroblasts. *Nat Rev Cancer* (2020) 20:174–86. doi: 10.1038/s41568-019-0238-1
 121. Dabbagh K, Laurent GJ, Shock A, Leoni P, Papakrivopoulou J, Chambers RC. Alpha-1-antitrypsin stimulates fibroblast proliferation and procollagen production and activates classical MAP kinase signalling pathways. *J Cell Physiol* (2001) 186:73–81. doi: 10.1002/1097-4652(200101)186:1<73::AID-JCP1002>3.0.CO;2-Q
 122. Reina-Campos M, Shelton PM, Diaz-Meco MT, Moscat J. Metabolic reprogramming of the tumor microenvironment by p62 and its partners. *Biochim Biophys Acta - Rev Cancer* (2018) 1870:88–95. doi: 10.1016/j.bbcan.2018.04.010
 123. Valencia T, Kim JY, Abu-Baker S, Moscat-Pardos J, Ahn CS, Reina-Campos M, et al. Metabolic reprogramming of stromal fibroblasts through p62-mTORC1 signaling promotes inflammation and tumorigenesis. *Cancer Cell* (2014) 26:121–35. doi: 10.1016/j.ccr.2014.05.004
 124. Yoshida GJ, Azuma A, Miura Y, Orimo A. Activated Fibroblast Program Orchestrates Tumor Initiation and Progression; Molecular Mechanisms and the Associated Therapeutic Strategies. *Int J Mol Sci* (2019) 20:2256. doi: 10.3390/ijms20092256
 125. Guttman O, Yossef R, Freixo-Lima G, Rider P, Porgador A, Lewis EC. alpha1-Antitrypsin modifies general NK cell interactions with dendritic cells and specific interactions with islet beta-cells in favor of protection from autoimmune diabetes. *Immunology* (2014) 144:530–9. doi: 10.1111/imm.12403
 126. Lewis EC. Expanding the clinical indications for alpha(1)-antitrypsin therapy. *Mol Med* (2012) 18:957–70. doi: 10.2119/molmed.2011.00196
 127. Churg A, Wang X, Wang RD, Meixner SC, Prydzial EL, Wright JL. Alpha1-antitrypsin suppresses TNF-alpha and MMP-12 production by cigarette smoke-stimulated macrophages. *Am J Respir Cell Mol Biol* (2007) 37:144–51. doi: 10.1165/rcmb.2006-0345OC

Conflict of Interest: The authors declare that the research was conducted in the absence of any commercial or financial relationships that could be construed as a potential conflict of interest.

Copyright © 2021 Janciauskiene, Wrenger, Günzel, Gründing, Golpon and Welte. This is an open-access article distributed under the terms of the Creative Commons Attribution License (CC BY). The use, distribution or reproduction in other forums is permitted, provided the original author(s) and the copyright owner(s) are credited and that the original publication in this journal is cited, in accordance with accepted academic practice. No use, distribution or reproduction is permitted which does not comply with these terms.



LRIG3 Suppresses Angiogenesis by Regulating the PI3K/AKT/VEGFA Signaling Pathway in Glioma

Chenghao Peng^{1,2}, Hanmin Chen¹, Youwei Li¹, Hang Yang³, Peizhong Qin⁴, Baojun Ma⁵, Qihong Duan², Baofeng Wang¹, Feng Mao¹ and Dongsheng Guo^{1*}

¹ Department of Neurosurgery, Tongji Hospital, Tongji Medical College, Huazhong University of Science and Technology, Wuhan, China, ² Department of Biochemistry and Molecular Biology, School of Basic Medicine, Huazhong University of Science and Technology, Wuhan, China, ³ Department of Neurology, Union Hospital, Tongji Medical College, Huazhong University of Science and Technology, Wuhan, China, ⁴ Department of Medical Genetics, School of Basic Medicine, Tongji Medical College, Huazhong University of Science and Technology, Wuhan, China, ⁵ Department of Neurosurgery, The Second Affiliated Hospital of Nantong University, Nantong University, Nantong, China

OPEN ACCESS

Edited by:

Marco Rossi,
University of Catanzaro, Italy

Reviewed by:

Swapna Chaudhuri,
Chittaranjan National Cancer
Institute, India
Shanmugarajan Krishnan,
Massachusetts General Hospital,
United States

*Correspondence:

Dongsheng Guo
Tjguodongsheng@163.com

Specialty section:

This article was submitted to
Cancer Molecular Targets
and Therapeutics,
a section of the journal
Frontiers in Oncology

Received: 25 October 2020

Accepted: 05 January 2021

Published: 25 February 2021

Citation:

Peng C, Chen H, Li Y, Yang H, Qin P,
Ma B, Duan Q, Wang B, Mao F and
Guo D (2021) LRIG3 Suppresses
Angiogenesis by Regulating the
PI3K/AKT/VEGFA Signaling
Pathway in Glioma.
Front. Oncol. 11:621154.
doi: 10.3389/fonc.2021.621154

High levels of microvessel density (MVD) indicate poor prognosis in patients with malignant glioma. Leucine-rich repeats and immunoglobulin-like domains (LRIG) 3, a potential tumor suppressor, plays an important role in tumor progression and may serve as a biomarker in many human cancers. However, its role and underlying mechanism of action in glioma angiogenesis remain unclear. In the present study, we used loss- and gain-of-function assays to show that LRIG3 significantly suppressed glioma-induced angiogenesis, both *in vitro* and *in vivo*. Mechanistically, LRIG3 inhibited activation of the PI3K/AKT signaling pathway, downregulating vascular endothelial growth factor A (VEGFA) in glioma cells, thereby inhibiting angiogenesis. Notably, LRIG3 had a significant negative correlation with VEGFA expression in glioma tissues. Taken together, our results suggest that LRIG3 is a novel regulator of glioma angiogenesis and may be a promising option for developing anti-angiogenic therapy.

Keywords: glioma, angiogenesis, LRIG3, vascular endothelial growth factor A, PI3K/AKT

INTRODUCTION

Currently, glioblastoma (GBM) represents the most common primary brain tumor in adults and carries a particularly poor prognosis (1). Despite the use of multimodal treatments, such as maximal surgical resection, chemotherapy, and radiotherapy, the average survival time of GBM patients, following diagnosis, is only 12 to 15 months (2, 3). This poor prognosis is mainly attributed to aberrant angiogenesis, high invasiveness, and therapeutic resistance.

Angiogenesis, a process in which new blood vessels develop from the existing vasculature, has been implicated in various physiological and pathological changes, such as tumor, development, and wound healing (4). Additionally, abnormal angiogenesis reportedly leads to proliferation, survival, and metastasis of tumors. High tumor microvessel density (MVD) has been shown to be a hallmark of GBM, with higher MVD levels associated with worse prognosis in patients (5, 6). Glioma

angiogenesis entails the coordination of multiple pro- and anti-angiogenic molecules, such as vascular endothelial growth factor (VEGF) family, endostatin, and angiostatin (7). An imbalance among these factors results in abnormal angiogenesis. To date, the precise mechanisms underlying the regulation of these angiogenesis-related factors are not fully understood.

The human leucine-rich repeats and immunoglobulin-like domains (LRIG) gene family comprises LRIG1, LRIG2, and LRIG3, which encode single-pass transmembrane proteins. LRIG genes are clinically relevant prognostic indicators in several human cancers and play various roles in tumor cell proliferation, migration, invasion, apoptosis, and chemosensitivity (8, 9). LRIG3 was the last gene to be discovered in this family and is frequently downregulated in human cancers (10–12). In fact, LRIG3 acts as a tumor suppressor in GBM, where it modulates proliferation, migration, and invasion of glioma cells by targeting the EGFR and MET signaling pathways (13, 14). Moreover, LRIG3 expression is significantly higher in low-grade gliomas than in high-grade gliomas (grades III and IV), and LRIG3 upregulation suggests a better prognosis in malignant glioma patients (14). However, the actual molecular mechanisms underlying LRIG3's role in angiogenesis are poorly understood.

In this study, we demonstrated that LRIG3 acted as an anti-angiogenic gene, inhibiting VEGFA *via* the PI3K/AKT signaling pathway. Our results suggested that LRIG3 is a potential target for the future development of therapeutic strategies against glioma angiogenesis.

MATERIALS AND METHODS

Cell Culture and Reagents

Human glioma cell lines, U87 and U251, were purchased from the American Type Culture Collection (ATCC; Manassas, VA, USA). The Human umbilical vein endothelial cell (HUVEC) line was purchased from the Cell Bank at the Shanghai Branch of Chinese Academy of Sciences (Shanghai, China). Glioma cells were cultured in Dulbecco's modified Eagle's medium (DMEM; Gibco), supplemented with 10% fetal bovine serum (FBS; Gibco) and 1% penicillin/streptomycin. HUVECs were cultured in Endothelial Cell Growth Medium-2 (EBM-2) Bulletkit (Lonza, Walkersville, MD, USA). All cells were maintained in a humidified incubator at 37°C and 5% CO₂. PI3K inhibitor LY294002 (Cat #S1105) and MEK inhibitor PD98059 (Cat #S1177) were purchased from Selleck (Houston, TX, USA).

Sample Collection and Study Approval

Twenty-eight glioma tissue samples were postoperatively obtained from patients at the Department of Neurosurgery, Tongji Hospital. Histological features of all specimens were confirmed by pathologists, according to the WHO criteria. A summary of patient characteristics is shown in **Supplementary Table S1**. This study was reviewed and approved by the Research Ethics Committee of Tongji Hospital, Tongji Medical College, Huazhong University of Science and Technology. Written informed consent was obtained from all participants before inclusion.

Conditioned Medium (CM)

Glioma cells were routinely cultured for 48 h, confluent cultures washed twice with serum-free medium, then incubated in serum-free EBM-2 medium for 24 h. The supernatant was harvested after conditioning, centrifuged at 2,000g at 4°C for 15 min, filtered through 0.22 µm Millipore filters, then supplemented with 0.5% serum and 1 ng/ml bFGF. The contents were frozen at –20°C until required.

Construction and Transduction of Lentiviral Vector

Lentiviral vectors were produced as previously described (15). Briefly, pLVX-DsRed-LRIG3 was constructed and transduced into U87 and U251 together with empty vector pLVX-DsRed, using Clontech's Lenti-XTM high-titer lentiviral packaging systems (Clontech Company, USA). The generated constructs were named LRIG3 and vector control groups, respectively.

siRNA Transfection

We adopted a siRNA-based approach to downregulate LRIG3. Summarily, three siRNA duplexes were designed to target LRIG3 and synthesized by GenePharma (Shanghai, China): siLRIG3-1 (sense (5'-3'): CCUUGAAACUUUGGACCUUTT; antisense (5'-3'): AAGGUCCAAAGUUUCAAGGTT), siLRIG3-2 (sense (5'-3'): GCUGGACCAUAACAACCUATT; antisense (5'-3'): UAGGUUGUUAUGGUCCAGCTT), siLRIG3-3 (sense (5'-3'): GGAGUAUACCACCAUCCUUTT; antisense (5'-3'): AAGGAUGGUGGUUAUCUCCTT). Cells were transiently transfected with the three siRNA duplexes (each 25 pmol) using Lipofectamine RNAiMAX transfection reagent (Thermo Fisher Scientific, USA) according to the manufacturer's instructions. After 48 h, RNA and proteins were isolated from the cells, then used to determine gene and protein expression *via* qRT-PCR and western blot assay, respectively.

Tube Formation Assay

Matrigel (10 mg/ml; 200 µl; BD Biosciences, CA, USA) was added into wells of a 24-well plate and polymerized for 30 min at 37°C. Thereafter, HUVECs were suspended in the CM, at a density of 1×10⁵/ml, then 200 µl of the cell suspension was added to each well followed by a 12-h incubation at 37°C and 5% CO₂. Capillary tube structures were observed, and representative images were photographed under a microscope (Carl Zeiss, Jena, Germany) at ×100 final magnification. The degree of tube formation was verified relative to the formation of tube length.

Transwell Migration Assay

Migration assays were performed using transwell chambers according to the manufacturer's protocol (Corning, USA). Briefly, CM was added to the lower chamber well to stimulate migration, homogeneous single-cell suspensions (2 × 10⁴/well) added to the upper chambers, then incubated for 24 h. Non-migrating cells were removed from the top well using a cotton swab, bottom cells fixed with 4% paraformaldehyde, and stained with 0.1% crystal violet. The migration rates were quantified under a microscope by counting migrated cells in five random

fields per well ($\times 100$ magnification). All assays were performed in sextuplicate and repeated at least three times.

Wound Healing Assay

Approximately 3×10^5 HUVECs were first seeded in 6-well dishes. When the monolayer culture reached about 90% confluency, a scratch wound was marked using a 200- μ l pipette tip, and all floating cells were washed off using PBS. Cells were cultured in CM at 37°C with 5% CO₂, then wound areas captured under a microscope (Carl Zeiss, Jena, Germany) at different time points to record the wound width.

3-(4, 5-Dimethyl-2-thiazolyl)-2, 5-diphenyl-2-H-tetrazolium Bromide (MTT) Assay

HUVECs growth and responsiveness to CM were determined using MTT assays. Summarily, cells (2×10^3 /well) were seeded into 96-well plates and cultured with CM for 24, 48, 72, 96, and 120 h. 20 μ l MTT reagent (5 mg/ml; Beyotime, Shanghai, China) was added to each well at the respective time point, and the plates incubated for 4 h at 37°C. Thereafter, the medium was replaced with 150 μ l of dimethyl sulfoxide (Sigma-Aldrich, USA), and absorbance was measured at 570 nm, with 630 nm used as the reference wavelength. All assays were performed in sextuplicate and repeated at least three times.

Western Blot Assay

Western blot assay was performed as previously described (16). Briefly, cells were first lysed in RIPA buffer, then equal amounts of protein separated on an 8 or 10% SDS-PAGE followed by electrotransfer onto a polyvinylidene difluoride membrane (Millipore, USA). The membranes were blocked, for 2 h, with 5% nonfat milk and immunoblotted with primary antibodies. After incubation with the appropriate secondary antibody, the membranes were visualized using the enhanced chemiluminescence detection system (BIO-RAD, USA). Immunoreactive bands were quantified using the densitometric analysis software (ImageJ, USA). Primary antibodies against LRIG3 (Cat #AF3495, R&D Systems), AKT (Cat #2920, Cell Signaling Technology), p-AKT (Ser473) (Cat #4060, Cell Signaling Technology), ERK (Cat #4696, Cell Signaling Technology), p-ERK (Thr202/Tyr204) (Cat #4370, Cell Signaling Technology), VEGFA (Cat #66828-1-Ig, Proteintech, Wuhan, China), and GAPDH (Cat #ab8245, Abcam) were used for Western blot assay. GAPDH was used as an internal control.

RNA Extraction and Quantitative Real-Time PCR (qRT-PCR)

Total RNA was extracted using the TRIzol reagent (Takara, Japan), then reverse transcribed to cDNA according to the instructions of the PrimeScript reverse transcriptase kit (Takara, Japan). qRT-PCR was performed using the TB Green™ Premix Ex Taq™ II (Takara, Japan) on an ABI 7500 real-time PCR system (Applied Biosystems, Foster City, CA, USA). Relative expression of target genes was calculated by $2^{-\Delta\Delta Ct}$ method, with GAPDH included as the reference gene. Experiments were performed in triplicate. All primer sequences are listed in **Supplementary Table S2**.

Enzyme-Linked Immunosorbent Assay (ELISA)

VEGFA concentrations in CM were measured according to the manufacturer's instructions of a commercial ELISA kit (Cat #DVE00) from R&D Systems.

Intradermal Angiogenesis Assay

Intradermal angiogenesis assay was performed as previously described (17). Briefly, male BALB/c nude mice (4–5 weeks old; $n = 6$ /group) were intradermally injected at the ventral skin surface with 1×10^6 tumor cells in 100 μ l PBS supplemented with 2% serum. The mice were sacrificed five days after tumor cell injection, then tumor-inoculated skin dissected and photographed using a digital camera. Tumor-directed capillaries were quantified by counting the number of newly formed blood vessels around the tumor-inoculated site.

Orthotopic Xenograft Models

Orthotopic xenograft models were established as previously described (16). Summarily, cells stably expressing LRIG3 or control cells (5×10^5) were first intracranially injected into male BALB/c nude mice (4–5 weeks old) ($n = 6$ /group), then kinetics of tumor formation estimated by T2-weighted MRI after every five days. PET/CT scanning was performed to evaluate blood flow changes in orthotopic tumors, when tumor growth was angiogenesis dependent corresponding to tumor volumes of 8 to 12 mm³ (18, 19). Thereafter, mice were anesthetized and perfused with 4% PFA, their brains harvested and embedded in paraffin. Quantification of MVD was performed as previously described (20). Briefly, areas of highest microvascular density were examined and counted under a microscope at $\times 100$ magnification. Results were expressed as the mean number of vessels \pm standard deviations (SD) per high power field ($\times 100$). All animal experiments were conducted in accordance with the guidelines of the Institutional Animal Care and Use Committee. All animal protocols used in this study were approved by the Ethical Committee of Tongji Hospital, Tongji Medical College, Huazhong University of Science and Technology.

Magnetic Resonance Imaging (MRI) of Orthotopic Mouse Tumors

MRI was performed on a 7 T horizontal bore Bruker small animal scanner. Summarily, mice were anesthetized using 2.5% isoflurane in 100% O₂, and maintained with 1% to 1.5% isoflurane in 100% O₂ delivered *via* a nose cone. Images were obtained using a T2-3D-RARE sequence (effective TE = 72 ms). Tumor sizes were determined using Amira v5.6.0 (FEI, USA).

PET/CT Scanning and Data Acquisition

PET/CT scanning was performed as previously described (21). Briefly, mice were anesthetized with 2% isoflurane, then intravenously injected with approximately 200 ± 10 μ Ci ¹³N-ammonia (¹³N-NH₃-H₂O). After 5 min of ¹³N-NH₃-H₂O uptake, the mice were anesthetized with 2% isoflurane and placed on a scanning bed. PET/CT images were obtained with the static mode for 5 min, followed by CT scan on the fast mode by the

TransPET Discoverist 180 system (Raycan Technology Co., Ltd, Suzhou, China). The PET images were reconstructed using the three-dimensional (3D) OSEM method with a voxel size of $0.5 \times 0.5 \times 0.5 \text{ mm}^3$, whereas CT images were reconstructed using the FDK algorithm with $256 \times 256 \times 256$ matrix. Images were displayed using the Pmod (Pmod Technologies LLC, Switzerland) Software, and their mean standardized uptake value (SUV) was calculated using the following formula: mean pixel value with the decay-corrected region-of-interest activity ($\mu\text{Ci/kg}$)/(injected dose [μCi]/weight [kg]).

Immunohistochemistry (IHC)

Immunohistochemical assays were performed on glioma and mouse xenograft tumor tissues as previously described (14). Expression levels of labeling were stratified and scored according to the following grading system: staining extensity was categorized as 1 ($\leq 10\%$ positive cells), 2 ($< 10\%$ and $\leq 30\%$ positive cells), 3 (< 30 and $\leq 50\%$ positive cells) or 4 ($> 50\%$ positive cells), whereas staining intensity was categorized as 0 (negative), 1 (weak), 2 (moderate) or 3 (strong). An overall score (0–12) was calculated for each case by multiplying the staining extensity with intensity score. Each sample was separately examined, then scored by two pathologists. In case of discrepancies in the scores, a discussion was held to reach a consensus.

Statistical Analysis

All data, from at least three independent experiments, were expressed as means \pm SD. Comparisons between groups were performed using a Student's *t*-test. The relationship between LRIG3 levels and VEGFA expression was analyzed using a Pearson's correlation analysis. All statistical analyses were performed using SPSS 18.0 statistical software package (IBM Corp, USA), with data followed by $p < 0.05$ considered statistically significant.

RESULTS

Ectopic Expression of LRIG3 Represses Glioma Cell-Promoted Angiogenesis *In Vitro*

To validate the effect of LRIG3 on angiogenesis, we performed *in vitro* gain-of-function analysis by overexpressing LRIG3 with a lentiviral vector in U87 and U251 cells. Western blots confirmed altered LRIG3 expression in glioma cells (Figure 1A). The wound healing assays and transwell assays revealed that ectopic expression of LRIG3 in U87 and U251 significantly suppressed the migration of HUVECs (Figures 1B, C). In addition, tube formation assay revealed that CM derived from

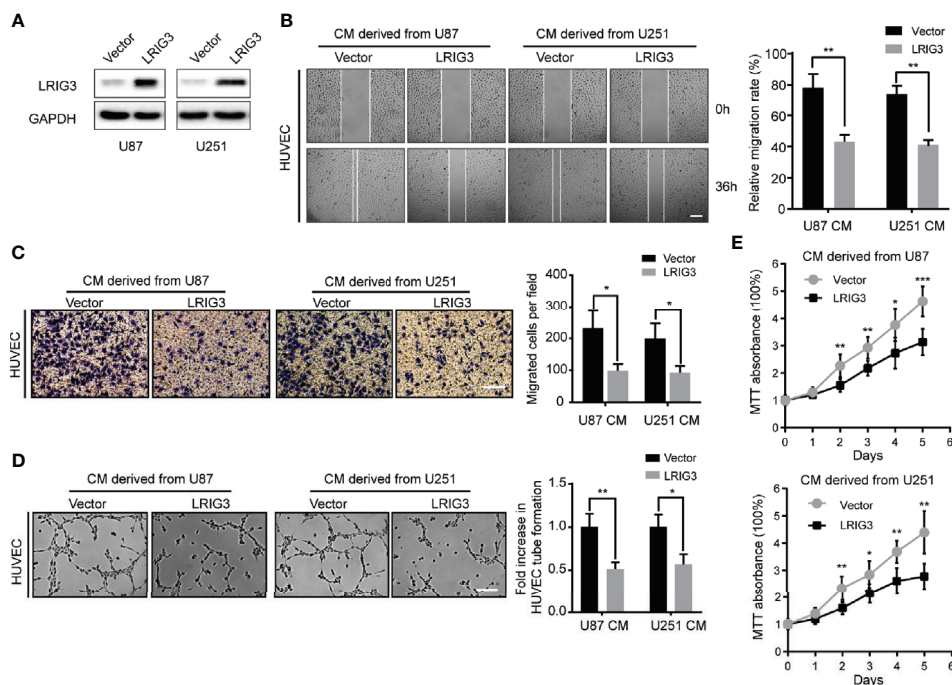


FIGURE 1 | Ectopic expression of LRIG3 reduces the pro-angiogenic activity of glioma cells *in vitro*. **(A)** Western blots showing levels of LRIG3 expression in the vector control and LRIG3-transduced glioma cells. GAPDH was used as an internal control. **(B)** Representative images (left) and quantification (right) of wound healing assays in HUVECs treated with CM derived from the vector control or LRIG3-transduced glioma cells. **(C)** Representative images (left) and quantification (right) of transwell migration assays of HUVECs treated with the indicated CM. **(D)** Representative images (left) and quantification (right) of HUVECs formed tube-like structures on Matrigel-coated plates with CM derived from the vector control or LRIG3-transduced glioma cells. **(E)** HUVEC viability was determined using the MTT assay. HUVECs were treated with CM derived from the indicated cells for the specific number of days. Data are means \pm SD of 3 replicates. * $p < 0.05$; ** $p < 0.01$; *** $p < 0.001$. CM, conditioned medium.

LRIG3 overexpressed cells significantly inhibited HUVECs tube formation relative to CM from vector control-infected cells (**Figure 1D**). Furthermore, MTT proliferation assay revealed significantly lower cell viability of HUVEC following treatment with CM derived from LRIG3 overexpressed glioma cells (**Figure 1E**). Collectively, these results suggest that overexpressing LRIG3 suppresses glioma cell-promoted angiogenesis *in vitro*.

LRIG3 Knockdown Enhances Pro-angiogenic Activity of Glioma Cells *In Vitro*

Since gain-of-LRIG3 could inhibit glioma cell-induced angiogenesis, we hypothesized that loss of LRIG3 could enhance the pro-angiogenic activity of glioma cells. Consequently, we transfected U87 and U251 cells with LRIG3 or control siRNAs (**Figure 2A**). Results indicated that CM derived from LRIG3 knockdown cells significantly increased the migration (**Figures 2B, C**), tube formation (**Figure 2D**), and cell viability (**Figure 2E**) of HUVECs relative to CM from siRNAs control infected cells. Taken together, these findings indicate that silencing LRIG3 enhances the pro-angiogenic activity of glioma cells *in vitro*.

LRIG3 Inhibits the Ability of Gliomas to Induce Angiogenesis *In Vivo*

We further investigated the role of LRIG3 in regulating the angiogenesis of glioma *in vivo* using intradermal angiogenesis assays and found that U87 cells stably overexpressing LRIG3 exhibited a significantly lower number of tumor-directed capillaries relative to cells transfected with the control vector (**Figures 3A, B**). Conversely, siLRIG3-transfected U87 cells attracted significantly more blood vessels compared to cells transfected with control siRNAs (**Figures 3A, B**). Parallel experiments performed in U251 cells revealed a similar trend. Next, we used intracranial xenograft mice to assess the effect of LRIG3 on angiogenesis and monitored tumor progression using MRI (**Figure 3C**). A $^{13}\text{N-NH}_3\text{-H}_2\text{O}$ PET scan performed on day 14 after tumor cell inoculation revealed that xenografts carrying LRIG3-overexpressing U87 cells exhibited a significantly lower $^{13}\text{N-NH}_3\text{-H}_2\text{O}$ uptake tumor/reference (T/R) ratio relative to the xenografts carrying control infected cells (**Figures 3C, D**). Parallel histological analysis of orthotopic xenograft tumors revealed significantly lower MVD in tumors formed by LRIG3-

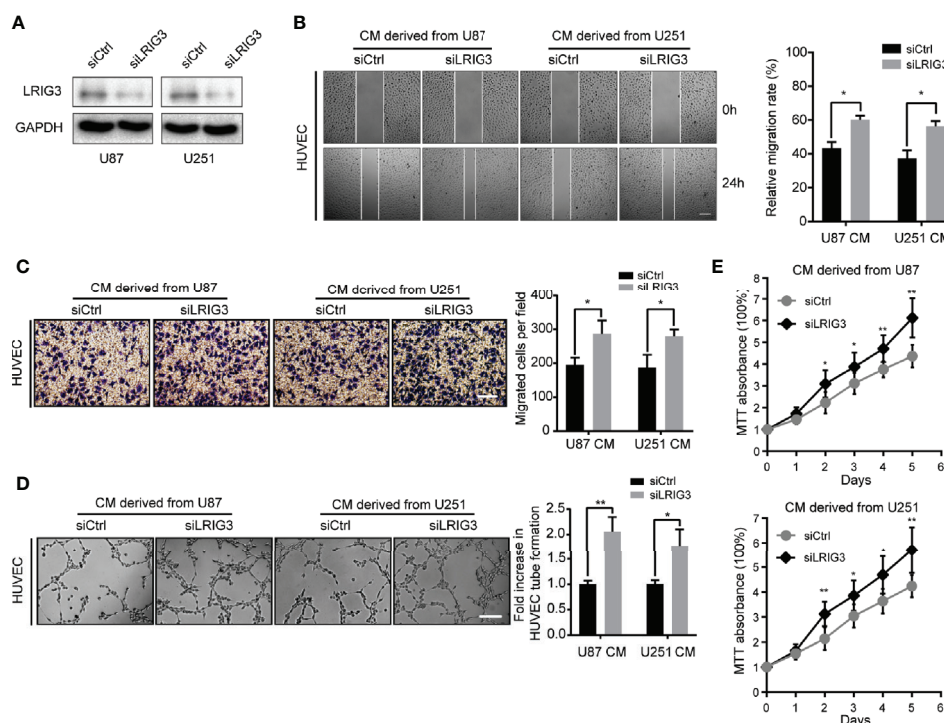


FIGURE 2 | Downregulation of LRIG3 enhances the pro-angiogenic activity of glioma cells *in vitro*. **(A)** Western blot analysis of LRIG3 expression in the siRNA control and LRIG3-silenced glioma cells. GAPDH was used as an internal control. **(B)** Representative images (left) and quantification (right) of wound healing assays of HUVECs treated with CM derived from the siRNA control or LRIG3-silenced glioma cells. **(C)** Representative images (left) and quantification (right) of transwell migration assays in HUVECs treated with the indicated CM. **(D)** Representative images (left) and quantification (right) of HUVECs formed tube-like structures on Matrigel-coated plates with CM derived from the siRNA control cells or LRIG3-silenced glioma cells. **(E)** HUVEC viability was determined using the MTT assay. HUVECs were treated with CM derived from the indicated cells for the specific number of days. Data are presented as means \pm SD of 3 independent replicates. * $p < 0.05$; ** $p < 0.01$. CM, conditioned medium.

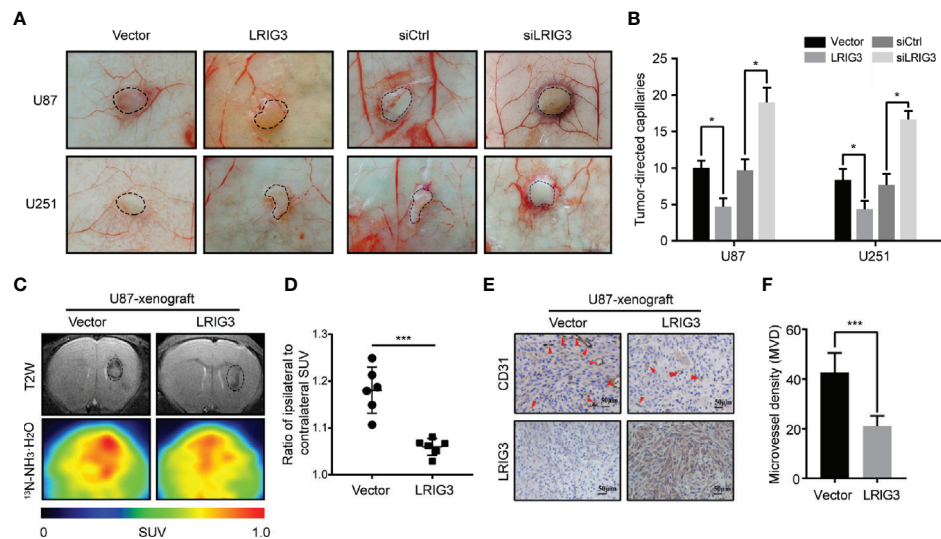


FIGURE 3 | LRIG3 affects the ability of gliomas to induce angiogenesis *in vivo*. Representative images (A) and quantification graphs (B) of the intradermal glioma tumors showing tumor-directed capillaries under different conditions: U87 and U251 cells transfected with the control vector and LRIG3; U87 and U251 cells transfected with the control and LRIG3 siRNAs. Dashed circles within the images show the tumor location. (C) Representative MRI and ^{15}N -H $_2$ O PET scan images of intracranial xenografts bearing LRIG3-overexpressing U87 cells or control cells, 14 days after tumor cell inoculation. (D) SUV ratio for the tumor to reference region (T/R) was used to determine the value for angiogenesis in the tumor, $n = 6/\text{group}$. (E) IHC analysis of LRIG3 and CD31 expression in intracranial xenografts generated from LRIG3-overexpressed U87 or control cells. (F) Quantification of CD31+ microvessel density in intracranial xenografts generated from LRIG3-overexpressed U87 or control cells. Data are means \pm SD of 3 independent replicates. $*p < 0.05$; $***p < 0.001$. MVD, microvessel density; PET, positron emission tomography; SUV, standardized uptake value; T/R, tumor/reference.

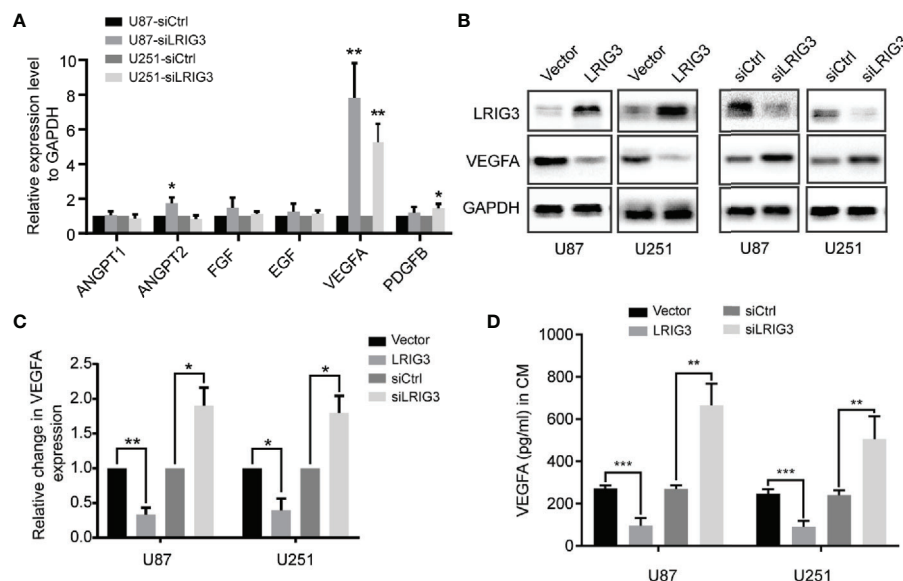


FIGURE 4 | LRIG3 inhibited glioma angiogenesis by regulating VEGFA expression. (A) qRT-PCR analysis targeting angiogenic factors in glioma cells transduced with LRIG3 and control siRNAs. (B) Western blot analysis of VEGFA, LRIG3, and GAPDH. (C) Integrated density of the bands was normalized to GAPDH in LRIG3 knockdown or overexpression glioma cells. (D) Levels of VEGFA protein in the CM from glioma cells with LRIG3 knockdown or overexpression were detected by ELISA. Data are means \pm SD of 3 independent replicates. $*p < 0.05$; $**p < 0.01$; $***p < 0.001$. CM, conditioned medium.

overexpressing U87 cells (Figures 3E, F). These results strongly indicate that LRIG3 overexpression suppresses glioma angiogenesis *in vivo*.

LRIG3 Modulates VEGFA Expression via the PI3K/AKT Signaling Pathway

To investigate the underlying mechanism, we performed qRT-PCR to quantify levels of mRNAs for angiogenesis-related factors in the glioma cells following LRIG3 knockdown or overexpression. Results showed that LRIG3 knockdown significantly elevated levels of VEGFA in U87 and U251 cells, whereas its overexpression significantly repressed these levels (Figure 4A, Supplementary Figures 1A–C). Moreover, western blots and ELISA results indicated that levels VEGFA protein were consistently upregulated and downregulated in LRIG3-knockdown and LRIG3-overexpressing glioma cells, respectively, compared to control cells (Figures 4B–D). These results indicate that VEGFA plays a critical effector role in LRIG3-regulated angiogenesis.

Our previous study has shown that LRIG3 functions as a tumor suppressor by attenuating phosphorylation of the ERK and AKT signaling pathways (13). Moreover, activation of these pathways has been associated with increased expression levels of angiogenic

factors, such as ANGPT2, COX2, and VEGFA, in glioma (22). To ascertain the pathway responsible for LRIG3-mediated VEGFA expression, we used the specific inhibitors of the ERK (PD98059) and AKT (LY294002) pathways to block their activation in glioma cells following LRIG3 knockdown. As shown in Figures 5A–C, there was no difference in basal ERK levels in U87 and U251 when PD98059 was added. However, the increased p-ERK level upon LRIG3 silencing was reduced on PD98059 addition. Besides, the decrease in p-Akt after LY294002 treatment was more pronounced in U87 as compared to U251. Moreover, the results indicated that inhibition of the AKT, not the ERK pathway, caused changes in VEGFA expression. Correspondingly, results from functional tests of HUVECs incubated with the indicated CM showed consistent results (Figures 5D–F). Taken together, these results affirm that LRIG3 modulates VEGFA expression *via* the PI3K/AKT signaling pathway.

Clinical Relevance of LRIG3, p-AKT, and VEGFA Expression in Gliomas

Finally, we validated the association between LRIG3 with p-AKT, and VEGFA in patients using IHC staining of these proteins in 28 glioblastoma specimens. Results revealed a significant

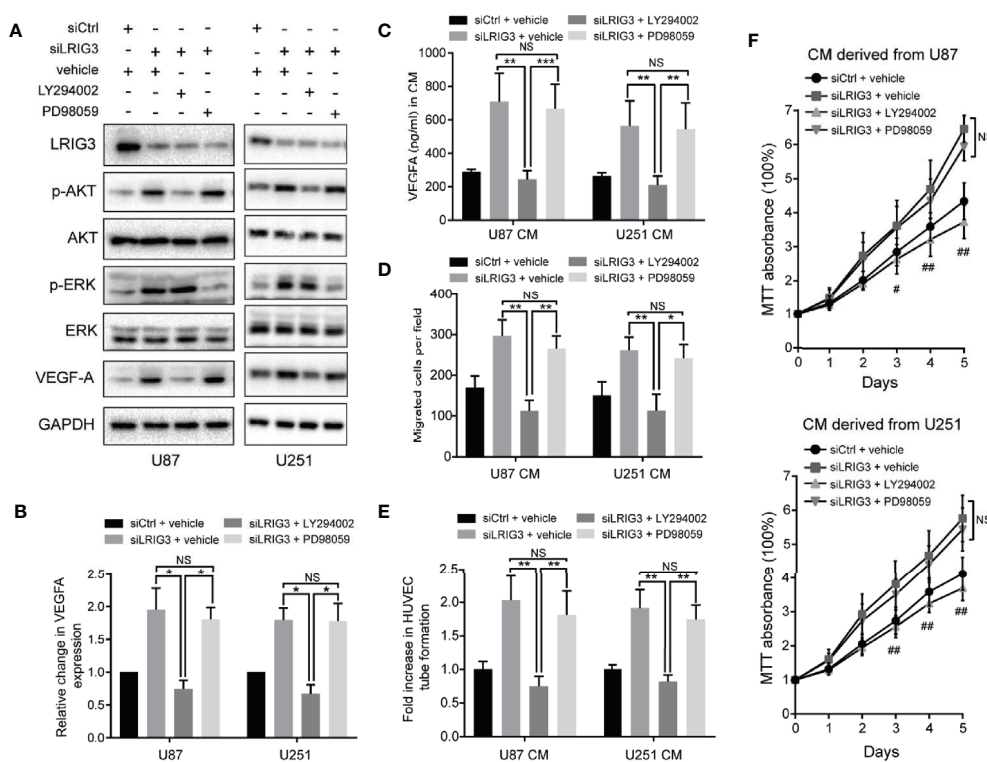


FIGURE 5 | LRIG3 modulates VEGFA expression via the PI3K/AKT signaling pathway. Western blots showing LRIG3, p-AKT, AKT, p-ERK, ERK, and VEGFA (A) alongside GAPDH (B) in the indicated glioma cells treated with the pathway inhibitors LY294002 (25μM), PD98059 (10μM), or DMSO vehicle for 24 h. (C) Levels of VEGFA protein in the CM from the indicated glioma cells were detected by ELISA. (D) Transwell migration assays in HUVECs treated with the indicated CM. (E) HUVECs formed tube-like structures with the indicated CM. (F) Cell viability of HUVECs was determined using the MTT assay. HUVECs were treated with the CM derived from the indicated cells for the specific number of days. Data are means ± SD of 3 independent replicates. * $p < 0.05$; ** $p < 0.01$; *** $p < 0.001$; # $p < 0.05$, siLRIG3 + LY294002 versus siLRIG3 + vehicle and siLRIG3 + PD98059; ## $p < 0.01$, siLRIG3 + LY294002 versus siLRIG3 + vehicle and siLRIG3 + PD98059. CM, conditioned medium.

correlation between LRIG3 and other proteins across these specimens. Specifically, tumors with high LRIG3 levels tended to express low levels of p-AKT and VEGFA, whereas the reverse was true for tumors with low LRIG3 levels (**Figures 6A, B**). Western blots corroborated the IHC results, with LRIG3 levels also strongly correlating with those of VEGFA in 10 freshly collected clinical glioma samples (**Figure 6C**). Together, these results affirmed the clinical relevance of the LRIG3/PI3K/AKT/VEGFA axis and confirmed these proteins play a vital role in the regulation of glioblastoma angiogenesis.

DISCUSSION

GBM, the most malignant brain tumor, is characterized by extensive neovascularization (23). Abnormal angiogenesis in

glioma is considered an essential factor for metastasis and resistance of chemoradiotherapy (24, 25). Previously, we demonstrated that LRIG3 is a critical tumor suppressor in glioma (13). However, its role in glioma angiogenesis remains unclear. Herein, we identified an anti-angiogenic signature for LRIG3 and showed that its presence downregulates VEGFA both *in vitro* and *in vivo*. Stepwise investigations revealed that the PI3K/AKT pathway has a major effect on the LRIG3-mediated VEGFA expression.

The LRIG gene family was discovered in a research on EGFR, which plays a critical role in cancer progression (26). The human LRIG proteins have similar structures: a signal peptide, 15 tandem leucine-rich repeats (LRRs), three immunoglobulin-like domains, a transmembrane segment, and an intracellular domain (27). Despite their structural similarity, they may have

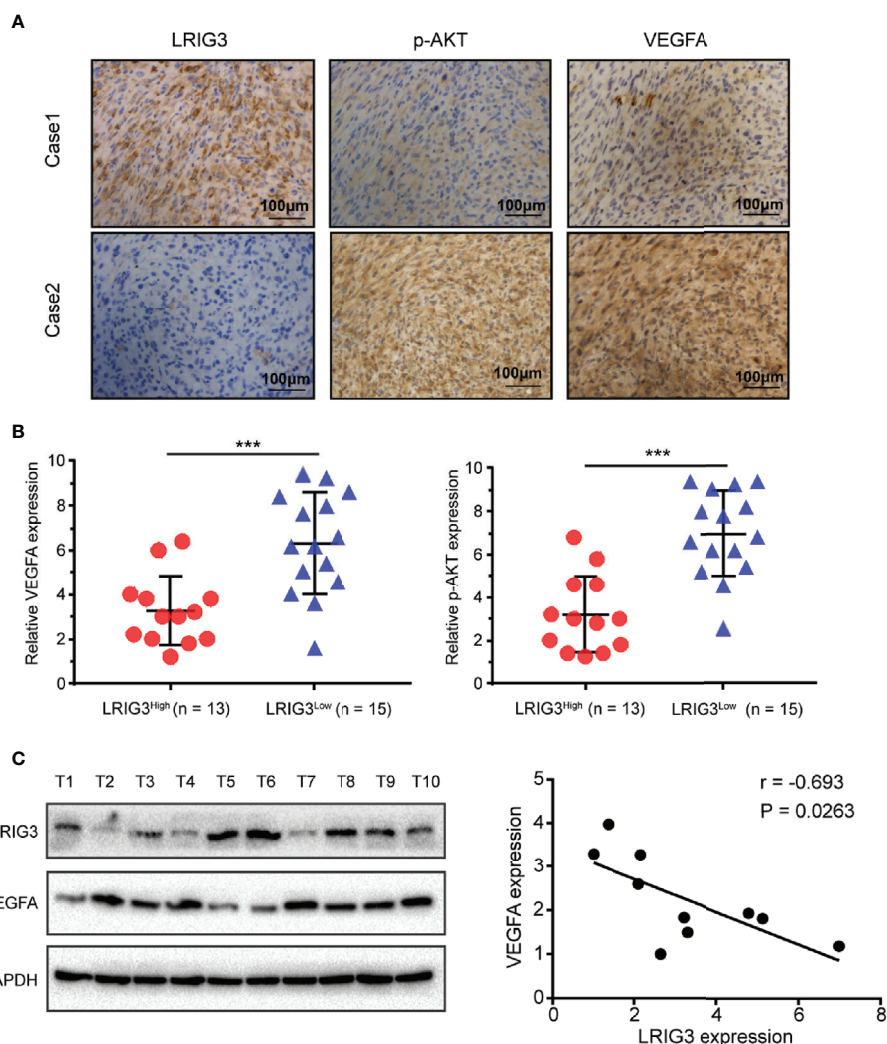


FIGURE 6 | Clinical relevance of LRIG3, p-AKT, and VEGFA expression in gliomas. **(A)** IHC staining targeting LRIG3, p-AKT, and VEGFA in two representative GBM specimens. Brown staining, positive immunoreactivity. **(B)** Relative levels of LRIG3, p-AKT, and VEGFA proteins in GBM specimens (with low and high LRIG3 expression levels in 28 GBM patients). **(C)** Expression analysis (left) and correlation (right) between LRIG3 and VEGFA expression in 10 freshly collected human glioma samples. Data are means \pm SD of 3 independent replicates. *** $p < 0.001$.

different biological functions. LRIG1 binds to EGFR with its LRRs and immunoglobulin-like domains, then increases ligand-induced receptor ubiquitination, inhibiting the EGFR signaling pathway (28). On the contrary, LRIG2 interacts with EGFR directly and promotes activation of the downstream signaling pathway (29). Besides, LRIG3 can inhibit activation of the Ras/ERK and PI3K/AKT pathways in glioma, indicating that LRIG3, similar to LRIG1, may have an antagonistic effect against LRIG2 (13, 14). Moreover, Zeng et al. showed that LRIG3 is required for the interaction between Dual-specificity phosphatase 6 (DUSP6) and ERK in colorectal cancer. In the absence of LRIG3, DUSP6 could hardly dephosphorylate ERK, suggesting that LRIG3 has potentially more complex biological functions (10). Recently, Yang et al. reported that LRIG2 promotes glioma angiogenesis through the EGFR/VEGFA pathway (30). In this study, our findings reveal the anti-angiogenic role of LRIG3 and affirm that LRIG3 has a functionally antagonistic relationship with LRIG2 in glioma angiogenesis.

Angiogenesis is a complex process regulated by a series of molecules. Among these cytokines, VEGFA is one of the most potent pro-angiogenic molecules. It is also a critical regulator of tumor angiogenesis and is highly expressed in malignant gliomas (31). High VEGFA levels in GBM are associated with increased tumor aggressiveness and poor survival rates (32). Functionally, VEGFA primarily interacts with the VEGFR1 and VEGFR2 receptors, activating downstream signaling pathways and promoting endothelial cells migration, proliferation, and tube formation (33). VEGFA-mediated angiogenesis has been a hallmark in glioblastoma, indicating the potential value of VEGFA-targeted treatments. However, bevacizumab, a humanized antibody targeting secreted VEGFA, did not significantly improve the overall survival of patients with GBM (34). Tamura et al. suggested that the alternative pro-angiogenic mechanisms, such as vascular co-option, vasculogenesis, and vasculogenic mimicry, are induced in the development of resistance to anti-VEGFA therapy (35). Moreover, the salvage angiogenic pathways, including c-MET and STAT3, are activated in the setting of bevacizumab treatment failure (36). In this study, we screened a panel of soluble angiogenic factors involved in vascular development. We found stable up-regulation of VEGFA mRNA and protein upon depletion of LRIG3, suggesting that VEGFA is the downstream target gene for LRIG3. Furthermore, our results demonstrated their clinical relevance in glioma specimens. As mentioned above, high levels of LRIG3 is associated with the downregulation of EGFR and MET signaling in malignant gliomas, supporting the idea that LRIG3 may be a novel target for anti-angiogenic therapy.

Multiple signaling pathways, including the ERK, AKT, STAT3, and JNK pathways, have been shown to modulate VEGFA expression (37). Previously, we demonstrated that LRIG3 functions as a tumor suppressor by inactivating the ERK and AKT signaling pathways (13). To further ascertain the most important pathway, we used specific inhibitors to suppress AKT and ERK phosphorylation and found that the AKT, and not the ERK pathway, plays a major role in the LRIG3-modulated VEGFA expression. Activation of the PI3K/AKT

pathway in glioma cells can increase VEGFA secretion, both *via* hypoxia-inducible factor 1 (HIF-1) dependent and independent mechanisms (25, 38). Additionally, the PI3K/AKT pathway's hyperactivation affects numerous biological processes in glioma, including angiogenesis, cytoskeletal rearrangement, cell proliferation, and vasculogenic mimicry formation (39, 40). Apart from these, VEGFA binding to VEGFR1 enhances a variety of signaling pathways, including the ERK and AKT pathways, leading to tumor invasion and migration (41). Whether LRIG3 has an inhibitory effect on this positive feedback loop warrants further investigation. Based on the results above, it is evident that LRIG3 represents a promising therapeutic target for developing anti-angiogenic strategies against gliomas.

Our study had several limitations. On the one hand, we only analyzed a series of classical angiogenesis-related factors, limiting the study's comprehensiveness. On the other, this was a single-center study with a small sample size. Multicenter data using larger clinical sample sizes are needed to validate our results. Further investigations are still required to identify the specific interactions between LRIG3 protein and the PI3K/AKT signaling pathway, as well as other relevant signaling pathways that might play potential roles in glioma angiogenesis.

In summary, we have demonstrated that LRIG3 inhibits angiogenesis in glioma. Specifically, our results show that LRIG3 suppresses expression and secretion of VEGFA, both *in vitro* and *in vivo*, by inactivating the PI3K/AKT signaling pathway. This novel LRIG3/PI3K/AKT/VEGFA axis provides new insights into the underlying mechanisms of glioma angiogenesis. This axis may be a potential target for developing therapeutic approaches for treating patients with malignant gliomas.

DATA AVAILABILITY STATEMENT

The original contributions presented in the study are included in the article/**Supplementary Material**. Further inquiries can be directed to the corresponding author.

ETHICS STATEMENT

The studies involving human participants were reviewed and approved by the Research Ethics Committee of Tongji Hospital, Tongji Medical College, Huazhong University of Science and Technology. The patients/participants provided their written informed consent to participate in this study. The animal study was reviewed and approved by Ethical Committee of Tongji Hospital, Tongji Medical College, Huazhong University of Science and Technology.

AUTHOR CONTRIBUTIONS

CP and DG designed the study. CP, HC, and YL collected cancer samples. CP, HY, PQ, and BM performed the experiments. CP

analyzed data and drafted the manuscript. BW, QD, and FM revised the manuscript. All authors contributed to the article and approved the submitted version.

FUNDING

This project was supported by the National Natural Science Foundation of China (grant no. 81874086) and the Natural

Science Foundation of Hubei Province, China (grant no. 2018CFB579).

SUPPLEMENTARY MATERIAL

The Supplementary Material for this article can be found online at: <https://www.frontiersin.org/articles/10.3389/fonc.2021.621154/full#supplementary-material>

REFERENCES

- Lapointe S, Perry A, Butowski NA. Primary brain tumours in adults. *Lancet* (2018) 392(10145):432–46. doi: 10.1016/S0140-6736(18)30990-5
- Wen PY, Kesari S. Malignant gliomas in adults. *N Engl J Med* (2008) 359(5):492–507. doi: 10.1056/NEJMra0708126
- Torre LA, Bray F, Siegel RL, Ferlay J, Lortet-Tieulent J, Jemal A. Global cancer statistics, 2012. *CA Cancer J Clin* (2015) 65(2):87–108. doi: 10.3322/caac.21262
- Carmeliet P. Angiogenesis in life, disease and medicine. *Nature* (2005) 438(7070):932–6. doi: 10.1038/nature04478
- Birlik B, Canda S, Ozer E. Tumour vascularity is of prognostic significance in adult, but not paediatric astrocytomas. *Neuropathol Appl Neurobiol* (2006) 32(5):532–8. doi: 10.1111/j.1365-2990.2006.00763.x
- Fan C, Zhang J, Liu Z, He M, Kang T, Du T, et al. Prognostic role of microvessel density in patients with glioma. *Med (Baltimore)* (2019) 98(9):e14695. doi: 10.1097/MD.00000000000014695
- Ameratunga M, Pavlakis N, Wheeler H, Grant R, Simes J, Khasraw M. Anti-angiogenic therapy for high-grade glioma. *Cochrane Database Syst Rev* (2018) 11:CD008218. doi: 10.1002/14651858.CD008218.pub4
- Lindquist D, Kvarnbrink S, Henriksson R, Hedman H. LRIG and cancer prognosis. *Acta Oncol* (2014) 53(9):1135–42. doi: 10.3109/0284186X.2014.953258
- Muller S, Lindquist D, Kanter L, Flores-Staino C, Henriksson R, Hedman H, et al. Expression of LRIG1 and LRIG3 correlates with human papillomavirus status and patient survival in cervical adenocarcinoma. *Int J Oncol* (2013) 42(1):247–52. doi: 10.3892/ijo.2012.1702
- Zeng K, Chen X, Xu M, Liu X, Li C, Xu X, et al. LRIG3 represses cell motility by inhibiting slug via inactivating ERK signaling in human colorectal cancer. *IUBMB Life* (2020) 72(7):1393–403. doi: 10.1002/iub.2262
- Chen Y, Wang Q, Wang M, Li M. Overexpressed LRIG3 gene ameliorates prostate cancer through suppression of cell invasion and migration. *Int J Biol Macromol* (2019) 124:1–9. doi: 10.1016/j.ijbiomac.2018.11.028
- Ranheim C, Lillsunde Larsson G, Hedman H, Lindquist D, Karlsson MG, Hellstrom AC, et al. Expression of LRIG proteins as possible prognostic factors in primary vaginal carcinoma. *PloS One* (2017) 12(8):e0183816. doi: 10.1371/journal.pone.0183816
- Guo D, Yang H, Guo Y, Xiao Q, Mao F, Tan Y, et al. LRIG3 modulates proliferation, apoptosis and invasion of glioblastoma cells as a potent tumor suppressor. *J Neurol Sci* (2015) 350(1–2):61–8. doi: 10.1016/j.jns.2015.02.015
- Cheng F, Zhang P, Xiao Q, Li Y, Dong M, Wang H, et al. The Prognostic and Therapeutic Potential of LRIG3 and Soluble LRIG3 in Glioblastoma. *Front Oncol* (2019) 9:447. doi: 10.3389/fonc.2019.00447
- Yang H, Mao F, Zhang H, Wang B, Wan F, Guo D, et al. Effect of over-expressed LRIG3 on cell cycle and survival of glioma cells. *J Huazhong Univ Sci Technol Med Sci* (2011) 31(5):667. doi: 10.1007/s11596-011-0579-9
- Peng C, Chen Z, Wang S, Wang HW, Qiu W, Zhao L, et al. The Error-Prone DNA Polymerase kappa Promotes Temozolomide Resistance in Glioblastoma through Rad17-Dependent Activation of ATR-Chk1 Signaling. *Cancer Res* (2016) 76(8):2340–53. doi: 10.1158/0008-5472.CAN-15-1884
- Nijaguna MB, Patil V, Urbach S, Shwetha SD, Sravani K, Hegde AS, et al. Glioblastoma-derived Macrophage Colony-stimulating Factor (MCSF) Induces Microglial Release of Insulin-like Growth Factor-binding Protein 1 (IGFBP1) to Promote Angiogenesis. *J Biol Chem* (2015) 290(38):23401–15. doi: 10.1074/jbc.M115.664037
- Folkman J. Tumor angiogenesis: therapeutic implications. *N Engl J Med* (1971) 285(21):1182–6. doi: 10.1056/NEJM197111182852108
- Kloepper J, Riedemann L, Amoozgar Z, Seano G, Susek K, Yu V, et al. Ang-2/VEGF bispecific antibody reprograms macrophages and resident microglia to anti-tumor phenotype and prolongs glioblastoma survival. *Proc Natl Acad Sci U S A* (2016) 113(16):4476–81. doi: 10.1073/pnas.1525360113
- Kunnumakkara AB, Guha S, Krishnan S, Diagaradjane P, Gelovani J, Aggarwal BB. Curcumin potentiates antitumor activity of gemcitabine in an orthotopic model of pancreatic cancer through suppression of proliferation, angiogenesis, and inhibition of nuclear factor-kappaB-regulated gene products. *Cancer Res* (2007) 67(8):3853–61. doi: 10.1158/0008-5472.CAN-06-4257
- Martin A, San Sebastian E, Gomez-Vallejo V, Llop J. Positron emission tomography with [(1)(3)N]ammonia evidences long-term cerebral hyperperfusion after 2h-transient focal ischemia. *Neuroscience* (2012) 213:47–53. doi: 10.1016/j.neuroscience.2012.03.050
- Zhu C, Kros JM, Cheng C, Mustafa D. The contribution of tumor-associated macrophages in glioma neo-angiogenesis and implications for anti-angiogenic strategies. *Neuro Oncol* (2017) 19(11):1435–46. doi: 10.1093/neuonc/nox081
- Jhaveri N, Chen TC, Hofman FM. Tumor vasculature and glioma stem cells: Contributions to glioma progression. *Cancer Lett* (2016) 380(2):545–51. doi: 10.1016/j.canlet.2014.12.028
- Phillips HS, Kharbanda S, Chen R, Forrest WF, Soriano RH, Wu TD, et al. Molecular subclasses of high-grade glioma predict prognosis, delineate a pattern of disease progression, and resemble stages in neurogenesis. *Cancer Cell* (2006) 9(3):157–73. doi: 10.1016/j.ccr.2006.02.019
- Fischer I, Gagner JP, Law M, Newcomb EW, Zagzag D. Angiogenesis in gliomas: biology and molecular pathophysiology. *Brain Pathol* (2005) 15(4):297–310. doi: 10.1111/j.1750-3639.2005.tb00115.x
- Ghiglione C, Carraway KL3, Amundadottir LT, Boswell RE, Perrimon N, Duffy JB. The transmembrane molecule kerkon 1 acts in a feedback loop to negatively regulate the activity of the Drosophila EGF receptor during oogenesis. *Cell* (1999) 96(6):847–56. doi: 10.1016/s0092-8674(00)80594-2
- Guo D, Holmlund C, Henriksson R, Hedman H. The LRIG gene family has three vertebrate paralogs widely expressed in human and mouse tissues and a homolog in Ascidacea. *Genomics* (2004) 84(1):157–65. doi: 10.1016/j.ygeno.2004.01.013
- Gur G, Rubin C, Katz M, Amit I, Citri A, Nilsson J, et al. LRIG1 restricts growth factor signaling by enhancing receptor ubiquitylation and degradation. *EMBO J* (2004) 23(16):3270–81. doi: 10.1038/sj.emboj.7600342
- Xiao Q, Tan Y, Guo Y, Yang H, Mao F, Xie R, et al. Soluble LRIG2 ectodomain is released from glioblastoma cells and promotes the proliferation and inhibits the apoptosis of glioblastoma cells in vitro and in vivo in a similar manner to the full-length LRIG2. *PloS One* (2014) 9(10):e111419. doi: 10.1371/journal.pone.0111419
- Yang HK, Chen H, Mao F, Xiao QG, Xie RF, Lei T. Downregulation of LRIG2 expression inhibits angiogenesis of glioma via EGFR/VEGF-A pathway. *Oncol Lett* (2017) 14(4):4021–8. doi: 10.3892/ol.2017.6671
- Tan Z, Chen K, Wu W, Zhou Y, Zhu J, Wu G, et al. Overexpression of HOXC10 promotes angiogenesis in human glioma via interaction with PRMT5 and upregulation of VEGFA expression. *Theranostics* (2018) 8(18):5143–58. doi: 10.7150/thno.27310
- Norden AD, Drappatz J, Wen PY. Novel anti-angiogenic therapies for malignant gliomas. *Lancet Neurol* (2008) 7(12):1152–60. doi: 10.1016/S1474-4422(08)70260-6

33. Baumgarten P, Blank AE, Franz K, Hattingen E, Dunst M, Zeiner P, et al. Differential expression of vascular endothelial growth factor A, its receptors VEGFR-1, -2, and -3 and co-receptors neuropilin-1 and -2 does not predict bevacizumab response in human astrocytomas. *Neuro Oncol* (2016) 18 (2):173–83. doi: 10.1093/neuonc/nov288
34. Batchelor TT, Reardon DA, de Groot JF, Wick W, Weller M. Antiangiogenic therapy for glioblastoma: current status and future prospects. *Clin Cancer Res* (2014) 20(22):5612–9. doi: 10.1158/1078-0432.CCR-14-0834
35. Tamura R, Tanaka T, Miyake K, Yoshida K, Sasaki H. Bevacizumab for malignant gliomas: current indications, mechanisms of action and resistance, and markers of response. *Brain Tumor Pathol* (2017) 34(2):62–77. doi: 10.1007/s10014-017-0284-x
36. Piao Y, Liang J, Holmes L, Henry V, Sulman E, de Groot JF. Acquired resistance to anti-VEGF therapy in glioblastoma is associated with a mesenchymal transition. *Clin Cancer Res* (2013) 19(16):4392–403. doi: 10.1158/1078-0432.CCR-12-1557
37. Onishi M, Ichikawa T, Kurozumi K, Date I. Angiogenesis and invasion in glioma. *Brain Tumor Pathol* (2011) 28(1):13–24. doi: 10.1007/s10014-010-0007-z
38. Liang W, Guo B, Ye J, Liu H, Deng W, Lin C, et al. Vasorin stimulates malignant progression and angiogenesis in glioma. *Cancer Sci* (2019) 110 (8):2558–72. doi: 10.1111/cas.14103
39. Karar J, Maity A. PI3K/AKT/mTOR Pathway in Angiogenesis. *Front Mol Neurosci* (2011) 4:51. doi: 10.3389/fnmol.2011.00051
40. Tuncel G, Kalkan R. Receptor tyrosine kinase-Ras-PI 3 kinase-Akt signaling network in glioblastoma multiforme. *Med Oncol* (2018) 35(9):122. doi: 10.1007/s12032-018-1185-5
41. Delgado-Bellido D, Serrano-Saenz S, Fernandez-Cortes M, Oliver FJ. Vasculogenic mimicry signaling revisited: focus on non-vascular VE-cadherin. *Mol Cancer* (2017) 16(1):65. doi: 10.1186/s12943-017-0631-x

Conflict of Interest: The authors declare that the research was conducted in the absence of any commercial or financial relationships that could be construed as a potential conflict of interest.

Copyright © 2021 Peng, Chen, Li, Yang, Qin, Ma, Duan, Wang, Mao and Guo. This is an open-access article distributed under the terms of the Creative Commons Attribution License (CC BY). The use, distribution or reproduction in other forums is permitted, provided the original author(s) and the copyright owner(s) are credited and that the original publication in this journal is cited, in accordance with accepted academic practice. No use, distribution or reproduction is permitted which does not comply with these terms.



HOTAIRM1 Promotes Malignant Progression of Transformed Fibroblasts in Glioma Stem-Like Cells Remodeled Microenvironment *via* Regulating miR-133b-3p/TGF β Axis

Haiyang Wang[†], Haoran Li[†], Qianqian Jiang, Xuchen Dong, Suwen Li, Shan Cheng, Jia Shi, Liang Liu, Zhiyuan Qian and Jun Dong^{*}

Department of Neurosurgery, The Second Affiliated Hospital of Soochow University, Suzhou, China

OPEN ACCESS

Edited by:

Cirino Botta,
Cosenza Hospital, Italy

Reviewed by:

Michele Sommariva,
University of Milan, Italy
Pirjo Spuul,
Tallinn University of Technology,
Estonia

*Correspondence:

Jun Dong
dongjun@suda.edu.cn

[†]These authors have contributed
equally to this work

Specialty section:

This article was submitted to
Cancer Molecular Targets
and Therapeutics,
a section of the journal
Frontiers in Oncology

Received: 05 September 2020

Accepted: 24 February 2021

Published: 19 March 2021

Citation:

Wang H, Li H, Jiang Q, Dong X, Li S,
Cheng S, Shi J, Liu L, Qian Z and
Dong J (2021) HOTAIRM1 Promotes
Malignant Progression of Transformed
Fibroblasts in Glioma Stem-Like Cells
Remodeled Microenvironment *via*
Regulating miR-133b-3p/TGF β Axis.
Front. Oncol. 11:603128.
doi: 10.3389/fonc.2021.603128

Recent studies have reported that cancer associated fibroblasts (CAFs) and glioma stem-like cells (GSCs) played active roles in glioma progression in tumor microenvironment (TME). Long non-coding RNAs (lncRNAs) have been found to be closely associated with glioma development in recent years, however, their molecular regulatory mechanisms on CAFs in GSCs remodeled TME kept largely unelucidated. Our study found that GSCs could induce malignant transformation of fibroblasts (t-FBs) based on dual-color fluorescence tracing orthotopic model. Associated with poor prognosis, lnc HOXA transcript antisense RNA, myeloid-specific 1 (HOTAIRM1) was highly expressed in high-grade gliomas and t-FBs. Depleting HOTAIRM1 inhibited the proliferation, invasion, migration, and even tumorigenicity of t-FB. Conversely, overexpression of HOTAIRM1 promoted malignancy phenotype of t-FB. Mechanistically, HOTAIRM1 directly bound with miR-133b-3p, and negatively regulated the latter. MiR-133b-3p partly decreased the promotion effect of HOTAIRM1 on t-FBs. Furthermore, transforming growth factor- β (TGF β) was verified to be a direct target of miR-133b-3p. HOTAIRM1 can modulate TGF β *via* competing with miR-133b-3p. Collectively, HOTAIRM1/miR-133b-3p/TGF β axis was involved in modulating t-FBs malignancy in TME remodeled by GSCs, which had the potential to serve as a target against gliomas.

Keywords: glioma stem-like cells, fibroblasts, tumor microenvironment, HOTAIRM1, malignant transformation

INTRODUCTION

Gliomas are the most prevalent primary intrinsic tumors in the central nervous system, and glioblastoma multiforme (GBM) accounts for nearly half of gliomas (1–3). Although the treatment is constantly optimized (4), GBM is regarded as one of the most malignant and aggressive cancer, which is characterized of poor prognosis and low overall survival. Recently, some studies

have focused on the interactions between GSCs and stromal cells in TME, which is regarded as crucial element for glioma progression recently (5).

Among the stromal cells in TME, fibroblasts are key components involved in progression and metastasis of various malignancies (6, 7). Chronic activation of peri-tumor fibroblasts by cancer cells leads to formation of a subgroup of cells generally known as cancer associated fibroblasts (CAFs) (8). As a significant crosstalk mediator between cancer and stroma in TME, fully exploring the roles of CAFs may help to develop new possible therapeutic approaches against gliomas (9). Local accumulation of CAFs in TME is related with poor prognosis (10, 11), CAFs can promote the proliferation and metastasis of breast cancer (12), endometrial cancer (13), adenocarcinoma of esophagogastric junction (14), melanoma (15), gastric cancer (16), etc. However, the roles of fibroblasts in gliomas TME, and their interactions or crosstalk with GSCs have not been fully elucidated up to now.

LncRNAs are a group of non-coding RNAs with over 200 nucleotides in length (17), which could activate/silence target gene on the level of transcription and/or post-transcription level (18). Emerging studies have declared that aberrant expression of lncRNAs is ubiquitous and relevant with multiple malignant phenotypes of tumors (19–21). LncRNA HOTAIRM1 is located in the HOX gene cluster and regulates the family of HOXA genes (22), which is associated with tumor progression, including colorectal (23), gastric (24), lung cancers (25), and pancreatic cancer (26), et al. However, the role of HOTAIRM1 played in interactions between GSCs and stromal cells in glioma microenvironment has never been reported previously.

Based on the findings that *in vivo* malignant transformation of fibroblasts with HOTAIRM1 upregulation after interaction with GSCs, further exploration the roles of HOTAIRM1 initiated molecular regulatory pathway on proliferation, invasion, migration, and tumorigenicity of t-FBs, will provide new experimental references for potential treatment strategy targeting on t-FBs in glioma microenvironment.

MATERIAL AND METHODS

Tumor Specimens, Experimental Animals, and Cell Culture

Surgical specimen from glioma patients were collected from the Department of Neurosurgery, the Second Affiliated Hospital of Soochow University with informed consent. The whole process obeyed the rules of the Ethics Committee of the Second Affiliated Hospital of Soochow University.

Balb/c nude mice expressing green fluorescent protein (GFP) were bred in specific pathogen free (SPF) experimental animal center in Soochow University (27). All of the animal studies adhered to the rules of the Ethics Committee of the Second Affiliated Hospital of Soochow University.

The GSCs-SU3 cells derived from surgical specimen of glioma patient (28) and were cultured in DMEM/F12 medium favored for neural stem cell growth (Gibco, USA) including 1x B27 Supplement (Gibco, USA), 20 ng/ml epidermal growth factor (EGF) (Gibco,

USA), and 20 ng/ml basic fibroblast growth factor (bFGF) (Gibco, USA). The normal human astrocyte cells (NHA), glioma cell lines (SNB19, A172, U343) were cultured in DMEM (Hyclone, USA) containing 10% fetal bovine serum (FBS) (BI, Israel). All cells were cultured in the incubator (SANYO, JP) at 37°C with 5% CO₂.

Establishment of Dual-Color Fluorescence Tracing Orthotopic GSCs Model

Human GSCs-SU3 cells (28) with red fluorescence protein (RFP) stable expression *via* lentivirus transfection (SU3-RFP) (**Supplementary Figures 1A, B**). GSCs-SU3RFP cells (1×10^6) were injected slowly into the caput nuclei caudate of 4 weeks old GFP Balb/c nude mice (15–20 g) with stereotaxic techniques (**Supplementary Figure 1C**). All mice were sacrificed 4 weeks later under general anesthesia, and the xenografts were harvested, fine minced, and digested with trypsin to prepare single-cell suspension. GSCs derived tumor cells (RFP+) and host derived tumor stromal cells (GFP+) in the xenograft parenchyma can be distinguished under fluorescence microscopic view (**Supplementary Figures 1D–F**). GFP+ cells with high proliferative capacity were mono-cloned with micropipetting techniques (**Supplementary Figures 1G, H**), and continued subculturing (**Supplementary Figures 1I, J**). Two of the mono-cloned GFP+ cells (positive for fibroblast makers α -SMA, vimentin, and S100A4) with unlimited proliferation ability (**Supplementary Figures 1K–M**), were named after transformed fibroblasts t-FB1 and t-FB2, respectively.

CCK8 Assay

Cells were seeded into 96-well plates at a density of 3,000 cells/well in 100 μ l DMEM. Ten μ l CCK8 reagent (Dojindo, Japan) was added into each well every 24 h and incubated for another 2 h at 37°C. Absorbance value at 450 nm was recorded with a spectrophotometer (Tecan, Switzerland).

Immunocytochemical Staining

Transformed fibroblasts were fixed with methanol for 20 min, then permeabilized with 0.25% Triton X-100 (Beyotime, China), and incubated in blocking solution for 1 h. The primary antibodies of α -SMA, vimentin, and S100A4 (CST, USA) were applied for 1 h, respectively. After washing with PBS for three times, the second antibody (Beyotime, China) was applied for 30 min. Finally, the cells were stained with diaminobenzidine (DAB) and hematoxylin, observed under fluorescence microscope (Zeiss, Germany) at a magnification of 200 \times .

Vector Construction and Cell Transfection

The short hairpin RNA (shRNA) targeting HOTAIRM1 (shHOTAIRM1-1 and shHOTAIRM1-2), the overexpression vector of HOTAIRM1, TGF- β , and the corresponding negative control, the miR-133b-3p mimics, inhibitors, and corresponding negative control, were all designed by GenePharma (Shanghai, China). The corresponding vectors and their controls were transfected into transformed fibroblasts according to the manufacturer's protocol.

Quantitative Real-Time Reverse Transcription PCR (qRT-PCR)

Total RNA was extracted with TRIzol (Invitrogen, USA). qRT-PCR was performed to evaluate the expression levels of HOTAIRM1, miR-133b-3p, and TGF- β . The expression of U6 and GAPDH was applied as control. The expression level was analyzed with $2^{-\Delta\Delta C_t}$ method.

5-Ethynyl-20-Deoxyuridine (EdU) Assay

Cells (5×10^4) were seeded in 24-well plates and cultured overnight. Then 300 μ l EdU (50 μ M) (RiboBio, China) was added in each well and incubated for 2 h. Then cells were fixed by 4% paraformaldehyde for 20 min and permeabilized by 0.5% TritonX-100 (Beyotime, China) for 20 min, dyed in 300 μ l Apollo dye solution (RiboBio, China) for 25 min. Cell nuclei were dyed with Hoechst (RiboBio, China) for 10–30 min. Cells were observed under an inverted fluorescence microscope (Zeiss, Germany) at a magnification of 200 \times . And then proportion of EdU positive cells was calculated.

Invasion Assay

Transwell chambers (Corning, USA) were coated with Matrigel (dilution 1:8; BD, USA). Then 120 μ l serum-free medium containing 5×10^4 cells was added in the upper chamber, 600 μ l complete medium containing 10% FBS was added in the lower chamber, then cultured for 24 h at 37°C. The cells on the upper surface were erased with cotton swabs. The cells on the lower surface were fixed with methanol for 30 min and stained with 0.1% crystal violet, cell images were captured with an inverted microscope (AMG, USA) at a magnification of 200 \times .

Wound Healing Assay

Cells were seeded on six-well plate and cultured at 37°C overnight. A 200 μ l pipette tip was applied to make wounds on monolayer cells. Cells were washed by PBS and cultured in DMEM without FBS. The cells were imaged with an inverted microscope (AMG, USA) at a magnification of 100 \times . Images of the wound area were analyzed *via* Image J software after 24 h (NIH, Bethesda, USA).

Luciferase Reporter Assay

The HOTAIRM1 fragment with the miRNAs binding sequences were inserted into the pMIR-REPORT vectors. Similarly, the 3'-UTR fragments of TGF- β with the miRNAs binding sequence were also inserted into pMIR-REPORT vectors. Transformed fibroblasts were transfected with the corresponding miRNAs and the reporter vectors. The mutated vectors were used as control. The duration of transfection was 36 h. Luciferase activity was evaluated by the Dual Luciferase Reporter Assay System (Promega, USA).

Western Blot

Total cell proteins were extracted with RIPA buffer (Beyotime Biotechnology, China). Twenty μ g total proteins were separated by 10% SDS-PAGE and transferred to PVDF membrane, then incubated with the primary antibodies against TGF- β (1:1,000,

CST, USA) and GAPDH (1:5,000, CST, USA) overnight. Then the membrane was incubated with the secondary antibody for 1 h. ECL method was used for visualization for quantitative analysis.

Enzyme Linked Immunosorbent Assay (ELISA)

Sample and the diluent buffer were added to the wells of the 96-well plate which was pre-coated with anti-TGF- β antibody (Abnova, USA), then shake the plate gently to mix thoroughly, and incubate at 37°C for 30 min. Discard the solution in the plate and fill each well completely with Wash Buffer (1 \times) and vortex gently on the shaker for 2 min. Repeat this procedure four more times, 50 μ l HRP conjugated anti-TGF- β antibody was added into each well. Incubate at 37°C for 30 min, then wash the plate for three times, following with adding 50 μ l TMB chromogenic reagent A and B, vortexing gently the plate on the shaker for 30 s, and incubating in dark at 37°C for 15 min, finally adding 50 μ l Stop solution into each well and mix thoroughly. The absorbance at 450 nm was detected with a spectrophotometer (Tecan, Switzerland).

Tumorigenicity Assay

Athymic Balb/c nude mice (4 weeks old, 15–20 g) were bred in the SPF animal center. Then 1×10^6 transformed fibroblasts with up/downregulation of HOTAIRM1 and the corresponding negative control were injected subcutaneously into the right flank of each mouse, respectively. After 5 weeks, all mice were sacrificed under general anesthesia, and the tumors were excised and weighed.

Statistical Analysis

All data were expressed as mean \pm SD and analyzed with t-test, one-way ANOVA, or two-way ANOVA using the software of Prism 7.0 (GraphPad Software, USA). P-value <0.05 was considered statistically significant (*p < 0.05; **p < 0.01; ***p < 0.001; ****p < 0.0001).

RESULTS

Overexpression of LncRNA HOTAIRM1 in Glioma Tissue/Cell Lines and Malignant Transformed Fibroblasts

HOTAIRM1 expression in gliomas was evaluated in The Cancer Genome Atlas (TCGA) database, indicating HOTAIRM1 upregulation in gliomas compared with adjacent normal brain tissue (**Figure 1A**). TCGA survival curve analysis of gliomas showed that the survival of patients with high HOTAIRM1 expression decreased significantly (**Figure 1B**). Clinical glioma samples (n = 10) were collected to further verify HOTAIRM1 expression, which was in accordance with the TCGA results (**Figure 1C**). RNA fluorescence *in situ* hybridization (FISH) demonstrated that HOTAIRM1 expression was positive correlated with glioma malignancy grades in tissues sections of clinical specimens (**Figure 1D**). In addition, HOTAIRM1

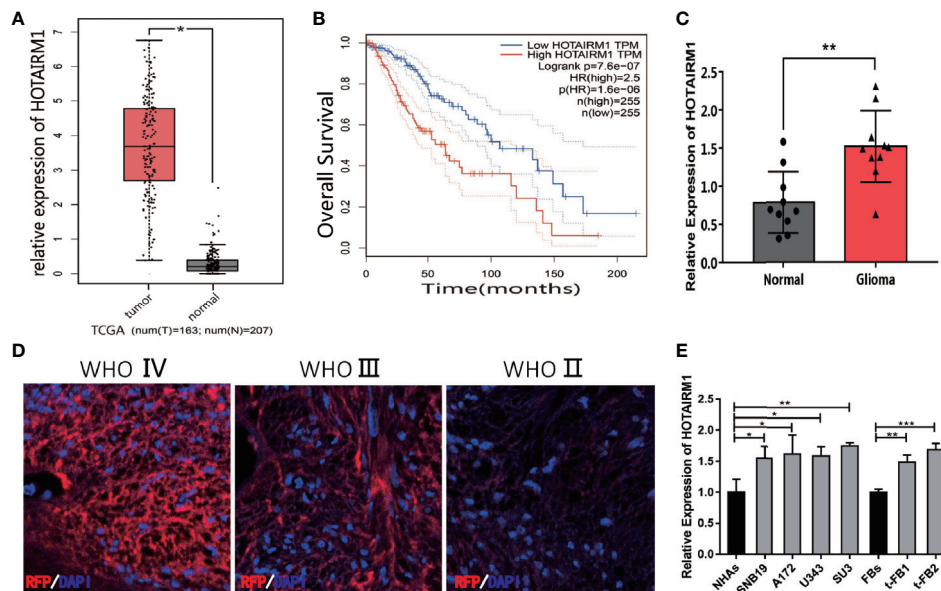


FIGURE 1 | Expression of HOTAIRM1 in malignant transformed fibroblasts (t-FBs) and glioma surgical specimens and cell lines. **(A)** HOTAIRM1 expression level between glioma and normal brain tissue in TCGA. * $p < 0.05$, Student's t test. **(B)** Overall survival rate of glioma patients in low HOTAIRM1 group and high HOTAIRM1 group. **(C)** HOTAIRM1 expression level in clinical glioma specimen ($n = 10$) and paired normal brain tissue ($n = 10$). ** $p < 0.01$, Student's t test. **(D)** HOTAIRM1 expression level in clinical specimen with different malignancy grade by RNA FISH assay. **(E)** HOTAIRM1 expression level in malignant transformed fibroblasts (t-FB), normal fibroblasts, glioma cell lines, and GSCs. * $p < 0.05$, ** $p < 0.01$, *** $p < 0.001$, one-way ANOVA.

expression was detected in the malignant transformed fibroblasts (t-FB1 and t-FB2), normal fibroblasts, glioma cell lines (SNB19, A172, U343), GSCs-SU3, and normal human astrocytes (NHAs), which disclosed HOTAIRM1 upregulation in glioma cell lines, GSCs, and transformed fibroblasts, when compared with NHAs and normal fibroblasts (Figure 1E).

HOTAIRM1 Downregulation Inhibited Proliferation, Invasion, Migration, and Tumorigenesis of Malignant Transformed Fibroblasts

After transfected with an shRNA targeting HOTAIRM1 (shHOTAIRM1-1 and shHOTAIRM1-2) in t-FB1 and t-FB2 cells, the transfection efficiency was validated by qRT-PCR (Figure 2A). EdU assay indicated that HOTAIRM1 downregulation decreased the proliferation ability of t-FB1 and t-FB2 cells (Figures 2B–D). Transwell assay showed that knock-down HOTAIRM1 expression resulted in significant decline of invasion ability of t-FB1 and t-FB2 cells (Figures 2E, F). Downregulation of HOTAIRM1 also remarkably weakened migration ability of t-FB1 and t-FB2 cells (Figures 2G–J), as shown in wound healing assay. Tumorigenicity assay indicated that HOTAIRM1 downregulation of transformed fibroblasts led to obvious decrease in both tumor volume and weight of subcutaneous implanted HOTAIRM1 knocking-down t-FB1/2 cells decreased obviously, compared with the control group (Figures 2K–P). To further investigate the effect of

HOTAIRM1 down-regulation in t-FB1 and t-FB2 cells on tumorigenicity ability of GSCs, *in vivo* combined inoculation of GSCs-SU3 and HOTAIRM1 downregulated t-FB1/2 cells was performed, the transplanted tumor volume and weight were significantly decreased, compared with the control group (Supplementary Figures 2A–F).

HOTAIRM1 Upregulation Promoted Proliferation, Invasion, Migration, and Tumorigenesis of Malignant Transformed Fibroblasts

To further validate the biological function of HOTAIRM1 in the malignant transformed fibroblasts, overexpression of HOTAIRM1 in t-FB1 and t-FB2 cells was achieved *via* transfection of HOTAIRM1, and verified by qRT-PCR (Figure 3A). EdU assay showed HOTAIRM1 upregulation enhanced the proliferation capacity of t-FB1 and t-FB2 cells *in vitro* (Figures 3B, C). The results of Transwell assays indicated that overexpression of HOTAIRM1 promoted the invasion of t-FB1 and t-FB2 cells (Figures 3D, E). Wound healing assay suggested that overexpression of HOTAIRM1 significantly increased the migration of t-FB1 and t-FB2 cells (Figures 3F, G). *In vivo* tumorigenicity assay also showed that overexpression of HOTAIRM1 in t-FB1/2 cells led to higher tumor volume and weight, compared with the control group (Figures 3H–M). To further investigate the effect of HOTAIRM1 overexpression of transformed fibroblasts on tumorigenicity of GSCs, *in vivo*

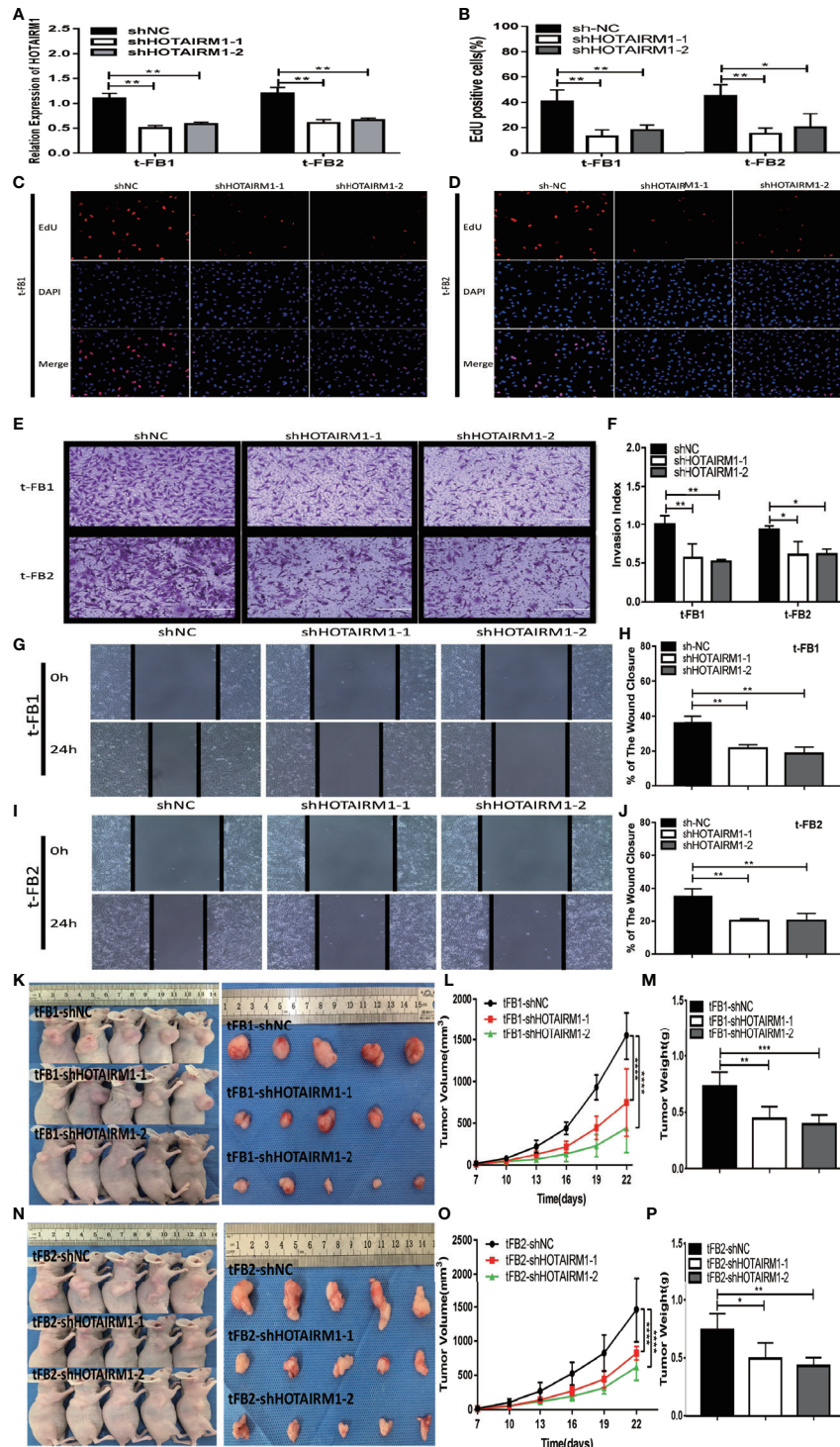


FIGURE 2 | HOTAIRM1 downregulation resulted in inhibition on proliferation, invasion, and migration abilities of malignant transformed fibroblasts. **(A)** HOTAIRM1 expression was analyzed by qRT-PCR in t-FB1/2 transfected with shNC, shHOTAIRM1-1, or shHOTAIRM1-2. $^{**}p < 0.01$, one-way ANOVA. **(B–D)** Proliferation ability was evaluated after HOTAIRM1 downregulation in t-FB1/2 using EdU assay. $^{*}p < 0.05$, $^{**}p < 0.01$, one-way ANOVA. **(E, F)** Invasion capacity was measured after HOTAIRM1 downregulation in t-FB1/2 by transwell assay. $^{*}p < 0.05$, $^{**}p < 0.01$, one-way ANOVA. **(G–J)** Migration capacity was detected after downregulation of HOTAIRM1 in t-FB1/2 by wound healing assay. $^{*}p < 0.01$, one-way ANOVA. **(K, N)** Tumorigenicity assay performed in nude mice by subcutaneous inoculation of t-FB1/2 cells transfected with shNC, shHOTAIRM1-1, or shHOTAIRM1-2, respectively. **(L, M, O, P)** Tumor growth curve and tumor weight of shNC, shHOTAIRM1-1, and shHOTAIRM1-2 group. $^{****}p < 0.0001$, two-way ANOVA; $^{*}p < 0.05$, $^{**}p < 0.01$, $^{***}p < 0.001$, one-way ANOVA.

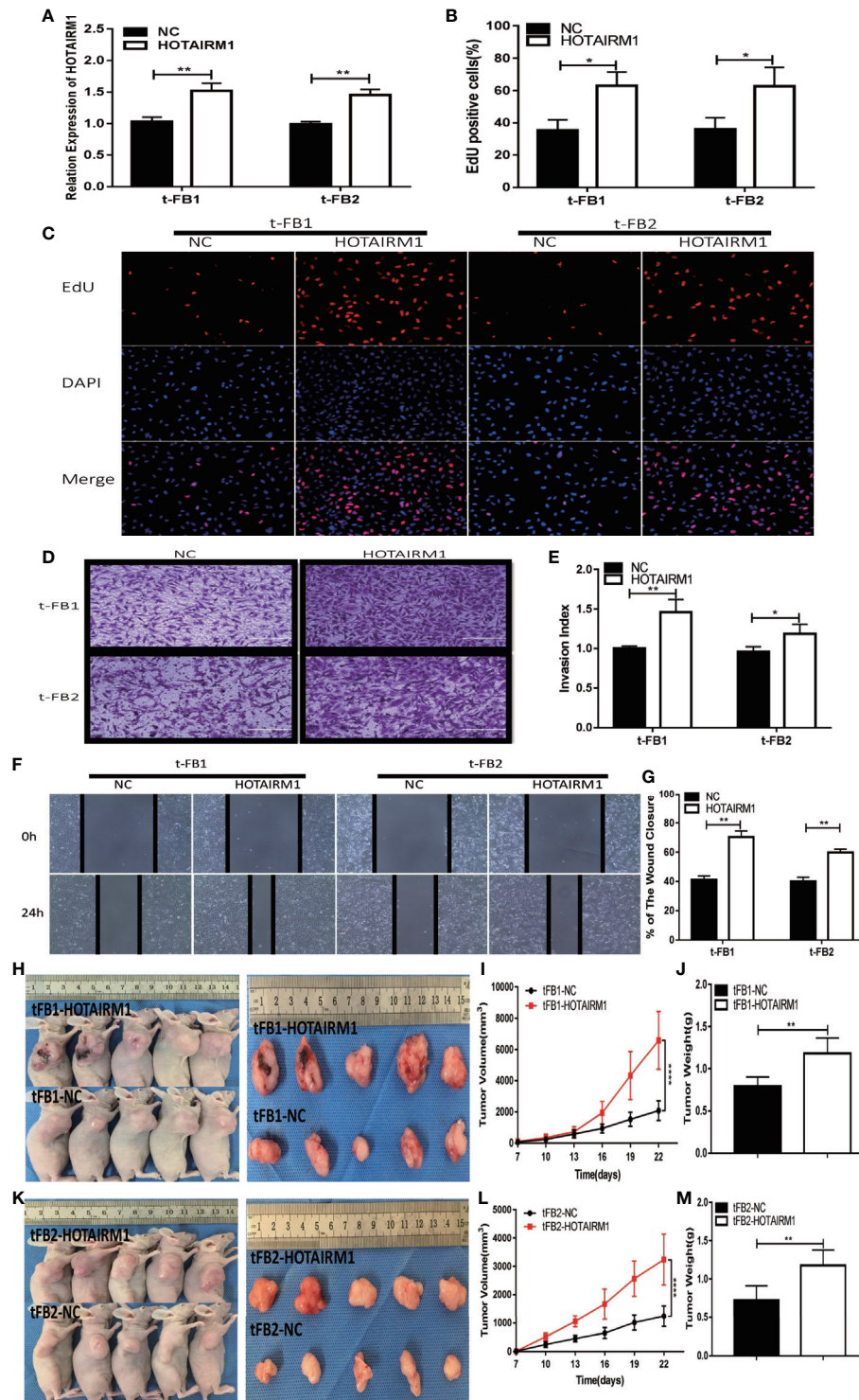


FIGURE 3 | HOTAIRM1 upregulation promoted proliferation, invasion, and migration of malignant transformed fibroblasts. **(A)** HOTAIRM1 expression was analyzed with qRT-PCR in t-FB1/2 transfected with HOTAIRM1 or NC. $^{**}p < 0.01$, Student's *t* test. **(B, C)** Proliferation ability was evaluated after HOTAIRM1 upregulation in t-FB1/2 using EdU assay. $^{*}p < 0.05$, Student's *t* test. **(D, E)** Invasion capacity was assessed after HOTAIRM1 upregulation in t-FB1/2 by transwell assay. $^{*}p < 0.05$, $^{**}p < 0.01$, Student's *t* test. **(F, G)** Migration ability was evaluated in t-FB1/2 with HOTAIRM1 overexpression by wound healing assay. $^{**}p < 0.01$, Student's *t* test. **(H, K)** Tumorigenicity was compared in murine subcutaneous tumor model between t-FB1/2 with NC or HOTAIRM1 transfection. **(I, J, L, M)** Tumor growth curve and tumor weight of NC and HOTAIRM1 transfection group. $^{****}p < 0.0001$, two-way ANOVA; $^{**}p < 0.01$, one-way ANOVA.

combined inoculation of GSCs-SU3 and HOTAIRM1 upregulated t-FB1/2 cells was performed, tumor volume and weight were increased, compared with the control group (Supplementary Figures 2G–L).

MiR-133b-3p Was a Direct Target of HOTAIRM1

To explore the role of competing endogenous RNA (ceRNA) on regulating biological activities of malignant transformed fibroblasts, the online database starBase (<http://starbase.sysu.edu.cn/>) was applied to identify the possible miRNA targets of HOTAIRM1. Potential binding sites between HOTAIRM1 and miR-133b-3p (Figure 4A) were predicted with bioinformatic analysis *via* starBase. Further verification with qRT-PCR found dramatic downregulation of miR-133b-3p expression in t-FB1/2 and glioma cell lines, compared with normal fibroblasts and NHAs (Figure 4B). Specifically, miR-133b-3p was negatively regulated by HOTAIRM1 in t-FB1/2 cells (Figures 4C, D). In order to clarify the direct interaction between miR-133b-3p and HOTAIRM1, wild type (WT) and mutant type (MUT) vector of HOTAIRM1 were constructed for luciferase activity assay, which showed that miR-133b-3p significantly inhibited the luciferase

activity of HOTAIRM1-WT (Figures 4E, F), indicating that miR-133b-3p was the direct target of HOTAIRM1.

MiR-133b-3p Inhibited Proliferation, Invasion, and Migration of Malignant Transformed Fibroblasts by Targeting TGF β

TGF β was one of the predicted downstream targets of miR-133b-3p according to bioinformatic analysis (Figure 5A). To further verify the direct bonding between miR-133b-3p and TGF β , TGF β -WT and TGF β -MUT vectors constructed for further luciferase activity assay (Figure 5A), which revealed that miR-133b-3p significantly weakened luciferase activity of TGF β -WT, compared with TGF β -MUT (Figures 5B, C). TGF β expression level was also detected with qRT-PCR in both glioma cell lines and t-FB1/2 cells, which showed TGF β was overexpressed in both glioma cell lines and transformed fibroblasts (Figure 5D).

To further explore the regulatory relationship between miR-133b-3p and TGF β , both of miR-133b-3p mimics and TGF β plasmid were transfected into t-FB1/2 cells. QRT-PCR, western blot assay, and ELISA showed that miR-133b-3p can inhibit

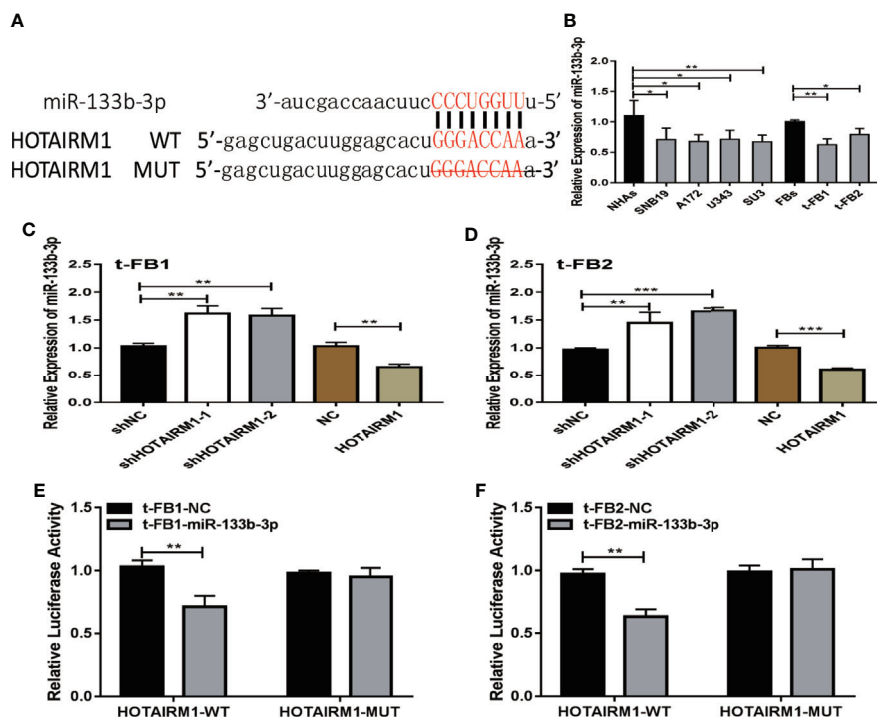


FIGURE 4 | MiR-133b-3p was verified to be a direct target of HOTAIRM1. **(A)** the binding site between miR-133b-3p and HOTAIRM1. Wild type (WT) and mutant type (MT) vector of HOTAIRM1 were constructed for luciferase activity assay. **(B)** MiR-133b-3p expression level was evaluated by qRT-PCR in t-FB1/2 and glioma cell lines. * $p < 0.05$, ** $p < 0.01$, one-way ANOVA. **(C, D)** qRT-PCR assay showed miR-133b-3p was negatively regulated by HOTAIRM1 in t-FB1/2. ** $p < 0.01$, *** $p < 0.001$, one-way ANOVA; ** $p < 0.01$, *** $p < 0.001$, Student's *t* test. **(E, F)** Luciferase reporter assay suggested that miR-133b-3p weakened the luciferase activity of HOTAIRM1-WT. ** $p < 0.01$, Student's *t* test.

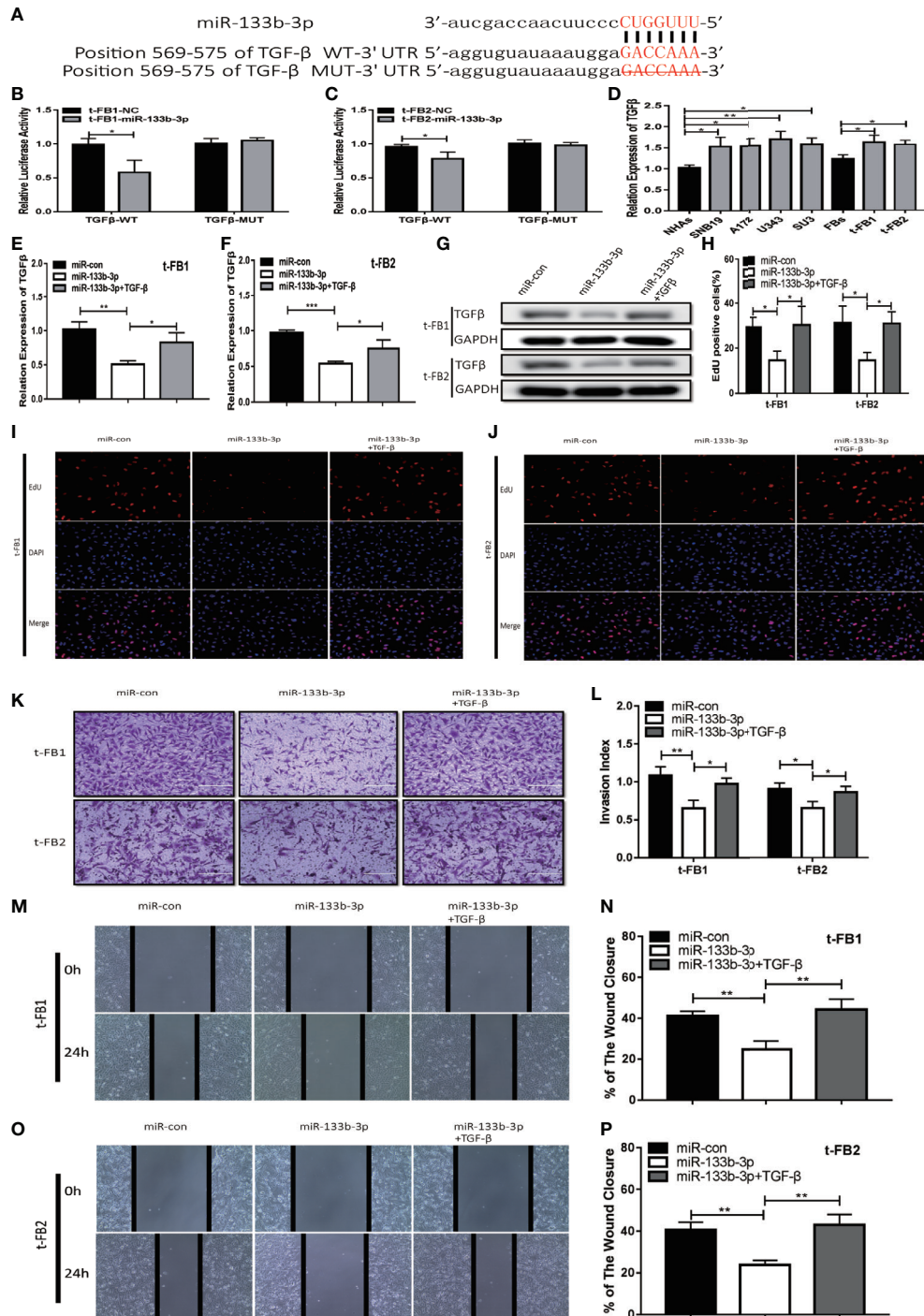


FIGURE 5 | Upregulation of miR-133b-3p can inhibit proliferation, invasion, and migration of transformed fibroblasts by targeting TGFβ. **(A)** The vector of TGFβ-WT and TGFβ-MUT were constructed for luciferase activity assay. **(B, C)** Luciferase reporter assay testified that miR-133b-3p significantly weakened the luciferase activity of TGFβ-WT. **p* < 0.05, Student's *t* test. **(D)** TGFβ expression level in t-FB1/2 and glioma cell lines. **p* < 0.05, ***p* < 0.01, one-way ANOVA. **(E–G)** qRT-PCR and western blot analysis of TGFβ expression in t-FB1/2 transfected with miR-133b-3p or miR-133b-3p together with TGFβ. **p* < 0.05, ***p* < 0.01, ****p* < 0.001, one-way ANOVA. **(H–J)** proliferation was analyzed in t-FB1/2 cells transfected with miR-133b-3p or TGFβ by EdU assay. **p* < 0.05, one-way ANOVA. **(K, L)** Invasion was evaluated in t-FB1/2 cells transfected with miR-133b-3p or TGFβ via transwell assay. **p* < 0.05, ***p* < 0.01, one-way ANOVA. **(M–P)** Migration was determined in t-FB1/2 transfected with miR-133b-3p or TGFβ by wound healing assays. ***p* < 0.01, one-way ANOVA.

TGF β expression, and this inhibition effect can be partially offset by TGF β plasmid transfection (Figures 5E–G; Supplementary Figures 3A, B). In addition, EdU assay showed miR-133b-3p decreased t-FB1/2 cells proliferation, and can be reversed by

TGF β overexpression (Figures 5H–J). Meanwhile, the weakened invasion and migration of t-FB1/2 cells induced by miR-133b-3p upregulation were partially offset by TGF β overexpression (Figures 5K–P).

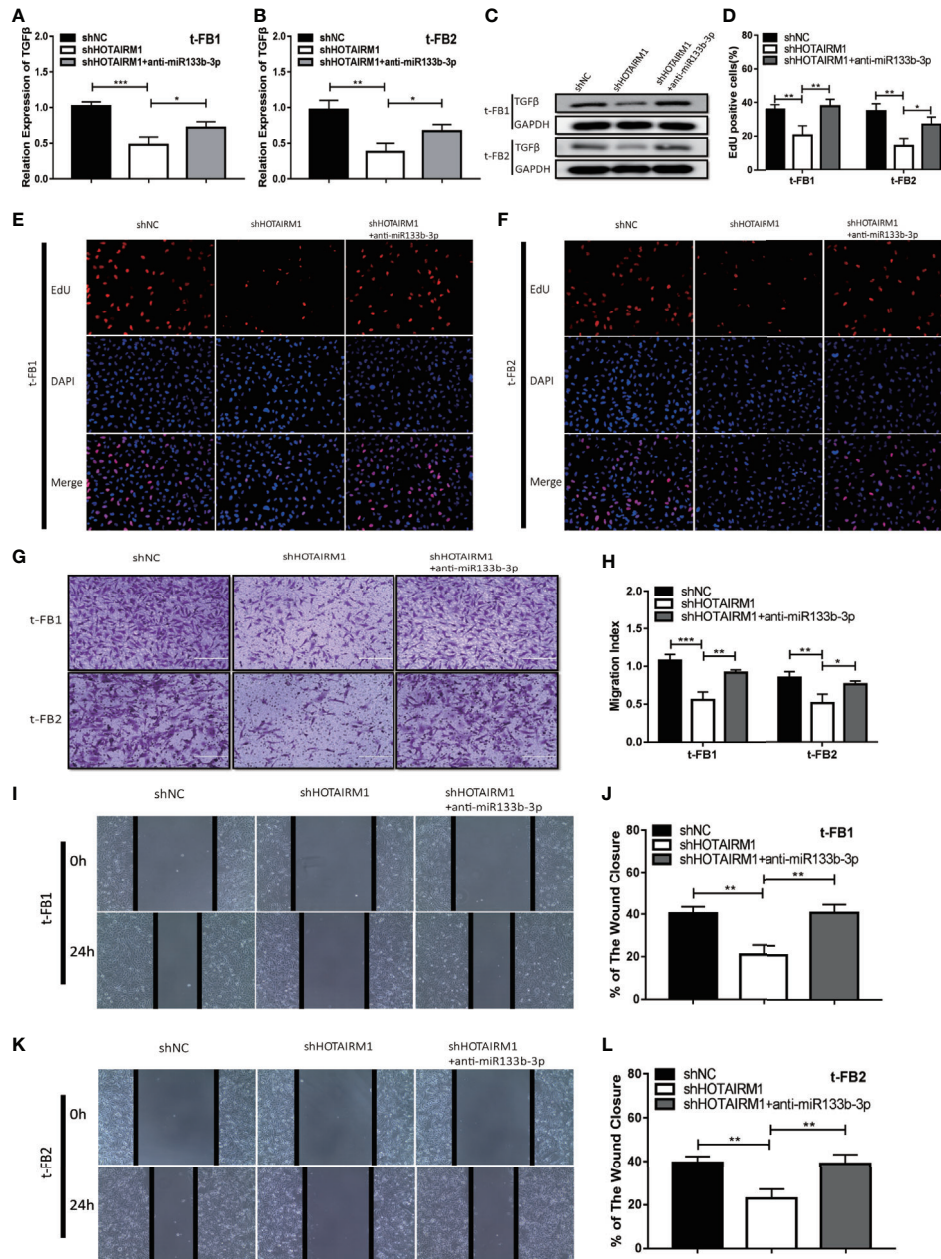


FIGURE 6 | HOTAIRM1 facilitated malignant transformed fibroblasts progression via regulating miR-133b-3p/TGF β axis. (A–C) qRT-PCR and Western blot analysis of TGF β expression in t-FB1/2 cells transfected with shHOTAIRM1 or shHOTAIRM1 together with miR-133b-3p inhibitors. *p < 0.05, **p < 0.01, ***p < 0.001, one-way ANOVA. (D–F) EdU assay was performed to evaluate the proliferation of t-FB1/2 cells transfected with shHOTAIRM1 or shHOTAIRM1 together with miR-133b-3p inhibitors. *p < 0.05, **p < 0.01, one-way ANOVA. (G, H) Invasion was evaluated in t-FB1/2 cells transfected with shHOTAIRM1 or shHOTAIRM1 together with miR-133b-3p inhibitors by transwell assay. *p < 0.05, **p < 0.01, ***p < 0.001, one-way ANOVA. (I–L) Migration was assessed in t-FB1/2 cells transfected with shHOTAIRM1 together with miR-133b-3p inhibitors by wound healing assay. **p < 0.01, one-way ANOVA.

HOTAIRM1 Facilitated Progression of Malignant Transformed Fibroblasts by Regulating miR-133b-3p/TGF β Axis

To elucidate the mechanism which HOTAIRM1 promoted malignancy of transformed fibroblasts *via* regulating miR-133b-3p/TGF β axis, t-FB1 and t-FB2 cells were transfected with shHOTAIRM1 or shHOTAIRM1 together with miR-133b-3p inhibitors. qRT-PCR, western blot assay, and ELISA suggested that shHOTAIRM1 can inhibit TGF β expression, which was partly offset by miR-133b-3p inhibitors (**Figures 6A–C; Supplementary Figures 3C, D**). Besides, EdU assay indicated shHOTAIRM1 decreased the proliferation of t-FB1/2 cells, which could be reversed by miR-133b-3p inhibitors (**Figures 6D–F**). Consistent with results of EdU assay, the weakened invasion and migration of t-FB1/2 cells induced by shHOTAIRM1 were partly rescued by miR-133b-3p inhibitors as well (**Figures 6G–L**).

DISCUSSION

In this study, glioma associated fibroblasts were found undergoing malignant transformation in GSCs remodeled tumor microenvironment. The role of lncHOTAIRM1 was highly associated with the pro-tumor abilities of transformed fibroblasts, including promoting proliferation, invasion, migration, and tumorigenesis on t-FBs. Further mechanistical studies suggested that HOTAIRM1 competitively bound miR-133b-3p to regulate the expression of TGF- β , thus producing obvious pro-tumor effect.

Most studies attributed treatment resistance and high recurrence of glioma to GSCs (29–31), which based on their infinite self-renewal capacity, persistent proliferation, and strong remodeling of TME (32–34). Despite the key roles of GSCs in tumor initiation, glioma microenvironment, including the relevant various stromal cells, interacted actively with GSCs, and played vital roles on GSCs initiated tissue remodeling processes. Various glioma biological processes were largely affected by TME (35), and targeting on TME has been the potential treatment strategy in recent years (36). Among stromal cells in glioma microenvironment, fibroblasts were essential for regulating glioma development (37–39). Normal fibroblasts maintained homeostasis, which was characterized of inertness and low levels of synthetic properties if they were not under any local microenvironment stress (40). When the intrinsic crosstalk between normal fibroblasts (NFs) and stroma changed due to education by cancer stem cells, NFs may acquire modified phenotypes and can converted into CAFs (41). Recent studies revealed that CAFs were main cancer-promoting components in TME, which were involved in carcinogenesis, proliferation, invasion, and chemoresistance (42–45), and the existence of CAFs implied poor prognosis in ovarian and breast cancer (43, 44). Yes-associated protein 1 (YAP1) was responsible for converting NFs into CAFs, thus facilitating prostate cancer development (46). However, the role

of fibroblasts in glioma microenvironment and how they interacted with GSCs kept largely unknown. *In vitro* studies showed CAFs were associated with glioma cell migration (38). Fibroblasts can differentiate from mesenchymal cells (47, 48), which can be recruited into glioma microenvironment. Our results verified malignant transformation of fibroblasts in glioma microenvironment induced by GSCs, and further disclosed that HOTAIRM1 played active roles on malignancy phenotype of t-FBs, which could be a potential target against gliomas.

Long non-coding RNAs were pivotal in molecular dysregulation of gliomas, including the aberrant expression profile of gliomas (49–51). Previous studies reported that lnc HOTAIRM1 can act as promoter or suppressor in tumor development: HOTAIRM1 exerted its tumor inhibitory effect through competitive combination with endogenous RNA in gastric cancer (24), head and neck tumor (52), it also can suppress tumor cell proliferation and promote cell apoptosis in hepatocellular carcinoma *via* inhibiting Wnt pathway (53). Besides, HOTAIRM1 can promote glioma progression through certain ceRNA networks (54–57). The role of HOTAIRM1 in transformation and malignant phenotype of fibroblasts in glioma microenvironment was explored in the current studies, which also disclosed that miR-133b-3p was the target of HOTAIRM1 and can inhibit biological behaviors of t-FBs. MiR-133b played tumor suppressing roles in several malignancies through regulating in gastric cancer (58), targeting Sox9 in breast cancer (59), negatively regulating EMP2 in glioma (60), targeting methyltransferase DOT1L in colorectal cancer (61), and targeting EGFR in esophageal squamous cell carcinoma (62). Our results supported that TGF β was the functional target of miR-133b-3p, miR-133b-3p can inhibit t-FBs *via* targeting TGF β .

In summary, the current studies showed that HOTAIRM1 was upregulated in t-FB and gliomas, it can promote malignant biological phenotype of t-FBs by regulating TGF β *via* miR-133b-3p. Therefore, the HOTAIRM1/miR-133b-3p/TGF β signal axis may serve as the potential therapeutic target against t-FBs in glioma microenvironment. However, our results were mainly based on an orthotopic xenograft tumor model, which may not fully reflect the real TME of glioma patients, which needs to be verified through high throughput single cell sequencing of glioma surgical specimens to confirm the molecular mechanisms regulating CAFs in glioma microenvironment.

DATA AVAILABILITY STATEMENT

The raw data supporting the conclusions of this article will be made available by the authors, without undue reservation.

ETHICS STATEMENT

The animal study was reviewed and approved by the ethics committee of Second Affiliated Hospital of Soochow University.

AUTHOR CONTRIBUTIONS

HW and JD conceived and designed the experiment. HW performed the experiments and wrote the manuscript. HL performed the statistical analyses and generated the figures. QJ and XD collected the public data. SL, SC, JS and LL collected the patient samples. ZQ and JD revised the manuscript. All authors contributed to the article and approved the submitted version.

FUNDING

This study was supported by grants from National Natural Science Foundation of China (NO. 81472739), Research and Practice Innovation Program for Postgraduates in Jiangsu (No. KYCX19_1982), and Clinical Special Disease Diagnosis and Treatment Technology in Suzhou, China (No. LCZX201807).

SUPPLEMENTARY MATERIAL

The Supplementary Material for this article can be found online at: <https://www.frontiersin.org/articles/10.3389/fonc.2021.603128/full#supplementary-material>

REFERENCES

- Latini F, Fahlstrom M, Berntsson SG, Larsson EM, Smits A, Ryttefjors M. A novel radiological classification system for cerebral gliomas: The Brain-Grid. *PLoS One* (2019) 14(1):e0211243. doi: 10.1371/journal.pone.0211243
- Sun G, Zhang C, Song H, Guo J, Li M, Cao Y. WZY-321, a novel evodiamine analog, inhibits glioma cell growth in an autophagy-associated manner. *Oncol Lett* (2019) 17(2):2465–72. doi: 10.3892/ol.2018.9847
- Hervey-Jumper SL, Berger MS. Insular glioma surgery: an evolution of thought and practice. *J Neurosurg* (2019) 130(1):9–16. doi: 10.3171/2018.10.JNS181519
- Prelaj A, Rebuzzi SE, Grassi M, Salvati M, D'Elia A, Buttarelli F, et al. Non-conventional temozolomide schedule as second-line treatment in recurrent malignant gliomas: Survival across disease and treatment subgroup analysis and review of the literature. *Mol Clin Oncol* (2019) 10(1):58–66. doi: 10.3892/mco.2018.1746
- Figueroa J, Phillips LM, Shahar T, Hossain A, Gumin J, Kim H, et al. Exosomes from Glioma-Associated Mesenchymal Stem Cells Increase the Tumorigenicity of Glioma Stem-like Cells via Transfer of miR-1587. *Cancer Res* (2017) 77(21):5808–19. doi: 10.1158/0008-5472.CAN-16-2524
- Cheteh EH, Augsten M, Rundqvist H, Bianchi J, Sarne V, Egevad L, et al. Human cancer-associated fibroblasts enhance glutathione levels and antagonize drug-induced prostate cancer cell death. *Cell Death Dis* (2017) 8(6):e2848. doi: 10.1038/cddis.2017.225
- Shahriari K, Shen F, Worre-Mahdi A, Liu Q, Gong Y, Garcia FU, et al. Cooperation among heterogeneous prostate cancer cells in the bone metastatic niche. *Oncogene* (2017) 36(20):2846–56. doi: 10.1038/onc.2016.436
- Kalluri R. The biology and function of fibroblasts in cancer. *Nat Rev Cancer* (2016) 16(9):582–98. doi: 10.1038/nrc.2016.73
- Shi L, Wang Z, Geng X, Zhang Y, Xue Z. Exosomal miRNA-34 from cancer-associated fibroblasts inhibits growth and invasion of gastric cancer cells in vitro and in vivo. *Aging (Albany NY)* (2020) 12(9):8549–64. doi: 10.18632/aging.103157
- Bochet L, Lhuede C, Dauvillier S, Wang YY, Dirat B, Laurent V, et al. Adipocyte-derived fibroblasts promote tumor progression and contribute to the desmoplastic reaction in breast cancer. *Cancer Res* (2013) 73(18):5657–68. doi: 10.1158/0008-5472.CAN-13-0530
- Yamashita M, Ogawa T, Zhang X, Hanamura N, Kashikura Y, Takamura M, et al. Role of stromal myofibroblasts in invasive breast cancer: stromal expression of alpha-smooth muscle actin correlates with worse clinical outcome. *Breast Cancer* (2012) 19(2):170–6. doi: 10.1007/s12282-010-0234-5
- Orimo A, Gupta PB, Sgroi DC, Arenzana-Seisdedos F, Delaunay T, Naeem R, et al. Stromal fibroblasts present in invasive human breast carcinomas promote tumor growth and angiogenesis through elevated SDF-1/CXCL12 secretion. *Cell* (2005) 121(3):335–48. doi: 10.1016/j.cell.2005.02.034
- Teng F, Tian WY, Wang YM, Zhang YF, Guo F, Zhao J, et al. Cancer-associated fibroblasts promote the progression of endometrial cancer via the SDF-1/CXCR4 axis. *J Hematol Oncol* (2016) 9:8. doi: 10.1186/s13045-015-0231-4
- Sugihara H, Ishimoto T, Yasuda T, Izumi D, Eto K, Sawayama H, et al. Cancer-associated fibroblast-derived CXCL12 causes tumor progression in adenocarcinoma of the esophagogastric junction. *Med Oncol* (2015) 32(6):618. doi: 10.1007/s12032-015-0618-7
- Whipple CA, Brinckerhoff CE. BRAF(V600E) melanoma cells secrete factors that activate stromal fibroblasts and enhance tumorigenicity. *Br J Cancer* (2014) 111(8):1625–33. doi: 10.1038/bjc.2014.452
- Wu X, Tao P, Zhou Q, Li J, Yu Z, Wang X, et al. IL-6 secreted by cancer-associated fibroblasts promotes epithelial-mesenchymal transition and metastasis of gastric cancer via JAK2/STAT3 signaling pathway. *Oncotarget* (2017) 8(13):20741–50. doi: 10.18632/oncotarget.15119
- Schmitt AM, Chang HY. Long Noncoding RNAs in Cancer Pathways. *Cancer Cell* (2016) 29(4):452–63. doi: 10.1016/j.ccell.2016.03.010
- Zhang Y, Yang G, Luo Y. Long non-coding RNA PVT1 promotes glioma cell proliferation and invasion by targeting miR-200a. *Exp Ther Med* (2019) 17(2):1337–45. doi: 10.3892/etm.2018.7083
- Guo LP, Zhang ZJ, Li RT, Li HY, Cui YQ. Influences of LncRNA SNHG20 on proliferation and apoptosis of glioma cells through regulating the PTEN/PI3K/AKT signaling pathway. *Eur Rev Med Pharmacol Sci* (2019) 23(1):253–61. doi: 10.26355/eurrev_201901_16771
- Sun S, Gong C, Yuan K. LncRNA UCA1 promotes cell proliferation, invasion and migration of laryngeal squamous cell carcinoma cells by activating Wnt/beta-catenin signaling pathway. *Exp Ther Med* (2019) 17(2):1182–9. doi: 10.3892/etm.2018.7097
- Yue C, Ren Y, Ge H, Liang C, Xu Y, Li G, et al. Comprehensive analysis of potential prognostic genes for the construction of a competing endogenous RNA regulatory network in hepatocellular carcinoma. *Oncotargets Ther* (2019) 12:561–76. doi: 10.2147/OTT.S188913

Supplementary Figure 1 | Glioma stem cells can induce malignant transformation of fibroblasts. (A) Patient-derived GSCs-SU3 cells had typical sphere-like cell clusters. (B) SU3 cells had stable RFP expression after RFP transfection. (C) Orthotopic tumor formation after SU3-RFP cells inoculated in transgenic GFP BALB/c athymic nude mice. (D–F) Primary culture of the xenograft tumor cells and observation under the fluorescence microscope. (G, H) GFP+ cells with high proliferation ability were mono-cloned in 96-well plates. (I, J) Subculture of the mono-cloned GFP+ cells. (K, L) the unlimited proliferation ability of GFP+ cells was measured by CCK8 assay. (M) GFP+ cells with high proliferation ability were positive for fibroblasts makers (α -SMA, vimentin, and S100A4).

Supplementary Figure 2 | Tumorigenicity assay by subcutaneous inoculation of GSCs-SU3 cells, and t-FB1/2 cells with HOTAIRM1 down-regulation or overexpression. (A, D) Tumorigenicity was compared in GSCs subcutaneous tumor model after simultaneous inoculation of t-FB1/2 cells with shNC, shHOTAIRM1-1, or shHOTAIRM1-2 transfection. (B, C, E, F) Tumor growth curve and tumor weight of shNC, shHOTAIRM1-1, and shHOTAIRM1-2 group. ****p < 0.0001, two-way ANOVA; **p < 0.01, one-way ANOVA. (G, J) Tumorigenicity was compared in GSCs subcutaneous tumor model after simultaneous inoculation of t-FB1/2 cells with NC or HOTAIRM1 transfection. (H, I, K, L) Tumor growth curve and tumor weight of NC and HOTAIRM1 transfection group. ****p < 0.0001, two-way ANOVA; ***p < 0.001, Student's t test.

Supplementary Figure 3 | ELISA to detect TGF β secretion. (A, B) Secretion of TGF β by t-FB1/2 cells which were transfected with miR-133b-3p or miR-133b-3p together with TGF β . (C, D) Secretion of TGF β by t-FB1/2 cells which were transfected with shHOTAIRM1 or shHOTAIRM1 together with miR-133b-3p inhibitors. *p < 0.05, **p < 0.01, one-way ANOVA.

22. Wang XQ, Dostie J. Reciprocal regulation of chromatin state and architecture by HOTAIRM1 contributes to temporal collinear HOXA gene activation. *Nucleic Acids Res* (2017) 45(3):1091–104. doi: 10.1093/nar/gkw966
23. Wan L, Kong J, Tang J, Wu Y, Xu E, Lai M, et al. HOTAIRM1 as a potential biomarker for diagnosis of colorectal cancer functions the role in the tumour suppressor. *J Cell Mol Med* (2016) 20(11):2036–44. doi: 10.1111/jcmm.12892
24. Lu R, Zhao G, Yang Y, Jiang Z, Cai J, Zhang Z, et al. Long noncoding RNA HOTAIRM1 inhibits cell progression by regulating miR-17-5p/ PTEN axis in gastric cancer. *J Cell Biochem* (2019) 120(4):4952–65. doi: 10.1002/jcb.27770
25. Tian X, Ma J, Wang T, Tian J, Zhang Y, Mao L, et al. Long Non-Coding RNA HOXA Transcript Antisense RNA Myeloid-Specific 1-HOXA1 Axis Downregulates the Immunosuppressive Activity of Myeloid-Derived Suppressor Cells in Lung Cancer. *Front Immunol* (2018) 9:473. doi: 10.3389/fimmu.2018.00473
26. Luo Y, He Y, Ye X, Song J, Wang Q, Li Y, et al. High Expression of Long Noncoding RNA HOTAIRM1 is Associated with the Proliferation and Migration in Pancreatic Ductal Adenocarcinoma. *Pathol Oncol Res* (2019) 25(4):1567–77. doi: 10.1007/s12253-018-00570-4
27. Lan Q, Chen Y, Dai C, Li S, Fei X, Dong J, et al. Novel enhanced GFP-positive congenic inbred strain establishment and application of tumor-bearing nude mouse model. *Cancer Sci* (2020) 111(10):3626–38. doi: 10.1111/cas.14545
28. Wan Y, Fei X, Wang Z, Jiang D, Chen H, Yang J, et al. Expression of miR-125b in the new, highly invasive glioma stem cell and progenitor cell line SU3. *Chin J Cancer* (2012) 31(4):207–14. doi: 10.5732/cjc.011.10336
29. Liu HW, Su YK, Bamodu OA, Hueng DY, Lee WH, Huang CC, et al. The Disruption of the β -Catenin/TCF-1/STAT3 Signaling Axis by 4-Acetyltanroquinonol B Inhibits the Tumorigenesis and Cancer Stem-Cell-Like Properties of Glioblastoma Cells, In Vitro and In Vivo. *Cancers* (2018) 10(12):491. doi: 10.3390/cancers10120491
30. Fan Y, Xue W, Schachner M, Zhao W. Honokiol Eliminates Glioma/Glioblastoma Stem Cell-Like Cells Via JAK-STAT3 Signaling and Inhibits Tumor Progression by Targeting Epidermal Growth Factor Receptor. *Cancers* (2018) 11(1):22. doi: 10.3390/cancers11010022
31. Matarredona E, Pastor A. Neural Stem Cells of the Subventricular Zone as the Origin of Human Glioblastoma Stem Cells. Therapeutic Implications. *Front Oncol* (2019) 9:779:779. doi: 10.3389/fonc.2019.00779
32. Yi L, Zhou X, Li T, Liu P, Hai L, Tong L, et al. Notch1 signaling pathway promotes invasion, self-renewal and growth of glioma initiating cells via modulating chemokine system CXCL12/CXCR4. *J Exp Clin Cancer Res* (2019) 38(1):339. doi: 10.1186/s13046-019-1319-4
33. Hu P, Li S, Tian N, Wu F, Hu Y, Li D, et al. Acidosis enhances the self-renewal and mitochondrial respiration of stem cell-like glioma cells through CYP24A1-mediated reduction of vitamin D. *Cell Death Dis* (2019) 10(1):25. doi: 10.1038/s41419-018-1242-1
34. Tao Z, Li T, Ma H, Yang Y, Zhang C, Hai L, et al. Autophagy suppresses self-renewal ability and tumorigenicity of glioma-initiating cells and promotes Notch1 degradation. *Cell Death Dis* (2018) 9(11):1063. doi: 10.1038/s41419-018-0957-3
35. Zhou J, Liu L, Yang T, Lu B. Prognostic and therapeutic value of CD103(+) cells in renal cell carcinoma. *Exp Ther Med* (2018) 15(6):4979–86. doi: 10.3892/etm.2018.6025
36. Deng F, Zhou R, Lin C, Yang S, Wang H, Li W, et al. Tumor-secreted dickkopf2 accelerates aerobic glycolysis and promotes angiogenesis in colorectal cancer. *Theranostics* (2019) 9(4):1001–14. doi: 10.7150/thno.30056
37. Quail DF, Joyce JA. The Microenvironmental Landscape of Brain Tumors. *Cancer Cell* (2017) 31(3):326–41. doi: 10.1016/j.ccell.2017.02.009
38. Trylcova J, Busek P, Smetana KJr, Balazova E, Dvorankova B, Mifkova A, et al. Effect of cancer-associated fibroblasts on the migration of glioma cells in vitro. *Tumour Biol* (2015) 36(8):5873–9. doi: 10.1007/s13277-015-3259-8
39. Charles NA, Holland EC, Gilbertson R, Glass R, Kettenmann H. The brain tumor microenvironment. *Glia* (2011) 60(3):502–14. doi: 10.1002/glia.21264
40. Asakawa M, Itoh M, Suganami T, Sakai T, Kanai S, Shirakawa I, et al. Upregulation of cancer-associated gene expression in activated fibroblasts in a mouse model of non-alcoholic steatohepatitis. *Sci Rep* (2019) 9(1):19601. doi: 10.1038/s41598-019-56039-0
41. Shen H, Yu X, Yang F, Zhang Z, Shen J, Sun J, et al. Reprogramming of Normal Fibroblasts into Cancer-Associated Fibroblasts by miRNAs-Mediated CCL2/VEGFA Signaling. *PloS Genet* (2016) 12(8):e1006244. doi: 10.1371/journal.pgen.1006244
42. Shen K, Luk S, Elman J, Murray R, Mukundan S, Parekkadan B. Suicide Gene-Engineered Stromal Cells Reveal a Dynamic Regulation of Cancer Metastasis. *Sci Rep* (2016) 6:21239. doi: 10.1038/srep21239
43. Vafaei F, Colvin EK, Mok SC, Howell VM, Samimi G. Functional prediction of long non-coding RNAs in ovarian cancer-associated fibroblasts indicate a potential role in metastasis. *Sci Rep* (2017) 7(1):10374. doi: 10.1038/s41598-017-10869-y
44. Zhu X, Wang K, Zhang K, Xu F, Yin Y, Zhu L, et al. Galectin-1 knockdown in carcinoma-associated fibroblasts inhibits migration and invasion of human MDA-MB-231 breast cancer cells by modulating MMP-9 expression. *Acta Biochim Biophys Sin (Shanghai)* (2016) 48(5):462–7. doi: 10.1093/abbs/gmw019
45. An Y, Liu F, Chen Y, Yang Q. Crosstalk between cancer-associated fibroblasts and immune cells in cancer. *J Cell Mol Med* (2020) 24(1):13–24. doi: 10.1111/jcmm.14745
46. Shen T, Li Y, Zhu S, Yu J, Zhang B, Chen X, et al. YAP1 plays a key role of the conversion of normal fibroblasts into cancer-associated fibroblasts that contribute to prostate cancer progression. *J Exp Clin Cancer Res* (2020) 39(1):36. doi: 10.1186/s13046-020-1542-z
47. Mishra P, Mishra P, Humeniuk R, Medina D, Alexe G, Mesirov J, et al. Carcinoma-associated fibroblast-like differentiation of human mesenchymal stem cells. *Cancer Res* (2008) 68(11):4331–9. doi: 10.1158/0008-5472.can-08-0943
48. Spaeth E, Dembinski J, Sasser A, Watson K, Klopp A, Hall B, et al. Mesenchymal stem cell transition to tumor-associated fibroblasts contributes to fibrovascular network expansion and tumor progression. *PloS One* (2009) 4(4):e4992. doi: 10.1371/journal.pone.0004992
49. Zong Z, Song Y, Xue Y, Ruan X, Liu X, Yang C, et al. Knockdown of LncRNA SCAMP1 suppressed malignant biological behaviours of glioma cells via modulating miR-499a-5p/LMX1A/NLR5 pathway. *J Cell Mol Med* (2019) 23(8):5048–62. doi: 10.1111/jcmm.14362
50. Jiang R, Tang J, Chen Y, Deng L, Ji J, Xie Y, et al. The long noncoding RNA lnc-EGFR stimulates T-regulatory cells differentiation thus promoting hepatocellular carcinoma immune evasion. *Nat Commun* (2017) 8:15129. doi: 10.1038/ncomms15129
51. Xiao Y, Zhu Z, Li J, Yao J, Jiang H, Ran R, et al. Expression and prognostic value of long non-coding RNA H19 in glioma via integrated bioinformatics analyses. *Aging (Albany NY)* (2020) 12(4):3407–30. doi: 10.18632/aging.102819
52. Zheng M, Liu X, Zhou Q, Liu G. HOTAIRM1 competed endogenously with miR-148a to regulate DLGAP1 in head and neck tumor cells. *Cancer Med* (2018) 7(7):3143–56. doi: 10.1002/cam4.1523
53. Zhang Y, Mi L, Xuan Y, Gao C, Wang YH, Ming HX, et al. LncRNA HOTAIRM1 inhibits the progression of hepatocellular carcinoma by inhibiting the Wnt signaling pathway. *Eur Rev Med Pharmacol Sci* (2018) 22(15):4861–8. doi: 10.26355/eurrev_201808_15622
54. Li X, Pang L, Yang Z, Liu J, Li W, Wang D. LncRNA HOTAIRM1/HOXA1 Axis Promotes Cell Proliferation, Migration And Invasion In Endometrial Cancer. *Onco Targets Ther* (2019) 12:10997–1015. doi: 10.2147/OTT.S222334
55. Liang Q, Li X, Guan G, Xu X, Chen C, Cheng P, et al. Long non-coding RNA, HOTAIRM1, promotes glioma malignancy by forming a ceRNA network. *Aging (Albany NY)* (2019) 11(17):6805–38. doi: 10.18632/aging.102205
56. Lin YH, Guo L, Yan F, Dou ZQ, Yu Q, Chen G. Long non-coding RNA HOTAIRM1 promotes proliferation and inhibits apoptosis of glioma cells by regulating the miR-873-5p/ZEB2 axis. *Chin Med J (Engl)* (2020) 133(2):174–82. doi: 10.1097/CM9.0000000000000615
57. Hao Y, Li X, Chen H, Huo H, Liu Z, Chai E. Over-expression of long noncoding RNA HOTAIRM1 promotes cell proliferation and invasion in human glioblastoma by up-regulating SP1 via sponging miR-137. *Neuroreport* (2020) 31(2):109–17. doi: 10.1097/WNR.0000000000001380
58. Cheng Y, Jia B, Wang Y, Wan S. miR-133b acts as a tumor suppressor and negatively regulates ATP citrate lyase via PPARgamma in gastric cancer. *Oncol Rep* (2017) 38(5):3220–6. doi: 10.3892/or.2017.5944
59. Wang QY, Zhou CX, Zhan MN, Tang J, Wang CL, Ma CN, et al. MiR-133b targets Sox9 to control pathogenesis and metastasis of breast cancer. *Cell Death Dis* (2018) 9(7):752. doi: 10.1038/s41419-018-0715-6

60. Zhang Q, Fan X, Xu B, Pang Q, Teng L. miR-133b acts as a tumor suppressor and negatively regulates EMP2 in glioma. *Neoplasma* (2018) 65(4):494–504. doi: 10.4149/neo_2018_170510N337
61. Lv L, Li Q, Chen S, Zhang X, Tao X, Tang X, et al. miR-133b suppresses colorectal cancer cell stemness and chemoresistance by targeting methyltransferase DOT1L. *Exp Cell Res* (2019) 385(1):111597. doi: 10.1016/j.yexcr.2019.111597
62. Zeng W, Zhu JF, Liu JY, Li YL, Dong X, Huang H, et al. miR-133b inhibits cell proliferation, migration and invasion of esophageal squamous cell carcinoma by targeting EGFR. *BioMed Pharmacother* (2019) 111:476–84. doi: 10.1016/j.biopha.2018.12.057

Conflict of Interest: The authors declare that the research was conducted in the absence of any commercial or financial relationships that could be construed as a potential conflict of interest.

Copyright © 2021 Wang, Li, Jiang, Dong, Li, Cheng, Shi, Liu, Qian and Dong. This is an open-access article distributed under the terms of the Creative Commons Attribution License (CC BY). The use, distribution or reproduction in other forums is permitted, provided the original author(s) and the copyright owner(s) are credited and that the original publication in this journal is cited, in accordance with accepted academic practice. No use, distribution or reproduction is permitted which does not comply with these terms.



YTHDF1 Is a Potential Pan-Cancer Biomarker for Prognosis and Immunotherapy

Jian Hu[†], Dongxu Qiu[†], Anze Yu, Jiao Hu, Hao Deng, Huihuang Li, Zhenglin Yi, Jinbo Chen^{*} and Xiongbing Zu^{*}

Department of Urology, Xiangya Hospital, Central South University, Changsha, China

OPEN ACCESS

Edited by:

Marco Rossi,
University of Catanzaro, Italy

Reviewed by:

Shanmugarajan Krishnan,
Massachusetts General Hospital,
United States
Kamaneh Montazeri,
Massachusetts General Hospital
Cancer Center, United States

*Correspondence:

Xiongbing Zu
zuxbxyyy@126.com
Jinbo Chen
chenjinbo1989@yahoo.com

[†]These authors have contributed
equally to this work

Specialty section:

This article was submitted to
Cancer Molecular
Targets and Therapeutics,
a section of the journal
Frontiers in Oncology

Received: 16 September 2020

Accepted: 06 April 2021

Published: 06 May 2021

Citation:

Hu J, Qiu D, Yu A, Hu J, Deng H, Li H,
Yi Z, Chen J and Zu X (2021) YTHDF1
Is a Potential Pan-Cancer Biomarker
for Prognosis and Immunotherapy.
Front. Oncol. 11:607224.
doi: 10.3389/fonc.2021.607224

Background: YTH N6-methyladenosine RNA binding protein 1 (YTHDF1) has been indicated proven to participate in the cross-presentation of tumor antigens in dendritic cells and the cross-priming of CD8+ T cells. However, the role of YTHDF1 in prognosis and immunology in human cancers remains largely unknown.

Methods: All original data were downloaded from TCGA and GEO databases and integrated via R 3.2.2. YTHDF1 expression was explored with the Oncomine, TIMER, GEPIA, and BioGPS databases. The effect of YTHDF1 on prognosis was analyzed via GEPIA, Kaplan-Meier plotter, and the PrognScan database. The TISIDB database was used to determine YTHDF1 expression in different immune and molecular subtypes of human cancers. The correlations between YTHDF1 expression and immune checkpoints (ICP), tumor mutational burden (TMB), microsatellite instability (MSI), and neoantigens in human cancers were analyzed via the SangerBox database. The relationships between YTHDF1 expression and tumor-infiltrated immune cells were analyzed via the TIMER and GEPIA databases. The relationships between YTHDF1 and marker genes of tumor-infiltrated immune cells in urogenital cancers were analyzed for confirmation. The genomic alterations of YTHDF1 were investigated with the c-BioPortal database. The differential expression of YTHDF1 in urogenital cancers with different clinical characteristics was analyzed with the UALCAN database. YTHDF1 coexpression networks were studied by the LinkedOmics database.

Results: In general, YTHDF1 expression was higher in tumors than in paired normal tissue in human cancers. YTHDF1 expression had strong relationships with prognosis, ICP, TMB, MSI, and neoantigens. YTHDF1 plays an essential role in the tumor microenvironment (TME) and participates in immune regulation. Furthermore, significant strong correlations between YTHDF1 expression and tumor immune-infiltrated cells (TILs) existed in human cancers, and marker genes of TILs were significantly related to YTHDF1 expression in urogenital cancers. YTHDF1 coexpression networks mostly participated in the regulation of immune response and antigen processing and presentation.

Conclusion: YTHDF1 may serve as a potential prognostic and immunological pan-cancer biomarker. Moreover, YTHDF1 could be a novel target for tumor immunotherapy.

Keywords: YTHDF1, prognosis, tumor microenvironment, immune infiltration, immunotherapy, human cancer

INTRODUCTION

N6-methyladenine (m6A), occurring in the N6-position of adenosine, is the most abundant modification of mRNA and noncoding RNAs in mammals (1–3). Moreover, it plays an essential role in RNA nucleation, RNA-protein interaction, mRNA metabolism, mRNA stability and splicing, and mRNA translation (4, 5). Under normal conditions, m6A molecules modify the processing of RNA by serving as “writers”, “erasers”, and “readers” (6, 7). However, abnormal expression of m6A molecules has been proven to promote tumorigenesis by affecting oncogene expression (8–10). Recent evidence reveals that m6A produces a marked effect on cancer development, such as proliferation, migration, and invasion (11), which means that m6A molecules may be promising prognostic biomarkers and therapeutic targets.

YTH N6-methyladenosine RNA binding protein 1 (YTHDF1) belongs to the YTH domain family, and acts as a “reader” of m6A-modified mRNAs. In the cytosol, YTHDF1 plays an essential role in RNA translation initiation by binding to initiation factors (4). Previous studies proved that tumor neoantigens could cause spontaneous antitumor immune responses and predict the response to cancer immunotherapies (12, 13). Recent studies have demonstrated that YTHDF1 plays a crucial role in cancer development and durable neoantigen-specific antitumor immunity (4). For example, YTHDF1 promotes the progression of lung cancer by participating in the m6A demethylase the ALKBH5 pathway (14). In colorectal cancer, YTHDF1 is regarded as an oncogene (15); In breast cancer, overexpression of YTHDF1 predicts worse survival (16). Furthermore, YTHDF1 inhibits the function of antitumor immune cells in the tumor microenvironment (TME) by acting on the infiltrated level of CD8+ T cells and natural killer cells. Blocking the YTHDF1 reactivates the inhibited antitumor immunity and synergistically improves the therapeutic efficacy of anti-PD-L1 inhibitors (17). All of the above studies indicate that YTHDF1 might be a promising prognostic and therapeutic pan-cancer biomarker.

Abbreviations: YTHDF1, YTH N6-methyladenosine RNA binding protein 1; ICP, immune checkpoints; TMB, tumor mutational burden; MSI: microsatellite instability; TILs, tumor immune-infiltrated cells; m6A, N6-methyladenine; TCGA, the Cancer Genome Atlas; ESTIMATE, Estimation of Stromal and Immune cells in Malignant Tumor tissues using Expression data; OS, overall survival; DFS, disease-free survival; RFS, relapse-free survival; ACC, adrenocortical carcinoma; BLCA, bladder urothelial carcinoma; BRCA, breast invasive carcinoma; CESC, cervical squamous cell carcinoma and endocervical adenocarcinoma; COAD, colon adenocarcinoma; READ, colon adenocarcinoma; ESCA, esophageal carcinoma; GBM, glioblastoma multiforme; HNSC, head and neck squamous cell carcinoma; KICH, kidney chromophobe; KIRC, kidney renal clear cell carcinoma; KIRP, kidney renal papillary cell carcinoma; LAML, acute myeloid leukemia; LGG, brain lower grade glioma; LIHC, liver hepatocellular carcinoma; LUAD, lung adenocarcinoma; LUSC, lung squamous cell carcinoma; MESO, mesothelioma; OV, ovarian serous cystadenocarcinoma; PAAD, pancreatic adenocarcinoma; PCPG, pheochromocytoma and paraganglioma; PRAD, prostate adenocarcinoma; READ, rectum adenocarcinoma; STAD, stomach adenocarcinoma; TGCT, testicular germ cell tumors; THCA, thyroid carcinoma; UCEC, uterine corpus endometrial carcinoma; UCS, uterine carcinosarcoma; TME, tumor microenvironment.

However, the role of YTHDF1 in prognosis and immunology in human cancers has seldomly been analyzed systematically. In this study, the role of YTHDF1 in prognosis and immunology in human cancers was comprehensively analyzed. Furthermore, the potential association between YTHDF1 expression and immune subtypes, molecular subtypes of different cancer types, promising immune biomarkers and tumor-infiltrating lymphocytes (TILs) in the TME was analyzed. In addition, we explored the effect of YTHDF1 expression in urogenital cancers to verify the results in human cancers. This study aimed to explore the potential of YTHDF1 in anticancer immunotherapy in human cancer, thus offering insight to a new antitumor strategy.

METHODS

Data and Software Availability

All original data were downloaded from The Cancer Genome Atlas (TCGA) (<https://cancergenome.nih.gov/>) and Gene Expression Omnibus (GEO) (<https://www.ncbi.nlm.nih.gov/geo/>) databases. Detailed information on human cancers and corresponding individual sample sizes is displayed in **Supplementary Table 1**. R 3.2.3 was used to integrate the original data and verify the results analyzed by the website database. All applied online web tools were introduced below.

Four Databases to Analyze YTHDF1 Expression in Human Cancers

The Oncomine database (<https://www.oncomine.org/resource/login.html>), TIMER database (<https://cistrome.shinyapps.io/timer/>), and GEPIA database (<http://gepia2.cancer-pku.cn/#analysis>) were used to compare YTHDF1 expression between human cancers and paired normal tissue (18–20). The BioGPS database (<http://biogps.org>) was used to analyze the expression profiles of YTHDF1 in different cancer and paired normal cell lines (21). In the Oncomine database, we set the thresholds to 0.001 for P-value and 1.5 for the fold change.

Three Databases to Analyze the Prognostic Value of YTHDF1 in Human Cancers

The GEPIA database (<http://gepia2.cancer-pku.cn/#analysis>), Kaplan-Meier Plotter database (<http://kmplot.com/analysis/>), and PrognoScan databases (<http://dna00.bio.kyutech.ac.jp/PrognoScan/index.html>) were used to explore the prognostic value of YTHDF1 expression in human cancers (20, 22, 23). The GEPIA database is an online website, and its analyzed tumor and normal tissue data were from the TCGA database. We used the GEPIA database to explore the correlation between YTHDF1 expression and overall survival (OS) and disease-free survival (DFS) in 33 cancer types. In the GEPIA database, the median YTHDF1 expression was used as a cutoff value to classify groups. The Kaplan-Meier Plotter database classifies groups by calculating an optimal cutoff value automatically. By using the Kaplan-Meier Plotter database, we identified the association between YTHDF1 expression and OS and relapse-free survival (RFS) in 21 cancer

types. Hazard ratios (HRs) with corresponding 95% confidence intervals (CIs) and log-rank P-values were calculated. Data on the Prognoscan website were also collected from the TCGA and GEO database. The prognostic value was considered statistically significant when the P-value was less than 0.05.

Database Applied to Analyze YTHDF1 Expression in Immune and Molecular Subtypes of Human Cancers

The TISIDB database (<http://cis.hku.hk/TISIDB/index.php>) is an online integrated repository portal collecting abundant human cancer datasets from the TCGA database (24). The correlations between YTHDF1 expression and immune or molecular subtypes of different cancer types were explored *via* the TISIDB database. Differences with a P-value < 0.05 were considered to be statistically significant.

Database Used to Analyze the Correlation Between YTHDF1 Expression and Immune Checkpoint (ICP) Genes, Tumor Mutational Burden (TMB), Microsatellite Instability (MSI), Neoantigen, and ESTIMATE of the TME in Human Cancers

The relationship between YTHDF1 expression and immune checkpoint (ICP) genes, biomarkers and ESTIMATE score in the TME was explored *via* the SangerBox website (<http://sangerbox.com/Tool>), which is a useful online platform for TCGA data analysis (25). Immune checkpoint (ICP) genes were selected according to a previous study (26). Tumor mutational burden (TMB), microsatellite instability (MSI), and neoantigens have been proved to be important biomarkers of the TME (27–29). ESTIMATE (Estimation of Stromal and Immune cells in Malignant Tumor tissues using Expression data) was an algorithm designed by Yoshihara et al. for predicting tumor purity in TME, and this algorithm included stromal score (that captures the presence of stroma 136 in tumor tissue), immune score (that represents the infiltration of immune cells in tumor 137 tissue), and estimate score (that infers tumor purity) (30). Correlations between YTHDF1 expression and the above TME biomarkers were explored *via* the SangerBox website. Differences with a P-value < 0.05 were considered to be statistically significant.

Three Databases Used to Analyze the Correlation Between YTHDF1 Expression and Immune Infiltration Cells and Their Marker Genes

We first explored the correlation between YTHDF1 expression and six immune cells (B cells, CD4+ T cells, CD8+ T cells, neutrophils, macrophages, and dendritic cells) in the TME of 31 human cancers *via* the SangerBox website. Then, the correlation between YTHDF1 expression and ten immune cells in the TME was explored in six urogenital cancers by the SangerBox website. These ten immune cells included B cells lineage, CB8+ T cells, cytotoxic lymphocytes, endothelial cells, fibroblasts, monocytic cells, myeloid dendritic cells, neutrophils, natural killer cells, and T cells. We reanalyzed the correlation between YTHDF1 expression and tumor infiltrating

lymphocytes (TILs) *via* the TIMER and GEPIA databases to verify the above results. The TIMER database (<https://cistrome.shinyapps.io/timer/>), which collected 10897 samples across 32 cancer types from TCGA, was created to analyze the level of tumor-associated immune cell infiltration in the TME (19, 31). Then, we verified the correlation between YTHDF1 expression and 24 tumor-infiltrating lymphocytes (TILs) in six urogenital cancers *via* the GEPIA database (20). These 24 tumor-infiltrating lymphocytes (TILs) were selected from a previous study (32), and detailed information is displayed in **Supplementary Table 2**. Finally, the TIMER database was used to explore the relationship between YTHDF1 expression and marker genes of the main immune cells, including B cells, CD8+ T cells, follicular helper T cells (Tfh), T-helper 1 (Th1) cells, T-helper 2 (Th2) cells, T-helper 9 (Th9) cells, T-helper 17 (Th17) cells, T-helper 22 (Th22) cells, Tregs cells, exhausted T cells, M1 macrophages, M2 macrophages, tumor-associated macrophages, monocytes, natural killer (NK) cells, neutrophils and dendritic cells (33–35). The difference at a P-value < 0.05 was considered to be statistically significant.

Database Used to Explore YTHDF1 Genomic Alterations in Six Urogenital Cancers

cBio Cancer Genomics Portal (c-BioPortal) (<http://cbioportal.org>) collected a multidimensional cancer genomics data set (36). Therefore, the c-BioPortal database was applied to explore YTHDF1 genomic alterations in six urogenital cancers.

Database Used to Explore YTHDF1 Expression in Different Clinical Subgroups of Six Urogenital Cancers

The UALCAN database (<http://ualcan.path.uab.edu>) collected RNA-seq and clinical data of 31 cancer types from TCGA (37), and it offered a useful platform to analyze gene expression in tumor and normal tissues. This database was used to analyze the relationship between individual gene expression and clinicopathological features in human cancers.

Database Used to Explore YTHDF1 Coexpression Networks

The LinkedOmics database (<http://www.linkedomics.org/login.php>) is a visual platform and is used to explore the gene expression profile (38). We used LinkedOmics to determine the YTHDF1 coexpression genes by using Pearson's correlation coefficient and showed the results *via* heat maps, and volcano plots. Then, we explored the Gene Ontology biological process (GO_BP), and KEGG pathways of YTHDF1 and its coexpression genes by using gene set enrichment analysis (GSEA).

RESULTS

YTHDF1 Is Significantly Differentially Expressed Between Tumors and Normal Tissues in Human Cancers

The Oncomine database showed that YTHDF1 mRNA levels were significantly higher in most human cancers, such as

bladder, brain and CNS, breast, cervical, colorectal, esophageal, head and neck, kidney, liver, lung, ovarian, pancreatic, prostate cancer, leukemia, melanoma, sarcoma, and other cancer types compared to the corresponding normal tissues. In contrast, YTHDF1 expression was significantly lower only in lymphoma (**Figure 1A**). The results from the TIMER database showed that YTHDF1 expression was significantly higher in BLCA (bladder urothelial carcinoma), BRCA (breast invasive carcinoma), CHOL (cholangiocarcinoma), COAD (colon adenocarcinoma), ESCA (esophageal carcinoma), HNSC (head and neck cancer), KICH (kidney chromophobe), KIRP (kidney renal papillary carcinoma), LIHC (liver hepatocellular carcinoma), LUAD (lung adenocarcinoma), LUSC (lung squamous cell carcinoma), PRAD (prostate adenocarcinoma), STAD (stomach adenocarcinoma) and UCEC (uterine corpus endometrial carcinoma) than in adjacent normal tissue. However, YTHDF1 mRNA expression was low only in THCA

(thyroid carcinoma) (**Figure 1B**). The results of the GEPIA database analysis are displayed as supplementary results of cancers without paired normal tissues in the TIMER database. Furthermore, the results showed that YTHDF1 mRNA expression was significantly high among most cancer types except LAML (acute myeloid leukemia), which was consistent with the Oncomine database results (**Figure 1C**). The expression of YTHDF1 in different cancer cell lines and normal tissues was investigated *via* the BioGPS database, and we found that YTHDF1 had a high expression level in almost all cancer cell lines. Ten cancer cell lines with the highest YTHDF1 expression level are displayed in **Figure 1D**. In normal cells, the YTHDF1 expression level in immune cells was the highest (**Figure 1E**). Detailed information is shown in **Supplementary Figure 1**. The above results suggested that YTHDF1 was overexpressed in cancer tissues and might participate in the process of immune regulation.

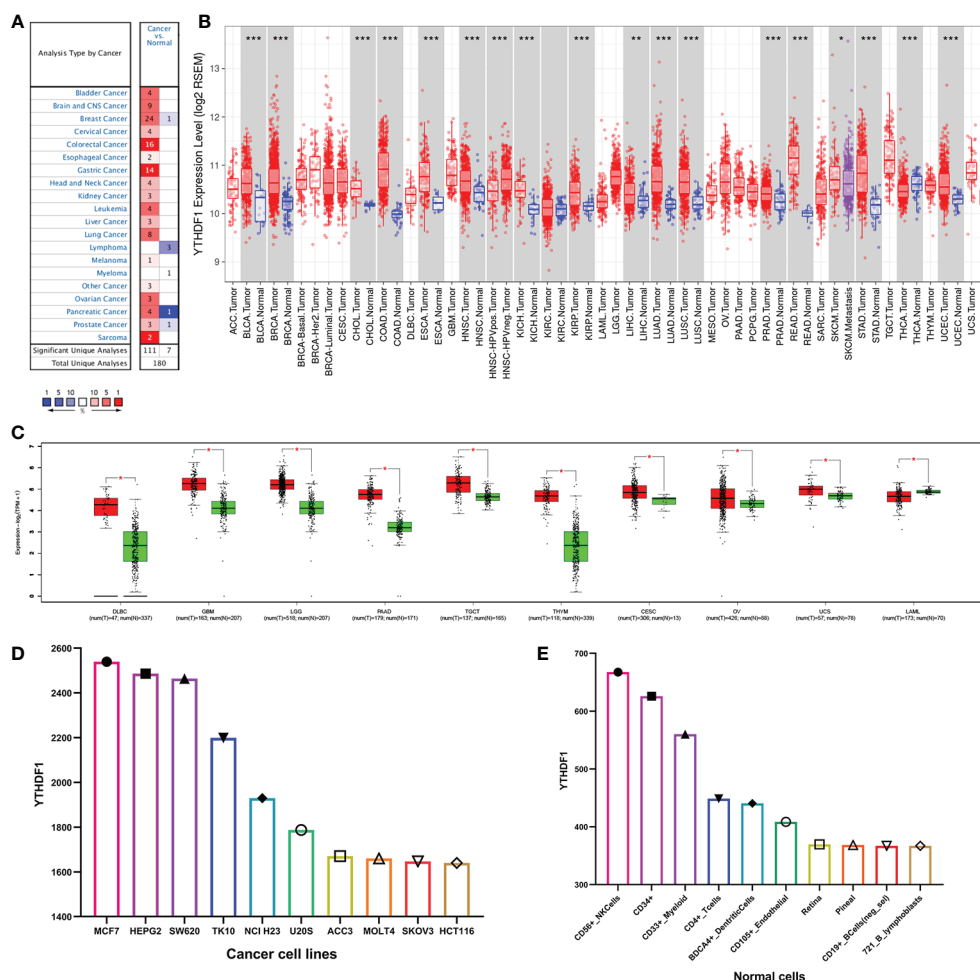


FIGURE 1 | YTHDF1 expression levels in human cancers. **(A)** YTHDF1 expression in different cancers and paired normal tissue in the Oncomine database. **(B)** YTHDF1 expression levels in different cancer types from the TCGA database analyzed by the TIMER database. (* $P < 0.05$, ** $P < 0.01$, *** $P < 0.001$). **(C)** YTHDF1 expression in several cancers and paired normal tissue in the GEPIA database. **(D)** the expression of YTHDF1 in different cancer cell lines analyzed by the BioGPS database. **(E)** the expression of YTHDF1 in normal tissue analyzed by the BioGPS database.

YTHDF1 Is a Prognostic Pan-Cancer Biomarker

The prognostic value of YTHDF1 expression in human cancers was analyzed by several databases. In GEPIA, we found that higher YTHDF1 expression was associated with poorer overall survival (OS) and disease-free survival (DFS) in LIHC (n = 364, OS: HR = 1.8, P = 0.0015; n = 364, DFS: HR = 1.6, P = 0.0018; **Figures 2A, B**), and UVM (uveal melanoma) (n = 78, OS: HR = 3.1, P = 0.027; n = 78, DFS: HR = 2.7, P = 0.034; **Figures 2C, D**). In addition, patients with higher YTHDF1 expression had poorer OS in mesothelioma (MESO) (n = 82, HR = 1.6, P = 0.049; **Figure 2E**) and uterine carcinosarcoma (UCS) (n = 740, HR = 2.2, P = 0.00097; **Figure 2F**), and also had poor DFS in BLCA (n = 400, HR = 1.5, P = 0.025; **Figure 2G**) and adrenocortical carcinoma (ACC) (n = 76, HR = 2, P = 0.046; **Figure 2H**). However, higher YTHDF1 expression was related to better OS and DFS in KIRC (kidney renal papillary cell carcinoma) (n = 516, OS: HR = 0.71, P = 0.031; n = 516, DFS: HR = 0.55, P = 0.0015; **Figures 2I, J**). In the Kaplan-Meier plotter database,

higher YTHDF1 expression was associated with poorer RFS in TGCT (testicular germ cell tumors) (n = 105, HR = 5.37, P = 0.011; **Figure 2K**) and KIRP (n = 183, HR = 3.56, P = 0.027; **Figure 2L**). More details of the relationship between YTHDF1 and OS or relapse-free survival (RFS) analyzed by the Kaplan-Meier plotter database are shown in **Supplementary Figure 2**. Furthermore, the correlation between YTHDF1 expression and survival in GEO datasets was evaluated by PrognScan. Higher expression of YTHDF1 showed worse survival in breast, soft tissue, bladder, lung and brain cancer. Details are shown in **Supplementary Table 3**. The above results proved that YTHDF1 expression closely related to the prognosis of various cancer types.

YTHDF1 Expression Is Related to Immune and Molecular Subtypes in Human Cancers

Next, the role of YTHDF1 expression on immune and molecular subtypes among human cancers was explored

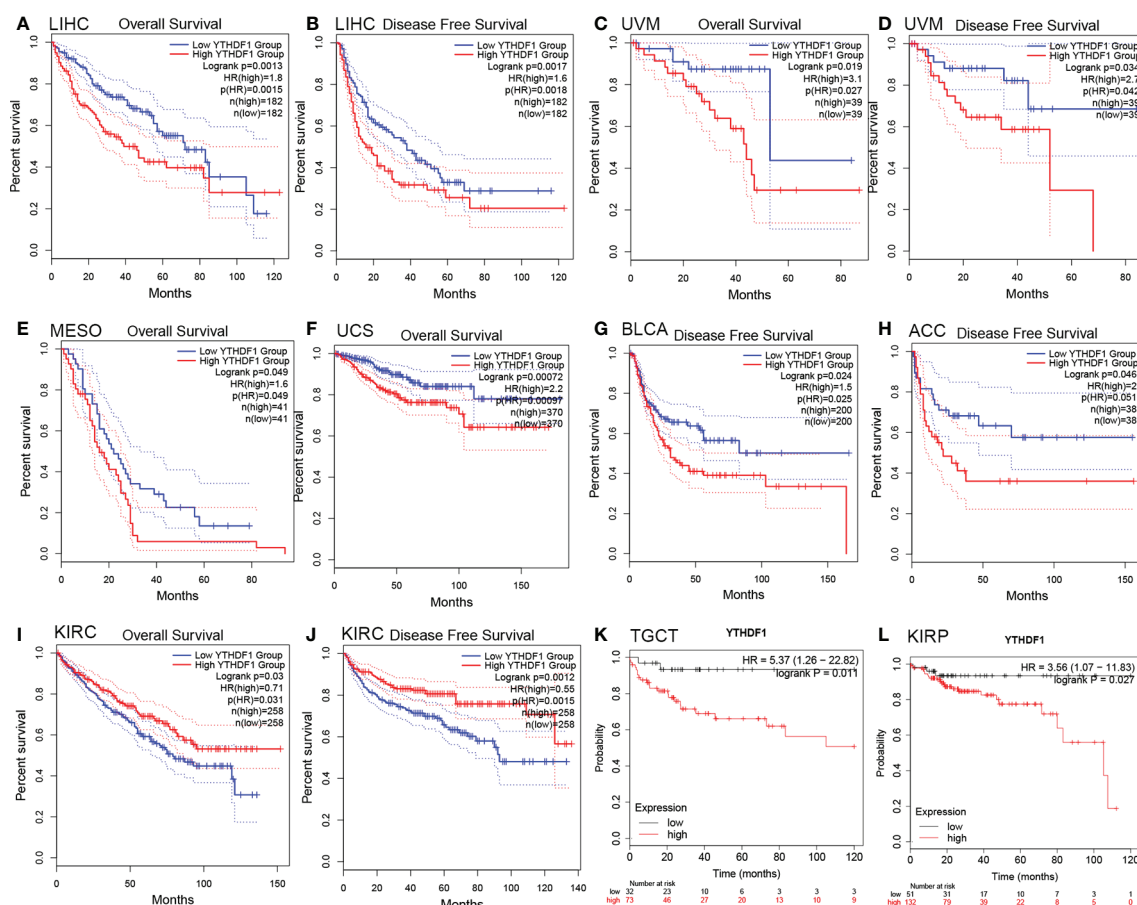


FIGURE 2 | Kaplan-Meier survival curve of human cancers with high and low YTHDF1 expression analyzed by the GEPIA database (**A–J**) and the Kaplan-Meier plotter database (**K, L**). (**A–D**) High YTHDF1 expression was related to worse OS and DFS in LIHC (n = 364) and UVM cohorts (n = 78). (**E, F**) High YTHDF1 expression was related to worse OS in MESO (n = 82) and UCS cohorts (n = 740). (**G, H**) High YTHDF1 expression was related to worse DFS in BLCA (n = 400) and ACC cohorts (n = 76). (**I, J**) High YTHDF1 expression was related to better OS and DFS in KIRC cohorts (n = 316). (**K, L**) higher YTHDF1 expression was related to poorer RFS in TGCT (n = 105) and KIRP (n = 183). OS, overall survival; DFS, disease free survival; RFS, relapse-free survival.

with the TISIDB website. Immune subtypes were classified into six types, including C1 (wound healing), C2 (IFN-gamma dominant), C3 (inflammatory), C4 (lymphocyte depleted), C5 (immunologically quiet) and C6 (TGF- β dominant). The results showed that YTHDF1 expression was related to different immune subtypes in BRCA, COAD, HNSC, KIRC, LGG (brain lower grade glioma), LUAD, LUSC, OV (ovarian serous cystadenocarcinoma), PRAD, SKCM (skin cutaneous melanoma), STAD, and UCEC (**Figure 3**). Additionally, YTHDF1 expression differed in different immune subtypes of one cancer type. Taking KIRC as an example, YTHDF1 showed high expression in C1 and C5 types and low expression in C2 types. For different molecular subtypes of cancers, a significant connection with YTHDF1 expression existed in BRCA, COAD, ESCA, HNSC, KIRP, LGG, LUSC, OV, PCPG (Pheochromocytoma and Paraganglioma), READ (rectum adenocarcinoma), STAD and UCEC (**Figure 4**). YTHDF1 expression in different immune and molecular subtypes of other cancers is shown in **Supplementary Figures 3, 4**. Based on the above results, we concluded that YTHDF1 expression differs in immune subtypes and molecular subtypes of various human cancer types.

YTHDF1 Expression Is Related to Immune Checkpoint (ICP) Genes in Human Cancers

Studies have proven that immune checkpoint (ICP) genes have a great influence on immune cell infiltration and immunotherapy (39). Subsequently, we explored the associations between YTHDF1 expression and ICP genes in human cancers to explore the potential of YTHDF1 in immunotherapy. Among 47 ICP genes, strong relationships with YTHDF1 expression were found in many types of cancer, such as GBM (glioblastoma multiforme), OV, LUSC, PRAD, UCEC, TGCT, KIRP, LIHC, BRCA, COAD, KIRC, THCA, LAML, LGG, KICH, and UVM (**Figure 5**). In OV, PRAD, UCEC, KIRP, LIHC, KIRC, LAML, LGG, KICH, and UVM, YTHDF1 expression was positively related to immune checkpoint genes, especially in LIHC, in which 32 of 47 immune checkpoint genes had connections with YTHDF1 expression. This suggests that YTHDF1 might coordinate the activity of these ICP genes in different signal transduction pathways, and potentially serve as an ideal immunotherapy target. And high YTHDF1 expression might predict good therapeutic efficacy of immunotherapy targeting ICP genes. In GBM, LUSC, TGCT, BRCA, COAD and THCA,

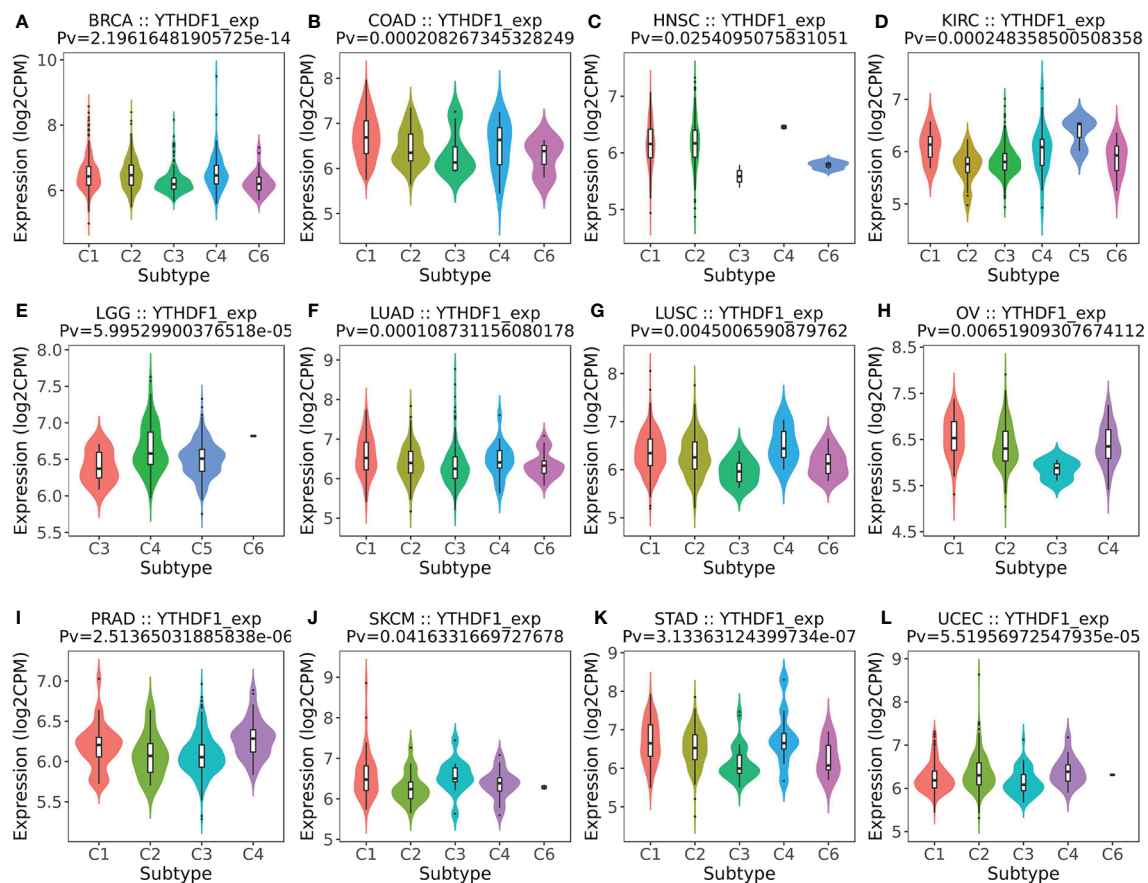


FIGURE 3 | The relationship between YTHDF1 expression and pan-cancer immune subtypes. (A) in BRCA, (B) in COAD, (C) in HNSC, (D) in KIRC, (E) in LGG, (F) in LUAD, (G) in LUSC, (H) in OV, (I) in PRAD, (J) in SKCM, (K) in STAD, (L) in UCEC.

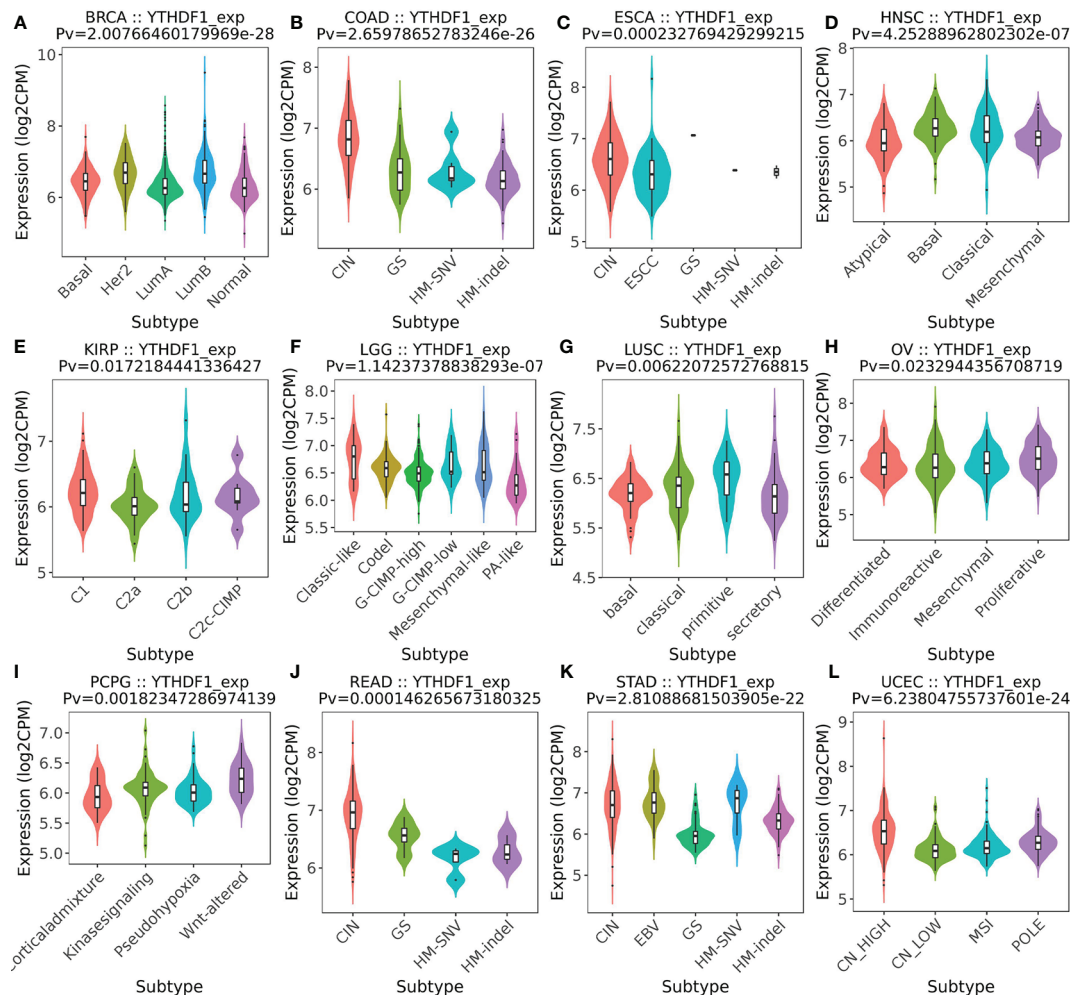


FIGURE 4 | The relationship between YTHDF1 expression and pan-cancer molecular subtypes. (A) in BRCA, (B) in COAD, (C) in ESCA, (D) in HNSC, (E) in KIRP, (F) in LGG, (G) in LUSC, (H) in OV, (I) in PCPG, (J) in READ, (K) in STAD, (L) in UCEC.

YTHDF1 is negatively related with ICP genes, which means that high YTHDF1 expression might predict unsatisfying immunotherapy outcomes when targeting ICP genes. On the other hand, YTHDF1 inhibitors might be potential alternative treatments. Thus, we hypothesized that YTHDF1, working as a potential pan-cancer biomarker or as a new immunotherapy target, may predict the immunotherapy response or achieve a promising therapeutic outcome, respectively.

YTHDF1 Expression Is Related to Tumor Mutational Burden (TMB), Microsatellite Instability (MSI), Neoantigen, and ESTIMATE

To explore the role of YTHDF1 in the immune mechanism and immune response of the tumor microenvironment (TME), we analyzed the correlations between YTHDF1 expression and TMB, MSI, and neoantigens. TMB, MSI, and neoantigens in tumor microenvironment are related to antitumor immunity and

could predict the therapeutic efficacy of tumor immunotherapy (13, 40–42). Our results showed that YTHDF1 expression had significant positive associations with TMB in LUAD, LUSC, BLCA, PAAD (pancreatic adenocarcinoma), SARC (sarcoma), BRCA, STAD, LGG, and ACC and negative relations in COAD and THCA (Figure 6A). For MSI, there were positive correlations with YTHDF1 expression in LUAD, LUSC, UCEC, BLCA, ESCA, and KIRC and negative correlations with YTHDF1 expression in PRAD, COAD, and DLBC (lymphoid neoplasm diffuse large B-cell lymphoma) (Figure 6B). Analyzing the relationships between YTHDF1 expression and neoantigens, we found that YTHDF1 expression was positively related to neoantigens in LUAD, BRCA, HNSC, LIHC, and LGG and negatively related to neoantigens in COAD (Figure 6C). Then, we explored the associations between YTHDF1 expression and three kinds of ESTIMATE (Figure 6D). The results indicated that there were strong positive correlations with YTHDF1 expression in LGG and negative correlations in ACC, PCPG, GBM, OV, LUAD,

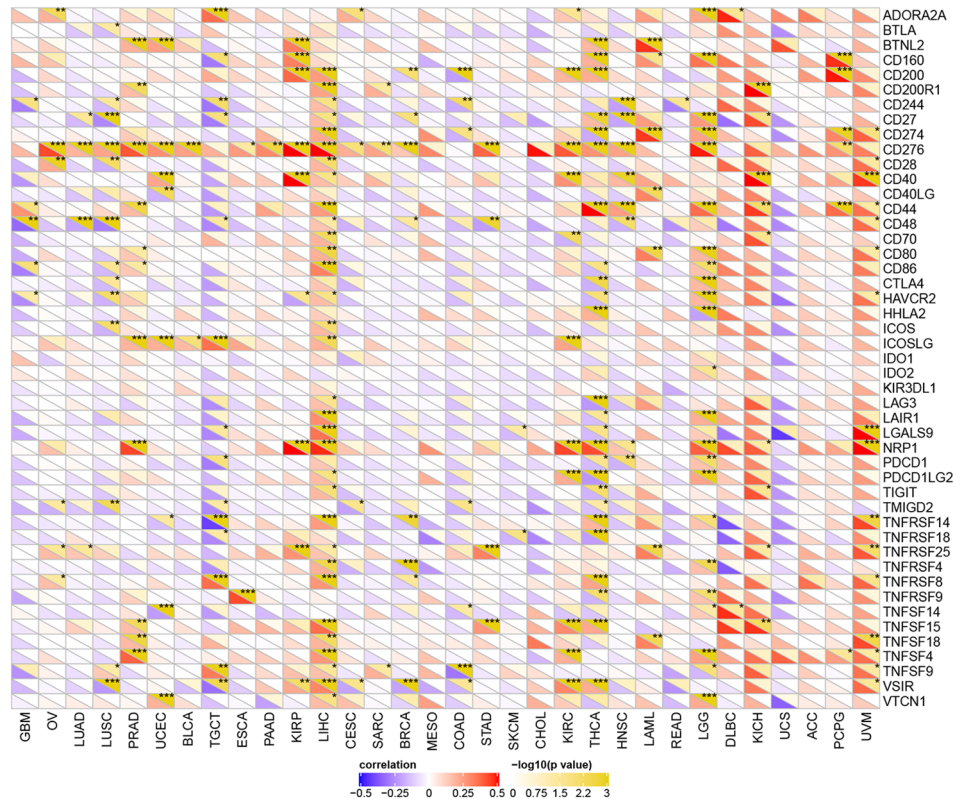


FIGURE 5 | The relationship between YTHDF1 expression and pan-cancer immune checkpoint genes. * $P < 0.05$; ** $P < 0.01$; *** $P < 0.001$.

LUSC, UCEC, BLCA, TGCT, PAAD, KIRP, CESC, BRCA, COAD, STAD, SKCM, KIRC, THCA, HNSC, READ, and UCS. The above results further verified our conjecture that YTHDF1 may influence antitumor immunity by regulating the composition and immune mechanism in the TME.

YTHDF1 Correlates With Immune Cell Infiltration in the TME in Human Cancers

After proving the differential YTHDF1 expression in different immune subtypes, we explored the potential correlation between YTHDF1 expression and immune cell infiltration in human cancers, and the results indicated that there was significant correlation in 31 cancer types. YTHDF1 expression had a strong relationship with dendritic cell in 12 cancer types, macrophage in 9 cancer types, neutrophil in 8 cancer types, CD8+ T cells in 13 cancer types, B cells in 10 cancer types and CD4+ T cells in 6 cancer types (**Figure 7A**). The TIMER database's results consisted of the above results, and all details are shown on **Supplementary Table 4**.

YTHDF1 Correlates With Immune Cell Infiltration and Their Gene Markers in TME in Urogenital Cancers

Next, we thoroughly analyze the connection between YTHDF1 expression and immune cell infiltration in six urogenital cancers.

The results showed that YTHDF1 expression was correlated with the infiltration levels of neutrophils in BLCA, CD8+ T cells, fibroblasts, monocytic cell lineage, myeloid dendritic cells, and neutrophils in KICH; endothelial cells, fibroblasts, monocytic cell lineage, and neutrophils in PRAD; B cell lineage, CD8+ T cells, fibroblasts, myeloid dendritic cells, neutrophils, and T cells in TGCT; endothelial cells, fibroblasts, monocytic cell lineage, neutrophils, and T cells in KIRC and endothelial cells, fibroblasts, monocytic cell lineage, myeloid dendritic cells and neutrophils in KIRC (**Figure 7B**). Next, we verified the above relationship *via* GEPIA and TIMER, and most results from those 2 databases were consistent with the above results. YTHDF1 expression was positively related to immune cells in all urogenital cancers except TGCT. Detailed information on the relationship between YTHDF1 expression and TILs in the GEPIA and TIMER databases is shown in **Supplementary Figures 5–10**. In general, the above results strongly identified that YTHDF1 expression influenced immune cell infiltration in urogenital cancers.

Then, we used the TIMER database to further explore the correlation between YTHDF1 expression and different marker subsets of immune cells in six urogenital cancers. The correlation was adjusted by purity to decrease the bias caused by clinical samples. The results showed that YTHDF1 was strongly connected with marker genes of macrophages, Th1 cells, Th2

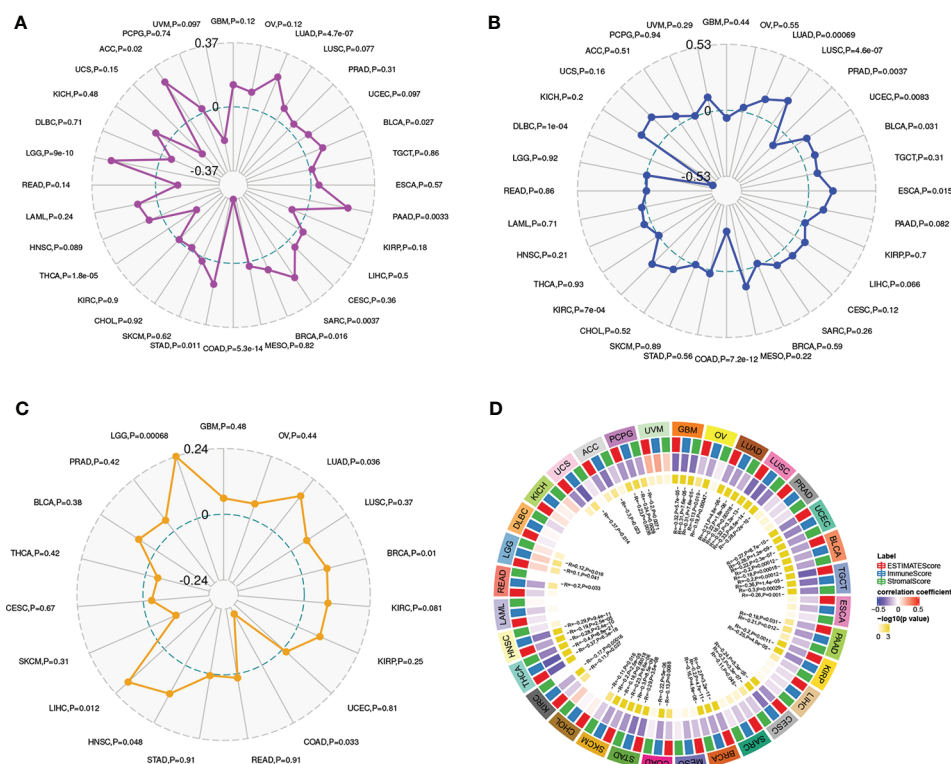


FIGURE 6 | The relationship between YTHDF1 expression and TMB (A), MSI (B), neoantigen (C) and ESTIMATE score (D) in human cancers. TMB, tumor mutational burden; MSI, microsatellite instability; MMR genes, mismatch repair genes; ESTIMATE, Estimation of Stromal and Immune cells in Malignant Tumor tissues using Expression data.

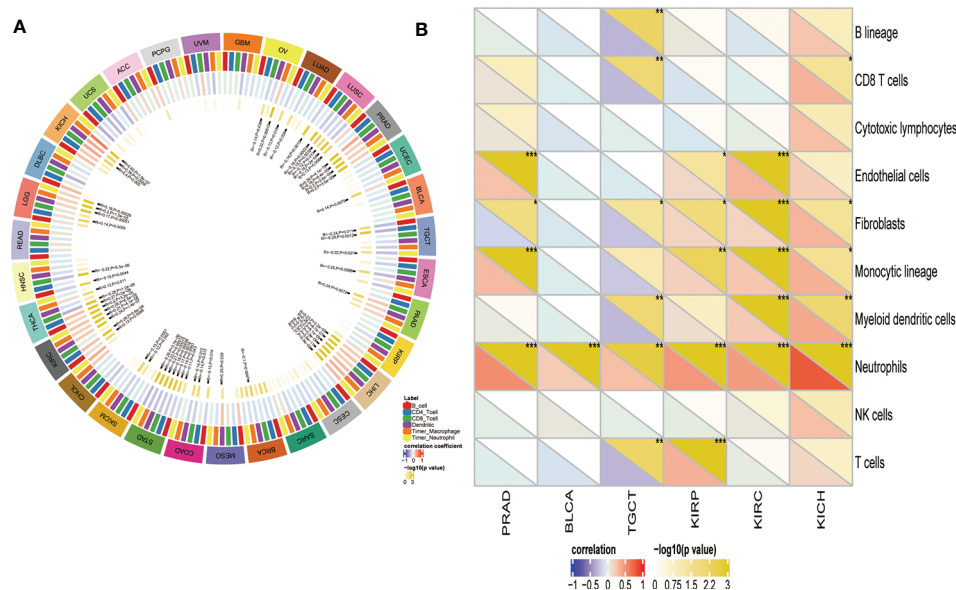


FIGURE 7 | The relationship between YTHDF1 expression and infiltrating immune cells of human cancers and urogenital cancers. (A) the relationship between YTHDF1 expression level and infiltrating levels of B cells, CD4+ T cells, CB8+ T cells, macrophages, neutrophils, dendritic cell in human cancers. (B) the relationship between YTHDF1 expression level and infiltrating levels of B cell lineages, CB8+ T cells, cytotoxic lymphocytes, endothelial cells, fibroblasts, monocytic cell lineages, myeloid dendritic cells, neutrophils, natural killer cells, T cells in six urogenital cancers. * $P < 0.05$; ** $P < 0.01$; *** $P < 0.001$.

TABLE 1 | Correlation between YTHDF1 and relate genes and markers of immune cells analyzed by TIMER.

Description	Gene markers	PRAD				BLCA			
		None		Purity		None		Purity	
		Cor	P	Cor	P	Cor	P	Cor	P
CD8+ T cell	CD8A	0.197	***	0.220	***	-0.044	0.380	0.015	0.772
	CD8B	0.141	**	0.134	**	-0.002	0.966	0.026	0.614
T cell (general)	CD3D	-0.011	0.808	-0.041	0.407	-0.124	*	-0.087	0.096
	CD3E	0.087	0.052	0.079	0.106	-0.077	0.120	-0.015	0.779
	CD2	0.119	**	0.089	0.070	-0.054	0.278	0.012	0.824
B cell	CD19	-0.041	0.356	-0.058	0.235	0.014	0.771	0.093	0.075
	CD79A	0.041	0.366	0.014	0.782	-0.051	0.304	0.011	0.833
Monocyte	CD86	0.260	***	0.226	***	-0.009	0.859	0.088	0.090
	CD115 (CSF1R)	0.229	***	0.193	***	-0.048	0.330	0.034	0.516
TAM	CCL2	0.156	***	0.168	***	0.006	0.900	0.109	*
	CD68	0.219	***	0.195	***	-0.030	0.546	0.007	0.901
	IL10	0.274	***	0.241	***	-0.018	0.724	0.088	0.091
M1 Macrophage	INOS (NOS2)	-0.097	*	-0.046	0.348	0.115	*	0.100	0.056
	IRF5	0.298	***	0.337	***	0.120	*	0.125	*
	COX2(PTGS2)	0.304	***	0.290	***	0.047	0.339	0.077	0.139
M2 Macrophage	CD163	0.310	***	0.276	***	-0.024	0.622	0.073	0.160
	VSIG4	0.251	***	0.220	***	-0.066	0.187	0.013	0.800
	MS4A4A	0.217	***	0.196	***	-0.052	0.292	0.037	0.476
Neutrophils	CD66b (CEACAM8)	0.031	0.490	0.047	0.339	0.122	*	0.092	0.079
	CD11b (ITGAM)	0.221	***	0.204	***	-0.015	0.761	0.085	0.105
	CCR7	0.158	***	0.149	**	0.039	0.431	0.096	0.066
Natural killer cell	KIR2DL1	0.101	*	0.109	*	-0.050	0.317	-0.020	0.698
	KIR2DL3	0.073	0.106	0.086	0.079	-0.065	0.187	-0.029	0.585
	KIR2DL4	0.234	***	0.258	***	-0.058	0.243	-0.019	0.717
	KIR3DL1	0.102	*	0.108	*	-0.040	0.418	-0.010	0.847
	KIR3DL2	0.092	*	0.062	0.209	-0.025	0.616	0.006	0.915
	KIR3DL3	0.000	0.997	-0.016	0.738	-0.023	0.645	-0.022	0.678
	KIR2DS4	0.030	0.499	0.039	0.430	-0.034	0.494	-0.003	0.952
Dendritic cell	HLA-DPB1	-0.005	0.904	-0.005	0.914	-0.051	0.304	0.028	0.596
	HLA-DQB1	0.095	*	0.086	0.079	-0.025	0.609	0.054	0.299
	HLA-DRA	0.214	***	0.216	***	0.009	0.863	0.095	0.069
	HLA-DPA1	0.200	***	0.181	***	-0.010	0.835	0.069	0.184
	BDCA-1(CD1C)	0.185	***	0.169	***	-0.069	0.163	-0.023	0.662
	BDCA-4(NRP1)	0.529	***	0.522	***	0.061	0.220	0.090	0.085
	CD11c (ITGAX)	0.218	***	0.233	***	-0.015	0.763	0.093	0.075
Th1	T-bet (TBX21)	0.135	**	0.161	***	-0.034	0.489	0.018	0.731
	STAT4	0.172	***	0.168	***	-0.032	0.525	0.029	0.580
	STAT1	0.557	***	0.546	***	0.157	**	0.223	***
	IFN- γ (IFNG)	0.139	**	0.120	*	-0.026	0.596	0.018	0.736
	TNF- α (TNF)	0.194	***	0.177	***	0.103	*	0.154	**
	IL12A	0.104	*	0.111	*	-0.047	0.341	0.016	0.762
	IL12B	0.173	**	0.118	*	-0.067	0.174	-0.018	0.733
Th2	GATA3	0.096	*	0.099	*	0.155	**	0.137	**
	STAT6	0.264	***	0.239	***	0.183	***	0.176	***
	STAT5A	0.166	***	0.166	***	0.048	0.338	0.099	0.057
	IL13	0.062	0.170	0.092	0.061	-0.126	*	-0.109	*
Tfh	BCL6	0.304	***	0.351	***	0.163	***	0.152	**
	IL21	0.084	0.061	0.088	0.073	0.039	0.429	0.089	0.089
Th17	STAT3	0.639	***	0.629	***	0.255	***	0.302	***
	IL17A	0.065	0.146	-0.008	0.866	0.033	0.512	0.047	0.372
Treg	FOXP3	0.274	***	0.300	***	0.074	0.135	0.166	**
	CCR8	0.370	***	0.340	***	0.144	**	0.234	***
	STAT5B	0.468	***	0.463	***	0.281	***	0.279	***
	TGF β (TGFB1)	0.134	**	0.179	***	-0.122	*	-0.145	**
T cell exhaustion	PD-1 (PDCD1)	0.033	0.459	0.061	0.212	-0.053	0.283	0.007	0.897
	CTLA4	0.044	0.323	0.047	0.338	-0.050	0.317	0.013	0.801
	LAG3	-0.124	**	-0.111	*	-0.040	0.419	0.021	0.692
	TIM-3 (HAVCR2)	0.235	***	0.227	***	-0.029	0.555	0.069	0.186
	GZMB	0.122	**	0.143	**	-0.115	*	-0.057	0.273

PRAD, prostate adenocarcinoma; BLCA: bladder urothelial carcinoma; TAM, tumor-associated macrophage; Th, T helper cell; Tfh, Follicular helper T cell; Treg, regulatory T cell; Cor, R value of Spearman's correlation; None, correlation without adjustment. Purity, correlation adjusted by purity. * $P < 0.05$; ** $P < 0.01$; *** $P < 0.001$.

cells, Tfh cells, Treg cells, and Th17 cells in urogenital cancers. For example, YTHDF1 expression had a strong association with STAT1 in Th1 cells, STAT6 in Th2 cells, STAT3 in Th17 cells, STAT5B in Treg cells, BCL6 in Tfh cells, and IRF5 in M1 macrophages in most cancer types (**Supplementary Table 5**). We used BLCA (n = 408) and PRAD (n = 497) as examples to demonstrate the potential immune function of YTHDF1 in urogenital cancers. According to the results of **Table 1**, YTHDF1 has a close connection with all included marker genes of monocytes, tumor-associated macrophages (TAMs), M2 Macrophages, Th1 cells and regulatory T cells (Tregs) in PRAD. However, YTHDF1 expression in BLCA does not have a strong link since it is only correlated with most marker genes of Th2 cells, and regulatory T cells (Tregs). Different relationships between YTHDF1 expression and gene markers of immune cell infiltration in PRAD and BLCA may explain why there are different survival outcomes in various cancer types. These results again indicate that YTHDF1 expression plays an essential role in the infiltration of immune cells in human cancers, and that YTHDF1 might regulate the function of immune cells by participating in a mechanism similar to that of marker genes.

YTHDF1 Gene and Expression Altered in Different Clinical Subgroups of Urogenital Cancers

Analysis of YTHDF1 genomic alterations in urogenital cancers was explored with the cBioPortal website. The results showed that genomic alterations of YTHDF1 occurred in 0.7% of patients (**Figure 8A**). The types of YTHDF1 gene alterations were diverse, resulting in changes in gene expression (**Figure 8B**). Copy number variation (CNV) mainly occurred in PRAD and BLCA, while no CNV occurred in KICH and TGCT (**Figure 8C**). Next, we used the UALCAN database to explore YTHDF1 expression in urogenital cancers with different clinical characteristics. Taking BLCA as an example, we found that YTHDF1 was significantly differentially expressed existed in different cancer stages, histological subtypes, patient sex, molecular subtypes, nodal metastasis status and TP53 mutation status of BLCA (**Figures 8D–I**). Additionally, differential YTHDF1 expression in another five urogenital cancers with different clinical characteristics is displayed in **Supplementary Figure 11**. All the above results suggested that YTHDF1 genomic alteration and differential expression indeed occur in cancer tissue, and might play an essential role in cancer onset and progression.

YTHDF1 Coexpression Networks Correlate With the Immune Response

The above results identified that YTHDF1 had a significant association with the prognosis and immunity of cancers. Next, we explored YTHDF1 coexpression networks using the LinkedOmics database to verify the potential function of YTHDF1 in tumor tissue, and used BLCA as an example to illustrate the potential effect. In BLCA, 1396 genes (dark red dots) were significantly positively related to YTHDF1, and 1143 genes (dark green dots) were negatively related (false discovery rate (FDR) < 0.01) (**Figure 9A**). A heat map was used to display

the top 50 genes positively and negatively correlated with YTHDF1 (**Figures 9B, C**). Moreover, all coexpressed genes were displayed in **Supplementary Table 6**. C20orf11, CSTF1, and LSM14B ($r = 0.631$) had the strongest association with YTHDF1 expression ($r = 0.696, 0.647, 0.631$ and $P = 1.90E-60, 9.72E-46, 6.43E-46$, respectively). Next, gene set enrichment analysis (GSEA) was used to determine the main gene ontology (GO) terms of YTHDF1 coexpression genes. We further analyzed the biological process categories of GO and found that YTHDF1 and its co-expression genes primarily participated in the regulation of immune response, leukocyte activation and inflammatory response (**Figure 9D**). Then, we carried out Kyoto Encyclopedia of Genes and Genomes (KEGG) pathway analysis, and the results showed that coexpressed genes were enriched in staphylococcus aureus infection, antigen processing and presentation, and cytokine-cytokine receptor interaction (**Figure 9E**). These results suggested that YTHDF1 expression might play an essential role in human cancers by regulating the immune response of the TME.

DISCUSSION

YTHDF1, a “reader” of m6A, impairs the activation of DCs and CD8+ T cells by increasing the translation of lysosomal cathepsins and thus degrading tumor neoantigens (4, 17). Moreover, in mice with low YTHDF1 expression, there was a higher level of CD8+ T cells and NK cells in the TME, which means enhanced immunosurveillance in the absence of YTHDF1 (17). Moreover, YTHDF1 also plays an important role in oncogenesis and tumor progression in various cancers. For example, YTHDF1 promotes the growth and progression of bladder cancer *via* the ITGA6-METTL3 pathway (43). In colorectal cancer, YTHDF1 plays a vital oncogenic role in cell self-renewal and differentiation *via* the Wnt/ β -catenin pathway (44). In addition, YTHDF1 also produces a marked effect on lung cancer growth and metastasis by mediating YAP expression and activity (14). Although anti-programmed death 1 (PD-1)/programmed death ligand-1 (PD-L1) drugs have achieved considerable clinical efficacy and durable response with low toxicity (45, 46), they are not effective for all cancer types or do not achieve ideal efficacy in all patients (47). A new study identified that YTHDF1 deficiency in classical dendritic cells enhanced the cross-presentation of tumor antigens and the cross-priming of CD8+ T cells, and the therapeutic efficacy of the anti-PD-L1 drug was improved after blocking YTHDF1 (17). The YTHDF1 inhibitor GB1107 was also proven to inhibit the growth and metastasis of lung adenocarcinoma *in vivo* (48). Consistent with our findings and hypothesis, GB1107 increased tumor M1 macrophage polarization and CD8+ T cell infiltration and potentiated the effects of a PD-L1 immune checkpoint inhibitor (48). Therefore, YTHDF1 can be used as a new anticancer immunotherapy drug target or in combination with known immune checkpoint inhibitors to enhance immune infiltration and responses in cancers. These studies indicated that YTHDF1 might be a promising target in antitumor immunotherapy. Furthermore, combining anti-PD-L1 drugs with YTHDF1 depletion could be used as a new antitumor strategy.

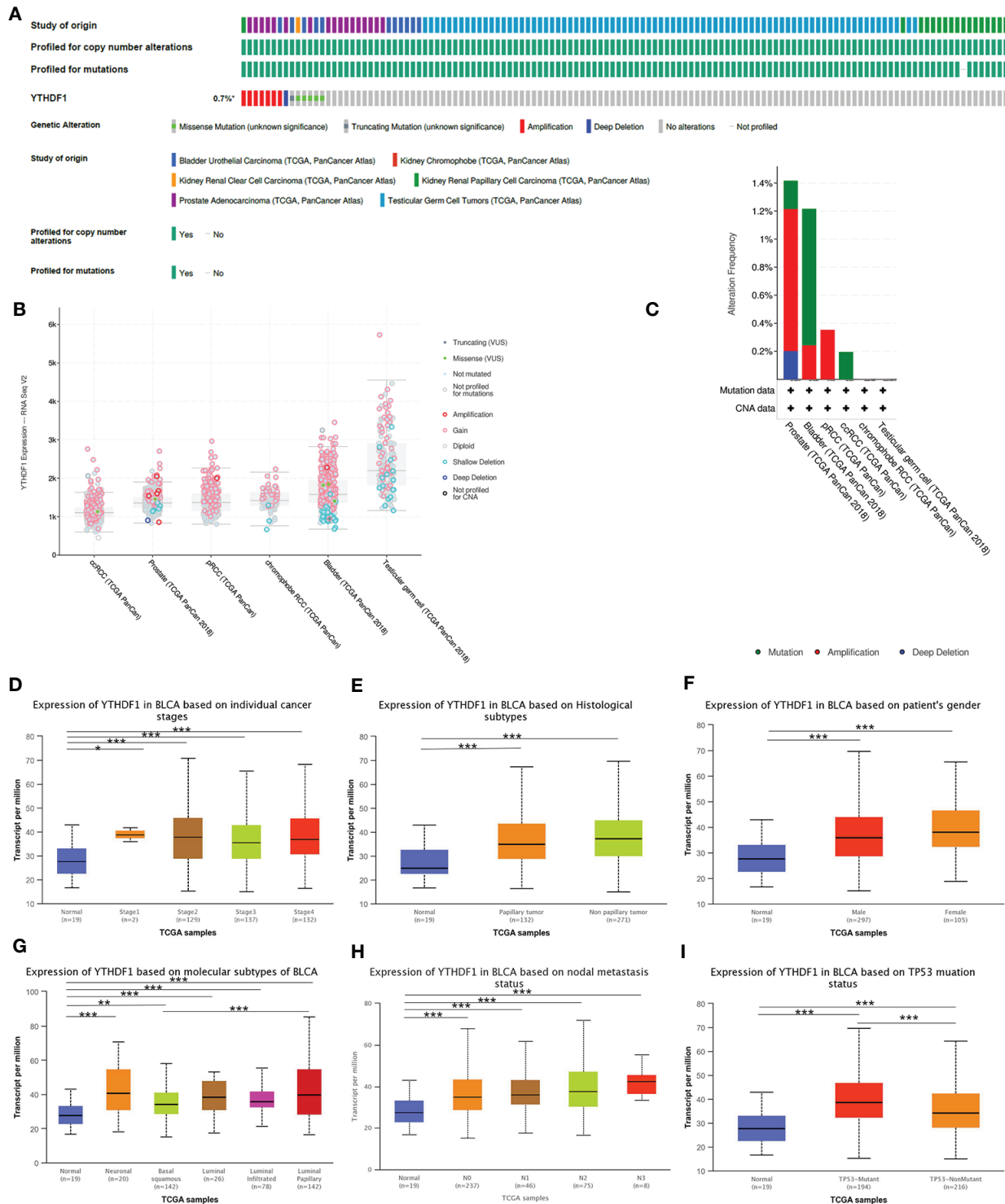


FIGURE 8 | YTHDF1 genomic alterations in six urogenital cancers analyzed by the cBioPortal database (A–C) and YTHDF1 differential expression in bladder cancer with different clinical subgroups (D–I) analyzed by the UALCAN database. (A) OncoPrint of YTHDF1 gene alterations in cancer cohort. (Different colors means different types of genetic alterations and amplification accounts for the largest proportion). (B) main type of YTHDF1 gene alterations in cancer groups. (C) Details of YTHDF1 gene alteration types in cancer cohort; (D–I) YTHDF1 differential expression in bladder cancer with individual cancer stages (n = 419) (D), histological subtypes (n = 422) (E), patient sex (n = 421) (F), molecular subtypes (n = 427) (G), nodal metastasis status (n = 385) (H), TP53 mutation status (n = 429) (I). (* $P < 0.05$, ** $P < 0.01$, *** $P < 0.001$).

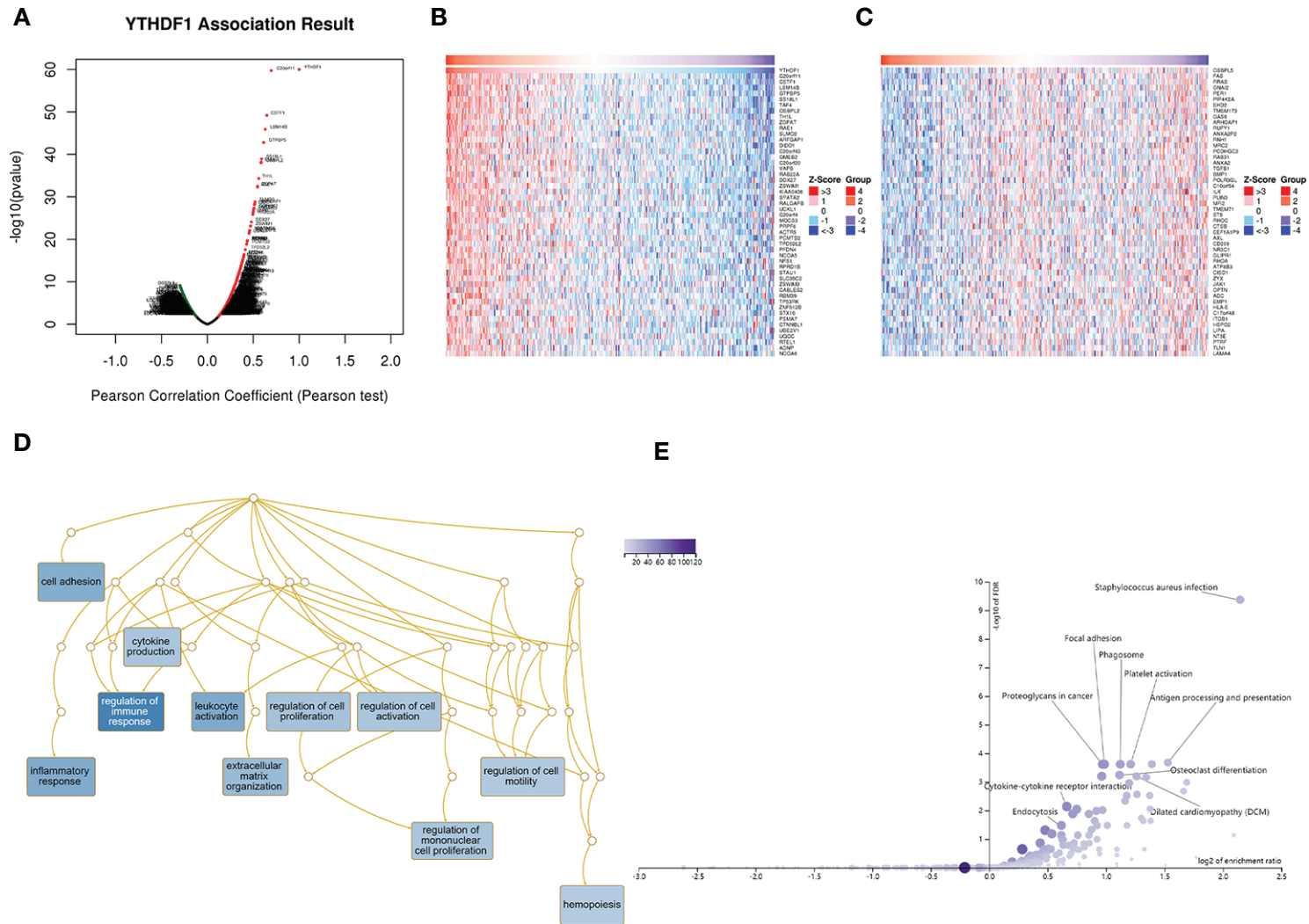


FIGURE 9 | YTHDF1 coexpression genes in BLCA analyzed by the LinkedOmics database. **(A)** Highly correlated genes of YTHDF1 tested by Pearson test in BLCA cohort. **(B, C)** Top 50 positive coexpression genes **(B)** and negative coexpression genes **(C)** of YTHDF1 in heat map in BLCA; **(D)** Directed acyclic graph of YTHDF1 GO analysis (biological process) in BLCA cohort. **(E)** Volcano plot of YTHDF1 KEGG pathways in BLCA cohort.

In the first step of our study, we used the Oncomine, TIMER, GEPIA, and BioGPS databases to determine the expression level of YTHDF1 in cancers and normal tissues. The results showed that YTHDF1 had significantly higher expression in most cancer types except lymphoma and THCA, which was consistent with previous studies in lung and colorectal cancer (14, 44). These results indicated that YTHDF1 indeed promotes oncogenesis and tumor progression in human cancers.

Next, the relationship between YTHDF1 expression and prognosis was explored. Similar to previous studies, high YTHDF1 expression patients had a worse prognosis in LIHC and TCGT (49, 50). In addition, in many other cancer types such as ACC, BLCA, MESO, UVM, LIHC, and UCS, high YTHDF1 expression meant worse prognosis, which proved that YTHDF1 was a potential prognostic pan-cancer biomarker. Then, we explored YTHDF1 expression in different immune subtypes and molecular subtypes of human cancers to determine its potential mechanism of action. The results showed that YTHDF1 expression was significantly different in different immune subtypes and molecular subtypes in most cancer types, which might prove that YTHDF1 is a promising diagnostic pan-cancer biomarker and participates in immune regulation. Moreover, we demonstrated that there were significant differences in YTHDF1 expression in different clinical subgroups of urogenital cancers, consistent with a previous study showing that YTHDF1 is expressed differently in KIRC at different stages (50). In fact, YTHDF1 differential YTHDF1 expression existed in all urogenital cancers with diverse clinical characteristics, which indicated that YTHDF1 might play a role in the growth and progression of cancers.

Tumor-infiltrating lymphocytes (TILs) in the TME have been proven to be an independent predictor of cancer patient prognosis and immunotherapeutic efficacy (51, 52). Our study demonstrated that YTHDF1 had a strong association with TILs and played an essential role in the TME. For example, YTHDF1 expression was strongly significantly related to CD8+ T cells, macrophages and dendritic cells. As a universal component of the TME, macrophages have been proven to contribute to immune evasion and suppression (53). The TME with low YTHDF1 expression contained higher levels of CD8+ T cells and natural killer (NK) cells in a mouse model, and enhanced the ability to DCs in cross-present of tumor antigens (17). In particular, in PRAD, we found that YTHDF1 expression has a close association with TILs in the TME. For example, YTHDF1 expression has a close association with IFN- γ in PRAD, which is regarded as a hallmark of antitumor immunity (54). Moreover, YTHDF1 expression is related to all of the examined marker genes of CD8+ T cells, monocytes, tumor-associated macrophages (TAMs), M2 macrophages, Th1 cells, and other known immune stimulatory and immune suppressive cytokines, which proves the potential immune function of YTHDF1 in PRAD.

Our study also found that YTHDF1 was negatively related to the immune, stromal and ESTIMATE scores of the TME in most human cancer types, but YTHDF1 expression was not always negatively related to TILs in human cancers, which indicated that YTHDF1 plays a different immune regulation role in various

cancer types. The correlation between YTHDF1 and tumor mutational burden (TMB), microsatellite instability (MSI), and neoantigens also proved that YTHDF1 closely related with the TME in human cancers. However, further experimental research to prove its function.

In our analysis of YTHDF1 coexpression networks, we found that YTHDF1 and its coexpression genes indeed took part in regulating the immune response and antigen processing and presentation. Furthermore, a previous study proved that anti-PD-L1 drugs achieved better therapeutic efficacy in YTHDF1 low expression conditions (17). A strong relationship between YTHDF1 and ICP genes was found, which provides a theoretical basis for combined molecular targeting immunotherapy for the future. In summary, the above results strongly indicated the potential of YTHDF1 as a target in anticancer immunotherapy.

However, even though we performed a comprehensive and systematic analysis on YTHDF1 and used different databases and R 3.2.2 for cross-verification, there are some limitations to this study. First, the microarray and sequencing data from different databases exhibited differences and lacked granularity and specificity, which might cause systematic bias. Second, *in vivo/in vitro* experiments are needed to prove our results on the potential function of YTHDF1, which could increase the credibility of our results. Third, even though we concluded that YTHDF1 expression was strongly related to immune cell infiltration and prognosis of human cancers, we lack direct evidence on YTHDF1 influencing prognosis by taking part in immune infiltration. Therefore, the mechanisms by which YTHDF1 participate in immune regulation remain unknown, and the exact pathway needs further study. Fourth, no anti-YTHDF1 therapeutic monoclonal antibodies have been evaluated in clinical trials. Therefore, we have no specific and complete cases with data to identify the benefit of anti-YTHDF1 targeting drugs in the survival of cancer models or inhibiting tumor growth. In the future, a prospective study of YTHDF1 expression and its role in human cancers' immune infiltration is needed, along with successful development and testing of a new antitumor immunotherapy drug targeting YTHDF1.

DATA AVAILABILITY STATEMENT

The datasets presented in this study can be found in online repositories. The names of the repository/repositories and accession number(s) can be found in the article/**Supplementary Material**.

AUTHOR CONTRIBUTIONS

JianH, DQ, AY and JiaoH were responsible for experimental design, experimental analysis and thesis writing. HD, HL, and ZY were responsible for data screening, collection and writing. JC and XZ were responsible for the guidance and review of the thesis. All authors contributed to the article and approved the submitted version.

FUNDING

We thank the National Natural Science Foundation of China (81902592), Hunan Province Key R&D Program (2019SK2202) and Xiangya Hospital Youth Fund (2018Q09) for the financial support. This article has not received sponsorship for publication.

ACKNOWLEDGMENTS

We thank everyone who provided support for this study. Thank You-e He and Belaydi Othmane for the helpful suggestions and language polishing on this manuscript.

SUPPLEMENTARY MATERIAL

The Supplementary Material for this article can be found online at: <https://www.frontiersin.org/articles/10.3389/fonc.2021.607224/full#supplementary-material>

Supplementary Figure 1 | YTHDF1 expression in different cancer cell lines (A) and normal tissue (B) investigated by the BioGPS database.

Supplementary Figure 2 | Kaplan-Meier survival curve of human cancers with high and low YTHDF1 expression analyzed by the Kaplan-Meier plotter database. (A–G) Overall survival of ESCA, HNSC, PPAD, PCPG, READ, THCA, and UCEC with high and low YTHDF1 expression (n = 80, 499, 177, 178, 165, and 502 respectively); (H–N) Progression-free survival of ESSC, HNSC, LUAD, PAAD, READ, STAD, and UCEC with high and low YTHDF1 expression (n = 54, 124, 300, 69, 47, 215, and 422, respectively).

Supplementary Figure 3 | Relationship between YTHDF1 expression and pan-cancer immune subtypes.

Supplementary Figure 4 | Relationship between YTHDF1 expression and pan-cancer molecular subtypes.

Supplementary Figure 5 | Correlation between YTHDF1 expression and 24 tumor infiltrating lymphocytes (TILs) in KICH analyzed by the GEPIA database.

Supplementary Figure 6 | Correlation between YTHDF1 expression and 24 tumor infiltrating lymphocytes (TILs) in PRAD analyzed by the GEPIA database.

Supplementary Figure 7 | Correlation between YTHDF1 expression and 24 tumor infiltrating lymphocytes (TILs) in KIRC analyzed by the GEPIA database.

Supplementary Figure 8 | Correlation between YTHDF1 expression and 24 tumor infiltrating lymphocytes (TILs) in KIRP analyzed by the GEPIA database.

Supplementary Figure 9 | Correlation between YTHDF1 expression and 24 tumor infiltrating lymphocytes (TILs) in BLCA analyzed by the GEPIA database.

Supplementary Figure 10 | Correlation between YTHDF1 expression and 24 tumor infiltrating lymphocytes (TILs) in TGCT analyzed by the GEPIA database.

Supplementary Figure 11 | YTHDF1 differential expression in five urogenital cancers with different clinical subgroups analyzed by the UALCAN database.

Supplementary Table 1 | Sample Numbers of the TCGA Cancer types and corresponding immune and molecular subtypes.

Supplementary Table 2 | Correlation between YTHDF1 expression and survival in the GEO datasets analyzed by the PrognScan database.

Supplementary Table 3 | Detailed relationship between YTHDF1 expression and pan-cancer immune cell infiltration in the tumor microenvironment.

Supplementary Table 4 | Relationship between YTHDF1 expression and related immune marker sets of urogenital cancers analyzed by the TIMER database.

Supplementary Table 5 | 24 tumors associated infiltrating lymphocytes (TILs) and their gene markers.

Supplementary Table 6 | YTHDF1 coexpression genes in urogenital cancers analyzed by the LinkedOmics database.

REFERENCES

- He L, Li H, Wu A, Peng Y, Shu G, Yin G. Functions of N6-methyladenosine and its Role in Cancer. *Mol Cancer* (2019) 18(1):176. doi: 10.1186/s12943-019-1109-9
- Dominissini D, Moshitch-Moshkovitz S, Schwartz S, Salmon-Divon M, Ungar L, Osenberg S, et al. Topology of the Human and Mouse M6a RNA Methylomes Revealed by M6a-Seq. *Nature* (2012) 485(7397):201–6. doi: 10.1038/nature11112
- Jia G, Fu Y, Zhao X, Dai Q, Zheng G, Yang Y, et al. N6-Methyladenosine in Nuclear RNA is a Major Substrate of the Obesity-Associated FTO. *Nat Chem Biol* (2011) 7(12):885–7. doi: 10.1038/nchembio.687
- Wang X, Zhao BS, Roundtree IA, Lu Z, Han D, Ma H, et al. N(6)-Methyladenosine Modulates Messenger RNA Translation Efficiency. *Cell* (2015) 161(6):1388–99. doi: 10.1016/j.cell.2015.05.014
- Wang X, Lu Z, Gomez A, Hon GC, Yue Y, Han D, et al. N6-Methyladenosine-Dependent Regulation of Messenger RNA Stability. *Nature* (2014) 505(7481):117–20. doi: 10.1038/nature12730
- Dang W, Xie Y, Cao P, Xin S, Wang J, Li S, et al. N(6)-Methyladenosine and Viral Infection. *Front Microbiol* (2019) 10:417. doi: 10.3389/fmicb.2019.00417
- Roignant JY, Sollier M. M(6)a in Mrna: An Ancient Mechanism for Fine-Tuning Gene Expression. *Trends Genet TIG* (2017) 33(6):380–90. doi: 10.1016/j.tig.2017.04.003
- Liu J, Eckert MA, Harada BT, Liu SM, Lu Z, Yu K, et al. M(6)a mRNA Methylation Regulates AKT Activity to Promote the Proliferation and Tumorigenicity of Endometrial Cancer. *Nat Cell Biol* (2018) 20(9):1074–83. doi: 10.1038/s41556-018-0174-4
- Vu LP, Pickering BF, Cheng Y, Zaccara S, Nguyen D, Minuesa G, et al. The N(6)-methyladenosine (M(6)a)-Forming Enzyme METTL3 Controls Myeloid Differentiation of Normal Hematopoietic and Leukemia Cells. *Nat Med* (2017) 23(11):1369–76. doi: 10.1038/nm.4416
- Li Z, Weng H, Su R, Weng X, Zuo Z, Li C, et al. Fto Plays an Oncogenic Role in Acute Myeloid Leukemia as a N(6)-Methyladenosine Rna Demethylase. *Cancer Cell* (2017) 31(1):127–41. doi: 10.1016/j.ccell.2016.11.017
- Liu ZX, Li LM, Sun HL, Liu SM. Link Between M6a Modification and Cancers. *Front Bioeng Biotechnol* (2018) 6:89. doi: 10.3389/fbioe.2018.00089
- Ott PA, Hu Z, Keskin DB, Shukla SA, Sun J, Bozym DJ, et al. An Immunogenic Personal Neoantigen Vaccine for Patients With Melanoma. *Nature* (2017) 547(7662):217–21. doi: 10.1038/nature22991
- Schumacher TN, Schreiber RD. Neoantigens in Cancer Immunotherapy. *Sci (New York NY)* (2015) 348(6230):69–74. doi: 10.1126/science.aaa4971
- Jin D, Guo J, Wu Y, Yang L, Wang X, Du J, et al. M(6)a Demethylase ALKBH5 Inhibits Tumor Growth and Metastasis by Reducing YTHDFs-mediated YAP Expression and Inhibiting Mir-107/LATS2-Mediated YAP Activity in NSCLC. *Mol Cancer* (2020) 19(1):40. doi: 10.1186/s12943-020-01161-1
- Nishizawa Y, Konno M, Asai A, Koseki J, Kawamoto K, Miyoshi N, et al. Oncogene c-Myc Promotes Epitranscriptome M(6)a Reader YTHDF1 Expression in Colorectal Cancer. *Oncotarget* (2018) 9(7):7476–86. doi: 10.18632/oncotarget.23554
- Liu L, Liu X, Dong Z, Li J, Yu Y, Chen X, et al. N6-Methyladenosine-Related Genomic Targets are Altered in Breast Cancer Tissue and Associated With Poor Survival. *J Cancer* (2019) 10(22):5447–59. doi: 10.7150/jca.35053
- Han D, Liu J, Chen C, Dong L, Liu Y, Chang R, et al. Anti-Tumour Immunity Controlled Through mRNA M(6)a Methylation and YTHDF1 in Dendritic Cells. *Nature* (2019) 566(7743):270–4. doi: 10.1038/s41586-019-0916-x

18. Rhodes DR, Kalyana-Sundaram S, Mahavisno V, Varambally R, Yu J, Briggs BB, et al. OncoPrint 3.0: Genes, Pathways, and Networks in a Collection of 18,000 Cancer Gene Expression Profiles. *Neoplasia (New York NY)* (2007) 9 (2):166–80. doi: 10.1593/neo.07112
19. Li T, Fan J, Wang B, Traugh N, Chen Q, Liu JS, et al. TIMER: A Web Server for Comprehensive Analysis of Tumor-Infiltrating Immune Cells. *Cancer Res* (2017) 77(21):e108–e10. doi: 10.1158/0008-5472.Can-17-0307
20. Tang Z, Kang B, Li C, Chen T, Zhang Z. GEPIA2: An Enhanced Web Server for Large-Scale Expression Profiling and Interactive Analysis. *Nucleic Acids Res* (2019) 47(W1):W556–w60. doi: 10.1093/nar/gkz430
21. Wu C, Jin X, Tsung G, Afrasiabi C, Su AI. BioGPS: Building Your Own Mash-Up of Gene Annotations and Expression Profiles. *Nucleic Acids Res* (2016) 44(D1):D313–6. doi: 10.1093/nar/gkv1104
22. Mizuno H, Kitada K, Nakai K, Sarai A. Prognoscan: A New Database for Meta-Analysis of the Prognostic Value of Genes. *BMC Med Genomics* (2009) 2:18. doi: 10.1186/1755-8794-2-18
23. Nagy A, Lanczky A, Menyhart O, Gyorffy B. Validation of miRNA Prognostic Power in Hepatocellular Carcinoma Using Expression Data of Independent Datasets. *Sci Rep* (2018) 8(1):9227. doi: 10.1038/s41598-018-27521-y
24. Ru B, Wong CN, Tong Y, Zhong JY, Zhong SSW, Wu WC, et al. TISIDB: An Integrated Repository Portal for Tumor-Immune System Interactions. *Bioinf (Oxford England)* (2019) 35(20):2400–2. doi: 10.1093/bioinformatics/btz210
25. Wang D, Wang Y, Zou X, Shi Y, Liu Q, Huan T, et al. FOXO1 Inhibition Prevents Renal Ischemia-Reperfusion Injury Via cAMP-response Element Binding Protein/PPAR- γ Coactivator-1 α -Mediated Mitochondrial Biogenesis. *Br J Pharmacol* (2020) 177(2):432–48. doi: 10.1111/bph.14878
26. Danilova L, Ho WJ, Zhu Q, Vithayathil T, De Jesus-Acosta A, Azad NS, et al. Programmed Cell Death Ligand-1 (PD-L1) and CD8 Expression Profiling Identify an Immunologic Subtype of Pancreatic Ductal Adenocarcinomas With Favorable Survival. *Cancer Immunol Res* (2019) 7(6):886–95. doi: 10.1158/2326-6066.Cir-18-0822
27. Bonneville R, Krook MA, Kautto EA, Miya J, Wing MR, Chen H-Z, et al. Landscape of Microsatellite Instability Across 39 Cancer Types. *JCO Precis Oncol* (2017) 1:PO.17.00073. doi: 10.1200/PO.17.00073
28. Chan TA, Yarchoan M, Jaffee E, Swanton C, Quezada SA, Stenzinger A, et al. Development of Tumor Mutation Burden as an Immunotherapy Biomarker: Utility for the Oncology Clinic. *Ann Oncol Off J Eur Soc Med Oncol* (2019) 30 (1):44–56. doi: 10.1093/annonc/mdy495
29. Rooney MS, Shukla SA, Wu CJ, Getz G, Hacohen N. Molecular and Genetic Properties of Tumors Associated With Local Immune Cytolytic Activity. *Cell* (2015) 160(1–2):48–61. doi: 10.1016/j.cell.2014.12.033
30. Yoshihara K, Shahmoradgol M, Martínez E, Vegesna R, Kim H, Torres-Garcia W, et al. Inferring Tumour Purity and Stromal and Immune Cell Admixture From Expression Data. *Nat Commun* (2013) 4:2612. doi: 10.1038/ncomms3612
31. Li B, Severson E, Pignon JC, Zhao H, Li T, Novak J, et al. Comprehensive Analyses of Tumor Immunity: Implications for Cancer Immunotherapy. *Genome Biol* (2016) 17(1):174. doi: 10.1186/s13059-016-1028-7
32. Miao YR, Zhang Q, Lei Q, Luo M, Xie GY, Wang H, et al. Immucellai: A Unique Method for Comprehensive T-Cell Subsets Abundance Prediction and its Application in Cancer Immunotherapy. *Advanced Sci (Weinheim Baden Wurttemberg Germany)* (2020) 7(7):1902880. doi: 10.1002/advs.201902880
33. Sousa S, Maatta J. The Role of Tumour-Associated Macrophages in Bone Metastasis. *J Bone Oncol* (2016) 5(3):135–8. doi: 10.1016/j.jbo.2016.03.004
34. Danaher P, Warren S, Dennis L, D'Amico L, White A, Disis ML, et al. Gene Expression Markers of Tumor Infiltrating Leukocytes. *J Immunother Cancer* (2017) 5:18. doi: 10.1186/s40425-017-0215-8
35. Siemers NO, Holloway JL, Chang H, Chasalow SD, Ross-MacDonald PB, Voliva CF, et al. Genome-Wide Association Analysis Identifies Genetic Correlates of Immune Infiltrates in Solid Tumors. *PloS One* (2017) 12(7):e0179726. doi: 10.1371/journal.pone.0179726
36. Gao J, Aksoy BA, Dogrusoz U, Dresdner G, Gross B, Sumer SO, et al. Integrative Analysis of Complex Cancer Genomics and Clinical Profiles Using the Cbioportal. *Sci Signaling* (2013) 6(269):pl1. doi: 10.1126/scisignal.2004088
37. Chandrashekar DS, Bashel B, Balasubramanya SAH, Creighton CJ, Ponce-Rodriguez I, Chakravarthi B, et al. Ualcan: A Portal for Facilitating Tumor Subgroup Gene Expression and Survival Analyses. *Neoplasia (New York NY)* (2017) 19(8):649–58. doi: 10.1016/j.neo.2017.05.002
38. Zhou G, Soufan O, Ewald J, Hancock REW, Basu N, Xia J. NetworkAnalyst 3.0: A Visual Analytics Platform for Comprehensive Gene Expression Profiling and Meta-Analysis. *Nucleic Acids Res* (2019) 47(W1):W234–41. doi: 10.1093/nar/gkz240
39. Topalian SL, Drake CG, Pardoll DM. Immune Checkpoint Blockade: A Common Denominator Approach to Cancer Therapy. *Cancer Cell* (2015) 27(4):450–61. doi: 10.1016/j.ccell.2015.03.001
40. Lee V, Murphy A, Le DT, Diaz LA Jr. Mismatch Repair Deficiency and Response to Immune Checkpoint Blockade. *Oncologist* (2016) 21(10):1200–11. doi: 10.1634/theoncologist.2016-0046
41. Peng M, Mo Y, Wang Y, Wu P, Zhang Y, Xiong F, et al. Neoantigen Vaccine: An Emerging Tumor Immunotherapy. *Mol Cancer* (2019) 18(1):128. doi: 10.1186/s12943-019-1055-6
42. Yarchoan M, Hopkins A, Jaffee EM. Tumor Mutational Burden and Response Rate to PD-1 Inhibition. *New Engl J Med* (2017) 377(25):2500–1. doi: 10.1056/NEJMc1713444
43. Jin H, Ying X, Que B, Wang X, Chao Y, Zhang H, et al. N(6)-Methyladenosine Modification of ITGA6 mRNA Promotes the Development and Progression of Bladder Cancer. *EBioMedicine* (2019) 47:195–207. doi: 10.1016/j.ebiom.2019.07.068
44. Bai Y, Yang C, Wu R, Huang L, Song S, Li W, et al. Ythdf1 Regulates Tumorigenicity and Cancer Stem Cell-Like Activity in Human Colorectal Carcinoma. *Front Oncol* (2019) 9:332. doi: 10.3389/fonc.2019.00332
45. Ma LJ, Feng FL, Dong LQ, Zhang Z, Duan M, Liu LZ, et al. Clinical Significance of PD-1/PD-Ls Gene Amplification and Overexpression in Patients With Hepatocellular Carcinoma. *Theranostics* (2018) 8(20):5690–702. doi: 10.7150/thno.28742
46. Meng X, Huang Z, Teng F, Xing L, Yu J. Predictive Biomarkers in PD-1/PD-L1 Checkpoint Blockade Immunotherapy. *Cancer Treat Rev* (2015) 41 (10):868–76. doi: 10.1016/j.ctrv.2015.11.001
47. Topalian SL, Hodi FS, Brahmer JR, Gettinger SN, Smith DC, McDermott DF, et al. Safety, Activity, and Immune Correlates of anti-PD-1 Antibody in Cancer. *New Engl J Med* (2012) 366(26):2443–54. doi: 10.1056/NEJMoa1200690
48. Vuong L, Kouverianou E, Rooney CM, McHugh BJ, Howie SEM, Gregory CD, et al. An Orally Active Galectin-3 Antagonist Inhibits Lung Adenocarcinoma Growth and Augments Response to PD-L1 Blockade. *Cancer Res* (2019) 79 (7):1480–92. doi: 10.1158/0008-5472.Can-18-2244
49. Zhao X, Chen Y, Mao Q, Jiang X, Jiang W, Chen J, et al. Overexpression of YTHDF1 Is Associated With Poor Prognosis in Patients With Hepatocellular Carcinoma. *Cancer Biomarkers Section A Dis Markers* (2018) 21(4):859–68. doi: 10.3233/cbm-170791
50. Lobo J, Barros-Silva D, Henrique R, Jerónimo C. The Emerging Role of Epitranscriptomics in Cancer: Focus on Urological Tumors. *Genes* (2018) 9 (11):552–73. doi: 10.3390/genes9110552
51. Azimi F, Scolyer RA, Rumcheva P, Moncrieff M, Murali R, McCarthy SW, et al. Tumor-Infiltrating Lymphocyte Grade is an Independent Predictor of Sentinel Lymph Node Status and Survival in Patients With Cutaneous Melanoma. *J Clin Oncol Off J Am Soc Clin Oncol* (2012) 30(21):2678–83. doi: 10.1200/jco.2011.37.8539
52. Ohtani H. Focus on TILs: Prognostic Significance of Tumor Infiltrating Lymphocytes in Human Colorectal Cancer. *Cancer Immun* (2007) 7:4.
53. Gajewski TF, Schreiber H, Fu YX. Innate and Adaptive Immune Cells in the Tumor Microenvironment. *Nat Immunol* (2013) 14(10):1014–22. doi: 10.1038/ni.2703
54. Grasso CS, Tsoi J, Onyshchenko M, Abril-Rodriguez G, Ross-Macdonald P, Wind-Rotolo M, et al. Conserved Interferon- γ Signaling Drives Clinical Response to Immune Checkpoint Blockade Therapy in Melanoma. *Cancer Cell* (2020) 39(1):122. doi: 10.1016/j.ccell.2020.11.015

Conflict of Interest: The authors declare that the research was conducted in the absence of any commercial or financial relationships that could be construed as a potential conflict of interest.

Copyright © 2021 Hu, Qiu, Yu, Hu, Deng, Li, Yi, Chen and Zu. This is an open-access article distributed under the terms of the Creative Commons Attribution License (CC BY). The use, distribution or reproduction in other forums is permitted, provided the original author(s) and the copyright owner(s) are credited and that the original publication in this journal is cited, in accordance with accepted academic practice. No use, distribution or reproduction is permitted which does not comply with these terms.

Advantages of publishing in Frontiers



OPEN ACCESS

Articles are free to read
for greatest visibility
and readership



FAST PUBLICATION

Around 90 days
from submission
to decision



HIGH QUALITY PEER-REVIEW

Rigorous, collaborative,
and constructive
peer-review



TRANSPARENT PEER-REVIEW

Editors and reviewers
acknowledged by name
on published articles

Frontiers

Avenue du Tribunal-Fédéral 34
1005 Lausanne | Switzerland

Visit us: www.frontiersin.org

Contact us: frontiersin.org/about/contact



REPRODUCIBILITY OF RESEARCH

Support open data
and methods to enhance
research reproducibility



DIGITAL PUBLISHING

Articles designed
for optimal readership
across devices



FOLLOW US

@frontiersin



IMPACT METRICS

Advanced article metrics
track visibility across
digital media



EXTENSIVE PROMOTION

Marketing
and promotion
of impactful research



LOOP RESEARCH NETWORK

Our network
increases your
article's readership